THE UNIVERSITY
of EDINBURGH

Targeting Aerobic Glycolysis in Breast and Ovarian Cancer

Chrysi Xintaropoulou

A thesis submitted in fulfilment of the requirements of the degree of

Doctor of Philosophy

University of Edinburgh

December 2016

Declaration

I, Chrysi Xintaropoulou, hereby declare that

- The present thesis has been composed by myself.
- The work in this thesis is solely my own work unless otherwise indicated, where credit to the contributor is clearly given.
- No part of the present work has been submitted for any other degree or professional qualification except as specified.

Chrysi Xintaropoulou

April 2017

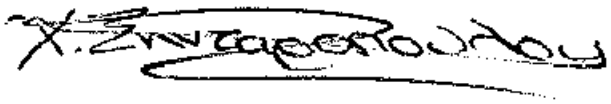

Scientific Abstract

Cancer cells, unlike normal tissue, frequently rely on glycolysis for the production of energy and the metabolic intermediates required for their growth regardless of cellular oxygenation levels. This metabolic reconfiguration, termed the Warburg effect, provides a potential strategy to preferentially target tumours from a therapeutic perspective. The present study sought to investigate the glycolytic phenotype of breast and ovarian cancer, and assess the possibility of exploiting several glycolytic targets therapeutically. Initially the growth dependency of breast and ovarian cancer cells on the availability of glucose was established. An array of 10 compounds reported to inhibit key enzymes of the glycolytic pathway were investigated and compared against an extended panel of breast and ovarian cancer cell line models. All inhibitors investigated, targeted against multiple points of the pathway, were shown to block the glycolytic pathway as demonstrated by glucose accumulation in the culture media combined with decreased lactate secretion, and attenuated breast and ovarian cancer cell proliferation in a concentration dependent manner. Furthermore their mechanism of action was investigated by flow cytometric analysis and their antiproliferative effect was associated with induction of apoptosis and G0/G1 cell cycle arrest. The glycolytic inhibitors were further assessed in combination strategies with established chemotherapeutic and targeted agents and several synergistic interactions, characterised by low combination index values, were revealed. Among them, 3PO (a novel PFKFB3 inhibitor) enhanced the effect of cisplatin in both platinum sensitive and platinum resistant ovarian cancer cells suggesting a strategy for treatment of platinum resistant disease. Furthermore robust synergy was identified between IOM-1190 (a novel GLUT1 inhibitor) and metformin, an antidiabetic inhibitor of oxidative phosphorylation, resulting in strong inhibition of breast cancer cell growth. This combination is proposed for the treatment of highly aggressive triple negative breast tumours. An additional objective of this research was to investigate the effect of the oxygen level on sensitivity to glycolysis inhibition. Breast cancer cells were found to be more sensitive to glycolysis inhibition in high oxygen conditions. This enhanced resistance at low oxygen levels was associated with upregulation of the targeted glycolytic enzymes as demonstrated at both the mRNA (by gene expression microarray profiling, Illumina BeadArrays) and protein level (by Western blotting). Manipulation of LDHA (Lactate Dehydrogenase A) by siRNA knockdown provided further evidence that downregulation of this target was sufficient to significantly suppress breast cancer cell proliferation. Finally, the expression of selected glycolytic targets was examined in a clinical tissue microarray set of a large cohort of ovarian tumours using quantitative immunofluorescence technology, AQUA.

The role of the glycolytic phenotype in ovarian cancer was suggested and interesting associations between the glycolytic profile and clear cell and endometrioid ovarian cancers revealed. Increased PKM2 (Pyruvate kinase isozyme M2) and LDHA expression were demonstrated in clear cell tumours and also low expression of these enzymes was significantly correlated with improved survival of endometrioid ovarian cancer patients. Taken together the findings of this study support the glycolytic pathway as a legitimate target for further investigation in breast and ovarian cancer treatment.

Lay Summary

Breast and ovarian cancer are two malignancies that present a major concern in public health care. Therefore there is an urgent need for novel targeted effective therapies. It is now well established that many cancer cells, unlike normal tissue, reduce their dependence on mitochondrial oxidative phosphorylation as their primary energy source and favour glycolysis. This altered metabolism, a defining feature of cancer, is expected to offer a strategy to preferentially kill cancer cells. The present study set out to investigate the glycolytic metabolism of breast and ovarian cancer, and assess the possibility of exploiting this alternative metabolic route for the development of novel cancer drug therapies. Initially it was established that proliferative growth of breast and ovarian cancer cells was dependent on glucose availability. The effects of a series of pharmacological tool compounds inhibiting key molecules of the pathway along with their mechanism of action were then examined. All compounds tested blocked the pathway and were shown to effectively target proliferation and growth of various breast and ovarian cancer cell line models. An additional objective of this research was to assess the metabolic inhibitors in combination strategies with common chemotherapeutic and targeted agents. Two novel promising strategies have been identified and are proposed for further evaluation. Glycolytic inhibitors were found to enhance the potency of platinum chemotherapy and sensitise resistant ovarian cancer cells to it. Also in combination with the antidiabetic drug metformin they produced robust synergistic effects on cell growth of relatively aggressive breast cancer cells. This study examined the impact of the oxygen level on the antiproliferative efficacy of the metabolic inhibitors and greater resistance to the compounds was demonstrated at low oxygen conditions. This was interpreted as due to the elevated expression of the target enzymes in these conditions. Finally, the expression of glycolytic targets of interest was evaluated in clinical tissue ovarian cancer samples. The importance of the glycolytic pathway in ovarian cancer was ascertained and furthermore, subgroups of tumours from which glycolytic enzymes could be used as survival markers or that could be more susceptible to glycolysis inhibition, were identified. Overall, this research makes a further contribution to our knowledge of the role of the glycolytic metabolism in breast and ovarian tumours and provides evidence that the glycolytic pathway is a promising target for breast and ovarian cancer treatment.

Publication

Part of this thesis was the basis for a published manuscript:

''A comparative analysis of inhibitors of the glycolysis pathway in breast and ovarian cancer cell line models''

Chrysi Xintaropoulou, Carol Ward, Alan Wise, Hugh Marston, Arran Turnbull,

Simon P. Langdon

Oncotarget 2015

DOI: 10.18632/oncotarget.4499

Manuscript included in Appendix 4.

All this work is dedicated

to my mother

Acknowledgments

I would like to take this opportunity to acknowledge certain people that without their contribution this thesis would not have been completed.

First and foremost I owe my deepest gratitude to my supervisors Dr Simon Langdon and Dr Carol Ward for their excellent guidance and valuable assistance throughout the past four and a half years. Both of them have supported me greatly, both scientifically and personally, throughout this period and especially in my final year that has been extremely difficult for me. Their influence and contribution on my academic progress were invaluable for me.

I also feel much obliged to my company supervisor Dr Alan Wise for his much appreciated support, valuable advice and guidance. In particular I owe a special thank you to everyone that used to work in TPP Global Development during my project, now called IOmet Pharma. They contributed significantly to my project. Meetings with them, even though extremely stressful for me at the very beginning, soon became enjoyable. Their constructive criticism and their 'out of the box' thinking were of great importance in my research.

Also I would like to thank the members of the committee of my first and second year examination board namely Dr Malcolm Walkinshaw, Dr Grant Stewart, Dr Hugh Marston and Prof David Harrison for their helpful comments and productive discussion regarding my project.

I also need to thank the Medical Research Scotland research charity for funding this project and Ms Alex Graham for her kindness and willingness to help in any situation.

I am very grateful to Dr Arran Turnbull for his assistance with the analysis of the AQUA and gene expression data as well as to Dr Elisabeth Freyer for her assistance with the FACS analysis. I would also like to give special thanks to James Meehan and Ed Jarman for our collaboration in the gene expression experiment. The tasks of sample collection, RNA extraction and RNA amplification were shared among the three of us.

I would especially like to say a big thank you to everyone in the Division of Pathology Labs for their support and for making three years of my life so enjoyable. My best friend Ghassan who shared an office with me for two years and made me laugh during many late evenings in the lab and supported me in his own unique way through our long 'psychotherapy' sessions. My dearests, Elaine and Helen, who always took 'special care' of me and we had great fun together in our outdoor lunches and beauty events. James and Carlos with whom we started

the journey of our PhDs at the same time and I have really enjoyed working together and sharing the lab and tissue culture room with them. Ed was the last addition to our group in my last year in the lab. Peter joined our office for almost a year and we had a good laugh together. And Kyle that I shared an office with the very first months in the lab and he gave me the ‘heads-up’ and made me feel welcome in his own way.

Finally, but most importantly, I would like to thank my whole family and especially my father George, my beloved siblings Andromache and Fotis and my partner Thodoris. Their unconditional love and ineffable support means everything to me. The final write up year of this project has been a tremendously difficult period in my life and without their encouragement and devotion I would never have made it here. Also I would like to thank my special friends Antonia, Aliki, Danae and Elena for just always being there and especially when I needed them the most.

Financial Support

I am grateful to Medical Research Scotland for support of this study.

List of Contents

Scientific Abstract 3

Lay Summary 7

Declaration 3

Publication 9

Acknowledgments 13

Financial Support 14

List of Contents 15

List of Abbreviations 23

CHAPTER 1: INTRODUCTION 31

1.1 Breast & Ovarian Cancer 31

1.1.1 Epidemiology of female malignancies 31

1.1.2 Breast Cancer 33

1.1.2.1 Risk factors 33

1.1.2.2 Diagnosis 33

1.1.2.3 Histopathological classification 34

1.1.2.4 Molecular classification 35

1.1.2.5 Treatment 36

1.1.3 Ovarian Cancer 38

1.1.3.1 Risk factors 38

1.1.3.2 Diagnosis 39

1.1.3.3 Histopathological classification 40

1.1.3.4 Molecular classification 41

1.1.3.5 Treatment 41

1.1.4 Limitations of current treatment approaches of breast & ovarian cancer 42

1.2 Tumour Metabolism 44

1.2.1 Warburg Effect 44

1.2.2 The reason behind aerobic glycolysis 46

1.2.3 The advantages of aerobic glycolysis 47

1.2.4 Glutaminolysis 49
1.2.4.1 Targeting Glutaminolysis 50

1.3 Hypoxia 51
1.3.1 Hypoxia Inducible Factor 1 52
1.3.2 Lactate 53

1.4 The glycolytic pathway and the major targets 54
1.4.1 Glucose Transporters 56
1.4.2 Hexokinase (HK) 61
1.4.3 Phosphofructokinase (PFK) 63
1.4.4 Pyruvate Kinase (PK) 64
1.4.5 Pyruvate Dehydrogenase Kinase 67
1.4.6 Lactate Dehydrogenase (LDH) 67

1.5 Targeting Glycolysis 70
1.5.1 Targeting Glucose Transport 71
1.5.1.1 Flavonoids – Phloretin & Quercetin 71
1.5.1.2 STF31 76
1.5.1.3 WZB117 77
1.5.1.4 IOM-1190 78
1.5.2 Targeting Hexokinase 79
1.5.3 Targeting PFKFB3 81
1.5.4 Targeting Pyruvate Dehydrogenase Kinase 83
1.5.5 Targeting Lactate Dehydrogenase 86
1.5.5.1 Oxamic acid 86
1.5.5.2 NHI-1 88

1.6 Combinatorial Therapeutic Approaches 89
1.6.1 Cytotoxic drugs – Cisplatin & Paclitaxel 90
1.6.2 Targeted agent – Trastuzumab 90
1.6.3 Metabolic targeted agent – Metformin 90

1.7 Aims & Objectives 91

CHAPTER 2: MATERIALS & METHODS 97

2.1 Mammalian Cell Culture 97

2.1.1 Cell lines 97
2.1.2 Cell culture conditions 98
2.1.3 Routine cell culture 99
2.1.4 Hypoxic cell culture 99
2.1.5 Cell cryopreservation in liquid nitrogen and recovery 100
2.1.6 Pharmacological tool compounds 100

2.2 Sulphorhodamine B assay (SRB) 101
2.2.1 Combinatorial treatments 101

2.3 Glucose uptake assay 102

2.4 Lactate assay 103

2.5 Annexin V apoptosis assay 105

2.6 Cell cycle flow cytometric analysis 106

2.7 Immunoblotting 107
2.7.1 Protein Extraction 107
2.7.2 Bicinchoninic Acid Assay (BCA) 107
2.7.3 Western Blotting 108

2.8 siRNA Knockdown 110

2.9 Immunofluorescence of clinical ovarian cancer tissues 111
2.9.1 Tissue Microarrays (TMAs) 111
2.9.2 Immunofluorescence 112
2.9.3 AQUA Image Analysis 113

2.10 Gene Expression Analysis 114
2.10.1 Sample collection 114
2.10.2 RNA Extraction 114
2.10.3 RNA Amplification 115
2.10.4 Concentration of Nucleic acids 115
2.10.5 Northern Blotting 115
2.10.6 Whole-Genome Direct Hybridisation and Data Normalisation 116

2.11 Statistical Analysis 117

CHAPTER 3: THE EFFECT OF METABOLIC INHIBITORS ON CELL PROLIFERATION 121

3.1 The effect of glucose and glutamine availability on cell growth of a panel of four breast and four ovarian cancer cell lines 121

3.2 The effect of glycolytic inhibitors on cell growth of a panel of four breast and four ovarian cancer cell lines 127

3.2.1 Targeting Glucose Transport 127

3.2.1.1 Phloretin & Quercetin 127

3.2.1.2 STF31 & WZB117 129

3.2.2 Targeting Hexokinase 130

- **3-Bromopyruvate** 130

3.2.3 Targeting Phosphofructokinase 131

- **3PO** 131

3.2.4 Targeting Pyruvate Dehydrogenase Kinase 131

- **Dichloroacetate** 132

3.2.5 Targeting Lactate Dehydrogenase 132

3.2.5.1 Oxamic acid 132

3.2.5.2 NHI-1 133

3.3 Exploration of the differential sensitivity of breast and ovarian cancer cell lines to glycolytic inhibitors 135

3.4 The effect of glycolytic inhibitors on cell growth of two pairs of chemosensitive - chemoresistant ovarian cancer cell lines 140

3.4.1 STF31 140

3.4.2 3PO 141

3.4.3 Oxamic acid 141

3.5 The effect of the novel GLUT1 inhibitor IOM-1190 142

3.5.1 The effect of IOM-1190 on cell growth of selected breast and ovarian cancer cell lines 142

3.5.2 The effect of IOM-1190 under different glucose concentrations 144

3.6 The effect of a glutaminolysis inhibitor on cell growth of a panel of four breast and four ovarian cancer cell lines 145

- **BPTES** 145

3.7 Discussion 146

3.7.1 Growth dependency of breast and ovarian cancer cell lines on nutrient availability 146
3.7.2 Growth inhibitory effect of glycolytic inhibitors on breast and ovarian cancer cell lines 149
3.7.3 Sensitivity to glycolytic inhibitors varies among cell lines 152
3.7.4 Comparing sensitivity to glycolysis inhibition with platinum sensitivity in ovarian cancer cell lines 154
3.7.5 Investigating the antiproliferative effect of the novel GLUT1 inhibitor IOM-1190 155
3.7.6 Growth inhibitory effect of a glutaminolytic inhibitor on breast and ovarian cancer cell lines 156

CHAPTER 4: THE EFFECT OF GLYCOLYTIC INHIBITORS ON BREAST CANCER CELLULAR FUNCTION 161

4.1 The effect of glycolytic inhibitors on induction of apoptosis 161

4.2 The effect of glycolytic inhibitors on cell cycle progression 168

4.3 The effect of glycolytic inhibitors on glucose uptake & lactate production 175

4.4 Knockdown of selected glycolytic enzymes 185
4.4.1 GLUT1 knockdown 185
4.4.2 LDHA knockdown 186
4.4.2.1 Effect of LDHA knockdown on LDHB expression 188
4.4.2.2 Effect of LDHA knockdown on cell proliferation 189
4.4.2.3 Effect of LDHA knockdown on lactate production 191

4.5 Discussion 191
4.5.1 The glycolytic inhibitors mainly induced apoptosis 191
4.5.2 The glycolytic inhibitors mainly caused cell cycle arrest at G0/G1 phase 194
4.5.3 The glycolytic inhibitors blocked the glycolytic pathway 195
4.5.4 Evaluation of glycolytic targets through siRNA knockdown 197

CHAPTER 5: COMBINING GLYCOLYTIC INHIBITORS WITH CHEMOTHERAPY AND TARGETED INHIBITORS 203

5.1 Combinations with cytotoxic drugs – Cisplatin & Paclitaxel 205
5.1.1 Cisplatin 205
5.1.1.1 3PO & Cisplatin 205
5.1.2 Paclitaxel 208

5.1.2.1 3PO & Paclitaxel 208
5.1.2.2 Oxamic acid & Paclitaxel 211

5.2 Combinations with targeted therapy – Trastuzumab 212
5.2.1 Oxamic acid & Trastuzumab 213
5.2.2 NHI-1 & Trastuzumab 214

5.3 Combinations with an antidiabetic drug – Metformin 215
5.3.1 IOM-1190 & Metformin 216
5.3.2 STF31 & Metformin 218
5.3.3 Phloretin & Metformin 221
5.3.4 Oxamic acid & Metformin 222
5.3.5 Dichloroacetate & Metformin 226

5.4 The effect of STF31 & Metformin combination on induction of apoptosis 228

5.5 The effect of glycolytic inhibitor combinations with Metformin on cell cycle progression 230

5.6 Discussion 233
5.6.1 Glycolytic inhibitors potentiated the antiproliferative effect of cisplatin and paclitaxel on breast and ovarian cancer cells 234
5.6.2 LDH inhibitors potentiated the antiproliferative effect of trastuzumab on breast cancer cells 236
5.6.3 Metformin potentiated the antiproliferative effect of glycolytic inhibitors on breast and ovarian cancer cells 238
5.6.4 Combinatorial treatment of STF31 and Metformin was associated with induction of apoptosis in breast cancer cells 241
5.6.5 Combinatorial treatments of glycolytic inhibitors and Metformin were associated with cell cycle arrest 242

CHAPTER 6: THE EFFECT OF VARYING OXYGEN LEVELS ON SENSITIVITY TO GLYCOLYTIC INHIBITION 247

6.1 The effect of glycolytic inhibitors on the growth of breast cancer cell lines under varying oxygen levels 247

6.2 Protein expression of glycolytic targets under varying oxygen levels 258
- Glucose Transporter 1 258
- Hexokinase II 260

- PFKFB3 261
- Pyruvate Dehydrogenase Kinase 1 262
- Lactate Dehydrogenase A 263

6.3 The antiproliferative effect of the novel GLUT1 inhibitor IOM-1190 under hypoxic conditions 265

6.3.1 The effect of the combination of IOM-1190 with metformin under hypoxic conditions 267

6.4 Analysis of the glycolytic pathway in hypoxia using transcriptomic data 268

6.4.1 Differentially expressed genes between hypoxic and normoxic breast cancer cells 269

6.4.2 Modulation of the glycolytic pathway in chronic hypoxic breast cancer cells 272

6.4.3 Modulation of selected glycolytic enzymes in breast cancer cells under varying conditions of hypoxia 273

6.5 Discussion 279

6.5.1 Breast cancer cells demonstrated increased sensitivity to glycolysis inhibition in high oxygen conditions 279

6.5.2 Resistance of breast cancer cells to glycolysis inhibition in hypoxia was associated with target overexpression 283

6.5.3 Breast cancer cells demonstrated enhanced sensitivity to the novel GLUT1 inhibitor IOM-1190 in low oxygen conditions 285

6.5.4 Upregulation of the glycolytic pathway in breast cancer cells under hypoxia at the transcriptomic level 287

CHAPTER 7: EVALUATION OF GLYCOLYTIC TARGETS IN OVARIAN TUMOURS 295

7.1 Expression of selected glycolytic enzymes in ovarian tumours 295

GLUT1 296

HKII 297

PKM2 297

LDHA 298

7.2 Association of the expression of glycolytic enzymes with ovarian cancer progression 299

7.3 Association of the expression of glycolytic enzymes with ovarian cancer histological subtype 301

7.4 Correlation of the expression of glycolytic enzymes with other markers 302

7.5 Association of the expression of glycolytic enzymes with clinical outcome **305**

7.6 Discussion **307**

CHAPTER 8: CONCLUDING DISCUSSION **317**

Appendix 1: Supplementary figures of Chapter 5 **325**

Appendix 2: Supplementary tables of Chapter 6 **331**

Appendix 3: Supplementary table of Chapter 7 **334**

Appendix 4: Published Manuscript **345**

BIBLIOGRAPHY **367**

List of Abbreviations

2-DG	2-Deoxy-D-glucose
3-D	Three-dimensional
3PO	3-(3-Pyridinyl)-1-(4-pyridinyl)-2-propen-1-one
5-FU	Fluorouracil
AACR	American association for cancer research
AAT	Aspartate aminotransferase
ABC	ATP-binding cassette transporters
ADP	Adenosine diphosphate
AJCC	American joint committee on cancer
AKT	Protein kinase B
ALDOC	Aldolase, fructose-bisphosphate C
AMP	Adenosine monophosphate
AMPK	5' adenosine monophosphate-activated protein kinase
ANOVA	Analysis of variance
APC/C	Anaphase-promoting complex/cyclosome
APS	Ammonium persulfate
AQUA	Automated quantitative analysis
AR	Androgen receptor
ATP	Adenosine triphosphate
BCA	Bicinchoninic acid assay
BRAF	v-Raf murine sarcoma viral oncogene homolog B
BRCA	Breast cancer susceptibility gene
CA125	Cancer antigen 125
CAIX	Carbonic anhydrase 9
CDK	Cyclin-dependent kinase
CI	Combination index
CO_2	Carbon dioxide
$CoCl_2$	Cobalt chloride
CRISPR	Clustered regularly interspaced short palindromic repeats
Cy5	Cyanine 5
DAPI	4',6-diamidino-2-phenylindole
DAVID	Database for annotation, visualization and integrated Discovery

DCIS	Ductal carcinoma in situ
DMA	5-(N,N-Dimethyl)amiloride hydrochloride
DMEM	Dulbecco's modified Eagle's medium
DMSO	Dimethyl sulfoxide
DNA	Deoxyribonucleic acid
DR5	Death receptor 5
EDTA	Ethylenediaminetetraacetic acid
EGFR	Epidermal growth factor receptor
ENO	Enolase
EORTC	European organisation for research and treatment of cancer
ER	Oestrogen receptor
ERK	Extracellular signal–regulated kinases
F1,6BP (FBP)	Fructose-1,6-bisphosphate
F2,6BP	Fructose-2,6-bisphospate
FBS	Fetal bovine serum
FDG	2-[^{18}F]fluoro-2-deoxyglucose (fluoro-deoxyglucose)
FDR	False discovery rate
FGFR	Fibroblast growth factor receptor
FIGO	International federation of gynaecology and obstetrics
FIH	Factor inhibiting HIF
FISH	Fluorescence *in situ* hybridization
GAPDH	Glyceraldehyde 3-phosphate dehydrogenase
GLUT	Glucose transporter
GO	Gene ontology
GPI	Glucose-6-phosphate isomerase
GSTZ	Glutathione S-transferase zeta
H	Histone
H2AX	H2A histone family, member X
H_2O_2	Hydrogen peroxide
HEPES	4-(2-hydroxyethyl)-1-piperazineethanesulfonic acid
HER2	Human epidermal growth factor receptor 2
HIF	Hypoxia-inducible factor

HK	Hexokinase
HNF1β	Hepatocyte nuclear factor
HNPCC	Hereditary nonpolyposis colorectal cancer
HRP	Horseradish peroxidase
IC_{50}	Half maximal inhibitory concentration
IDC	Invasive ductal carcinoma
IDH	Isocitrate dehydrogenase
IF	Immunofluorescence
IGF	Insulin-like growth factor
Igmm	Institute of genetics and molecular medicine
IHC	Immunohistochemistry
IL	Interleukin
Ki	Inhibitory constant
KRAS	v-Ki-ras2 Kirsten rat sarcoma viral oncogene homolog
LDH	Lactate dehydrogenase
MAPK	Mitogen-activated protein kinase
MCT	Monocarboxylate transporter
MELAS	Mitochondrial myopathy, encephalopathy, lactic acidosis and stroke-like episodes
mM	Millimolar
mmHg	Millimetre of mercury
mTOR	Mammalian target of rapamycin
MTS	3-(4,5-dimethylthiazol-2-yl)-5-(3-carboxymethoxyphenyl)-2-(4-sulfophenyl)-2H-tetrazolium
MTT	3-(4,5-dimethylthiazol-2-yl)-2,5-diphenyltetrazolium bromide
NAD+	Oxidised nicotinamide adenine dinucleotide
NADH	Reduced nicotinamide adenine dinucleotide
NAMPT	Nicotinamide phosphoribosyltransferase
NAPRT	Nicotinate phosphoribosyltransferase
NCBI	National centre for biotechnology information
NCI	National cancer institute
NFκB	Nuclear factor kappa-light-chain-enhancer of activated B cells
NHE	Na^+-H^+ exchanger
NHI	N-hydroxyindole-based inhibitor
NIH	National institutes of health

NST	Invasive carcinoma of no special type
O_2	Oxygen
OD	Optical density
ODD	Oxygen-dependent degradation domain
OXPHOS	Oxidative phosphorylation
PARP	Poly ADP ribose polymerase
PBS	Phosphate-buffered saline
PBS-T	PBS 0.05% Tween 20
PDH	Pyruvate dehydrogenase
PDHK	Pyruvate dehydrogenase kinase
PEP	Phosphoenolpyruvate
PET	Positron emission tomography
PFK	Phosphofructokinase
PFKFB	6-phosphofructo-2-kinase/fructose-2,6-bisphosphatase
PGK	Phosphoglycerate kinase
PGM	Phosphoglucomutase
PI	Propidium iodide
PI3K	Phosphoinositol 3 kinase
PK	Pyruvate kinase
PPP	Pentose phosphate pathway
PR	Progesterone receptor
PVDF	Polyvinylidene difluoride membrane
qRT-PCR	Quantitative real-time polymerase chain reaction
QS	Quercetin-50,8-di-sulfonate
Rb	Retinoblastoma
RNA	Ribonucleic acid
RNAi	RNA interference
ROCA	Risk of ovarian cancer algorithm
ROS	Reactive oxygen species
RPMI	Roswell park memorial institute medium
SDS-PAGE	Sodium dodecyl sulphate polyacrylamide gels electrophoresis
SERM	Selective estrogen receptor modulator
siRNA	Small interfering ribonucleic acid

SLC	Solute carrier family
Snail	Zinc finger protein SNAI1
SRB	Sulforhodamine B
STAT3	Signal transducer and activator of transcription 3
STR	Short tandem repeat
TCA	Trichloroacetic acid
TCA cycle	Tricarboxylic acid cycle
TEMED	Tetramethylethylenediamine
TIGAR	TP53-induced glycolysis and apoptosis regulator
TMA	Tissue microarray
TNF	Tumour necrosis factor
TNM	Tumour, node and metastasis classification of malignant tumours
TRAIL	Tumour necrosis factor-related apoptosis-inducing ligand
UK	United Kingdom
US	United States
V-ATPase	Vacuolar-type H^+-ATPase
VDAC	Voltage-dependent anion channel
VEGFR	Vascular endothelial growth factor receptor
VHL	von Hippel–Lindau tumour suppressor
WB	Western blotting
WHO	World health organisation
XTT	2,3-bis-(2-methoxy-4-nitro-5-sulfophenyl)-2H-tetrazolium-5-carboxanilide
µM	Micromolar

Chapter 1

Chapter 1: Introduction

1.1 Breast & Ovarian Cancer

Examining the glycolytic profile of breast and ovarian cancer cell line models as well as exploiting several glycolytic targets therapeutically were the main objectives of this study. A brief introduction regarding these two malignancies is given below.

1.1.1 Epidemiology of female malignancies

Breast cancer is undeniably the most frequently diagnosed female malignancy accounting for 30% of all new female cases each year in the UK. The ovary is the fifth most common female cancer site with ovarian cancer accounting for 4% of all female cancer cases. According to Cancer Research UK, as presented in Figure 1.1, in 2012 nearly 51,000 women were diagnosed with breast cancer in the UK and approximately 7,000 with ovarian cancer [1].

Breast cancer is the second most common cause of female cancer deaths, following lung cancer, accounting for approximately 15% of all cancer related deaths among women each year in the UK. Ovarian cancer, being the most lethal among all gynaecological malignancies, is the fifth most common cause of cancer deaths in women, responsible for nearly 6% of female cancer mortality (Figure 1.2). The survival rates for both types of cancer have been improving over the last few years; this is attributed to better awareness, earlier diagnosis and treatment advances. Nevertheless in 2012 nearly 12,000 women died from breast cancer and 4,300 from ovarian cancer in the UK [1]. The American Cancer Society estimates that this year (2016) more than 40,000 women in the US will succumb to breast cancer and more than 14,000 to ovarian cancer [2].

Both breast and ovarian cancer present a major concern in public health care and further research to enhance our understanding and develop further treatment opportunities is urgently needed and of great importance.

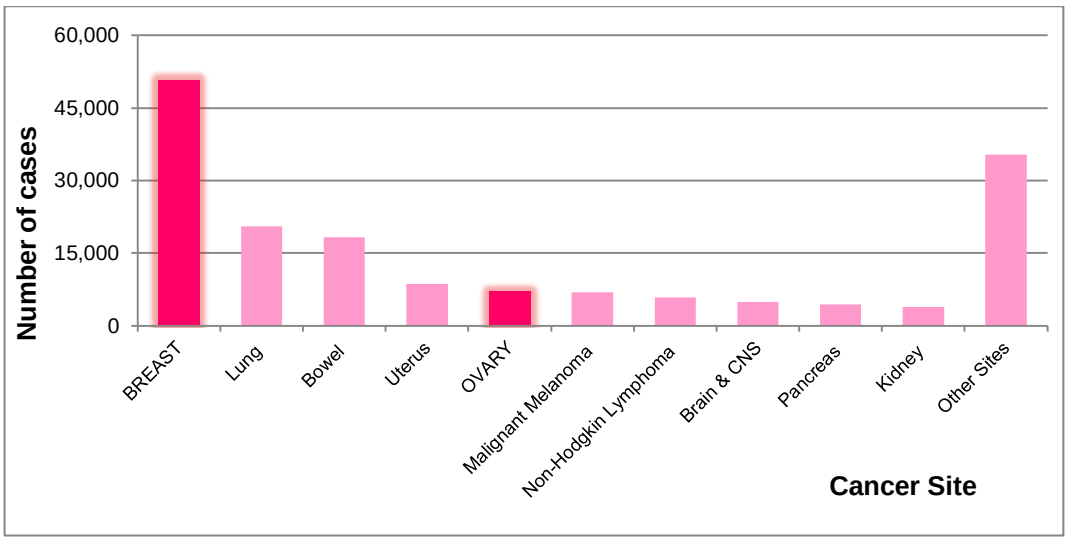

Figure 1.1: The most commonly diagnosed female cancers in the UK in 2012 [1]

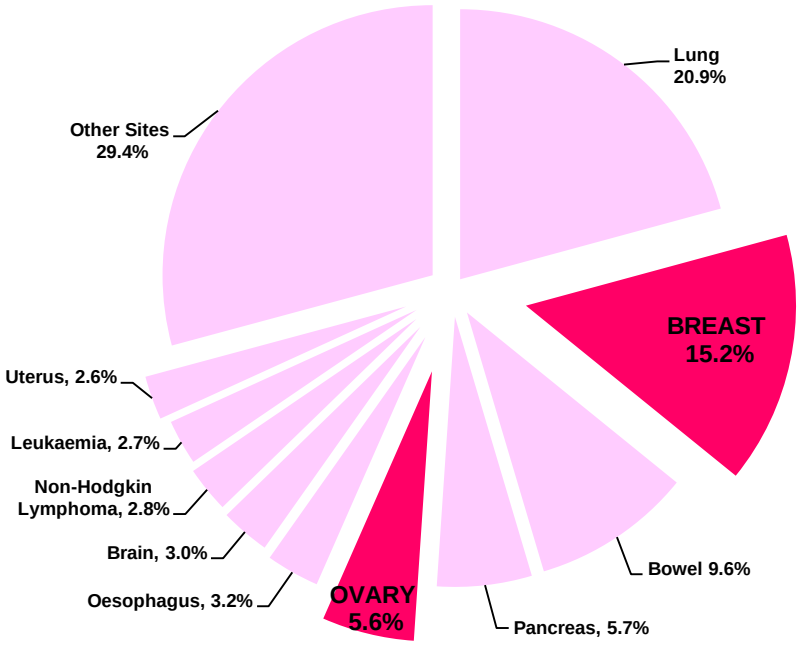

Figure 1.2: Female cancer mortality in the UK in 2012 [1]

1.1.2 Breast Cancer

1.1.2.1 Risk factors

A single cause for breast cancer has not been described but several factors have been linked to the disease. The best-documented risk factors are gender and increasing age. A woman in the UK is estimated to have a 1 in 8 chance of being diagnosed with breast cancer during her lifetime. Men are rarely affected with around 400 cases diagnosed in the UK in 2012 [1]. The malignancy is more frequent in women around menopause with 80% of cases occurring in women aged 50 and over [1]. Natural hormonal changes are considered to play an important role in breast cancer development. Early menarche, late menopause as well as nulliparity are associated with an elevated risk of occurrence. In contrast prolonged breastfeeding and young age at childbearing are described to have protective value. Extensive exogenous hormone intake during hormone replacement therapy is a well-defined risk factor contributing to a higher incidence of breast carcinogenesis. Among further factors that have been suggested to increase the risk of breast cancer are obesity for postmenopausal women, alcohol consumption and exposure to radiation [2-5].

Individuals with a first-degree relative diagnosed with breast cancer have an elevated risk of developing the disease. Approximately 10% of breast cancer incidences in the Western world are attributed to familial predisposition. The most important and best characterised susceptibility genes are the tumour suppressor genes BRCA1 and BRCA2. Germline mutations in these DNA repair genes are associated with up to 80% cumulative lifetime risk of breast cancer occurrence. Several polymorphisms in additional genes have also been identified along with rare familial predisposing syndromes including the Li-Fraumeni (TP53 germline mutations) and the Cowden syndrome (PTEN germline mutations) [6, 7]. Women with prior history of benign breast lesions like atypical hyperplasia have significantly elevated risk of developing malignant breast carcinomas [3-5].

1.1.2.2 Diagnosis

The U.K. NHS breast screening programme offers an X-ray mammogram test to women aged between 50 and 70 every three years [8]. Women with symptoms, most frequently a palpable lump in the breast, or with suspicious screening results are referred to a specialist breast clinic for triple assessment. This involves clinical examination, a mammography and possibly an ultrasound scan as well as a needle or a core biopsy for histological investigation [8-10].

Following pathological examination of the biopsy material, tumours are graded and staged. Breast tumours are graded based on the Bloom-Richardson histological grading system with a scoring scale ranging from 1 to 3. This system provides an indication of 'the degree of potential malignancy' with grade 1 tumours being well differentiated while grade 3 tumours are poorly differentiated [11]. The most broadly used staging system for breast cancer is the American Joint Committee on Cancer (AJCC) TNM staging system. Tumours are classified based on their size, their lymph node status and the presence of distant metastasis. A five-year relative survival rate is statistically predicted for patients with similarly staged disease [12].

1.1.2.3 Histopathological classification

The vast majority of breast malignancies are adenocarcinomas, at a percentage greater than 95%, originating from the same segment of the mammary gland terminal duct lobular unit [13]. However, breast cancer is a very heterogeneous group of diseases that exhibit great diversity not only clinically but histologically and genetically as well. Pathologists have developed a classification system based on the morphological and cytological characteristics of tumours. Breast cancer is broadly categorised as either *in situ* or invasive carcinoma. *In situ* carcinoma is non-invasive, confined to the breast epithelium and is classified as either ductal or lobular [14, 15]. Ductal carcinoma *in situ* (DCIS) is considerably more frequent accounting for almost one quarter of all breast cancer cases diagnosed each year. It is considered a precursor lesion that could potentially evolve into invasive malignancy but it is currently debatable as to how aggressively it should be treated. In many cases DCIS would not develop further and therefore a considerable issue of overdiagnosis undoubtedly exists. DCIS is classically subdivided into five subtypes according to the architectural characteristics of the tumour (comedo, cribriform, micropapillary, papillary and solid) [16]. Invasive (infiltrating) carcinomas constitute a group of heterogeneous highly proliferative malignancies that have penetrated the stroma through the basement membrane. Multiple histological subtypes of invasive carcinomas are recognised accounting for up to 25% of all breast cancer cases. The most common specific subtypes include invasive lobular, tubular, cribriform, medullary, mucinous, papillary, micropapillary, apocrine and metaplastic. However almost 80% of all invasive tumours cannot be classified as a special histological type and are collectively designated as invasive carcinoma of no special type (NST), previously called invasive ductal carcinoma (IDC) [14, 15].

1.1.2.4 Molecular classification

Routine use of molecular markers has been incorporated into everyday clinical practice. The expression levels of the oestrogen receptor (ER), progesterone receptor (PR) and the human epidermal growth factor 2 (HER2) are examined through immunohistochemistry (IHC) and fluorescence *in situ* hybridisation (FISH). Determination of the status of these biomarkers enables stratification of breast cancer patients predicting their clinical outcome and their response to targeted therapies [17, 18].

In the last decade novel high-throughput gene expression microarray technology has enhanced our understanding of breast cancer heterogeneity. In their seminal study, Perou *et al* classified breast tumours into distinct molecular subgroups based on their gene expression profile [19]. The intrinsic subtypes identified have been further confirmed from a number of studies and are broadly recognised and associated with distinct clinical outcomes and survival predictions. Breast tumours are clustered into two main groups; the ER positive luminal group, subdivided into luminal A and luminal B subgroups and the ER negative group subdivided into HER2 positive, basal-like and normal breast-like carcinomas [14, 15, 18]. Luminal tumours are the most common group accounting for around 60% of all breast cancer cases. They have a similar expression pattern with mammary luminal epithelial cells and they also express genes related with an active ER pathway. Luminal A (ER^+, PR^+, $HER2^-$) tumours are more common and generally have low histological grade. Luminal B (ER^+, $PR^{+/-}$, $HER2^{+/-}$) tumours demonstrate increased expression of proliferation-related genes and tend to have poorer prognosis. The HER2 positive (ER^-, PR^-, $HER2^+$) subtype comprises up to 20% of all breast cancers. These tumours overexpress the HER2 gene along with several other genes related to the pathway and are associated with poor prognostic outcome. The basal-like (ER^-, PR^-, $HER2^-$) subtype contains 15% of all breast cancer patients including the vast majority of BRCA1 cases. These tumours have a similar expression pattern with mammary myoepithelial cells and normal basal epithelial cells and they also express basal cytokeratins 5, 6 and 17. They are mostly aggressive tumours of high histological grade. Normal breast-like cancers have a gene-expression profile similar to adipose tissue of normal breasts and they account for 5% of all diagnoses [15, 18, 20, 21]. Recently additional molecular subgroups have been identified. Claudin-low (ER^-, PR^-, $HER2^-$) tumours have a genetic profile similar to that of mammary stem cells and are characterised by an epithelial to mesenchymal transition phenotype. The apocrine (ER^-, AR^+, PR^-, $HER2^{+/-}$) subtype is characterised by the expression of androgen receptors and an active AR pathway [18, 22].

1.1.2.5 Treatment

There are five main modalities currently available in clinical practice for breast cancer treatment. These include surgery, chemotherapy, radiotherapy, endocrine therapy and targeted therapies. Most frequently two or more types of therapy are combined to achieve the optimal result. The treatment strategy is decided based on the stage and grade of the disease, the general health of the patient as well as the nodal status and the molecular characteristics of the tumour [2, 8-10].

Surgery is considered the most effective treatment for breast cancer and is used as first-line management for the vast majority of patients excluding those presenting with advanced metastatic disease or weak elderly patients. Two different clinical approaches are currently in use; breast conserving surgery and mastectomy. In breast conserving surgery, also called lumpectomy, only the tumour is removed along with a margin of the surrounding healthy tissue. Breast conserving surgery is followed by post-operative radiotherapy meaning high-energy x-ray ionizing irradiation. Adjuvant radiation therapy destroys any residual cancer cells and reduces the possibility of local recurrence [23]. Mastectomy ranges from simple mastectomy to modified radical mastectomy and radical mastectomy depending on whether the axillary lymph nodes and the pectoral muscles respectively are removed along with the entire breast. Less disfiguring operations include skin sparing and nipple sparing mastectomy. Many women choose to undergo reconstructive surgery following a mastectomy. This can be an immediate or delayed procedure and usually saline or silicone implants are used or even tissue from a different part of the patient's body (autologous reconstruction). Recent studies based on a twenty-year randomised trial demonstrate that women offered breast conserving surgery followed by adjuvant radiotherapy had equivalent outcome and survival rates to women who underwent mastectomy [24]. Axillary lymph node dissection for further histological examination is a crucial procedure for staging and dictates patient further management. To avoid highly invasive techniques like axillary node clearance and the possible risk of lymphoedema in patients with clinically negative axilla, sentinel node biopsy is frequently performed. Using a radioactive isotope and a blue dye, surgeons identify the sentinel nodes to which lymph fluid drains from the tumour and which have the highest probability of metastasis [25]. Systemic therapy is usually offered after surgery regardless of the nodal status and significantly reduces the risk of metastasis and regional recurrence [2, 8-10].

Chemotherapy involves the cyclical co-administration of multiple cytotoxic agents. The most commonly used regimens include the anthracyclines (doxorubicin, daunorubicin), the

taxanes (paclitaxel, docetaxel), antimetabolites (fluorouracil) and alkylating agents (cyclophosphamide, carboplatin). Chemotherapy is most commonly used in the adjuvant setting for patients with increased risk of recurrence [26]. However in cases with inoperable tumours it may be offered preoperatively (neoadjuvant setting) to shrink the tumours and make them resectable or allow breast conserving surgery in cases where tumour size exceeds recommendations [2, 8-10, 27].

Around two-thirds of all breast tumours express hormone receptors and are highly dependent on oestrogen and/or progesterone to stimulate their growth. Endocrine therapy blocks hormone action and plays a critical role in the treatment of luminal cancers; it is used both in adjuvant and neoadjuvant settings [5, 8-10]. Tamoxifen is a selective estrogen receptor modulator (SERM), acts as an ER antagonist and is used for the treatment of pre-menopausal women. It has been shown that tamoxifen adjuvant therapy with a 5 year duration reduces the recurrence probability and the mortality rate [28]. Aromatase inhibitors block the synthesis of oestrogen from androgens through inhibition of the aromatase enzyme in peripheral fatty tissues. Letrozole, anastrozole and exemestane are currently used for the treatment of postmenopausal women with hormone-receptive tumours [29].

Molecular targeted therapies involve inhibitors targeting specific pathways crucial for the growth and recurrence of tumours. Trastuzumab is a humanised monoclonal antibody that binds to the extracellular domain of the HER2 receptor inhibiting the activation of downstream signalling pathways. Twelve months of adjuvant trastuzumab significantly increases survival rate and is the standard treatment for HER2 positive breast cancer patients combined with chemotherapy or as monotherapy [30-32]. Trastuzumab emtansine, previously referred as T-DM1, is an antibody- drug conjugate of Trastuzumab with the cytotoxic agent emtansine. It allows targeted delivery of chemotherapy to HER2 positive cancer cells and is approved as a single-agent for the treatment of advanced, metastatic HER2 positive tumours pre-treated with trastuzumab and a taxane [33]. Lapatinib is a dual EGFR/HER2 tyrosine kinase inhibitor. It is approved for the treatment of advanced stage tumours and can be effective in trastuzumab resistant disease. Pertuzumab is a humanised monoclonal HER2 antibody that inhibits the receptor's heterodimerisation. It is used in combination with trastuzumab and chemotherapy for neoadjuvant treatment of early stage HER2 positive tumours or for adjuvant treatment of advanced metastatic HER2 tumours [31, 34, 35]. Everolimus targets the mTOR complex 1 (mammalian target of rapamycin) inhibiting the mTOR signalling pathway. It is approved in combination with exemestane for the treatment of postmenopausal women with advanced hormone receptor positive tumours

resistant to nonsteroidal aromatase inhibitors [36]. Palbociclib inhibits cyclin-dependent kinases 4 and 6 (CDK4 and CDK6) and it has recently been approved for the treatment of postmenopausal women with hormone receptor positive metastatic tumours in combination with letrozole [2, 37]. Multiple targeted agents inhibiting different pathways have been developed and are currently undergoing clinical trials to assess their efficacy and potential benefit in advanced breast cancer [38].

1.1.3 Ovarian Cancer

1.1.3.1 Risk factors

The specific aetiology of ovarian cancer has not been identified yet, but several risk factors have been described. The predominant risk factor for ovarian cancer is age. Every woman in the UK is considered to have a 1 in 52 chance of being diagnosed with ovarian cancer during her lifetime. However nearly three-quarters of ovarian cancer cases are diagnosed in postmenopausal women aged 55 and over [1]. The number of a woman's lifetime ovulation cycles is correlated with the risk of ovarian cancer occurrence. Oral contraception, multiple pregnancies and prolonged breastfeeding are considered of protective value. Hormonal factors have also been linked to development of the disease. Hormone replacement therapy as well as ovarian stimulation treatment and infertility itself have been associated with an elevated risk of ovarian carcinogenesis. Women who suffered from endometriosis or polycystic ovarian syndrome may also face an elevated risk. Several lifestyle factors including genital use of talcum powder, obesity and tobacco smoking have also been suggested to increase ovarian cancer risk but studies are inconclusive [39-43].

A strong family history of ovarian or breast cancer is a well-established risk factor for ovarian cancer. It is estimated that up to 10% of ovarian cancer incidences are attributable to hereditary genetic predisposition [39-43]. Germ-line mutations in the high-penetrance susceptibility genes BRCA1 and BRCA2 are associated with up to 50% and 30% respectively lifetime risk of developing ovarian cancer [7, 44-46]. Women with such mutations are frequently offered prophylactic bilateral salpingo-oophorectomy after childbearing to eliminate the risk of ovarian cancer occurrence [44, 46]. The hereditary nonpolyposis colon cancer syndrome (HNPCC/ formerly known as Lynch syndrome) caused by germline mutations in the DNA mismatch repair genes (predominantly MSH2 and MLH1) confers a cumulative lifetime ovarian cancer risk equal to 12% [45-47].

1.1.3.2 Diagnosis

Ovarian cancer has a high mortality rate and this is attributed to the fact that almost 80% of cases are diagnosed at an advanced stage which is correlated with poor survival. Disease is mainly asymptomatic at early stages and even advanced disease symptoms are difficult to recognise. Clinical indications including abdominal distension, pelvic or abdominal pain, and changes in urinary or bowel habits are atypical and are usually misinterpreted as non-malignant aetiology. A palpable ovarian mass, ascites or pleural effusions mostly present when disease has already metastasised beyond the ovaries [39, 43, 48]. A screening programme for ovarian cancer is not currently in use. Diagnosis is based on a transvaginal ultrasonography and detection of high serum CA125 levels and is confirmed by surgical biopsy. The glycoprotein CA125 has been investigated as an ovarian cancer biomarker but it lacks the required specificity and sensitivity to be used as a screening tool. Several benign conditions including endometriosis, menstruation or pregnancy can elevate CA125 blood levels [39, 43, 48]. Research trials show that it has no value in being implemented in the general population as a screening tool, as it did not reduce mortality rates for ovarian cancer. However recent studies indicate that sequential CA125 measurements interpreted by a mathematical algorithm (ROCA- Risk of Ovarian Cancer Algorithm) may offer a promising strategy to calculate ovarian cancer risk [49, 50].

Women with suspected ovarian cancer usually undergo laparotomy surgery. Diagnosis is confirmed through histopathological examination of the biopsy material and tumours are graded and staged. A histological grading system is followed classifying well differentiated tumours as grade 1, moderately differentiated as grade 2 whereas poorly differentiated tumours are classified as grade 3 [1]. The FIGO staging classification system (established from the International Federation of Gynaecology and Obstetrics) based on the tumour size and the presence of lymph node and distant metastasis is typically used. Stage I tumours are confined to the ovaries, stage II tumours have spread into the pelvis, stage III tumours have spread into the peritoneal cavity and may have lymph node involvement while final stage IV tumours have metastasised into distant organs [2, 39, 43, 46]. The most common sites of ovarian cancer metastasis include the liver, spleen, stomach and lungs. Survival rate is highly dependent on the stage classification with stage I tumours typically having a 90% five year relative survival rate as opposed to only 5% of stage IV tumours [1].

1.1.3.3 Histopathological classification

Over 90% of ovarian tumours are of epithelial origin traditionally considered to arise from malignant transformation of the epithelium lining the ovaries or cortical inclusion cysts [51]. Epithelial ovarian tumours constitute a greatly heterogeneous group of diseases. The World Health Organisation (WHO) classifies epithelial ovarian tumours based on their histopathological and morphological features into four major histotypes exhibiting substantial heterogeneity. These are serous, endometrioid, clear cell and mucinous carcinomas. Less common histotypes include mixed, transitional cell (Brenner tumours) and undifferentiated tumours [52-57]. Serous is the most common histological subtype accounting for approximately 70% of all diagnosed ovarian cancer cases. Serous carcinomas are commonly diagnosed at advanced stage (III and IV). They usually present a combination of architectural patterns including papillary, glandular and solid and frequently contain calcified structures called psammoma bodies [52-54]. Two different types of serous carcinomas having distinct pathogeneses and molecular profiles are characterised; low grade and high grade serous tumours. High grade serous tumours present great resemblance to the fimbrial epithelium of the fallopian tubes and it is proposed that they may have fallopian origin [52, 55-59]. They are also associated with BRCA1 and BRCA2 abnormalities. Endometrioid adenocarcinomas account for 10% of ovarian tumours and are usually diagnosed at an early stage. They have glandular or papillary morphology resembling the normal endometrial epithelium and are often associated with endometriosis. Clear cell carcinomas have similar frequency to endometrioid tumours and are also frequently diagnosed at an early stage. They are characterised by typical hobnail shaped cells with clear cytoplasm. Clear cell tumours may be associated with endometriosis and exhibit chemoresistance correlated with poor outcome. Mucinous tumours are rare and constitute less than 3% of ovarian cancers. They usually have glandular architecture with typical cells containing mucin-filled cytoplasm. Mucinous cancer cells resemble those of the gastrointestinal epithelium [52-54]. Recent evidence strongly challenges the notion of universal origin from the ovarian epithelium and suggests that a substantial proportion of the tumours traditionally considered of exclusive ovarian origin only relate to the ovary secondarily [57, 60]. The histotypes exhibit distinctive gene expression signatures and interestingly a correlation has been demonstrated between the gene expression profile of normal differentiated fallopian tube epithelium and serous carcinomas, endometrial epithelium and endometrioid and clear cell tumours as well as colonic mucosa and mucinous tumours [51, 61]. Mixed ovarian tumours are often diagnosed when two histologically distinct types exist in the same tumour each one with at least 10% presence. A frequently

occurring combination is that of endometriosis associated histotypes, endometrioid with clear cell. An epithelial ovarian tumour is diagnosed as undifferentiated when it lacks histological differentiation and cannot be classified in another way. It is a group of clinically aggressive heterogeneous tumours usually associated with poor prognosis [52-54, 56].

1.1.3.4 Molecular classification

Based on distinctive carcinogenetic pathways and molecular profiles, Kurman *et al.* classified ovarian tumours into two major groups named type I and type II. Type I tumours account for roughly a quarter of all diagnosed cases; low grade serous, endometrioid, clear cell and mucinous carcinomas are included. Type II mainly involves high grade serous and undifferentiated carcinomas. Type I tumours are slow growing, confined to the ovaries at diagnosis, well differentiated and have gradually progressed from established benign precursor lesions (e.g. endometriosis and borderline tumours). In contrast, type II tumours are aggressive, poorly differentiated and are considered to develop *de novo* since no precursor lesion has been identified. The molecular signatures of the two types are distinct and differ greatly. Type I tumours are characterised by genetic stability and mutations at KRAS, KRAF, PTEN are frequently detected. In contrast type II tumours are genetically remarkably unstable and are defined by TP53 mutations [59, 62-64].

1.1.3.5 Treatment

The standard treatment of ovarian cancer is debulking surgery followed by systemic platinum and taxol-based chemotherapy. Cytoreductive surgery involves abdominal hysterectomy, bilateral salpingo-oophorectomy, pelvic lymphadenectomy and omentectomy aiming to eradicate disease. It has been shown that lower residual tumour volume is of crucial importance for improved clinical outcome. Adjuvant chemotherapy is offered to high-risk patients both at early and advanced stages. Intraperitoneal chemotherapy administration has been studied and proved more effective compared to the standard intravenous delivery route in certain situations. However, it has not been universally adopted because of several toxicity and practical implications [65-68]. The gold standard first-line treatment is a combination of platinum analogues (cisplatin or carboplatin which cause DNA crosslinking) and taxanes (paclitaxel or docetaxel which inhibit microtubule depolymerisation). It has been shown that optimally debulked women with low grade and early stage disease (FIGO stages IA and IB) do not benefit from chemotherapy [39, 65, 67]. Complete remission is observed in up to 80% of early stage patients and 50% of patients with advanced disease [67, 69]. Following treatment patients are frequently monitored though physical examination, scanning and CA125 measurements. Inevitably many patients

relapse. Second line treatment of recurrent disease depends on the disease free interval following completion of initial therapy. Platinum sensitive disease (relapse after at least 6 months) is likely to respond to a subsequent carboplatin – paclitaxel combination. In contrast for platinum insensitive (relapse within 6 months) and platinum refractory disease (progress even during platinum treatment) different cytotoxic agents usually as monotherapy are employed including the pegylated liposomal doxorubicin, topotecan and gemcitabine. Because of the low response rates these patients are preferred candidates for clinical trials and investigational studies of novel therapeutic strategies [65, 67, 70]. Radiation therapy and hormonal therapy are rarely used for ovarian cancer treatment.

Several novel targeted molecular therapies hold promise for improved outlook of ovarian cancer patients. Olaparib is a small molecule PARP (poly (ADP)-ribose polymerase) inhibitor used for the treatment of ovarian cancer patients who are carriers of BRCA germline mutations and have advanced disease. Based on a synthetic lethality strategy, PARP inhibitors cause the accumulation of DNA single strand breaks and if the homologous recombination DNA repair pathway is impaired due to loss of function of the BRCA tumour suppressor genes, cell cycle arrest and cell death are induced. It is now realised that BRCA deficiency also occurs in many sporadic ovarian cancers, especially high grade serous carcinomas, and these patients can potentially benefit from PARP inhibition [71, 72]. Bevacizumab is a recombinant humanised monoclonal antibody targeting the vascular endothelial growth factor A (VEGFA). Clinical trials showed promising results of the use of this angiogenesis inhibitor as monotherapy or in combination with traditional chemotherapy even for advanced platinum resistance disease [67, 69, 73-75].

1.1.4 Limitations of current treatment approaches of breast & ovarian cancer

Substantial progress has been made for the treatment of breast and ovarian cancer documented by the significant improvement of the survival rates of both diseases in the last few decades. Nevertheless major challenges still remain to be faced.

An issue of vital importance is the side effect profiles of conventional chemotherapeutic agents which are usually very distressing. Unfortunately, chemotherapy can have a serious impact on the patient's quality of life, without always guaranteeing a beneficial response. Common side effects include gastrointestinal complications (nausea, vomiting, constipation or diarrhoea), myelosuppression (increased infection risk, bleeding and fatigue), loss of appetite as well as hair loss [1, 2, 8]. Systemic hormonal and targeted therapies are usually

well tolerated with limited symptoms however there are still significant challenges. For example tamoxifen causes menopausal symptoms (hot flushes, irregular menstrual periods), trastuzumab causes cardiotoxicity and bevacizumab has been associated with gastrointestinal perforation, hypertension and thrombosis [32, 69, 73].

Endocrine and HER2 targeted therapies present great advances in the treatment of breast cancer improving greatly the disease free survival and the clinical outcome for the benefiting subgroups. However disease recurrence following endocrine therapy and clinical resistance to trastuzumab present major clinical issues. Furthermore treatment of triple negative tumours remains challenging because of the limited treatment options and the consequent poor survival rates [76].

Quantitation of protein expression levels of ER and HER2 receptors determines the use of endocrine and HER2 targeted therapy. Gene expression analysis and molecular classification of breast cancers could improve prediction of therapeutic response and also identify specific key regulators of each molecular subtype to enable development of novel targeted therapies [77].

Regarding ovarian cancer, even though platinum based chemotherapy has high response rates, it is estimated that approximately 70% of patients will relapse with resistant disease. The median progression free survival is calculated equal to 18 months [67, 69]. Recurrent disease is generally untreatable and current treatment is only palliative [39, 68]. Even platinum sensitive recurrent disease is retreated with the same agent again and again until eventually resistance develops and patients succumb to their disease.

It should be realised that under the umbrella term ovarian cancer several diseases are included with distinct morphological and molecular characteristics and different aetiology. Ovarian cancer histotypes should not be regarded as a single homogenous disease and separate therapeutic approaches for each of them should be developed [78]. For example clear cell tumours exhibit chemoresistance and cytotoxic chemotherapy may be inappropriate since there is little proven benefit [67, 79, 80]. Specific treatment modalities should be developed for these tumours using different cytotoxic regimens and targeted agents. Novel high-throughput technologies and large-scale gene expression profiling studies should be used to identify novel molecular targets for drug development.

It is apparent that there is an urgent need for the development of novel less-toxic treatments for these dreadful female malignancies.

1.2 Tumour Metabolism

1.2.1 Warburg Effect

It would be irrational to commence an analysis of cancer cell metabolism without first mentioning the renowned biochemist Otto Heinrich Warburg (Figure 1.3). In the 1920s, almost a century ago he made an outstanding observation showing that cancer cells exhibit increased production of lactic acid from glucose [81]. In his seminal study *On the origin of cancer cells* he identified a metabolic alteration as the sole pivotal cause responsible for the loss of cell differentiation and carcinogenesis. Warburg demonstrated that because of an irreversible 'injury of respiration' cancer cells rely on lactic fermentation for energy production [82-85].

Figure 1.3: Nobel Laureate Otto Heinrich Warburg (1883-1970)

He was awarded the Nobel Prize in Physiology or Medicine in 1931 "for his discovery of the nature and mode of action of the respiratory enzyme"

[86]

Non-malignant differentiated cells in the presence of oxygen (O_2) metabolise glucose to carbon dioxide (CO_2) in their mitochondrial tricarboxylic acid cycle (TCA) and generate their required energy through oxidative phosphorylation. Only under low oxygen conditions are they forced to utilise breakdown of glucose to lactate in the cytoplasm. However most cancer cells rely on glycolysis as their primary source of energy regardless of oxygen availability (Figure 1.4) [87, 88]. The persistence of glycolysis even under aerobic conditions is termed aerobic glycolysis or the Warburg effect; as it was first called by Racker in 1972 [89]. The metabolic alteration of tumours is nowadays well substantiated, extensively demonstrated in a wide variety of cancers and considered a 'hallmark' of advanced malignancy [90, 91]. Hanahan and Weinberg in their key review *Hallmarks of Cancer: The Next Generation* were the first to recognise the metabolic reprogramming of tumours as a hallmark of tumourigenesis [92]. The exact contribution of the glycolytic pathway to energy production is highly dependent on the cell type and the oxygenation level. Nevertheless it has been estimated that many tumour cells under aerobic conditions produce up to 60% of their ATP requirement through glycolysis [93, 94].

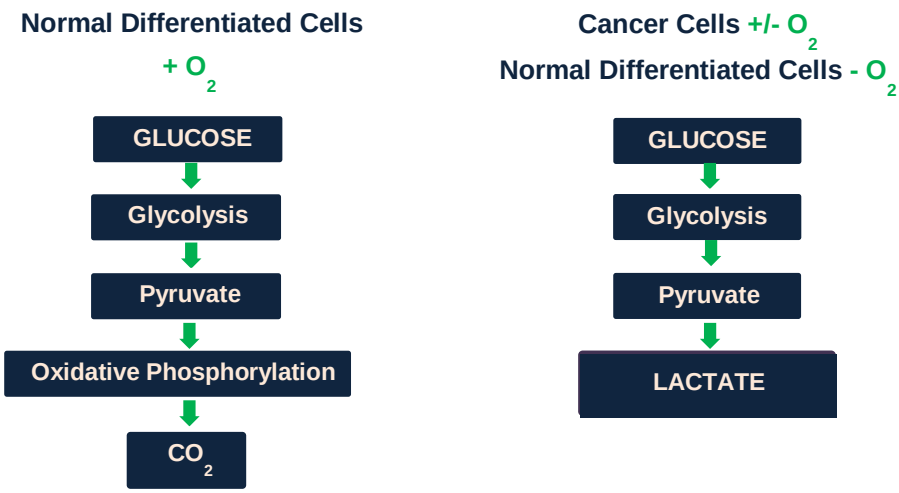

Figure 1.4: Simplistic schematic emphasising the alteration in cancer cell metabolism in the presence of oxygen.

The avid uptake of glucose by tumours has been exploited clinically with the use of 2-[^{18}F]fluoro-2-deoxyglucose positron emission tomography (FdG-PET) [95, 96]. This imaging technique was first developed in the late 1980s and approved in 1998 for detection, staging and monitoring of treatment response and relapse of most human cancers [97]. This traceable glucose analogue is administered to the patient and follows the metabolic route of glucose. It enters the cells through glucose transporters, gets phosphorylated by hexokinase and subsequently undergoes isomerisation. However it cannot be further catabolised and accumulates inside cells where it can be visualised and quantified reflecting the rate of glucose uptake which is enhanced in malignant tissues [95-97]. This non-invasive, sensitive technique is a valuable, universal tool in oncology and presents a direct translation of the Warburg effect into clinical practice.

The metabolic deregulation is evidently not a unique feature of malignancy [87, 88, 98]. A similar metabolic switch is also observed in unicellular organisms exhibiting exponential growth in an abundant nutrient environment and also in differentiated cells engaged in proliferative metabolism such as stimulated lymphocytes and proliferating fibroblasts [87, 98, 99]. It has been suggested that the glycolytic pathway has been selected by evolution to fulfil the special needs of rapidly proliferating cells [87, 98, 99].

In his day Warburg's theory was profoundly disregarded but recently it has regained a lot of interest and Warburg's contribution is universally recognised. In the last two decades, tumour metabolism has played a leading role in cancer research with tremendous therapeutic implications [93, 94, 100-105].

1.2.2 The reason behind aerobic glycolysis

According to Warburg's hypothesis the reason behind the high rate of glycolysis in cancer cells is a defect in their mitochondria that impairs aerobic respiration. However it is now recognised that mitochondrial function is retained intact in most cancer cells and oxidative phosphorylation contributes significantly to ATP generation depending on O_2 availability [90, 99]. In Warburg's day using Warburg's own data, Weinhouse resolutely contradicted the idea of a respiratory defect in cancer cells, but he did confirm the unquestionable elevated rate of glycolysis found by Warburg [84, 106].

Many factors contribute to the metabolic alteration of tumours including oncogenic transformation, the tumour microenvironment and mitochondrial DNA mutations. Aberrations in oncogenes and tumour suppressor genes can dictate and strictly regulate the metabolic alterations of tumours [83, 90, 91, 96, 107]. Akt, the serine-threonine kinase, downstream signalling effector of the phosphatidylinositol 3-kinase (PI3K), plays a critical role in the regulation of glucose metabolism [104, 108]. Akt activation promotes the metabolic switch to the glycolytic pathway and induces translocation of the Glucose transporter 4 (GLUT4) to the plasma membrane [104, 109, 110]. Further downstream in the same signalling pathway, Akt-mediated mTORC1 activation leads to increased GLUT1 levels through upregulation of mRNA translation [111]. It has also been proposed that Akt regulates the translocation of specific hexokinase isoforms (HKI and HKII) to the outer mitochondrial membrane and their interaction with the mitochondrial voltage-dependent anion channel (VDAC) enabling access to the mitochondrial ATP and promoting an advanced glycolytic rate. Through a mechanism that is not completely understood, Akt mediated hexokinase mitochondrial association prevents cytochrome c release and induction of apoptosis [112]. Constitutively active transformed c-Myc stimulates glycolysis and drives the overexpression of multiple glycolytic targets including GLUT1, GLUT4, Hexokinase, Pyruvate kinase and LDHA [104, 113, 114]. TIGAR (TP53-induced glycolysis and apoptosis regulator), a well characterised p53 regulator, attenuates glycolysis reducing the level of fructose-2,6-bisphosphate in the presence of a functional tumour suppressor p53 [104, 115]. It has also been demonstrated that p53 stimulates mitochondrial respiration by directly upregulating synthesis of cytochrome c oxidase-2, essential for the formation of the cytochrome c oxidase complex [116]. Another crucial factor is that the primary role of mitochondria is switched from energy generation to anabolic biosynthesis through aberrant oncogenic signalling [90]. The TCA cycle generates intermediates used for the biosynthesis of lipids and proteins through the process of cataplerosis [88].

Preferential expression of specific isoforms of glycolytic enzymes is also crucial for the glycolytic phenotype of tumours [96]. The most extensively studied is the M2 pyruvate kinase isoform. Furthermore amplification of glycolytic enzymes has also been described. Rempel *et al* demonstrated a five-fold amplification of Hexokinase II in a hepatoma cell line compared to normal hepatocytes [117].

The tumour microenvironment selects for cells adapted in hypoxic conditions. Stabilization of the transcription factor HIF-1α (Hypoxia Inducible Factor) stimulates glycolysis and upregulates the majority of enzymes related to the glycolytic pathway. It has been demonstrated through certain mechanisms that the HIF-1α subunit can be stabilised even in the presence of oxygen [107, 118]. Activation of mTOR as well as several oncogenes including Src, H-Ras and PI3K has been linked to HIF induction. The β domain of the von Hippel–Lindau (VHL) gene product binds the HIF-1α subunits leading to their oxygen dependent polyubiquitylation and proteasomal degradation. Subsequently, the inactivation of the VHL tumour suppressor gene, which is strongly associated with renal-cell carcinomas, inhibits HIF-1α degradation [119]. Moreover Lu *et al* suggested that the glycolytic pathway itself, through its final product pyruvate, promotes HIF-1α stability independently of the oxygenation level [120]. Recently it has also been shown that accumulation of succinate due to loss-of-function of succinate dehydrogenase results in prolyl hydroxylase inhibition and HIF-1α stabilisation irrespective of O_2 availability [83, 118, 121]. HIF regulation is described in greater detail in section 1.3.1.

Even though it is well established that mitochondrial function in tumours is in general not impaired, it has been demonstrated that mitochondrial DNA mutations contribute in certain cases to the glycolytic phenotype of tumours [83, 94, 96, 100, 107]. Moreover somatic or germline mutations in nuclear genes encoding TCA cycle enzymes might partially compromise mitochondrial respiration. It has been shown that succinate dehydrogenase and fumarate hydratase act as tumour suppressor genes in certain tumour types [88, 121].

1.2.3 The advantages of aerobic glycolysis

The metabolic switch of cancer cells involves an apparent paradox taking into consideration that glycolysis is a much less efficient pathway stoichiometrically for the production of ATP. Indeed the glycolytic pathway generates two ATP molecules per glucose molecule as opposed to 36 molecules generated through complete mitochondrial oxidation of glucose [87, 107, 122]. The abundant energy production of oxidative phosphorylation (OXPHOS) is the basis of the Pasteur Effect which describes the inhibition of glycolysis when O_2 is available [122, 123].

But what could be the reason behind this unprofitable, in terms of ATP generation, metabolic selection within tumours? First of all it has been suggested that for cancer cells nutrients are in many cases abundant. It is likely that malignant tissues maintain a constant affluent nutrient supply through blood circulation that enables a high rate of ATP production through the glycolytic pathway [87]. It has been shown that regardless of the high proliferation rate, cancer cells typically demonstrate high ATP/ADP and NADH/ NAD^+ ratios proving that resources are usually not scarce [87].

The 'metabolic reprogramming' is an adaptation to fulfil the immense anabolic requirements of highly proliferative malignant tissues, providing the precursors needed to support biosynthesis. Glycolysis and biosynthetic pathways provide the cells with energy and the metabolic intermediates needed for cell growth and biosynthesis of macromolecules [87, 88, 91, 98, 122]. Amino acid, fatty acid and nucleotide biosynthesis demands consumption of a large amount of carbon precursors in the form of α-ketoacids, acetyl-CoA or ribose in addition to ATP. Mitochondrial enzymes play a leading role in anabolic reactions. On the other hand vast ATP production through oxidative phosphorylation would compromise biosynthesis because of the lack of reducing equivalents and also jeopardise constant glucose uptake because of an elevated ATP/ADP ratio. Highly elevated ATP levels suppress glycolysis inhibiting allosterically phosphofructokinase (PFK) [98, 123, 124].

The metabolic alteration of cancer cells is proposed to provide them with a selective advantage for survival and growth in the low O_2 tumour microenvironment. As tumours grow and expand away from a functional blood supply, glycolysis is an evolutionary adaptation of cells to survive and thrive in a hypoxic environment [91, 102, 125]. Furthermore the acidic microenvironment from the vast amount of released lactate, offers cancer cells a selective growth advantage promoting motility and invasion (discussed in greater detail in section 1.3.2) [125, 126].

Another important aspect is that the metabolic switch offers a survival advantage protecting tumours from intracellular reactive oxygen species (ROS). An elevated level of oxidative phosphorylation in aerobic conditions would result in extensive ROS production that would induce oxidative stress and ROS-associated apoptosis. It has been repeatedly suggested that elevated glycolysis is a protective mechanism for cancer cells from oxidative stress [85, 93, 99].

1.2.4 Glutaminolysis

Glutamine is the most abundant amino acid in blood circulation and a nutrient of major importance to proliferating tumour cells. Glutaminolysis is an alternative metabolic pathway playing a crucial role in many tumours [127-130]. In 1979 Reitzer *et al* demonstrated that HeLa cells are highly dependent on glutamine for the production of energy. They reported that glutamine was the exclusive energy source when cells were cultured in fructose or galactose while contributing to energy generation at a level exceeding 65% in the presence of glucose [131]. More recently DeBerardinis *et al* examined the metabolism of glioblastoma cells using nuclear magnetic resonance spectroscopy. They documented that highly glycolytic tumour cells maintained a functional TCA cycle and engaged in glutamine metabolism to generate intermediates (anaplerosis) as well as reducing equivalents (NADPH) [132]. Although glutamine is a non-essential amino acid that can be synthesised from glutamate and ammonia by glutamine synthetase, it has been observed that many cancer cells require elevated amounts of glutamine for survival and growth [127-130].

Glutamine is transported into the cell by specific glutamine transporters. Once inside the cell glutamine is hydrolysed to glutamate by glutaminase. Subsequently glutamate is converted to α-ketoglutarate either through oxidative deamination by glutamate dehydrogenase or through a transamination reaction catalysed by aminotransferases. α-ketoglutarate is then directed to the TCA cycle for oxidation. It should also be mentioned that glutamate is a precursor of the redox regulator and major antioxidant glutathione [98, 130].

Cancer cell addiction to glutamine can be interpreted in several ways. First of all, glutamine provides nitrogen for amino acid synthesis as well as for the synthesis of purines and pyrimidines supporting the anabolic growth of tumours. Furthermore glutamine along with amino acid abundance activates mTORC1 and downstream signalling pathways promoting protein synthesis and tumour growth. Finally glutamine is a primary substrate of the mitochondrial TCA cycle contributing to biosynthetic precursors and NADPH generation and subsequently to macromolecular synthesis as well as energy production [98, 127-129]. It is well substantiated that c-Myc oncogenic transformation promotes glutamine addiction upregulating glutamine transporters and enzymes involved in glutamine catabolism (glutaminase) [127-130, 133, 134].

1.2.4.1 Targeting Glutaminolysis

The dependency of many tumours on glutamine can be exploited for preferential targeting of glutamine 'addicted' cancer cells. Several approaches to target glutamine metabolism for cancer therapy have been suggested and are currently under investigation [128, 129].

Glutaminase catalyses the conversion of glutamine to glutamate. Hydrolytic cleavage of glutamine generates glutamate along with an ammonium ion. BPTES (Figure 1.5) [Bis-2-(5-phenylacetamido-1,3,4-thiadiazol-2-yl)ethyl sulphide] is a small molecule, identified as a glutaminase inhibitor through a library screen in 2002. Five years later, Robinson *et al* performed extensive kinetic analyses and characterised the compound as a selective non-competitive inhibitor of the kidney glutaminase isoform. BPTES presents no structural similarity to either glutamine or glutamate and binds with high affinity to both the free enzyme as well as the enzyme-substrate complex. The authors suggested that the mechanism of inhibition involves restriction of phosphate-mediated allosteric activation and formation of inactive stable tetramers [135].

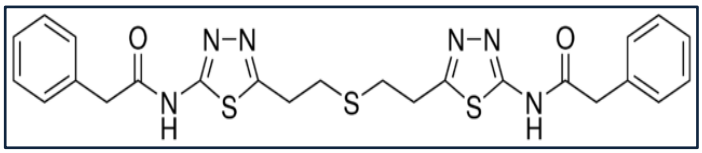

Figure 1.5:
BPTES
Linear Formula: $C_{24}H_{24}N_6O_2S_3$
Molecular Weight: 524.68
K_i value: 3μM
[135, 136]

Le *et al* performed isotope-resolved metabolomic studies and investigated the metabolism of Myc-activated P493 human Burkitt lymphoma cells. They reported that Myc induced both glucose and glutamine metabolism. However a functional glutamine-dependent TCA cycle under low O_2 or glucose-deprived conditions was substantiated. Glutaminase inhibition confirmed the crucial role of glutamine metabolism for tumour survival and growth. BPTES inhibited cell proliferation and impaired ATP production, elevating ROS levels, in P493 cells under both normoxic and hypoxic conditions. Attenuation of tumour growth in xenograft *in vivo* models was also demonstrated [137]. Isocitrate dehydrogenase 1 (IDH1) catalyses the oxidative decarboxylation of isocitrate to α-ketoglutarate. This enzyme is frequently mutated in gliomas and acute myelogenous leukemia. The mutants perform a different distinct reaction generating 2-hydroxyglutarate from α-ketoglutarate. Seltzer *et al* demonstrated that BPTES can preferentially suppress the growth of glioma cancer cells bearing IDH1 mutations by attenuating glutaminase activity and eliminating α-ketoglutarate levels [138]. These findings were further verified by Emadi *et al* who documented that primary acute myelogenous leukemia cells expressing mutant IDH were highly dependent on glutamine

metabolism and selectively sensitive to glutaminase BPTES-mediated inhibition [139]. A very interesting recent study conducted by Hudson and colleagues associated ovarian cancer platinum resistance with c-Myc upregulated glutamine metabolism. Platinum resistant ovarian cancer cells proved highly dependent on glutamine availability and upregulation of glutamine transporters and glutaminase was observed. Interestingly, analysis of three publicly available ovarian cancer patient microarray datasets revealed a significant correlation between elevated glutaminase expression and poor survival. A synergistic interaction between BPTES and cisplatin was reported and indicated by induction of apoptosis. Furthermore, BPTES was able to sensitise platinum resistant ovarian cancer cells to cisplatin treatment [140].

A novel selective glutaminase inhibitor named CB-839 (Calithera BioSciences) demonstrated preclinical antitumour activity across a range of tumour types. Phase I dose escalation trials in solid and haematological tumours are currently conducted [141].

1.3 Hypoxia

As mentioned earlier, hypoxia is a well substantiated characteristic of the microenvironment of advanced solid tumours. Several previous studies have documented that at least 50% of locally advanced solid tumours contain hypoxic and anoxic areas; a typical feature that does not correlate with the histological grade, the pathological stage nor any other clinical parameter. Substantial heterogeneity in the oxygenation status of individual tumours as well as among separate tumours has been extensively described [142-144]. Vaupel *et al* reported that at least 40% of examined breast carcinomas exhibited hypoxic tissue regions with O_2 tensions ranging from 0 to 2.5mmHg [144, 145]. They also revealed considerable variability in oxygenation even between breast tumours sharing identical histology, stage and grade [145]. Variability among separate tumours has proved greater than heterogeneity among areas of the same tumour [142, 143, 145]. Furthermore, it has been shown that relapsed lesions are more hypoxic compared to their primary counterparts [142-144].

Hypoxia in tumours, defined as O_2 tension lower than 2.5mmHg, develops because of a disturbed balance between O_2 availability and consumption [142-144]. Heterogeneously distributed alternating normoxic, hypoxic, anoxic necrotic as well as re-oxygenated areas are a common pattern of solid malignancies. This phenomenon results from the chaotic architecture of tumour microvessels and is termed ‘Cycling hypoxia’ [146]. Perfusion-limited hypoxia, referred as acute hypoxia, may occur as a consequence of insufficient O_2

delivery due to a functionally or structurally damaged microvasculature network and abnormalities of microcirculation. Additionally diffusion limited hypoxia, referred as chronic hypoxia, emerges due to extended diffusion distances as growing tumours expand further than 100 to 200μm away from blood capillaries [146, 147] [142-144]. Marked variability in blood flow of tumours has been reported ranging from zero and in some cases even exceeding that of surrounding healthy tissue. However O_2 extraction is typically deficient leading to reduced O_2 tensions [148]. Interestingly abnormal tumour microvasculature has been shown to stimulate the extraction of glucose as opposed to O_2 thus promoting the Warburg phenotype [148]. Other aetiologies of tumour oxygen deficiency include treatment-related anaemia or plasma-perfused microvessels [142-144].

Hypoxia disrupts cellular homeostasis and suppresses proliferation. In response to hypoxia, cells reduce their protein synthesis rate and frequently undergo p53-dependent or BCL2-regulated apoptotic cell death or even necrosis [142, 143]. The minimum O_2 requirement for normal cellular function is estimated at 1mmHg. Bellow this threshold, cell cycle arrest at the G1/S phase is induced [143]. However, oxygen deficiency plays a pivotal role in tumour progression through critical hypoxia-induced genome and proteome changes. Hypoxia has been associated with a clinically aggressive phenotype, resistance to radiation therapy and limited response to several chemotherapeutic agents (e.g. anthracyclines, carboplatin) [142-144]. Moreover, a considerable amount of literature confirms that hypoxic areas in tumours correlate with adverse clinical outcome and poor survival in a wide range of malignancies [142-144]. In line with this it has been suggested that pre-treatment oxygenation status could serve as a useful survival prognostic marker [144].

1.3.1 Hypoxia Inducible Factor 1

Cellular response to conditions of low oxygen availability is mainly coordinated by the transcription factor HIF-1 which plays a major role in tumour progression. HIF-1 was first described through the identification of a hypoxia-response element in the erythropoietin gene [149, 150]. It is a heterodimer of constitutively and ubiquitously expressed HIF-1α and HIF-1β subunits and has a basic–helix-loop-helix structure [147, 151]. The HIF-1β subunit, also named the aryl hydrocarbon-receptor nuclear translocator, is a typical subunit of several transcription factors [149]. HIF-1α, even though continually synthesised, undergoes rapid ubiquitination and proteasomal degradation in the presence of O_2 [152, 153]. In high O_2 tensions, HIF-1α gets hydroxylated by highly-conserved prolyl hydroxylases [153, 154]. Hydroxylated HIF-1α is recognised by the von Hippel-Lindau (VHL) tumour suppressor protein which binds directly to the oxygen-dependent degradation (ODD) domain of the

subunit and attracts the E3 ubiquitin-protein ligase complex [119, 153, 155, 156]. The factor inhibiting HIF-1 (FIH-1), utilising molecular O_2, hydroxylates an asparagine residue of HIF blocking its transactivation and suppressing its transcriptional activity [153, 157, 158]. In hypoxic conditions, hydroxylation and subsequent degradation is inhibited due to O_2 deprivation, leading to HIF-1α accumulation. In addition to substrate depletion, mitochondrial ROS inactivate the hydroxylases through oxidation of the ferrous ions in their catalytic centre [118, 159]. Stabilised HIF-1α is then translocated to the nucleus where it dimerises with the HIF-1β subunit to form the transcriptionally active complex [150]. HIF-1 induction is tightly regulated in response to O_2 tension; it is degraded promptly when O_2 availability is restored in hypoxic cells having a half-life lower than 5 min [149, 150].

Activated HIF-1 coordinates oxygen homeostasis and mediates adaptive responses to hypoxia via transcriptional activation of target genes [151, 153]. These responses include angiogenesis and erythropoiesis, promoting enhanced O_2 delivery, as well as metabolic reprogramming eliminating O_2 utilisation [149, 153]. HIF-1 induces the expression of SLC2A1 and SLC2A3 genes, encoding glucose transporters GLUT1 and GLUT3; and upregulates virtually all enzymes involved in the glycolytic pathway [118]. Indeed nine out of the ten glycolytic enzymes are known to be HIF-1 inducible. PDHK1 (pyruvate dehydrogenase kinase) is a HIF-1 target that suppresses mitochondrial respiration redirecting ATP synthesis to glycolysis through inhibition of the mitochondrial enzyme PDH (pyruvate dehydrogenase) [118, 160, 161]. Furthermore HIF-1 induces the expression of BNIP3 leading to selective mitochondrial autophagy [118].

Activation of HIF-1 resulting either from the hypoxic tumour microenvironment or uncoupled from changes in cellular oxygenation levels plays a critical role in carcinogenesis and tumour progression. A tight cooperation has been revealed between HIF-1 and deregulated oncogenic transcription factor c-Myc stimulating the glycolytic phenotype of tumours through upregulation of glycolytic enzymes [159, 162].

1.3.2 Lactate

Lactate generated by the glycolytic pathway was long considered merely a waste metabolic product however it is now well established that it plays a crucial role in carcinogenesis and tumour progression [163]. Lactate is transported in and out of cells via four monocarboxylate transporters MCT1-MCT4; members of a large solute carrier family. These are proton-linked proteins containing 12 transmembrane helices, intracellular terminal regions and a distinct cytosolic loop in-between the 6^{th} and the 7^{th} domain [164, 165]. The principal lactate transporters in tumour cells are MCT1 and the hypoxia inducible MCT4.

Highly glycolytic tumours export large amounts of lactate into the extracellular milieu. Lactate tumour levels have been extensively associated with treatment resistance and adverse clinical outcome [163]. Specifically secreted lactate has been shown to induce the expression of proinflammatory cytokines IL-23 and IL-17 in macrophages or monocytes and stimulated tumour-infiltrating immune cells. The proinflammatory response is well associated with tumour progression and distant metastases [166]. Furthermore it has been demonstrated that the lactate efflux impairs the tumour specific adaptive immune response. The acidic tumour microenvironment hinders the glycolytic metabolism of activated cytotoxic T cell lymphocytes as due to the lack of a concentration gradient, the lactic acid produced by tumour infiltrating immune cells cannot be efficiently removed. As a result their function is undermined as evidenced by reduced cytokine production [167]. An additional proposed role for lactate is that of a signalling molecule. It has been demonstrated that lactate released from tumour cells can be taken up by endothelial cells and can initiate a proangiogenic response through activation of the NFκB and IL-8 autocrine pathway, stimulating cell migration [168].

Lactate shuttling between tumour cells has been described. It has recently been realised that lactate may fuel the oxidative metabolism of tumour cells growing in an oxygenated microenvironment. Use of lactate as an alternative metabolic fuel has been observed in several non-malignant tissues including the liver and skeletal muscles. Sonveaux *et al* identified a metabolic symbiosis between hypoxic tumour cells that produce lactate which is then oxidised and used as an energy source from the subpopulation of tumour cells growing under high O_2 tensions. In this way glucose is spared for the highly glycolytic hypoxic tumour cell compartment located in great distance from a functional blood supply [122, 165, 169, 170]. MCT1 is considered the premier regulator of this symbiotic relationship and has been proposed as an attractive antitumour target [122, 169, 170].

1.4 The glycolytic pathway and the major targets

The glycolytic pathway comprises a series of ten enzymatic cytoplasmic reactions (Figure 1.6). One molecule of glucose is catabolised in the cytoplasm to two molecules of pyruvate generating two ATP and two NADH molecules [93, 100, 105, 122].

Glucose is transported into the cell by glucose transporters and gets phosphorylated to glucose-6-phosphate by hexokinase. Glucose-6-phosphate can be redirected to the pentose phosphate pathway and metabolised to ribose-5-phosphate for nucleotide synthesis.

Alternatively glucose-6-phosphate is converted to fructose-6-phosphate by isomerase and then a second phosphate group is added by 6-phosphofructo-1-kinase generating fructose-1,6-bisphosphate. In a series of consecutive steps in the second energy-yielding phase of the pathway, fructose-1,6-bisphosphate is metabolized to phosphoenolpyruvate through the intermediate products glyceradehyde-3-phosphate, 1,3-diphosphoglycerate, 3-phosphoglycerate and 2-phosphoglycerate. The enzymes catalysing these reactions are: aldolase, glyceraldehyde-3-phosphate dehydrogenase, phosphoglycerate kinase, phosphoglycerate mutase and enolase. Subsequently, pyruvate kinase transforms phosphoenolpyruvate to pyruvate. Differentiated tissues under aerobic conditions direct pyruvate into the mitochondrial TCA cycle for oxidative phosphorylation. In contrast tumour cells mainly convert pyruvate to lactate by lactate dehydrogenase, which is released through monocarboxylate transporters [93, 100].

The glycolytic pathway can be summarised in the following reaction: Glucose+2ADP → 2ATP+2 Lactate+$2H^+$+$2H_2O$ (Figure 1.6). The glycolytic components of particular interest to this study will be presented below.

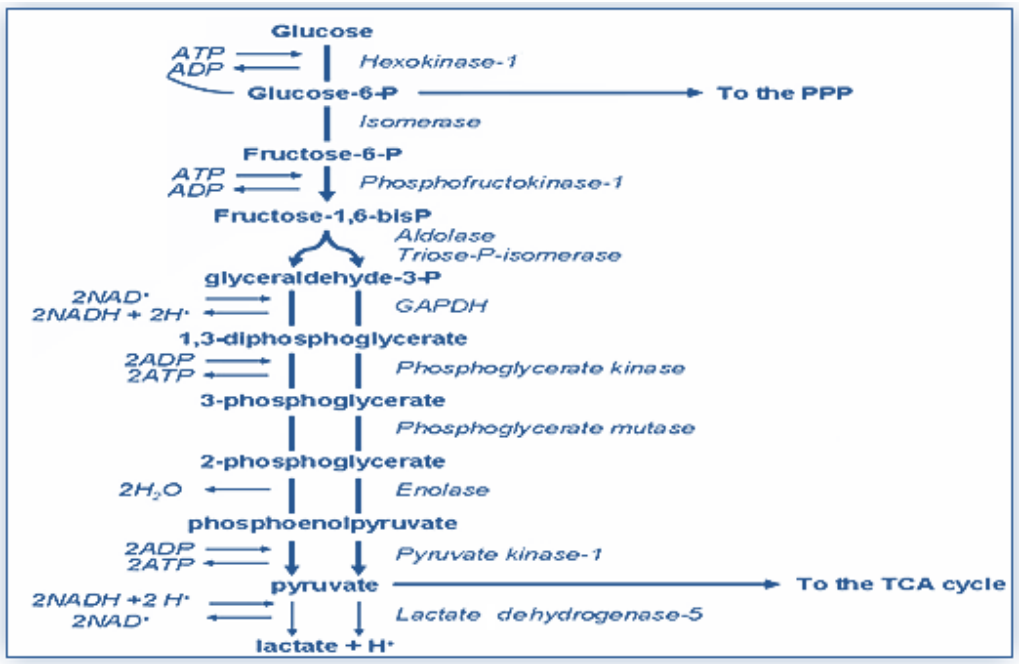

Figure 1.6: Representation of the glycolytic metabolic pathway and the enzymes catalysing its reactions. Figure adapted from Porporato *et al* [122]. PPP and TCA indicate the pentose phosphate pathway and the tricarboxylic acid cycle respectively.

1.4.1 Glucose Transporters

Proliferative cells demand a constant supply of nutrients to support biosynthesis and growth. This requirement is usually met by increased expression of nutrient transporters. Membrane glucose import into the cytosol is a key rate-limiting step for glycolysis and cellular proliferation. Glucose transporters (GLUTs) mediate the facilitated (energy independent) bidirectional diffusion of glucose and other hexone molecules across the plasma membrane in favour of the concentration gradient [171-176]. The GLUTs are members of the SLC2A gene family of transporters – solute carrier family 2A. The family comprises 14 isoforms each one of them containing 12 highly conserved transmembrane alpha helices and a N-linked glycosylation site. Three different classes of transporters are distinguished based on their sequence similarities. Class I comprises the extensively studied GLUT1-GLUT4; also known as classical transporters, as well as GLUT14, which is considered a gene duplication of GLUT3. The different isoforms display distinct tissue-specific expression patterns and substrate affinity [172-177]. GLUT1/ SLC2A1 is ubiquitously expressed, highly abundant in erythrocytes, and facilitates basal glucose transport in most tissues. The transport of glucose across the blood brain barrier is exclusively mediated by this transporter. GLUT1 plays an important role in tumourigenesis and is found overexpressed in the vast majority of transformed cells [171, 173-177]. GLUT2/ SLC2A2 shows low affinity for glucose and is expressed primarily in pancreatic islet cells, the intestinal epithelium and hepatocytes. It has also been associated with some neoplasms [172, 173, 175-177]. GLUT3/ SLC2A3 is a high-affinity transporter predominantly found in neurons and the testes. Abnormal expression has been described in several tumour types [171, 175-177]. GLUT4/ SLC2A4 is an insulin responsive transporter abundantly expressed in adipose tissue as well as skeletal and cardiac muscles. Even though its role is best characterised in insulin related disorders, including obesity and type II diabetes, upregulation in some tumours has been documented [171, 175-177]. GLUT5/ SLC2A5 belongs in Class II and presents high specificity for fructose. It is primarily expressed in the kidneys and small intestine but is also induced in some cancers [172, 173, 176, 177].

Among the transporters GLUT1 has the most universal and pivotal role in tumourigenesis. GLUT1 upregulation has been described in many different tumour types and is typically associated with tumour progression and poor prognosis [174-176]. In a study conducted by Carvalho *et al* IHC staining of tissue microarray (TMA) slides comprising 1955 samples of different tumour types revealed variable GLUT1 expression in the different neoplasms. Sarcomas, lymphomas, melanomas and hepatoblastomas were the only exceptions suggested to rely on another transporter for glucose uptake [178].

A considerable amount of literature indicates the crucial role of GLUT1 in breast tumours. Grover-McKay *et al* performed a comparative study of GLUT isoform protein expression against breast cancer cell line invasiveness. The non-invasive MCF7, the moderately invasive MDA-MB-435 and the highly invasive MDA-MB-231 cell lines were used and Western blot analysis was conducted. Interestingly, GLUT1 expression was correlated with breast cancer cell invasive potential while in contrast GLUT2 and GLUT5 presented an inverse correlation. GLUT3 expression was higher in MDA-MB-435 cells and GLUT4 was not detected in any of the cell lines [179]. In a more recent *in vitro* study the expression of GLUTs was compared between MCF7 and MDA-MB-231 cells based on Northern blot analysis. Xu *et al* reported that both cell lines express GLUT1, with the triple negative cell line exhibiting significantly higher levels, as well as the fructose transporter GLUT5, which is undetectable in healthy breast tissue. GLUT3 was found specifically expressed only in MDA-MB-231. The authors correlated the elevated GLUT1 and GLUT3 expression with the invasive and aggressive phenotype of the multidrug resistant MDA-MB-231 line [180]. In an IHC study conducted by Brown and Wahl contradicting the previous *in vitro* results GLUT3 and GLUT5 were not detected in any of the 12 breast cancer samples and 8 lymph node metastases examined. GLUT2 was mildly expressed in all tissues and GLUT4 was only detected in a subgroup of them. In contrast GLUT1 was overexpressed in all primary tumours and metastases. Membranous as well as cytoplasmic expression along with remarkable intratumoral and intertumoral staining variability were reported [181]. Unlike Brown, Younes *et al* assessed GLUT1 expression in 118 breast tumours and reported that less than half of them (42%) were positive for GLUT1. The discrepancy with Brown's results was attributed other than population variability to the staining technique and antibody specificity. Nevertheless GLUT1 expression was correlated with high proliferative index, as determined by ki-67 positivity, and higher nuclear grade [182]. In a subsequent study Brown *et al* showed that GLUT1 was expressed in 61% of 27 untreated breast cancer tissue sections. GLUT1 immunostaining was both membranous and cytoplasmic and was described as heterogeneous with higher expression observed in advanced stage tumours. Interestingly FDG uptake was associated with GLUT1 expression and not HKII [183]. Following IHC staining of 100 invasive ductal carcinoma samples Kang *et al* reported positive GLUT1 staining in 47% of the samples and correlated GLUT1 overexpression with negative ER and PR status and higher nuclear grade. Notably GLUT1 expression was significantly correlated with disease-free survival along with tumour size and lymph node involvement [184]. A more recent study conducted by Jang *et al* confirms that GLUT1 expression correlates with tumour grade, absence of ER and PR and triple-negative phenotype. The authors recorded

GLUT1 immunoreactivity in 38% of 276 invasive ductal tumours and 43% of 58 lymph node metastases. GLUT1 was also proposed as an independent prognostic marker as the transporter's expression was significantly correlated with poor disease-free and overall survival [185]. Pinheiro *et al* examined GLUT1 expression in 124 invasive breast tumours and reported immunoreactivity in 46% of the samples. GLUT1 expression was correlated with the expression of the hypoxia marker CAIX as well as MCT1 but not MCT4. Significant associations between GLUT1 upregulation and advanced tumour grade, absence of PR, basal-like subtype as well as high proliferative activity (ki-67) were further confirmed. However no association with the survival outcome was identified [186]. Krzeslak *et al* followed a slightly different approach and assessed GLUT1 mRNA and protein expression in 70 breast cancers using Q-PCR and Western blotting. GLUT1 was expressed in 50% of the samples at both the mRNA and protein level and the expression was higher in poorly differentiated tumours. Elevated GLUT3 expression in high grade tumours was also observed [187]. However in the literature there is substantial controversy regarding GLUT1 expression in normal mammary epithelium. In both his studies Brown along with Krzeslak and Jang described GLUT1 expression in normal and hyperplastic benign breast tissue [181, 183, 185, 187]. However, others, including Younes and Kang, failed to detect GLUT1 expression in normal breast epithelial cells [182, 184, 186]. Kang *et al* attributed the contradictory findings to the sensitivity of the various immunostaining protocols as well as to differential GLUT1 expression during the various phases of the menstrual cycle [184]. Another study by Alo *et al* documented GLUT1 expression in 31% (out of 48 samples) of normal breast tissues adjacent to in situ breast carcinomas and 36% (out of 28) of adjacent typical/atypical hyperplastic tissues. It should be noted that this is an additional study correlating GLUT1 expression with invasive phenotype and advanced tumour grade based on immunostaining of 66 breast carcinomas [188].

In reviewing the literature the pivotal role of GLUT1 in ovarian tumourigenesis is also revealed. Cantuaria *et al* argued that GLUT1 is critical for the malignant transformation of ovarian epithelia. The authors evaluated GLUT1 expression following an IHC streptavidin labelled biotin protocol in 21 borderline and 82 malignant epithelial ovarian tumours. GLUT1 was observed in 95 and 99% of the lesions respectively, while normal ovarian epithelium was mostly negative. GLUT1 expression was gradually elevated from borderline to high-grade malignant tumours and was correlated with the grade and histology of the tumours; serous carcinomas were found to express higher GLUT1 levels compared to other histotypes [189]. In a follow-up study the authors examined GLUT1 expression in 113 primary ovarian tumour tissues and observed immunoreactivity in 86% of the samples. In the

subgroup of advanced stage tumours GLUT1 overexpression was correlated significantly with clinical response to chemotherapy and poor disease free survival [190]. An interesting study conducted by Kalir *et al* corroborated the previous findings and demonstrated negative GLUT1 staining in normal and benign ovarian epithelial tissue, moderate expression in borderline tumours and strong expression in malignant tumours (54 out of 56 ovarian adenocarcinomas were stained positively) [191]. Rudlowski *et al* further confirmed previous findings of progressive GLUT1 expression from benign ovarian tissue (n=16) and borderline tumours (n=16) to malignant ovarian adenocarcinoma (n=78) as demonstrated by IHC, Western blotting analysis as well as *in situ* hybridisation. However in this study GLUT1 expression was not correlated with either the tumour grade, nor the histological subtype or the survival outcome. Weak GLUT3 expression was observed in both benign and tumour lesions while none of the GLUT2 and GLUT4 were found [192]. Contradictory findings were published by Tsukioka and colleagues who demonstrated strong GLUT1, GLUT3 and GLUT4 expression in ovarian adenocarcinomas. The authors examined 154 ovarian tumours using IHC and found the transporters expressed in 99, 93 and 84% respectively and their expression was correlated with angiogenesis and VEGF. GLUT1 along with GLUT4 were significantly higher in serous carcinomas compared to clear cell tumours and their expression was correlated with tumour stage [193]. In a more recent study Semaan *et al* examined GLUT1 expression in 213 primary ovarian tumours by IHC and correlated GLUT1 expression with tumour proliferation and microvessel density but not angiogenesis. Furthermore based on a univariate survival analysis elevated GLUT1, ki-67 and CD34 levels were significantly associated with poor clinical outcome. Also overexpression of GLUT1 in highly proliferative advanced stage tumours was shown to have a significant impact on optimal cytoreduction [194]. Cho *et al* performed genome wide microarray analysis and compared the gene expression profiles of developed ovarian cancer cell lines against benign ovarian tissue. GLUT1 was among the differentially expressed genes that were found remarkably overexpressed in ovarian malignancy. Subsequently the authors detected GLUT1 expression in each of the 50 examined ovarian tumour tissues and reported overexpression in serous carcinomas as well as a significant association with the survival outcome [195]. Lamkin *et al* adopted a totally different perspective and proved that glucose may have prognostic value in ovarian carcinogenesis. They examined the pre-surgical plasma glucose levels of ovarian cancer patients and demonstrated that high glucose levels were correlated with compromised survival rates and elevated risk of disease recurrence [196].

Overexpression of GLUTs in tumours is attributed to aberrant oncogenic growth factor signalling. As previously described hypoxia and HIF-1 induce GLUT1 and GLUT3 expression [118]. The PI3K/ Akt/ mTOR signalling pathway upon cytokine activation is highly associated with GLUT1 upregulation at the transcriptional and post-translational levels [197]. Activation of the serine/ threonine kinase Akt has been shown to induce GLUT1 gene transcription [198]. Several signals including insulin as well as *ras* and *src* oncogenic transformation have been described to stimulate the transporter's expression [197-199]. Insulin has been shown to induce both GLUT1 mRNA transcription and translation while an opposite effect has been observed for GLUT4 [111]. *KRAS* and *BRAF* transformation have also been associated with GLUT1 upregulation. Interestingly, Yun *et al* demonstrated that glucose deprivation can induce *KRAS* pathway mutations in colorectal cancer cells [200]. Another study conducted by Chen *et al* revealed that elevated GLUT1 expression upon *HRAS* transformation is mediated by HIF-1α upregulation and subsequent transactivation of the *glut1* promoter [201]. Other than aberrant growth factor signalling nutrient starvation is also described to contribute to GLUT upregulation. Impaired tumour blood supply may also trigger the overexpression of nutrient transporters [171]. On the other hand the tumour suppressor p53 is evidenced to repress the expression of the GLUT1 and GLUT4 transporters [202].

GLUT1 is considered a very attractive target for cancer therapy. A study conducted by Young *et al* demonstrated that GLUT1 knockdown suppressed mammary tumour growth in athymic nude mice. On the other hand GLUT1 overexpression stimulated tumour growth in the same *in vivo* model [203]. Several compounds inhibiting glucose transport have been identified and novel specific GLUT1 inhibitors have been recently synthesised attracting great interest [102]. Finally it should be mentioned that the GLUT1 deficiency syndrome is a treatable disorder transmitted through autosomal dominant inheritance. Impaired glucose transport into the brain is typically associated with infantile seizures, developmental delay and movement disorders. Various different mutations have been identified in the SLC2A1 gene combined with extended phenotypic diversity. It should be highlighted that the syndrome is somewhat treatable with a ketogenic diet (high fat, low carbohydrate diet) as ketone bodies can enter the central nervous system and provide an alternative energy source for the brain [177, 204].

1.4.2 Hexokinase (HK)

Hexokinase catalyses the first rate-controlling irreversible reaction of the glycolytic pathway; phosphorylating glucose to glucose-6-phosphate coupled with ATP de-phosphorylation [205-207]. This phosphorylation traps glucose inside the plasma membrane and determines its fate to follow the glycolytic pathway [205]. Four different mammalian isoforms have been identified; referred to as HKI, HKII, HKIII and HKIV. The first three of these present high affinity for glucose and their kinase activity is subjected to strong inhibition by the phosphorylation product [206, 208]. They have evolved through duplication of an ancestral glucokinase gene resembling that encoding HKIV [205, 206, 208]. Among the different isoforms, HKII is considered to play a pivotal role in carcinogenesis [205, 206]. Rapidly produced glucose-6-phosphate from cancer cells follows the glycolytic pathway for ATP production or is directed to the pentose phosphate pathway for NADPH and biosynthetic precursor generation [205, 206].

HKII is bound to the outer mitochondrial membrane anchored to the voltage-dependent anion channel (VDAC) via a binding domain at the amino-terminus. HKII preferentially utilises the ATP synthesised by the mitochondrial ATP synthase transferred by the adenine nucleotide translocator, and avoids strong inhibition from the generated glucose-6-phosphate [112, 205, 207, 209]. Due to its position in the mitochondrial membrane HKII plays a critical anti-apoptotic role promoting cancer cell survival [112, 205-207, 209]. Pastorino *et al* revealed that HKII prevents mitochondrial interaction of the proapoptotic protein Bax thus inhibiting Bax-induced apoptosis [112, 209, 210]. Furthermore Azoulay-Zohar *et al* showed that mitochondrial-bound hexokinase suppresses the formation of the mitochondrial permeability transition pore thereby inhibiting the release of cytochrome c [205, 211]. According to Roberts *et al*, HKII also regulates a protective glucose sensing mechanism mediated by mTORC1 inhibition and subsequent autophagy induction in glucose deprivation conditions. They recently demonstrated that the phosphorylation product, glucose-6-phosphate, not only suppresses the kinase activity of the enzyme and its mitochondrial localisation but also inhibits mTORC1 binding and autophagy activation [212, 213].

HKII is not expressed in most healthy mammalian tissues excluding insulin-responsive tissues such as skeletal muscle and the heart [205, 206]. Nevertheless it is overexpressed in many tumours [206]. The overexpression of HKII can be explained through both genetic and transcriptional events. Firstly, as previously mentioned, Rempel *et al* have demonstrated a five-fold amplification of the HKII gene in a hepatoma cell line [117, 214]. Furthermore it has been shown that normal hepatocytes express exclusively HKIV as HKII expression is

inhibited at the epigenetic level because of extensive methylation. Nonetheless in hepatocellular carcinomas HKIV is silenced and HKII expression is activated by demethylating agents [205, 207, 215]. Enhanced transcription has been extensively demonstrated in tumours and is attributed to *cis*-element promoter activation by protein kinase-A, protein kinase-C, HIF-1, p53 as well as glucose, glucagon and insulin [205, 207, 214].

Several studies have examined the role of HKII in breast and ovarian cancer. Brown *et al* examined HKII expression in a cohort of 27 untreated primary breast tumours by IHC. They found HKII cytoplasmic expression in 79% of the samples, not always correlating with GLUT1 expression. No association was observed between HKII expression and FDG uptake [183]. In a recent study Sato-Tadano *et al* identified HKII as a HIF-1α induced gene associated with breast cancer recurrence based on microarray gene expression analysis. Examining 118 breast tumours using IHC they detected HKII expression in 44% of them while expression in normal and benign tissues was considerably lower. The authors reported an association between HKII expression and the histological grade as well as expression of the proliferation marker Ki-67 and disease recurrence. HKII was proposed as a useful independent prognostic factor of disease-free survival in breast cancer patients [216]. Palmieri *et al* performed a small scale gene expression analysis examining differentially expressed genes between primary breast tumours and metastatic disease in the brain and observed a trend of HK overexpression in metastatic lesions. Indeed following IHC staining in a cohort of 123 resected brain metastases of breast cancer, HKII was found expressed in 77% of the samples and a significant association between HKII overexpression and poor clinical outcome was revealed [217].

Regarding the role of HKII in ovarian cancer a search of the existing literature revealed several studies. Suh *et al* examined HKII expression in 111 ovarian cancer samples following an IHC protocol. They reported a correlation between HKII overexpression and chemoresistance, defined as disease recurrence within 6 months of treatment completion. HKII overexpression was demonstrated as a prognostic factor for early disease recurrence and was significantly associated with reduced progression-free survival [218]. In 2014 Jin *et al* investigated HKII expression in ovarian tumour samples using IHC and qRT-PCR. Significantly elevated HKII expression was observed in malignant tissues compared to healthy and benign ones, as well as poorly-differentiated compared to well-differentiated lesions. HKII overexpression was associated with serous histogenesis, an association confirmed at both the mRNA and protein level [219].

1.4.3 Phosphofructokinase (PFK)

PFK1 (6-phosphofructo-1-kinase) catalyses the transfer of a phosphate group from ATP to fructose-6-phosphate. This irreversible reaction yields one molecule of ADP along with one fructose-1,6-bisphosphate (F1,6BP) molecule. It is the first committed step of glycolysis regulating the rate of the whole pathway. Elevated PFK1 activity is detected in many tumours as a result of oncogenic transformation [220, 221]. PFK1 is a complex tetramer composed of three different subunits in a tissue dependent manner. The three subunits, each encoded by a separate gene, are PFKM, PFKL and PFKP predominantly found in muscles, the liver and platelets respectively. PFK1 being a critical control point of the glycolytic pathway is tightly regulated. The enzyme is inhibited by lactate and citrate as well as fatty acids. However the most powerful PFK1 inhibitor is ATP. Likewise AMP activates PFK1 since both molecules reflect the cellular energy state [220, 221]. Nonetheless the most potent allosteric activator of PFK1 is fructose-2,6-bisphospate (F2,6BP) which promotes high glycolytic flux regardless of the ATP content. F2,6BP is both synthesised (fructose-6-phospate phosphorylation) and degraded (F2,6BP dephosphorylation) by a family of bifunctional enzymes called 6-phosphofructo-2-kinase/fructose-2,6-bisphosphatases (PFKFB) [220-222]. The kinase catalytic domain (PFK2 activity) is in the amino-terminus of a single polypeptide within a homodimeric protein complex while the bisphosphatase domain is in the carboxyl-terminus. Four different mammalian isozymes have been identified, encoded by separate genes and referred to as PFKFB1-4. As opposed to the other three isozymes, PFKFB3 presents a significant bias towards kinase enzymatic activity favouring F2,6BP synthesis (actual kinase: phosphatase activity ratio 740:1) [220-222].

PFKFB3 is hypoxia inducible, frequently overexpressed in tumours and considered to play a critical role in tumourigenesis [220-222]. Atsumi *et al* examined PFKFB3 mRNA and protein expression *in situ* in 60 human tumour samples. They reported that PFKFB3 was overexpressed in neoplastic cells; including lung, breast, colon and ovarian carcinomas, compared to their corresponding healthy tissues [223]. The upregulation of PFKFB3 during neoplastic transformation has been justified in many ways. Firstly, multiple repeat copies of the AUUUA instability motif have been observed in the 3' untranslated region (3'UTR) of the PFKFB3 mRNA stimulating transcriptional activity [224]. Novellasdemunt *et al* identified a progesterone response element in the PFKFB3 promoter and showed that binding of the progesterone receptor following progestin hormonal treatment induced transactivation of PFKFB3 transcription in breast cancer cells [225]. Moreover, it has been shown that AMPK-mediated extensive phosphorylation of a serine residue in the carboxyl-terminal region is crucial for the elevated PFKFB3 kinase activity observed in tumours

[226]. Telang *et al* identified PFKFB3 as a key metabolic mediator of *ras* oncogenic transformation. Paradoxically they observed reduced F2,6BP cellular levels in immortalised or *ras* transformed cells in spite of PFKFB3 overexpression. The authors attributed the reduction to a compensation feedback mechanism or increased glycolytic utilisation [227]. Almeida *et al* demonstrated that under physiological conditions PFKFB3 is constantly degraded in neurons via ubiquitination by the E3 ubiquitin ligase anaphase-promoting complex/cyclosome (APC/C)- Cdh1. Inactivation of the ligase activator Cdh1 at the restriction point of G1 phase is required for transition to S phase and induction of proliferation and glycolysis [228]. Interestingly, Garcia-Cao *et al* indicated that the tumour-suppressor PTEN downregulates PFKFB3 by promoting APC/C-Cdh1 complex activity and subsequently PFKFB3 degradation [229].

An additional role in regulation of cellular proliferation and cell cycle progression in a glycolysis-independent manner has been attributed to PFKFB3. Several PFKFB3 splice variants with distinct carboxyl-terminal domains have been noted in tumours. A key study conducted by Yalcin *et al* revealed nuclear localisation of the most prevalent PFKFB3 splice variant in tumours and demonstrated that nuclear F2,6BP activated Cdk1 resulting in phosphorylation and degradation of the cell cycle inhibitor p27 [230]. In a recent follow-up study the authors verified that PFKFB3 knockdown suppressed Cdk1 activity while elevating p27 levels and induced apoptosis via cell cycle arrest at G1/S phase [231]. De Bock *et al* revealed new insight into the roles of PFKFB3 as an angiogenesis regulator. They observed that PFKFB3 promoted vessel sprouting of highly glycolytic endothelial cells as well as lamellipodia formation and migration, a function mediated by an association between the enzyme and F-actin [232]. Additionally, Seo *et al* recently described PFKFB3 as a protective regulator of redox homeostasis. They reported that elevated ROS levels lead to S-glutathionylation of PFKFB3 attenuating its enzymatic activity and reducing F2,6BP generation. Subsequently the impaired glycolytic rate stimulated the pentose phosphate pathway influx and reduced glutathione production contributing to ROS detoxification [233].

1.4.4 Pyruvate Kinase (PK)

Pyruvate kinase catalyses the irreversible conversion of phosphoenolpyruvate (PEP) to pyruvate coupled with ADP phosphorylation which is the final rate-limiting step of the glycolytic pathway. Four different mammalian isoforms have been identified encoded by two separate genes. The L and R isoforms, found mainly in liver and erythrocytes respectively, are encoded by the *Pklr* gene using different promoters [234, 235]. M1 and M2 isoforms are splice variants of the *Pkm* gene. Mutually exclusive alternative splicing results

in the M1 isoform comprising exon 9, whereas M2 isoform comprises exon 10. The two isoforms differ in 23 amino acids encoding the inter-subunit contact domain associated with tetrameric formation [234-236]. PKM1 is constitutively active and present in many differentiated tissues including skeletal muscles and the brain while PKM2 is the predominant isoform of highly proliferative cells and embryonic tissues as well as cancer cells [234, 235]. Aberrant activation of the oncogenic transcription factor c-Myc has been shown to upregulate the transcription of heterogeneous nuclear ribonucleoproteins responsible for PKM2 specific splicing, i.e. exon 9 exclusion, resulting in preferential PKM2 overexpression in tumours [236].

PKM2 is found overexpressed in various tumour types and plays a pivotal role in carcinogenesis [234, 237]. Two different PKM2 forms have been described. The tetrameric form presents high affinity to PEP and is catalytically active while the dimeric form has low affinity to the enzyme's substrate and is virtually inactive. The interconversion is regulated by the upstream glycolytic metabolite fructose-1,6-bisphosphate (FBP) which acts as an allosteric activator inducing the formation of tetramers [234, 235, 237]. The low enzymatic activity isoform regulates the rate of the glycolytic pathway and leads to the accumulation of glycolytic intermediates stimulating the biosynthetic pathways. In this way, PKM2 balances energy production with channelling carbon sources for the biosynthesis of nucleic acids, proteins and lipids [235, 237, 238].

The dimeric:tetrameric ratio determines PKM2 activity and is tightly regulated [234, 237]. Evidence of oncogenic growth factor regulation was first provided by Christofk *et al*. In 2008 they demonstrated that PKM2 binds directly to phosphotyrosine peptides provoking the release of the bound allosteric activator FBP thereby suppressing PKM2 catalytic activity [239]. A year later Hitosugi *et al* reported that aberrant growth factor receptor tyrosine kinase signalling causes PKM2 phosphorylation resulting in interruption of FBP binding. Inhibiting the formation of highly active PKM2 tetramers favours anabolic pathways and the glycolytic tumour phenotype promoting tumour growth [240].

Other than fulfilling the tumour metabolic requirements, additional roles have been attributed to PKM2 [234, 237]. In 2012, Gao *et al* demonstrated that while tetrameric PKM2 is a pyruvate kinase, PKM2 dimer acts as an active protein kinase regulating gene transcription and promoting cancer cell proliferation. They provided evidence that dimeric PKM2 locates in the nucleus and phosphorylates *stat3* stimulating the transcription of a number of stat3 target genes [241]. In parallel Yang *et al* revealed that PKM2 regulates cell cycle progression and promotes tumour development through an interaction with β-catenin.

They showed that EGFR growth stimulation promotes PKM2 nuclear translocation where it binds and transactivates the c-Src-phosphorylated β-catenin. The interaction of the two proteins enhances cyclin-D1 expression through histone H3 acetylation and dissociation of histone deacetylase 3 from the *CCND1*gene promoter [242]. In a follow-up study conducted by the same group, it was reported that PKM2 binds directly to and phosphorylates histone H3 following EGFR activation; a modification essential for the induction of cyclin-D1 and c-Myc expression and consequently tumour progression [243]. Another key study by Luo *et al* revealed a feedback-loop interaction between PKM2 and HIF-1, mediating tumour metabolic transformation and transactivation of HIF-1 target genes. PKM2 being a HIF-1 induced gene itself, containing a hypoxia response element within the first intron, was found to coactivate HIF-1 enhancing its transcriptional activity. Hydroxylation of nuclear PKM2 by prolyl hydroxylase 3 (in the PKM2-specific domain in exon 10) promotes PKM2- HIF-1α interaction which stimulates HIF-1 binding to hypoxia response elements, recruitment of coactivators (p300) and therefore expression of HIF-1 target genes [244, 245].

Solid evidence of the fundamental role of PKM2 in tumourigenesis came firstly from Christofk *et al* in 2008. PKM2 proved essential for the glycolytic phenotype of tumours and it was shown that replacing the M2 isoform with M1 increased oxygen consumption and reduced tumour growth of human lung cancer cells in nude mouse xenografts [246]. In the same vein, in 2012 Anastasiou *et al* demonstrated that small molecule activation of PKM2, similarly to expression of the constitutively active PKM1 isoform, attenuated tumour growth in xenograft mouse models. The identified compounds bind specifically to PKM2, at a distinct site from that of FBP binding, and stimulate tetramer formation [238, 247]. Vander Heiden *et al* followed a different approach and through a library screening assay they identified a small-molecule selective PKM2 inhibitor that inhibited glycolysis and caused cytotoxicity to H1299 human lung cancer cells [248]. Both approaches, activation and inhibition, have been considered legitimate antitumour strategies [102, 104, 105]. Even though PKM2 emerges as an attractive target for cancer therapy some recent studies have challenged the notion of a switch from PKM1 to PKM2 expression during malignant transformation [249, 250]. Evidence of PKM2 expression in several normal differentiated tissues has been demonstrated and PKM2 isoform specificity in proliferating tissues has been questioned [234, 249, 250]. Along the same lines Cortes-Cros *et al* documented that dual knockdown of both PKM1 and PKM2 isoforms was required to attenuate colorectal cancer cell proliferation *in vitro* while PKM2 knockdown or total depletion of PK activity had no significant effect on tumour growth in established xenografts *in vivo* [251].

1.4.5 Pyruvate Dehydrogenase Kinase

Pyruvate Dehydrogenase Complex (PDC) is composed of three enzymatic components; pyruvate dehydrogenase (E1-PDH), dihydrolipoamide acetyltransferase (E2) and dihydrolipoamide dehydrogenase. Mitochondrial PDC catalyses the irreversible oxidative decarboxylation of pyruvate generating acetyl-CoA and CO_2 with a concomitant reduction of NAD+ to NADH. It is a tightly regulated link of cytosolic glycolysis with the mitochondrial TCA cycle, determining the fate of pyruvate between glycolytic lactate secretion and oxidative phosphorylation [252-254]. PDC is inhibited through PDH phosphorylation by a family of enzymes named Pyruvate Dehydrogenase Kinases (PDHKs). Phosphorylated PDH gets reactivated via dephosphorylation mediated by pyruvate dehydrogenase phosphatases. PDHKs regulate glucose homeostasis and are considered to be involved in several metabolic diseases including cancer [252, 254]. Four different PDHK isozymes with tissue specific distribution have been identified in humans. Acetyl-CoA and NADH act as allosteric activators of these enzymes while in contrast coenzyme A, NAD+, ADP and pyruvate inhibit their function [252-254].

PDHK1 is a direct HIF-1 target and plays a critical role in neoplastic transformation promoting the glycolytic phenotype of tumours. Inactivation of PDC, following PDHK1-mediated PDH phosphorylation, suppresses mitochondrial respiration and pro-apoptotic signals and eliminates ROS production favouring tumour progression [160, 252, 255]. PDHK1 is upregulated in tumours by HIF-1 and c-Myc. Additional activation has recently been demonstrated by Hitosugi *et al* through oncogenic tyrosine kinase signalling. They reported that tyrosine kinases, including Fibroblast growth factor receptor 1 (FGFR1) localised to the mitochondria phosphorylate PDHK1 stimulating glycolysis and tumour development [256].

1.4.6 Lactate Dehydrogenase (LDH)

LDH catalyses the interconversion of pyruvate to lactate along with concomitant oxidation of NADH to NAD^+. The final reversible reaction of the glycolytic pathway is a critical rate limiting step as regeneration of NAD^+ is essential to maintain the glycolytic flux. Human LDH belongs to the family of L-specific enzymes that use NAD^+ as a cofactor. LDH is a homo- or hetero-tetrameric enzyme composed from two different subunits, LDHA and LDHB. The two subunits are highly conserved, characterised by great sequence homology (reaching 75%) and are encoded by two separate genes *ldha* and *ldhb* respectively [257-259]. The LDHA (also known as LDHM-muscle) subunit is mostly detected in anaerobic tissues

such as skeletal muscle and liver while LDHB (also known as LDHH-heart) is the predominant subunit of tissues with aerobic metabolism including cardiac muscle, brain and kidneys. Five different isozymes have been identified depending on the subunit synthesis- LDH1 (H_4 or LDHB), LDH2 (M_1H_3), LDH3 (M_2H_2), LDH4 (M_3H_1) and LDH5 (M_4 or LDHA as it is herein referred). LDH5 along with isozymes with an excess of LDHA chains are mostly detected in anaerobic tissues favouring lactate generation whereas LDH1 and isozymes enriched in LDHB chains are kinetically more efficient in catalysing the conversion of lactate to pyruvate. The different isozymes have distinct electrophoretic mobility and kinetic features; with LDHA being the slowest moving and having the highest affinity to pyruvate [257-259]. An additional subunit named LDHC encoded by a separate *ldhc* gene, exhibiting high homology to the other two LDH genes, has been identified. The relevant LDHX (LDHC4) sixth isozyme is expressed exclusively in the testes and to a lesser extent in oocytes. LDHX is the predominant isozyme of spermatozoa and has been associated with male fertility [260, 261].

LDH is a well characterised and extensively studied enzyme family since it was first isolated back in the early 1930s. Elevated LDH serum level is used as an indication of tissue damage and is an important biomarker of several acute medical conditions that cause a rapid release of the enzyme into the blood; including myocardial, liver, skeletal muscle as well as neoplastic disorders [257, 258, 262]. Besides that, LDHA overexpression has been observed in various tumour types and is considered to have a crucial role in tumourigenesis. It is broadly associated with poor clinical outcome and resistance to therapy [257-259, 262]. Regarding breast and gynaecological malignancies Koukourakis *et al* demonstrated that LDHA expression was upregulated in 60% of breast, endometrial and ovarian adenocarcinomas compared to healthy control tissues. LDHA exhibited a cytoplasmic and nuclear expression pattern and was associated with HIF1α expression. In the same study LDH serum levels were found to be significantly increased only in endometrial and ovarian cancer patients suggesting that LDHA upregulation may not be the only factor contributing to elevated LDH activity in the bloodstream [263]. A recent study conducted by Dennison *et al* revealed that even though LDHA is widely overexpressed in breast tumours, LDHB exhibits differential expression. mRNA microarray data analysis of a panel of breast cancer cell lines identified LDHB as a bimodal expressed gene. In patient datasets LDHB was found expressed specifically in glycolytic basal-like tumours and overexpression was associated with response to neoadjuvant chemotherapy and disease relapse in triple-negative tumours [264]. Conversely, LDHB silencing due to promoter hypermethylation has been observed in several cancer types [265]. LDHA overexpression in breast tumours was also demonstrated

by Wang *et al*. In this study the authors correlated LDHA expression with tumour size but no other clinicopathological features using 49 breast cancer tissue samples. Additionally LDHA shRNA knockdown was shown to attenuate tumour growth in both *in vitro* and *in vivo* breast cancer models and induce oxidative stress and mitochondrial- mediated apoptosis [266].

Upregulation of LDHA in tumours is mainly attributed to HIF1 and Myc transcription factors [262]. Additionally, activation through oncogenic receptor tyrosine kinases has been described. FGFR1 (Fibroblast growth factor receptor 1) directly phosphorylates LDHA and enhances its enzymatic activity; promoting tetrameric formation and NADH- cofactor binding [267]. LDHA is mainly cytoplasmic, engaging in the glycolytic pathway. However it has been demonstrated that LDH localises also in the nucleus where it acts as a single-stranded DNA binding protein regulating gene transcription through interaction with the DNA polymerase α primase complex [268]. Further evidence has been provided by Luo and colleagues who showed that LDH is involved in the transcriptional activator complex of the histone 2B (H2B) gene and is essential for the attachment of the complex to the gene promoter. LDH along with GAPDH (glyceraldehyde-3-phosphate dehydrogenase) regulate the NAD^+/NADH cellular redox status which plays a critical role in H2B optimal transcription and S-phase progression [269, 270].

LDHA constitutes a promising anticancer target and has recently attracted a lot of interest. Conversion of pyruvate to lactate at the very bottom of the glycolytic pathway is specific to cancer cells and is expected to have very limited effect on normal cells that primarily oxidise pyruvate in their mitochondrial TCA cycle. It should be mentioned that individuals genetically deficient for LDHA are viable, relatively healthy and face only minor symptoms especially following intense physical activity [257, 258]. LDH knockdown has proved to have a major impact on tumour physiology; reduced LDHA activity promoted mitochondrial respiration, decreased mitochondrial membrane potential and suppressed tumour growth [271]. To date several LDH inhibitors have been identified and some of them have shown promising antitumour activity [102, 257, 258]. Additionally, LDH has been suggested as an attractive antimalarial target and inhibition of the LDH isozyme of the protozoan of the genus *Plasmodium* that causes malaria has gained a lot of interest recently [257, 258].

1.5 Targeting Glycolysis

The deregulated cellular metabolism of tumour cells and their preferential reliance on glycolysis opens a promising therapeutic window. The propensity of cancer cells to favour a glycolytic metabolism has been characterised as their Achilles' heel and signifies a viable vulnerability option promising to preferentially target tumours highly dependent on the pathway sparing normal differentiated cells. The array of enzymes comprising the glycolytic pathway can be exploited as potential targets for selective cancer treatment [93, 94, 100-105, 272].

Several glycolytic inhibitors have recently emerged exhibiting promising anticancer activity both *in vitro* and *in vivo*; nevertheless very few have reached clinical trials to date [94, 100-102, 105, 122]. The effect of glycolysis inhibition on breast cancer and even more on ovarian cancer remains to be thoroughly investigated. In the present study ten glycolytic inhibitors (Figure 1.7) targeting five prime components of the pathway were selected and compared against a panel of breast and ovarian cancer cell lines. The inhibitors are presented in detail below.

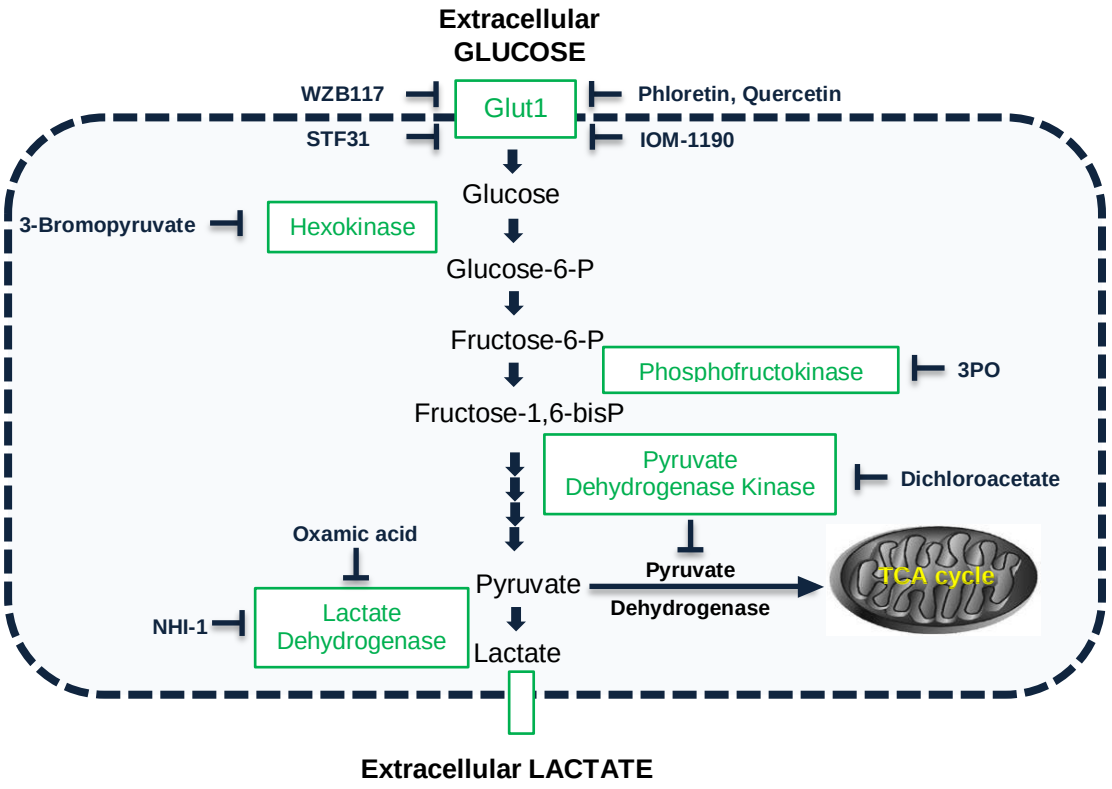

Figure 1.7: Representation of selected components of the glycolysis pathway and the glycolytic inhibitors used in this study. Figure adapted from Xintaropoulou *et al.*, 2015 [273].

1.5.1 Targeting Glucose Transport

1.5.1.1 Flavonoids – Phloretin & Quercetin

Flavonoids represent a substantial group of over 4,000 natural polyphenolic substances ubiquitously distributed in the plant kingdom. They are secondary metabolites; benzo-γ-pirone derivatives synthesised from the aromatic amino acids phenylalanine and tyrosine along with acetate units, and fulfil numerous diverse biological roles in plant physiology. They act as the coloured pigments of crops and flowers, contribute to developmental and defence mechanisms of plants and are generally involved in several processes including photosensitisation, morphogenesis and photosynthesis [274, 275]. Flavonoids are essential constituents of the human daily diet as they abundantly occur in fruits, vegetables, seeds, herbs as well as olive oil and red wine. It has been estimated that on average we consume roughly 1g of flavonoids on a daily basis [274, 275].

Various remarkable pharmacological responses have been linked with these 'natural therapeutic drugs' as they are also referred to. Antioxidant, anti-inflammatory, anti-allergic, anti-hyperglycaemic, oestrogenic as well as hepato-protective and cardio-protective properties, among many others, have all been attributed to them [274-276]. Of particular interest to this study, flavonoids have been shown to inhibit glucose transmembrane transport and have demonstrated notable preclinical antiproliferative effects [274-277]. The inhibition of glucose transport has been reported to be sensitive to pH variation since maximal effect has been observed at low pH that causes the dissociation of the molecules [277]. Phloretin and Quercetin are representative members of the large family of flavonoids.

Phloretin (Figure 1.8) [2′,4′,6′-trihydroxy-3-(4-hydroxyphenyl)-propiophenone], the aglucone of phloridzin, is mainly found in plants of the *Rosaceae* family, including pears and apples. This phytochemical is considered a natural nonsteroidal estrogen and has been described as a protein kinase C inhibitor [278, 279]. The reversible binding of Phloretin to the erythrocyte membrane and the selective inhibition of glucose efflux have been well documented [277, 280]. Chalcone Phloretin has been described as the most potent flavonoid in terms of glucose transport blockage [277].

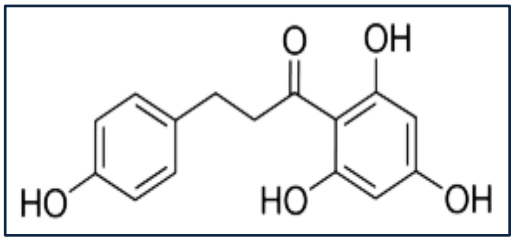

[136, 277]

Figure 1.8:
Phloretin
Linear Formula: $C_{15}H_{14}O_5$
Molecular Weight: 274.27
K_i value: 0.37±0.03μM (at pH 6.5)

Phloretin-mediated antitumour effects have been demonstrated in several models both *in vitro* and *in vivo*. More than two decades ago Nelson *et al* reported that phloridzin and phloretin inhibited the growth of Fisher bladder carcinoma and rat mammary adenocarcinoma cells *in vivo* [281]. In a follow up study the authors attributed the antiproliferative effect to inhibition of glucose transmembrane transport [282]. Kobori *et al* documented induction of apoptosis in B16 mouse melanoma 4A5 cells following Phloretin treatment. Apoptotic cell death was linked with inhibition of glucose transport as extracellular glucose was shown to prevent Phloretin action. The authors suggested that glucose transport inhibition is mainly responsible for the antitumour effect of Phloretin [278]. In a following study the authors reported that induction of apoptosis in B16 cells was mediated by Bax and caspase activation while a different mechanism was found responsible for the apoptotic cell death of HL60 human leukemia cells that was associated with protein kinase C inhibition [283]. Wu *et al* demonstrated induction of apoptosis in a human hepatocellular carcinoma cell line while cells could be rescued by glucose pretreatment. Additionally Phloretin attenuated the growth of HepG2 xenograft bearing mice suppressing FdG uptake. GLUT2 upregulation was evidenced in hepatoma cells as well as patient samples and the Phloretin effect was correlated with GLUT2 glucose transport inhibition [284]. Regarding breast cancer Kim *et al* presented induction of apoptosis in H-Ras transformed MCF10A mammary cells upon Phloretin treatment. Activation of MAPKs (Mitogen-Activated Protein Kinases – JNK and p38) and caspase-3 were documented followed by upregulation of p53 and Bax as well as Bcl-xl downregulation [279]. The same molecular mechanisms underlying Phloretin-mediated apoptotic cell death were verified in a very recent study conducted by Min and colleagues. Inhibition of proliferation and migration of non-small cell lung carcinoma A549 cells as well as attenuation of tumour growth of xenograft models were demonstrated [285]. Gonzalez-Menendez *et al* compared the effect of different flavonoids on androgen sensitive and insensitive prostate cancer cells. With respect to Phloretin they reported that it exhibits a potent antiproliferative effect regardless of androgen receptor signalling. They observed that Phloretin treatment suppressed glucose uptake leading to GLUT1 and GLUT4 upregulation without affecting the localisation of the transporters. Furthermore, based on docking simulation studies with a bacterial GLUT

homolog they predicted that Phloretin interacts with a conserved area near the active site centre of GLUT1 and GLUT4 blocking glucose binding [286].

Combinatorial interaction between Phloretin and common chemotherapeutic agents has also been evidenced. In a key study Cao *et al* examined GLUT1 expression in primary colon and breast tumours and noticed that GLUT1 was overexpressed especially in hypoxic regions with extensive necrosis. Phloretin was shown to reduce glucose uptake to 60% in SW620 colon cancer cells and proved able to resensitise both hypoxia-induced resistant as well as multi-drug resistant colon cancer and leukemia cells to daunorubicin, exclusively under hypoxic conditions [287]. Similarly, Yang *et al* documented that Phloretin enhanced the antitumour effect of Paclitaxel on *in vitro* and *in vivo* hepatocellular carcinoma models. The combination of the agents induced apoptotic cell death mediated by caspases 3,8 and 9 activation [288].

Quercetin (Figure 1.9) (3,3´,4´,5,7-pentahydroxyflavone) has been referred to as the most frequently consumed flavonoid [275, 289]. It is abundant in the form of glycosides in several components of the human diet including caper, chili peppers, cocoa beans, red onions, dill and fennel. A wide range of physiological actions have been attributed to this phytochemical however the underlying molecular mechanisms are not completely understood yet [289-291]. It is worth mentioning that the U.S. National Institutes of Health clinical trials website lists 45 different Quercetin related trials referring to an impressive range of conditions including Alzheimer's disease, anaemia, asthma, diabetes, hypertension, inflammation and obesity; emphasising the fascinating pleiotropic nature of this natural compound. Relative to carcinomas 4 studies were found. Isoquercetin (hydrolysed *in vivo* to Quercetin) as adjunct therapy for renal cell carcinoma patients treated with first-line sunitinib (ClinicalTrials.gov Identifier: NCT02446795), effect of Quercetin on green tea polyphenol uptake in prostate tissue of prostate cancer patients undergoing radical prostatectomy (ClinicalTrials.gov Identifier: NCT01912820), cancer associated thrombosis and isoquercetin (ClinicalTrials.gov Identifier: NCT02195232) and a pilot study evaluating broccoli sprouts in patients with advanced pancreatic ductal adenocarcinoma that receive palliative chemotherapy (ClinicalTrials.gov Identifier: NCT01879878). All these trials are currently recruiting participants [292].

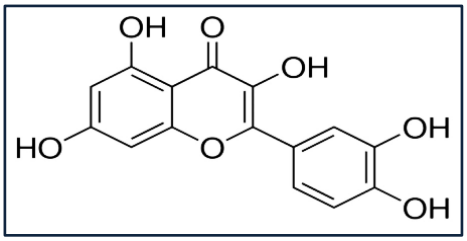

Figure 1.9:
Quercetin
Linear Formula: $C_{15}H_{10}O_7$
Molecular Weight: 302.24
K_i value: 0.93±0.28 μM

[136, 277]

Quercetin is considered a phytoestrogen with antioxidant properties at low concentrations while potent oxidative apoptotic action is presented at high concentrations. Potent chemopreventive action is attributed to this phytochemical. Multiple intracellular targets including heat shock proteins, protein kinases and topoisomerases as well as inhibition of certain signalling pathways have been described. Antitumour activity has been demonstrated in several types of cancer including breast, colon, lung, bladder and melanoma [289-291, 293]. Of particular interest to this study competitive binding of Quercetin to GLUT1 has been documented [294]. Moreover Quercetin has been shown to inhibit glucose uptake by isolated rat adipocytes and direct inhibition of GLUT4 has been suggested [295]. Inhibition of glucose uptake by MCF7 as well as MDA-MB-231 breast cancer cells in a concentration dependent manner has also been evidenced by Moreira *et al* [296].

Selected recent publications regarding breast and ovarian cancer will be discussed here. In 2013 Deng *et al* examined the effect of Quercetin on MCF7 breast cancer cells. Quercetin treatment attenuated breast cancer cell proliferation, induced apoptosis and G0/G1 phase cell cycle arrest. The apoptotic effect was linked with a reduction in mRNA and protein of the apoptotic inhibitor survivin [297]. The exact same antiproliferative observations regarding apoptotic cell death and G0/G1 cell cycle arrest characterised by survivin suppression were also documented for the ovarian cancer cell SKOV3 by Ren *et al* [298]. In another very recent study Ranganathan *et al* verified the apoptotic effect of Quercetin on MCF7 cells and reported selectivity over the triple negative MDA-MB-231 breast cancer cell line. Treatment with the flavonoid was shown to reduce the levels of the Twist oncogene and also suppress cyclin D1 and phospho-p38MAPK expression [299]. In contrast Tao *et al* presented similar sensitivity from the two breast lines. Caspase-3 dependent apoptotic cell death was linked with miR-146a upregulation and was also confirmed *in vivo* [300]. Seo *et al* examined the effect of Quercetin on the HER2-overexpressing BT-474 breast cancer cell line. Induction of caspase dependent apoptosis corroborating previous findings was demonstrated along with suppression of the STAT3 signalling pathway [301]. Zhang *et al* compared the effect of Quercetin with that of its sulphated derivative QS (quercetin-50,8-di-sulfonate) on MCF7 cells. QS proved more potent in attenuating cell proliferation, blocking cell cycle at the S

phase and inducing apoptotic cell death in a ROS dependent manner [302]. Very recently Liao *et al* synthesised two novel alkylated derivatives of Quercetin, 7-O-butylquercetin and 7-O-geranylquercetin. Both agents exhibited greater cytotoxicity to MCF7 cells compared to the parental compound. They were associated with induction of caspase-independent apoptosis [303]. Zhao *et al* demonstrated great antitumour activity *in vivo* using a MCF7 xenograft nude mouse model. Quercetin treatment attenuated tumour growth, reduced Ki-67 expression and promoted tumour necrosis without any side-effects being reported. Additionally the phytochemical exhibited potent antiangiogenic action compromising microvessel density, downregulating VEGF and VEGFR2 and inhibiting calcineurin [304].

Several studies have demonstrated a synergistic effect between Quercetin and common therapeutic modalities. Wang *et al* reported that Quercetin reversed tamoxifen resistance in breast cancer cells. The authors established a tamoxifen resistant cell line and observed that Quercetin significantly enhanced the cytotoxic effect of tamoxifen. The combination promoted induction of apoptosis and resulted in reduced HER2 and upregulated ERα levels [305]. Minaei *et al* provided evidence that nanoparticle-conjugated Quercetin (to achieve enhanced bioavailability) sensitised MCF7 cells to doxorubicin, augmenting apoptosis induction [306]. As regards combinations in ovarian cancer models, Maciejczyk *et al* demonstrated that Quercetin sensitised ovarian cancer cells to paclitaxel and cisplatin [307]. This finding was verified by Yang *et al* who showed that Quercetin pre-treatment sensitised ovarian cancer cells to cisplatin both *in vitro* and *in vivo* and alleviated cisplatin nephrotoxicity. Quercetin provoked endoplasmic reticulum stress and suppressed STAT3 signalling downregulating its target genes including Bcl-2 [308]. Yi *et al* documented that Quercetin enhanced TRAIL-induced (tumor necrosis factor-related apoptosis-inducing ligand) cytotoxicity in ovarian cancer cells *in vitro* (SKOV3, OVCAR3 and TOV21G cell lines) as well as in SKOV3 mouse xenografts. Synergistic apoptotic cell death was associated with caspase activation, enhanced ROS generation and DR5 (TRAIL binding – death receptor 5) upregulation [309]. Twenty years ago a first in class phase I clinical trial was published. A patient with cisplatin resistant disease reported a remarkable decline in serum CA125 levels following Quercetin intravenous treatment. Similarly α-fetoprotein serum concentration was diminished in a hepatoma patient. Quercetin was generally well tolerated and was correlated with tyrosine kinase inhibition [310]. An interesting very recent case report study revealed that oral Quercetin (up to 2g per day) along with cyclophosphamide resulted in complete radiological response with minimal adverse effects and fatigue improvement in a male with advanced metastatic bladder cancer [311].

1.5.1.2 STF31

In 2011 Chan *et al* performed a high-throughput chemical synthetic lethal screen to discover agents that specifically target VHL deficient renal cell carcinomas. STF31 (Figure1.10) [4-[[[[4-(1,1-Dimethylethyl)phenyl]sulfonyl]amino]methyl]-N-3-pyridinylbenzamide] is a pyridyl-anilino-thiazole that belongs to the second class of the 3-series small-molecules identified to exhibit selective cytotoxicity in cells that have lost a functional VHL tumour suppressor gene. In their characterisation study the authors argued that STF31 impairs the glycolytic metabolism of VHL deficient tumours by binding specifically to the GLUT1 transporter. Based on molecular modelling STF31 was predicted to interact directly with the central pore of the transporter and was shown to inhibit glucose uptake and induce necrotic cell death selectively in glycolytic cancer cells harbouring a VHL mutation. Interestingly elevated GLUT2 expression proved able to prevent the STF31 cytotoxic effect in renal cell cancer cells. *In vivo* efficacy of the compound was also demonstrated. A soluble STF31 analogue impaired glucose uptake, as monitored by FDG-PET, and attenuated tumour growth of mice with VHL-defective renal cell carcinoma xenografts without any apparent toxicity to normal tissue including the brain [312].

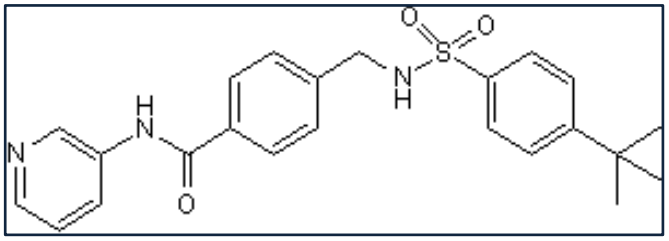

Figure 1.10:
STF31
Linear Formula: $C_{23}H_{25}N_3O_3S$
Molecular Weight: 423.53

[313]

In a very recent study Matsumoto *et al* reported the effectiveness of STF31 against myeloma cell lines. The authors examined the glucose uptake and the expression of glucose transporters in multiple myeloma cell lines and demonstrated a cytotoxic effect specifically on cell lines with upregulated GLUT1 expression. STF31 was shown to impair glucose uptake of these cell lines and was associated with induction of caspase-8 dependent apoptotic cell death. A very interesting finding of this study was that STF31 enhanced the cytotoxic effect of first-line anti-myeloma regimens including doxorubicin, bortezomib and melphalan [314].

However three years after the first identification of the compound, in 2014, Adams *et al* claimed that the main cellular target of STF31 is nicotinamide phosphoribosyl-transferase (NAMPT), an enzyme involved in NAD^+ regeneration. They performed a large-scale cancer cell line sensitivity profiling study and observed that the response pattern to STF31 was highly correlated to that of established NAMPT inhibitors. Based on whole genome next-

generation sequencing data of clones resistant to a more potent STF31 analogue (referred to as compound 146) they attributed the resistance to a recurrent mutation in the NAMPT gene. It was also demonstrated that STF31 inhibits the enzymatic activity of recombinant NAMPT and cells can be rescued from the cytotoxic effects of the small molecule by co-treatment with nicotinic acid, a substrate for NAMPT independent NAD^+ recycling (providing a functional nicotinate phosphoribosyl-transferase isoform 1 NAPRT1, an enzyme involved in the NAD^+ recycling pathway, is expressed) [315]. In agreement with these, a small molecule with identical structure was among the compounds characterised as potent direct NAMPT inhibitors in a fragment-based identification study conducted by Dragovich and colleagues [316]. Along the same line Kropp *et al* recognised STF31 as a NAMPT inhibitor attributing its metabolic effects on NAD^+ depletion. This study demonstrated that the compound was effective in eliminating the undifferentiated human pluripotent stem cells under several culture conditions with minimal toxicity to differentiated cells [317].

1.5.1.3 WZB117

In 2010 Liu *et al* reported the identification of a group of novel synthetic small molecules inhibiting basal glucose transport. Among these compounds WZB27 and WZB115 were presented as potent growth inhibitors of breast and lung cancer cell lines while exhibiting minimal toxicity on normal cells. Induction of caspase-3 dependent and p53 independent apoptotic cell death as well as a synergistic interaction with cisplatin and paclitaxel were also demonstrated [318]. In a follow-up study, two years later, the representative structural analogue WZB117 (Figure 1.11) [3-Fluoro-1,2-phenylene-bis(3-hydroxybenzoate)] was characterised as a novel selective GLUT1 inhibitor. The compound exhibited potent antiproliferative activity in lung and breast cancer cell line models and proved more effective under hypoxic conditions. Remarkable antitumour efficacy was also demonstrated *in vivo* in A549 lung tumour bearing nude mice with limited side-effects. Glucose transport inhibition in human red blood cells that are exclusively dependent on GLUT1 indicated that WZB117 is a specific GLUT1 inhibitor. Ligand docking studies revealed that inhibitor-transporter binding comprises 3 hydrogen bonds in the central channel of GLUT1. WZB117 treatment suppressed glucose uptake and lactate production and decreased intracellular ATP levels leading to AMPK phosphorylation. The mechanism of action of the effective GLUT1 inhibitor was also examined; G1 cell cycle arrest along with senescence were observed and followed by subsequent necrosis [319].

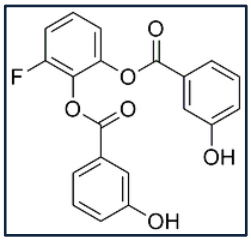

[320]

Figure 1.11:
WZB117
Linear Formula: $C_{20}H_{13}FO_6$
Molecular Weight: 368.3

In 2014 Liu *et al* investigated 5-fluorouracil (5-FU) resistance in colon cancer. They generated a 5-FU resistant colon cancer cell line and observed that resistance was associated with increased GLUT1 expression and elevated glucose uptake. WZB117 was used to overcome 5-FU resistance in colon cancer cells and a synergistic interaction between the two agents was demonstrated [321]. Along the same lines Zhao *et al* very recently reported a link between glycolysis and radiation therapy resistance (radioresistance) in breast cancer. GLUT1 upregulation accompanied with a stimulated glycolytic metabolism were documented in radioresistant breast cancer cells as well as radioresistant patient tumour samples. Interestingly GLUT1 overexpression reduced sensitivity to radiation therapy while GLUT1 knockdown conferred the opposite effect. A synergistic inhibitory interaction was presented between WZB117 and radiation and furthermore the GLUT1 inhibitor proved able to resensitise radioresistant breast cancer cells to treatment. The synergism was attributed to the decreased GLUT1 levels (both mRNA and protein) and the suppression of glucose metabolism following WZB117 treatment [322]. Another study by Shibuya *et al* examined the role of GLUT1 in the self-renewal capacity of cancer stem cells. They documented that WZB117 treatment attenuated the self-renewal and tumour initiating ability of highly glycolytic cancer stem cells in both *in vitro* and *in vivo* models [323].

1.5.1.4 IOM-1190

In 2014 IOmet Pharma patented the identification of a series of novel best-in-class specific GLUT1 inhibitors [324]. One of the lead molecules, IOM-1190 (Figure 1.12), was provided for this study to complement the array of glycolytic inhibitors used. Official characterisation of the compound has not been published yet; however Dr Alan Wise presented initial information in the 26th EORTC-NCI-AACR Symposium on 'Molecular Targets and Cancer Therapeutics' in November 2014.

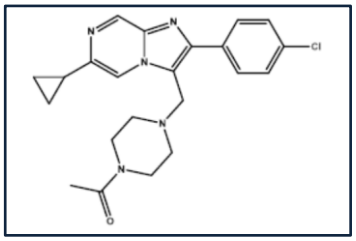

Figure 1.12:
IOM-1190
Molecular Weight: 526

The compound, possessing an imidazo[1,2-a]pyrazine core, was identified through a small molecule diversity study and was presented as a potent (low nM potency) and selective GLUT1 inhibitor. Suppression of 2-DG uptake and lactate production were demonstrated in A549 lung cancer cells along with evidence of induction of rapid apoptotic cell death. Competitive action against 2-DG for GLUT1 binding was reported and high affinity GLUT1 binding of radiolabelled compound was documented. Furthermore, a synergistic interaction was demonstrated between an optimised analogue and metformin in lung, melanoma and glioma cancer cell lines promoting ATP depletion and cell death.

1.5.2 Targeting Hexokinase

3-bromopyruvate (3BP) (Figure 1.13) (3-Bromo-2-oxopropionic acid) is a small molecule and a synthetic analogue of pyruvate and lactate that directly inhibits mitochondrial bound HKII. It has consistently demonstrated potent anticancer activity in both *in vitro* and *in vivo* model systems [325, 326]. 3BP is a strong alkylating agent that exerts its antitumour activity mainly through inhibition of glycolysis and cellular ATP depletion [325, 326]. Furthermore it has been shown that 3BP through a covalent modification of cysteine residues of HKII causes dissociation of the enzyme from the mitochondrial membrane and promotes the release of apoptosis inducing factor into the cytoplasm [327]. It has also been suggested that through HKII inhibition, low 3BP concentrations cause shortage of biosynthetic precursors hindering anabolic reactions [326, 328]. Potent inhibitory action has been described in various cancer cell line models including pancreatic, hepatocellular, melanoma, glioblastoma and mammary [325].

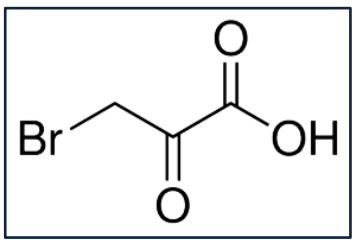

Figure 1.13:
Bromopyruvic acid
Linear Formula: $BrCH_2COCOOH$
Molecular Weight: 166.96

[136]

Majkowska-Skrobek *et al* demonstrated a cytotoxic inhibitory effect in a human myeloma cell line induced by intracellular ATP depletion. The authors described increased tumour specificity of 3BP action compared to normal peripheral blood cells which correlated with increased uptake due to MCT1 overexpression [329]. Along the same line Queiros *et al* in their study presented induction of apoptosis in breast cancer cell lines following 3BP treatment. Interestingly, they observed that pre-treatment with the carboxylic acid butyrate enhanced 3BP cytotoxicity particularly in the most resistant ER-negative cell line. The authors attributed the butyrate effect to MCT4 upregulation and increased membrane localisation of MCT1 [330]. Xu *et al* documented that leukaemia and colon cancer cells with impaired mitochondrial function due to hypoxic conditions or mitochondrial defects, as well as cells with a multidrug resistant phenotype, were found to be particularly sensitive to 3BP. 3BP induced ATP-depletion related apoptotic cell death associated with Bad dephosphorylation, and Bax translocation to the mitochondria and enhanced the cytotoxic effect of doxorubicin, vincristine and cytarabine. 3BP treatment was proposed as a promising strategy to overcome multidrug resistance [331]. In their study Icard *et al* reported that 3BP treatment induced cell death even in platinum-resistant mesothelioma cells as well as improved the survival of nude mice bearing mesothelioma tumours [332]. Recently Zou *et al* showed induction of apoptosis in nasopharyngeal carcinoma cell lines following 3BP treatment [333]. Another study by Wintzell *et al* provided evidence that a multi-resistant ovarian cancer cell population resembling cancer stem cells, developed from the SKOV3 cell line through repeated treatment with increasing concentrations of cisplatin, was sensitive to 3BP [334].

The first *in vivo* system in which the anti-tumour effect of 3BP was examined in was the VX2 tumour implanted into a rabbit liver. In 2001 Ko *et al* described the VX2 tumour as highly glycolytic and sensitive to 3BP treatment delivered via the hepatic artery, with no marked side-effects reported [335]. In a following study, three years later the same author using a hepatocellular carcinoma model in the rat, demonstrated that 3BP eradicated the tumours that had developed in all 19 animals studied, exhibiting 100% efficacy; while no toxicity or recurrence were observed [336]. Another study conducted by Buijs *et al* reported that 3BP treatment selectively reduced FDG uptake in breast tumours in a rat model suggesting that 3BP did not affect the glucose metabolism of healthy tissues [337]. Three years ago Ko *et al* published a case study of the first human patient treated with a specially formulated 3BP. It was a young Caucasian male suffering from advanced stage fibrolamellar hepatocellular carcinoma. 3BP treatment was not associated with any major toxicities and effectively prolonged the patient's survival, improving his quality of life [338]. In 2014 a

second case was reported by El Sayed *et al*. A male patient with metastatic stage IV melanoma received 3BP intravenous infusions. The authors described minimal adverse effects; nevertheless the antitumour activity was modest. This was attributed to the elevated tumour glutathione level and co-administration of a glutathione depletor was suggested [339].

3BP as a potent alkylating agent inhibits other metabolic enzymes as well [326, 328]. Among 3BP targets another glycolytic enzyme glyceraldehyde-3-phosphate dehydrogenase (GAPDH) as well as the mitochondrial succinate dehydrogenase have been described [326, 328, 340, 341]. In a recent study Kwiatkowska *et al* showed that 3BP inhibits several enzymes in glutathione metabolism and causes an imbalance in the cellular redox state increasing ROS production. They illustrated increased sensitivity of MDA-MB-231 breast cancer cells through induction of oxidative stress compared to the non-invasive MCF7 cell line [342]. Overall, it has been claimed that because of targeting key metabolic enzymes impairing both the glycolytic pathway and mitochondrial respiration, and taking into consideration the demonstrations of tumour specificity and low toxicity profile, 3BP could play a leading role in cancer treatment in the near future [102, 328]. Because of its structural similarity to lactate, 3BP is taken up specifically by tumour cells through MCTs and exerts potent antitumour activity [102].

1.5.3 Targeting PFKFB3

In 2008 Clem *et al* identified a competitive inhibitor of PFKFB3 using computational modelling and virtual database *in silico* screening. 3PO (Figure 1.14) [3-(3-Pyridinyl)-1-(4-pyridinyl)-2-propen-1-one] is a novel small molecule, dipyridinyl-propenone based compound. In their characterisation study, the authors demonstrated that 3PO reduced intracellular F2,6BP levels, glucose uptake and lactate production followed by an induction of G2-M phase cell cycle arrest in Jurkat T cell leukemia cells. Selective sensitivity of ras-transformed bronchial epithelial cells along with a cytostatic effect in several tumour cell line models, including MDA-MB-231 breast cancer cells, was demonstrated. PFKFB3 overexpression was shown to induce resistance to 3PO while the enzyme's deletion enhanced the sensitivity of Jurkat cells, suggesting that PFKFB3 is critical for the observed tumour growth inhibition. Finally, 3PO treatment suppressed tumour growth *in vivo* in mice bearing leukaemia, lung and breast adenocarcinoma xenografts with no adverse effects documented. The authors mentioned that even though 3PO was identified as a specific PFKFB3 inhibitor; due to the high homology between the different PFKFB isozymes simultaneous inhibition of any of them cannot be excluded [343]. Recently Klarer *et al*

reported that the metabolic stress induced by PFKFB3 inhibition activates autophagy as a protective pro-survival mechanism in response to glucose starvation. 3PO treatment of HCT-116 colon adenocarcinoma cells increased ROS production and induced autophagy, as demonstrated by increased levels of the autophagy marker LC3-II, reduced p62 levels and detection of autophagosomal structures. It was shown that co-treatment with autophagy inhibitors can enhance 3PO antitumour efficacy both *in vivo* and *in vitro* [344].

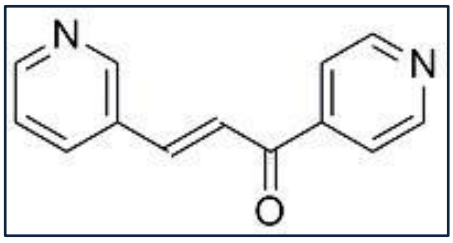

Figure 1.14:
3PO
Linear Formula: $C_{13}H_{10}N_2O$
Molecular Weight: 210.2
K_i value: 25±9μM

[320, 343]

Several very recent studies have revealed supplementary effects of 3PO treatment other than glycolysis inhibition. Trefely *et al* performed a global human genome kinase screening combined with siRNA knockdown and among others they identified PFKFB3 as a kinase involved in the insulin growth factor (IGF) signalling pathway. Indeed they showed that 3PO treatment of 3T3-L1 adipocytes impaired insulin-dependent GLUT-4 membrane localisation and Akt kinase activity as demonstrated through decreased phosphorylation of downstream substrates [345]. An antiangiogenic effect of 3PO was revealed in another recent study by Schoors *et al*. The authors reported that the PFKFB3 inhibitor impaired vessel sprouting in both *in vivo* and *in vitro* models. Even though 3PO treatment had only a partial and temporary effect on glycolysis decrement, it attenuated pathological angiogenesis and enhanced the antivascular activity of VEGFR inhibitors in ocular and inflammatory mouse models [346]. Furthermore Telang *et al* suggested 3PO as a T cell immunosuppressive agent. 3PO treatment was shown to suppress glycolytic metabolism and activation of T cells and also impaired T cell dependent immunity of *in vivo* mouse models [347].

In 2011 Seo *et al* published the structure based development of another novel small molecule competitive PFKFB3 inhibitor named N4A and its potent derivative YNI. The authors reported reduced F2,6BP levels, glycolysis inhibition and cell death in HeLa cells validating PFKFB3 inhibition as a promising strategy for cancer treatment [348].

Two years later, in 2013, Clem *et al* published the identification of an optimised derivative of 3PO, 100 times more active against enzymatic PFKFB3. PFK15 [1-(4-pyridinyl)-3-(2-quinolinyl)-2-propen-1-one] has a quinolinyl ring substituted for a pyridinyl ring. The second generation compound presented markedly enhanced potency and pharmacokinetic

properties and induced apoptosis in tumour cells both *in vitro* and *in vivo*. PFK15 suppressed glucose uptake and attenuated tumour growth in several tumour xenograft models [349]. A related compound termed PFK158 is currently undergoing a phase I safety clinical trial in patients with advanced solid malignancies (ClinicalTrials.gov Identifier: NCT02044861) [350]. The study was initiated in January 2014 and initial results are expected soon [102, 350, 351].

1.5.4 Targeting Pyruvate Dehydrogenase Kinase

Dichloroacetate (DCA) is a pyruvate analogue (Figure 1.15), a small molecule that inhibits PDHK. PDHK inhibition restrains PDH phosphorylation and subsequent PDC activation. Hence pyruvate metabolism is redirected from glycolysis and lactate production to oxidative phosphorylation. DCA is a generic drug with great oral bioavailability that was described almost fifty years ago in 1969. DCA has been used clinically for decades to alleviate the symptoms of lactic acidosis and ketoacidosis of several inherited mitochondrial diseases [352, 353]. Nonetheless DCA has been associated with nerve toxicity and because of its potency in high millimolar concentrations off-target effects cannot be excluded. A randomised placebo-controlled trial in 30 patients suffering from MELAS (mitochondrial myopathy, encephalopathy, lactic acidosis and stroke-like episodes) syndrome was discontinued because of peripheral neuropathy [354]. However another randomised double-blinded trial in 21 children with congenital lactic acidosis reported that DCA was well tolerated [355]. Actually it has been shown that DCA plasma clearance and consequently toxicity are inversely associated with age as well as haplotype genetic variability in the glutathione transferase zeta 1 gene (GSTZ1). GSTZ1 catalyses DCA biotransformation and dehalogenates it to glyoxylate [353, 356].

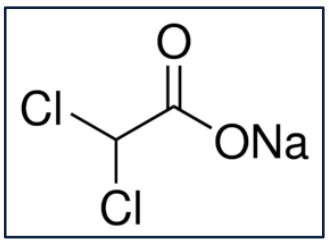

[136]

Figure 1.15:
Sodium dichloroacetate
Linear Formula: Cl_2CHCO_2Na
Molecular Weight: 150.92

Antitumour activity of DCA has been extensively demonstrated in a wide spectrum of cancer types *in vitro* (including pancreatic, prostate, colon, lung, leukaemia, neuroblastoma, endometrial) as well as several *in vivo* tumour models [255, 352, 353]. Of particular interest to this study Saed *et al* provided evidence that DCA induced apoptosis via oxidative stress in

epithelial ovarian cancer cell lines. It was shown that DCA reduced the expression of key redox regulator enzymes (myeloperoxidase and inducible nitric oxide synthase) as well as HIF-1α, upregulated superoxide dismutase and subsequently increased caspase 3 activity [357]. Regarding breast cancer, Sun *et al* demonstrated that DCA treatment attenuated proliferation in a panel of breast cancer cell lines; sensitivity ranged from 20 to 80% after a 4 day treatment, without affecting the growth of a control non-cancerous line (MCF-10A). Even though an increase in caspase 3/7 activity was observed, induction of apoptosis was not detected, differing from several studies showing apoptotic cell death in various cancer types. Furthermore an antitumour effect was presented *in vivo* in a highly metastatic breast adenocarcinoma rat model [358]. In a follow up study the authors demonstrated that DCA upregulated the ATP synthase β subunit leading to increased ATP and ROS production and inhibited HIF-1α in breast cancer cells. Moreover DCA was shown to enhance the cytotoxic effect of arsenic trioxide, an anti-mitochondrial agent used for the treatment of acute promyeloid leukaemia, and this combination profoundly suppressed c-Myc and HIF-1α expression [359]. Similarly DCA was found unable to induce apoptosis in a panel of breast cancer cell lines by Gang *et al*; however DCA treatment reinforced the apoptotic effect of PENAO [4-(N-(S-penicillaminylacetyl)amino) phenylarsonous acid] another mitochondrial inhibitor targeting the adenine nucleotide translocase, by an oxidative stress-related mechanism due to enhanced ROS generation [360].

In a key study conducted by Bonnet and co-workers it was shown that DCA reverses the function of mitochondria in tumours and induces apoptosis selectively in cancer cells. DCA stimulates glucose oxidation, decreases the membrane potential of hyperpolarised mitochondria and promotes mitochondria-induced apoptosis through the release of pro-apoptotic signals, ROS production and activation of K^+ channels [361]. Sutendra *et al* revealed an antiangiogenic role of DCA. They demonstrated that PDHK inhibition elevated H_2O_2 levels and induced p53 activation and nuclear localisation resulting in decreased HIF-1α transcriptional activity. HIF-1α inhibition reduced the expression of HIF-1α target genes and suppressed angiogenesis in cancer cells both *in vitro* and *in vivo* [362]. Although the DCA antitumour effect is generally associated with ROS mediated mitochondrial apoptosis some recent indications of autophagy have been reported. In 2014 Lin *et al* documented increased expression of the autophagy marker LC3B II, cell cycle arrest and induction of autophagy following DCA treatment of colorectal and prostate cancer cell lines and *in vivo* HT29 colorectal tumour xenografts. Autophagy was associated with mTOR inhibition and ROS production while negligible necrosis and apoptosis were detected. MCT1 upregulation

was also observed and the authors suggested that DCA may also act as a potential competitive MCT1 inhibitor [363].

Aiming to enhance the potency and specificity of PDK inhibition, several attempts to develop a DCA structural analogue have been described [353]. Among them mitaplatin [c,t,c-[Pt(NH3)2(O2CHCl2)2Cl2]] has gained a lot of interest. It is a fusion compound that upon reduction from the negative intracellular redox potential releases cisplatin and two DCA units. A dual killing mechanism is accomplished through cisplatin-mediated DNA crosslinks as well as DCA mitochondrial targeting. Mitaplatin reduces mitochondrial membrane potential and induces apoptosis and nuclear degradation specifically in cancer cells [364].

Early phase trials using DCA in cancer patients have been reported. The first-in-human DCA study was conducted in 2010 by Michelakis and colleagues in five patients with glioblastoma multiforme. Peripheral neuropathy was the only clinically significant toxicity noted; nevertheless it was reversible and mitigated with a lower, yet clinically relevant dosage. Three of the patients (one with recurrent disease and the other two with newly diagnosed tumours receiving DCA in combination with chemotherapy and radiotherapy) presented radiologic regression and four patients in total were stable upon completion of a 15 month DCA treatment and alive 3 months afterwards. Additionally, the authors treated ex vivo, 49 tissue specimens collected from patients with glioblastoma, and reported that DCA treatment normalised mitochondrial hyperpolarisation, induced ROS production and p53 activation leading to apoptosis and suppressed HIF-1α and tumour angiogenesis [365]. Dunbar *et al* conducted a phase I trial in 15 patients with advanced recurrent gliomas or brain metastasis from primary tumours outside the central nervous system. Dosing was effectively adjusted according to GSTZ1 genotype and no clinically significant adverse effects were observed. Eight patients received DCA treatment for at least 1 four-week cycle and they were reported as clinically stable [356]. Another open-label phase II study in patients with advanced stage non−small cell lung cancer and metastatic breast cancer was designed by Garon *et al* and was terminated prematurely in 2014 due to limited participation and lack of clinical benefit [366]. Finally Strum *et al* published a noteworthy case report of a 46 year old male individual with relapsed non-Hodgkin's lymphoma after standard chemotherapy. The authors documented complete remission over 4 years following DCA monotherapy without any toxicity [367]. A considerable amount of evidence suggests that DCA warrants further investigation and may play a critical role in cancer therapy in the next few years.

1.5.5 Targeting Lactate Dehydrogenase

1.5.5.1 Oxamic acid

Oxamic acid (Figure 1.16) is an established pyruvate analogue (a structural isostere of pyruvic acid) described as a well characterised substrate-like competitive inhibitor of LDH. It is a non-selective inhibitor demonstrating an inhibitory effect on both LDHA and LDHB isoforms. Additionally inhibition of the *Plasmodium* LDH isoform has been reported and Oxamic acid has gained a lot of interest as a potential antimalarial agent [368]. Several N-substituted derivatives have been synthesised [368].

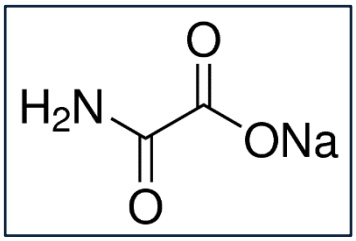

Figure 1.16:
Sodium oxamate
Linear Formula: $C_2H_2NO_3Na$
Molecular Weight: 111.03
Ki value: 136.3µM (vs pyruvate)
[136, 369]

Promising antiproliferative effect of Oxamic acid has been extensively reported mainly *in vitro* using various types of cancer cell line models. Fiume *et al* demonstrated that Oxamic acid supressed lactic acid production and attenuated the proliferation of two hepatocellular carcinoma cell lines. Treatment with the LDH inhibitor was associated with elevated PUMA levels indicating increased cell death [370]. In a follow-up study the authors confirmed the Oxamic acid-mediated glycolysis inhibition through reduced lactate production in a hepatocellular carcinoma cell line. Additionally they demonstrated that Oxamic acid enhanced the antiproliferative effect of kinase inhibitors. This was attributed to reduced ATP levels following LDH inhibition, competing with the kinase inhibitors for binding to the same site of oncogenic protein kinases [371]. A key study by Zhao *et al* demonstrated that Oxamic acid attenuated tumour growth of several HER2-positive and trastuzumab-resistant breast cancer cell lines as well as xenograft nude mice models of trastuzumab sensitive and resistant breast cancer. Interestingly Oxamic acid enhanced the antitumour effect of trastuzumab and helped overcome trastuzumab resistance in both *in vitro* and *in vivo* breast cancer models [372]. Similarly, Zhou *et al* published a synergistic interaction between Oxamic acid and taxol in breast cancer cell lines. Oxamic acid was found to be effective in inhibiting proliferation of MDA-MB-435 breast cancer cells as well as a taxol resistant derivative line, which exhibited even greater sensitivity to the combination of taxol with Oxamic acid. The LDH inhibitor was able to resensitise taxol resistant breast cancer cells to taxol, triggering apoptotic cell death [373]. Another recent study conducted by Miskimins and collaborators demonstrated a very modest antitumour effect of Oxamic acid against a

tonsil cancer cell line (E6E7Ras) and a CT26 colon cancer mouse model. Nonetheless, a synergistic effect was revealed between the LDH inhibitor and phenformin, a biguanide, shown to be a more potent inhibitor of mitochondrial respiratory chain complex I than metformin. The combination proved effective in various cancer cell lines as well as *in vivo* in immune competent syngeneic mice. Reduced lactate production, increased ROS generation, ATP depletion and induction of apoptotic and PARP-dependent cell death were reported [374].

Regarding the mechanism of action of Oxamic acid, Zhai *et al* reported that treatment with the LDH inhibitor induced mitochondrial oxidative stress-mediated apoptosis in nasopharyngeal carcinoma cells. Cell cycle arrest at G_2/M phase was demonstrated and correlated with downregulation of the CDK1/ cyclin B1 kinase complex. Additionally, Oxamic acid was shown to suppress tumour growth in nasopharyngeal cancer cell lines and enhance the antitumour effect of ionising radiation in both *in vitro* and *in vivo* nasopharyngeal tumour models. The radio-sensitising effect of the LDH inhibitor was associated with increased ROS generation augmenting the DNA damage [375]. In 2014 Yang *et al* published that non-small cell lung cancer cells presented a differential response to Oxamic acid treatment. They reported that Oxamic acid induced apoptosis in H1395 cells along with G_2/M cell cycle arrest. However, a protective autophagic response was recorded for the more resistant A549 cell line coupled with G_0/G_1 quiescence. Autophagy was associated with activation of glycogen synthase kinase-3β and subsequent inhibition of the Akt/mTOR signalling pathway, a known negative regulator of autophagy. It was suggested that autophagy inhibition could be a promising strategy to overcome LDH inhibition resistance. Another noteworthy observation of this study was that HBE normal lung epithelial cells were found considerably less sensitive to Oxamic acid treatment [376]. In the same vein a very recent study conducted by Zhao and colleagues confirmed induction of protective autophagy following Oxamic acid treatment in gastric cancer cells. It was demonstrated that Oxamic acid attenuated proliferation of gastric cancer cell lines and promoted autophagy which was correlated with elevated ROS production and inhibition of the Akt/mTOR signalling pathway. Interestingly, autophagy inhibition by chloroquine was shown to enhance the antiproliferative effect of Oxamic acid as well as apoptotic cell death [377].

Oxamic acid is a rather non-specific LDH inhibitor as inhibition of aspartate aminotransferase (AAT), an enzyme involved in the malate-aspartate NADH shuttle, has also been confirmed. Thornburg *et al* conducted enzymatic studies and demonstrated that the

compound inhibits both LDHA and AAT recombinant enzymes. It was shown that Oxamic acid only modestly affected glucose uptake and lactate production of breast cancer cells while inhibition of the TCA mitochondrial cycle and reduced O_2 consumption were reported. However, evidence was provided that Oxamic acid treatment selectively inhibited the proliferation of MDA-MB-231 breast cancer cells compared with normal mammary epithelial cells and also suppressed the growth of established breast tumour xenografts in athymic mice [369]. Besides multiple confirmed metabolic targets the compound is also characterised by low potency as high concentrations in the millimolar range are demanded to exert antitumour activity and membrane permeability is limited due to its polar nature. Unfortunately such high concentration levels have proved challenging for *in vivo* experiments [368, 371].

1.5.5.2 NHI-1

In 2011 Granchi *et al* published the identification of a series of N-hydroxy-2-carboxy-substituted indoles synthesised specifically as LDHA inhibitors. NHI-1 (Figure 1.17) [1-Hydroxy-6-phenyl-4-(trifluoromethyl)-1Hindol-2-carboxylic acid] is the most promising of these N-hydroxyindole-based (NHI) inhibitors, also referred as compound 1j, competitive for both the substrate-pyruvate as well as the cofactor-NADH. In their characterisation study the authors showed that NHI-1 reduced lactate production of HeLa cells and attenuated tumour growth, inducing apoptotic cell death, of various cancer cell lines including ovarian, mesothelioma and pancreatic. Specificity for the LDHA isoform over LDHB as well as enhanced efficacy under hypoxic conditions has also been demonstrated [378].

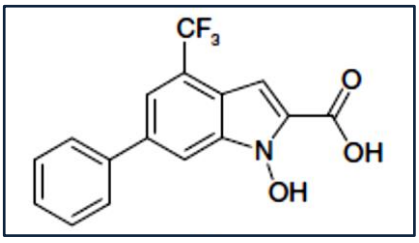

[368, 378]

Figure 1.17:
NHI-1
Linear Formula: $C_{16}H_{10}F_3NO_3$
Molecular Weight: 321.25
Ki value: 4.7±0.5μM (vs pyruvate)
8.9±1.3μM (vs NADH)

In a follow-up study the authors confirmed the antiproliferative activity of NHI compounds in two pancreatic carcinoma cell lines particularly under hypoxic conditions. Several analogues modifying the aryl-substituents of the standard NHI scaffold were synthesised and characterised as potent and selective LDHA inhibitors [379]. Two years later, in 2013, the authors performed a comparative study between NHI compounds and novel malonic derivatised LDHA inhibitors synthesised by AstraZeneca UK. In this analysis the methyl ester NHI-2 [methyl 1-hydroxy-6-phenyl-4-(trifluoromethyl)-1H-indole-2-carboxylate] was identified as a very potent LDHA inhibitor exhibiting great antiproliferative activity and

enhanced cell-membrane permeability [380]. Many derivatives of the original NHI scaffold have been synthesised in subsequent studies [368]. In 2014 Maftouh *et al* described a synergistic interaction between NHI-1 (as well as NHI-2) and gemcitabine; a chemotherapeutic nucleoside analogue, in pancreatic ductal adenocarcinoma. The LDHA inhibitor was particularly effective in attenuating proliferation of the pancreatic cancer cell lines PANC-1 and LPC006 in low O_2 conditions, inducing apoptosis and inhibiting growth and invasion of 3D spheroid culture models. It was also shown that NHI-1 treatment resulted in reduced expression of metalloproteinases as well as cancer-stem-like cell markers. The synergism with gemcitabine was evidenced by impaired cellular proliferation and migration, induction of apoptosis and S phase cell cycle arrest; and was attributed to elevated levels of phosphorylated active gemcitabine metabolites (deoxy-nucleotides) [381].

1.6 Combinatorial Therapeutic Approaches

Inhibition of the glycolytic pathway is recognised as a promising therapeutic strategy especially for tumours with impaired mitochondrial function. Tumours harbouring mitochondrial defects or hypoxic ones are expected to be preferentially sensitive to glycolysis inhibition. It should be mentioned that these conditions are associated with increased resistance to common therapies [100, 103, 104, 331]. However even though it is widely accepted that many tumours are more reliant on the glycolytic pathway it is undeniable that ATP generation through oxidative phosphorylation, to a certain extent, also occurs [100, 103, 104].

Combinatorial treatments of glycolytic inhibitors with traditional therapeutics are considered the best way to achieve optimal therapeutic efficacy and complete ATP depletion. Indeed combination regimes have always attracted considerable attention and are a major area of growing interest. Several successful combinations have recently been identified and glycolytic inhibitors have proved able to resensitise resistant cells to conventional regimens [100, 103, 104, 382, 383]. Other than enhanced antitumour effect and an optimal therapeutic index an additional benefit of combinational strategies is reduced adverse effects since the doses used for both agents are considerably lower than monotherapy.

Some combinatorial studies involving inhibitors of particular interest were mentioned earlier. Even though exploiting glycolysis inhibition to enhance the effect of traditional agents has recently emerged as a powerful strategy, so far only a few studies have been conclusive and such combinations have not progressed into clinical practice to date. The main purpose of this part of the research was to investigate novel combinations of glycolytic inhibitors with traditional agents. Some information regarding the selected agents is given below.

1.6.1 Cytotoxic drugs – Cisplatin & Paclitaxel

Cisplatin is a platinum based chemotherapeutic agent widely used for the treatment of several tumours among them bladder, testicular, brain as well as lung cancers. Its main mechanism of action involves DNA cross-links, preferentially binding to purine bases on the DNA, causing DNA damage. In this way cell division is inhibited, DNA repair mechanisms are activated and eventually apoptotic cell death is induced. Cisplatin is associated with severe side effects including nephrotoxicity, neurotoxicity, cardiotoxicity and myelosuppression. Cisplatin-refractory disease frequently develops and hence combinatorial treatments with other antitumour agents are currently under investigation, aiming to alleviate adverse effects and overcome resistance [384, 385]. As previously mentioned cisplatin or its analogue carboplatin along with paclitaxel is the first line treatment for ovarian cancer [39].

Paclitaxel belongs to the taxane family; it is a natural compound derived from the pacific yew tree *Taxus brevifolia*. It exhibits potent antitumour activity and is extensively used for the treatment of breast, ovarian, pancreatic and lung tumours as well as Kaposi's sarcoma. It is an important agent of chemotherapeutic regimens in combination with other drugs. Paclitaxel is a mitotic agent that binds specifically to polymerised tubulin. It stabilises microtubule formation, inhibiting depolymerisation and cell division and leads to cell cycle arrest and cell death. Paclitaxel is associated with the common side effects of cytotoxic agents such as hair loss, sickness, diarrhoea and limb numbness [386-388].

1.6.2 Targeted agent – Trastuzumab

Trastuzumab is a humanised monoclonal antibody that binds to the extracellular domain of the HER2 receptor inhibiting the activation of downstream signalling pathways. It is used for the treatment of HER2 positive breast cancer tumours (as described in section 1.1.2.5) [32].

1.6.3 Metabolic targeted agent – Metformin

Metformin is a biguanide used for first-line treatment of type 2 diabetes mellitus. It is the most widely prescribed antidiabetic medication based on its established anti-hyperglycaemic efficacy (reducing hepatic gluconeogenesis) coupled with low toxicity profile and low cost. Metformin reduces insulin resistance and blood glucose levels through inhibition of mitochondrial respiratory chain complex 1 leading to reduced ATP production and subsequent AMPK activation [389, 390].

A considerable amount of epidemiologic meta-analysis studies have associated metformin with a decreased incidence of several malignancies as well as with improved clinical outcome and reduced cancer-related mortality of diabetic cancer patients [390-392]. In

recent years, a large and growing body of literature has revealed potent antitumour activity. Antiproliferative action has been extensively demonstrated in preclinical studies in several types of cancer. Furthermore great attention has been focused in combinatorial studies with other antitumour agents. Evidence has been provided that metformin enhanced the cytotoxic effect of several agents including cisplatin, paclitaxel and doxorubicin [389, 391]. A number of clinical trials have recently been conducted or are currently underway investigating the effect of metformin on various cancer types as monotherapy or combined with chemotherapeutic drugs [389-392]. The antitumour effect of metformin is mainly attributed to AMPK activation and mTOR inhibition along with activation of T cell tumour immune response [389-392].

1.7 Aims & Objectives

The ultimate aim of this project was to explore the role of aerobic glycolysis in two major female malignancies, breast and ovarian cancer. Furthermore this study set out to identify a translatable glycolytic target as well as a legitimate combinatorial strategy for the development of novel metabolic cancer drug therapies.

An overview of the aims and objectives of each results chapter of this thesis is presented below in Table 1.1.

Thesis Chapters	**Overview of Aims & Objectives**
Chapter 3	Assess the growth dependency of breast and ovarian cancer cell line models on glucose and glutamine availability.
	Examine the growth inhibitory effect of several compounds reported to inhibit key enzymes of the glycolytic pathway against panels of breast and ovarian cancer cell lines.
Chapter 4	Investigate the mechanism of action of these agents using Annexin V and cell cycle flow cytometric analysis.
	Examine the effect of each compound on glucose uptake and lactate production.
	Evaluate two major glycolytic targets, GLUT1 and LDHA, using siRNA knockdown.
Chapter 5	Examine the efficacy of novel combinatorial strategies among glycolytic inhibitors and established cytotoxic and targeted therapies.
Chapter 6	Investigate the effect of the oxygen level on sensitivity to glycolysis inhibition.
	Investigate the effect of the oxygen level on the expression of the glycolytic enzymes at both the mRNA and protein level.
Chapter 7	Examine the expression of four selected glycolytic targets (GLUT1, HKII, PKM2 and LDHA) on a clinical tissue microarray set of ovarian cancers using quantitative immunofluorescence technology.
	Correlate the expression of the targets with the histological subtype, the stage of the disease and the survival outcome.

Table 1.1: Overview of the aims and objectives in each results chapter.

To date there hasn't been a detailed comparative study of multiple metabolic inhibitors in these tumour types. To address this, a panel of breast and ovarian cancer cell lines were cultured under varying concentrations of glucose and glutamine with the aim of developing an understanding of the growth dependency of these cancer models on availability of these two major nutrients. Ten commercially available pharmacological tool compounds reported to inhibit five main components of the glycolytic pathway (GLUT1, HKII, PFKFB3, PDH1 and LDHA) were selected. These included both established inhibitors (Phloretin, Quercetin, 3BP, DCA and Oxamic acid) as well as novel agents (STF31, WZB117, IOM-1190, 3PO and NHI-1) (Figure 1.7). The array of glycolytic inhibitors were compared against a panel of four breast and four ovarian cancer cell line models as well as a panel of two pairs of chemosensitive and chemoresistant ovarian cancer cell lines using a cell proliferation assay. The differential effects of the compounds as growth inhibitors on these cell lines were investigated. Comparisons were made between the sensitivity of the two cancer types and a hypothesised association between chemoresistance and resistance to glycolysis inhibition was examined. Correlations between the sensitivity of the cell lines to different inhibitors as well as with the expression of the glycolytic targets and cellular growth rate were explored. A glutaminase inhibitor (BPTES) was employed to examine sensitivity to the glutaminolytic pathway and give a comprehensive view of the metabolic phenotype of breast and ovarian cancer. (Chapter 3)

Secondly, the mechanism of action of the agents targeted against multiple points of the pathway was assessed using Annexin V and cell cycle flow cytometric analysis. Additionally *in vitro* cell-based biochemical glucose uptake and lactate assays were developed to assess the effect of each compound on the glycolytic pathway. Two major targets of interest at the very top and bottom of the glycolytic pathway, GLUT1 and LDHA, were selected for further evaluation using siRNA knockdown. (Chapter 4)

Thirdly, the main aim of this study was to explore interactions between glycolytic inhibitors and established cytotoxic and targeted therapies. Based on previously published data it was hypothesised that glycolytic inhibitors may sensitise cancer cells to established therapies. Novel combinations between cisplatin, paclitaxel or trastuzumab with inhibitors of the glycolytic pathway were investigated and evaluated quantitatively by their combination index values. The antidiabetic drug metformin, an inhibitor of mitochondrial oxidative phosphorylation was employed for a combinatorial strategy aiming for complete ATP depletion and subsequent induction of cell death. The mechanism of action as regards induction of apoptosis and cell cycle arrest of potentially promising combinations was

examined using flow cytometry. The purpose of this work was to identify successful synergistic combinations of glycolytic inhibitors and traditional agents and propose them for further *in vivo* assessment. (Chapter 5)

Fourthly, this study sought to explore the effect of the oxygen level on the expression of the glycolytic enzymes and sensitivity to their inhibition. The effect of the array of glycolytic inhibitors was investigated across a range of oxygenation levels (21%, 7%, 2% and 0.5% O_2), since most experimental studies in the field have only focused on normoxic conditions which are less relevant to the tumour microenvironment. The response to glycolysis inhibition under varying oxygen levels was interpreted through examination of the protein expression of the drug targets in the exact same conditions. The modulation of the relevant glycolytic targets was examined under the selected range of oxygen levels by Western blotting. Additionally the mRNA levels of the enzymes of the glycolytic pathway were analysed in breast cancer cells cultured in hypoxia for different periods of time using gene expression microarray profiling. This study intended to investigate the effect of glycolysis inhibition under varying oxygenation levels and attempt to interpret the results based on the expression of the glycolytic enzymes at both the mRNA and protein level. (Chapter 6)

Fifthly, in the final chapter of this thesis the expression of four selected glycolytic targets (GLUT1, HKII, PKM2 and LDHA) were examined on a clinical tissue microarray of 469 human ovarian cancers using quantitative immunofluorescence technology. The expression of the targets was correlated with the histological subtype, the stage of the disease and the survival outcome. Far too little is known regarding the clinical value of the glycolytic pathway in ovarian cancer and these experiments sought to enhance our current understanding and reveal subtypes of tumours in which glycolysis inhibition might be more beneficial. (Chapter 7)

Overall this study aimed to elucidate further the role of aerobic glycolysis in breast and ovarian cancer and to evaluate the possibilities of therapeutic exploitation of the Warburg effect in these malignancies.

Chapter 2

Chapter 2: Materials & Methods

All laboratory experiments in this study, unless otherwise stated, were carried out in the Division of Pathology Laboratories, Western General Hospital, University of Edinburgh.

2.1 Mammalian Cell Culture

2.1.1 Cell lines

A panel of four breast and four ovarian cancer cell lines were used in the majority of the experiments in this study. MCF7, MDA-MB-231, HBL100 and BT549 are human breast adenocarcinoma cell lines. The **MCF7** cell line was isolated in 1970 from a pleural effusion of a 69-year old Caucasian female with invasive ductal carcinoma. It has a luminal transcription profile and expresses oestrogen and progesterone receptors [393]. **MDA-MB-231** was derived from a pleural effusion of a 51-year old Caucasian woman [394, 395]. It has an invasive basal B phenotype and is a triple negative cell line. **HBL100** was isolated from the milk of a 27-year old Caucasian nursing mother. It has an epithelial basal B morphology and does not express oestrogen or progesterone receptors [396]. **BT549** was established from an invasive ductal tumour of a 72-year old Caucasian woman in 1978. It has basal B epithelial morphology and does not express oestrogen or progesterone receptors [394, 395].

MCF7-HER2 (originally named MCF-7/HER2–18) is a HER2 overexpressing MCF7 cell line. It was a kind gift from the Osborne/Schiff laboratory, Baylor College of Medicine, USA and was available in the laboratory [397]. This cell line was included in the gene expression experiment presented in Chapter 6, section 6.4. **MDA-MB-361** is a human breast adenocarcinoma cell line originating from a metastatic site in the brain of a 40-year old Caucasian woman suffering from breast adenocarcinoma. It has luminal epithelial phenotype and expresses oestrogen and HER2 receptors [394, 395]. This cell line was used for combinatorial studies of glycolytic inhibitors with a monoclonal HER2 antibody (Chapter 5, section 5.2).

OVCAR5, TOV112D, OVCAR3 and CAOV3 are human ovarian adenocarcinoma cell lines with epithelial morphology. **OVCAR5** was isolated in 1982 from the ascitic fluid of a 67-year old Caucasian female with progressive ovarian adenocarcinoma who had not received any cytotoxic treatment. **TOV112D** was established in 1992 from a 42-year old woman of French- Canadian origin with early onset, stage III, endometrioid carcinoma [395]. **OVCAR3** was derived in 1982 from the malignant ascites of a 60-year old Caucasian female with progressive ovarian adenocarcinoma. The patient had already been treated with

chemotherapy [398]. **CAOV3** was established from the primary tumour of a 54-year old Caucasian woman [395].

PEA1-PEA2 and PEO1-PEO4 are two ovarian cancer cell line pairs derived from two patients with ovarian adenocarcinoma at different stages of platinum-based chemotherapy. The first cell line pair was derived from a patient with poorly-differentiated ovarian adenocarcinoma. The **PEA1** cell line was established from a pleural effusion prior to treatment while **PEA2** was established 6 months later from peritoneal ascites of platinum-resistant, relapsed disease. The second cell line pair was derived from malignant peritoneal ascites of a patient with poorly- differentiated serous adenocarcinoma. **PEO1** was derived from relapsed disease 22 months after combined chemotherapy and was shown to be sensitive to platinum-based agents. **PEO4** was established 10 months later from resistant progressive disease. These two paired cell lines, each of them derived from a single patient at different times during treatment; provide an excellent model for studying differences between platinum sensitive and platinum resistant disease (Figure 2.1) [399, 400].

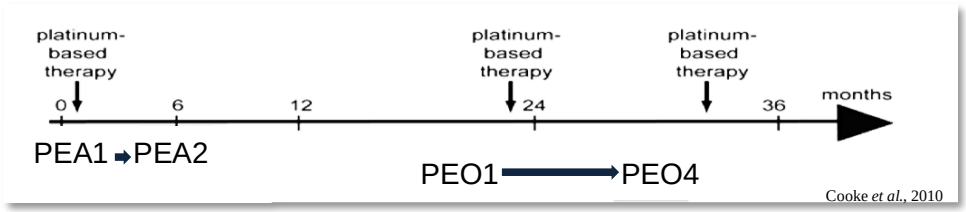

Figure 2.1: Timeline explaining how the ovarian cancer cell line pairs, PEA1-PEA2 and PEO1-PEO4, have been established from two patients with poorly-differentiated ovarian adenocarcinoma at different stages of platinum-based chemotherapy. Figure adapted from Cooke et al., 2010 [400].

All cell lines used in this study were authenticated using Short Tandem Repeat profiling (STR) and had been subjected to mycoplasma testing.

2.1.2 Cell culture conditions

All cell line experimental work was conducted in aseptic sterile conditions in a class II Laminar Air Flow hood at room temperature. Cells were incubated in a humidified atmosphere of 5% CO_2 at 37^{o}C.

The panel of four breast and four ovarian cancer cell lines (MCF7, MDA-MB-231, HBL100, BT549, OVCAR5, TOV112D, OVCAR3 and CAOV3) as well as the MCF7-HER2 and the MDA-MB-361 cell lines were all maintained in Dulbecco's Modified Eagle Medium without HEPES modification (DMEM, 31885/ Thermo Fisher Scientific), containing low glucose (5.56mM), Sodium Pyruvate (1mM) and L-glutamine (3.97mM). The two ovarian cancer cell line pairs (PEA1-PEA2, PEO1-PEO4) were maintained in Roswell Park Memorial

Institute Medium 1640 (RPMI 1640, 21875/ Thermo Fisher Scientific) containing 11.11mM glucose and 2mM L-glutamine. In both cases the media contained phenol red and were supplemented with 10% heat inactivated fetal bovine serum FBS (Fetal Bovine Serum, South America origin, 10270106/ Thermo Fisher Scientific) and 1% Penicillin-Streptomycin (Penicillin-Streptomycin 10,000 U/mL, 15140122/ Thermo Fisher Scientific). For the MCF7-HER2 cell line, the medium was supplemented with 800μg/mL of Geneticin (G418 Geneticin, 10131035/ Thermo Fisher Scientific).

In the deprivation experiments presented in Chapter 3 section 3.1 where the effect of glucose and glutamine availability on cell growth of different cell lines was examined; medium without glucose or glutamine was used (DMEM, A14430/ Thermo Fisher Scientific). Phenol red free media were supplemented with 10% heat inactivated dialysed fetal bovine serum (26400036/ Thermo Fisher Scientific) and 1% Penicillin-Streptomycin. In the glucose and glutamine depleted medium the desired concentration of nutrients, D-Glucose (G8270/ Sigma Aldrich) and L-Glutamine (G7513/ Sigma Aldrich) was added, respectively. For the glucose treatments a standard 4mM glutamine concentration was added while for glutamine treatments a constant 5.56mM glucose concentration was used. These concentrations were selected to be consistent with the content of DMEM medium used for the rest of the experiments.

2.1.3 Routine cell culture

Cells were routinely maintained in T175cm^3 tissue culture flasks and were sub-cultured at least once a week, when reaching 70-80% confluence as described below. Medium was discarded and cells were washed with preheated phosphate buffered saline (PBS tablets Dulbecco A, BR0014G/ Oxoid™). Cells were then incubated for a few minutes with a trypsin/EDTA solution (Trypsin-EDTA 0.05%, 25300062/ Thermo Fisher Scientific) at 37^{o}C to cause cell detachment. The enzyme was neutralised by addition of serum-containing medium and cell suspension was centrifuged at 1,200rpm for 5min. Pelleted cells were resuspended in fresh media and passaged into new flasks at a ratio of 1:10. When setting up an experiment cells were counted using a Neubauer hemocytometer and were seeded in cell culture plates or dishes at the desired dilution.

2.1.4 Hypoxic cell culture

Hypoxia experiments presented in Chapter 6, were conducted at 37^{o}C with 5% CO_2 using the H35 Hypoxystation (Don Whitley Scientific, Shipley, UK). The oxygen level was set at 7, 2 or 0.5%. Prior to hypoxic cell culture all reagents (e.g. media, PBS) were allowed to fully

adapt to each oxygen level for at least 6h. Cells were preadapted to the oxygen level for different periods of time depending on the specific requirements of each experiment.

2.1.5 Cell cryopreservation in liquid nitrogen and recovery

For long term storage cells were preserved in liquid nitrogen tanks at -196^{o}C. To prepare cells for cryopreservation they were detached and pelleted as described above (section 2.1.3). Then the pellet was resuspended in a solution containing 10% Dimethylsulphoxide (DMSO) in serum. The suspension was aliquoted in cryovials that were kept in a -70^{o}C freezer overnight before being transferred to the liquid nitrogen tank (Institute of Genetics and Molecular Medicine, University of Edinburgh).

To recover cells from liquid nitrogen, cryovials were defrosted rapidly and their content was transferred into preheated medium. Cell suspension was centrifuged at 1,200rpm for 5min to remove DMSO. Finally, cell pellet was resuspended into fresh medium and transferred into flasks for culture. Cells were only used for experiments two weeks after recovery from liquid nitrogen.

2.1.6 Pharmacological tool compounds

The pharmacological tool compounds used in the present study are listed in the table below (Table 2.1). The solvent used to prepare stock solutions as well as the supplier company and the catalogue number of each of the compounds is indicated.

Compounds	**Solvent**	**Catalogue No/Supplier company**
Phloretin	DMSO	P7912/ Sigma Aldrich
Quercetin	DMSO	Q4951/ Sigma Aldrich
STF31	DMSO	4484/ Tocris Bioscience
WZB117	Ethanol	400036/ Merck Millipore
IOM-1190	DMSO	provided by IOmet Pharma
3-bromopyruvate	PBS	16490/ Sigma Aldrich
3PO	DMSO	525330/ Merck Millipore
Dichloroacetate	PBS	347795/ Sigma Aldrich
Oxamic acid	PBS	O2751/ Sigma Aldrich
NHI-1	DMSO	provided by IOmet Pharma
BPTES	DMSO	SML0601/ Sigma Aldrich
Metformin	PBS	2864/ Tocris Bioscience

Table 2.1: Pharmacological tool compounds used in the present study. The solvent as well as the supplier company and the catalogue number of each of the compounds are indicated.

Cisplatin (Teva UK Limited), Paclitaxel (Actavis) and Trastuzumab (Roche Pharmaceuticals) were kindly provided from Western General Hospital Pharmacy, Edinburgh.

2.2 Sulphorhodamine B assay (SRB)

The SRB assay is a colorimetric cell density assay based on the quantification of cellular protein content [401]. It was used in this study to examine the efficacy of glycolytic inhibitors as growth inhibitors and to measure compound-induced cytotoxicity.

Cells were seeded in flat-bottom 96-well plates at the appropriate density based on the proliferation rate of each cell line and the duration of the treatment. After a 48h incubation cells were treated with or without the relevant treatment as indicated (final volume 200µl). A series of 10 dilutions with 1:2 steps of each inhibitor in six replicates was applied. Once the treatment period was completed cell monolayers were fixed on the day of treatment (Day 0 control) and on selected time points thereafter with cold 25% trichloroacetic acid (TCA, Sigma Aldrich - 50µl per well). After a 60min incubation at 4^{o}C TCA was discarded and plates were thoroughly washed under running tap water to remove any residuals and left to dry. Then cell monolayers were stained with 0.4% SRB dye solution (Sigma Aldrich - 50µl per well) and after 30min at room temperature unbound excess dye was removed by 1% glacial acetic acid (VWR International) washes. Once plates dried, the protein bound stain was solubilised in 10mM Tris buffer solution pH 10.5 (Sigma Aldrich - 150µl per well). Finally after 60min at room temperature absorbance was measured at 540nm with a spectrophotometer microplate reader (BP800, Biohit Health Care).

Analysis: Measurements were corrected for background absorbance and values are presented as percentage of absorbance of untreated control. The half maximal inhibitory concentration (IC_{50}), indicating the concentration needed to reduce cell viability by half, was used as a quantitative indication of the effectiveness of each compound as a cancer cell growth inhibitor. IC_{50} values were generated through sigmoidal concentration response curves fitted using the XL fit tool within Microsoft Excel.

2.2.1 Combinatorial treatments

In Chapter 5 glycolytic inhibitors were assessed in interaction studies with traditional drugs. For these treatments a range of different concentrations of a glycolytic inhibitor were combined with a constant fixed concentration, around the IC_{20} or less, of the other drug. Both drugs were delivered at the same time. Concentration response curves of each examined combination along with curves of the two compounds as single agents were analysed using

the Calcusyn Software. To quantitatively evaluate the effectiveness of each combination index values were generated for each combination point indicating synergism, additivity or antagonism. Indication of the CI values is presented in Table 2.2 [402].

CI value	Indication
<0.1	very strong synergism
0.1 – 0.3	strong synergism
0.3 – 0.7	synergism
0.7 – 0.85	moderate synergism
0.85 – 0.9	slight synergism
0.9 – 1.1	nearly additive
1.1 – 1.2	slight antagonism
1.2 – 1.45	moderate antagonism
1.45 – 3.3	antagonism
3.3 – 10	strong antagonism
>10	very strong antagonism

Table 2.2: Indication of combination index values generated through Calcusyn Software. Figure adapted from Ian A. Cree, *Cancer Cell Culture*, 2011 [402].

2.3 Glucose uptake assay

The effect of glycolytic inhibitors on glucose uptake was examined using the Amplex Red Glucose/Glucose Oxidase Assay Kit (A22189/ Thermo Fisher Scientific). MCF7 and HBL100 breast cancer cells were seeded in 12-well plates at a density of $2x10^5$ cells per well. After a 24h incubation cells were treated or not with a glycolytic inhibitor as indicated. A range of three different concentrations of each of the inhibitors was used; selected by taking into consideration the corresponding IC_{50} concentration determined from the SRB assays (Chapter 3). Culture media was collected after a 24h treatment and the concentration of glucose was determined using the kit based on the following principle.

The Amplex Red Glucose/Glucose Oxidase Assay Kit provides a sensitive colorimetric method for detecting glucose through two coupled enzymatic reactions depicted in Figure 2.2. Glucose oxidase reacts with D-glucose and generates D-gluconolactone and H_2O_2. The H_2O_2 produced then reacts stoichiometrically with the Amplex Red reagent; reaction catalysed by Horseradish Peroxidase (HRP), and forms the fluorescent product resorufin. This oxidation product can be detected either fluorometrically or spectrophotometrically [403].

The concentration of glucose in the culture media was measured using the kit according to the manufacturer's instructions. A 96-well plate format with triplicates was applied. Samples were diluted 1:50 with the provided reaction buffer (50mM sodium phosphate buffer pH 7.4) in a final volume of 50µl and were incubated with 50µl of the glucose reagent solution. This was prepared in reaction buffer containing 100µM Amplex Red reagent, 0.2 U/ml HRP and 2U/ml glucose oxidase. Reactions were incubated for 30min at room temperature, protected from light. Finally absorbance was measured at 540nm with a spectrophotometer microplate reader. The glucose standard curve generated through the assay is presented in Figure 2.3.

Analysis: Measurements were corrected for background absorbance subtracting the value of the no-glucose control. Data are presented as mean optical density of 3 replicates. To evaluate the statistical significance of differences between treated samples and untreated controls one-way ANOVA and the Tukey-Kramer multiple comparisons test were used.

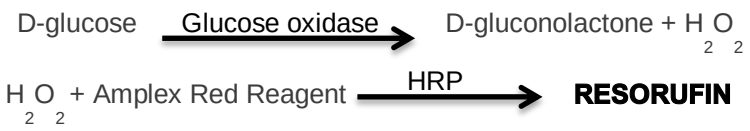

Figure 2.2: Principle of coupled enzymatic reactions used for the detection of glucose [403].

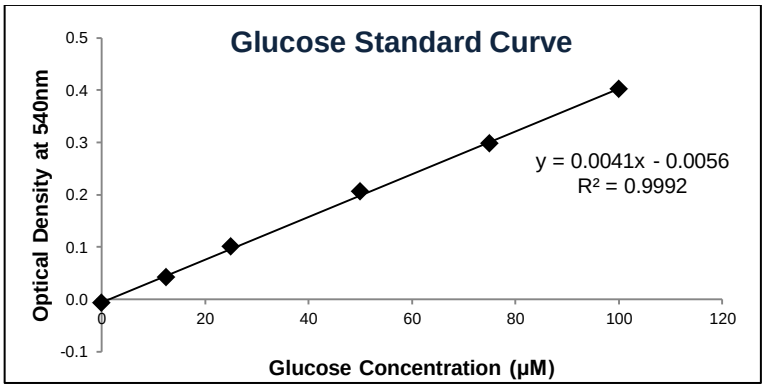

Figure 2.3: Glucose standard curve generated through the Amplex Red Glucose/Glucose Oxidase Assay for glucose concentrations of 0 to 100µM.

2.4 Lactate assay

The effect of glycolytic inhibitors on lactate production was examined using the Lactate Assay Kit (735-10/ Trinity Biotech). Lactate concentration was measured in the same samples used for the glucose assay; culture media collected after a 24h treatment with the glycolytic inhibitors as described above. The concentration of lactate was determined using the kit based on the following principle.

The Lactate Assay Kit provides a sensitive colorimetric method for detecting lactate through two coupled enzymatic reactions depicted in Figure 2.4. Lactate oxidase reacts with L-lactic acid and generates pyruvate and H_2O_2. The produced H_2O_2 then reacts stoichiometrically with chromogen precursors; reaction catalysed by Horseradish Peroxidase (HRP), and forms a coloured dye. This oxidation product can be detected spectrophotometrically [404].

The amount of lactate in the culture media was measured using the kit according to the manufacturer's instructions. A 96-well plate format with triplicates was applied. 2µl of sample were incubated with 200µl of the lactate reagent solution. This was reconstituted by the addition of 20ml dH_2O to the solid reagent provided. Reactions were incubated for 7min at room temperature, protected from light. Finally absorbance was measured at 540nm with a spectrophotometer microplate reader. The lactate standard curve generated through the assay is presented in Figure 2.5.

Analysis: Measurements were corrected for background absorbance subtracting the value of a no-lactate control. Data are presented as mean optical density of 3 replicates. To evaluate the statistical significance of differences between treated samples and untreated controls one-way ANOVA and the Tukey-Kramer multiple comparisons test were used.

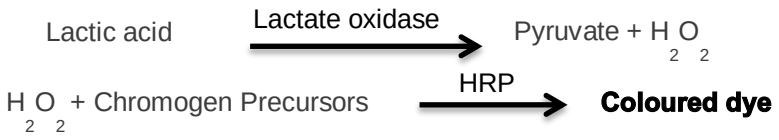

Figure 2.4: Principle of coupled enzymatic reactions used for the detection of lactate [404].

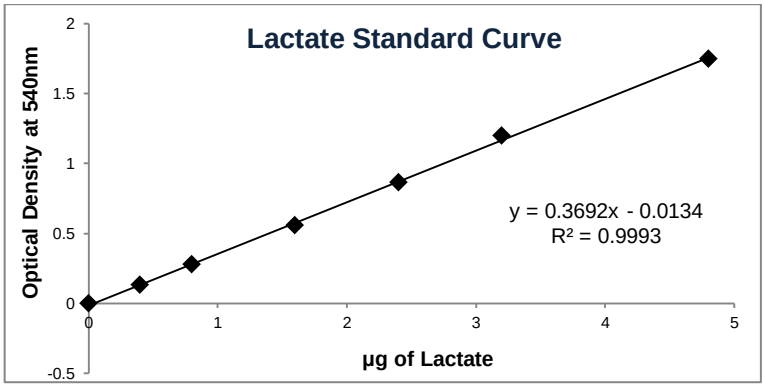

Figure 2.5: Lactate standard curve generated through the Lactate Assay for lactate levels of 0 to 4.8µg.

2.5 Annexin V apoptosis assay

To quantitatively determine the percentage of cells undergoing apoptosis following treatment with glycolytic inhibitors; dual staining with annexin V, conjugated with the fluorochrome FITC, and propidium iodide (PI) was conducted along with flow cytometric analysis. Detection of compound-induced cell death was performed using the FITC Annexin V Apoptosis Detection Kit I (556547/ BD Pharmingen). The kit was used according to the manufacturer's instructions [405].

MCF7 or MDA-MB-231 (for combinatorial treatments in Chapter 5, section 5.4) breast cancer cells were seeded in 6-well plates at a density of $3x10^5$ cells per well. After a 24h incubation cells were treated with or without a glycolytic inhibitor as indicated. Culture media was collected after a 24 or 48h treatment and cells were washed twice with ice-cold PBS. Culture media along with PBS used for washes were all collected in a universal 30ml tube labelled for each sample to ensure collection of floating apoptotic cells. Adherent cells were then incubated for a few minutes with an Accutase solution (A6964/ Sigma Aldrich) at 37^oC to cause cell detachment. The Accutase enzymes were neutralised by addition of serum-containing medium and the suspension of all cells collected was centrifuged at 1,200rpm for 5min. Pelleted cells were resuspended in the provided binding buffer (diluted in dH_2O - 600µl). 100µl of the solution was transferred in a microcentrifuge tube and 10µl FITC annexin V along with 10µl PI was added. Samples were gently vortexed and incubated for 15min at room temperature, protected from light before 400µl binding buffer was added in each tube. Finally measurements of PI and FITC-conjugated annexin V fluorescence of 30,000 events for each sample were taken using the BD Accuri C6 (BD Biosciences) flow cytometer (Institute of Genetics and Molecular Medicine, University of Edinburgh) within 1h after staining.

Analysis: Analysis of measurements was performed using the BD Accuri C6 flow cytometer. Annexin V versus PI (FL1 versus FL2) two-dimensional scatter plots of single cell gated populations were generated. Controls of unstained and single stained cells with either FITC-annexin or PI were used to determine the required compensation of the cytometer and the proper position of the quadrant markers. Annexin V and PI negative cells were identified as live intact cells. Double positive cells were identified as end stage apoptotic cells. Annexin V single positive cells were considered early apoptotic while PI single positive cells as necrotic. The proportion of cells in each subpopulation was determined.

FACs analysis was conducted with the assistance of Elisabeth Freyer, Institute of Genetics and Molecular Medicine, Western General Hospital, University of Edinburgh.

2.6 Cell cycle flow cytometric analysis

To assess whether treatment with glycolytic inhibitors had an impact on cell cycle progression staining with the red fluorescent propidium iodide (PI) was conducted along with flow cytometric analysis. The FxCycle PI/RNase Staining Solution (F10797/ Thermo Fisher Scientific) was used according to the manufacturer's instructions [406]. The percentage of cells in various stages of the cell cycle following treatment with glycolytic inhibitors was determined through measurement of the DNA content.

MCF7 or MDA-MB-231 (for combinatorial treatments in Chapter 5, section 5.5) breast cancer cells were seeded in 6-well plates at a density of $1x10^6$ cells per well. After a 24h incubation cells were treated or not with a glycolytic inhibitor as indicated. Adherent cells were harvested using trypsin/EDTA solution as described in section 2.1.3. Floating apoptotic cells were not used for cell cycle analysis experiments. After centrifugation the supernatant was discarded and the cell pellet was collected in a microcentrifuge tube. Pelleted cells were resuspended in 300μl 50% FBS in PBS. Cells were fixed adding dropwise 700μl ice-cold 70% ethanol in dH_2O while gently vortexing. Fixed samples were stored overnight at 4^oC. The following day samples were centrifuged at 1,200rpm for 10min and the supernatant was discarded gently. To ensure that all fixative was removed cells were washed twice by re-suspension in 1,000μl PBS, centrifugation at 1,200 rpm for 10 minutes, and supernatant discarded. Following washes the cell pellet was resuspended in 500μl of FxCycle PI/RNase Staining Solution. DNase-free Ribonuclease A was included in the staining solution to enable DNA specific binding of PI. Samples were gently vortexed and incubated for 30min at room temperature, protected from light and finally were analysed using the BD LSRFORTESSA (BD Biosciences) flow cytometer (Institute of Genetics and Molecular Medicine, University of Edinburgh).

Analysis: Analysis of measurements was performed using the BD FACSDIVA Software (BD Biosciences). Forward scatter versus side scatter (FS versus SS) two-dimensional scatter plots of single cell populations were gated and PI histograms were generated indicating the DNA content in X-axis against the number of cells in the Y-axis. Cells during G0/G1 phase, prior to DNA synthesis, have one set of paired chromosomes. During S phase cells replicate their DNA and have variable DNA content, increased compared to the diploid chromosomal amount. While during G2/M phase cells have already doubled their DNA content containing two sets of paired chromosomes. The proportion of cells in various stages of the cell cycle was determined.

FACs analysis was conducted with the assistance of Elisabeth Freyer, Institute of Genetics and Molecular Medicine, Western General Hospital, University of Edinburgh.

2.7 Immunoblotting

2.7.1 Protein Extraction

Cells were seeded in cell culture dishes and were incubated until reaching approximately 70-80% confluence. Then dishes were transferred on ice, medium was discarded and cells were washed with ice cold PBS before being lysed in 400µl ice-cold isotonic lysis buffer (50mM Tris pH7.5, 5mM EGTA pH8.5, 150mM NaCl supplemented as presented in Table 2.3). Cells were then scraped and left for 15min for lysis to occur. Subsequently lysates were collected in a microcentrifuge tube and centrifuged at 13,000g for 6min at 4ºC. Pelleted cell debris was discarded and lysate supernatant was collected and stored at -70ºC.

For experiments in Chapter 6, section 6.2 cells were seeded in cell culture dishes and were incubated in the Hypoxystation under the indicated O_2 conditions for the indicated period of time (24, 48 or 72h). Dishes were removed from the Hypoxystation only after cells were washed with ice cold PBS preadapted to the respective oxygen level and then were lysed as previously described.

Component	Quantity in 10ml	Catalogue No/Supplier company
Complete Protease Inhibitor Tablet	1 tablet	11836153001/ Roche
Phosphatase Inhibitor Cocktail 2	100µl	P5726/ Sigma Aldrich
Phosphatase Inhibitor Cocktail 3	100µl	P0044/ Sigma Aldrich
Aprotinin	50µl	A6279/ Sigma Aldrich
Triton-X 100	100µl	X100/ Sigma Aldrich

Table 2.3: Additional contents of isotonic lysis buffer -50mM Tris pH7.5, 5mM EGTA pH8.5, 150mM NaCl.

2.7.2 Bicinchoninic Acid Assay (BCA)

To quantify the protein concentration of the lysates the BCA assay was used. Protein samples were diluted 1:10 in dH_2O in a final volume of 50µl. The BCA reagent was prepared containing 1 volume of copper sulphate (C2284/ Sigma Aldrich) in 50 volumes of BCA solution (B9643/ Sigma Aldrich). 1ml of the reagent was added to each sample and then they were incubated at 60^{o}C for 15 min. Finally, 200µl of each sample was loaded in 96-well plates and absorbance was measured at 540nm with a spectrophotometer microplate reader. A protein standard solution 1mg/ml (P0914/ Sigma Aldrich) was used to generate a standard

curve as presented in Figure 2.6 and through this the protein concentration of samples was determined.

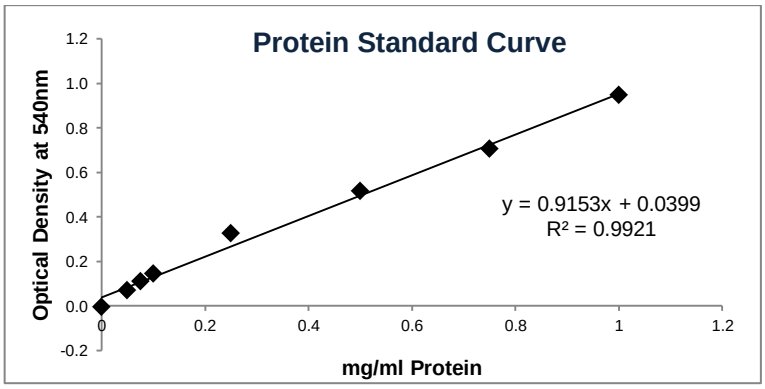

Figure 2.6: Protein standard curve generated through the BCA Assay for protein concentrations of 0 to 1mg/ml.

2.7.3 Western Blotting

Samples were prepared containing 40µg of protein diluted in 4x Laemmli Sample Buffer (1610747/ Bio-Rad Laboratories). Complete lysis buffer was used to equalise the volume of each protein sample. Sodium dodecyl sulphate polyacrylamide gels (SDS-PAGE) were constructed as presented in Table 2.4 using the mini-Protean equipment (Bio-Rad Laboratories). Protein samples were denatured at 90^{o}C for 5 min and loaded onto the polyacrylamide gel along with two markers the Spectra Multicolor High Range Protein Ladder (26625/ Thermo Fisher Scientific) and the Prestained Protein Marker, Broad Range (P7708L/ New England Biolabs). Electrophoresis was conducted in Tris-Glycine, SDS buffer at 80V for 15min and subsequently at 180V for 45-60min depending on the molecular weight of the target protein.

Component	10% Resolving Gel	6% Stacking Gel
30% Acrylamide	6.75	1.8
1M Tris pH 8.85	7.5	-
0.375M Tris pH 6.8	-	5
dH_2O	5.55	8
10% SDS	0.2	0.15
Temed (Tetramethylethylenediamine)	0.05	0.05
10% APS (Ammonium persulfate)	0.05	0.05

Table 2.4: Contents of SDS-PAGE gels, quantities indicated are ml required for 2 gels.

When electrophoresis was completed separated proteins were transferred onto a methanol-activated Immobilon-P polyvinylidene difluoride (PVDF) membrane (Merck Millipore) using the Protean Transfer Cell equipment (Bio-Rad Laboratories). Transfer was conducted at 100V for 90min at 4^{o}C in ice-cold Tris-Glycine transfer buffer. Following transfer the membrane was blocked in 1:1 Odyssey Blocking Buffer (LI-COR Biosciences) / PBS for 60min at room temperature. The membrane was then washed with PBS-0.1% Tween 20 (PBS-T, Sigma Aldrich) three times for 5min each before an overnight incubation in primary antibody solution at 4^{o}C was performed. The antibodies used in the present study along with their host, the dilution factor used as well as the supplier company and the catalogue number are listed in Table 2.5. Odyssey Blocking Buffer/ PBS or 5%w/v bovine serum albumin (BSA, Sigma Aldrich) in PBS-0.1% Tween 20 (for GLUT1 and PDHK1) were used as primary antibody diluent.

Antibody	**Host**	**WB Dilution**	**Catalogue No/Supplier company**
GLUT1	rabbit	1:15,000	07-1401/ Merck Millipore
HKII	rabbit	1:3,000	2867/ Cell Signaling Technology
PFKFB3	rabbit	1:800	13123/ Cell Signaling Technology
PDHK1	rabbit	1:1,500	3820/ Cell Signaling Technology
LDHA	rabbit	1:3,000	3582/ Cell Signaling Technology
LDHB	mouse	1:5,000	ab85319 / Abcam
α tubulin	mouse	1:10,000	ab7291/ Abcam
β actin	rabbit	1:10,000	ab8227/ Abcam

Table 2.5: Primary antibodies used for WB in the present study. Antibodies' host, used dilution as well as the supplier company and the catalogue number are indicated.

The following day the membrane was washed with PBS-T three times for 5min each before secondary fluorescent antibodies raised against the species of the primary antibody were applied (Table 2.6). Secondary antibodies were diluted in Odyssey Blocking Buffer/ PBS supplemented with 0.001% SDS and incubation lasted for 45min at room temperature, protected from light. Three final 5min PBS-T washes were performed and then the membrane was left to dry remaining always in the dark. Finally it was scanned on the Odyssey scanner (LI-COR Biosciences) using two infrared channels at wavelengths of 700nm and 800nm enabling visualisation of two separate targets simultaneously.

Antibody	**Host**	**WB Dilution**	**Catalogue No/Supplier company**
Anti-rabbit IR Dye 800CW	goat	1:10,000	926-32211/ LI-COR Biosciences
Anti-mouse IR Dye 680LT	goat	1:10,000	926-68020/ LI-COR Biosciences

Table 2.6: Secondary antibodies used for WB in the present study. Antibodies' host, used dilution as well as the supplier company and the catalogue number are indicated.

Analysis: Densitometry analysis was conducted using the Odyssey Infrared Imaging System software (LI-COR Biosciences) and target protein's expression was normalised to the respective expression of a loading control (either α tubulin or β actin).

2.8 siRNA Knockdown

Four individual predesigned siRNA oligos and a pool with a mixture of the four sequences targeting two glycolytic enzymes, GLUT1 (/SLC2A1) and LDHA, were acquired from the ON-TARGETplus series of GE Healthcare Dharmacon. Specifications of the siRNA sequences are presented in Table 2.7. The siRNA oligos were resuspended in RNase-free siRNA Buffer (B-002000-UB/ Dharmacon) to generate a 20μM stock which was aliquoted and stored at -70ºC. The standard transfection protocol suggested by the manufacturer was followed.

Target gene	**ON-TARGETplus**	**Targeted Region Target Sequence**	**Catalogue No**
SLC2A1	SMART pool	-	L-007509-02
	Individual	ORF GUAUGUGGGUGAAGUGUCA	J-007509-06
	Individual	ORF AGACAUGGGUCCACCGCUA	J-007509-07
	Individual	ORF CAAAUUUCAUUGUGGGCAU	J-007509-08
	Individual	ORF ACUCAUGACCAUCGCGCUA	J-007509-18
LDHA	SMART pool	-	L-008201-00
	Individual	Non-Coding, ORF GGAGAAAGCCGUCUUAAUU	J-008201-05
	Individual	ORF GGCAAAGACUAUAAUGUAA	J-008201-06
	Individual	Non-Coding, ORF UAAGGGUCUUUACGGAAUA	J-008201-07
	Individual	3'UTR, Non-Coding, ORF AAAGUCUUCUGAUGUCAUA	J-008201-08

Table 2.7: ON-TARGETplus siRNAs used in the present study. The targeted region as well as the catalogue number is indicated. Supplier company: GE Healthcare Dharmacon.

MCF7 and MDA-MB-231 breast cancer cells were seeded in 6-well plates at a density of $3x10^5$ cells per well using DMEM medium as described in section 2.1.2 supplemented with FBS but containing no antibiotics. Cells were incubated for 24h before being transfected. Two separate microcentrifuge tubes were prepared one containing the desired amount from the 20μM siRNA stock solution and the other 4μl of DharmaFECT 1 Transfection Reagent (T-2001/ Dharmacon), both in a final volume of 200μl FBS and antibiotic-free medium. The contents of each tube were mixed gently and incubated for 5min at room temperature. Subsequently, the two tubes were combined in a total volume of 400μl, mixed carefully and incubated for 20min at room temperature. Meanwhile, medium was discarded from cells and after a PBS wash 1ml antibiotic-free medium was added. When the 20min incubation was completed 600μl antibiotic-free medium was added to the transfection mix before this was added to the cells dropwise and while shaking the plate gently. Transfected cells were then incubated for the indicated period of time.

Each experiment included the following; untreated cells, mock cells treated only with transfection reagent (but no siRNA sequence) as well as a negative control- cells transfected with a non-targeting siRNA sequence (D-001810-01/ Dharmacon). Lysates of transfected samples were collected and efficiency of knockdown was assessed at the protein level through Western blotting; comparing the expression of the targeted protein between transfected and mock treated cells.

2.9 Immunofluorescence of clinical ovarian cancer tissues

2.9.1 Tissue Microarrays (TMAs)

The TMAs used in the present study were obtained from the Division of Pathology Laboratories, Western General Hospital, University of Edinburgh. Primary tissue of 469 ovarian carcinomas had been collected from patients treated in the Edinburgh Cancer Centre the period between 1991 and 2006 prior to treatment. Tissues were formalin-fixed and paraffin-embedded and using a microtome sections were cut and cores were mounted onto TMA slides. Three separate TMA replicates containing cores of 469 ovarian tumours had been constructed. The study was approved by the Lothian Research Ethics Committee (08/S1101/41). No informed consent (written or verbal) was obtained for use of retrospective tissue samples from the patients within this study, most of whom were deceased, since this was not deemed necessary by the Ethics Committee. The TMA material was provided by the Edinburgh Experimental Cancer Medicine Centre (ECMC ID: SR319). The cohort characteristics are summarized in Table A3 in the Appendix.

2.9.2 Immunofluorescence

TMA slides were deparaffinised in xylene (twice for 5min each time) and then rehydrated in graded ethanol solutions (99%, 99%, 80% and 50% for 2min each). Following a wash in running tap water, heat-induced antigen retrieval was performed by pressure cooking in sodium citrate buffer at pH6 (18ml 0.1M citric acid, 82ml 0.1M sodium citrate, 900μl dH_2O). Slides were then left to cool and after a 5min wash in 0.05% PBS Tween 20 (PBS-T) were incubated in a 3% hydrogen peroxide solution for 10min to block any endogenous peroxidase activity. Following an additional PBS-T 5min wash non-specific binding was blocked by a 10min incubation in serum-free protein block (X0909/ DAKO). Primary antibodies were diluted in antibody diluent (S0809/ DAKO) and were applied for an overnight incubation at 4ºC (Table 2.8). The selected primary rabbit antibodies had been validated for the used protocol and optimal dilutions had been identified.

Antibody	**Host**	**IF Dilution**	**Catalogue No/Supplier company**
GLUT1	rabbit	1:300	07-1401/ Merck Millipore
HKII	rabbit	1:50	2867/ Cell Signaling Technology
LDHA	rabbit	1:400	3582/ Cell Signaling Technology
PKM2	rabbit	1:100	3198 / Cell Signaling Technology

Table 2.8: Antibodies used for IF in the present study. Antibodies' host, used dilution as well as the supplier company and the catalogue number are indicated.

The following day the tissue sections were washed with PBS-T, three times for 5min each, and then were incubated with the second primary mouse anti-cytokeratin antibody (M3515/ DAKO) diluted 1:25 in the same antibody diluent in order to mask the tumour areas. This incubation was performed at room temperature, lasted 1h and was followed by three additional PBS-T washes. To enable epithelial mask visualisation slides were then incubated with the secondary goat anti-mouse antibody conjugated with Alexa Fluor 555 (A21422/ Thermo Fisher Scientific) diluted 1:25 in the goat anti-rabbit peroxidase-conjugated Envision reagent (K4003/ DAKO). The duration of this incubation was 90min, it was conducted at room temperature protected from light and was followed by three PBS-T washes. Target visualisation was implemented by a 10min incubation with Cyanine 5 (Cy5) Tyramide, diluted at 1:50 in amplification diluent (SAT705A001KT/ PerkinElmer), at room temperature protected from light. Subsequently, tissue sections were washed three times with PBS-T as previously and dehydrated in 80% ethanol for 1min. Finally, slides were counterstained with 45μl Prolong Gold Antifade Mountant with DAPI (4', 6-diamidino-2-

phenylindole) (P-36931/ Thermo Fisher Scientific) to visualise the nuclei and a coverslip was mounted.

2.9.3 AQUA Image Analysis

The expression of glycolytic targets in clinical ovarian tumours was quantitatively evaluated by Automated Quantitative Analysis (AQUA). High resolution monochromatic images of each TMA core were captured at 20x objective using an Olympus AX-51 epifluorescence microscope and were analysed by the AQUAnalysis software. DAPI, Cy-3 and Cy-5 filters were applied to visualise the nuclei, the cytokeratin tumour mask and the target protein respectively. The Cy-5 fluorescent signal intensity of the target antigen was quantified in each image pixel. A quantitative score was attributed in each histospot based on the average Cy5 signal in the cytoplasmic compartment within the epithelial tumour mask, as this was identified from the cytokeratin Cy3 stain. Damaged cores or cores containing imaging errors as well as those consisting of less than 5% epithelium were excluded from further analysis.

Analysis: Target expression in the cytoplasmic compartment of each core was quantified and assigned an AQUA score. Data were filtered and only samples that had at least two replicate values were considered. Expression values were averaged from either two or three replicates. The expression of examined glycolytic targets was compared across the different pathological stages and histological types of ovarian tumours using one-way ANOVA and statistical significance was determined by the Tukey's multiple comparisons test. Furthermore, the expression of the glycolytic enzymes was correlated with expression of several proliferation, apoptosis and signalling markers described previously for the same cohort. Spearman nonparametric correlation and network analysis were conducted using TMA Navigator. Correlation heatmaps were generated using the same server (http://www.tmanavigator.org/). Expression data of different markers had been log2 transformed, mean-centred and quantile-normalised to compensate for differences in the staining. Association of glycolytic targets expression with clinical outcome was assessed using Kaplan-Meier analysis. The X-Tile tool was used to define optimised cut-off values. Miller–Siegmund P-value correction was applied and the Log-Rank survival analysis test was performed to determine statistical significance.

Data analysis was conducted with the assistance of Dr Arran Turnbull, Edinburgh Breast Cancer Now Research Team, Division of Pathology Laboratories, Western General Hospital, University of Edinburgh.

2.10 Gene Expression Analysis

Gene expression experiment was conducted in collaboration with James Meehan and Ed Jarman.

2.10.1 Sample collection

Gene expression analysis was performed using MCF7, MCF7-HER2, MDA-MB-231 and HBL100 breast cancer cell lines. Gene expression changes were examined under four different conditions: normoxic cells cultured at 21% O_2, acute hypoxic cells cultured at 0.5% O_2 for 24h, chronic hypoxic cells cultured at 0.5% O_2 for 10 weeks and cells treated with 400µM $CoCl_2$ (Cobalt Chloride) for 24h to chemically mimic hypoxia.

Breast cancer cells were seeded in cell culture dishes and incubated accordingly in the conditions mentioned above. Cells were then trypsinised as described in section 2.1.3 and the cell suspension was centrifuged at 1,200rpm for 5min. $3x10^6$ pelleted cells were collected in microcentrifuge tubes and kept at -70^{o}C. Samples were prepared in 3 biological replicates.

2.10.2 RNA Extraction

Total RNA was extracted and purified using the miRNeasy Mini Kit (217004/ Qiagen) according to the manufacturer's instructions [407]. 1ml of QIAzol lysis reagent (phenol and guanidine thiocyanate solution included in the kit) along with one steel ball was added in each sample tube. Cells were homogenised in the lysis reagent using the TissueLyser (Qiagen) for 5min at 50Hz at room temperature. Subsequently, 240µl of Chloroform was added and following a centrifugation for 15 min at 13000rpm at 4°C the homogenates were separated into aqueous and organic phases. 500µl of the upper aqueous phase was carefully extracted and 750µl of 100% ethanol was added to provide a suitable binding environment for RNA molecules. Samples were then applied onto RNeasy Mini columns and after a centrifugation at 13000rpm for 15 sec at room temperature RNA was attached to the membranes and the filtrates were discarded. Columns were washed with 350µl RWT buffer followed by an additional centrifugation and discarding of the flow-through. Contaminating DNA was removed by incubating with 80µl of DNAse mix (1:8 DNAse in RDD buffer, Qiagen) for 15min at room temperature. Further washing steps with 350µl RWT buffer and 500µl RPE buffer (twice) followed by additional centrifugations ensured removal of other contaminants. Finally RNA was eluted in 30µl of RNase-free water. The concentration as well as the quality of the RNA was assessed using the spectrophotometer Nanodrop 2000c (Thermo Fisher Scientific). RNA samples were stored -70°C.

2.10.3 RNA Amplification

The RNA was biotinylated and amplified using the Illumina TotalPrep RNA Amplification Kit (AMIL1791/ Thermo Fisher Scientific) according to the manufacturer's instructions [408]. Samples were prepared containing 500ng RNA in a final volume of 11μl Nuclease-free H_2O and were incubated with 9μL of Reverse Transcription Master Mix, containing the T7 Oligo(dT) Primer, for 2h at 42°C. Through the reactions the first strand cDNA with a T7 promoter sequence was synthesised. From the single stranded cDNA a double stranded dsDNA was then synthesised through incubating with 80μl of Second Strand Master Mix for 2h at 16°C. DNA polymerase and RNase H were included in the master mix to enable simultaneous synthesis of the second strand cDNA and RNA degradation. Subsequently the synthesised cDNA was purified; 250μl of cDNA Binding Buffer were added to each sample and the mixture was filtered through a cDNA Filter Cartridge, 500μl of Wash Buffer was then applied and the cDNA was eluted in 20μl 55°C Nuclease-free H_2O. Once purification was completed 7.5μl of IVT Master Mix was added to each cDNA sample and they were incubated for 14h at 37°C for the synthesis of cRNA. The following day the in vitro transcription was ceased by adding 75μl Nuclease-free H_2O and then the synthesised cRNA was purified. 350μl of cRNA Binding Buffer was added to each cRNA sample followed by 250μl 100% ethanol and then the mixture was filtered through a cRNA Filter Cartridge. Finally 650μl Wash Buffer was applied to each sample and the cRNA was eluted in 200μl 55°C Nuclease-free H_2O. The concentration as well as the quality of the cRNA was assessed using the spectrophotometer Nanodrop 2000c.

2.10.4 Concentration of Nucleic acids

In some cases the concentration of the amplified RNA was not adequate for hybridization and it was necessary to concentrate particular samples by precipitation with NH_4OAc (ammonium acetate). 20μl of 7.5M NH_4OAc along with 550μl 100% ethanol was added to the eluted cRNA sample and the mixture was incubated for 30 min at -20°C. Following a centrifugation for 15min at top speed at 4°C, the pellet was washed with 500μl 70% ice-cold ethanol. Finally an additional centrifugation was performed, residual ethanol was removed and the pelleted RNA was resuspended in 50μl Nuclease-free H_2O.

2.10.5 Northern Blotting

Ten cRNA samples were randomly selected to test biotin incorporation following amplification through northern blotting. Samples were prepared containing 2μl 1M NaOH, 0.25μl 200mM EDTA pH8.2 and 2.75μl cRNA. After being heated at 100°C for 10min samples were blotted carefully onto a Biodyne B nylon membrane (Thermo Fisher

Scientific). The membrane was then rinsed in Saline-Sodium Citrate buffer (Sigma Aldrich) and then incubated in 1:1 Odyssey Blocking Buffer/ PBS supplemented with 1% SDS for 60min at room temperature. Finally the IR Dye 800CW Streptavidin (925-32230/ LI-COR Biosciences) at 1:10,000 dilution was used as a secondary detection reagent and the membrane was scanned on the Odyssey scanner as described in section 2.7.3. All cRNA samples examined were properly biotinylated (Figure 2.7).

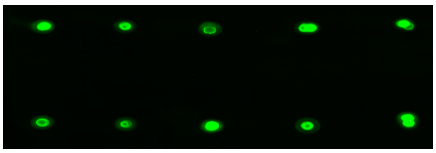

Figure 2.7: Biotin incorporated into the labelled cRNA samples was detected by fluorophore labelled streptavidin through Northern blotting.

2.10.6 Whole-Genome Direct Hybridisation and Data Normalisation

Labelled RNA was hybridised to HumanHT-12 v4 whole-genome expression BeadChip (BD-103-0204/ Illumina). Each array on the chip targets 47,000 probes derived from the National Centre for Biotechnology Information Reference Sequence (NCBI) Release 38 (2009). Samples were carefully distributed over 4 chips, each one containing 12 samples. The Direct Hybridisation Assay along with scanning of the hybridised chips on the Illumina iScan System was performed at the Hologic healthcare and diagnostics company (Manchester). Image data were processed with the Illumina GenomeStudio Software and a raw dataset was generated containing a quantitative level of expression intensity for each probe sequence. Data were filtered using the Illumina probe detection P-value and undetected probes were excluded ($P>0.05$ in at least n-3 samples). Probe profiles were log2 transformed and quantile normalised using the lumi Bioconductor package within the statistical software package R. Data were re-annotated to Ensembl gene identifiers mapping the probe sequences to Ensembl genes.

Analysis: Data were subjected to paired and unpaired Rank Products analysis. Hierarchical clustering was performed on mean-centred data using Cluster. Functional gene analysis was performed using the online pathway annotation tool DAVID Bioinformatics Resources 6.7 (https://david.ncifcrf.gov/). Gene Ontology (GO) enrichment analysis was conducted in the Revigo server (http://revigo.irb.hr/). Heatmaps of differentially expressed genes were generated using TM4 microarray software suite's Multiple Experiment Viewer. Log2 fold change expression values calculated between hypoxic and normoxic conditions for each cell line were used and genes were clustered by Euclidean distance. To evaluate the statistical

significance of expression differences of specific genes of interest under different conditions one-way ANOVA and the Dunnett's multiple comparisons test were used.

Data analysis was conducted with the assistance of Dr Arran Turnbull, Edinburgh Breast Cancer Now Research Team, Division of Pathology Laboratories, Western General Hospital, University of Edinburgh.

2.11 Statistical Analysis

Unless otherwise mentioned statistical tests were undertaken using the GraphPad Prism software version 6.0.

Chapter 3

Chapter 3: The effect of metabolic inhibitors on cell proliferation

Glycolysis and glutaminolysis both play a pivotal role in the metabolism of tumours and targeting of these pathways is considered an exploitable promising anticancer strategy [88, 272]. The primary aim of this chapter was to investigate the growth inhibitory effects of several compounds targeting the glycolytic and glutaminolytic pathways in a panel of breast and ovarian cancer cell lines. Initially the growth dependency of these cancer cell line models on the availability of the basic metabolic substrates (glucose and glutamine) was examined.

3.1 The effect of glucose and glutamine availability on cell growth of a panel of four breast and four ovarian cancer cell lines

The aim of these experiments was to develop an understanding of the metabolic profile of breast and ovarian cancer cell lines by investigating their growth dependency on glucose and glutamine availability. The effect of varying concentrations of the main nutrient sources on cancer cell growth was examined. A panel of four breast and four ovarian cancer cell lines was cultured in the presence of variable glucose and glutamine concentrations and cancer cell proliferation was examined by SRB assay after a 5-day incubation period. Growth was compared with controls completely deprived of glucose or glutamine. These experiments were conducted in glucose and glutamine depleted medium. For the glucose treatments a standard 4mM glutamine concentration was applied while for glutamine treatments a constant 5.56mM glucose concentration was used. These concentrations were selected based on the content of the standard medium used for the majority of experiments of this study.

The following graphs illustrate the average optical density value generated through an SRB assay against increasing concentration of glucose or glutamine. A duplicate control for complete glucose or glutamine depletion conditions (the first two columns of each graph) was used to establish a baseline of growth under complete deprivation. The statistical significance of differences with the depleted controls was determined by one-way ANOVA and the Tukey-Kramer multiple comparisons test. Experiments were conducted at least twice and representative results are presented.

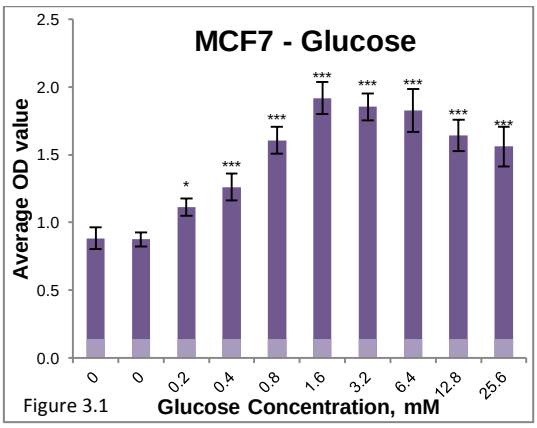

Figure 3.1

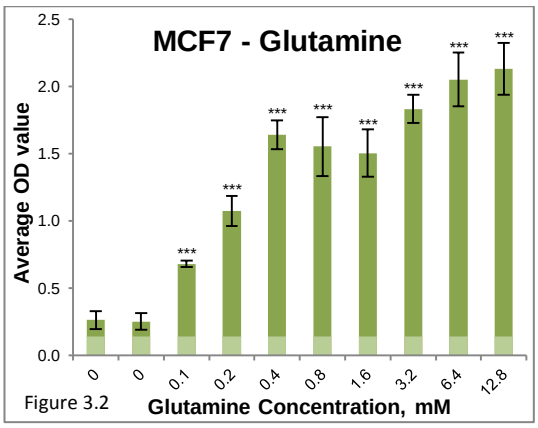

Figure 3.2

Figures 3.1 & 3.2: Optical density values of MCF7 breast cancer cells treated with glucose concentrations between 0-25.6mM and glutamine concentrations between 0-12.8mM for a five day period. Optical density was determined by an SRB assay. Mean results of 6 replicates are reported and error bars represent standard deviations. Faint coloration at the bottom of the columns represents OD value on the day of treatment (Day 0). Statistical significance indications: * P<0.05, *** P<0.001 compared with the average of no glucose/ no glutamine controls (one-way ANOVA followed by Tukey-Kramer multiple comparisons test). Representative data of 3 independent experiments are presented.

Figure 3.1 presents the effect of different glucose concentrations on MCF7 breast cancer cell growth in the presence of a constant 4mM glutamine concentration. MCF7 cells were able to grow in the absence of glucose increasing their cell number six fold compared to the number of cells on day 0. Maximal optimal growth was observed at glucose concentrations of 1.6mM or more. In contrast MCF7 cell growth proved highly dependent on glutamine concentration. Figure 3.2 presents the effect of different glutamine concentrations on MCF7 breast cancer cell growth in the presence of 5.56mM glucose. It can be observed that MCF7 cells were unable to proliferate at zero glutamine concentration. They required a minimum concentration of 0.1mM glutamine to proliferate.

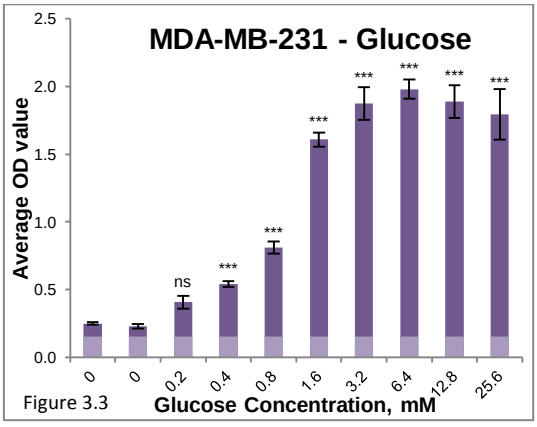

Figure 3.3

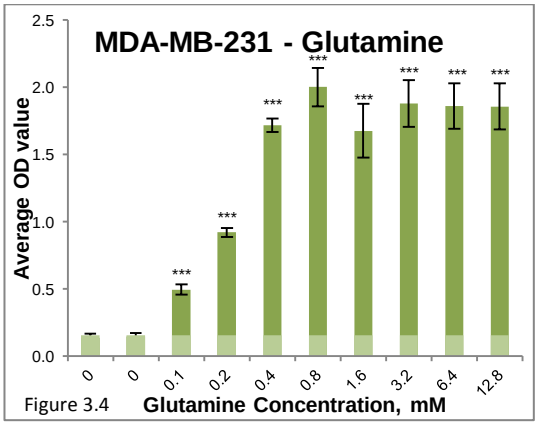

Figure 3.4

Figures 3.3 & 3.4: Optical density of MDA-MB-231 breast cancer cells treated with glucose concentrations between 0-25.6mM and glutamine concentrations between 0-12.8mM for a five day period. Optical density was determined by an SRB assay. Mean results of 6 replicates are reported and error bars represent standard deviations. Faint coloration at the bottom of the columns represents OD value on the day of treatment (Day 0). Statistical significance indications: ns not significant P>0.05, *** P<0.001 compared with the average of no glucose/ no glutamine controls (one-way ANOVA followed by Tukey-Kramer multiple comparisons test). Representative data of 3 independent experiments are presented.

As demonstrated in Figures 3.3 and 3.4 MDA-MB-231 cells were unable to proliferate when deprived of either glucose or glutamine. These cells proved reliant on both nutrients to grow.

A significant increase in cell proliferation was only observed at a concentration of 0.4mM glucose compared to the no-glucose control. In contrast, 0.1mM glutamine was adequate to significantly increase the cell number compared to the no glutamine samples.

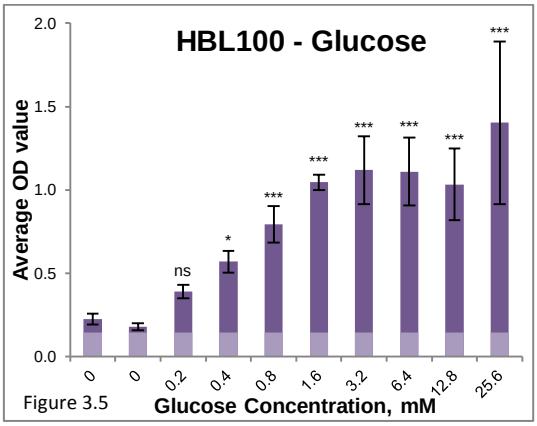

Figure 3.5

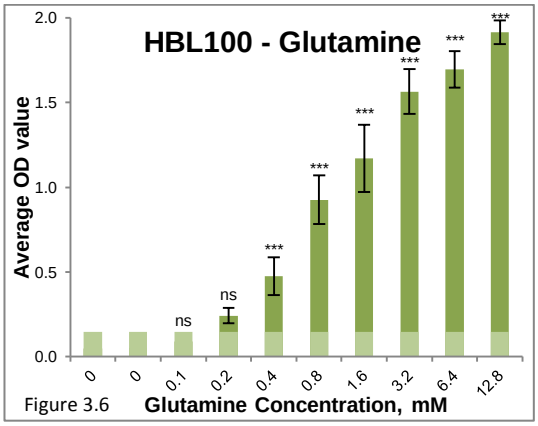

Figure 3.6

Figures 3.5 & 3.6: Optical density of HBL100 breast cancer cells treated with glucose concentrations between 0-25.6mM and glutamine concentrations between 0-12.8mM for a five day period. Optical density was determined by an SRB assay. Mean results of 6 replicates are reported and error bars represent standard deviations. Faint coloration at the bottom of the columns represents OD value on the day of treatment (Day 0). Statistical significance indications: ns not significant P>0.05, * P<0.05, *** P<0.001 compared with the average of no glucose/ no glutamine controls (one-way ANOVA followed by Tukey-Kramer multiple comparisons test). Representative data of 3 independent experiments are presented.

HBL100 cells also demonstrated strong reliance on both glucose and glutamine for cell growth. As can be observed in Figures 3.5 and 3.6, HBL100 cells could not proliferate if lacking glucose or glutamine. A significant induction in cell proliferation was only observed after addition of 0.4mM glucose and 0.4mM glutamine compared to the depleted controls.

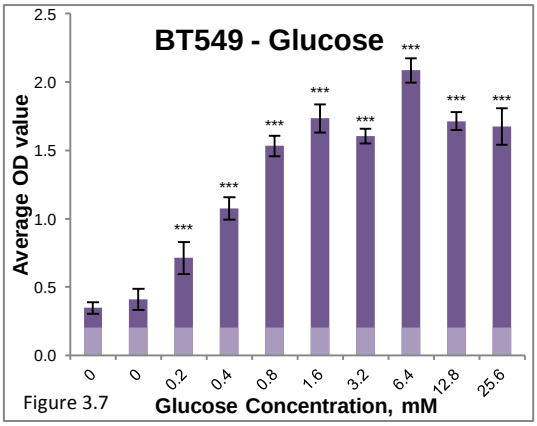

Figure 3.7

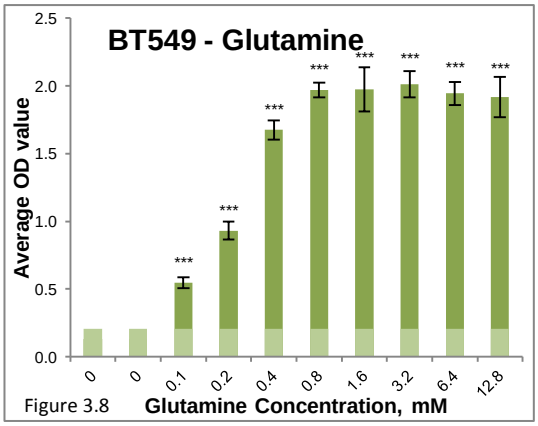

Figure 3.8

Figures 3.7 & 3.8: Optical density of BT549 breast cancer cells treated with glucose concentrations between 0-25.6mM and glutamine concentrations between 0-12.8mM for a five day period. Optical density was determined by an SRB assay. Mean results of 6 replicates are reported and error bars represent standard deviations. Faint coloration at the bottom of the columns represents OD value on the day of treatment (Day 0). Statistical significance indication: *** P<0.001 compared with the average of no glucose/ no glutamine controls (one-way ANOVA followed by Tukey-Kramer multiple comparisons test). Representative data of 3 independent experiments are presented.

Figures 3.7 and 3.8 present the response of BT549 cells to variable concentrations of these nutrients. These cells proved dependent on glutamine availability for growth as they were

found completely unable to proliferate when glutamine was depleted. A glutamine concentration equal to 0.1mM was sufficient to significantly induce growth compared to the zero glutamine control. In contrast, BT549 cells were able to double their cell number even in a completely glucose free environment.

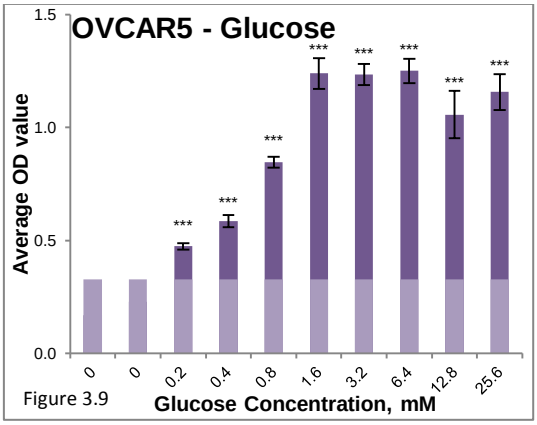

Figure 3.9

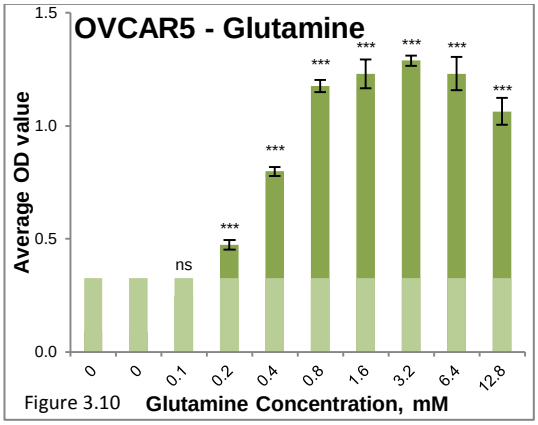

Figure 3.10

Figures 3.9 & 3.10: Optical density of OVCAR5 ovarian cancer cells treated with glucose concentrations between 0-25.6mM and glutamine concentrations between 0-12.8mM for a five day period. Optical density was determined by an SRB assay. Mean results of 6 replicates are reported and error bars represent standard deviations. Faint coloration at the bottom of the columns represents OD value on the day of treatment (Day 0). Statistical significance indications: ns not significant P>0.05, *** P<0.001 compared with the average of no glucose/ no glutamine controls (one-way ANOVA followed by Tukey-Kramer multiple comparisons test). Representative data of 2 independent experiments are presented.

Figures 3.9 and 3.10 show that OVCAR5 cells were not able to proliferate when cultured in a no glucose or no glutamine environment for five days, and were strongly reliant on both substrates for proliferation. 0.2mM of glucose or glutamine was essential for significant growth then higher concentration led to higher growth rate until a plateau was reached with a maximal cell number at a concentration of 1.6mM glucose and 0.8mM glutamine.

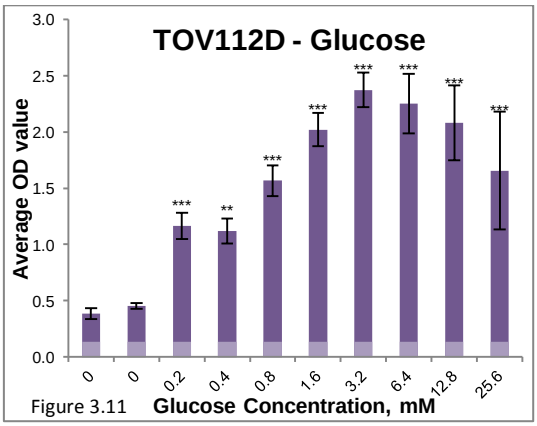

Figure 3.11

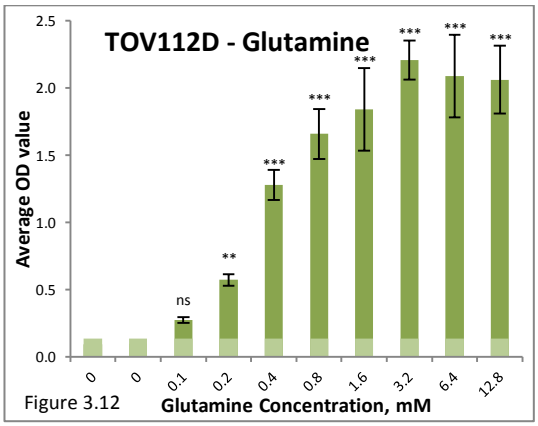

Figure 3.12

Figures 3.11 & 3.12: Optical density of TOV112D ovarian cancer cells treated with glucose concentrations between 0-25.6mM and glutamine concentrations between 0-12.8mM for a five day period. Optical density was determined by an SRB assay. Mean results of 6 replicates are reported and error bars represent standard deviations. Faint coloration at the bottom of the columns represents OD value on the day of treatment (Day 0). Statistical significance indications: ns not significant P>0.05, ** P<0.01, *** P<0.001 compared with the average of no glucose/ no glutamine controls (one-way ANOVA followed by Tukey-Kramer multiple comparisons test). Representative data of 2 independent experiments are presented.

Figures 3.11 and 3.12 depict the response of TOV112D ovarian cancer cells to different glucose and glutamine concentrations. These cells showed a threefold increase in their cell number in the absence of glucose while in contrast no proliferation was observed in glutamine depleted conditions. They demonstrated a minimum glutamine requirement of 0.2mM for statistically significant proliferation.

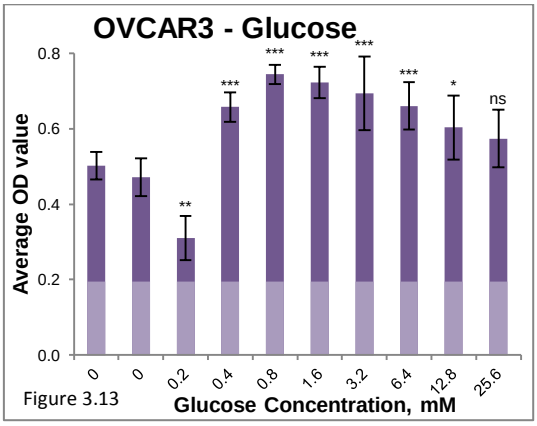

Figure 3.13

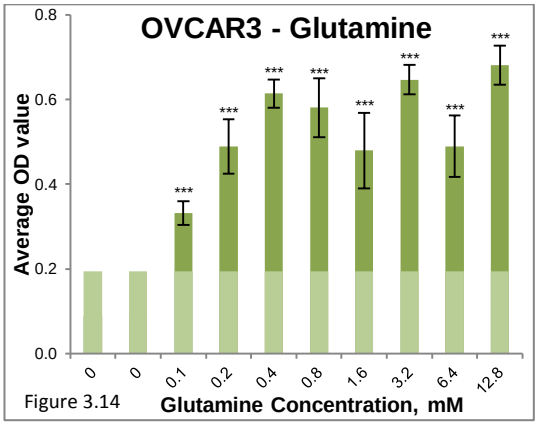

Figure 3.14

Figures 3.13 & 3.14: Optical density of OVCAR3 ovarian cancer cells treated with glucose concentrations between 0-25.6mM and glutamine concentrations between 0-12.8mM for a five day period. Optical density was determined by an SRB assay. Mean results of 6 replicates are reported and error bars represent standard deviations. Faint coloration at the bottom of the columns represents OD value on the day of treatment (Day 0). Statistical significance indications: ns not significant P>0.05, * P<0.05, ** P<0.01, *** P<0.001 compared with the average of no glucose/ no glutamine controls (one-way ANOVA followed by Tukey-Kramer multiple comparisons test). Representative data of 2 independent experiments are presented.

OVCAR3 cells were able to proliferate and increase their cell number up to 2.5 times despite a 5-day glucose depletion as presented in Figure 3.13. An interesting observation is that OVCAR3 cells were found unable to maintain proliferation at 0.2mM glucose and their cell number was significantly reduced while maximal growth was observed at 0.8mM. In contrast Figure 3.14 suggests that they rely strongly on glutamine. OVCAR3 cells could not proliferate in the absence of glutamine. A concentration of 0.1mM glutamine was essential for growth resulting in a statistically significant higher cell number in comparison to the zero glutamine control.

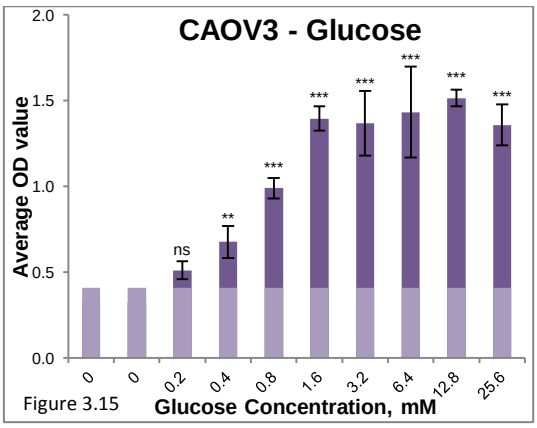

Figure 3.15

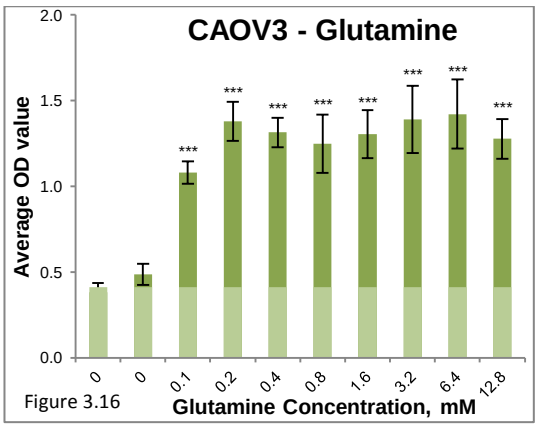

Figure 3.16

Figures 3.15 & 3.16: Optical density of CAOV3 ovarian cancer cells treated with glucose concentrations between 0-25.6mM and glutamine concentrations between 0-12.8mM for a five day period. Optical density was determined by an SRB assay. Mean results of 6 replicates are reported and error bars represent standard deviations. Faint coloration at the bottom of the columns represents OD value on the day of treatment (Day 0). Statistical significance indications: ns not significant P>0.05, ** P<0.01, *** P<0.001 compared with the average of no glucose/ no glutamine controls (one-way ANOVA followed by Tukey-Kramer multiple comparisons test). Representative data of 2 independent experiments are presented.

In Figures 3.15 and 3.16 evidence is provided of a strong reliance on both glucose and glutamine for CAOV3 ovarian cancer cell proliferation. CAOV3 cells were unable to grow when glucose or glutamine were not present in the culture medium. In comparison to the control samples, cells demonstrated significant growth when cultured with a minimum of 0.4mM glucose or 0.1mM glutamine.

Interestingly, marked variation was observed in the growth requirements of these key nutrients among the different breast and ovarian cancer cell lines. The table below demonstrates the minimum glucose and glutamine concentration required by each cell line for significant growth compared to growth on the day of treatment (day 0). It should be noted that statistical significance indications in the above figures refer to growth comparison with the average growth of the no glucose/ no glutamine controls and not the growth on day 0.

Cell Line	Minimum Glucose Concentration required for significant growth	Minimum Glutamine Concentration required for significant growth
MCF7	0mM	0.1mM
MDA-MB-231	0.2mM	0.1mM
HBL100	0.2mM	0.2mM
BT549	0mM	0.1mM
OVCAR5	0.2mM	0.2mM
TOV112D	0mM	0.2mM
OVCAR3	0mM	0.1mM
CAOV3	0.4mM	0.1mM

Table 3.1: Minimum glucose or glutamine concentration required by a panel of breast and ovarian cancer cell lines to achieve significant growth following a five day treatment under a range of glucose and glutamine concentrations respectively. All values are significant at the $P<0.001$ level.

3.2 The effect of glycolytic inhibitors on cell growth of a panel of four breast and four ovarian cancer cell lines

An array of glycolytic inhibitors, targeted against multiple points of the glycolytic pathway, were selected and compared against a panel of four breast and four ovarian cancer cell lines. Cancer cell proliferation was examined by the SRB assay after a 5-day treatment period. Experiments were conducted at least twice and representative results are presented.

3.2.1 Targeting Glucose Transport

GLUT1 is a member of the SLC transporter family that enables glucose to enter the cells. It is abundantly expressed in most human tissues and found overexpressed in many cancers [171, 173-177]. Several compounds reported to inhibit glucose transmembrane transport were compared in this study.

3.2.1.1 Phloretin & Quercetin

Phloretin and Quercetin are flavonoids described to inhibit glucose transmembrane transport [277]. Figures 3.17 and 3.18 present the concentration response curves of these compounds for a panel of four breast cancer cell lines generated through an SRB assay. They depict the percentage of cell number remaining after a 5-day treatment with increasing concentrations of the compounds.

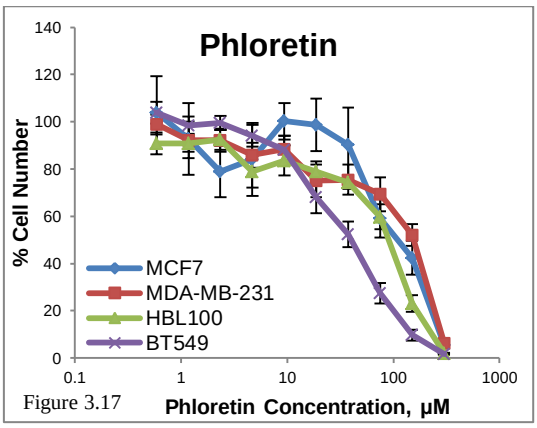

Figure 3.17

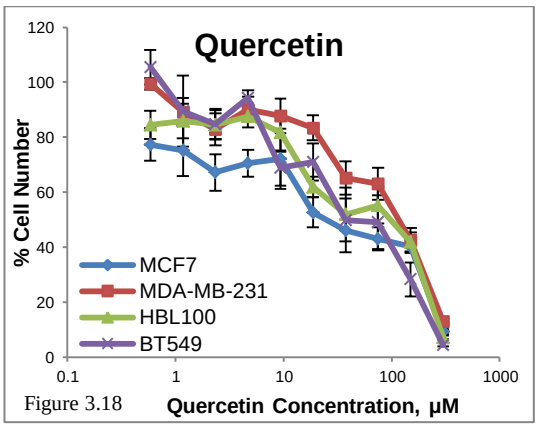

Figure 3.18

Figures 3.17 & 3.18: Concentration response curves of breast cancer cells treated with Phloretin (3.17) and Quercetin (3.18) concentrations between 0.6-300µM for a five day period. Cell viability was determined by an SRB assay. Mean results of 6 replicates are reported and error bars represent standard deviations. Values are shown as a percentage of control. A constant 0.3% DMSO concentration was used across the whole curve in both cases. Representative data of 5 independent experiments are presented.

Both compounds inhibited the cell proliferation of all four breast cancer cell lines in a concentration dependent manner. The IC_{50} values ranged from 36 to 135µM for Phloretin and from 44 to 105µM for Quercetin, as shown in Table 3.2. Both compounds shared the same pattern of sensitivity between the different cell lines. BT549 cells were found to be more sensitive to both compounds while MDA-MB-231 cells were less sensitive.

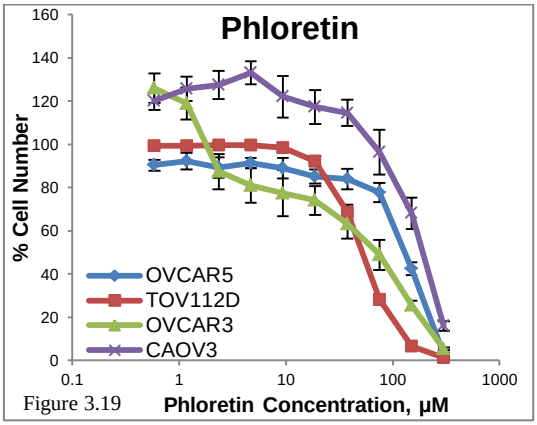

Figure 3.19

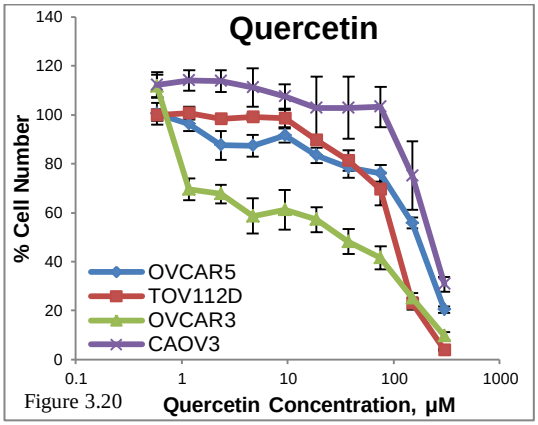

Figure 3.20

Figures 3.19 & 3.20: Concentration response curves of ovarian cancer cells treated with Phloretin (3.19) and Quercetin (3.20) concentrations between 0.6-300µM for a five day period. Cell viability was determined by an SRB assay. Mean results of 6 replicates are reported and error bars represent standard deviations. Values are shown as a percentage of control. A constant 0.3% DMSO concentration was used across the whole curve in both cases. Representative data of 5 independent experiments are presented.

Figures 3.19 and 3.20 present the concentration response curves of Phloretin and Quercetin for a panel of four ovarian cancer cell lines. All four cell lines were sensitive to both compounds and presented IC_{50} values that ranged between 51 and 197µM for Phloretin and 21 to 240µM for Quercetin. TOV112D presented greater sensitivity to Phloretin and OVCAR3 to Quercetin. CAOV3 cells were found to be more resistant to both flavonoids.

3.2.1.2 STF31 & WZB117

STF31 and WZB117 are both recently identified compounds described as specific GLUT1 inhibitors [312, 319].

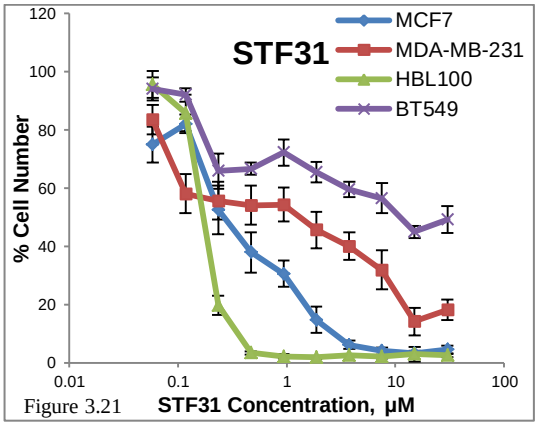

Figure 3.21

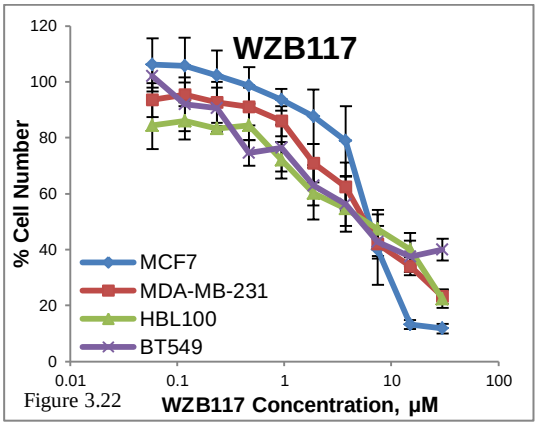

Figure 3.22

Figures 3.21 & 3.22: Concentration response curves of breast cancer cells treated with STF31 (3.21) and WZB117 (3.22) concentrations between 0.06-30µM for a five day period. Cell viability was determined by an SRB assay. Mean results of 6 replicates are reported and error bars represent standard deviations. Values are shown as a percentage of control. A constant 0.3% DMSO concentration was used across the whole STF31 curve and a constant 0.3% Ethanol concentration was used across the whole WZB117 curve. Representative data of 3 independent experiments are presented.

Figures 3.21 and 3.22 present the effect of STF31 and WZB117 on cell proliferation of the breast cancer cell panel. STF31 exhibited an interesting differential effect between the cell lines. Three of them were very sensitive to this compound, presenting IC_{50} values in the range of 173 (HBL100) to 813nM (MDA-MB-231), while BT549 cells were almost resistant to the compound with an IC_{50} value of 18µM. Regarding WZB117 all four breast cancer cell lines presented similar sensitivities with an IC_{50} value of around 6µM.

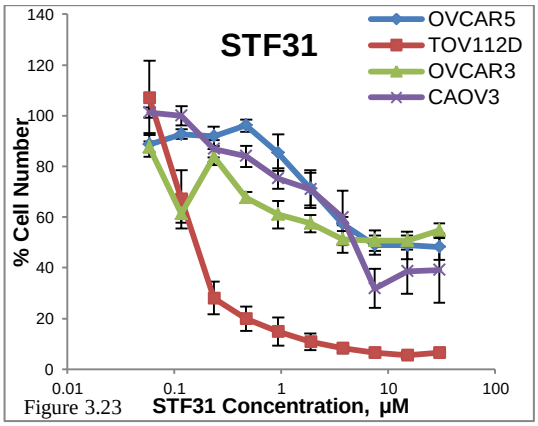

Figure 3.23

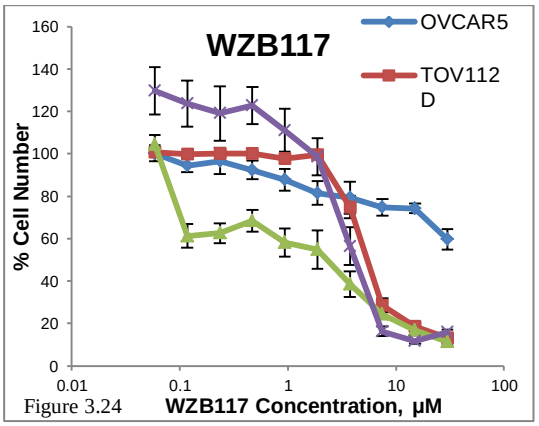

Figure 3.24

Figures 3.23 & 3.24: Concentration response curves of ovarian cancer cells treated with STF31 (3.23) and WZB117 (3.24) concentrations between 0.06-30µM for a five day period. Cell viability was determined by an SRB assay. Mean results of 6 replicates are reported and error bars represent standard deviations. Values are shown as a percentage of control. A constant 0.3% DMSO concentration was used across the whole STF31 curve

and a constant 0.3% Ethanol concentration was used across the whole WZB117 curve. Representative data of 3 independent experiments are presented.

Figures 3.23 and 3.24 depict the effect of STF31 and WZB117 on the selected ovarian cancer cell lines. The four cell lines presented great differences in their response to these compounds. Regarding STF31, TOV112D was very sensitive with an IC_{50} value equal to 154nM while OVCAR3 was completely resistant to the range of the concentrations used. Similar differences were also observed for WZB117. OVCAR3 cells were very sensitive presenting an IC_{50} value of 1.4μM while in contrast OVCAR5 cells proved resistant to this compound. The other two cell lines had similar sensitivity to the examined breast cancer cells.

3.2.2 Targeting Hexokinase

Hexokinase catalyses the first rate-limiting reaction of the glycolytic pathway and phosphorylates glucose to glucose-6-phosphate. 3-Bromopyruvate (3BP) inhibits the mitochondrial bound hexokinase II [325, 326].

- **3-Bromopyruvate**

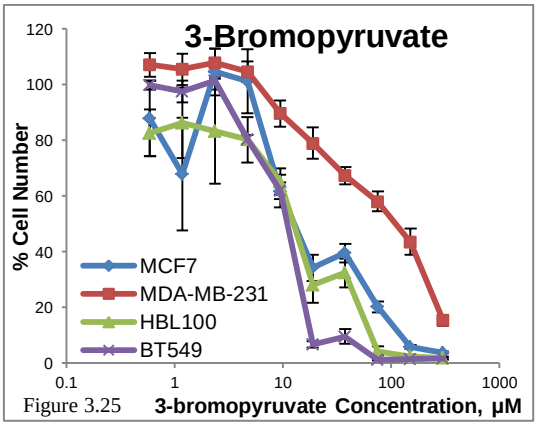

Figure 3.25

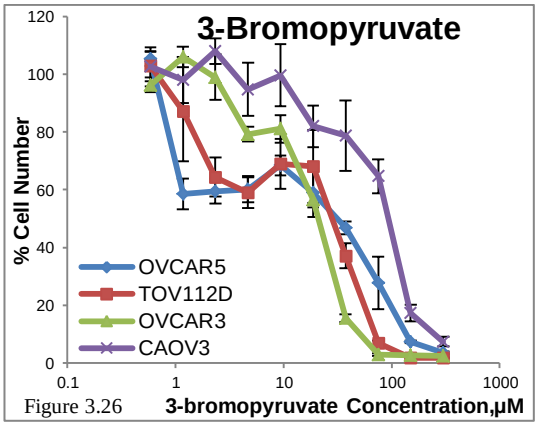

Figure 3.26

Figures 3.25 & 3.26: Concentration response curves of breast (3.25) and ovarian (3.26) cancer cells treated with 3-bromopyruvate concentrations between 0.6-300μM for a five day period. Cell viability was determined by an SRB assay. Mean results of 6 replicates are reported and error bars represent standard deviations. Values are shown as a percentage of control. Representative data of 3 independent experiments are presented.

Figures 3.25 and 3.26 indicate the effects of 3BP on cell viability of the panels of breast and ovarian cancer cell lines respectively. Both groups of cancer cells presented similar sensitivities to this agent. Among breast cancer cell lines, BT549 was more sensitive with an IC_{50} value of 10μM whereas MDA-MB-231 was the least sensitive, having an IC_{50} value equal to 84μM. Between the ovarian cancer cell lines TOV11D was the most sensitive and CAOV3 the least sensitive, with IC_{50} values of 16 and 84 μM respectively.

3.2.3 Targeting Phosphofructokinase

PFK1 catalyses the second rate-limiting reaction of the glycolytic pathway adding a second phosphate group to glucose-6-phosphate. PFKFB3 is a component of Fru-2,6-BP which is an allosteric activator of PFK1. 3PO is a recently identified PFKFB3 inhibitor [343].

- **3PO**

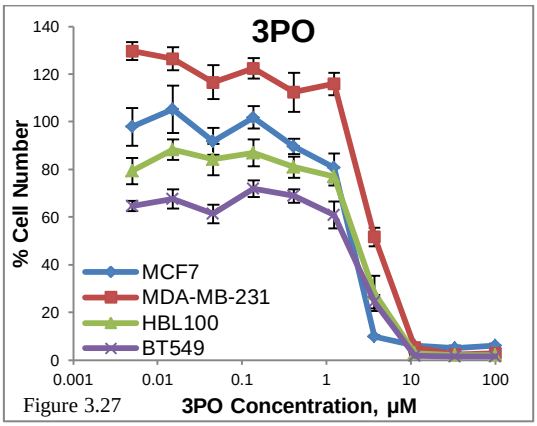

Figure 3.27

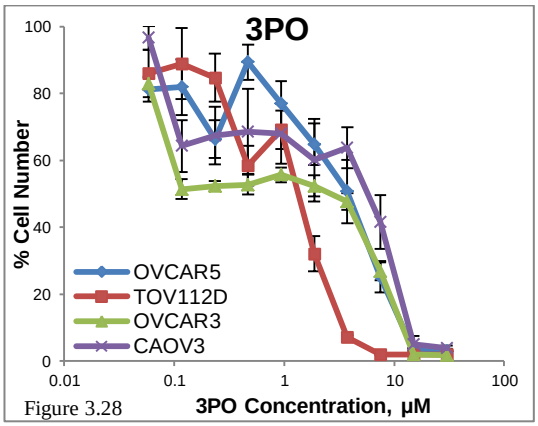

Figure 3.28

Figures 3.27 & 3.28: Concentration response curves of breast (3.27) and ovarian (3.28) cancer cells treated with 3PO concentrations between 0.005-100µM (3.27) and between 0.06-30µM (3.28) for a five day period. Cell viability was determined by an SRB assay. Mean results of 6 replicates are reported and error bars represent standard deviations. Values are shown as a percentage of control. A constant 1% and 0.3% DMSO concentration was used respectively across the curves. Representative data of 2 independent experiments are presented.

Figures 3.27 and 3.28 demonstrate the response of the breast and ovarian cell panel to 3PO treatment. Breast cancer cell lines had a similar response to this compound with an IC_{50} value around 2µM. MDA-MB-231 cells were found slightly more resistant (IC_{50} 4µM). Between the ovarian cancer cell lines TOV112D was the most sensitive with an IC_{50} value as low as 1µM and CAOV3 the most resistant with an IC_{50} value almost six fold higher.

3.2.4 Targeting Pyruvate Dehydrogenase Kinase

PDHK1 phosphorylates and inactivates PDH. Dichloroacetate (DCA) is a well-established PDHK1 inhibitor leading to redirection of ATP synthesis through mitochondrial oxidative phosphorylation [352, 353].

- **Dichloroacetate**

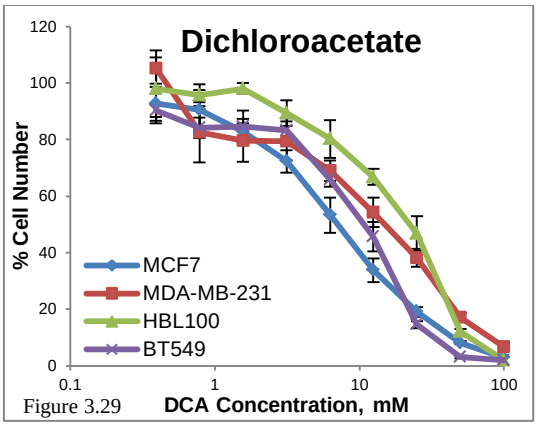

Figure 3.29

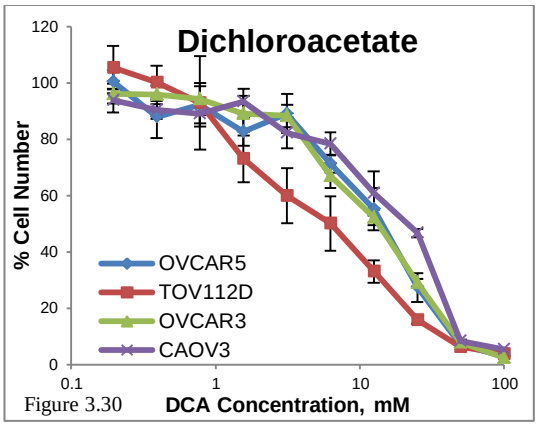

Figure 3.30

Figures 3.29 & 3.30: Concentration response curves of breast (3.29) and ovarian (3.30) cancer cells treated with Dichloroacetate concentrations between 0.4-100mM for a five day period. Cell viability was determined by an SRB assay. Mean results of 6 replicates are reported and error bars represent standard deviations. Values are shown as a percentage of control. Representative data of 5 independent experiments are presented.

DCA was effective in inhibiting breast and ovarian cancer cell proliferation in the millimolar concentration range (Figures 3.29 and 3.30). HBL100 was the most resistant breast cancer cell line (IC_{50} 19mM) and MCF7 the most sensitive one (IC_{50} 7mM). Having similar IC_{50} values CAOV3 and TOV112D were the least and most sensitive ovarian cancer cell lines respectively.

3.2.5 Targeting Lactate Dehydrogenase

LDHA catalyses the final step of the glycolytic pathway converting pyruvate to lactate.

3.2.5.1 Oxamic acid

Oxamic acid is an established LDH inhibitor [368].

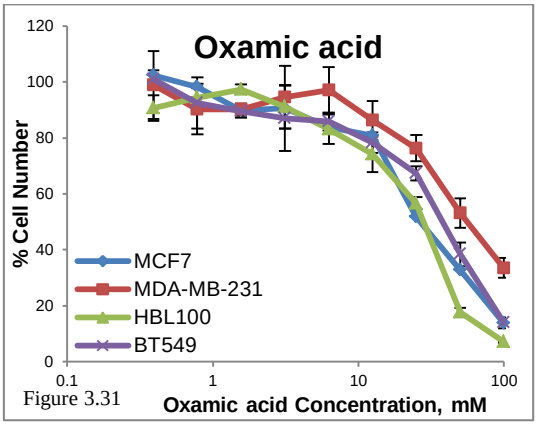

Figure 3.31

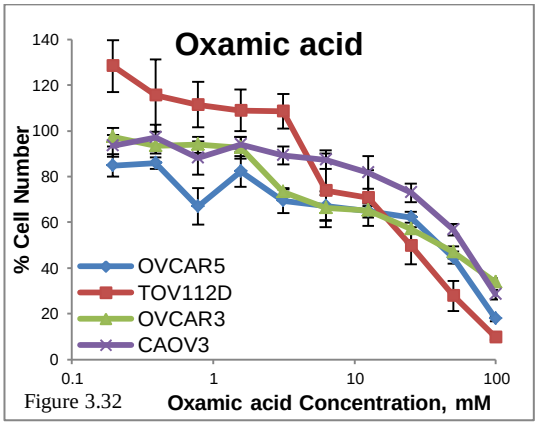

Figure 3.32

Figures 3.31 & 3.32: Concentration response curves of breast (3.31) and ovarian (3.32) cancer cells treated with Oxamic acid concentrations between 0.4-100mM for a five day period. Cell viability was determined by an SRB assay. Mean results of 6 replicates are reported and error bars represent standard deviations. Values are shown as a percentage of control. Representative data of 5 independent experiments are presented.

The above graphs present the effect of Oxamic acid on cell proliferation of the panel of breast and ovarian cancer cells respectively (Figures 3.31&3.32). Oxamic acid attenuated cell proliferation of both panels in the millimolar concentration range. MDA-MD-231 was the most resistant breast cancer cell line with an IC_{50} value of 60mM while MCF7 and HBL100 were the most sensitive cell lines having an IC_{50} value of 30mM. Among the ovarian cancer cell lines CAOV3 was the most resistant and TOV112D the most sensitive. Their IC_{50} values were analogous to the respective breast lines.

3.2.5.2 NHI-1

NHI-1 was described recently by Granchi *et al* as a specific LDHA inhibitor [378].

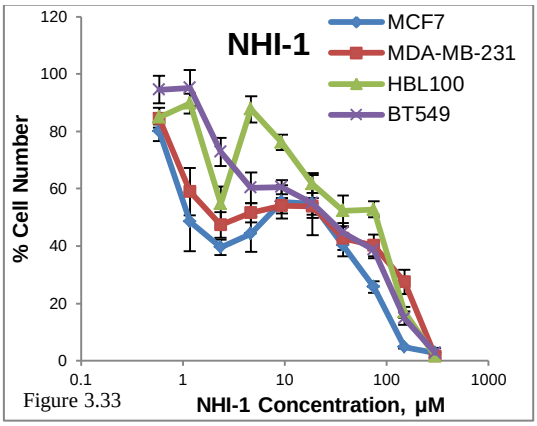

Figure 3.33

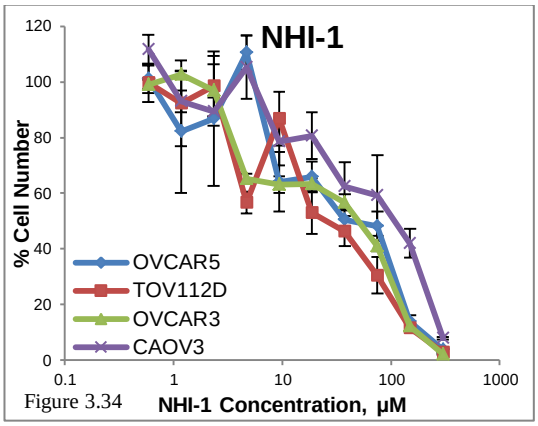

Figure 3.34

Figures 3.33 & 3.34: Concentration response curves of breast (3.33) and ovarian (3.34) cancer cells treated with NHI-1concentrations between 0.6-300µM for a five day period. Cell viability was determined by an SRB assay. Mean results of 6 replicates are reported and error bars represent standard deviations. Values are shown as a percentage of control. A constant 0.3% DMSO concentration was used across the whole curve in both cases. Representative data of 2 independent experiments are presented.

NHI-1 was more effective than Oxamic acid in inhibiting cancer cell proliferation, requiring much lower concentrations (Figures 3.33&3.34). MCF7 was the most sensitive breast cancer cell line to this compound among those examined, presenting an IC_{50} value of 8µM. In contrast, the ovarian CAOV3 was certainly the most resistant of all examined cell lines with an IC_{50} value of 90µM. Among the breast cancer cell lines, HBL100 presented the greatest resistance having an IC_{50} value equal to 53µM.

The IC_{50} concentrations are summarised in Tables 3.2 and 3.3.

IC_{50} values	Targeted Enzyme	MCF-7	MDA-MB-231	HBL100	BT549
Phloretin (µM)	GLUT1	122	135	69	36
Quercetin (µM)	GLUT1	44	105	76	44
STF31 (µM)	GLUT1	0.31	0.81	0.17	18
WZB117 (µM)	GLUT1	6.4	6.3	5.2	6.6
3-bromopyruvate (µM)	HKII	18	84	15	10
3PO (µM)	PFKFB3	2.1	3.8	2.7	2.3
Dichloroacetate (mM)	PDHK1	6.8	13	19	9.1
Oxamic acid (mM)	LDH	28	58	27	39
NHI-1 (µM)	LDHA	8	20	53	22

Table 3.2: Summary of the IC_{50} concentrations generated for four breast cancer cell lines after a five day treatment with 9 glycolytic inhibitors. The targeted glycolytic enzyme is indicated.

IC_{50} values	Targeted Enzyme	OVCAR5	TOV112D	OVCAR3	CAOV3
Phloretin (µM)	GLUT1	119	51	54	197
Quercetin (µM)	GLUT1	154	94	21	240
STF31 (µM)	GLUT1	7.4	0.15	>30	4.9
WZB117 (µM)	GLUT1	>30	5.9	1.4	4.3
3-bromopyruvate (µM)	HKII	20	16	20	84
3PO (µM)	PFKFB3	3.9	1.2	2.8	5.8
Dichloroacetate (mM)	PDHK1	14	5.5	13	20
Oxamic acid (mM)	LDH	38	24	34	59
NHI-1 (µM)	LDHA	45	28	35	91

Table 3.3: Summary of the IC_{50} concentrations generated for four ovarian cancer cell lines after a five day treatment with 9 glycolytic inhibitors. The targeted glycolytic enzyme is indicated.

3.3 Exploration of the differential sensitivity of breast and ovarian cancer cell lines to glycolytic inhibitors

To explore the reasons for the differential effects of the glycolytic inhibitors on the panel of cell lines, the expression of the glycolytic targets of interest was first examined in whole cell lysates of the panel of breast and ovarian cancer cell lines. Figure 3.35 shows the Western blotting results for GLUT1, HKII, PFKFB3 and LDHA protein expression in the various cell lines. The four glycolytic enzymes were found present in all eight cell lines. Figures 3.36, 3.37 and 3.38 present the results of the quantitative densitometric analysis of the immunoblots. Data were normalised to α tubulin expression. GLUT1, HKII and LDHA expression was comparable among the different breast and ovarian cell lines. Based on the loading control data MCF7 and OVCAR5 cells had increased GLUT1 level compared to the other cell lines. OVCAR3 cells presented higher HKII expression. Regarding PFKFB3, OVCAR3 and CAOV3 ovarian cancer cells expressed higher levels of this target. For the other cell lines the expression was low and difficult to quantify. OVCAR5 and OVCAR3 cells had slightly higher LDHA expression compared to the other cell lines.

It was hypothesised that the differences observed in the sensitivity of the cell lines to the various glycolytic inhibitors (Tables 3.2&3.3) could possibly be explained by differential expression of the glycolytic enzymes. The IC_{50} values obtained for the panel of eight cell lines when treated with different glycolytic inhibitors were correlated with the protein expression level of the respective glycolytic target. Spearman r nonparametric correlation values are summarised in Table 3.4. No significant correlation was found between sensitivity to any of the inhibitors and expression of the inhibitor target (two-tailed P values> 0.05).

It was next investigated whether the rate of proliferation of each cell line could have an impact on cellular response to glycolytic inhibitors. As illustrated in Figures 3.39 and 3.40, sensitivity to two of the glycolytic inhibitors was revealed to correlate significantly with the proliferation rate of the different cell lines. Sensitivity to STF31 was found to correlate with the cell growth rate at p=0.0368 level, as well as sensitivity to Oxamic acid at the p=0.0046 level. Cell lines with the fastest growth rates presented increased sensitivity to these inhibitors while in contrast the slowest proliferating ones were found more resistant to both of them.

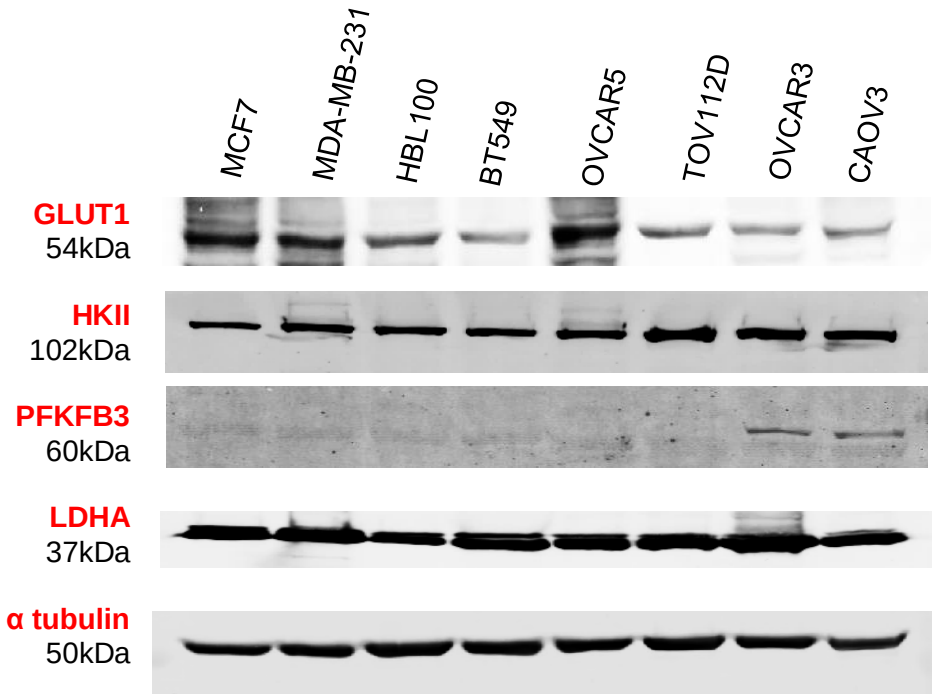

Figure 3.35: GLUT1, HKII, PFKFB3 and LDHA protein expression detected through Western blotting in a panel of 4 breast and 4 ovarian cancer cell lines. Alpha tubulin was used as a loading control (n=1).

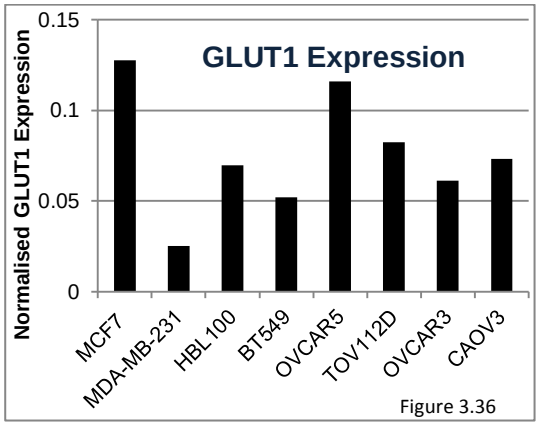

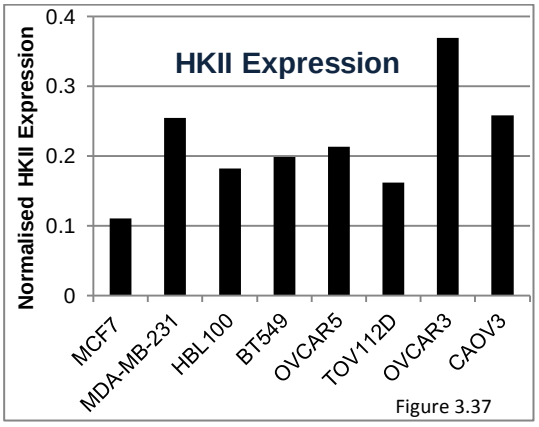

Figures 3.36 & 3.37: GLUT1, HKII and LDHA protein expression detected through Western blotting in a panel of 4 breast and 4 ovarian cancer cell lines. Densitometry analysis was conducted using the Odyssey Infrared Imaging System software (Licor) and data were normalised to α tubulin expression.

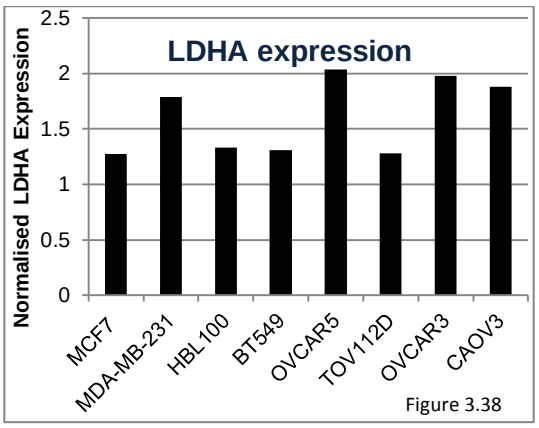

Figure 3.38: LDHA protein expression detected through Western blotting in a panel of 4 breast and 4 ovarian cancer cell lines. Densitometry analysis was conducted using the Odyssey Infrared Imaging System software (Licor) and data were normalised to α tubulin expression.

IC_{50} – Target protein expression NONPARAMETRIC CORRELATION	**Spearman r**	**two-tailed P value**
Phloretin	0.1667	0.7033
Quercetin	0.2381	0.5821
STF31	-0.3571	0.3894
WZB117	0.2381	0.5821
3-bromopyruvate	0.6347	0.0962
Oxamic acid	0.2431	0.2431
NHI-1	0.5952	0.1323

Table 3.4: Spearman nonparametric correlation of the IC_{50} concentrations generated for 4 breast and 4 ovarian cancer cell lines when treated with the indicated glycolytic inhibitors for a five-day period with the protein expression of the respective target.

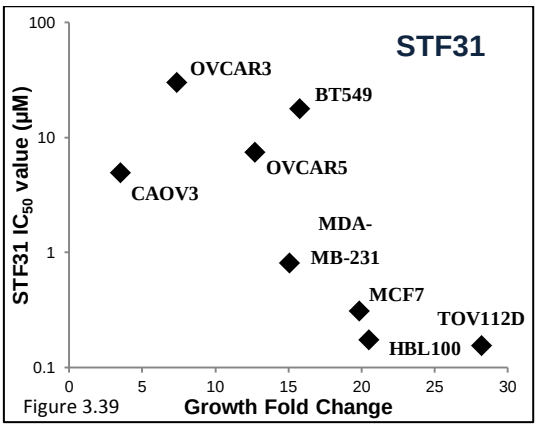

Figure 3.39

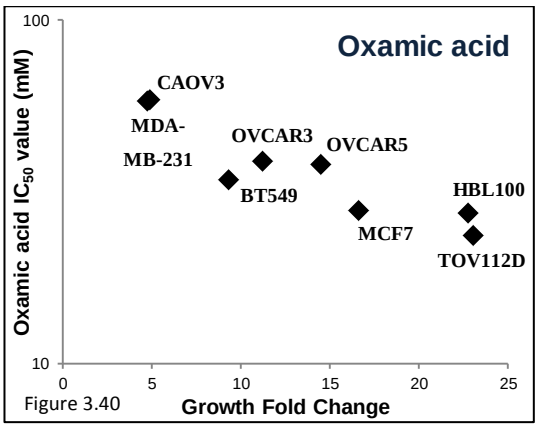

Figure 3.40

Figures 3.39 & 3.40: IC_{50} concentrations generated for 4 breast and 4 ovarian cancer cell lines when treated with STF31 and Oxamic acid for a five-day period plotted against growth fold change of the respective cell line. For STF31: Spearman nonparametric correlation r=-0.7619 and two-tailed P value 0.0368; characterised significant. For Oxamic acid: Spearman nonparametric correlation r=-0.9048 and two-tailed P value 0.0046; characterised very significant.

Pearson correlation	Phloretin	Quercetin	STF31	WZB117	3-BP	3PO	DCA	Oxamic acid	NHI-1
Phloretin		**0.018**	0.53	0.93	**0.017**	**0.010**	0.22	**0.049**	0.19
Quercetin	**0.018**		0.88	0.94	0.07	**0.015**	0.14	0.097	**0.019**
STF31	0.53	0.88		0.63	0.62	0.88	0.89	0.71	0.99
WZB117	0.93	0.94	0.63		0.99	0.58	0.38	0.98	0.38
3-BP	**0.017**	0.07	0.62	0.99		**0.024**	0.24	**0.002**	0.29
3PO	**0.010**	**0.015**	0.88	0.58	**0.024**		**0.021**	**0.009**	**0.03**
DCA	0.22	0.14	0.89	0.38	0.24	**0.021**		0.21	**0.011**
Oxamic acid	**0.049**	0.097	0.71	0.98	**0.002**	**0.009**	0.21		0.30
NHI-1	0.19	**0.019**	0.99	0.38	0.29	**0.03**	**0.011**	0.30	

Table 3.5: Pearson correlation of each pair of IC_{50} concentrations of nine glycolytic inhibitors generated for 4 breast and 4 ovarian cancer cell lines treated for a five-day period. Statistically significant Person P-values ($P < 0.05$) are shown in bold.

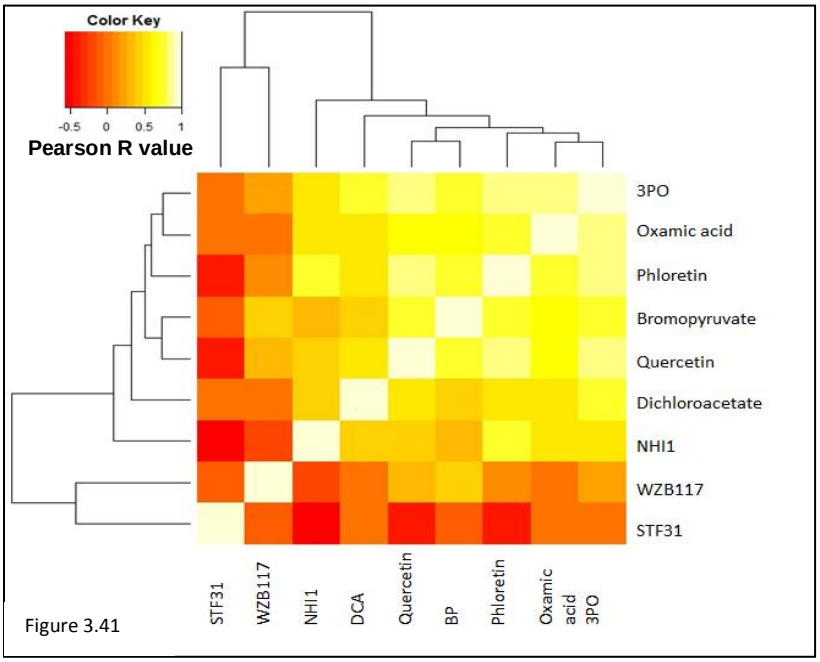

Figure 3.41: Correlation heatmap of pairs of IC_{50} concentrations of nine glycolytic inhibitors generated for 4 breast and 4 ovarian cancer cell lines treated for a five-day period. Positive Person R correlation values are displayed in bright white colours while negative Pearson R correlation values in dark red colours.

It was observed that two particular cell lines presented greater resistance to the majority of glycolytic inhibitors; MDA-MB-231 among the breast cancer cell lines and CAOV3 among the ovarian cancer cell lines (Tables 3.2&3.3). In order to develop a better understanding of the differential sensitivity of the cell lines to glycolysis inhibition the generated IC_{50} concentrations were correlated with each other. Table 3.5 presents the Pearson correlation P values of pairs of IC_{50} concentrations obtained for the panel of breast and ovarian cancer cell lines when treated with the nine glycolytic inhibitors. In Figure 3.41 is shown a correlation heatmap that illustrates the Pearson R correlation values. Positive R correlation values are displayed in bright white colours while negative R values are displayed in dark red colours. Seven of the inhibitors (Phloretin, Quercetin, 3BP, 3PO, DCA, Oxamic acid and NHI-1) had IC_{50} values that generated positive R values when compared to each other; visualised in the bright yellow square of the heatmap. Only two of the array of compounds, STF31 and WZB117 in the first branch of the dendrogram, gave IC_{50} values that did not correlate significantly with any of the other inhibitors. Negative R values are visualised in the dark red border of the bottom and left side of the heatmap.

3.4 The effect of glycolytic inhibitors on cell growth of two pairs of chemosensitive - chemoresistant ovarian cancer cell lines

PEA1-PEA2 and PEO1-PEO4 are two ovarian cancer cell line pairs established from two patients with ovarian adenocarcinoma. The first cell line of each pair is platinum sensitive while the second one was acquired after platinum resistance had been established [399, 400]. The effect of three selected glycolytic inhibitors on these cell lines was examined.

3.4.1 STF31

Figures 3.42 and 3.43 show the response of the two ovarian cancer cell line pairs to STF31 treatment. In both cases the two cell lines of each pair responded similarly to the GLUT1 inhibitor. The PEA2 cell line was found to be slightly more resistant compared to its paired platinum naïve line PEA1, with an IC_{50} value of 1.3μM against 0.9μM. In contrast the platinum-resistant line PEO4, having an IC_{50} value of 1.3μM, showed increased sensitivity to the inhibitor compared to its paired platinum-sensitive line PEO1, with an IC_{50} value of 1.5μM (Table 3.6).

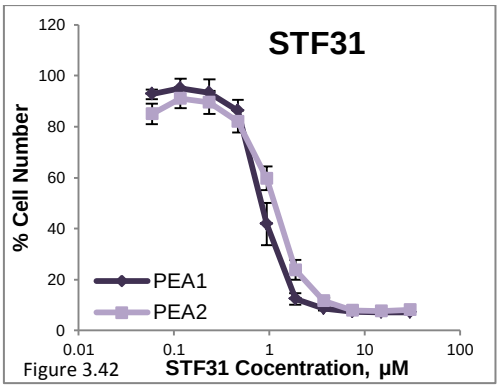

Figure 3.42

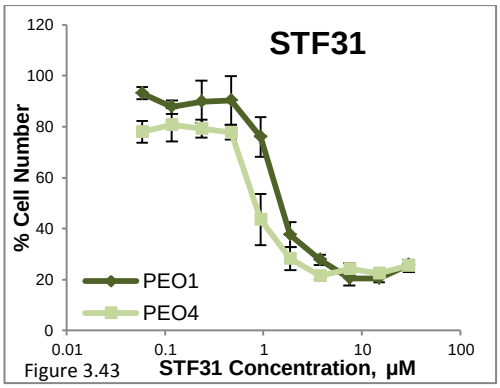

Figure 3.43

Figures 3.42 & 3.43: Concentration response curves of ovarian cancer cell line pairs treated with STF31 concentrations between 0.06-30μM for a four day period. Cell viability was determined by an SRB assay. Mean results of 6 replicates are reported and error bars represent standard deviations. Values are shown as a percentage of control. A constant 0.3% DMSO concentration was used across the whole curve in both cases. Representative data of 3 independent experiments are presented.

3.4.2 3PO

Results of 3PO treatment for the two ovarian cancer cell line pairs are shown in Figures 3.44 and 3.45. In both cases sensitivity to the PFKFB3 inhibitor coincided with platinum sensitivity. Both platinum resistant cell lines presented greater resistance to 3PO compared to their platinum sensitive paired cell lines. Both of them had a twofold higher IC_{50} value compared to the corresponding values of the platinum sensitive cell lines (Table 3.6).

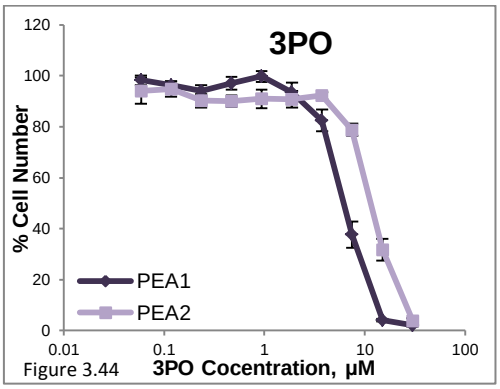

Figure 3.44

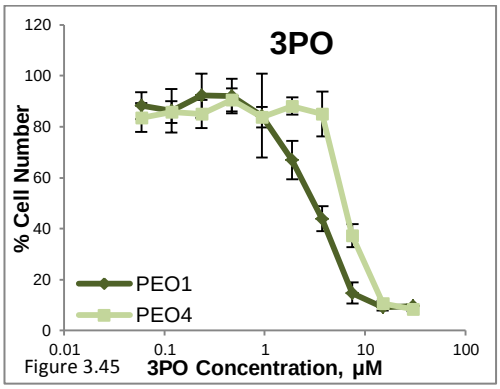

Figure 3.45

Figures 3.44 & 3.45: Concentration response curves of ovarian cancer cell line pairs treated with 3PO concentrations between 0.06-30µM for a four day period. Cell viability was determined by an SRB assay. Mean results of 6 replicates are reported and error bars represent standard deviations. Constant 0.3% DMSO concentration was used across the whole curve in both cases. Representative data of 3 independent experiments are presented.

3.4.3 Oxamic acid

The figures below present the results of the two ovarian cancer cell line pairs when treated with Oxamic acid (Figures 3.46&3.47). The first pair responded similarly to the LDH inhibitor with an almost identical IC_{50} value of 16mM. Regarding the second pair, the PEO4 platinum resistant cell line proved to be more resistant to Oxamic acid, having an IC_{50} value threefold higher than the corresponding value of PEO1 (Table 3.6).

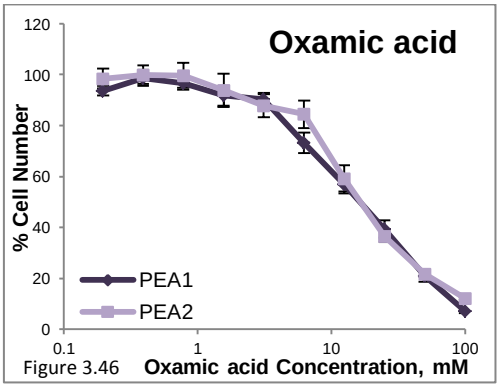

Figure 3.46

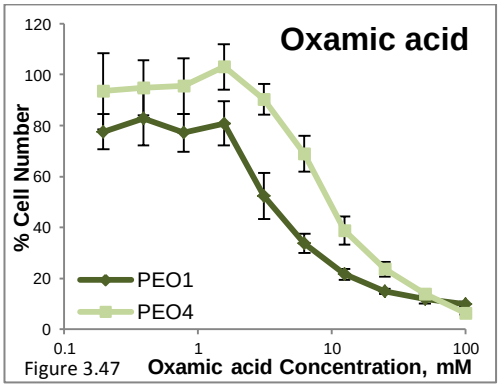

Figure 3.47

Figures 3.46 & 3.47: Concentration response curves of ovarian cancer cell line pairs treated with Oxamic acid concentrations between 0.4-100mM for a four day period. Cell viability was determined by an SRB assay. Mean results of 6 replicates are reported and error bars represent standard deviations. Values are shown as a percentage of control. Representative data of 3 independent experiments are presented.

IC_{50} values	1st pair		2nd pair	
	PEA1	**PEA2**	**PEO1**	**PEO4**
STF31 (μM)	0.86	1.3	1.5	0.88
3PO (μM)	6.3	11.9	3	6.8
Oxamic acid (mM)	16	17.6	3.8	10.1

Table 3.6: Summary of the IC_{50} concentrations generated for two ovarian cancer cell line pairs after a four day treatment with three glycolytic inhibitors.

3.5 The effect of the novel GLUT1 inhibitor IOM-1190

3.5.1 The effect of IOM-1190 on cell growth of selected breast and ovarian cancer cell lines

IOM-1190 is a novel selective GLUT1 inhibitor [324]. The effect of this inhibitor on cell proliferation of two breast cancer cell lines (MCF7 and MDA-MB-231) as well as the two pairs of chemosensitive - chemoresistant ovarian cancer cell lines (PEA1-PEA2 and PE01-PE04) described above was examined. Cancer cell proliferation was examined by the SRB assay.

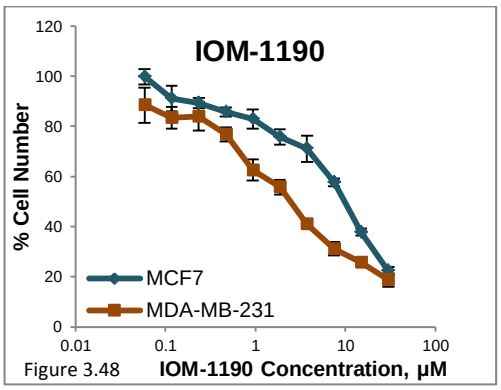

Figure 3.48

IC_{50} values	MCF-7	MDA-MB-231
IOM-1190 (μM)	8.6	2.4

Table 3.7: Summary of the IC_{50} concentrations generated for two breast cancer cell lines after a three day treatment with IOM-1190.

Figure 3.48: Concentration response curves of two breast cancer cell lines treated with IOM-1190 concentrations between 0.06-30μM for a three day period. Cell viability was determined by an SRB assay. Mean results of 6 replicates are reported and error bars represent standard deviations. Values are shown as a percentage of control. A constant 0.3% DMSO concentration was used across the whole curve. Representative data of 3 independent experiments are presented.

Figure 3.48 depicts the concentration response curves of two breast cancer cell lines, the ER positive MCF7 and the triple negative MDA-MB-231, when treated with IOM-1190 for three days. As shown in Table 3.7 MDA-MB-231 cells, with an IC_{50} value of 2μM, appeared to be almost four times more sensitive to this inhibitor compared to MCF7 cells.

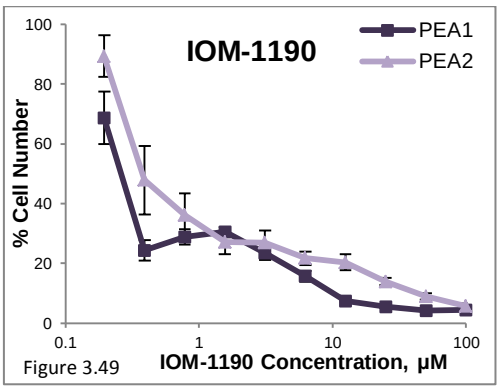

Figure 3.49

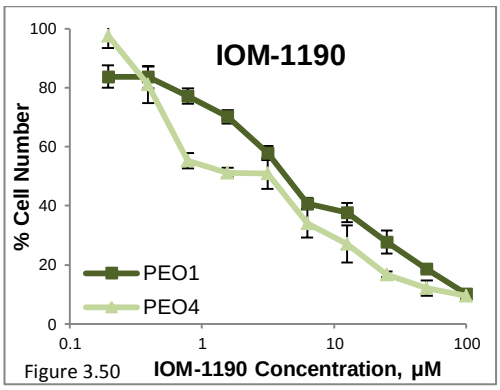

Figure 3.50

Figures 3.49 & 3.50: Concentration response curves of ovarian cancer cell line pairs treated with IOM-1190 concentrations between 0.2-100µM for a four day period. Cell viability was determined by an SRB assay. Mean results of 6 replicates are reported and error bars represent standard deviations. Values are shown as a percentage of control. A constant 1% DMSO concentration was used across the whole curve in both cases. Representative data of 2 independent experiments are presented.

IC_{50} values	1st pair		2nd pair	
	PEA1	**PEA2**	**PEO1**	**PEO4**
IOM-1190 (µM)	0.28	0.46	4.8	1.6

Table 3.8: Summary of the IC_{50} concentrations generated for two ovarian cancer cell line pairs after a four day treatment with IOM-1190.

Figures 3.49 and 3.50 demonstrate the effect of IOM-1190 on cell proliferation of two ovarian cancer cell line pairs. The compound effectively attenuated cell proliferation of both chemosensitive and chemoresistant cell lines. The first pair of cell lines responded in a similar way and presented similar sensitivity to the inhibitor. PEA1 had an IC_{50} value equal to 280nM and PEA2 equal to 460nM. In contrast, the PEO4 platinum-resistant cell line presented greater sensitivity having a threefold lower IC_{50} value (equal to 1.6µM) compared to the platinum sensitive PEO1 cell line (Table 3.8).

3.5.2 The effect of IOM-1190 under different glucose concentrations

The effect of IOM-1190 on MCF7 and MDA-MB-231 cell lines was examined under two different conditions; low glucose 5.56mM (as used in every experiment of this study) and high glucose 25mM.

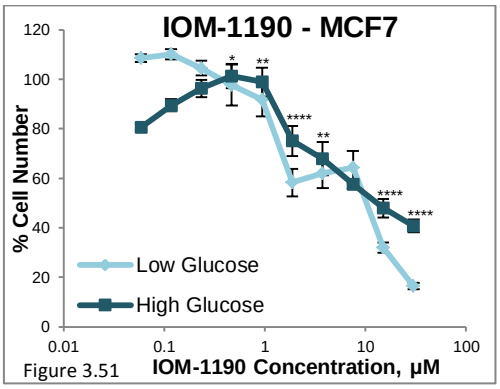

Figure 3.51

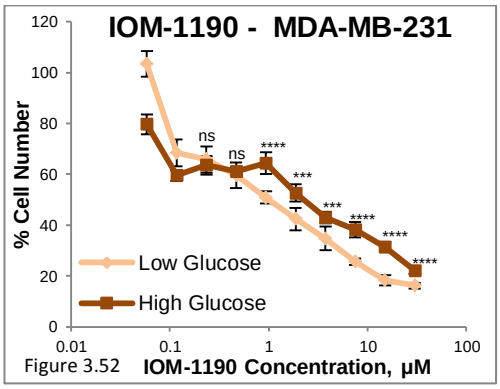

Figure 3.52

Figures 3.51 & 3.52: Concentration response curves of two breast cancer cell lines treated with IOM-1190 concentrations between 0.06-30µM under two different conditions of low and high glucose. Cell viability was determined by an SRB assay after a three day treatment. Mean results of 6 replicates are reported and error bars represent standard deviations. Values are shown as a percentage of control. A constant 0.3% DMSO concentration was used across the whole curve in both cases. Statistical significance indications: ns not significant P>0.05, * P<0.05, ** P<0.01, *** P<0.001, **** P<0.0001 (two-tailed P value generated from unpaired t-test, n=1).

IC_{50} values	MCF7		MDA-MB-231	
	Low glucose	High Glucose	Low glucose	High Glucose
IOM-1190 (µM)	7.8	10.3	0.78	2.34

Table 3.9: Summary of the IC_{50} concentrations generated for two breast cancer cell lines after a three day treatment with IOM-1190 under two different conditions of low and high glucose.

Figures 3.51 and 3.52 indicate the response of MCF7 and MDA-MB-231 cells to IOM-1190 treatment in the presence of a low or high glucose environment. Both cell lines presented greater resistance to the compound under high glucose conditions. The data demonstrated that MDA-MB-231 cells had a threefold increase in their IC_{50} value in the presence of high concentration of glucose compared to low glucose conditions. MCF7 cells presented a modest increase in their IC_{50} value (Table 3.9).

3.6 The effect of a glutaminolysis inhibitor on cell growth of a panel of four breast and four ovarian cancer cell lines

- **BPTES**

It is well established that many tumours have elevated glutamine metabolism [127-130]. Glutaminase catalyses the conversion of glutamine to glutamate which is the first reaction of the glutaminolytic pathway. BPTES, a selective glutaminase inhibitor, was used in this study and compared against the panel of four breast and four ovarian cancer cell lines described above [135]. Cancer cell proliferation was examined by the SRB assay after a 5-day treatment period.

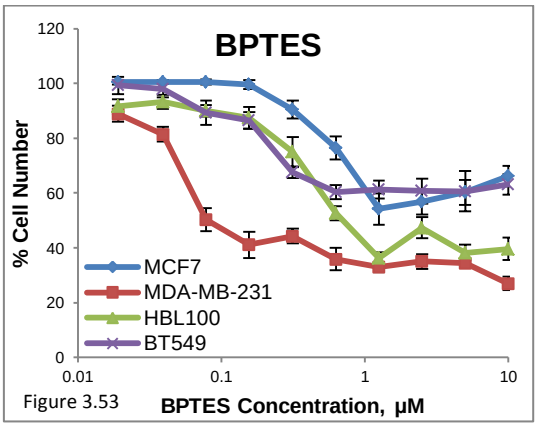

Figure 3.53

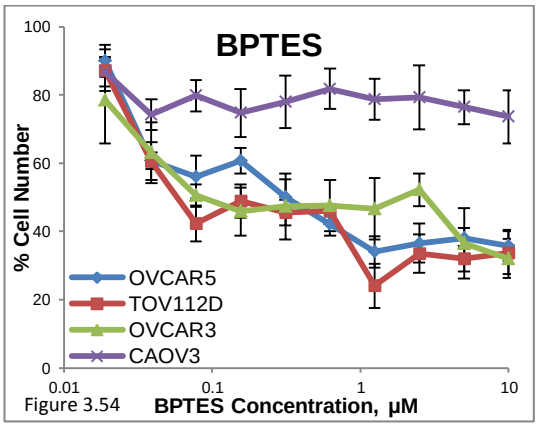

Figure 3.54

Figures 3.53 & 3.54: Concentration response curves of breast (3.53) and ovarian (3.54) cancer cells treated with BPTES concentrations between 0.02-10µM for a five day period. Cell viability was determined by an SRB assay. Mean results of 6 replicates are reported and error bars represent standard deviations. Values are shown as a percentage of control. A constant 0.1% DMSO concentration was used across the whole curve in both cases. Representative data of 2 independent experiments are presented.

Figures 3.53 and 3.54 present the results of the breast and ovarian cancer cell lines treated with BPTES. Great variation is demonstrated in the response of the different cell lines to this inhibitor. Regarding the breast cancer cell lines, MDA-MB-231 was very sensitive to BPTES, with an IC_{50} value equal to 80nM, while MCF7 and BT549 were found to be highly resistant to it in the range of the concentrations used. Between the ovarian cancer cell lines OVCAR5 and OVCAR3 cells were also found to be very sensitive, with IC_{50} values a little higher than 100nM, while in contrast CAOV3 cells demonstrated resistance to the compound even when used at concentrations as high as 10µM (Table 3.10).

IC_{50} values	**MCF-7**	**MDA-MB-231**	**HBL100**	**BT549**
BPTES (µM)	N/A	0.08	0.66	N/A

IC_{50} values	**OVCAR5**	**TOV112D**	**OVCAR3**	**CAOV3**
BPTES (µM)	0.18	0.8	0.12	N/A

Table 3.10: Summary of the IC_{50} concentrations generated for four breast and four ovarian cancer cell lines after a five day treatment with BPTES. N/A stands for not achieved in the range of tested concentrations.

3.7 Discussion

3.7.1 Growth dependency of breast and ovarian cancer cell lines on nutrient availability

The initial aim of this study was to develop an understanding of how the growth of breast and ovarian cancer cell lines were influenced by varying the concentrations of glucose and glutamine. The mean physiological level of glucose in the plasma is approximately 5mM; with a maximum concentration of 9mM after eating and a minimum of 3mM following physical exercise or moderate fasting [409]. Nevertheless the concentration of glucose in malignant tissues is significantly lower than their normal counterparts (up to 10 fold) in consequence of augmented glucose consumption and abnormal tumour microvasculature [410]. The majority of *in vitro* cell culture studies are typically conducted at a supraphysiological 25mM D-glucose concentration (the concentration present in DMEM medium 4500mg/L) to allow sufficient energy and maximal growth; however in the present metabolic study a lower glucose environment (5.56mM), closer to the physiological glucose level, was selected for the experiments. Glutamine is the most abundant free amino acid with a concentration reaching 0.7-0.9mM in the plasma [411, 412]. All the experiments in this study, similar to the majority of cancer research literature, were conducted with 4mM L-glutamine. The first question in this study sought to determine the growth of a panel of selected breast and ovarian cancer cell lines under a range of glucose and glutamine concentrations as well as in conditions of complete deprivation of each metabolic substrate.

The most interesting observation from the breast cancer data is that MDA-MB-231 and HBL100 cells were completely unable to proliferate in the absence of glucose. For both cell lines a significant induction in cell proliferation was only observed after addition of 0.4mM glucose compared to the no-glucose controls (Figures 3.3&3.5). The other two breast cancer

cell lines behaved in a different way. MCF7 cells were able to proliferate and increase their cell number by an impressive six fold when glucose was depleted; compared to the number of cells on the day of treatment (day 0). In the same conditions, BT549 cells doubled their cell number (Figures 3.1&3.7). All four examined breast cancer cell lines demonstrated maximal growth when cultured at 1.6mM glucose and above that concentration a plateau of growth was reached. The ovarian cancer cell lines demonstrated similar differences in the ability to grow in the absence of glucose. TOV112D and OVCAR3 were both able to increase their cell number up to threefold in glucose depleted conditions while in contrast OVCAR5 and CAOV3 were unable to grow when glucose was not present in the culture medium (Figures 3.9, 3.11, 3.13&3.15). Particularly for CAOV3 cells, a relatively high concentration equal to 0.4mM was essential for significant growth. Interestingly OVCAR5, TOV112D and CAOV3 cells reached a plateau of maximal growth at 1.6mM glucose, similar to the breast lines. In contrast OVCAR3 cells demonstrated optimal growth when cultured in a low glucose environment of 0.4mM. The observed differential sensitivity to glucose limitation corroborates the findings of Birsoy *et al*. In their study the authors developed a novel cell culture system ensuring constant low glucose availability and reported that cancer cells respond differently to glucose limitation. Based on RNAi pool screen data of metabolic genes, they identified that oxidative phosphorylation upregulation was of major importance for adaptation to a low glucose environment and correlated sensitivity to low glucose with mitochondrial mutations or deficient glucose utilisation [410].

As regards glutamine growth requirements, three out of four breast cancer cell lines (MCF7, MDA-MB-231 and BT549) were found unable to proliferate under zero glutamine availability. For these cell lines a minimum concentration of 0.1mM glutamine was required to achieve significant proliferation while optimal growth was observed between 0.4 and 0.8mM with no significant difference in growth under higher glutamine concentrations (Figures 3.2, 3.4&3.8). In contrast HBL100 cells required a minimum concentration of 0.4mM glutamine to significantly induce growth compared to the glutamine depleted control while higher glutamine concentration led to higher growth rate with the maximal cell number observed at the highest tested concentration of 12.8mM (Figure 3.6). With respect to the ovarian cancer cell lines an interesting finding is that none of the examined lines was able to show any sign of growth when glutamine was not present in the culture medium (Figures 3.10, 3.12, 3.14&3.16). Another finding of note is that OVCAR3 and CAOV3 cells demonstrated maximal growth at a low glutamine concentration, equal to 0.4 and 0.2mM respectively, whereas OVCAR5 and TOV112D demanded a concentration higher than 0.8mM to achieve optimal growth. A very interesting recent study linked ovarian cancer cell

glutamine dependency with invasive capability. Nonetheless the current study has been unable to support this association as proliferative growth of OVCAR3 cells, considered of low invasive potential was not found independent of glutamine as previously described [413]. This discrepancy could possibly be attributed to the prolonged incubation of 5 days under glutamine depleted conditions whereas previous findings do not exceed a 3 day 'treatment'.

Results from this set of experiments are consistent with those of Mathews *et al* who demonstrated that glucose and glutamine deprivation had a significant effect on HeLa cell survival. They documented that low glucose and glutamine availability and especially complete depletion impaired cancer cell viability and induced morphological changes even after a rapid 2h exposure [414]. Glucose deprivation has been extensively associated with oxidative stress [414, 415]. Aykin-Burns *et al* attributed the increased sensitivity of breast cancer cells to glucose withdrawal (and subsequently to glucose inhibition) compared to normal mammary epithelial cells, to the pro-oxidant status mediated by elevated ROS production [415]. In line with these findings Graham *et al* also confirmed the association between the metabolic reconfiguration of tumours and increased sensitivity to glucose deprivation. They linked glucose depletion with elevated tyrosine kinase signalling and ROS mediated cell death [416]. Regarding glutamine dependency Yuneva *et al* associated glutamine withdrawal with apoptotic cell death in cells bearing an activated Myc oncogene. Apoptosis was not related to DNA damage nor ATP depletion but only to deficiency of Krebs cycle intermediates [417].

Taken together these findings highlight that both breast and ovarian cancer cell growth is highly dependent on the availability of the major metabolic substrates, glucose and glutamine. The most striking observation is that none of the examined cell lines was able to proliferate in glutamine depleted conditions. Furthermore only four of the cell lines, two breast (MCF7 and BT549) and two ovarian (TOV112D and OVCAR3) achieved minimal growth when deprived of glucose (Table 3.1). The evidence of strong reliance on both glucose and glutamine for breast and ovarian cancer cell proliferation indicates that targeting of these metabolic pathways could potentially be therapeutically exploited and provide a promising strategy for the treatment of these female malignancies. Nevertheless it could be argued that the cell lines might have adapted metabolically to prolonged culture in a nutrient-rich *in vitro* environment and this might compromise the present findings. Further research is required to establish growth dependencies in *in vivo* experimental conditions.

3.7.2 Growth inhibitory effect of glycolytic inhibitors on breast and ovarian cancer cell lines

The effect of several inhibitors targeting key enzymes of the glycolytic pathway was then investigated in this study. Upstream components of the pathway (GLUT1, HKII and PFKFB3), the downstream target LDH along with PDHK1, an important regulator of the mitochondrial PDH complex, were selected and targeted with pharmacological tool compounds (Figure 1.7). Initially the growth inhibitory effect of these agents against a panel of breast and ovarian cancer cell lines was examined by the SRB assay after a 5-day treatment period.

Even though the tetrazolium-based MTT [3-(4,5-dimethylthiazol-2-yl)-2,5-diphenyl-2H-tetrazolium bromide] assay has been considered the 'gold-standard' of *in vitro* cytotoxicity assays several concerns have recently been raised and its accuracy has been questioned [418, 419]. The MTT assay, as well as other tetrazolium-based assays including the XTT and MTS, is based on the enzymatic reduction of a tetrazolium salt to the water insoluble formazan by metabolically active cells [420]. Recent evidence suggests that the MTT assay may interfere with several compounds containing oxido-reductive properties, including the glycolytic inhibitors 3BP, 2-deoxyglucose and lonidamine; generating false positive results thus indicating enhanced cellular viability [418, 419]. In contrast, the SRB assay is independent of metabolic function and exclusively based on the cellular protein content. Therefore it was selected here as more suitable for the study of metabolic inhibitors. Indeed this assay has gained a lot of ground in preclinical compound screening and is now the assay of choice in the Developmental Therapeutics Programme of the USA National Cancer Institute (NCI-60 Human Tumor Cell Lines Screen) [418, 421].

The most important finding of this set of experiments is that every single inhibitor tested attenuated breast and ovarian cancer cell proliferation in a concentration-dependent manner. Each of the examined compounds exhibited distinct inhibitory potency while each cell line demonstrated differential sensitivity to the same inhibitor. Recently developed agents, including STF31, WZB117 and 3PO were considerably more effective in inhibiting cancer cell proliferation compared to more established compounds like DCA and Oxamic acid that required higher concentrations (Tables 3.2&3.3).

A limitation of these experiments lies in the absence of a non-malignant control cell line that would allow a comparison of the effect of glycolysis inhibition between benign and malignant cells. Nevertheless selectivity towards cancers cells has already been demonstrated for several of these inhibitors namely STF31, 3BP, DCA and Oxamic acid

[312, 329, 358, 369]. Through metabolic plasticity normal cells are expected to tolerate glycolytic inhibition more readily and be able to generate ATP through mitochondrial respiration using alternative energy sources (fatty acids and amino acid) [100].

GLUT1 plays a critical role in breast and ovarian tumourigenesis and has been validated as a promising therapeutic target. GLUT1 overexpression has been extensively associated with poor clinical outcome and adverse prognosis [174-176]. Two flavonoids, reported to inhibit glucose transmembrane transport were compared with two novel GLUT1 inhibitors. STF31 and WZB117 proved more potent compared to the phytochemicals Phloretin and Quercetin (Figures 3.17 to 3.24). A striking observation is the differential effect of the novel inhibitors among the cell lines. STF31 was associated with remarkable cytotoxicity against HBL100 breast and TOV112D ovarian cancer cells with an IC_{50} concentration lower than 0.2μM. In contrast BT549 breast and OVCAR3 ovarian cancer cells presented great resistance in the examined range of concentrations (Figures 3.21&3.23). Likewise, while the four breast cancer cell lines along with two ovarian lines (TOV112D and CAOV3) responded to WZB117 treatment in a similar manner, with IC_{50} values between 5 and 6μM; OVCAR3 cells were considerably more sensitive (IC_{50} value equal to 1.4μM) whereas OVCAR5 cells were found absolutely resistant to the compound (Figures 3.22&3.24).

Based on previously presented growth dependency data it was anticipated that cell lines able to grow in glucose depleted conditions would be less sensitive to GLUT1 inhibition compared to cell lines that proved unable to proliferate in the absence of glucose. However this does not appear to be the case. BT549 as well as TOV112D and OVCAR3 were the most Phloretin sensitive breast and ovarian cancer cell lines respectively. Nevertheless all these cell lines had proved able to proliferate when deprived of glucose (Table 3.1). Similarly for MCF7 and BT549 among the breast lines as well as OVCAR3 among the ovarian lines that were the most sensitive to Quercetin. This discrepancy might be attributed to the pleiotropic nature of these phytochemicals as both have a wide range of biological effects beyond inhibition of glucose transport [274, 275]. Indeed the growth inhibitory effect of the next-generation GLUT1 inhibitor STF31 seems more consistent with the glucose growth reliance of the cell lines. BT549 and OVCAR3 cells, both demonstrating the ability to grow in glucose depleted conditions, showed resistance to the compound. Furthermore since all four compounds are considered to target the same molecule they would be expected to have a more comparable effect among the cell lines. A possible explanation for this is that some of these compounds are likely to have additional off-target effects, for example they may not target selectively GLUT1 but other glucose transporters as well.

Regarding previous research a thorough literature review did not reveal any information for antiproliferative action of the traditional phytochemical Phloretin against the breast nor the ovarian cancer cell line models used in this study; similarly for STF31. With respect to Quercetin and WZB117, data for only one of the cell lines (MCF7) was identified. Sensitivity of MCF7 breast cancer cells to Quercetin and WZB177 is consistent with findings from previous studies. The IC_{50} values detected here for MCF7 cells when treated with Quercetin and WZB117 are 44 and 6.4μM respectively as opposed to 37 and 10μM (approximate figure from supplementary data) that were previously reported [299, 319].

HKII is the mitochondrial-associated isoform upregulated in many types of cancer [206]. Specifically for breast and ovarian tumours HKII upregulation has been linked with disease recurrence [216, 218]. The synthetic pyruvate analogue, 3BP, effectively inhibited tumour cell growth of breast and ovarian cancer cell lines (Figures 3.25&3.26). The two cancer types responded in a similar way to HKII inhibition with all examined cell lines demonstrating IC_{50} values between 10 and 20μM. Only two of the lines, the MDA-MB-231 breast and the CAOV3 ovarian, were at least fourfold less sensitive (IC_{50} values higher than 80μM). The similar response to this inhibitor demonstrated by the majority of examined cell lines might be an indication that they all express similar levels of this target or have comparable activities. This remains to be further investigated.

PFKFB3 catalyses the synthesis of F2,6BP the allosteric activator of PFK1. PFKFB3 overexpression has been documented in several tumour types including breast and ovarian cancers [223]. 3PO was confirmed as a potent growth inhibitor of both breast and ovarian cancer cell lines generating low IC_{50} values (Figures 3.27&3.28). Sensitivity of MDA-MB-231 cells corroborates previous findings of Clem *et al* [343]. In the same study 3PO was shown to inhibit MDA-MB-231 xenograft tumour growth. It is therefore likely that the other breast and ovarian lines demonstrating similar or even enhanced sensitivity to PFKFB3 inhibition compared to MDA-MB-231 cells may also have *in vivo* potential.

DCA targets PDHK1 preventing PDH phosphorylation and therefore stimulating mitochondrial glucose oxidation [352]. DCA was effective in attenuating breast and ovarian cancer cell proliferation in a concentration dependent manner (Figures 3.29&3.30). However this compound required higher concentrations in the millimolar range. Sensitivity of MCF7 cells to PDHK1 inhibition corroborated previous published data by Sun *et al* [358]. The low potency of the compound renders it challenging to achieve relevant therapeutic levels clinically. Nevertheless the high bioavailability and impressive *in vivo* and preclinical data of the compound suggest it is a valuable tool especially for combinatorial strategies [352, 366].

LDHA, the enzyme catalysing the reduction of pyruvate at the bottom of the glycolytic pathway, is the final target of interest in this study. LDHA upregulation has been reported in breast and ovarian cancers compared to normal tissues [263]. Two inhibitors, an established pyruvate analogue along with a novel LDHA selective inhibitor were compared here. Both compounds induced a concentration-dependent decline of viable cancer cell number (Figures 3.31 to 3.34). Nevertheless NHI-1 demonstrated significantly greater growth inhibitory potency compared to Oxamic acid.

These experiments provide evidence that nine compounds targeting key components of the glycolytic pathway inhibited breast and ovarian cancer cell proliferation in a concentration-dependent way. Interestingly both cancer types presented similar sensitivities to these inhibitors. It should be mentioned that Phloretin, 3BP, 3PO, DCA and NHI-1 presented a clear cytotoxic effect in the majority of cell lines whereas Quercetin, WZB117 and Oxamic acid suppressed cancer cell proliferation in a cytostatic way, since for the latter compounds the optical density measurements at the final day of treatment were higher than the corresponding values on the day of treatment (day 0) thus indicating that at least the initial number of treated cells was viable even following treatment with the highest concentration of these compounds for 5 days.

On searching the literature, this work appears to be the first comparative study of an extended array of glycolytic inhibitors against breast and ovarian cancer cell line panels. There is little published data on the effect of the majority of these compounds on breast cancer and particularly on ovarian cancer lines. Taken together these results provide evidence that breast and ovarian cancer cell proliferative growth is dependent on the glycolytic pathway which may have therapeutic implications. The glycolytic pathway was validated as a legitimate target for cancer treatment.

3.7.3 Sensitivity to glycolytic inhibitors varies among cell lines

The noteworthy variation in IC_{50} concentrations indicates that the different breast and ovarian cancer cell lines exhibit diverse responses to the glycolytic inhibitors (Tables 3.2&3.3). The protein expression of the targeted glycolytic enzymes was examined in the panel of breast and ovarian cancer cell lines through Western blotting. GLUT1, HKII and LDHA expression did not differ markedly between these cell lines (Figures 3.36 to 3.38). Furthermore no association was identified between the expression of the targeted glycolytic enzyme and sensitivity to the corresponding inhibitor (Table 3.4).

Nevertheless an interesting correlation between inhibitor response and proliferation rate was detected. It was revealed that sensitivity to two of the inhibitors targeting the top and bottom of the glycolytic pathway, STF31 and Oxamic acid, correlated significantly with the growth rate of the cell lines (Figures 3.39&3.40). Thus the differential response of cancer cells to these compounds could be attributed to growth rate differences. The fastest growing cell lines appeared more sensitive to these agents (lower IC_{50} values) compared to the slower growing ones that presented greater resistance to glycolysis inhibition (higher IC_{50} values). It could conceivably be hypothesised that faster growing cells are likely to be more dependent on the glycolytic pathway for biosynthetic precursor and energy generation in order to sustain their rapid proliferation and hence are more sensitive to inhibition of the pathway.

Another interesting observation was that two of the cell lines demonstrated remarkable resistance to the majority of the tested inhibitors; MDA-MB-231 breast cancer cells and CAOV3 ovarian cancer cells (Tables 3.2&3.3). MDA-MB-231 is a triple negative cell line characterised as highly invasive; elevated resistance to several antitumour agents including tumour necrosis factor-α (TNFα) and taxol has previously been documented [422]. Furthermore Gaglio *et al* reported that MDA-MB-231 cells, harbouring an oncogenic K-Ras, exhibit enhanced glycolytic activity and upregulation of several glycolytic enzymes [423]. It is possible therefore that upregulation of the glycolytic targets is responsible for the decreased sensitivity to glycolytic inhibitors, as higher concentration of a compound could be required to target higher level of an enzyme. For further support it should also be mentioned that it has been reported that the Warburg is the dominant metabolic phenotype of triple negative tumours [424]. As regards CAOV3, this is a primary ovarian cancer cell line that carries a nonsense mutation in the p53 gene and multiple copies of the PIK3CA oncogene [425, 426]. P53 is a well-established metabolic regulator promoting the glycolytic switch when it is inactivated [116]. Another relevant aspect is that CAOV3 is the slowest growing cell line among the ones tested here (Figures 3.39&3.40). Hence, it seems likely that the observed increased resistance to glycolysis inhibition could be related to the slow proliferation rate.

A very significant finding to emerge from the analysis of these experiments is that sensitivity of the panel of breast and ovarian cancer cell lines to the vast majority of the glycolytic inhibitors (7 out of 9 compounds) appeared correlated with each other. Phloretin, Quercetin, 3-BP, 3PO, DCA, Oxamic acid and NHI-1 generated IC_{50} concentrations that gave high Pearson R correlation values when compared in pairs (Figure 3.41). This association of sensitivity to each pair of inhibitors could serve as a fundamental indication that all these

compounds have a similar mode of action sharing a common target, i.e. the glycolytic pathway. STF31 and WZB117 formed an exception and did not correlate with sensitivity to any of the other agents. This could possibly be attributed to off-target effects. Indeed, regarding STF31 inhibition of NAMPT has been evidenced [315-317].

Finally, for the above analyses, breast and ovarian cancer cell lines were collectively considered as cancer cells and analysed together. Even though it is far from homogenous the panel of eight cancer cell lines was essential to get statistically significant correlations.

3.7.4 Comparing sensitivity to glycolysis inhibition with platinum sensitivity in ovarian cancer cell lines

PEA1-PEA2 and PEO1-PEO4 are two ovarian cancer cell line pairs each derived from a single patient with ovarian adenocarcinoma at different stages of platinum treatment. The first cell line of each pair is responsive to platinum therapy while the second one exhibits resistance to it [399, 400]. These two pairs represent a valuable model to study platinum sensitive and resistant ovarian cancer. Recent evidence associated drug resistance with an elevated dependency on the glycolytic phenotype however much less is known as to whether glycolysis inhibition could be exploited against resistant disease [427]. This set of experiments investigated the sensitivity of platinum sensitive and resistant ovarian cancer cells to glycolytic inhibitors. Three compounds were selected targeted against three major components of the glycolytic pathway; the upstream transporter GLUT1, the downstream target LDHA and the intermediate regulator PFKFB3.

Targeting all three major components of glycolysis proved effective in attenuating ovarian cancer cell proliferation in a concentration dependent manner regardless of platinum sensitivity (Figures 3.42 to 3.47). These findings provide evidence that inhibition of the glycolytic pathway could be a promising strategy for the treatment of platinum resistant disease.

The PEO1-PEO4 pair appeared considerably more sensitive to the glycolytic inhibitors compared to the PEA1 and PEA2 lines. Interestingly, PEA1 and PEA2 cells responded in a very similar way to STF31 and Oxamic acid. In contrast the platinum resistant cell line of both pairs appeared more resistant to PFKFB3 inhibition, demonstrating a twofold increase in the IC_{50} value. Likewise the platinum resistant PEO4 line had reduced sensitivity to Oxamic acid. In contrast the same cell line presented more sensitivity to STF31 compared to its paired platinum-responsive line PEO1 (Table 3.6).

3.7.5 Investigating the antiproliferative effect of the novel GLUT1 inhibitor IOM-1190

Several compounds reported to inhibit glucose transport have been used in this study. However concerns have been raised and their specificity has been questioned. The two flavonoids, Phloretin and Quercetin, are pleiotropic in nature and as discussed in the Introduction (section 1.5.1.1) have been associated with a wide range of biological effects [274, 275]. Moreover recent evidence has linked the STF31-mediated antiproliferative effect with NAMPT inhibition [59-61]. For that reason a novel compound specifically inhibiting GLUT1 was sought and investigated.

IOM-1190 is the lead compound of a series of specific GLUT1 inhibitors identified very recently by IOmet Pharma [324]. The effect of this novel inhibitor on cell proliferation of a pair of breast cancer cell lines as well as the previously mentioned chemosensitive and chemoresistant ovarian cancer cell line pairs was investigated. IOM-1190 demonstrated remarkable antiproliferative action against breast as well as ovarian cancer cell lines both resistant and sensitive to platinum therapy generating low IC_{50} values (Figures 3.48 to 3.50).

The most striking finding was the enhanced sensitivity of the MDA-MB-231 triple negative breast cancer cells compared to MCF7 cells (Table 3.7). This contradicts earlier findings showing that MDA-MB-231 cells were more resistant to a collection of 9 glycolytic inhibitors compared to the ER positive cell line (Table 3.2). Nevertheless it is in agreement with the nutrient growth dependency experiments presented in section 3.1. MDA-MB-231 cellular growth proved highly dependent on glucose availability as cells were unable to proliferate when glucose was depleted. This strong reliance could possibly be interpreted as an indication of enhanced sensitivity to inhibition of glucose transport. Triple negative tumours are highly aggressive and with limited treatment options thus the observed sensitivity to a novel agent is a very important and encouraging finding [428].

As regards the ovarian cancer cell line pairs, an interesting observation was the elevated sensitivity of the PEA1 and PEA2 lines, compared to the other ovarian cancer cell pair, a finding that is in contrast with the results from the previously examined glycolytic inhibitors (Table 3.6). The PEA1 line appeared remarkably sensitive to the GLUT1 inhibitor with an IC_{50} value as low as 280nM, 17 times lower than the corresponding value of the other platinum sensitive line PEO1. Another noteworthy observation is that this platinum sensitive line PEO1 was considerably more resistant to IOM-1190 compared to its paired platinum resistant line PEO4, with a threefold higher IC_{50} concentration (Table 3.8).

Overall IOM-1190 proved a very potent inhibitor with a strong antiproliferative effect on widely considered resistant lines, including the triple negative MDA-MB-231 and the platinum resistant PEO4 cell lines.

The next question addressed was whether sensitivity to this novel GLUT1 inhibitor would be affected by the concentration of glucose in the culture medium. Therefore MCF7 and MDA-MB-231 cells were treated with IOM-1190 under low glucose (5.56mM) and high glucose conditions (25mM). Interestingly the effect on both cell lines proved dependent on glucose availability and both of them appeared more sensitive to the agent in a low glucose environment (Table 3.9). Even though especially for MCF7 the effect was only marginal this finding is in agreement with data presented by Dr Alan Wise in the 26th EORTC-NCI-AACR Symposium given that the molecule was reported to have a substrate competitive mechanism of action [429]. These data indicated that A549 lung cancer cells were eightfold more sensitive to IOM-1190 when treated in 5mM glucose medium compared to a high glucose 17mM environment. Glucose sensitive cytotoxicity is also in agreement with findings from Liu *et al* on another GLUT1 inhibitor. They reported that high glucose concentration was able to alleviate the growth inhibitory effect of WZB115 on H1299 non-small cell lung cancer cells suggesting this as an indication of basal glucose transport inhibition [318].

3.7.6 Growth inhibitory effect of a glutaminolytic inhibitor on breast and ovarian cancer cell lines

Previously it was demonstrated that breast and ovarian cancer cell growth was highly dependent on glutamine availability (section 3.1). The effect of glutaminolysis inhibition was therefore examined in the previously mentioned panel of four breast and four ovarian cancer cell lines. BPTES is as a selective non-competitive glutaminase inhibitor. This agent induced a concentration dependent reduction in the number of both breast and ovarian viable cancer cells (Figures 3.53&3.54). The compound demonstrated a cytostatic mechanism of action since the maximal growth inhibitory effect observed for any of the cell lines was around 80% following a 5-day incubation with the highest concentrations used in the present study. Antiproliferative action against the selected cell line models has not been previously reported.

BPTES exhibited an interesting differential effect among the various cell lines. MDA-MB-231 was by far the most sensitive breast cancer cell line with an IC_{50} value as low as 80nM. This sensitivity confirms the association between oncogenic K-ras transformation and elevated dependence on glutamine for anaplerosis as demonstrated by Gaglio *et al* [423].

Moreover HBL100 cells proved considerably more sensitive compared to MCF7 and BT549 cells. This seems in agreement with glutamine growth requirements presented above. HBL100 cancer cells proved highly reliant on glutamine as they required high glutamine availability (equal to 0.4mM) to achieve significant growth compared to the glutamine depleted control and also they were responsive to high glutamine concentrations by increasing cellular proliferation (Figure 3.6).

Among ovarian cancer cell lines OVCAR3, OVCAR5 and TOV112D presented a similar response to glutaminase inhibition with the latter being around fourfold less sensitive. An interesting observation was that CAOV3 cells demonstrated resistance to BPTES. This result is consistent with findings from the glutamine growth dependency experiments. CAOV3 cells were unresponsive to high glutamine availability. Maximal growth was achieved with concentrations as low as 0.2mM glutamine and remained unaffected even with a concentration as high as 12.8mM. It is also worth mentioning that in glutamine depleted conditions CAOV3 cells were not able to proliferate nevertheless they were able to sustain their cell number as the average OD value of the no glutamine controls was comparable to the respective value on the day of treatment (Figure 3.16). It is possible that if the duration of glutamine 'treatments' was shorter than 5 days CAOV3 cells might be able to proliferate even in the absence of glutamine and prove completely independent of glutamine as resistance to glutaminase inhibition indicates.

Taken together BPTES proved a potent inhibitor of breast and ovarian cancer cell proliferation. Inhibition of glutamine catabolism therefore also seems a promising therapeutic strategy for these cancer types.

Chapter 4

Chapter 4: The effect of glycolytic inhibitors on breast cancer cellular function

4.1 The effect of glycolytic inhibitors on induction of apoptosis

The mechanism by which the glycolytic inhibitors attenuate cancer cell proliferation was next examined. Flow cytometric analysis of cells double stained with annexin V conjugated with the fluorochrome FITC, and propidium iodide, was conducted. Annexin V is a calcium-dependent phospholipid binding protein that binds with high affinity to phosphatidylserine when it is translocated and exposed in the outer cellular membrane of apoptotic cells [430, 431]. PI is a vital dye that binds to the nucleic acids of cells that have lost the integrity of their cellular membrane [432]. The double staining and the subsequent flow cytometric analysis enabled the differentiation of a cell population treated with several glycolytic inhibitors in four distinct categories as presented in the following two-dimensional scatter plots. In these plots the annexin V fluorescent signal is indicated in the y-axis and the PI signal in the x-axis. Annexin V and PI negative cells, in the lower left quadrant, are considered intact live cells. Annexin V high and PI low cells, in the upper left quadrant are characterised as early apoptotic. The upper right quadrant represents cells in late apoptotic stages stained with both Annexin V and PI. And finally the lower right quadrant with cells stained only with PI represents necrotic cells [430, 431]. Cells in the upper region (upper left and upper right quadrants), stained positive for annexin V, were collectively characterised as cells undergoing apoptosis.

For this experiment MCF7 breast cancer cells were used and were treated for 24 and 48 h with the nine glycolytic inhibitors described in previous chapters. The concentrations used for each compound were based on previously acquired SRB data presented in Chapter 3 section 3.2. The mechanism of cell death involved in the end point of the sigmoidal concentration response curves was investigated. The concentration used for each of the compounds was associated with maximal growth inhibition in the SRB assays following a 5-day treatment and was anticipated to have a significant effect on cell viability even as early as 24h. Two time points (24h and 48h) were selected to give a clear picture of the apoptotic process.

Untreated Cells

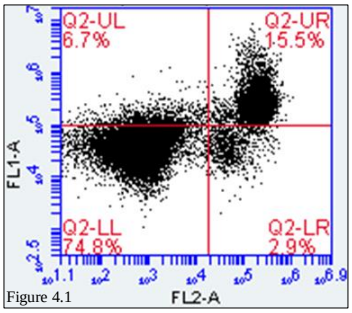

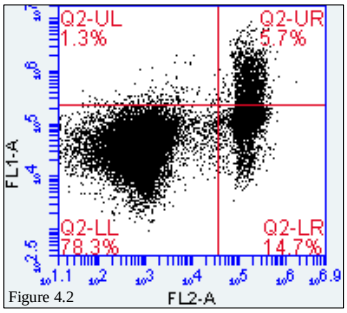

Figures 4.1 & 4.2: Flow cytometric analysis of untreated MCF7 breast cancer cells at 24 and 48h. FL1 (annexin V) versus FL2 (PI) scatter plots of gated cells double stained with FITC-conjugated annexin V and propidium iodide are presented. The percentage of cells in each quadrant is indicated in red (n=1).

Figures 4.1 and 4.2 present the flow cytometric analysis of untreated MCF7 cells at 24 and 48h respectively. At both time points the majority of cells (75 and 78% respectively) were found viable and non-apoptotic, annexin V and PI negative. It is interesting that at 24h 6.7% of the cells were classified as early apoptotic (annexin V positive, PI negative) and 15.5% late apoptotic (annexin V and PI positive). At 48h the percentage of apoptotic cells was lower (7% compared to 22.2%), however increased necrosis was observed (14.7% against 2.9% at 24h). The untreated controls were used to define the baseline levels of apoptotic and necrotic cells at each time point. Untreated samples were collected at 24 and 48h and the culture medium was not changed before then.

300μM Phloretin

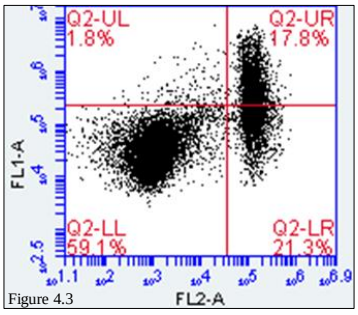

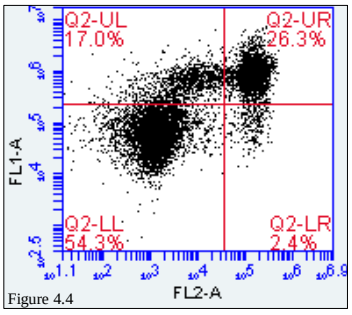

Figures 4.3 & 4.4: Flow cytometric analysis of MCF7 breast cancer cells treated with 300μM Phloretin for 24 and 48h. FL1 (annexin V) versus FL2 (PI) scatter plots of gated cells double stained with FITC-conjugated annexin V and propidium iodide are presented. The percentage of cells in each quadrant is indicated in red (n=1).

Figures 4.3 and 4.4 show the annexin V versus PI plots of gated MCF7 cells treated with 300µM Phloretin for 24 and 48h, respectively. It is apparent that the percentage of viable cells has decreased compared to the untreated controls and it is similar at both time points at 59.1 and 54.3% respectively. At 24h the PI positively stained population increased compared to the untreated control, reaching 21.3%, indicating increased necrosis. After 48h treatment, a marked induction of both early and late apoptosis was noted. Annexin V positive cells increased to 43.3% from 7% for the untreated cells. The percentage of necrosis was low; consisting of only 2.4% of the whole cell population.

300µM Quercetin

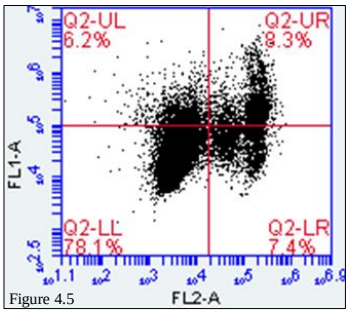

Figure 4.5

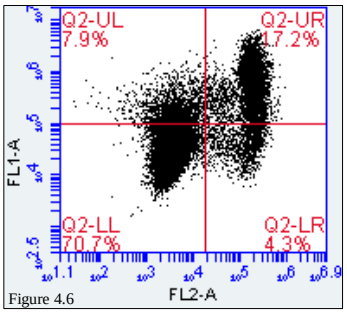

Figure 4.6

Figures 4.5 & 4.6: Flow cytometric analysis of MCF7 breast cancer cells treated with 300µM Quercetin for 24 and 48h. FL1 (annexin V) versus FL2 (PI) scatter plots of gated cells double stained with FITC-conjugated annexin V and propidium iodide are presented. The percentage of cells in each quadrant is indicated in red (n=1).

The results of flow cytometric analysis of MCF7 cells treated with 300µM Quercetin for 24 and 48h are presented in Figures 4.5 and 4.6. The number of live cells is similar to the corresponding value of the untreated controls. At 24h a marginal increase of PI positively stained, necrotic cells can be observed (from 2.9 to 7.4%). With respect to the 48h time point, an induction of both early and late apoptosis was detected. The percentage of cells in the upper left quadrant increased from 1.3 to 7.9% while in the upper right quadrant from 5.7 to 17.2%.

30µM STF31

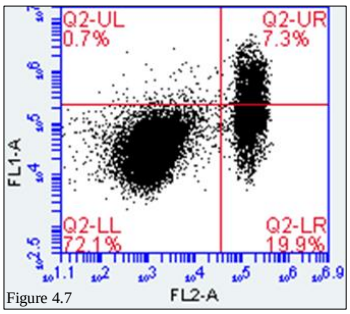

Figure 4.7

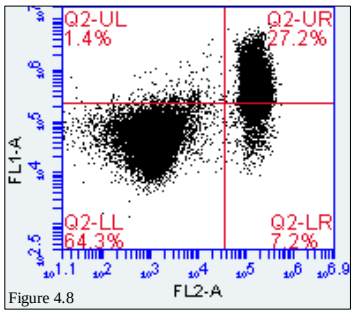

Figure 4.8

Figures 4.7 & 4.8: Flow cytometric analysis of MCF7 breast cancer cells treated with 30µM STF31 for 24 and 48h. FL1 (annexin V) versus FL2 (PI) scatter plots of gated cells double stained with FITC-conjugated annexin V and propidium iodide are presented. The percentage of cells in each quadrant is indicated in red (n=1).

Scatter plots generated through flow cytometric analysis of MCF7 cells treated with 30µM STF31 for 24 and 48h are depicted in Figures 4.7 and 4.8. At 24h the proportion of live cells was almost unaffected. However an induction of necrotic cell death was seen (from 2.9 to 19.9%). After a 48h treatment with STF31 MCF7 cells presented a fivefold increase of late apoptotic cells, stained positive for both annexin V and PI. It is interesting that the percentage of early apoptotic cells remained the same.

30µM WZB117

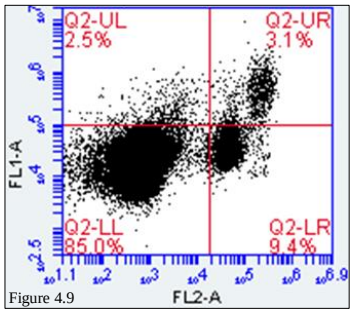

Figure 4.9

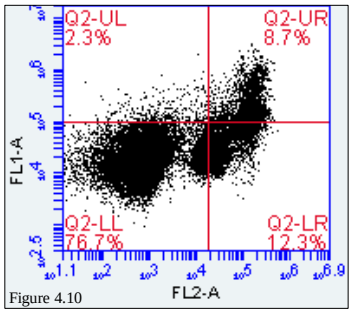

Figure 4.10

Figures 4.9 & 4.10: Flow cytometric analysis of MCF7 breast cancer cells treated with 30µM WZB117 for 24 and 48h. FL1 (annexin V) versus FL2 (PI) scatter plots of gated cells double stained with FITC-conjugated annexin V and propidium iodide are presented. The percentage of cells in each quadrant is indicated in red (n=1).

Figures 4.9 and 4.10 present the scatter plots of gated MCF7 cells treated with 30µM WZB117 for 24 and 48h. Treatment with this particular GLUT1 inhibitor did not affect the viability of cancer cells at either of the time points, since live cells at 24h were quantified at 85% of the measured population, 10% higher than the respective percentage of the untreated sample. Nonetheless, a threefold increase of necrotic cells, positively stained only with PI, can be observed after 24h treatment. At 48h a modest increase of both early and late apoptosis was observed. Annexin V positively stained cells increased from 7% in the control to 11%.

300µM 3BP

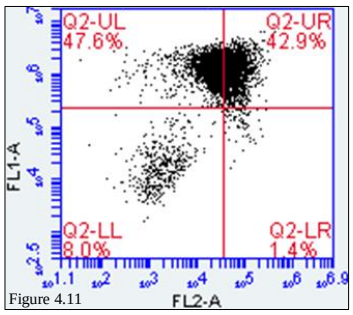

Figure 4.11

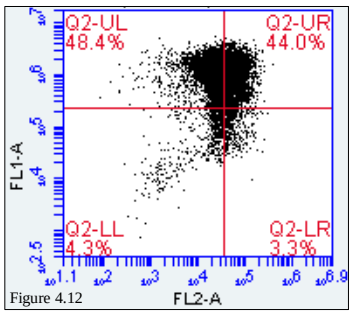

Figure 4.12

Figures 4.11 & 4.12: Flow cytometric analysis of MCF7 breast cancer cells treated with 300µM 3-bromopyruvate for 24 and 48h. FL1 (annexin V) versus FL2 (PI) scatter plots of gated cells double stained with FITC-conjugated annexin V and propidium iodide are presented. The percentage of cells in each quadrant is indicated in red (n=1).

Figures 4.11 and 4.12 reveal that 3BP has a very marked impact on cell viability through the apoptotic process. At least 90% of a population of MCF7 cells treated with 300μM 3BP for 24 or 48h underwent apoptotic cell death (cells stained positive with annexin V). A balanced marked induction of both early and late apoptosis was observed.

30μM 3PO

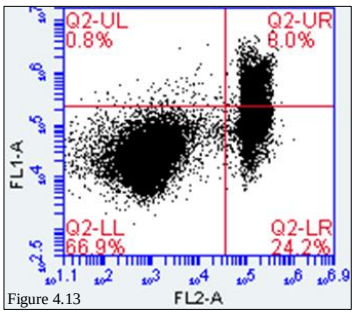

Figure 4.13

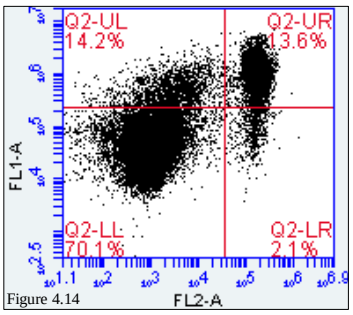

Figure 4.14

Figures 4.13 & 4.14: Flow cytometric analysis of MCF7 breast cancer cells treated with 30μM 3PO for 24 and 48h. FL1 (annexin V) versus FL2 (PI) scatter plots of gated cells double stained with FITC-conjugated annexin V and propidium iodide are presented. The percentage of cells in each quadrant is indicated in red (n=1).

The annexin V versus PI two-dimensional scatter plots acquired from the flow cytometric analysis of MCF7 cells treated with 3PO for 24 and 48h are depicted in Figures 4.13 and 4.14. An eightfold increase of cells stained positively for PI, in the lower right quadrant, suggesting necrosis, can be observed after treatment with 30μM 3PO for 24h compared to the untreated control. On the other hand at 48h the level of necrosis is very limited (2.1%) while there is an evident induction of apoptosis. The percentage of cells in early apoptotic stages increased eleven times and a twofold increase of late apoptosis was observed as well.

100mM DCA

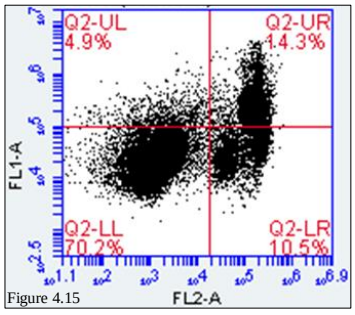

Figure 4.15

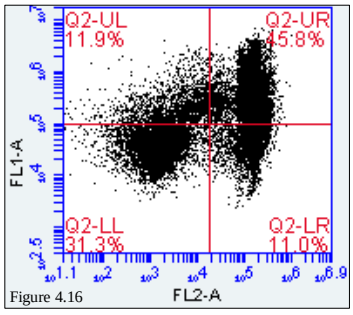

Figure 4.16

Figures 4.15 & 4.16: Flow cytometric analysis of MCF7 breast cancer cells treated with 100mM Dichloroacetate for 24 and 48h. FL1 (annexin V) versus FL2 (PI) scatter plots of gated cells double stained with FITC-conjugated annexin V and propidium iodide are presented. The percentage of cells in each quadrant is indicated in red (n=1).

A 24h treatment with 100mM DCA resulted in increased necrosis. As shown in Figure 4.15 the percentage of cells in the lower right quadrant increased to 10.5% from 2.9% in the untreated control. In Figure 4.16, evidence is provided that treatment with the PDHK1 inhibitor induces apoptosis at 48h. The percentage of live intact cells was reduced two and a half times and a marked increase in apoptosis was observed. Early apoptotic cells, annexin V positive, presented a nine fold increase while late apoptotic cells, annexin V and PI positive, increased eight fold.

100mM Oxamic acid

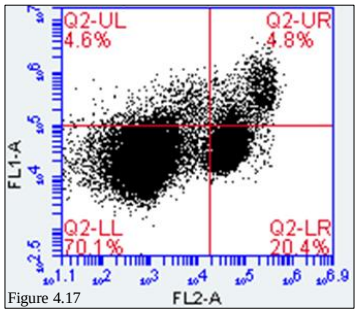

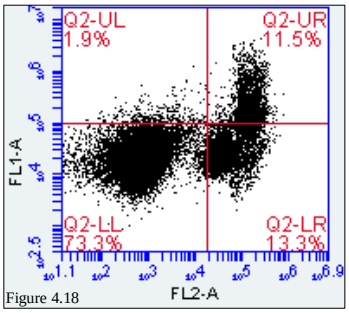

Figures 4.17 & 4.18: Flow cytometric analysis of MCF7 breast cancer cells treated with 100mM Oxamic acid for 24 and 48h. FL1 (annexin V) versus FL2 (PI) scatter plots of gated cells double stained with FITC-conjugated annexin V and propidium iodide are presented. The percentage of cells in each quadrant is indicated in red (n=1).

Plots of gated cells through flow cytometric analysis after a 24 and 48h treatment with 100mM Oxamic acid are presented in Figures 4.17 and 4.18. At both time points there was a modest 5% decline in the number of live cells compared to the respective control sample. Nevertheless a sevenfold increase in the proportion of necrotic cells was observed at 24h. Regarding the 48h time point the percentage of late apoptotic cells, in the upper right quadrant was found to be doubled.

300µM NHI-1

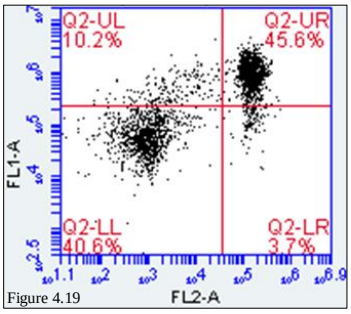

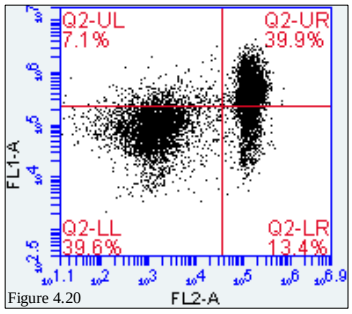

Figures 4.19 & 4.20: Flow cytometric analysis of MCF7 breast cancer cells treated with 300µM NHI-1 for 24 and 48h. FL1 (annexin V) versus FL2 (PI) scatter plots of gated cells double stained with FITC-conjugated annexin V and propidium iodide are presented. The percentage of cells in each quadrant is indicated in red (n=1).

Evidence that NHI-1 inhibits cancer cell growth through induction of apoptotic cell death is provided in Figures 4.19 and 4.20. Live intact cells are reduced almost by half when treated with 300μM NHI-1 for either 24 or 48h compared to the untreated control samples. A large increase in apoptotic cells stained positive for annexin V was observed at both time points. At 24h a threefold increase of late apoptotic cells was presented. As regards the 48h time point the increase of cells in the upper left quadrant was more impressive at the fivefold level while a similar threefold increase was presented for late apoptotic cells.

The following charts illustrate the percentage of live, apoptotic and necrotic cell populations as quantified after cell cytometric analysis of MCF7 cells treated with the nine glycolytic inhibitors. Results are related to the respective populations of an untreated control. Figure 4.21 presents the results after a 24h treatment with the indicated inhibitors while in Figure 4.22 48h treatment's results are presented.

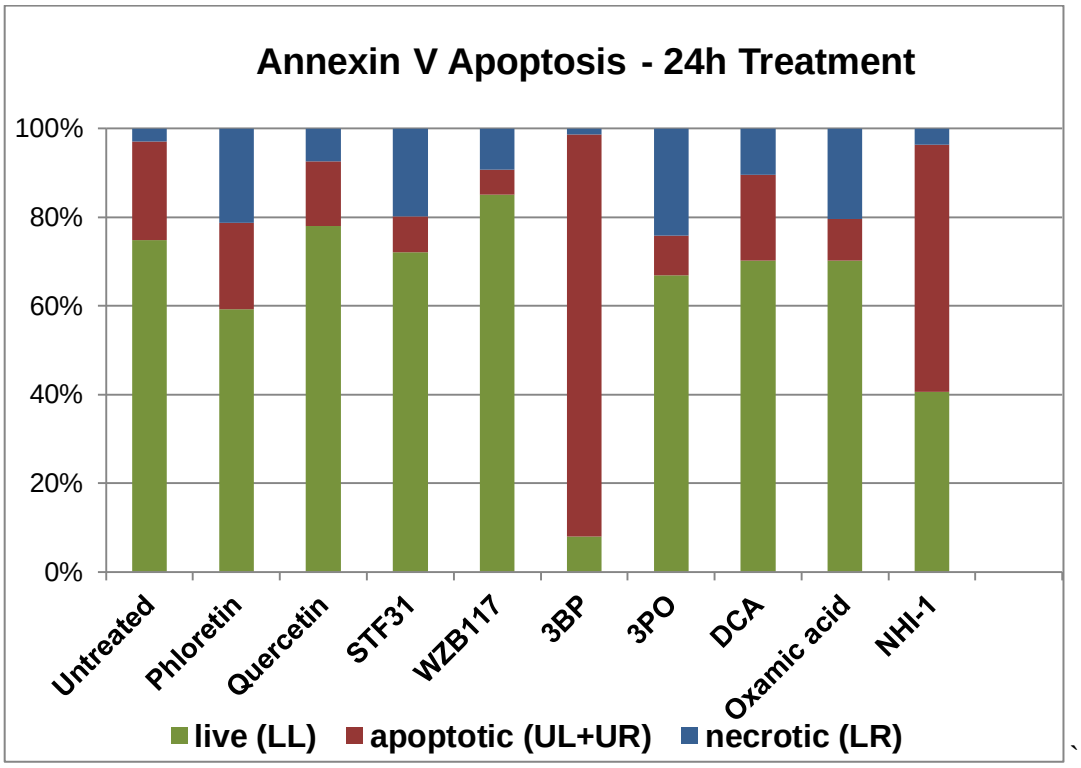

Figure 4.21: Quantification of percentages of apoptotic, necrotic and live MCF7 cells when treated with 9 glycolytic inhibitors for 24h compared to an untreated control, as generated through flow cytometric analysis.

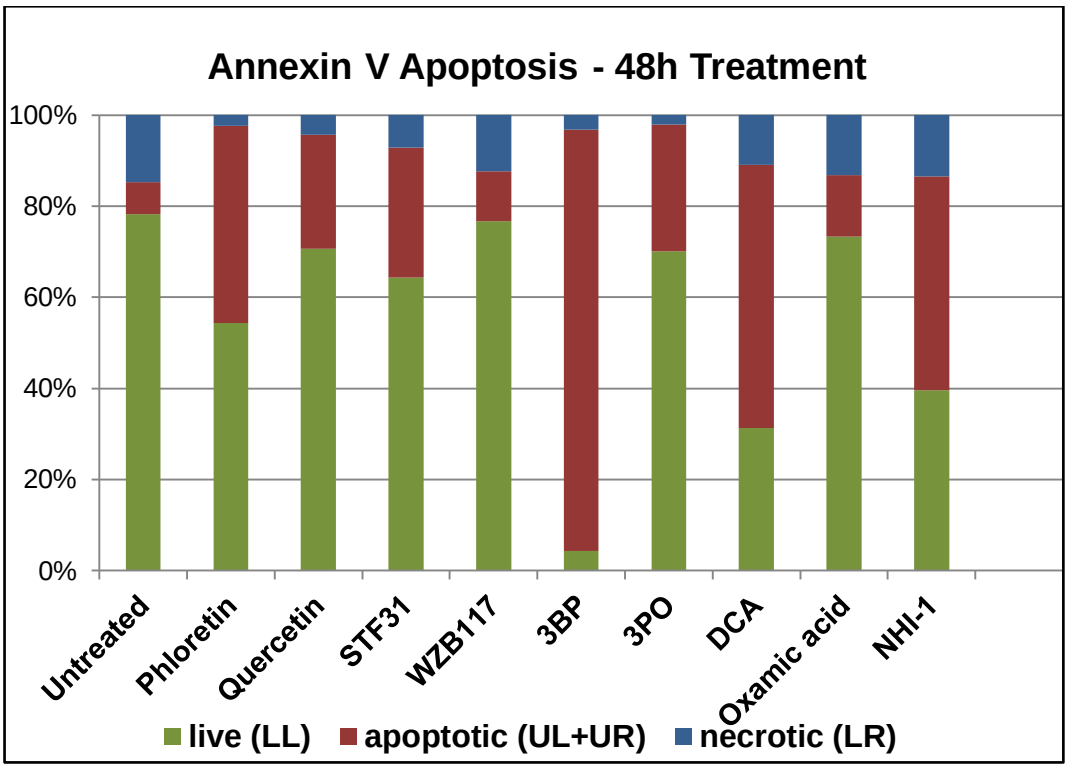

Figure 4.22: Quantification of percentages of apoptotic, necrotic and live MCF7 cells when treated with 9 glycolytic inhibitors for 48h compared to an untreated control, as generated through flow cytometric analysis.

4.2 The effect of glycolytic inhibitors on cell cycle progression

The cell cycle of eukaryotic cells consists of two separate stages; interphase and mitosis. Interphase includes three distinct phases, G1, S and G2 phases. During G1 phase (1st gap) cells grow and engage to increased biosynthetic activity. S phase is defined by DNA synthesis and cells replicate their chromosomal DNA. G2 phase (2nd gap) prepares cells for division and finally during Mitosis (M phase) each cell divides into two genetically identical daughter cells. G0 phase describes non proliferative quiescent fully differentiated cells [433]. For the purpose of the analysis here G0 and G1 phases, as well as G2 and M phases, are described as one phase as they have a uniform DNA content.

To assess whether treatment with various inhibitors of the glycolytic pathway had an impact on cell cycle progression flow cytometric analysis was performed. Propidium iodide (PI) a fluorescent dye that binds stoichiometrically to nucleic acids was used. Pre-treatment with

DNase-free Ribonuclease A enabled DNA specific binding. Through flow cytometry, the relative DNA content of samples treated with nine different glycolytic inhibitors for 24h was quantified. The histogram plots presented below show gated single cell populations according to their cellular DNA content. The PI fluorescent signal was proportional to the amount of DNA and separation of cells into three different categories was enabled. Cells during G0/G1 phase (P3), prior to DNA synthesis, have one set of paired chromosomes (diploid DNA). During S phase (P4) cells replicate their DNA and have variable DNA content, increased compared to the diploid chromosomal amount. In G2/M phase (P5) cells have already doubled their DNA content containing two sets of paired chromosomes (tetraploid DNA) [433, 434]. For these experiments fixed and permeabilised MCF7 breast cancer cells were used. Since great levels of cellular death were previously observed in the apoptosis flow cytometry analysis, lower concentrations of the compounds were used here to ensure the number of adherent live cells required to run the cell cycle analysis.

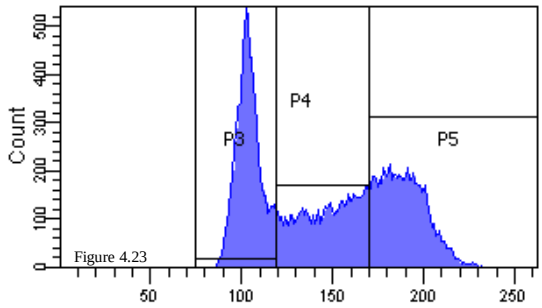

Untreated Cells	
G0/G1	36.4
S	29.6
G2/M	34

Figure 4.23: Flow cytometric analysis of cellular DNA content of untreated MCF7 breast cancer cells at 24h. In the histogram fluorescence of the DNA bound propidium iodide, indicating the DNA content in X- axis, is plotted against the number of cells in the Y-axis. The percentage of cells in each cell cycle phase is demonstrated on the right (n=1).

The DNA content of MCF7 breast cancer cells in exponential growth was analysed through flow cytometry. The variation of the fluorescence intensity of PI was used to differentiate cells in each phase of the cell cycle. The percentage of cells at the G0/G1 phase (P3) was calculated at 36.4% of the total cell population. Cells at the G2/M phase (P5), containing twice the amount of DNA of G1 cells, were calculated 34%. Finally 29.6% of the total cell population were at the S phase (P4) and had an intermediate amount of DNA between that of G1 and G2 cells (Figure 4.23). The cell cycle distribution of the untreated control was used as reference to develop an understanding of the mechanism of the antiproliferative action of the glycolytic inhibitors.

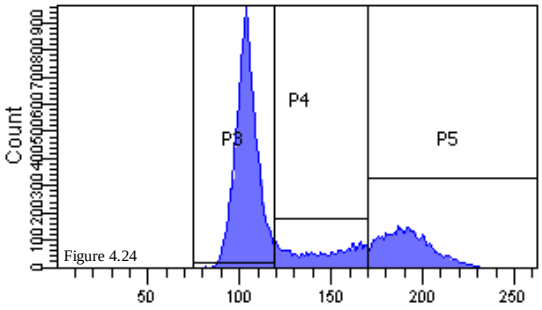

150µM Phloretin	
G0/G1	60.9
S	15.1
G2/M	24

Figure 4.24: Flow cytometric analysis of cellular DNA content of MCF7 breast cancer cells treated with 150µM Phloretin for 24h. In the histogram fluorescence of the DNA bound propidium iodide, indicating the DNA content in X- axis, is plotted against the number of cells in the Y-axis. The percentage of cells in each cell cycle phase is demonstrated on the right (n=1).

Figure 4.24 provides evidence that Phloretin inhibits MCF7 cancer cell growth through cell cycle arrest in G1 phase. Treatment with 150µM Phloretin for 24h caused an accumulation of cells in the G0/G1 phase and inhibited G1-S transition. As shown in the above figure the percentage of cells found in the G0/G1 phase almost doubled and a corresponding decrease of cells in the S and G2/M phases was observed. Percentage of cells in the S phase decreased to 15.1% and in the G2/M phase to 24% compared to 29.6 and 34% respectively in the untreated control.

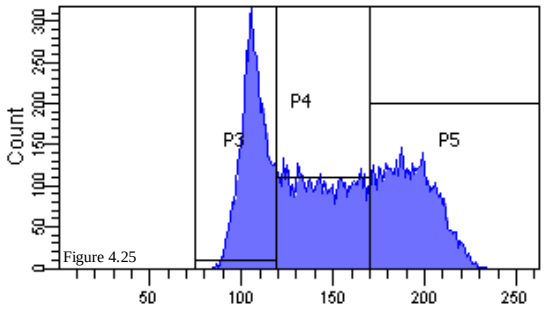

300µM Quercetin	
G0/G1	31
S	34.6
G2/M	34.4

Figure 4.25: Flow cytometric analysis of cellular DNA content of MCF7 breast cancer cells treated with 300µM Quercetin for 24h. In the histogram fluorescence of the DNA bound Propidium Iodide, indicating the DNA content in X- axis, is plotted against the number of cells in the Y-axis. The percentage of cells in each cell cycle phase is demonstrated on the right (n=1).

The percentage of MCF7 cells treated with 300µM Quercetin for 24h, in each stage of the cell cycle is presented in Figure 4.25. Quercetin treatment proved associated with cell cycle arrest in the S phase. The proportion of cells in the S phase was found 34.6% compared to 29.6% in the untreated control while percentage of cells in the G2/M phase remained unaffected. In contrast number of cells in the G0/G1 phase decreased from 36.4 to 31%.

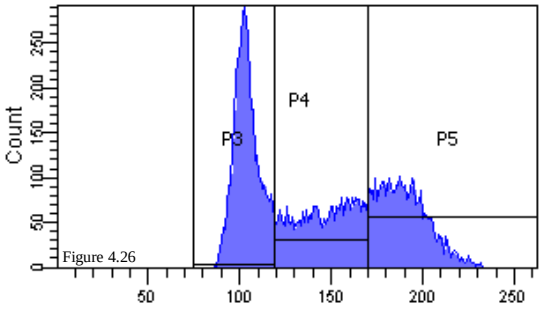

30µM STF31	
G0/G1	39
S	29.3
G2/M	31.7

Figure 4.26: Flow cytometric analysis of cellular DNA content of MCF7 breast cancer cells treated with 30µM STF31 for 24h. In the histogram fluorescence of the DNA bound propidium iodide, indicating the DNA content in X- axis, is plotted against the number of cells in the Y-axis. The percentage of cells in each cell cycle phase is demonstrated on the right (n=1).

The DNA histogram in Figure 4.26 illustrates the effect of STF31 on cell cycle progression. It shows that treatment with 30µM STF31 for 24h restricted cancer cells in the G0/G1 phase of the cell cycle. The number of cells in the G0/G1 phase increased by 7% compared to the untreated control while in the S phase remained the same.

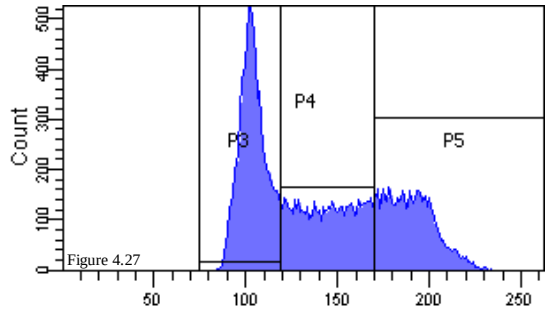

30µM WZB117	
G0/G1	40.5
S	31.3
G2/M	28.2

Figure 4.27: Flow cytometric analysis of cellular DNA content of MCF7 breast cancer cells treated with 30µM WZB117 for 24h. In the histogram fluorescence of the DNA bound propidium iodide, indicating the DNA content in X- axis, is plotted against the number of cells in the Y-axis. The percentage of cells in each cell cycle phase is demonstrated on the right (n=1).

Figure 4.27 depicts the DNA cell cycle profile of cells treated with 30µM WZB117 for 24h. Following WZB117 treatment cells appeared to arrest in the G0/G1 and S phases. The percentage of cells in the G0/G1 and S phases increased by 11 and 5% respectively compared to the untreated cells. Accordingly a profound decline of cells in the G2/M phase, from 34 to 28.2% was detected.

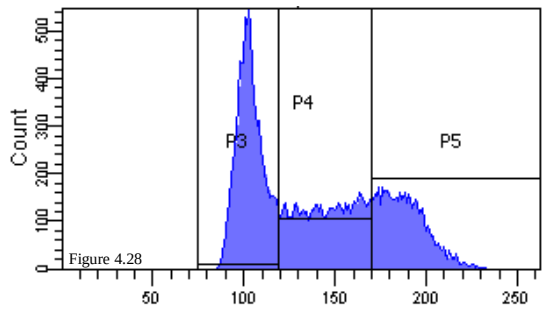

50µM 3-bromopyruvate	
G0/G1	41.4
S	32
G2/M	26.6

Figure 4.28: Flow cytometric analysis of cellular DNA content of MCF7 breast cancer cells treated with 50µM 3-bromopyruvate for 24h. In the histogram fluorescence of the DNA bound propidium iodide, indicating the DNA content in X- axis, is plotted against the number of cells in the Y-axis. The percentage of cells in each cell cycle phase is demonstrated on the right (n=1).

The DNA content frequency histogram generated through flow cytometry analysis of MCF7 cells treated with 50µM 3BP is depicted in Figure 4.28. It can be observed that a 24h hour treatment with 3BP resulted in an evident arrest in the G0/G1 and S phases of the cell cycle. The proportion of cells in these phases increased 14 and 8% respectively compared to the untreated sample. Progression to cell division was strongly inhibited which was demonstrated by a 22% reduction of cells in G2/M phase.

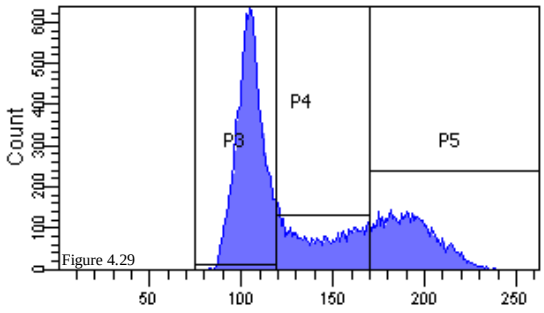

15µM 3PO	
G0/G1	52.1
S	21.8
G2/M	26.1

Figure 4.29: Flow cytometric analysis of cellular DNA content of MCF7 breast cancer cells treated with 15µM 3PO for 24h. In the histogram fluorescence of the DNA bound propidium iodide, indicating the DNA content in X- axis, is plotted against the number of cells in the Y-axis. The percentage of cells in each cell cycle phase is demonstrated on the right (n=1).

Figure 4.29 illustrates the quantitation of DNA content of MCF7 cells treated with 15µM 3PO for 24h. Cells presented a clear arrest in the G1 phase while progression to DNA replication and the later stages of the cell cycle were restricted. An accumulation of cells in the G0/G1 phase was observed, with the number of cells increased by 43% compared to the untreated control. Cell numbers in the S and G2/M phases appeared decreased and were calculated at 21.8 and 26.1% respectively compared to 29.6 and 34% that were initially seen in controls.

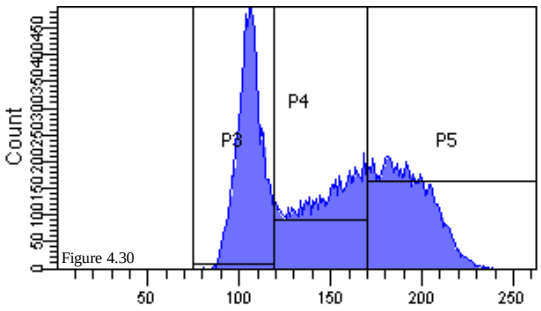

100mM Dichloroacetate	
G0/G1	33.8
S	30.9
G2/M	35.3

Figure 4.30: Flow cytometric analysis of cellular DNA content of MCF7 breast cancer cells treated with 100mM Dichloroacetate for 24h. In the histogram fluorescence of the DNA bound propidium iodide, indicating the DNA content in X- axis, is plotted against the number of cells in the Y-axis. The percentage of cells in each cell cycle phase is demonstrated on the right (n=1).

Figure 4.30 demonstrates that DCA treatment did not have a remarkable effect on cell cycle progression. A 24h treatment with 100mM DCA increased the cell number in the S and G2/M phases from 29.6 to 30.9% and from 34 to 35.3% respectively compared to the untreated control. However these shifts are only marginal and cannot substantiate a cell cycle arrest.

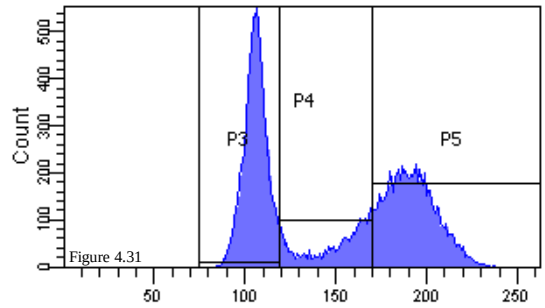

100mM Oxamic acid	
G0/G1	43.8
S	14.3
G2/M	41.9

Figure 4.31: Flow cytometric analysis of cellular DNA content of MCF7 breast cancer cells treated with 100mM Oxamic acid for 24h. In the histogram fluorescence of the DNA bound propidium iodide, indicating the DNA content in X- axis, is plotted against the number of cells in the Y-axis. The percentage of cells in each cell cycle phase is demonstrated on the right (n=1).

The histogram plot in Figure 4.31 was generated through PI flow cytometric analysis of MCF7 cells treated with 100mM Oxamic acid for 24h. It can be observed that treatment with the LDH inhibitor induced a cell cycle arrest in G0/G1 and G2/M phases. The proportion of cells in these two phases was increased by 20 and 23% respectively while the percentage of cells in the DNA replication phase was reduced by half compared to the untreated control.

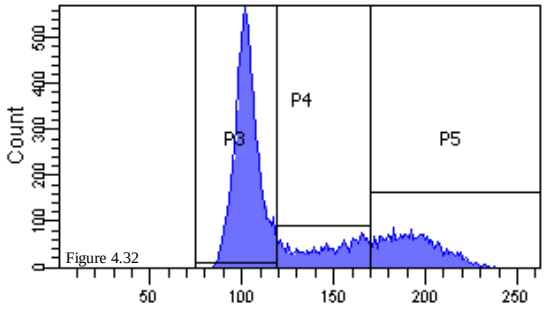

Figure 4.32

150µM NHI-1	
G0/G1	60.5
S	17.2
G2/M	22.3

Figure 4.32: Flow cytometric analysis of cellular DNA content of MCF7 breast cancer cells treated with 150µM NHI-1 for 24h. In the histogram fluorescence of the DNA bound propidium iodide, indicating the DNA content in X- axis, is plotted against the number of cells in the Y-axis. The percentage of cells in each cell cycle phase is demonstrated on the right (n=1).

The analysis of cell cycle progression with PI DNA staining of MCF7 cells treated with 150µM NHI-1 for 24h is depicted in Figure 4.32. It can be observed that the anticancer effect of the novel LDHA inhibitor can be correlated with an apparent cell cycle arrest in the G1 phase. Cells in the G1 phase increased by 66% compared to the untreated control while cells in the S and G2/M phases declined to 17.2 and 22.3% respectively from 29.6 and 34%.

The following chart illustrates the proportion of cells in the G0/G1, S and G2/M phases of the cell cycle as quantified after cell cytometric analysis of MCF7 cells treated with the nine glycolytic inhibitors for 24h. Results are related to the respective populations of an untreated control.

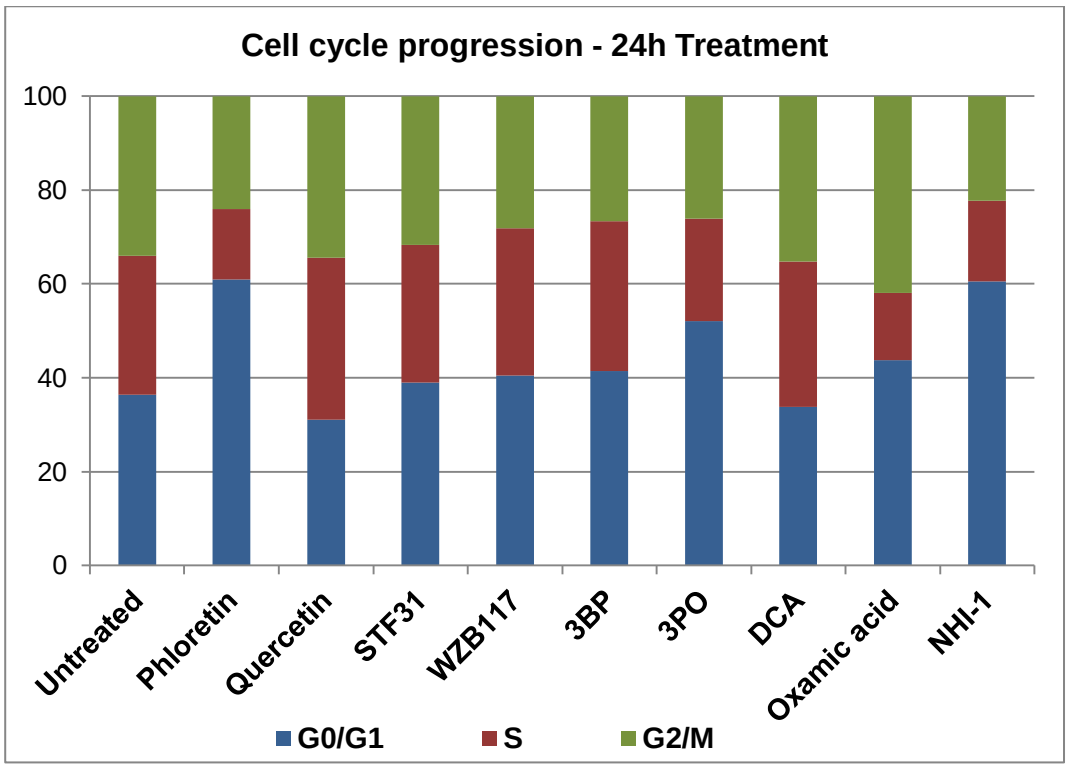

Figure 4.33: Quantification of percentages of MCF7 cells in the G0/G1, S and G2/M phases of the cell cycle when treated with 9 glycolytic inhibitors for 24h compared to an untreated control, as generated through flow cytometric analysis.

4.3 The effect of glycolytic inhibitors on glucose uptake & lactate production

The next aim of this chapter was to investigate the effect of the selected array of compounds as inhibitors of the glycolytic pathway. Glucose is the 'fuel' of the glycolytic pathway while lactate is its final end product; therefore the effect of the glycolytic inhibitors on glucose uptake and lactate production was examined. Taken together, these two measurements provide an indication of the activity of the pathway. Two breast cancer cell lines were selected for these experiments; MCF7 and HBL100. Breast cancer cells were treated for 24h with each of the glycolytic inhibitors and then the culture medium was collected. In these samples the concentrations of both glucose and lactate were measured. The following figures depict the amount of glucose (in green colour) and the amount of lactate (in red colour) measured in the culture medium of the indicated breast cancer cell line when treated with each of the glycolytic inhibitors for 24 h. A range of three different concentrations of each of the compounds was used; selected by taking into consideration the corresponding IC_{50} concentration determined from the SRB assays (Table 3.2, section 3.2). Low concentrations were used to minimise the antiproliferative effect of the compounds. Measurements were

compared to an untreated control using one-way ANOVA and the Tukey-Kramer multiple comparisons test.

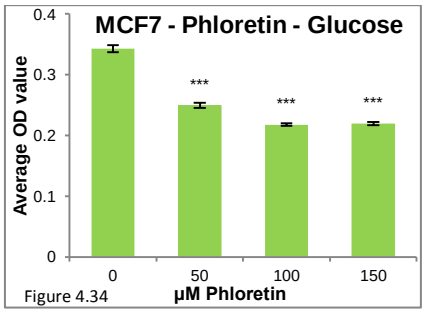

Figure 4.34

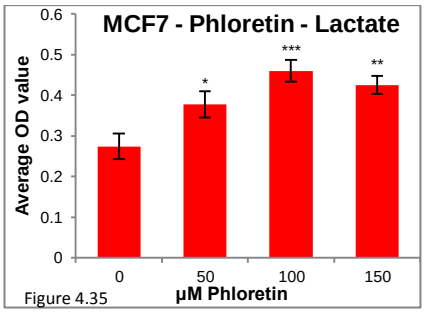

Figure 4.35

Figures 4.34 & 4.35: Extracellular glucose (in green colour) remaining in the culture medium of MCF7 breast cancer cells in parallel with lactate production (in red colour) after a 24h treatment with 50, 100 or 150µM Phloretin. Mean results of 3 replicates are reported and error bars represent standard deviations. Statistical significance indications: * P<0.05, ** P<0.01, *** P<0.001 compared with untreated control (one-way ANOVA followed by Tukey-Kramer multiple comparisons test). Representative data of 2 independent experiments are presented.

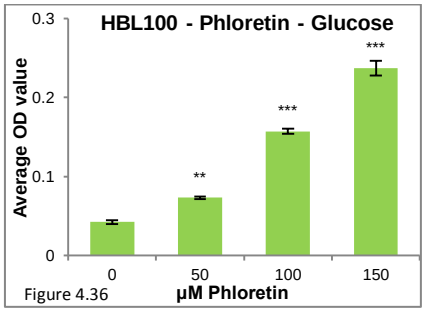

Figure 4.36

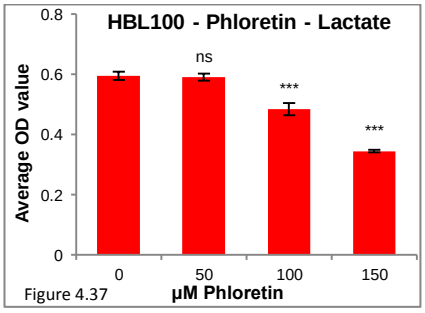

Figure 4.37

Figures 4.36 & 4.37: Extracellular glucose (in green colour) remaining in the culture medium of HBL100 breast cancer cells in parallel with lactate production (in red colour) after a 24h treatment with 50, 100 or 150µM Phloretin. Mean results of 3 replicates are reported and error bars represent standard deviations. Statistical significance indications: ns not significant P>0.05, ** P<0.01, *** P<0.001 compared with untreated control (one-way ANOVA followed by Tukey-Kramer multiple comparisons test). Representative data of 2 independent experiments are presented.

Phloretin has been described as an inhibitor of glucose transmembrane transport [277]. However, Phloretin had a differential effect in the two examined breast cancer cell lines. As shown in Figures 4.34 and 4.35, Phloretin treatment decreased the amount of glucose remaining in the culture medium of MCF7 cells and also increased the production of lactate. This is the opposite result expected from an inhibitor targeting the glycolytic pathway. Conversely, Phloretin treatment had the anticipated effect on HBL100 cells where increasing concentrations of Phloretin caused an increase in the concentration of glucose measured in the culture medium after a 24h treatment and a decrease in the production of lactate (Figures 4.36&4.37).

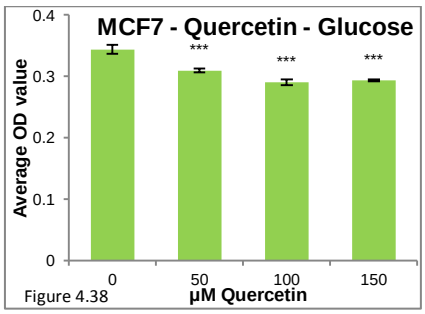

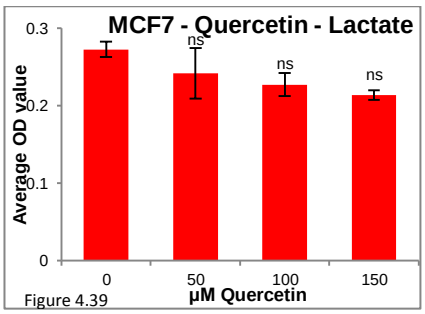

Figures 4.38 & 4.39: Extracellular glucose (in green colour) remaining in the culture medium of MCF7 breast cancer cells in parallel with lactate production (in red colour) after a 24h treatment with 50, 100 or 150µM Quercetin. Mean results of 3 replicates are reported and error bars represent standard deviations. Statistical significance indications: ns not significant P>0.05, *** P<0.001 compared with untreated control (one-way ANOVA followed by Tukey-Kramer multiple comparisons test). Representative data of 2 independent experiments are presented.

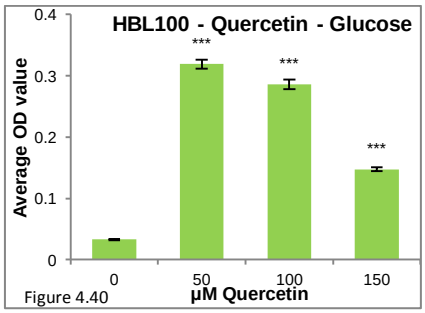

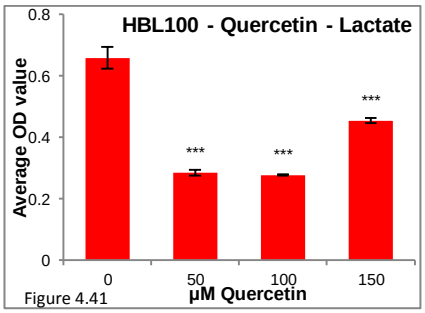

Figures 4.40 & 4.41: Extracellular glucose (in green colour) remaining in the culture medium of HBL100 breast cancer cells in parallel with lactate production (in red colour) after a 24h treatment with 50, 100 or 150µM Quercetin. Mean results of 3 replicates are reported and error bars represent standard deviations. Statistical significance indications: ns not significant P>0.05, *** P<0.001 compared with untreated control (one-way ANOVA followed by Tukey-Kramer multiple comparisons test). Representative data of 2 independent experiments are presented.

Similarly to Phoretin, the two breast cancer cell lines responded differently to the second flavonoid Quercetin, which is also reputed to inhibit glucose transport [277]. As shown in Figures 4.38 and 4.39, Quercetin caused a reduction in the leftover concentration of glucose and had no significant effect on the measurement of lactate in the culture medium of MCF7 cells. In contrast, HBL100 cells responded as would be anticipated to a glycolytic inhibitor. Quercetin treatment resulted in a large increase of the remaining glucose and a concurrent depletion of the lactate produced (Figures 4.40 and 4.41). An interesting unexpected observation is that 150µM Quercetin seem to have a lesser effect on the glucose and lactate levels of this cell line compared to the lower concentrations of the compound.

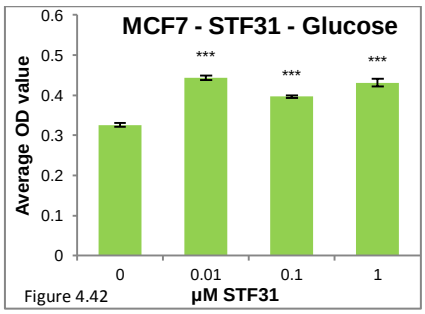

Figure 4.42

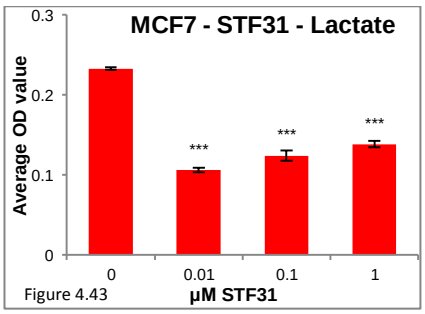

Figure 4.43

Figures 4.42 & 4.43: Extracellular glucose (in green colour) remaining in the culture medium of MCF7 breast cancer cells in parallel with lactate production (in red colour) after a 24h treatment with 0.01, 0.1 or 1µM STF31. Mean results of 3 replicates are reported and error bars represent standard deviations. Statistical significance indication: *** P<0.001 compared with untreated control (one-way ANOVA followed by Tukey-Kramer multiple comparisons test).

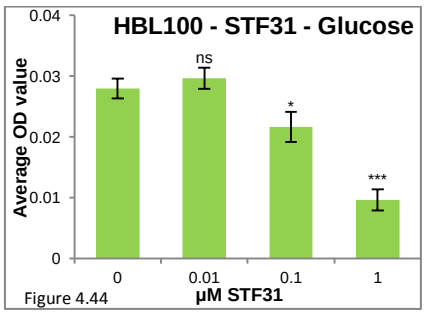

Figure 4.44

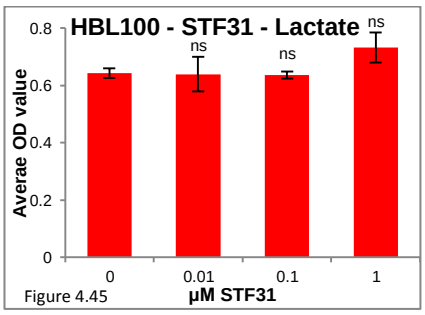

Figure 4.45

Figures 4.44 & 4.45: Extracellular glucose (in green colour) remaining in the culture medium of HBL100 breast cancer cells in parallel with lactate production (in red colour) after a 24h treatment with 0.01, 0.1 or 1µM STF31. Mean results of 3 replicates are reported and error bars represent standard deviations. Statistical significance indications: ns not significant P>0.05, * P<0.05, *** P<0.001 compared with untreated control (one-way ANOVA followed by Tukey-Kramer multiple comparisons test). Representative data of 2 independent experiments are presented.

Figures 4.42 to 4.45 illustrate the effect of the GLUT1 inhibitor STF31 on glucose uptake and lactate production of MCF7 and HBL100 cells respectively. STF31 treatment led to accumulation of glucose in the culture medium of MCF7 cells coupled with a significant reduction in lactate generation. On the other hand HBL100 cells demonstrated an unexpected decrease in glucose concentrations while lactate production remained unaffected by STF31 treatment.

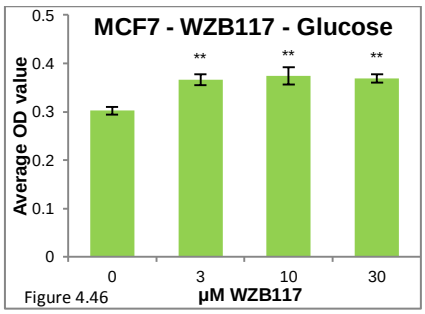

Figure 4.46

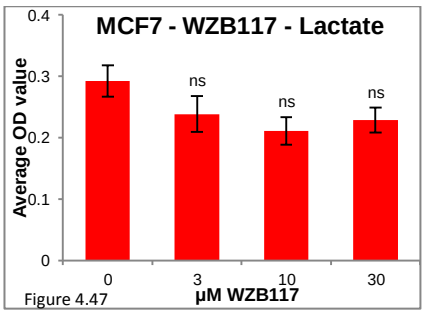

Figure 4.47

Figures 4.46 & 4.47: Extracellular glucose (in green colour) remaining in the culture medium of MCF7 breast cancer cells in parallel with lactate production (in red colour) after a 24h treatment with 3, 10 or 30µM WZB117. Mean results of 3 replicates are reported and error bars represent standard deviations. Statistical significance indications: ns not significant P>0.05, ** P<0.01 compared with untreated control (one-way ANOVA followed by Tukey-Kramer multiple comparisons test). Representative data of 3 independent experiments are presented.

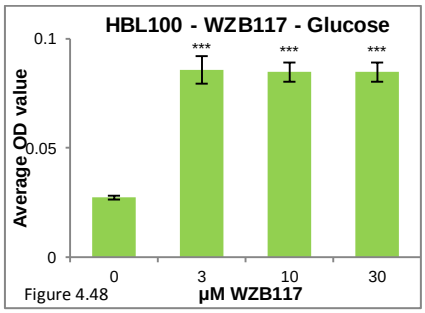

Figure 4.48

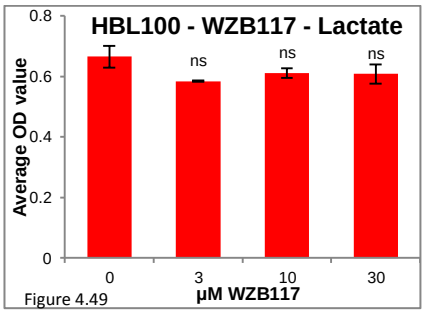

Figure 4.49

Figures 4.48 & 4.49: Extracellular glucose (in green colour) remaining in the culture medium of HBL100 breast cancer cells in parallel with lactate production (in red colour) after a 24h treatment with 3, 10 or 30µM WZB117. Mean results of 3 replicates are reported and error bars represent standard deviations. Statistical significance indications: ns not significant P>0.05, *** P<0.001 compared with untreated control (one-way ANOVA followed by Tukey-Kramer multiple comparisons test). Representative data of 3 independent experiments are presented.

Figures 4.46 and 4.48 reveal that the GLUT1 inhibitor WZB117 induced accumulation of glucose in the culture medium of both breast cancer cell lines. Even the lowest tested concentration of 3µM was adequate to cause the maximal observed effect and higher concentrations did not cause any additional increase. The effect was more profound on HBL100 cells ($p<0.001$). In contrast no statistically significant differences were detected in lactate production after WZB117 treatment in both cell lines (Figures 4.47&4.49).

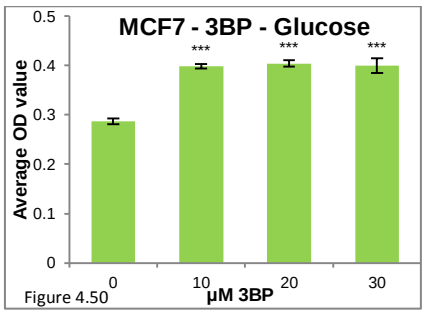

Figure 4.50

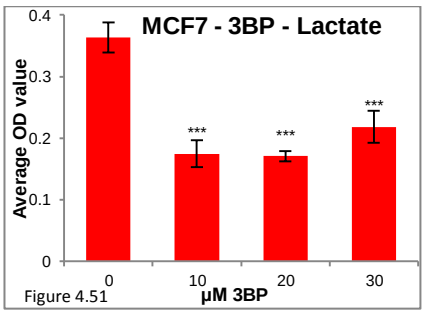

Figure 4.51

Figures 4.50 & 4.51: Extracellular glucose (in green colour) remaining in the culture medium of MCF7 breast cancer cells in parallel with lactate production (in red colour) after a 24h treatment with 10, 20 or 30µM 3-bromopyruvate. Mean results of 3 replicates are reported and error bars represent standard deviations. Statistical significance indication: *** P<0.001 compared with untreated control (one-way ANOVA followed by Tukey-Kramer multiple comparisons test). Representative data of 3 independent experiments are presented.

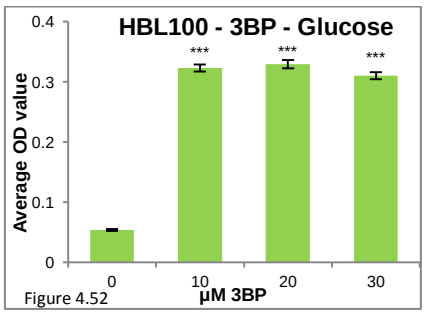

Figure 4.52

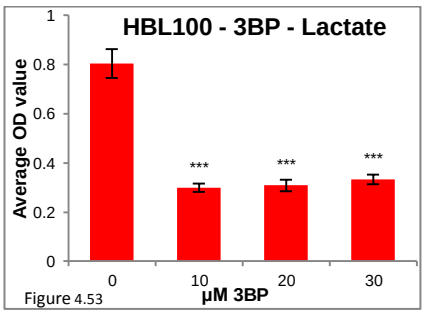

Figure 4.53

Figures 4.52 & 4.53: Extracellular glucose (in green colour) remaining in the culture medium of HBL100 breast cancer cells in parallel with lactate production (in red colour) after a 24h treatment with 10, 20 or 30µM 3-bromopyruvate. Mean results of 3 replicates are reported and error bars represent standard deviations. Statistical significance indication: *** P<0.001 compared with untreated control (one-way ANOVA followed by Tukey-Kramer multiple comparisons test). Representative data of 3 independent experiments are presented.

As shown in Figures 4.50 to 4.53, the HKII inhibitor 3BP had a marked impact on glucose and lactate measurements in the culture medium of both MCF7 and HBL100 cells. The effect was consistent with inhibition of the glycolytic pathway. In both cell lines a large increase in glucose combined with a massive reduction in the secreted lactate can be observed. The lowest tested concentration of 10µM 3BP produced a maximal effect and with higher concentrations no additional response could be detected.

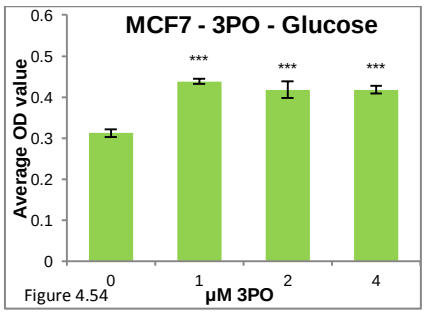

Figure 4.54

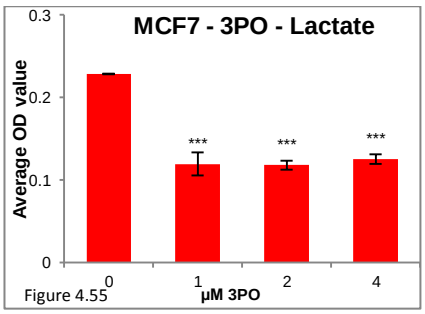

Figure 4.55

Figures 4.54 & 4.55: Extracellular glucose (in green colour) remaining in the culture medium of MCF7 breast cancer cells in parallel with lactate production (in red colour) after a 24h treatment with 1, 2 or 3µM 3PO. Mean results of 3 replicates are reported and error bars represent standard deviations. Statistical significance indication: *** P<0.001 compared with untreated control (one-way ANOVA followed by Tukey-Kramer multiple comparisons test). Representative data of 3 independent experiments are presented.

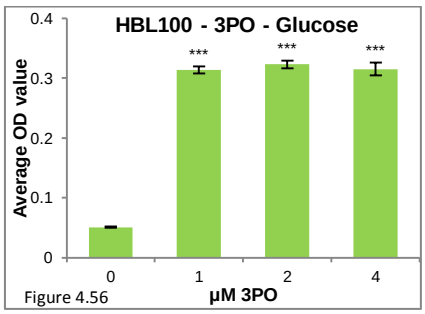

Figure 4.56

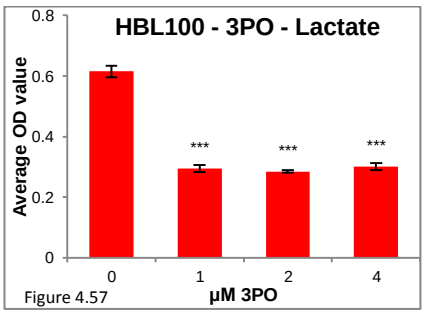

Figure 4.57

Figures 4.54 & 4.55: Extracellular glucose (in green colour) remaining in the culture medium of HBL100 breast cancer cells in parallel with lactate production (in red colour) after a 24h treatment with 1, 2 or 3µM 3PO. Mean results of 3 replicates are reported and error bars represent standard deviations. Statistical significance indication: *** P<0.001 compared with untreated control (one-way ANOVA followed by Tukey-Kramer multiple comparisons test). Representative data of 3 independent experiments are presented.

In Figures 4.54 to 4.57, evidence is provided that 3PO effectively blocks the glycolytic pathway. Treatment with the PFKFB3 inhibitor resulted in accumulation of glucose, which was more notable in HBL100 cells, while lactate production decreased to 50% compared to the untreated controls in both cell lines. Interestingly, after treatment with a concentration as low as 1µM the inhibition of the pathway reached a plateau.

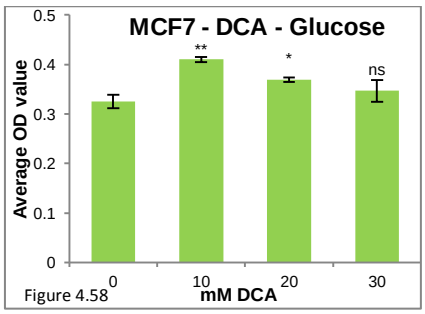

Figure 4.58

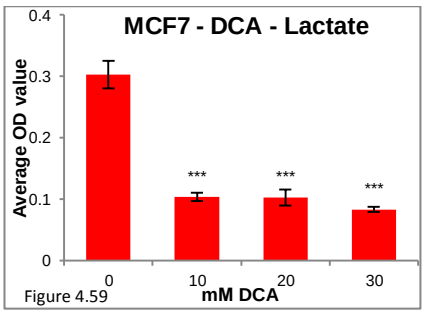

Figure 4.59

Figures 4.58 & 4.59: Extracellular glucose (in green colour) remaining in the culture medium of MCF7 breast cancer cells in parallel with lactate production (in red colour) after a 24h treatment with 10, 20 or 30mM Dichloroacetate. Mean results of 3 replicates are reported and error bars represent standard deviations. Statistical significance indications: ns not significant P>0.05, * P<0.05, ** P<0.01, *** P<0.001 compared with untreated control (one-way ANOVA followed by Tukey-Kramer multiple comparisons test). Representative data of 2 independent experiments are presented.

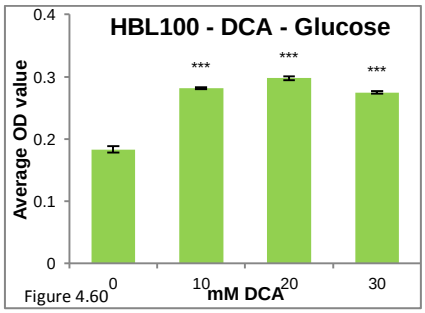

Figure 4.60

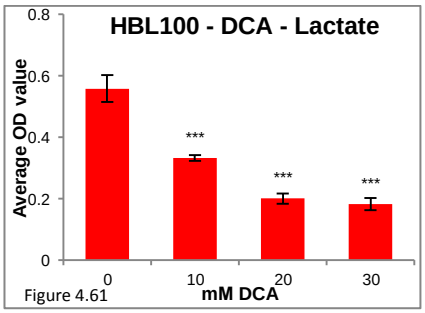

Figure 4.61

Figures 4.60 & 4.61: Extracellular glucose (in green colour) remaining in the culture medium of HBL100 breast cancer cells in parallel with lactate production (in red colour) after a 24h treatment with 10, 20 or 30mM Dichloroacetate. Mean results of 3 replicates are reported and error bars represent standard deviations. Statistical significance indications: ns not significant P>0.05, * P<0.05, ** P<0.01, *** P<0.001 compared with untreated control (one-way ANOVA followed by Tukey-Kramer multiple comparisons test). Representative data of 2 independent experiments are presented.

Figures 4.58 to 4.61 confirm that PDHK1 inhibition suppresses glycolysis. DCA increased the concentration of glucose that remained in the culture medium after a 24h treatment in both breast cancer cells lines. It is noteworthy that the accumulation of glucose for HBL100 cells was more significant compared to MCF7. Regarding the results obtained from the lactate assay DCA reduced the amount of lactate produced to 30% in both cell lines compared to the untreated controls.

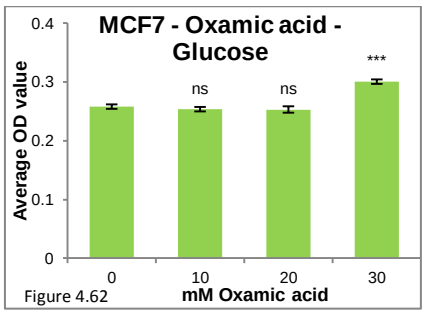

Figure 4.62

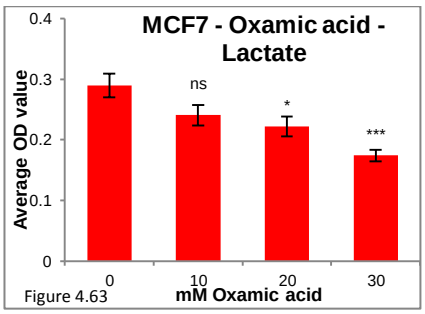

Figure 4.63

Figures 4.62 & 4.63: Extracellular glucose (in green colour) remaining in the culture medium of MCF7 breast cancer cells in parallel with lactate production (in red colour) after a 24h treatment with 10, 20 or 30mM Oxamic acid. Mean results of 3 replicates are reported and error bars represent standard deviations. Statistical significance indications: ns not significant P>0.05, * P<0.05, *** P<0.001 compared with untreated control (one-way ANOVA followed by Tukey-Kramer multiple comparisons test). Representative data of 3 independent experiments are presented.

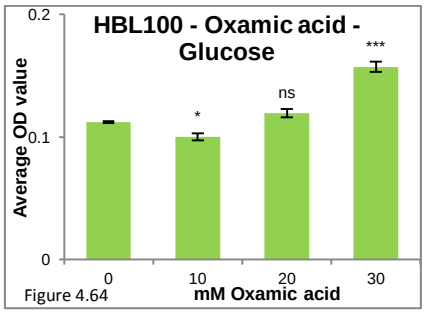

Figure 4.64

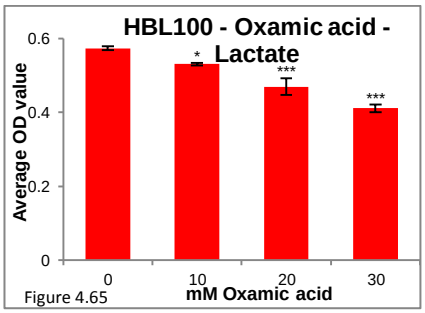

Figure 4.65

Figures 4.64 & 4.65: Extracellular glucose (in green colour) remaining in the culture medium of HBL100 breast cancer cells in parallel with lactate production (in red colour) after a 24h treatment with 10, 20 or 30mM Oxamic acid. Mean results of 3 replicates are reported and error bars represent standard deviations. Statistical significance indications: ns not significant P>0.05, * P<0.05, *** P<0.001 compared with untreated control (one-way ANOVA followed by Tukey-Kramer multiple comparisons test). Representative data of 3 independent experiments are presented.

Figures 4.62 to 4.65 demonstrate that LDH inhibition leads to blockade of the glycolytic pathway. A high concentration of 30mM Oxamic acid was required for both breast cancer cell lines to induce a statistically significant accumulation of glucose. In contrast it can be observed that increasing concentrations of Oxamic acid resulted in decreasing lactate production up to 60 and 70% for MCF7 and HBL100 cells respectively.

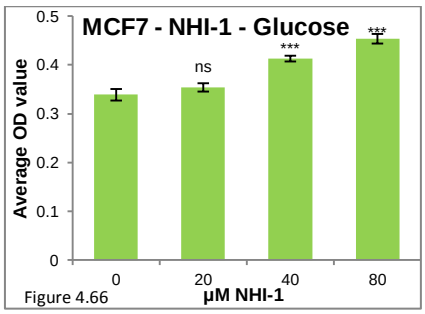

Figure 4.66

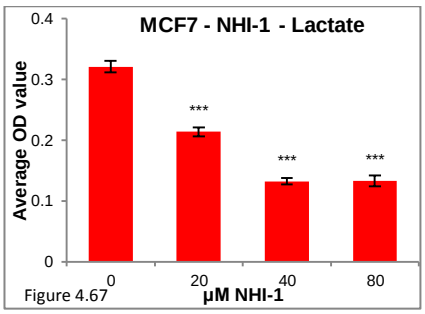

Figure 4.67

Figures 4.66 & 4.67: Extracellular glucose (in green colour) remaining in the culture medium of MCF7 breast cancer cells in parallel with lactate production (in red colour) after a 24h treatment with 20, 40 or 80µM NHI-1. Mean results of 3 replicates are reported and error bars represent standard deviations. Statistical significance indications: ns not significant P>0.05, *** P<0.001 compared with untreated control (one-way ANOVA followed by Tukey-Kramer multiple comparisons test). Representative data of 2 independent experiments are presented.

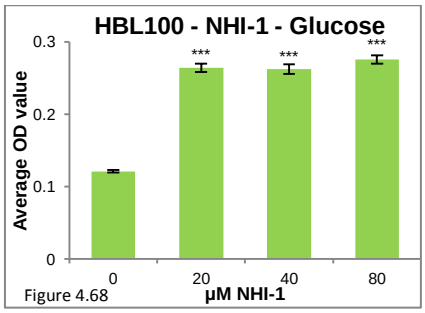

Figure 4.68

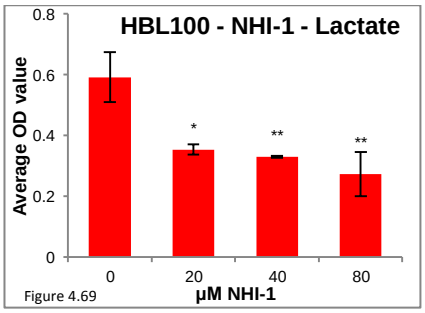

Figure 4.69

Figures 4.68 & 4.69: Extracellular glucose (in green colour) remaining in the culture medium of HBL100 breast cancer cells in parallel with lactate production (in red colour) after a 24h treatment with 20, 40 or 80µM NHI-1. Mean results of 3 replicates are reported and error bars represent standard deviations. Statistical significance indications: * P<0.05, ** P<0.01, *** P<0.001 compared with untreated control (one-way ANOVA followed by Tukey-Kramer multiple comparisons test). Representative data of 2 independent experiments are presented.

The effects of NHI-1 on glucose uptake and lactate production on the breast cancer cell lines are compared in Figures 4.66 to 4.69. As expected from an inhibitor targeting LDHA, NHI-1 treatment caused a marked depletion of lactate in the culture medium. Lactate production was found decreased to around 40% in both cell lines compared to the untreated controls. The effect of NHI-1 treatment on glucose uptake of MCF7 cells was modest. Only the higher concentrations of 40 and 80µM resulted in a statistically significant increase of the remaining glucose in the culture medium. In contrast regarding HBL100 cells, 20µM of NHI-1 was adequate to result in a great accumulation of glucose.

4.4 Knockdown of selected glycolytic enzymes

To further elucidate the role of glycolytic enzymes and evaluate them as potential therapeutic targets for cancer treatment, gene downregulation was attempted. Two promising targets at the top and bottom of the glycolytic pathway, GLUT1 and LDHA, were selected for assessment after their inhibitors had been investigated (Chapter 3 section 3.2 growth inhibition, Chapter 4 apoptosis induction, cell cycle arrest, inhibition of the glycolytic pathway).

siRNA mediated gene knockdown was utilised to examine the glycolytic targets of interest. Four different predesigned siRNA oligos and a pool with a mixture of the four sequences were utilised as described in Chapter 2 section 2.8. MCF7 and MDA-MB-231 breast cancer cells were used for transfection experiments. An optimisation process was followed to identify the optimal conditions achieving high transfection efficiency coupled with minimal cellular toxicity. Three controls were used in every experiment; untreated cells, mock cells treated only with transfection reagent as well as a negative control transfected with a non-targeting random sequence. Lysates of transfected samples were collected and efficiency of knockdown was assessed at the protein level through Western blotting.

4.4.1 GLUT1 knockdown

Efficient GLUT1 knockdown was not achieved in the present study even though a thorough optimisation process was followed. Several cell densities of two breast cancer cell lines were tried combined with three different volumes of the transfection reagent as recommended by the manufacturer. A concentration range (5, 10, 25, 50, 100nM) was used for each of the single oligonucleotides and the pool and also transfection duration of 24, 48, 72 and 120h was attempted. Unfortunately none of these was successful. A representative result of a 72h transfection of MCF7 breast cancer cells is presented below in Figure 4.70. GLUT1 expression in the transfected samples remained unaffected compared to expression in mock treated cells.

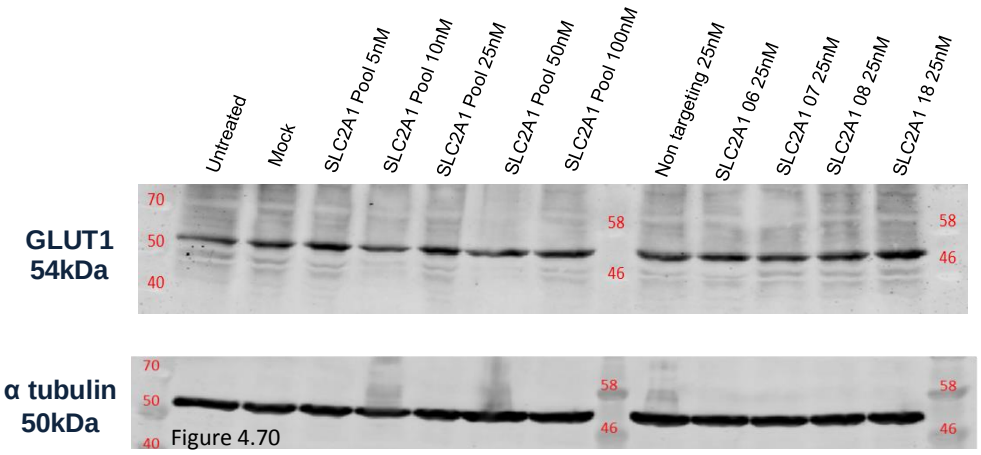

Figure 4.70: GLUT1 protein expression detected through Western blotting in MCF7 siRNA transfected cells. Transfection lasted for 72h and the following siRNA sequences were used: non targeting (25nM), SLC2A1 Pool (5, 10, 25, 50, 100nM), SLC2A1 06 (25nM), SLC2A1 07 (25nM), SLC2A1 08 (25nM) and SLC2A1 18 (25nM). Expression was compared to mock cells, treated only with transfection reagent. Alpha tubulin was used as a loading control. Representative data of 12 independent experiments are presented.

4.4.2 LDHA knockdown

In contrast to GLUT1, significant LDHA knockdown was achieved after targeting with oligonucleotides specific to LDHA. Different concentrations of the four siRNA sequences and the pool of the four sequences combined were tried under various conditions. Optimal conditions allowing high transfection efficiency were identified. A representative Western blot from the optimisation process is presented in Figure 4.71. The densitometric analysis of a 96h transfection experiment of MCF7 cells is depicted in Figure 4.72. It can be observed that transfection with the pool or with two of the sequences as single oligonucleotides resulted in significant LDHA knockdown. The two sequences that gave optimal results were selected for further experiments. The sequence 06 at 25nM and the sequence 08 at 50nM reduced LDHA expression to 19 and 5% respectively compared to mock treated cells.

Similar results were also obtained for MDA-MB-231 breast cancer cells. The respective immunoblots and the normalised expression analysis for the triple negative cell line are presented in Figures 4.73 and 4.74. These demonstrate that the two selected sequences, after a 96h transfection period, reduced LDHA expression to 7 and 9% respectively.

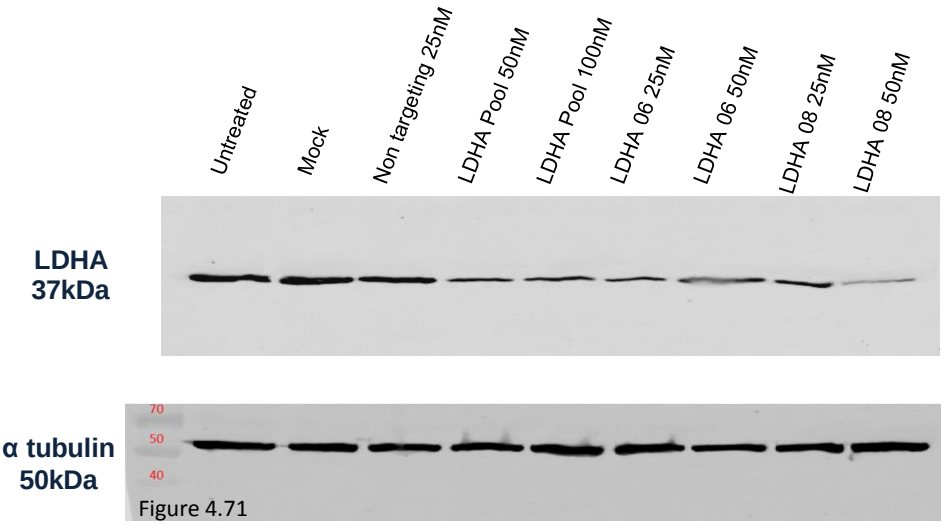

Figure 4.71: LDHA protein expression detected through Western blotting in MCF7 siRNA transfected cells. Transfection lasted for 96h and the following siRNA sequences were used: non targeting (25nM), LDHA Pool (50, 100nM), LDHA 06 (25, 50nM) and LDHA 08 (25, 50nM). Expression was compared to mock cells, treated only with transfection reagent. Alpha tubulin was used as a loading control. Representative data of 5 independent experiments are presented.

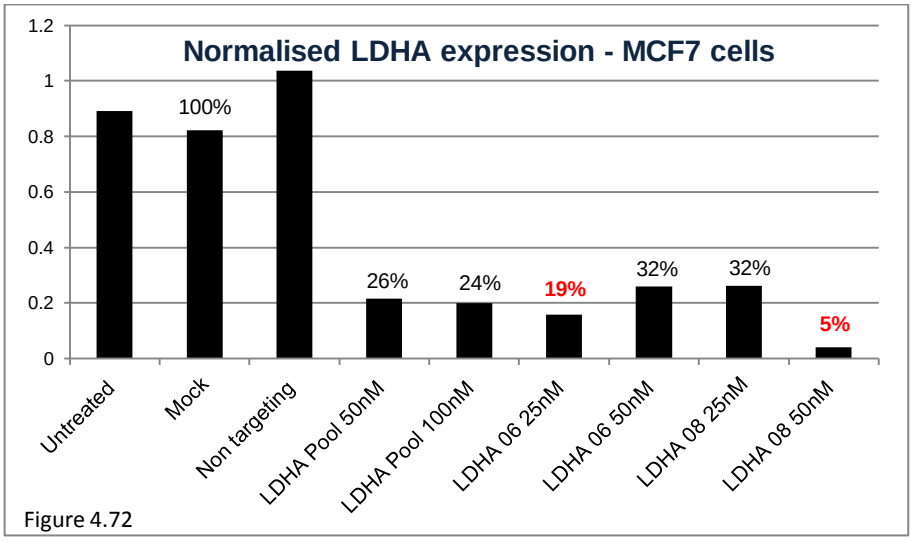

Figure 4.72: LDHA protein expression detected through Western blotting in MCF7 siRNA transfected cells. Transfection lasted for 96h and the following siRNA sequences were used: non targeting (25nM), LDHA Pool (50, 100nM), LDHA 06 (25, 50nM) and LDHA 08 (25, 50nM). Expression was compared to mock cells, treated only with transfection reagent (percentages shown). Densitometry analysis was conducted using the Odyssey Infrared Imaging System software (Licor) and data were normalised to α tubulin expression.

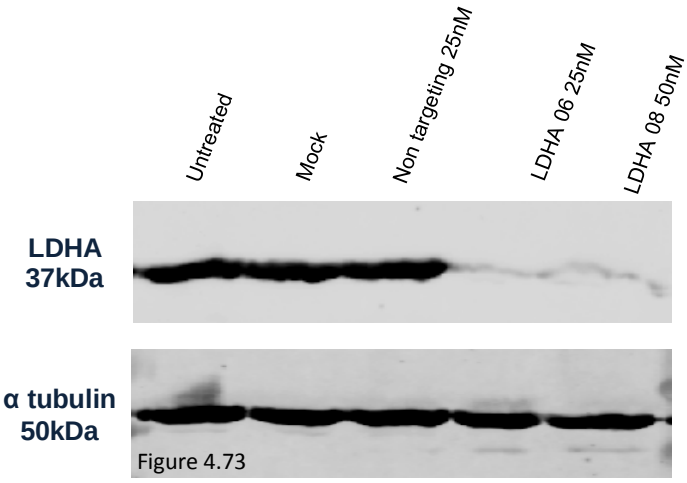

Figure 4.73: LDHA protein expression detected through Western blotting in MDA-MB-231 siRNA transfected cells. Transfection lasted for 96h and the following siRNA sequences were used: non targeting (25nM), LDHA 06 (25nM) and LDHA 08 (50nM). Expression was compared to mock cells, treated only with transfection reagent. Alpha tubulin was used as a loading control. Representative data of 5 independent experiments are presented.

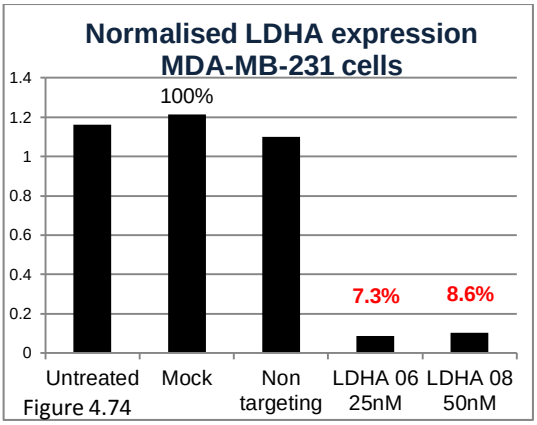

Figure 4.74: LDHA protein expression detected through Western blotting in MDA-MB-231 siRNA transfected cells. Transfection lasted for 96h and the following siRNA sequences were used: non targeting (25nM), LDHA 06 (25nM) and LDHA 08 (50nM). Expression was compared to mock cells, treated only with transfection reagent (percentages shown). Densitometry analysis was conducted using the Odyssey Infrared Imaging System software (Licor) and data were normalised to α tubulin expression.

4.4.2.1 Effect of LDHA knockdown on LDHB expression

The effect of LDHA siRNA knockdown on the expression of the other LDH subunit (LDHB) was also examined. Figure 4.75 shows LDHB expression in samples transfected with LDHA siRNAs. The corresponding densitometry analysis results are presented in Figure 4.76. This indicates that the siRNA effect was specific to the A subunit. It can be observed that the same oligonucleotides that reduced LDHA expression to 7% had no effect on LDHB expression.

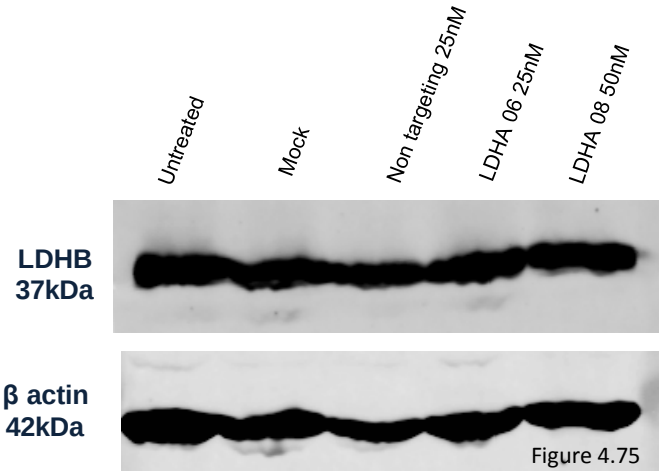

Figure 4.75: LDHB protein expression detected through Western blotting in MDA-MB-231 cells transfected with LDHA siRNAs. Transfection lasted for 96h and the following siRNA sequences were used: non targeting (25nM), LDHA 06 (25nM) and LDHA 08 (50nM). Beta actin was used as a loading control. Representative data of 2 independent experiments are presented.

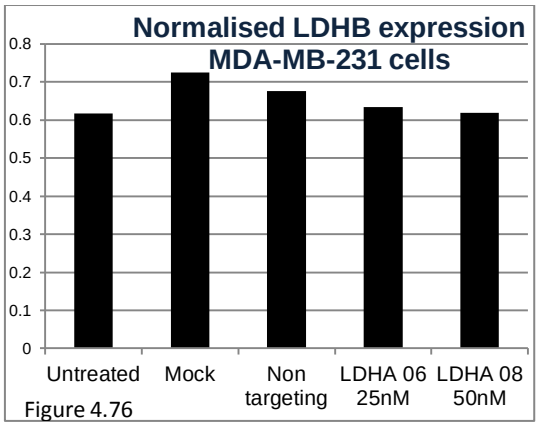

Figure 4.76: LDHB protein expression detected through Western blotting in MDA-MB-231 cells transfected with LDHA siRNAs. Transfection lasted for 96h and the following siRNA sequences were used: non targeting (25nM), LDHA 06 (25nM) and LDHA 08 (50nM). Densitometry analysis was conducted using the Odyssey Infrared Imaging System software (Licor) and data were normalised to β actin expression.

4.4.2.2 Effect of LDHA knockdown on cell proliferation

The effect of LDHA knockdown on cell proliferation was examined. MCF7 cells were transfected with the 06 and 08 siRNA oligos and incubated for 96h at 21% O_2 and 0.5% O_2. Cancer cell viability was examined by the SRB assay. Measurements were compared to mock treated cells using one-way ANOVA and the Tukey-Kramer multiple comparisons test.

Figure 4.77 demonstrates that the two siRNA sequences reduced cell growth to 58 and 40% in normoxic conditions compared to mock treated cells. This effect of LDHA knockdown on cell proliferation is roughly equivalent to the corresponding effect of 10mM Oxamic acid and 10μM NHI-1. The concentration response curves of the two LDH inhibitors were generated through a parallel experiment and are presented in Figures 4.79 and 4.80. Cells presented slightly less sensitivity to LDHA knockdown when cultured at 0.5% O_2 (Figure 4.78). Under hypoxic conditions cell density was reduced to 73 and 45% of the mock control from the two oligos.

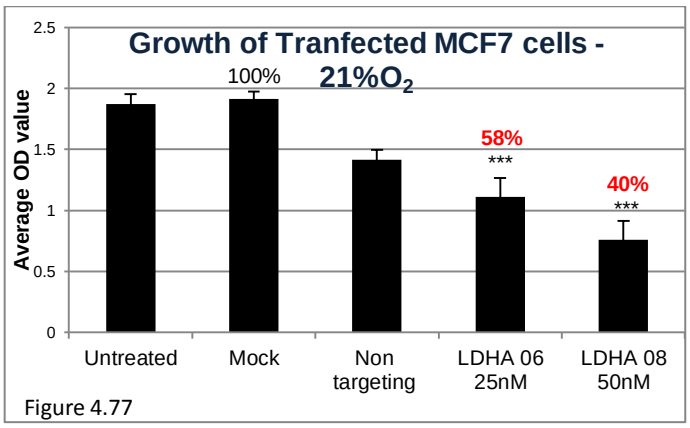

Figure 4.77

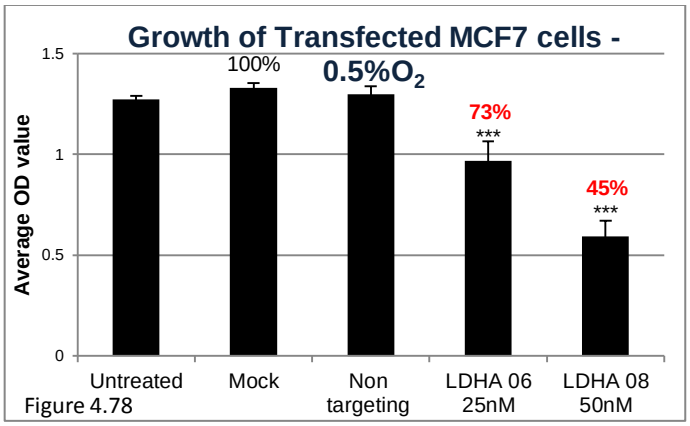

Figure 4.78

Figures 4.77 & 4.78: Optical density of MCF7 breast cancer cells transfected with LDHA siRNAs for a 96h period at 21 or 0.5%O_2. The following siRNA sequences were used: non targeting (25nM), LDHA 06 (25nM) and LDHA 08 (50nM). Optical density was determined by an SRB assay. Mean results of 6 replicates are reported and error bars represent standard deviations. Growth was compared to mock cells, treated only with transfection reagent (percentages shown). Statistical significance indications: *** P<0.001 compared to mock treated control (one-way ANOVA followed by Tukey-Kramer multiple comparisons test). Representative data of 3 independent experiments are presented.

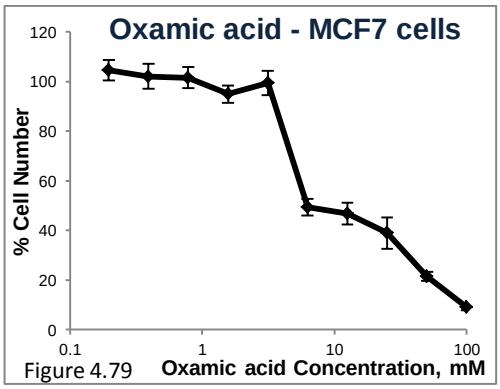

Figure 4.79

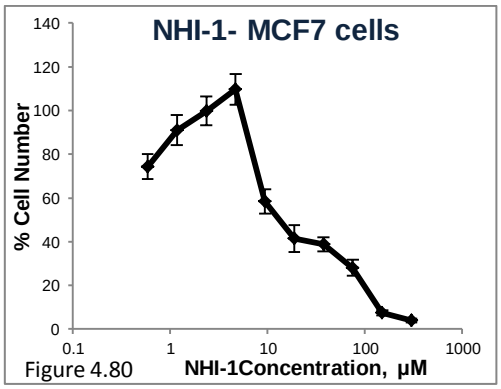

Figure 4.80

Figures 4.79 & 4.80: Concentration response curves of MCF7 breast cancer cells treated with Oxamic acid concentrations between 0.2-100mM and NHI-1 concentrations between 0.6-300µM for 96h. Cell viability was determined by an SRB assay. Mean results of 6 replicates are reported and error bars represent standard deviations. Values are shown as a percentage of control. A constant 0.3% DMSO concentration was used across the whole NHI-1 curve. Representative data of 2 independent experiments are presented.

4.4.2.3 Effect of LDHA knockdown on lactate production

The effect of LDHA knockdown on lactate production was examined. MDA-MB-231 cells were transfected with the 06 and 08 siRNA sequences for 96h. Immediately after the transfection period was terminated, cells were incubated with fresh culture medium for 4h. Then the medium was collected and extracellular lactate was measured following the protocol described in Chapter 2 section 2.4. Measurements were normalised to the protein content to compensate for differences in the cell number and are presented as μg lactate per 1000 μg/ml of protein. As demonstrated in Figure 4.81 lactate production proved unaffected by LDHA knockdown, even though LDHA expression in these specific samples was measured at less than 10% compared to expression of mock treated cells.

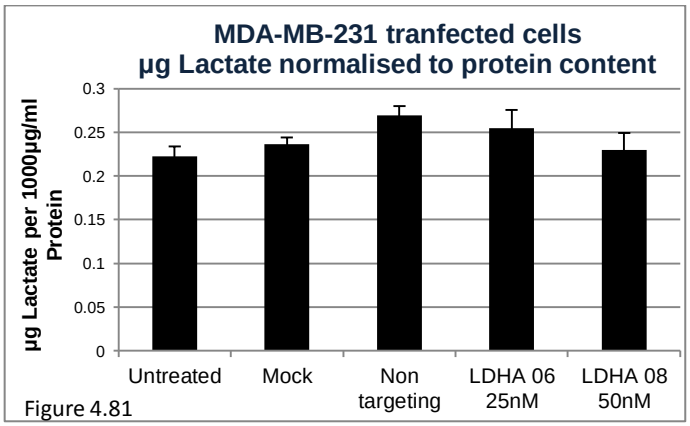

Figure 4.81: Extracellular lactate production in the culture medium of transfected MDA-MB-231 breast cancer cells. Measurements were normalised to protein content and are presented as μg lactate per 1000 μg/ml of protein. The following siRNA sequences were used: non targeting (25nM), LDHA 06 (25nM) and LDHA 08 (50nM). Mean results of 3 replicates are reported and error bars represent standard deviations. Representative data of 7 independent experiments are presented.

4.5 Discussion

4.5.1 The glycolytic inhibitors mainly induced apoptosis

The mechanism of action of the glycolytic inhibitors was examined by flow cytometry. MCF7 breast cancer cells were treated with high concentrations of nine glycolytic inhibitors for 24 or 48h and double stained with FITC-conjugated annexin V and PI. Flow cytometric analysis differentiated the treated cell population in four separate groups; viable intact cells (double negative), early apoptotic cells (annexin V positive), late apoptotic cells (double positive) and necrotic cells (PI positive).

Evidence that the mechanism of action of high concentrations of the glycolytic inhibitors after a 24h treatment is associated with necrotic cell death was obtained. A notable increase of necrotic cells, stained positive for PI, was observed for the vast majority of the compounds after 24h of treatment compared to untreated cells. At 24h the proportion of untreated necrotic cells was 3% whereas cells treated with 300μM Phloretin for 24h showed 21% necrosis, 300μM Quercetin for 24h 7%, 30μM STF31 for 24h 20%, 30μM WZB117 for 24h 9%, 30μM 3PO for 24h 24%, 100mM DCA for 24h 11% and 100mM Oxamic acid for 24h 20% (Figure 4.57).

In contrast a 48h treatment with the same high concentrations of the glycolytic inhibitors resulted in induction of both early and late apoptosis compared to the untreated control. All 9 of these inhibitors were shown to induce apoptosis following a 48h treatment of breast cancer cells as demonstrated by a pronounced increase of annexin V positive cells. Apoptotic untreated cells at 48h were quantified at 7% whereas cells treated with 300μM Phloretin for 48h showed 43% apoptosis, 300μM Quercetin for 48h 25%, 30μM STF31 for 48h 29%, 30μM WZB117 for 48h 11%, 300μM 3BP for 48h 92%, 30μM 3PO for 48h 28%, 100mM DCA for 48h 58%, 100mM Oxamic acid for 48h 13% and 300μM NHI-1 for 48h 47% (Figure 4.58).

The selected compounds were associated with more than one mode of cell death via different signalling routes at different time courses. It seems that they lead to necrosis after a short treatment period while longer incubation is associated with apoptotic cell death suggesting that apoptosis is not an immediate process following treatment with these compounds. Nonetheless great levels of cellular death are in agreement with results obtained by the SRB assays in Chapter 3 section 3.2 demonstrating that the same concentrations of these inhibitors eliminated breast cancer cellular populations following a 5-day treatment.

Traditionally, it has been argued that nutrient withdrawal and blocking of the glycolytic pathway depletes cellular ATP levels and renders cells unable to engage in an ATP demanding death process. Indeed it has been extensively demonstrated that glycolysis inhibition leads to necrotic cell death as cells are unable to undergo ATP dependent apoptosis [435]. Among the compounds of interest in this study the novel GLUT1 inhibitors, STF31 and WZB117, have been associated with necrotic cell death in the literature [312, 319]. However the concentrations used in these published studies were considerably lower compared to the ones used here.

Glucose starvation and glycolysis inhibition has also been linked with ROS mediated oxidative stress [414, 415]. Apoptotic cell death following treatment with the majority of these compounds is in agreement with earlier studies. Phloretin treatment has been associated with induction of apoptosis in several tumour types including melanoma, hepatocellular carcinoma and breast cancer cell lines [278, 279, 284]. Quercetin has been shown repeatedly to induce apoptosis in breast and ovarian cancer cell lines [297-301]. Apoptotic cell death of breast cancer cells following 3BP treatment has also been documented [330]. DCA and Oxamic acid have also been associated with apoptotic cell death in several cancer types [357, 375, 376]. Similarly the novel LDHA inhibitor, NHI-1, was reported to cause apoptosis in various cancer cell line models [378]. In this study breast cancer cells were consistently found to undergo apoptosis following 3BP and NHI-1 treatment for either 24 or 48h in line with previous findings [330, 378]. Nevertheless it should be highlighted that the concentrations used in this study are high and therefore results are not directly comparable.

An important finding is that the mechanistic response of these breast cancer cells to all nine inhibitors was very similar at both time points. This is consistent with a likely shared action and targeting of a common pathway. However these data should be interpreted with caution as it could conceivably be argued that the high concentrations used may produce off-target effects, and therefore cannot be exclusively associated with glycolysis inhibition. The main aim of these experiments was to investigate the mechanism of cell death associated with the maximal growth inhibitory effect of an array of inhibitors as observed in the SRB assays presented in Chapter 3.

A source of weakness here is that this experiment was only conducted once and there is only one set of data suggesting that it should be interpreted with caution. Further work is required to explain this shift from necrotic to apoptotic cell death between 24 and 48h of treatment with glycolytic inhibitors. ATP measurements, determination of PARP cleavage levels as well as expression of pro-apoptotic and necrotic cellular markers would be essential to develop a full picture of the antiproliferative mechanism of action of these compounds.

A growing body of literature associates the growth inhibitory effect of several of these compounds with autophagy. Examples include studies demonstrating that 3PO induced an autophagic response in HCT-116 colon cancer cells, DCA in colorectal and prostate cancer cell lines and Oxamic acid in A549 lung cancer cells as well as in SGC7901 and BGC823 gastric cancer cells [344, 363, 376, 377]. Autophagy is a regulated degradation process of cytosolic components within lysosomes. The role of autophagy in cancer is not completely

clarified yet. There is evidence suggesting that it promotes survival, tumour growth and aggressiveness serving as a protective response to metabolic stress [436, 437]. Combinatorial treatment with autophagy inhibitors has been shown to enhance the efficacy of some of these agents [344, 377]. It would be interesting to examine the levels of autophagy markers like LC3-II following treatment with the array of glycolytic inhibitors and determine the role of autophagy in the models of interest here.

4.5.2 The glycolytic inhibitors mainly caused cell cycle arrest at G0/G1 phase

An objective of this study was to further assess whether the antiproliferative effect of several glycolytic inhibitors could be associated with cell cycle arrest. MCF7 breast cancer cells were treated with the panel of nine glycolytic inhibitors for 24h and then fixed and stained with PI. Flow cytometric analysis enabled the separation of each population into three groups based on the cellular DNA content as this was indicated by variation of the fluorescence intensity of PI; cells in the G0/G1 phase, the S phase and the G2/M phase. As great levels of cellular death were previously observed in the apoptosis assay lower concentrations of the compounds were used here to investigate cell cycle progression.

The DNA content frequency histograms generated through flow cytometric analysis and quantification of cells in the different phases of the cell cycle suggested that the glycolytic inhibitors are predominantly associated with cell cycle arrest at the G0/G1 phase. While 36% of untreated cells were found at the G0/G1 phase, for cells treated with 150μM Phloretin the percentage increased to 61%, 15μM STF31 to 39%, 15μM WZB117 to 41%, 50μM 3BP to 41%, 15μM 3PO to 52%, 100mM Oxamic acid to 44% and 150μM NHI-1 to 61%. The accumulation of cells in the G0/G1 phase and inhibition of the G1-S transition was more profound following Phloretin and NHI-1 treatment. It should also be mentioned that Oxamic acid induced a concomitant G2/M phase cell cycle arrest, increasing the proportion of cells in this phase from 34% in the untreated control to 42%. A different response was observed from Quercetin that was associated with cell cycle arrest in the S phase. The number of cells in the S phase was increased to 35% compared to 30% in the untreated sample. Following DCA treatment no considerable effect in the percentage of cells in the various stages of the cell cycle was detected (Figure 4.69).

In the literature the information regarding the effect of these compounds on cell cycle progression is limited. Quercetin was shown to induce G0/G1 cell cycle arrest in breast and ovarian cancer cells contradicting the findings of the current study [297, 298]. However a more potent sulphated derivative of Quercetin was associated with S phase cell cycle arrest in MCF7 cells supporting the present findings [302]. Consistent with current results

WZB117 was previously found to block the cell cycle at the G0/G1 phase in A549 lung cancer cells [319]. In contrast 3PO was documented to induce G2/M phase cell cycle arrest in Jurkat T cell leukemia cells [343]. A similar effect has also been observed following DCA treatment in HCT116 colon cancer cells while G0/G1 arrest was reported for another colorectal cancer cell line HT29 and PC3 prostate cancer cells [363]. G2/M phase cell cycle arrest has also been observed after Oxamic acid treatment of CNE-1 and CNE-2 nasopharyngeal carcinoma cells as well as H1395 lung cancer cells. However G0/G1 arrest was detected in a different lung cancer cell line, A549, similar to the compound's effect on MCF7 breast cancer cells evidenced here. Nevertheless it should be mentioned that the concentrations of the compounds used in this experiment are higher that the concentrations used in many of the mentioned studies. Furthermore, the major limitation of this experiment is that it was only conducted once and proper statistical analysis unfortunately cannot be performed.

The main finding of this section is that almost every glycolytic inhibitor examined induced G0/G1 quiescence in breast cancer cells, inhibiting the transition into the DNA synthesis S phase. The major regulator of the G1/S cell cycle checkpoint is the tumour suppressor gene retinoblastoma (Rb) that binds and inhibits the transcription factor E2F. Phosphorylation of the Rb by CDK complexes (Cyclin D-CDK 4/6 and Cyclin E-CDK 2) dissociates E2F enabling gene transcription and DNA replication [438]. Investigation of the pRb and CDK levels would further enlighten the cell cycle arrest in breast cancer cells treated with glycolytic inhibitors.

4.5.3 The glycolytic inhibitors blocked the glycolytic pathway

The experiments in this section provide evidence that the nine glycolytic inhibitors studied block the glycolytic pathway. Each of the examined compounds induced accumulation of glucose along with decline in the amount of produced lactate in the media of breast cancer cells treated for 24h with each agent (Figures 4.34 to 4.69). This is supportive evidence that this set of compounds indeed targets the glycolytic pathway.

Two breast cancer cell lines were used in these experiments. It should be highlighted that at least for one of them the anticipated effect consistent with glycolysis inhibition was documented for every single compound. Some discrepancy was observed for the GLUT1 inhibitors as treatment with the two flavonoids, Phloretin and Quercetin, reduced the amount of glucose remaining in the culture medium of MCF7 cells and increased lactate production. Similarly STF31 treatment had the same unexpected effect on HBL100 cells. As mentioned in the literature review, both phytochemicals inhibited glucose efflux in human erythrocytes

and STF31 impaired glucose uptake and lactate production in renal cell carcinoma cells [277, 312]. However it is known that the two flavonoids are associated with a wide range of biological effects other than inhibition of glucose transport and STF31 has recently been characterised as a NAMPT inhibitor [274, 275, 315]. Regarding WZB117 while a significant increase in the remaining glucose in the culture medium of both cell lines was detected, this study has been unable to demonstrate any significant effect on the measurement of lactate. This contradicts earlier findings from Liu *et al* who showed that WZB117 treatment decreased the amount of produced lactate in A549 non–small cell lung cancer cells even after 6h of treatment [319]. The rest of the compounds resulted in a consistent increase in the concentration of glucose that remained in the culture medium after a 24h treatment in both breast cancer cells lines combined with a decrease in the extracellular lactate levels secreted. It should be mentioned that even when the bottom of the pathway was targeted an effect on glucose uptake was apparent signifying the tight allosteric regulation of the glycolytic enzymes.

A noteworthy observation is that for the majority of the compounds (including STF31, WZB117, 3BP and 3PO) the lowest concentration used induced the maximal observed response while higher concentrations did not have any additional effect. This possibly indicates that inhibition of each glycolytic enzyme can affect glucose uptake and lactate secretion to a certain extent. It was also observed that changes in the levels of glucose and lactate were mostly more profound for the ER negative HBL100 breast cancer cell line compared to the ER positive MCF7. Interestingly this relatively modest response from MCF7 cells did not coincide with resistance to the inhibitors (Table 3.2). However it corroborates previous findings suggesting that HBL100 cells demonstrated stronger reliance on glucose availability for cell growth as they were not able to proliferate in glucose depleted conditions (Table 3.1).

Another caveat is that it cannot be excluded that a proportion of the observed effect is attributed to the antiproliferative effect of the inhibitors. Ideally glucose and lactate measurements should be normalised to the cell number. However the concentrations used were selected based on the corresponding IC_{50} concentrations generated from the SRB assays following a 5-day treatment (Chapter 3), whereas here incubations lasted only 24h. Therefore the anticipated antiproliferative effect from such low concentrations at only 24h is minimal. Another possibility to minimise even more the antiproliferative effect of the inhibitors could be to examine glucose uptake and lactate production following shorter time period of inhibitor exposure for example 4h.

The present study makes a further contribution to our understanding of the mechanism mediating the antiproliferative effect of glycolytic inhibitors in breast cancer cells. Induction of apoptosis along with G0/G1 cell cycle arrest are identified as key elements of the action of these compounds. However, it is important to bear in mind that inhibition of the glycolytic pathway was detected at much lower concentrations compared to the ones used in the flow cytometry experiments. It is therefore likely that the enhanced apoptosis and cell cycle arrest observed could not be exclusively attributed to inhibition of the glycolytic pathway (since this was demonstrated in considerably lower concentrations) and additional off-target effects should be taken into consideration.

4.5.4 Evaluation of glycolytic targets through siRNA knockdown

The final section of this chapter sought to evaluate further selected glycolytic enzymes as anticancer targets using siRNA mediated gene knockdown. Inhibition of multiple molecules of the glycolytic pathway using an array of inhibitors was previously investigated in this study (Chapter 3). Among the compounds used the novel inhibitors IOM-1190 and NHI-1, targeting GLUT1 and LDHA respectively, were identified as valuable pharmacological tool compounds and potent cancer cell growth inhibitors. The two targeted glycolytic enzymes, at the top and bottom of the glycolytic pathway, were demonstrated to be promising therapeutic targets and were selected for further assessment using siRNA mediated gene downregulation.

This study was unable to achieve significant GLUT1 silencing by siRNA despite extensive optimisation experiments that took into consideration every suggestion of the manufacturer. Different plating cell densities of two breast cancer cell lines were used with a range of volumes of the transfection reagent and a dose curve of each of the five siRNAs (four single oligos and the pool) while transfection duration ranged from 24 to 120h. Unfortunately GLUT1 downregulation was not accomplished. A representative example of the GLUT1 knockdown experiments is presented in Figure 4.70.

Since significant LDHA knockdown was achieved, this indicates that optimal transfection conditions were successfully identified. This suggests that ineffective GLUT1 downregulation was not related to transfection efficiency as the protocol was successfully optimised and validated, but target related. Nevertheless effective GLUT1 silencing by siRNA oligos or shRNA vectors has been previously documented [323, 439, 440]. Interestingly in their study Shibuya *et al* reported that sustained GLUT1 siRNA knockdown required repeated transfection 3 or 4 days following the initial transfection [323].

GLUT1 has a very short half-life, much shorter than the average degradation rate of cellular proteins. Sargeant *et al* calculated GLUT1 protein half-life equal to 19h in 3T3-L1adipocytes while another study reported 6h in L6 myotubes [441, 442]. This rapid turnover rate might render the assessment of the knockdown at the protein level problematic. Further experimentation should ideally examine the mRNA level using PCR as siRNA transfection is a direct RNA specific process and short time points for immediate downregulation can be investigated. Alternatively CRISPR gene editing technology could be employed to ensure precise and efficient GLUT1 knockdown [443].

Another possible explanation for ineffective knockdown of GLUT1 might be the specificity of the antibody used. Because the siRNA manufacturer guarantees GLUT1 specific silencing, it is possible that the antibody is not GLUT1 specific and is binding to other GLUTs as well. It is known that both MCF7 and MDA-MB-231, the breast cancer cell lines used, express other glucose transporters [179, 180].

On the other hand LDHA silencing was achieved. All four single siRNA oligonucleotides as well as the pool of four combined, accomplished significant LDHA knockdown (Figure 4.72). The sequences that demonstrated highest target downregulation efficiency were used in the experiments that followed in MCF7 and MDA-MB-231 cells.

The specificity of LDHA silencing with respect to LDHB expression was then investigated. Even though the two subunits share a high level of homology selective LDHA protein knockdown was documented. LDHA siRNA transfection resulted in a depletion of LDHA protein levels (up to 93%) without affecting LDHB expression in MDA-MB-231 cells (Figure 4.75).

The most interesting finding of this section was that LDHA knockdown significantly attenuated breast cancer cell proliferation. It was observed that the two siRNA oligonucleotides following a 96h transfection period reduced the cell density of MCF7 breast cancer cells to 58 and 40% respectively at 21% O_2 compared to mock treated cells (Figure 4.77). The antiproliferative effect of LDHA silencing was comparable to the corresponding effect of 10mM Oxamic acid and 10μM NHI-1, the two LDH inhibitors used in this study (Figures 4.79&4.80). These findings are consistent with previous studies. Fantin *et al* demonstrated that shRNA mediated LDHA knockdown impaired the proliferation rate of breast cancer cells, stimulated mitochondrial oxidative phosphorylation and also suppressed their tumorigenic potential *in vivo* [271]. In line with these Sheng *et al* reported that lentiviral RNAi-induced LDHA downregulation attenuated the growth of hepatocellular

carcinoma cells, increased ROS production and resulted in apoptotic cell death. Moreover it inhibited invasion *in vitro* and supressed metastasis in an *in vivo* xenograft model [444]. More recently Allison *et al* documented that LDHA knockdown induced apoptosis in cancer cells associated with oxidative stress [445].

The effect of LDHA knockdown on cell proliferation was also examined at 0.5% O_2. Under hypoxic conditions transfection with the two selected siRNA sequences resulted in a reduction of the cell number to 73 and 45% respectively compared to mock treated control cells (Figure 4.78). It was noted that breast cancer cells were less sensitive to LDHA silencing under hypoxic conditions. This is consistent with enhanced sensitivity presented to LDH inhibitors at 21% O_2 conditions demonstrated in Chapter 6 section 6.1. It is known that LDHA, as a verified HIF-1 target, is upregulated in hypoxia [446]. However this finding does not support previous research. Fantin *et al* reported that the effect of LDHA knockdown on the proliferation rate of breast cancer cells was greater in hypoxic conditions [271].

Taken together these findings provide additional evidence that LDHA is a legitimate target for anticancer treatment. Suppressing LDHA expression in breast cancer cells *in vitro* was sufficient to significantly impair their proliferation. LDHA is a tumour specific enzyme that plays a key role in the glycolytic phenotype of cancer cells. It is responsible for NAD+ regeneration which is essential to sustain the glycolytic flux. Most importantly normal cells predominantly rely on mitochondrial respiration for energy generation and LDHA inhibition is anticipated to cause minimal toxicity [257, 258].

Finally an unexpected finding was that LDHA silencing did not affect lactate production. It was observed that even though LDHA protein expression was reduced at least by 90% compared to mock treated cells following siRNA transfection the lactate levels secreted surprisingly remained unaffected (Figure 4.81). This result is difficult to interpret and differs from previous findings. In their study Allison *et al* reported inhibition of the glycolytic pathway, indicated by 30% reduced lactate production, following LDHA silencing in HCT116 colorectal cancer cells [445].

The glycolytic pathway is not the exclusive source of intracellular lactate as it is also generated, to a lesser extent, by the catabolism of alanine and other amino acids. Nevertheless LDH is the only characterised enzyme that catalyses the reduction of pyruvate to lactate [447]. Thus another enzyme cannot be implicated in lactate formation following LDHA knockdown. However a possibility might be that in the absence of LDHA increased LDHB protein turnover could be responsible for lactate generation. It is known that both

isozymes can catalyse the interconversion of pyruvate to lactate even though each one is more efficient in catalysing the reaction in a specific direction [258]. Nevertheless if this was the case LDHB would possibly be expected to negate the observed antiproliferative effect. Also LDHB protein expression was found to remain unaffected following LDHA silencing. Another possible explanation might be that the expression of LDHA in MDA-MB-231 cells is so high that even a fraction of the expressed protein can produce the same levels of lactate. In line with this it has been demonstrated that MDA-MB-231 triple negative cells have a highly glycolytic phenotype and upregulated LDHA levels [423]. Several questions regarding this finding remain unanswered and warrant further investigation.

Chapter 5

Chapter 5: Combining glycolytic inhibitors with chemotherapy and targeted inhibitors

The efficacy of an array of glycolytic inhibitors in attenuating cancer cell proliferation has been described in Chapter 3. However their value as monotherapy for breast and ovarian cancer treatment is likely to be limited as relatively high concentrations are required to achieve the desired antitumour effect. Combination treatment is currently carried out for most tumour types and therefore the effects of several glycolytic inhibitors were assessed in combination strategies with traditional drugs. There are two primary aims of this section. Firstly to attempt to improve the efficacy of currently used therapeutics using glycolytic inhibitors and to investigate the possibility of resensitising cancer cells to treatment to which they had developed resistance. Secondly, to explore novel combinations of inhibitors that could potentially be developed as future treatment strategies.

A range of co-treatments with two cytotoxic drugs, a monoclonal HER2 antibody and an antidiabetic inhibitor of oxidative phosphorylation were conducted. Cisplatin is a platinum-based chemotherapy drug that causes DNA crosslinking and is widely used for the treatment of ovarian cancer [384]. Paclitaxel (Taxol) is a chemotherapy drug that binds to microtubules and inhibits tubulin depolymerisation. It is commonly used for the treatment of both breast and ovarian cancer [387]. Trastuzumab (Herceptin) is a humanised monoclonal HER2 antibody. It is mainly used for the treatment of HER2-positive breast cancers [32]. Finally, metformin inhibits mitochondrial oxidative phosphorylation and is widely used for the treatment of type 2 diabetes. Recently it has attracted great interest as it exhibits antiproliferative action [389-392].

In these experiments a range of different concentrations of each glycolytic inhibitor were used in combination with a constant fixed concentration, around the IC_{20} or less, of the other drug. Both drugs were delivered at the same time and cancer cell proliferation was examined by the SRB assay after a 3-day treatment period. Along with each co-treatment, in every experiment, single drug concentration response curves of both compounds were performed. Data were analysed using the Calcusyn software. Combination Index values (CI) were generated for each combination point providing a quantitative evaluation of the combination efficacy. A detailed indication of the CI values can be seen in Chapter 2 section 2.2.1. Briefly, values lower than 0.8 suggest synergy, values between 0.8 and 1.2 imply additivity while values higher than 1.2 indicate antagonism.

Three paired cancer cell-line models were used in these experiments. One breast cancer cell line pair, the ER positive cell line MCF7 and the triple negative MDA-MB-231 cell line and two chemosensitive - chemoresistant ovarian cancer cell line pairs, PEA1-PEA2 and PEO1-PEO4, which were previously described in Chapter 2 section 2.1.1. The high HER2 MDA-MB-361 breast cancer cell line was also used in one set of studies investigating trastuzumab. Co-treatments with cisplatin were only conducted in ovarian cancer cell lines, as platinum-based regimens are first line treatment for ovarian cancer.

Glycolytic Inhibitor	Traditional Drug	Cell Lines generating synergistic combination points
IOM-1190	Metformin	MCF7, MDA-MB-231
Phloretin	Metformin	PEO1
	Cisplatin	none
STF31	Metformin	all tested
	Cisplatin	none
	Paclitaxel	none
3PO	Metformin	none
	Cisplatin	PEA1, PEA2, PEO1, PEO4
	Paclitaxel	PEA1, PEA2, PEO1, PEO4
Oxamic acid	Metformin	all tested
	Cisplatin	none
	Paclitaxel	MCF7, MDA-MB-231
	Trastuzumab	MDA-MB-361
NHI-1	Metformin	none
	Cisplatin	none
	Paclitaxel	none
	Trastuzumab	MDA-MB-361
Dichloroacetate	Metformin	MCF7, MDA-MB-231
	Cisplatin	none

Table 5.1: Summary of the combination treatments examined in this study. Cell lines for which each combination was found successful, generating at least one treatment point characterised as synergistic, are indicated.

Table 5.1 summarises the combination treatments that were examined in this study. The last column indicates the cell lines for which each particular combination was found to successfully produce at least one treatment point that could be characterised as synergistic (CI<0.8). The most interesting combinations identified are presented in detail below. Representative examples of unfavourable non-synergistic combinations can be seen in the Appendix (Figures A1.4 to A1.7).

5.1 Combinations with cytotoxic drugs – Cisplatin & Paclitaxel

5.1.1 Cisplatin

The interaction between cisplatin and several glycolytic inhibitors (Phloretin, STF31, 3PO, Oxamic acid, NHI-1, DCA) was examined. Among them 3PO was found able to enhance the potency of the cytotoxic agent.

5.1.1.1 3PO & Cisplatin

The PFKFB3 inhibitor was able to enhance the effect of cisplatin on two ovarian cancer cell line pairs, as shown in Figures 5.1 and 5.2 for the cell lines PEA1 and PEA2 and Figures 5.5 and 5.6 for PEO1 and PEO4 respectively. The fixed concentration of cisplatin was selected for each cell line based on its growth inhibitory effect. For example, in PEA2 cells, 4μM of cisplatin was required to produce a similar inhibitory effect on cell number to that of 1μM cisplatin on PEA1 cells. A synergistic interaction between the two compounds is observed. In these graphs, the blue line indicates the concentration response curve of the glycolytic inhibitor given alone. The green line demonstrates the effect of a constant concentration of cisplatin on cell viability, while in red, the combination curve of a range of 7 different 3PO concentrations combined with a fixed concentration of cisplatin is shown. The asterisks on the red line indicate synergistic combination points with CI values lower than 0.8. The growth inhibition effect of each combination point along with the CI values generated through the Calcusyn Software is presented in tables in the Appendix (Tables A1.1&A1.2). The most successful combination point for each cell line, the one characterised by the lowest CI value, is presented in greater detail in the separate column charts below (Figures 5.3&5.4).

The platinum naïve PEA1 line was found slightly more sensitive to the combination of 3PO with cisplatin compared to the platinum-resistant line PEA2 as it was characterised by lower CI values. As can be seen in Figure 5.3 1.9μM 3PO had no growth inhibitory effect on PEA1 cells; 1μM cisplatin reduced the cell number to 89% while the combination of both resulted in a reduction of the cell number to 49% compared to the untreated controls. For this

combination a CI value equal to 0.22 was generated which indicates strong synergism. When the same 3PO concentration was combined with 4μM cisplatin the cell number of PEA2 cells was reduced to 52%. The CI value for this combination was 0.5 indicating synergy. The IC_{50} values of the combination concentration response curves were roughly fivefold lower compared to the respective values of the 3PO curves for both cell lines (Table 5.2).

The other ovarian cancer cell line pair also proved sensitive to this combination. Figures 5.7 and 5.8 show that 3.8μM 3PO combined with 0.5 or 1μM cisplatin generated a synergistic combination for PEO1 and PEO4 cells respectively; characterised by a CI value equal to 0.6 in both cases. The IC_{50} values of the combination curves were found to be 2.6 and 1.6 times lower compared to the single 3PO treatment curves of the two cell lines (Table 5.2).

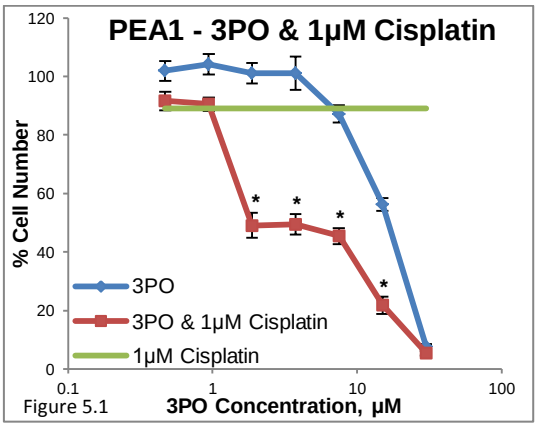

Figure 5.1

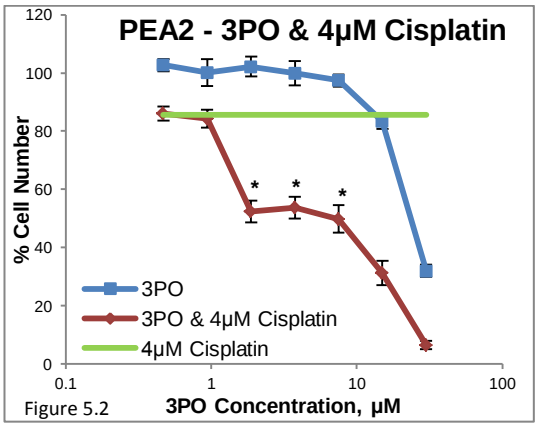

Figure 5.2

Figures 5.1 & 5.2: Concentration response curves of PEA1 (5.1) and PEA2 (5.2) ovarian cancer cells treated with 3PO concentrations between 0.5-30μM alone (blue line) or combined with a constant concentration of Cisplatin (red line). Cell viability was determined by an SRB assay after a three day treatment. Mean results of 6 replicates are reported and error bars represent standard deviations. Values are shown as a percentage of control. In green the effect of 1μM (PEA1) or 4μM (PEA2) Cisplatin on cell viability is presented. Asterisks indicate synergistic combination points with Combination Index values lower than 0.8. Representative data of 3 independent experiments are presented.

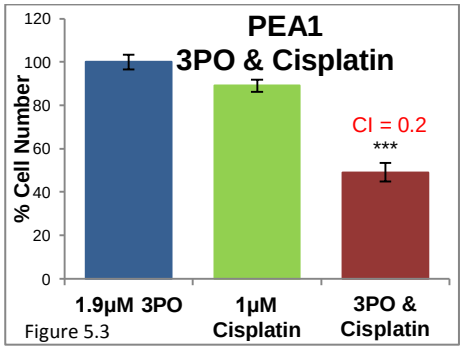

Figure 5.3

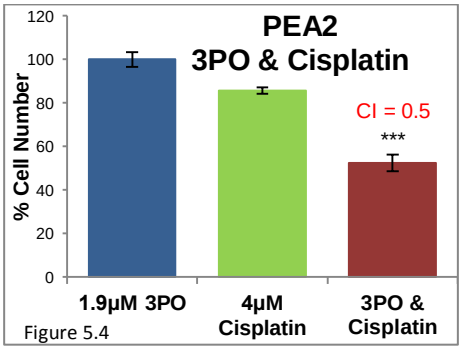

Figure 5.4

Figures 5.3 & 5.4: Effect of 1.9μM 3PO, 1μM Cisplatin and their combination on cell viability of PEA1 cells (5.3) as well as effect of 1.9μM 3PO, 4μM Cisplatin and their combination on cell viability of PEA2 cells (5.4). Mean results of 6 replicates are reported and error bars represent standard deviations. The respective Combination Index values generated through Calcusyn are indicated. Statistical significance indications: *** P<0.001 compared to 3PO single treatment (two-tailed P value generated from unpaired t-test).

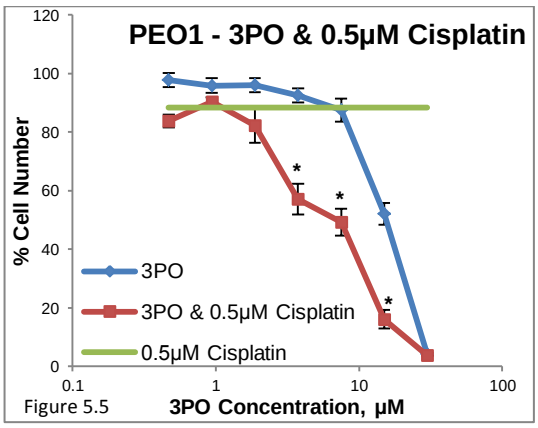

Figure 5.5

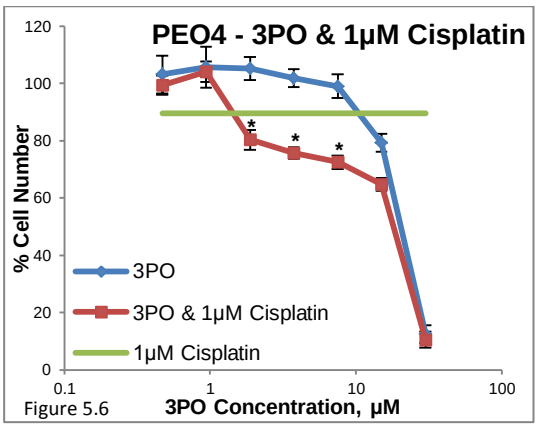

Figure 5.6

Figures 5.5 & 5.6: Concentration response curves of PEO1 (5.5) and PEO4 (5.6) ovarian cancer cells treated with 3PO concentrations between 0.5-30µM alone (blue line) or combined with a constant concentration of Cisplatin (red line). Cell viability was determined by an SRB assay after a three day treatment. Mean results of 6 replicates are reported and error bars represent standard deviations. Values are shown as a percentage of control. In green the effect of 0.5µM (PEO1) or 1µM (PEO4) Cisplatin on cell viability is presented. Asterisks indicate synergistic combination points with Combination Index values lower than 0.8. Representative data of 3 independent experiments are presented.

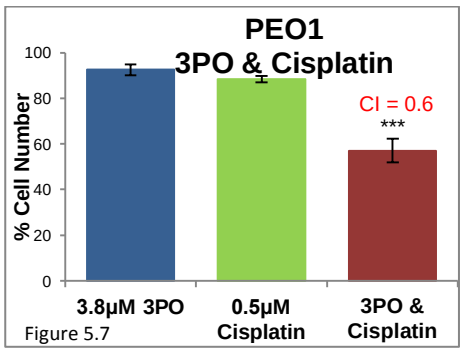

Figure 5.7

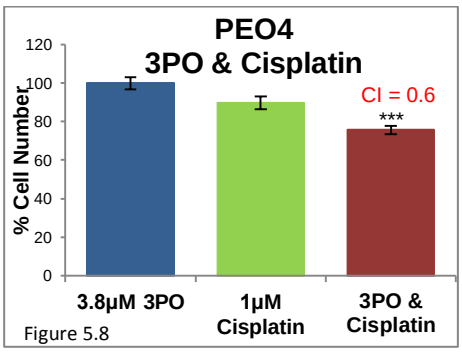

Figure 5.8

Figures 5.7 & 5.8: Effect of 3.8µM 3PO, 0.5µM Cisplatin and their combination on cell viability of PEO1 cells (5.7) as well as effect of 3.8µM 3PO, 1µM Cisplatin and their combination on cell viability of PEO4 cells (5.8). Mean results of 6 replicates are reported and error bars represent standard deviations. The respective Combination Index values generated through Calcusyn are indicated. Statistical significance indications: *** P<0.001 compared to 3PO single treatment (two-tailed P value generated from unpaired t-test).

IC_{50} values (µM)	1st pair		2nd pair	
	PEA1	**PEA2**	**PEO1**	**PEO4**
3PO	16.4	25.6	15.5	22.3
3PO & Cisplatin	3.8	5.1	5.9	13.9

Table 5.2: Summary of the IC_{50} concentrations generated for two ovarian cancer cell line pairs when treated with 3PO alone or combined with Cisplatin.

5.1.2 Paclitaxel

In this study paclitaxel was assessed in combination strategies with STF31, 3PO, Oxamic acid and NHI-1. Of these glycolytic inhibitors, 3PO and Oxamic acid were found to enhance the potency of paclitaxel.

5.1.2.1 3PO & Paclitaxel

Figures 5.9 and 5.10 show that the combination of 3PO with paclitaxel was very effective in inhibiting growth of the PEA1 and PEA2 cell lines, generating low CI values for all 3PO concentrations used. While 1.9μM 3PO and 1nM paclitaxel did not affect PEA1 cell number when delivered by themselves, their combination caused a 50% reduction in cell number (Figures 5.11&5.12). Similarly the same growth inhibition effect was caused by the combination of 0.9μM 3PO with 2nM paclitaxel in PEA2 cells. The CI values attributed to these combinations were 0.1 and 0.3 respectively both characterised as strong synergy. Moreover, as shown in Table 5.3 the IC_{50} values of the combination curves of the two cell lines were found at least threefold lower compared to the values of the 3PO single treatment curves.

The efficacy of this combination on the other ovarian cancer cell line pair was different. Figure 5.13 shows that for the platinum-sensitive line PEO1 the combination of 3PO with paclitaxel generated synergistic CI values for the whole range of 3PO concentrations used. As an example, Figure 5.15 demonstrates that while 0.9μM 3PO and 2nM paclitaxel reduced the percentage of cell number to 95 and 91% respectively, when combined together the inhibitory effect reached 47% (CI=0.5). In contrast, for the platinum-resistant line PEO4 the CI values generated for the lowest 3PO concentrations revealed additivity and moderate antagonism (Figure 5.14). Only a concentration as high as 15μM 3PO produced a synergistic interaction (CI=0.6, Figure 5.16). The differences between the two cell lines with regards to the efficacy of the combination is also reflected in the modification of the IC_{50} values (Table 5.3). PEO1 cells increased their sensitivity to the combination of the drugs tenfold compared to their sensitivity to 3PO single treatment while a modest twofold reduction in the IC_{50} value of the combination curve occurred in PEO4 cells.

The interaction between 3PO and paclitaxel was also examined in breast cancer cell lines but was not found effective under the particular conditions of the present study.

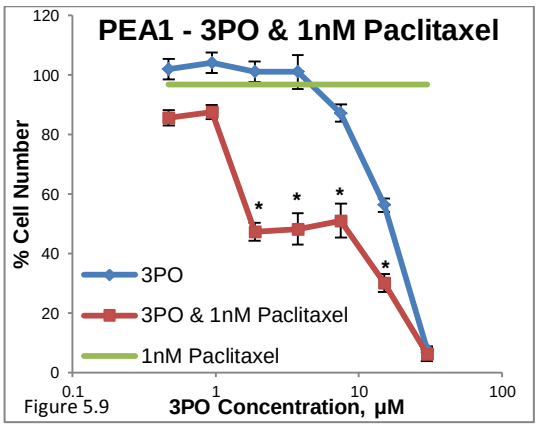

Figure 5.9

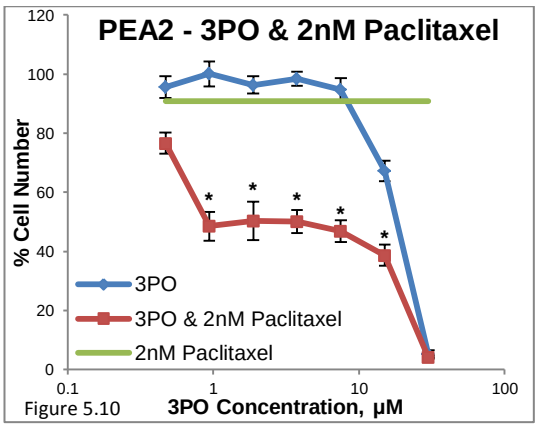

Figure 5.10

Figures 5.9 & 5.10: Concentration response curves of PEA1 (5.9) and PEA2 (5.10) ovarian cancer cells treated with 3PO concentrations between 0.5-30µM alone (blue line) or combined with a constant concentration of Paclitaxel (red line). Cell viability was determined by an SRB assay after a three day treatment. Mean results of 6 replicates are reported and error bars represent standard deviations. Values are shown as a percentage of control. In green the effect of 1nM (PEA1) or 2nM (PEA2) Paclitaxel on cell viability is presented. Asterisks indicate synergistic combination points with Combination Index values lower than 0.8. Representative data of 3 independent experiments are presented.

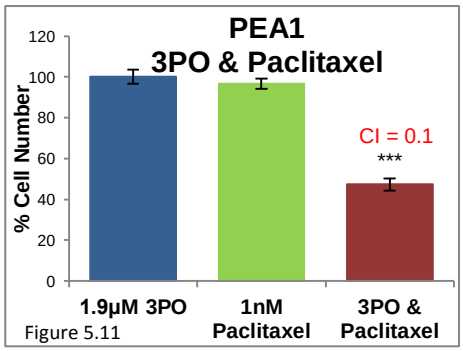

Figure 5.11

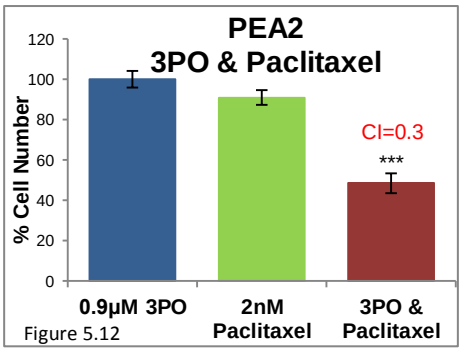

Figure 5.12

Figures 5.11 & 5.12: Effect of 1.9µM 3PO, 1nM Paclitaxel and their combination on cell viability of PEA1 cells (5.11) as well as effect of 0.9µM 3PO, 2nM Paclitaxel and their combination on cell viability of PEA2 cells (5.12). Mean results of 6 replicates are reported and error bars represent standard deviations. The respective Combination Index values generated through Calcusyn are indicated. Statistical significance indications: *** P<0.001 compared to 3PO single treatment (two-tailed P value generated from unpaired t-test).

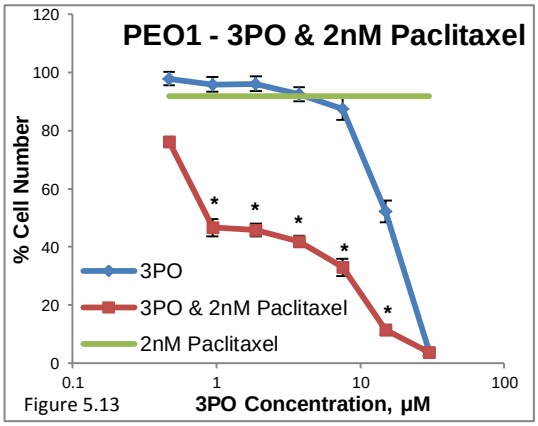

Figure 5.13

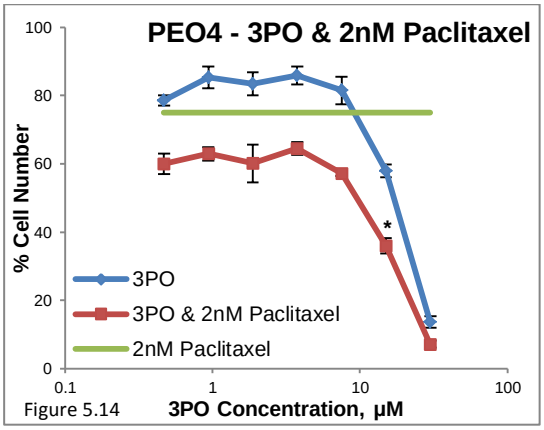

Figure 5.14

Figures 5.13 & 514: Concentration response curves of PEO1 (5.13) and PEO4 (5.14) ovarian cancer cells treated with 3PO concentrations between 0.5-30µM alone (blue line) or combined with 2nM Paclitaxel (red line). Cell viability was determined by an SRB assay after a three day treatment. Mean results of 6 replicates are reported and error bars represent standard deviations. Values are shown as a percentage of control. In green the effect of 2nM Paclitaxel on cell viability is presented. Asterisks indicate synergistic combination points with Combination Index values lower than 0.8. Representative data of 3 independent experiments are presented.

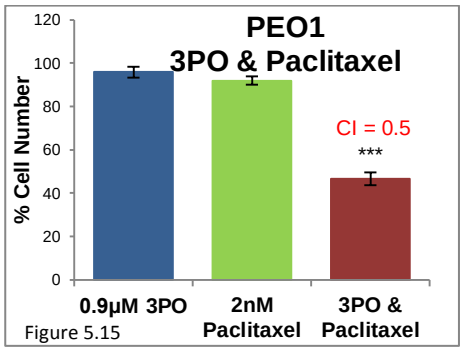

Figure 5.15

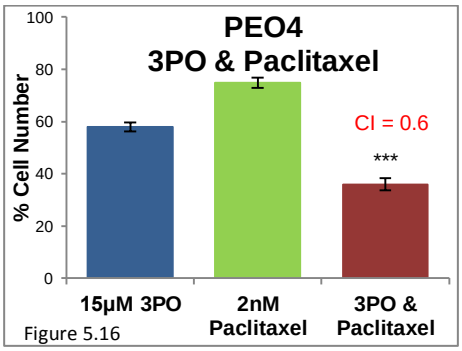

Figure 5.16

Figures 5.15 & 5.16: Effect of 0.9µM 3PO, 2nM Paclitaxel and their combination on cell viability of PEO1 cells (5.15) as well as effect of 15µM 3PO, 2nM Paclitaxel and their combination on cell viability of PEO4 cells (5.16). Mean results of 6 replicates are reported and error bars represent standard deviations. The respective Combination Index values generated through Calcusyn are indicated. Statistical significance indications: *** P<0.001 compared to 3PO single treatment (two-tailed P value generated from unpaired t-test).

IC_{50} values (µM)	1st pair		2nd pair	
	PEA1	**PEA2**	**PEO1**	**PEO4**
3PO	16.4	18.4	15.5	17
3PO & Paclitaxel	4.3	5.4	1.6	7.9

Table 5.3: Summary of the IC_{50} concentrations generated for two ovarian cancer cell line pairs when treated with 3PO alone or combined with Paclitaxel.

5.1.2.2 Oxamic acid & Paclitaxel

A favourable interaction between Oxamic acid and paclitaxel was identified in the breast cancer cell lines. Figures 5.17 and 5.18 illustrate that Oxamic acid enhanced the effect of paclitaxel on both MCF7 and MDA-MB-231 cells. Low synergistic CI values were generated only for the lower Oxamic acid concentrations used. As shown in Figure 5.19, 9.4mM Oxamic acid reduced the MCF7 cell number to 76% and 1nM paclitaxel to 93% compared to the untreated controls. However when the two drugs were combined the cell number was reduced to 49% (CI=0.5). Regarding MDA-MB-231 cells, Figure 5.20 depicts that while 4.7mM Oxamic acid and 1nM paclitaxel caused 5 and 10% growth inhibition respectively their combination resulted in 63% cell viability (CI=0.4). Both cell lines demonstrated a twofold lower IC_{50} value of the concentration response curves when Oxamic acid was combined with a fixed low concentration of paclitaxel compared to the respective values of Oxamic acid single treatment (Table 5.4).

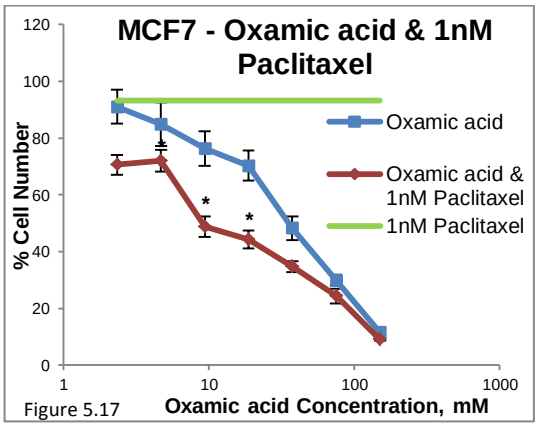

Figure 5.17

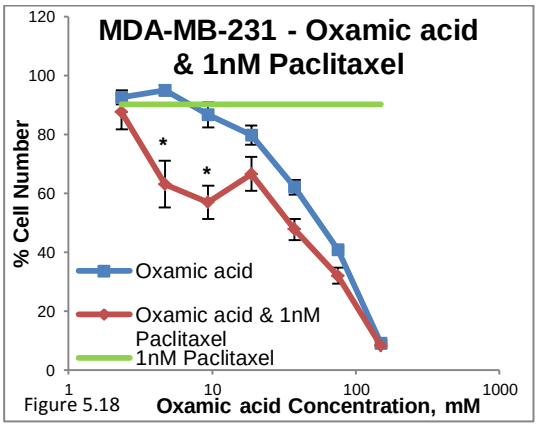

Figure 5.18

Figures 5.17 & 5.18: Concentration response curves of MCF7 (5.17) and MDA-MB-231 (5.18) breast cancer cells treated with Oxamic acid concentrations between 2.3-150mM alone (blue line) or combined with 1nM Paclitaxel (red line). Cell viability was determined by an SRB assay after a three day treatment. Mean results of 6 replicates are reported and error bars represent standard deviations. Values are shown as a percentage of control. In green the effect of 1nM Paclitaxel on cell viability is presented. Asterisks indicate synergistic combination points with Combination Index values lower than 0.8. Representative data of 2 independent experiments are presented.

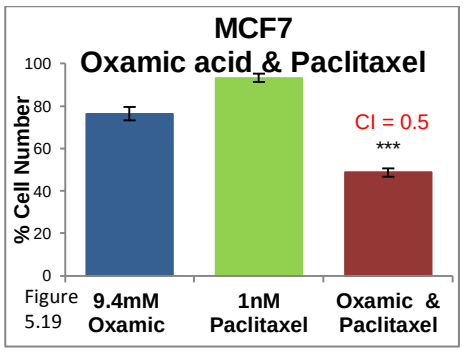

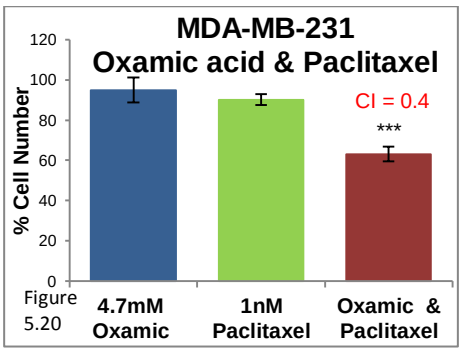

Figures 5.19 & 5.20: Effect of 9.4mM Oxamic acid, 1nM Paclitaxel and their combination on cell viability of MCF7 cells (5.19) as well as effect of 4.7mM Oxamic acid, 1nM Paclitaxel and their combination on cell viability of MDA-MB-231 cells (5.20). Mean results of 6 replicates are reported and error bars represent standard deviations. The respective Combination Index values generated through Calcusyn are indicated. Statistical significance indications: *** P<0.001 compared to Oxamic acid single treatment (two-tailed P value generated from unpaired t-test).

IC_{50} values (mM)	MCF7	MDA-MB-231
Oxamic acid	33.1	49.7
Oxamic acid & Paclitaxel	12	22.3

Table 5.4: Summary of the IC_{50} concentrations generated for two breast cancer cell lines when treated with Oxamic acid alone or combined with Paclitaxel.

5.2 Combinations with targeted therapy – Trastuzumab

The HER2-high MDA-MB-361 cell line was used for experiments with trastuzumab in this study. Figure 5.21 indicates that trastuzumab had an invariable cytostatic effect on MDA-MB-361 cells; reducing the percentage of cell number to 80% over the whole range of concentrations used (0.3-160µg/ml). For that reason the examined combinations could not be analysed through Calcusyn, as the software requires a sigmoidal growth inhibition curve from both single agents to describe quantitatively a combination and generate CI values. Positive interactions were identified between trastuzumab and two LDH inhibitors.

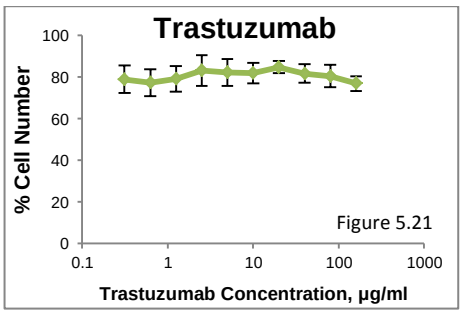

Figure 5.21: Concentration response curve of MDA-MB-361 breast cancer cells treated with Trastuzumab concentrations between 0.31-160µg/ml for a three day period. Cell viability was determined by an SRB assay. Mean results of 6 replicates are reported and error bars represent standard deviations. Values are shown as a percentage of control.

5.2.1 Oxamic acid & Trastuzumab

Figure 5.22 demonstrates that Oxamic acid enhanced the efficacy of trastuzumab on MDA-MB-361 cells as a growth inhibitor. Oxamic acid was used in combination with four separate trastuzumab concentrations. The glycolytic inhibitor had similar effects on the efficacy of trastuzumab, even when different concentrations of trastuzumab were examined. As the combination of the two agents is more effective than each agent separately their interaction is characterised as synergistic. Examples of the synergistic action are depicted in Figures 5.23 and 5.24. When 1.6 or 12.5mM Oxamic acid, both of which had no effect on cell viability were combined with either 10 or 40µg/ml trastuzumab, the cell number was reduced to 50%.

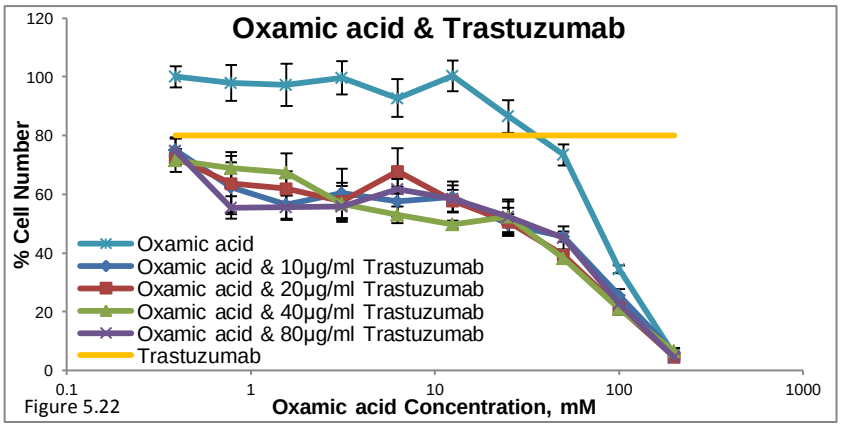

Figure 5.22: Concentration response curves of MDA-MB-361 breast cancer cells treated with Oxamic acid concentrations between 0.4-200mM alone (light blue line) and combined with 10µg/ml (blue line), 20µg/ml (red line), 40µg/ml (green line) or 80µg/ml (purple line) Trastuzumab. Cell viability was determined by an SRB assay after a three day treatment. Mean results of 6 replicates are reported and error bars represent standard deviations. Values are shown as a percentage of control. In yellow the effect of Trastuzumab on cell viability is indicated. Representative data of 3 independent experiments are presented.

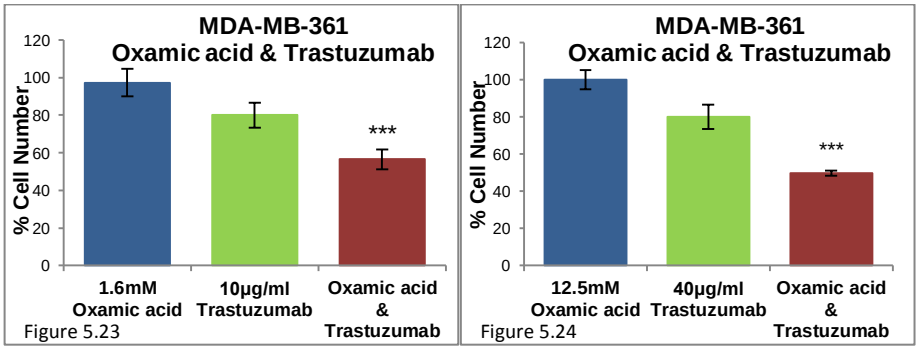

Figures 5.23 & 5.24: Effect of 1.6mM Oxamic acid, 10µg/ml Trastuzumab and their combination (5.23) as well as of 12.5mM Oxamic acid, 40µg/ml Trastuzumab and their combination (5.24) on cell viability of MDA-MB-361 cells. Mean results of 6 replicates are reported and error bars represent standard deviations. Statistical significance indications: *** P<0.001 compared to Oxamic acid single treatment (two-tailed P value generated from unpaired t-test).

5.2.2 NHI-1 & Trastuzumab

NHI-1 augmented the action of Trastuzumab as a cancer cell proliferation inhibitor. The novel LDHA inhibitor was used in combination with four separate trastuzumab concentrations (Figure 5.25). The addition of NHI-1 had a greater effect on the lowest concentration of trastuzumab (5µg/ml) compared to the higher concentrations of 20 and 40µg/ml. Interestingly when even lower concentrations were used equal to 0.1 and 0.5µg/ml (Figures 5.26 and 5.27) a synergistic interaction was identified. Figures 5.28 and 5.29 show that a combination of 1.2 or 37.5µM NHI-1, both of which have no effect on cell viability by themselves, with 5 or 0.1µg/ml trastuzumab respectively resulted in a cell number lower than 50%. It is apparent that the effect of the drugs in combination is greater than each separately.

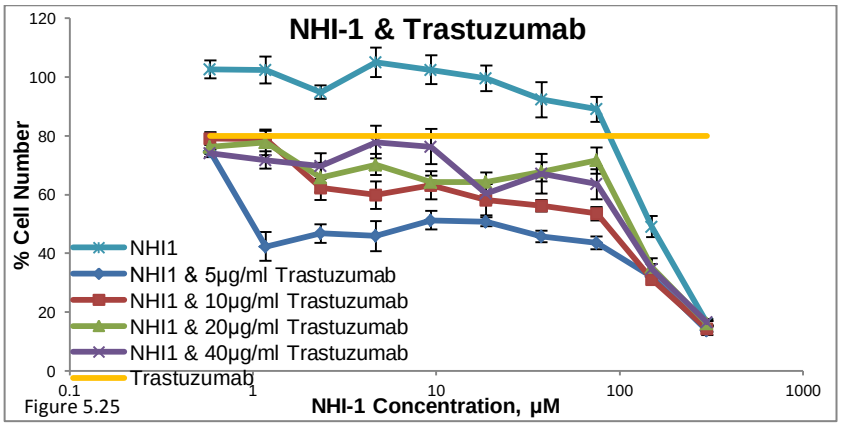

Figure 5.25

Figure 5.25: Concentration response curves of MDA-MB-361 breast cancer cells treated with NHI-1 concentrations between 0.6-300µM alone (light blue line) and combined with 5µg/ml (blue line), 10µg/ml (red line), 20µg/ml (green line) or 40µg/ml (purple line) Trastuzumab. Cell viability was determined by an SRB assay after a three day treatment. Mean results of 6 replicates are reported and error bars represent standard deviations. Values are shown as a percentage of control. In yellow the effect of Trastuzumab on cell viability is indicated. A constant 0.3% DMSO concentration was used across the whole curve in all cases. Representative data of 3 independent experiments are presented.

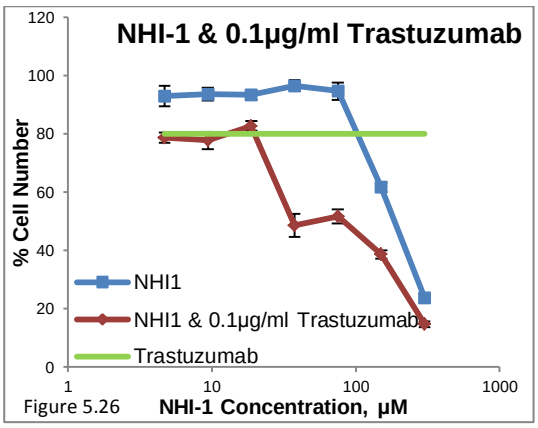

Figure 5.26

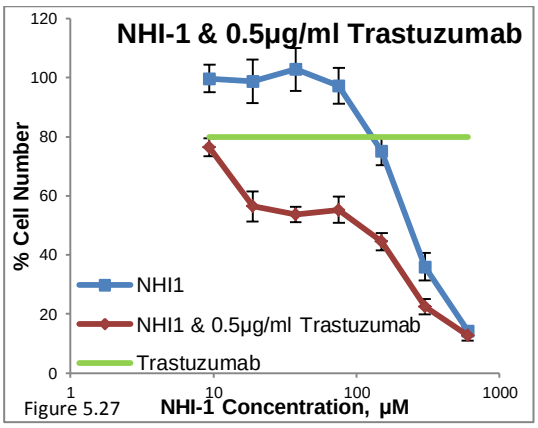

Figure 5.27

Figures 5.26 & 5.27: Concentration response curves of MDA-MB-361 breast cancer cells treated with NHI-1 concentrations between 4.7-300µM (5.26) and 9.4-600µM (5.27) alone (blue line) or combined with 0.1µg/ml (5.2.6) and 0.5µg/ml Trastuzumab (red line). Cell viability was determined by an SRB assay after a three day treatment. Mean results of 6 replicates are reported and error bars represent standard deviations. Values are shown as a percentage of control. In green the effect of Trastuzumab on cell viability is indicated. Representative data of 2 independent experiments are presented.

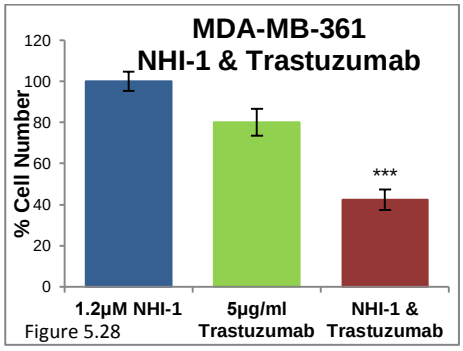

Figure 5.28

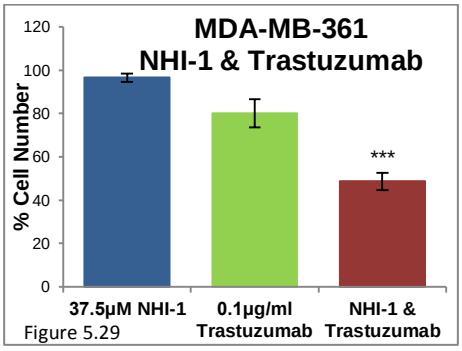

Figure 5.29

Figures 5.28 & 5.29: Effect of 1.2µM NHI-1, 5µg/ml Trastuzumab and their combination (5.28) as well as of 37.5µM NHI-1, 0.1µg/ml Trastuzumab and their combination (5.29) on cell viability of MDA-MB-361 cells. Mean results of 6 replicates are reported and error bars represent standard deviations. Statistical significance indications: *** P<0.001 compared to NHI-1 single treatment (two-tailed P value generated from unpaired t-test).

5.3 Combinations with an antidiabetic drug – Metformin

In the present study metformin was assessed in combination strategies with several glycolytic inhibitors. Interestingly a synergistic interaction was demonstrated with five of these compounds while antagonistic combinations were identified with 3PO and NHI-1.

Concentration response curves of metformin for the panel of breast and ovarian cancer cell lines used in these experiments justifying the range of concentrations used are included in the Appendix (Figures A1.1 to A1.3).

5.3.1 IOM-1190 & Metformin

The strongest synergistic combination that was identified in the present study was between the novel GLUT1 inhibitor IOM-1190 and metformin. Figure 5.30 shows that 1 or 2mM metformin enhanced greatly the potency of the GLUT1 inhibitor on MCF7 breast cancer cells. Similarly Figure 5.33 indicates that the effect of IOM-1190 on MDA-MB-231 cells was markedly augmented by the addition of 1 or 4mM metformin. The potency of these combinations is evident from the CI values. All the values generated for the whole range of used concentrations are very low indicating strong synergy. Some examples for MCF7 cells are emphasised in Figures 5.31 and 5.32. It is depicted that 0.9μM IOM-1190 reduced the cell number to 82% and 1 and 2mM metformin to 99 and 94% respectively. When IOM-1190 was combined with these two metformin concentrations the cell number was reduced to 41 and 13%. The CI values describing these combinations are 0.2 and 0.04 indicating strong and very strong synergism respectively. Regarding the triple negative cell line similar synergistic combinations are presented in Figures 5.34 and 5.35. It is shown that while 0.5μM IOM-1190 reduced the percentage of cell number to 71% and the two metformin concentrations used to 99 and 75%, when IOM-1190 was combined with each of metformin concentrations cell number was reduced to 31 and 11%. The attributed CI values to these combinations were 0.1 and 0.04 respectively indicating very strong synergism. The great efficacy of the combinations is also reflected in the very low IC_{50} values of the combination curves (Table 5.5).

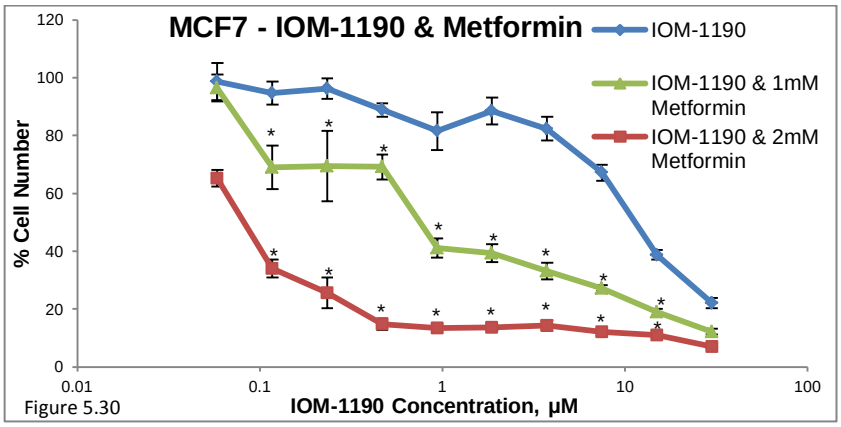

Figure 5.30: Concentration response curves of MCF7 breast cancer cells treated with IOM-1190 concentrations between 0.06-30μM alone (blue line) and combined with 1mM (green line) or 2mM Metformin (red line). Cell viability was determined by an SRB assay after a three day treatment. Mean results of 6 replicates are reported and error bars represent standard deviations. Values are shown as a percentage of control. A constant 0.3% DMSO concentration was used across the whole curve in all cases. Asterisks indicate synergistic combination points with Combination Index values lower than 0.8 (n=1).

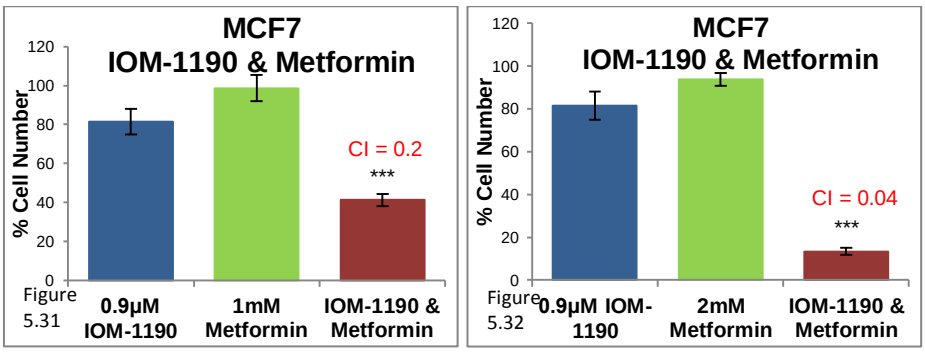

Figures 5.31 & 5.32: Effect of 0.9μM IOM-1190, 1mM Metformin and their combination (5.31) as well as effect of 0.9μM IOM-1190, 2mM Metformin and their combination (5.32) on cell viability of MCF7 cells. Mean results of 6 replicates are reported and error bars represent standard deviations. The respective Combination Index values generated through Calcusyn are indicated. Statistical significance indications: *** P<0.001 compared to IOM-1190 single treatment (two-tailed P value generated from unpaired t-test).

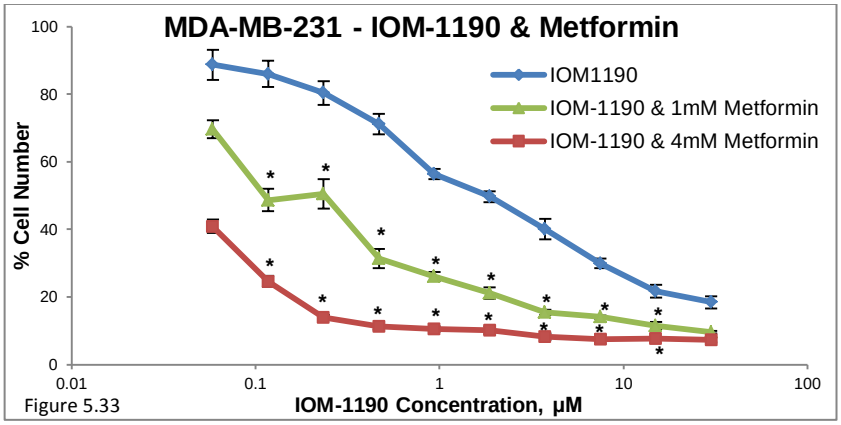

Figure 5.33: Concentration response curves of MDA-MB-231 breast cancer cells treated with IOM-1190 concentrations between 0.06-30μM alone (blue line) and combined with 1mM (green line) or 4mM Metformin (red line). Cell viability was determined by an SRB assay after a three day treatment. Mean results of 6 replicates are reported and error bars represent standard deviations. Values are shown as a percentage of control. A constant 0.3% DMSO concentration was used across the whole curve in all cases. Asterisks indicate synergistic combination points with Combination Index values lower than 0.8 (n=1).

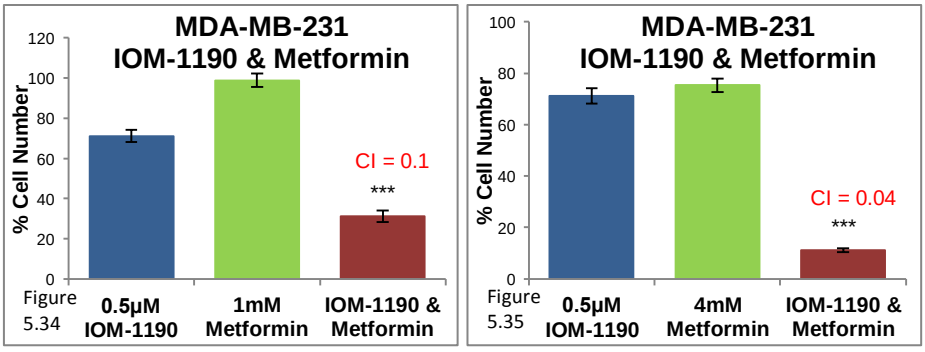

Figures 5.34 & 5.35: Effect of 0.5μM IOM-1190, 1mM Metformin and their combination (5.34) as well as effect of 0.5μM IOM-1190, 4mM Metformin and their combination (5.35) on cell viability of MDA-MB-231 cells. Mean results of 6 replicates are reported and error bars represent standard deviations. The respective Combination Index values generated through Calcusyn are indicated. Statistical significance indications: *** P<0.001 compared to IOM-1190 single treatment (two-tailed P value generated from unpaired t-test).

IC_{50} values (μM)	IOM-1190	IOM-1190 & 1mM Metformin	IOM-1190 & 2/4mM Metformin
MCF7	12.5	0.8	0.08
MDA-MB-231	1.9	0.2	<0.06

Table 5.5: Summary of the IC_{50} concentrations generated for two breast cancer cell lines when treated with IOM-1190 alone or combined with two different Metformin concentrations.

5.3.2 STF31 & Metformin

Another effective combination identified was between STF31 and metformin. The effect of the GLUT1 inhibitor on both breast and ovarian cancer cell lines was enhanced by metformin. Figures 5.36 and 5.37 depict the synergistic action of the two agents on MCF7 and MDA-MB-231 cells. The lowest CI value presented from MCF7 cells was 0.4 when 0.9μM STF31 was combined with 2mM metformin. The single agents reduced the cell number to 84 and 85% respectively however when combined the cell number was reduced to 37% (Figure 5.38). As regards the triple negative cell line Figure 5.39 demonstrates that the effect on cell viability of 1.9μM STF31 was 78%, of 3mM metformin 87% whereas their combination produced 37% cell number; giving a synergistic CI value equal to 0.2.

A synergistic interaction between STF31 and metformin was also observed for the ovarian cancer cell line pair PEA1 and PEA2. As shown in Figures 5.40 and 5.41 low CI values were generated for both cell lines. Strong synergy at the level of a CI value equal to 0.1 was demonstrated for both. Examples of the combination of 0.9μM STF31 with 1mM metformin are presented in Figures 5.42 and 5.43. The effect of this concentration of the GLUT1 inhibitor on the cell number of the platinum naïve cell line was 48%, of metformin 99% whilst their combination resulted in cell number reduced to 22%. The respective percentages for the platinum resistant line were 93% for STF31, 90% for metformin and 49% for the combination. A large shift of the IC_{50} values of the combination growth inhibition curves, compared to the STF31 single treatment curves, was observed for both breast and ovarian cancer cell lines (Table 5.6).

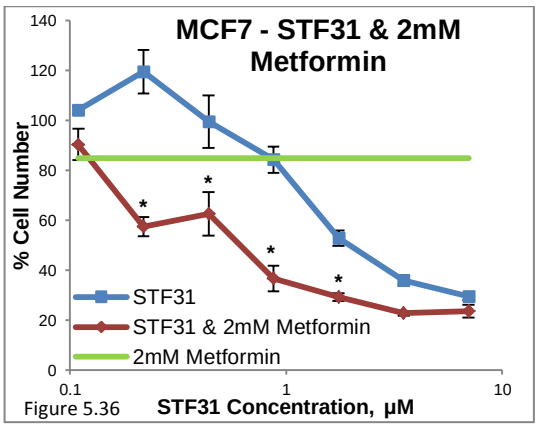

Figure 5.36

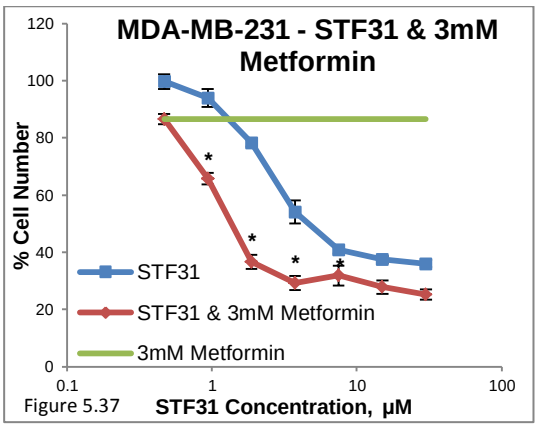

Figure 5.37

Figures 5.36 & 5.37: Concentration response curves of MCF7 (5.36) and MDA-MB-231 (5.37) breast cancer cells treated with STF31 concentrations between 0.1-7µM (MCF7) and 0.5-30µM (MDA-MB-231) alone (blue line) or combined with a constant concentration of Metformin (red line). Cell viability was determined by an SRB assay after a three day treatment. Mean results of 6 replicates are reported and error bars represent standard deviations. Values are shown as a percentage of control. In green the effect of 2mM(MCF7) or 3mM (MDA-MB-231) Metformin on cell viability is presented. Asterisks indicate synergistic combination points with Combination Index values lower than 0.8. Representative data of 3 independent experiments are presented.

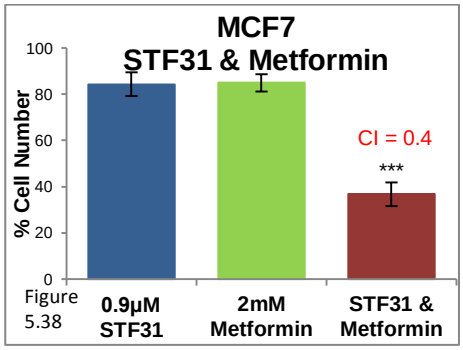

Figure 5.38

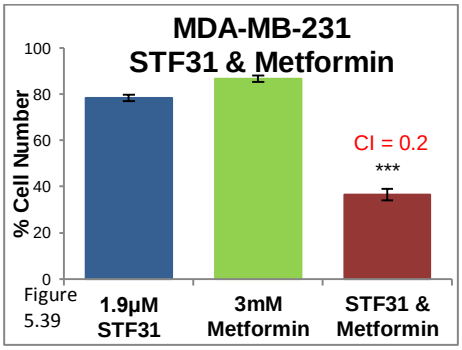

Figure 5.39

Figures 5.38 & 5.39: Effect of 0.9µM STF31, 2mM Metformin and their combination on cell viability of MCF7 cells (5.38) as well as effect of 1.9µM STF31, 3mM Metformin and their combination on cell viability of MDA-MB-231 cells (5.39). Mean results of 6 replicates are reported and error bars represent standard deviations. The respective Combination Index values generated through Calcusyn are indicated. Statistical significance indications: *** P<0.001 compared to STF31 single treatment (two-tailed P value generated from unpaired t-test).

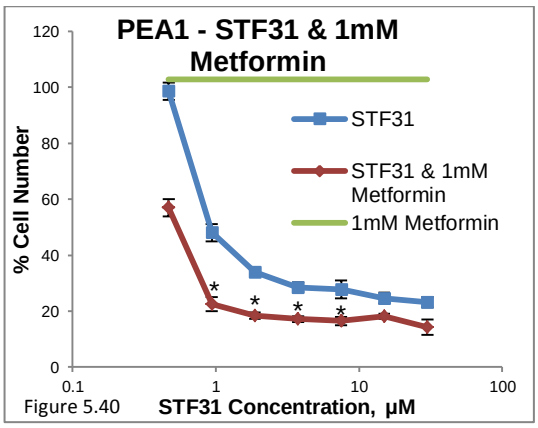

Figure 5.40

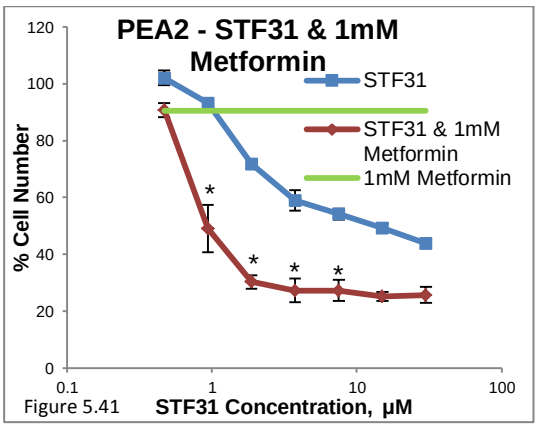

Figure 5.41

Figures 5.40 & 5.41: Concentration response curves of PEA1 (5.40) and PEA2 (5.41) ovarian cancer cells treated with STF31 concentrations between 0.5-30µM alone (blue line) or combined with 1mM Metformin (red line). Cell viability was determined by an SRB assay after a three day treatment. Mean results of 6 replicates are reported and error bars represent standard deviations. Values are shown as a percentage of control. In green the effect of 1mM Metformin on cell viability is presented. Asterisks indicate synergistic combination points with Combination Index values lower than 0.8. Representative data of 2 independent experiments are presented.

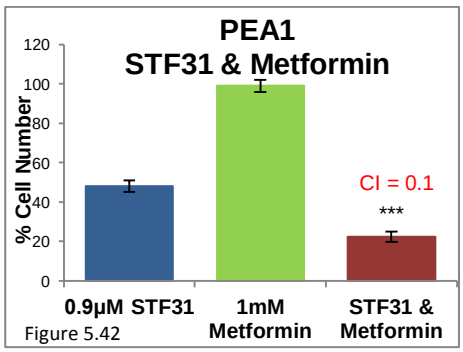

Figure 5.42

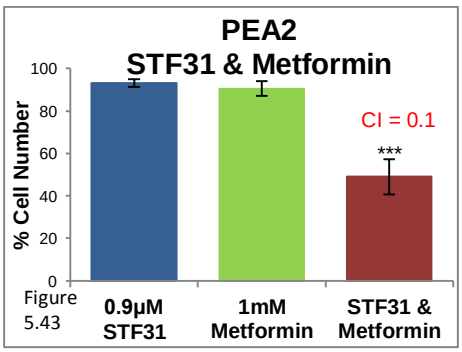

Figure 5.43

Figures 5.42 & 5.43: Effect of 0.9µM STF31, 1mM Metformin and their combination on cell viability of PEA1 (5.42) and PEA2 cells (5.43). Mean results of 6 replicates are reported and error bars represent standard deviations. The respective Combination Index values generated through Calcusyn are indicated. Statistical significance indications: *** P<0.001 compared to STF31 single treatment (two-tailed P value generated from unpaired t-test).

IC_{50} values (µM)	Breast cancer cell lines		Ovarian cancer cell lines	
	MCF7	**MDA-MB-231**	**PEA1**	**PEA2**
STF31	1.9	4.4	0.9	9.4
STF31 & Metformin	0.5	1.3	0.5	0.9

Table 5.6: Summary of the IC_{50} concentrations generated for one breast and one ovarian cancer cell line pair when treated with STF31 alone or combined with Metformin.

5.3.3 Phloretin & Metformin

An effective interaction between Phloretin and metformin was characterised for PEO1 ovarian cancer cells and is depicted in Figure 5.44. The combination was not found effective for platinum resistant ovarian cancer cell lines nor for breast lines. A synergistic action between the two compounds for the platinum sensitive line was observed only for the lower Phloretin concentrations examined. An example is presented in Figure 5.45. Even though 18.8μM of the flavonoid and 3mM metformin did not affect PEO1 cell viability their combination appeared to reduce the cell number to 60% (CI=0.4). Furthermore the IC_{50} value of the combination curve was 50% lower than the value of Phloretin single treatment (Table 5.7).

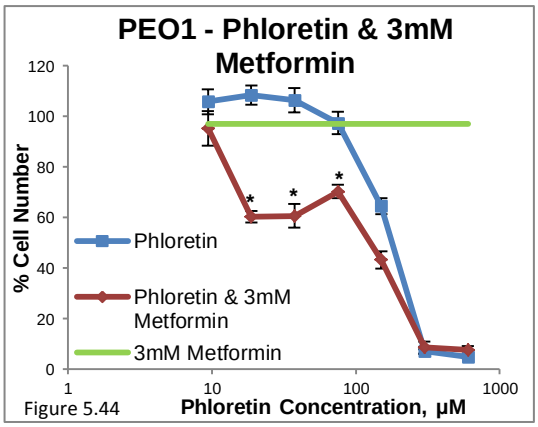

Figure 5.44: Concentration response curves of PEO1 ovarian cancer cells treated with Phloretin concentrations between 9.4-600μM alone (blue line) or combined with 3mM Metformin (red line). Cell viability was determined by an SRB assay after a three day treatment. Mean results of 6 replicates are reported and error bars represent standard deviations. Values are shown as a percentage of control. In green the effect of 3mM Metformin on cell viability is presented. Asterisks indicate synergistic combination points with Combination Index values lower than 0.8 (n=1).

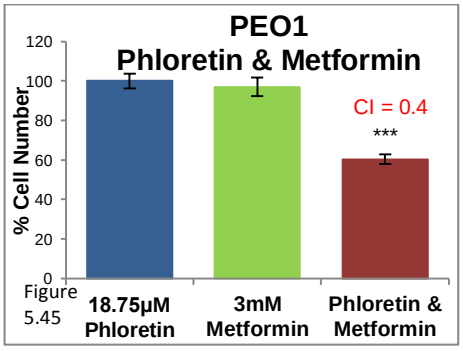

IC_{50} values (μM)	PEO1
Phloretin	175.8
Phloretin & Metformin	87.7

Table 5.7: Summary of the IC_{50} concentrations generated for one ovarian cancer cell line when treated with Phloretin alone or combined with Metformin.

Figure 5.45: Effect of 18.8μM Phloretin, 3mM Metformin and their combination on cell viability of PEO1 cells. Mean results of 6 replicates are reported and error bars represent standard deviations. The respective Combination Index value generated through Calcusyn is indicated. Statistical significance indication: *** P<0.001 compared to Phloretin single treatment (two-tailed P value generated from unpaired t-test).

5.3.4 Oxamic acid & Metformin

A promising positive interaction between Oxamic acid and metformin was identified and found to have universal effectiveness in all cancer cell lines, both breast and ovarian, that were examined. Figures 5.46 and 5.47 present a synergistic interaction between the two agents in MCF7 and MDA-MB-231 breast cancer cells. Equally low CI values (between 0.3 and 0.4) were generated for both the ER positive and the triple negative breast cancer cell line. According to Figure 5.48, 18.5mM Oxamic acid reduced MCF7 cell number to 70% and 2mM metformin to 75% while their combination reached a 68% growth inhibition. Regarding MDA-MB-231 cells as shown in Figure 5.49, 37.5mM Oxamic acid caused a reduction of the cell number to 62%, 4mM metformin to 85% and their combination to 22%.

Figures 5.50 and 5.51 demonstrate a synergistic interaction between the LDH inhibitor and metformin in the first ovarian cancer cell line pair PEA1 and PEA2; while Figures 5.54 and 5.55 are for PEO1 and PEO4 lines. The combination was very effective for all four cell lines producing very low CI values. An interesting observation though is that while the second pair of cell lines presented similar sensitivity to the combination; the platinum naïve line PEA1 was more sensitive compared to its paired platinum resistant line generating CI values even lower than 0.1. The synergistic interaction for this cell line pair is demonstrated in Figures 5.53 and 5.54. The combination of 3.1mM Oxamic acid with 1mM metformin reduced PEA1 cell number to 18% in contrast to a 10% and 2% growth inhibition presented from each compound alone (CI=0.05). Similarly 12.5mM Oxamic acid combined with 1mM metformin reduced PEA2 cell number to 48% compared to 81 and 95% when used as single agents (CI=0.3). Figures 5.56 and 5.57 depict examples of synergistic action for the other ovarian cancer cell line pair. It is shown that 3.1mM of the LDH inhibitor reduced the percentage of PEO1 cell number to 92% and 2mM metformin to 94% whereas the combination of both resulted in 29% cell viability (CI=0.2). Regarding the platinum resistant line PEO4 the combination of 6.3mM Oxamic acid with 2mM metformin caused 75% growth inhibition while each of the drugs alone were 19 and 1% respectively (CI=0.1).

Along with the low CI values generated, the efficacy of the combination of Oxamic acid with the widely prescribed antidiabetic drug is also demonstrated from the IC_{50} values of the combination curves, which were much lower compared to the values for Oxamic acid alone for all six cell lines that were examined (Table 5.8).

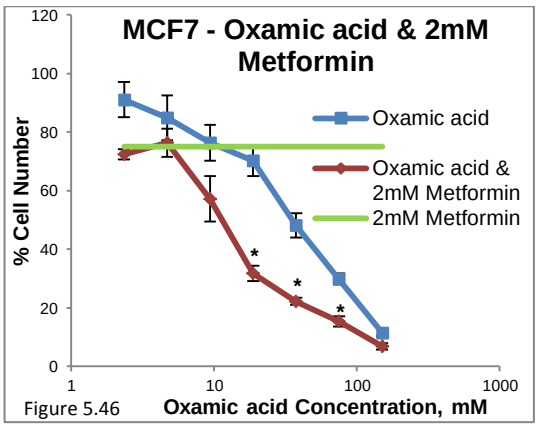

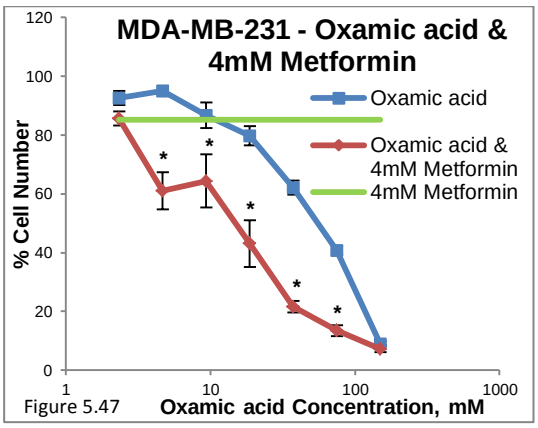

Figures 5.46 & 547: Concentration response curves of MCF7 (5.46) and MDA-MB-231 (5.47) breast cancer cells treated with Oxamic acid concentrations between 2.3-150mM alone (blue line) or combined with a constant concentration of Metformin (red line). Cell viability was determined by an SRB assay after a three day treatment. Mean results of 6 replicates are reported and error bars represent standard deviations. Values are shown as a percentage of control. In green the effect of 2mM (MCF7) or 4mM (MDA-MB-231) Metformin on cell viability is presented. Asterisks indicate synergistic combination points with Combination Index values lower than 0.8. Representative data of 2 independent experiments are presented.

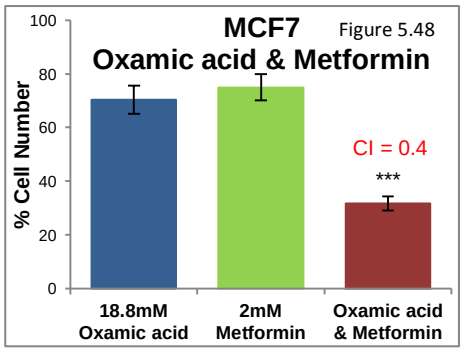

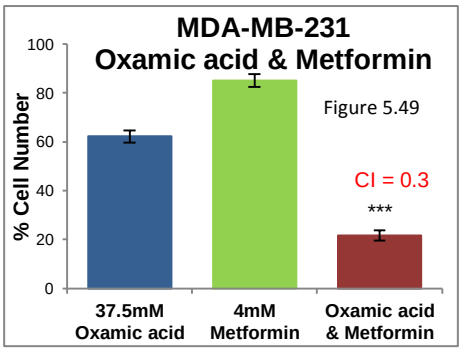

Figures 5.48 & 5.49: Effect of 18.8mM Oxamic acid, 2mM Metformin and their combination on cell viability of MCF7 cells (5.48) as well as effect of 37.5mM Oxamic acid, 4mM Metformin and their combination on cell viability of MDA-MB-231 cells (5.49). Mean results of 6 replicates are reported and error bars represent standard deviations. The respective Combination Index values generated through Calcusyn are indicated. Statistical significance indications: *** P<0.001 compared to Oxamic acid single treatment (two-tailed P value generated from unpaired t-test).

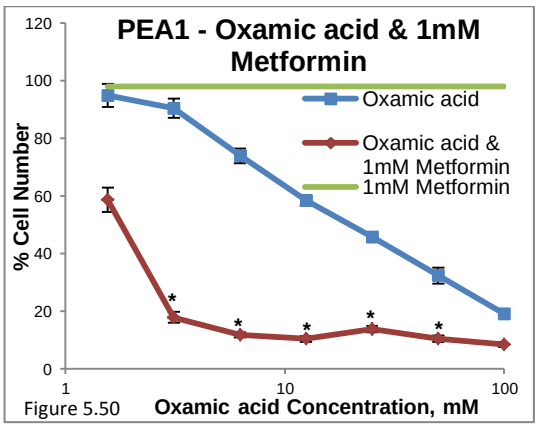

Figure 5.50

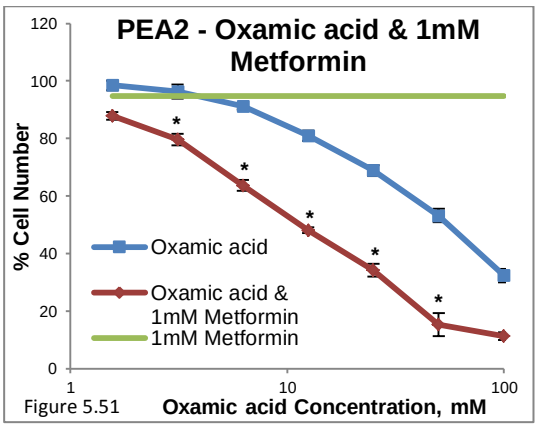

Figure 5.51

Figures 5.50 & 5.51: Concentration response curves of PEA1 (5.50) and PEA2 (5.51) ovarian cancer cells treated with Oxamic acid concentrations between 1.56-100mM alone (blue line) or combined with 1mM Metformin (red line). Cell viability was determined by an SRB assay after a three day treatment. Mean results of 6 replicates are reported and error bars represent standard deviations. Values are shown as a percentage of control. In green the effect of 1mM Metformin on cell viability is presented. Asterisks indicate synergistic combination points with Combination Index values lower than 0.8. Representative data of 3 independent experiments are presented.

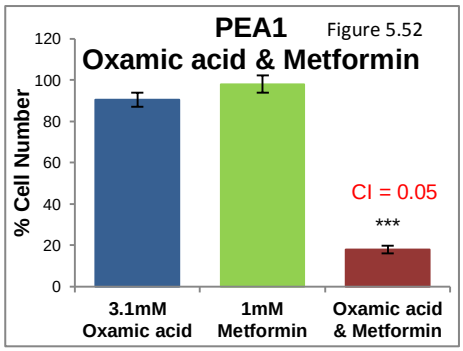

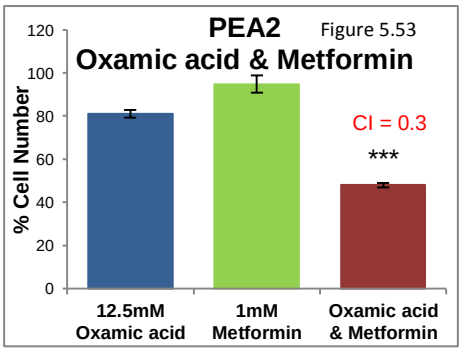

Figures 5.52 & 5.53: Effect of 3.1mM Oxamic acid, 1mM Metformin and their combination on cell viability of PEA1 cells as well as effect of 12.5mM Oxamic acid, 1mM Metformin and their combination on cell viability of PEA2 cells. Mean results of 6 replicates are reported and error bars represent standard deviations. The respective Combination Index values generated through Calcusyn are indicated. Statistical significance indications: *** $P<0.001$ compared to Oxamic acid single treatment (two-tailed P value generated from unpaired t-test).

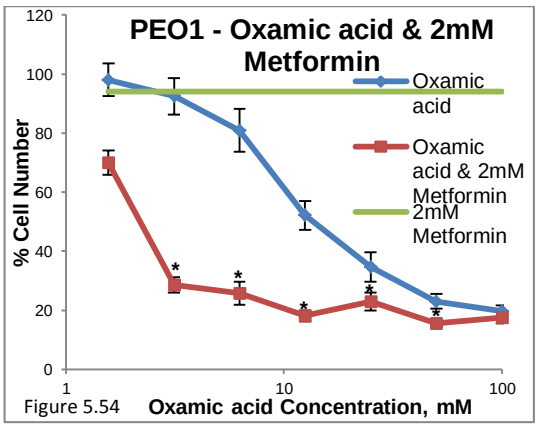

Figure 5.54

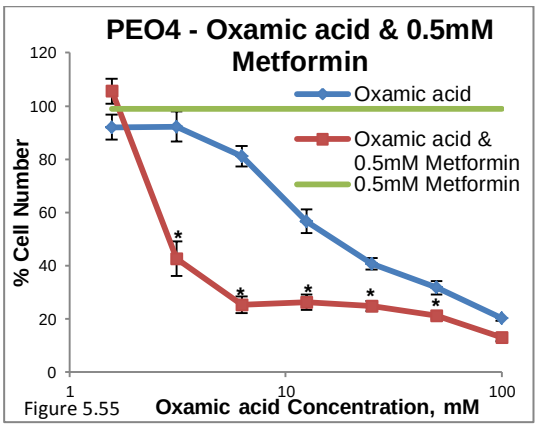

Figure 5.55

Figures 5.54 & 5.55: Concentration response curves of PEO1 (5.54) and PEO4 (5.55) ovarian cancer cells treated with Oxamic acid concentrations between 1.56-100mM alone (blue line) or combined with a constant concentration of Metformin (red line). Cell viability was determined by an SRB assay after a three day treatment. Mean results of 6 replicates are reported and error bars represent standard deviations. Values are shown as a percentage of control. In green the effect of 2mM (PEO1) or 0.5mM (PEO4) Metformin on cell viability is presented. Asterisks indicate synergistic combination points with Combination Index values lower than 0.8. Representative data of 3 independent experiments are presented.

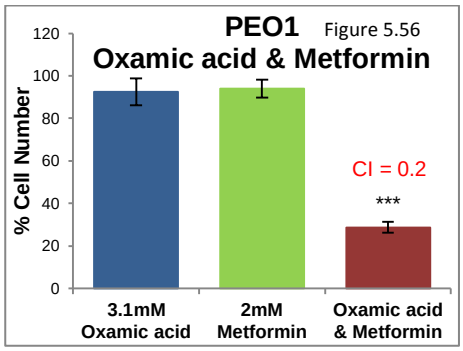

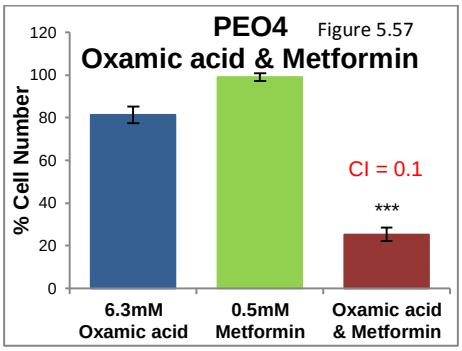

Figures 5.56 & 5.57: Effect of 3.1mM Oxamic acid, 2mM Metformin and their combination on cell viability of PEO1 cells as well as effect of 6.3mM Oxamic acid, 0.5mM Metformin and their combination on cell viability of PEO4 cells. Mean results of 6 replicates are reported and error bars represent standard deviations. The respective Combination Index values generated through Calcusyn are indicated. Statistical significance indications: *** P<0.001 compared to Oxamic acid single treatment (two-tailed P value generated from unpaired t-test).

IC_{50} values (mM)	Breast cancer cell lines		Ovarian cancer cell line pairs			
	MCF7	**MDA-MB-231**	**PEA1**	**PEA2**	**PEO1**	**PEO2**
Oxamic acid	33.1	49.7	18.8	19	14.5	18
Oxamic acid & Metformin	10.8	12.2	1.7	11.5	2	2.7

Table 5.8: Summary of the IC_{50} concentrations generated for one breast and two ovarian cancer cell line pairs when treated with Oxamic acid alone or combined with Metformin.

5.3.5 Dichloroacetate & Metformin

Figures 5.58 and 5.59 provide evidence of a synergistic interaction between DCA and metformin for MCF7 and MDA-MB-231 cells. The inhibitor of oxidative phosphorylation was found to enhance the efficacy of DCA only on breast cancer cell lines. The triple negative cell line was found more sensitive to the combination as very low CI values were generated suggesting strong synergism. Examples of the synergistic interaction are presented in Figures 5.60 and 5.61. Combination of 6.3mM DCA with 1mM metformin reduced the percentage of MCF7 cell number to 45% compared to 69 and 88% cell number that was caused from each of them alone (CI=0.4). As for MDA-MB-231 cells 3.1mM DCA did not affect the cell number, 3mM metformin reduced the cell number to 87% and their combination to 57% (CI=0.2). Sensitivity to the combination of the drugs was at least 50% higher compared to the use of the PDHK1 inhibitor alone; as this was quantified by an IC_{50} value of the combination curve lower than the one of the DCA curve (Table 5.9).

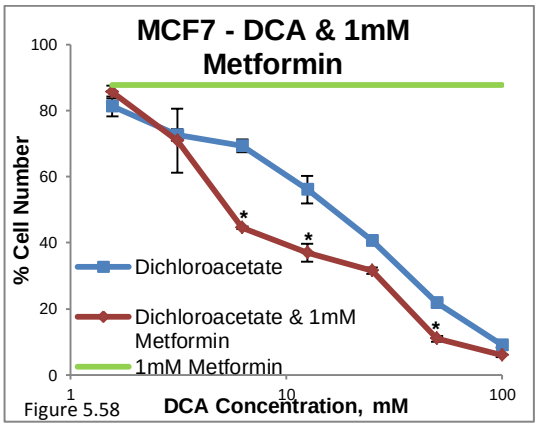

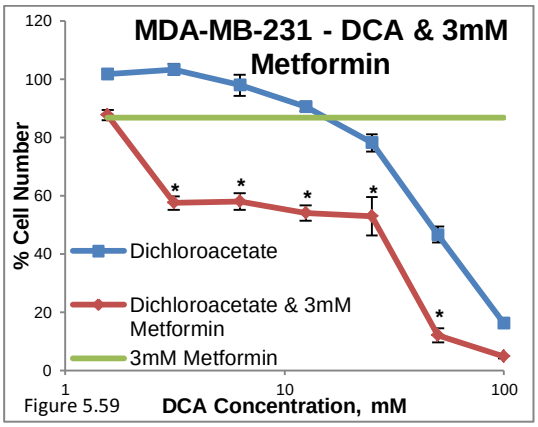

Figures 5.58 & 5.59: Concentration response curves of MCF7 (5.58) and MDA-MB-231 (5.59) breast cancer cells treated with Dichloroacetate concentrations between 1.56-100mM alone (blue line) or combined with a constant concentration of Metformin (red line). Cell viability was determined by an SRB assay after a three day treatment. Mean results of 6 replicates are reported and error bars represent standard deviations. Values are shown as a percentage of control. In green the effect of 1mM (MCF7) or 3mM (MDA-MB-231) Metformin on cell viability is presented. Asterisks indicate synergistic combination points with Combination Index values lower than 0.8 (n=1).

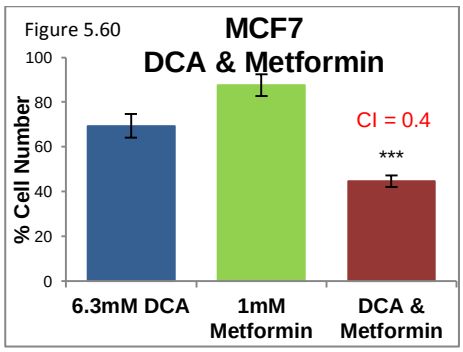

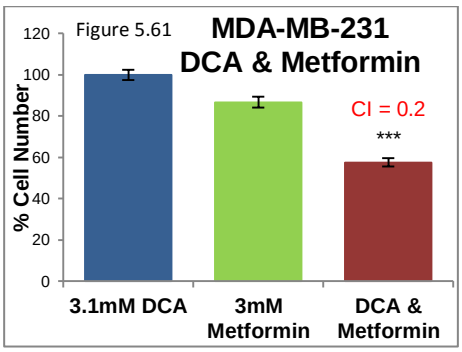

Figures 5.60 & 5.61: Effect of 6.3mM DCA, 1mM Metformin and their combination on cell viability of MCF7 cells (5.60) as well as effect of 3.1mM DCA, 3mM Metformin and their combination on cell viability of MDA-MB-231 cells (5.61). Mean results of 6 replicates are reported and error bars represent standard deviations. The respective Combination Index values generated through Calcusyn are indicated. Statistical significance indications: *** P<0.001 compared to DCA single treatment (two-tailed P value generated from unpaired t-test).

IC_{50} values (mM)	MCF7	MDA-MB-231
Dichloroacetate	14.9	47.5
Dichloroacetate & Metformin	6.5	27.9

Table 5.9: Summary of the IC_{50} concentrations generated for two breast cancer cell lines when treated with Dichloroacetate alone or combined with Metformin.

The following table summarises the most successful combinations that were identified in this study (Table 5.10). These combinations produced promising effects in breast and ovarian cancer cell lines and merit further investigation as possible treatments.

Glycolytic Inhibitor	Traditional Drug	Breast Cancer Cell Lines	Ovarian Cancer Cell Lines
IOM-1190	Metformin	✚	
STF31	Metformin	✚	✚
3PO	Cisplatin		✚
3PO	Paclitaxel		✚
Oxamic acid	Metformin	✚	✚
Oxamic acid	Trastuzumab	✚	
NHI-1	Trastuzumab	✚	

Table 5.10: Summary of the most successful combinations identified in this study.

5.4 The effect of STF31 & Metformin combination on induction of apoptosis

The combination of STF31 with metformin was identified as a very successful combination on both breast and ovarian cancer cell lines. The mechanism of antiproliferative action of this combination was examined through flow cytometric analysis of double stained MDA-MB-231 cells with FITC-conjugated annexin V and propidium iodide. Figures 5.62 and 5.63 present the scatter plots of gated cells treated with 4μM STF31, 4mM metformin and their combination for 24 and 48h. Data illustrates that combination treatment of the two drugs inhibited cancer cell growth through induction of apoptotic cell death. Regarding cells treated with the combination of STF31 with metformin for 24h the population undergoing apoptosis stained positive with annexin V (upper region) was quantified at 8.1%; this represented an increase of 100% compared to the respective percentages of cells treated with each of the agents alone. After a 48h combination treatment late apoptotic cells, positively stained with annexin V and PI (upper right quadrant), reached 14.3% when the same population after single treatment with either 4μM STF31 or 4mM metformin was found to be 4.5 and 7.1% respectively.

Scatter plots of untreated MDA-MB-231 control cells can be seen in the Appendix (Figures A1.8&A1.9).

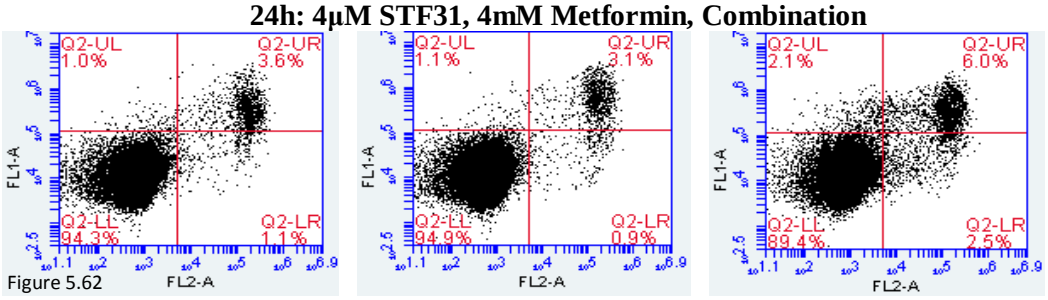

Figure 5.62

Figure 5.62: Flow cytometric analysis of MDA-MB-231 breast cancer cells treated with 4μM STF31, 4mM Metformin and their combination for 24h. FL1 (annexin V) versus FL2 (PI) scatter plots of gated cells double stained with FITC-conjugated annexin V and propidium iodide are presented. The percentage of cells in each quadrant is indicated in red (n=1).

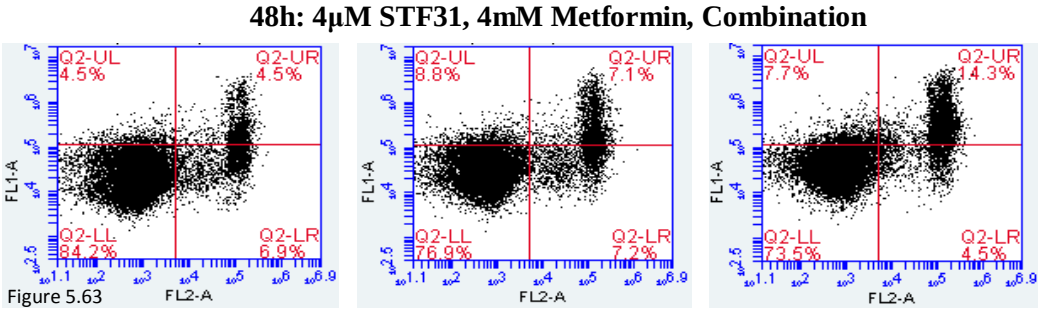

Figure 5.63: Flow cytometric analysis of MDA-MB-231 breast cancer cells treated with 4µM STF31, 4mM Metformin and their combination for 48h. FL1 (annexin V) versus FL2 (PI) scatter plots of gated cells double stained with FITC-conjugated annexin V and propidium iodide are presented. The percentage of cells in each quadrant is indicated in red (n=1).

Figures 5.64 and 5.65 illustrate the percentage of live, apoptotic and necrotic cell populations as quantified after cell cytometric analysis of MDA-MB-231 cells treated with STF31 and metformin alone or combined for 24 or 48h.

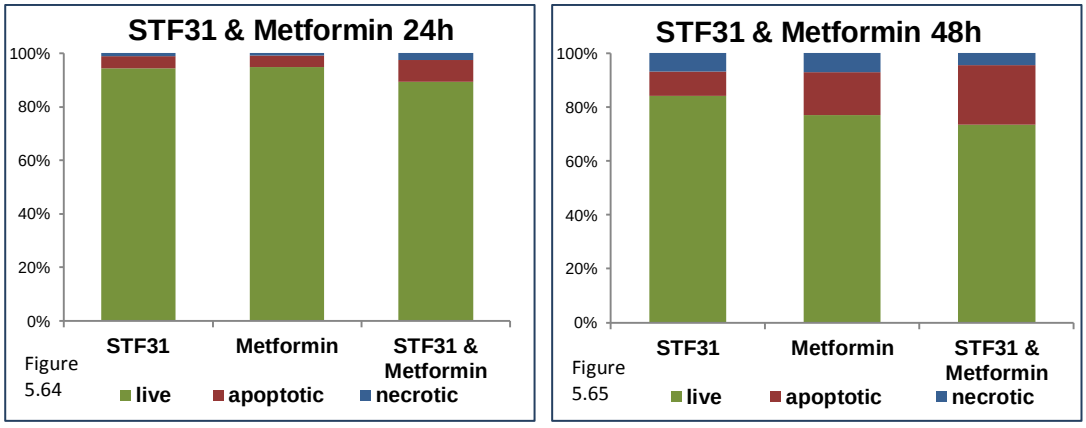

Figures 5.64 & 5.65: Quantification of percentages of apoptotic, necrotic and live MDA-MB-231 cells when treated with STF31 and Metformin alone or combined for 24 or 48h, as generated through flow cytometric analysis.

5.5 The effect of glycolytic inhibitor combinations with Metformin on cell cycle progression

To examine whether the combinations of glycolytic inhibitors with metformin had an impact on cell cycle progression, compared to their use as single agents, flow cytometric analysis was performed. PI fluorescent staining was used to separate MDA-MB-231 cell populations in different phases of the cell cycle according to their cellular DNA content. The histogram plots presented below illustrate the effect of the combinations of three glycolytic inhibitors, IOM-1190, STF31 and Oxamic acid, with metformin on cell cycle progression. Figure 5.66 demonstrates that combination treatment of IOM-1190 with metformin was associated with cell cycle arrest in the G2 phase. The proportion of cells in this phase of the cell cycle was found to be 54.2%, doubled compared to the respective percentages of single treated cells. Figure 5.67 indicates that combination treatment of MDA-MB-231 cells with STF31 and metformin did not have any additional effect on cell cycle progression compared to treatment with each of the drugs alone. The distribution of double treated cells in each stage of the cell cycle was similar to that of cells treated with them as single agents. Co-treatment of Oxamic acid with metformin was associated with cell cycle arrest in G1 phase. As shown in Figure 5.68 the percentage of co-treated cells found in the G1 phase was 66.4% compared to 57.6 and 52.85% for cells treated with either Oxamic acid or metformin. A corresponding decrease of cells in G2/M phases was observed.

Histogram plots of untreated MDA-MB-231 control cells can be seen in the Appendix (Figure A1.10).

0.5μM IOM-1190, 4mM Metformin, Combination

Figure 5.66

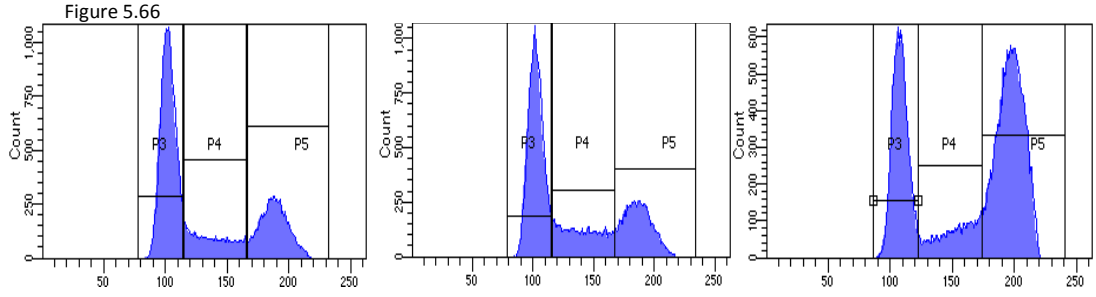

	0.5µM IOM-1190	4mM Metformin	IOM-1190 & Metformin
G0/G1	55	52.85	32.6
S	17.5	21.4	13.2
G2/M	27.5	25.75	54.2

Figure 5.66 & Table 5.11: Flow cytometric analysis of cellular DNA content of MDA-MB-231 breast cancer cells treated with 0.5µM IOM-1190, 4mM Metformin and their combination for 24h. In the histograms fluorescence of the DNA bound propidium iodide, indicating the DNA content in X-axis, is plotted against the number of cells in the Y-axis. The percentage of cells in each cell cycle phase is demonstrated in the complementary table (n=1).

4µM STF31, 4mM Metformin, Combination

Figure 5.67

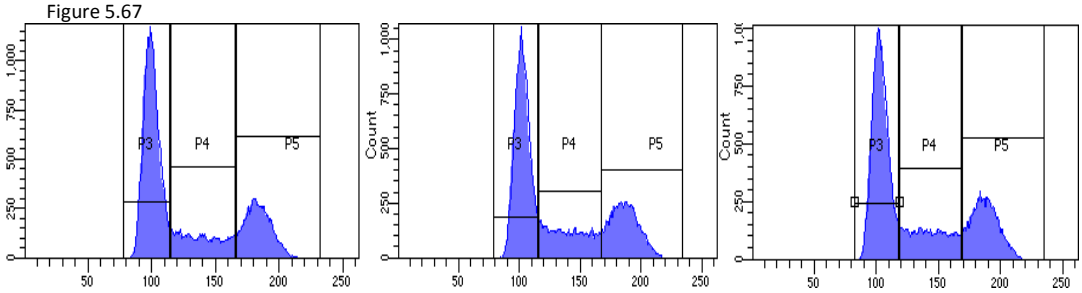

	4µM STF31	4mM Metformin	STF31 & Metformin
G0/G1	55.9	52.85	50.5
S	18.9	21.4	22.2
G2/M	25.2	25.75	27.3

Figure 5.67 & Table 5.12: Flow cytometric analysis of cellular DNA content of MDA-MB-231 breast cancer cells treated with 4µM STF31, 4mM Metformin and their combination for 24h. In the histograms fluorescence of the DNA bound propidium iodide, indicating the DNA content in X-axis, is plotted against the number of cells in the Y-axis. The percentage of cells in each cell cycle phase is demonstrated in the complementary table (n=1).

20mM Oxamic acid, 4mM Metformin, Combination

Figure 5.68

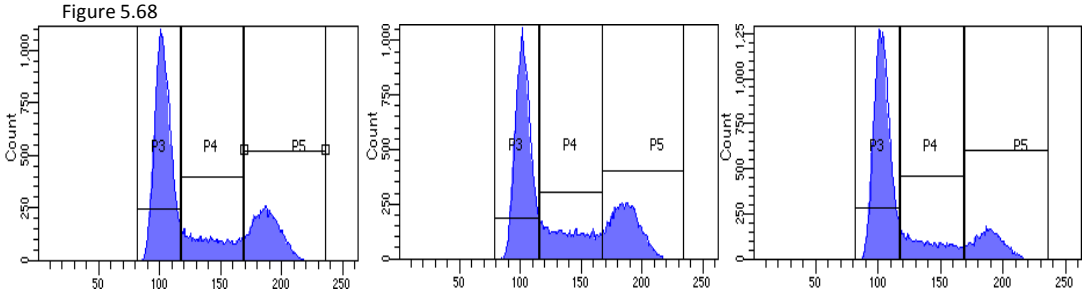

	20mM Oxamic acid	4mM Metformin	Oxamic acid & Metformin
G0/G1	57.6	52.85	66.4
S	18.4	21.4	17.2
G2/M	24	25.75	16.4

Figure 5.68 & Table 5.13: Flow cytometric analysis of cellular DNA content of MDA-MB-231 breast cancer cells treated with 20mM Oxamic acid, 4mM Metformin and their combination for 24h. In the histograms fluorescence of the DNA bound propidium iodide, indicating the DNA content in X-axis, is plotted against the number of cells in the Y-axis. The percentage of cells in each cell cycle phase is demonstrated in the complementary table (n=1).

Figures 5.69 to 5.71 illustrate the proportion of cells in the G0/G1, S and G2/M phases of the cell cycle as quantified after cell cytometric analysis of MDA-MB-231 cells treated with IOM-1190, STF31, Oxamic acid and Metformin alone or combined for 24h.

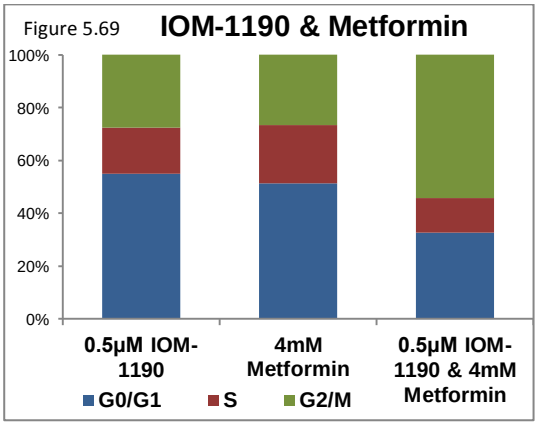

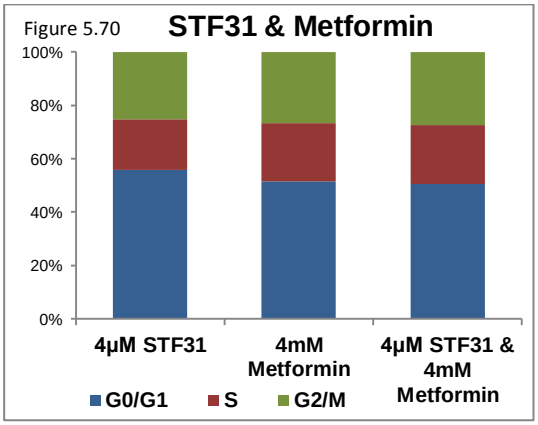

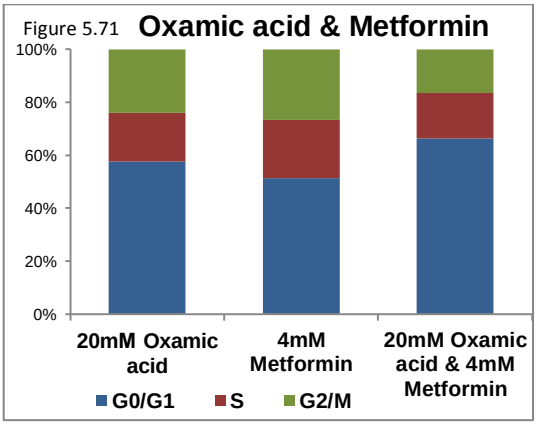

Figures 5.69 to 5.71: Quantification of percentages of MDA-MB-231 cells in the G0/G1, S and G2/M phases of the cell cycle when treated with IOM-1190, STF31, Oxamic acid and Metformin alone or combined for 24h, as generated through flow cytometric analysis.

5.6 Discussion

Currently, the administration of antitumour therapy generally involves combinatorial strategies of several therapeutic agents. Drug combinations aim to augment the therapeutic benefit, reduce the adverse effects and delay or ideally hinder resistance [448]. Synergism can be defined as an effective drug interaction where one agent enhances the effect of the other and the combination of them both is more efficient than each of them individually. In contrast antagonism refers to the case where two agents used together are less effective than each of them separately with one opposing the other's action [402].

The median-drug effect analysis method is a mathematical model commonly used for the analysis of the effectiveness of drug interaction studies. It was developed by Chou and Talalay and assumes sigmoidal concentration response curves from both single agents and their combination [402, 448]. CI values were generated based on this method using the Calcusyn Software. In this way each combination point was characterised quantitatively as synergistic, additive or antagonistic. However, the mathematical algorithm is unreliable when growth inhibition is minimal (around 100% growth) or maximal (almost 0% growth) and for that reason edge values near each end point of the sigmoidal curves were excluded from every analysis.

The combinatorial experiments of this study were designed involving simultaneous drug exposure and a non-constant concentration ratio. A range of different concentrations with 1:2 dilution steps of the glycolytic inhibitors were combined with a fixed concentration, around the IC_{20} or less, of the established drug. In this set of experiments the constant concentration of the non-glycolytic inhibitor was selected based on its growth inhibition effect. The main aim was to use a low clinically relevant concentration (below the IC_{20} of the single drug inhibition curve) that would have roughly the same growth inhibitory effect between each cell line pair. Therefore for example a higher concentration of cisplatin was used for the platinum resistant PEA2 line compared to the platinum naïve PEA1 line to achieve a comparable antiproliferative effect (4μM compared to 1μM – Figures 5.1&5.2).

The main goal of the current chapter of this thesis was to investigate the efficacy of novel combinatorial strategies among glycolytic inhibitors and traditional therapeutics. Among a wide range of investigated combinations (Table 5.1) only the ones that proved effective generating low CI values and were considered promising for further evaluation have been presented. Representative examples of non-effective combinations are included in the

Appendix (Figures A1.4 to A1.7). Nevertheless it should be highlighted that this refers to the current experimental design and conditions. It is not unlikely that a different experimental setting for example sequential (non-simultaneous) delivery or a different cell line model could generate different results.

5.6.1 Glycolytic inhibitors potentiated the antiproliferative effect of cisplatin and paclitaxel on breast and ovarian cancer cells

Resistance to common chemotherapeutic agents has been associated with the deregulated reliance of tumours on the glycolytic pathway. It has been suggested that targeting the metabolic phenotype of tumours may enhance the efficacy of chemotherapy regimens and moreover resensitise tumour cells to treatment to which they had developed resistance [382, 383]. Possible proposed mechanisms predict glycolysis inhibition reducing cellular ATP levels and compromising the activation of resistance pathways or attenuating tumour growth promoting induction of apoptosis and hindering the adaptation to chemotherapeutic treatment [382, 383].

The interaction between cisplatin and a range of glycolytic inhibitors was examined in this study (Table 5.1). Cisplatin is the most extensively used drug for the treatment of ovarian cancer however resistance frequently emerges [385]. A dilution series of certain compounds targeting the glycolytic pathway was used in combination with a fixed concentration of the platinum analogue. It was observed that the PFKFB3 inhibitor 3PO significantly enhanced the anticancer effect of cisplatin in four ovarian cancer cell line models. The platinum naïve cell line PEA1 was particularly sensitive to the combination of 3PO with cisplatin generating CI values as low as 0.2 indicating strong synergism. For the platinum sensitive line of the other pair, PEO1, the combination was also effective, however the lowest synergistic CI value observed was in the range of 0.6. Interestingly both platinum resistant lines, PEA2 and PEO4, were also responsive to this combination with lowest CI values detected equal to 0.5 and 0.6 for each cell line respectively (Figures 5.1 to 5.8). This is an important finding suggesting that combinatorial treatment of cisplatin with 3PO could reverse the platinum resistant phenotype and may be an effective strategy against platinum-resistant ovarian tumours. It should be noted that the concentrations of the two drugs that gave the lowest CI values are relatively low and potentially achievable in *in vivo* experiments.

Paclitaxel is an anti-mitotic agent extensively used for the treatment of both breast and ovarian cancer. A favourable interaction was identified in this study between the PFKFB3

inhibitor and paclitaxel. 3PO combined with paclitaxel presented synergistic anticancer action on ovarian cancer cells. Both PEA1 and PEA2 lines of the first ovarian cancer cell line pair were very sensitive to this combination. Very low CI values indicating strong synergism were generated for both of them. Interestingly this was not the case for the other pair. While synergistic CI values were detected for the platinum sensitive PEO1 line its paired platinum resistant PEO4 line responded to the combination showing moderate antagonism. Synergism was only observed when a high concentration of 3PO equal to 15μM was used but this defeats the main purpose of the combination being to use low concentrations of the individual agents and cannot be considered promising (Figures 5.9 to 5.16). Nevertheless the effectiveness of the combination in the other lines including the resistant PEA2 line suggests that this combination might have *in vivo* potential. On searching the literature, this research appears to be the first providing direct evidence of a synergistic interaction between 3PO and widely used chemotherapeutic cytotoxic agents.

To date a number of studies have revealed that certain compounds targeting the glycolytic metabolism of tumours might improve the therapeutic index of chemotherapeutic cytotoxic agents mainly through reduction of the ATP levels selectively in malignant cells [382, 383]. Similar to this study's observations Liu *et al* reported synergistic antitumour action between the GLUT1 inhibitor WZB117 and cisplatin or paclitaxel [319]. Another glucose transport inhibitor, the phytochemical Phloretin, has been shown to potentiate the cytotoxic effect of daunorubicin promoting apoptosis and also sensitised resistant leukaemia and colon cancer cells to the anthracycline exclusively under hypoxic conditions [287]. Nakano *et al* documented that the HKII inhibitor 3BP enhanced the anticancer effects of daunorubicin and doxorubicin in leukaemia and myeloma cells both *in vitro* and *in vivo*. The glycolytic inhibitor diminished the cellular ATP levels which led to inactivation of the ATP-binding cassette transporters (ABC) therefore preventing the agent's efflux from malignant cells [449]. Synergistic antitumour activity has also been evidenced among DCA and 5-fluorouracil in colon cancer cell lines demonstrating elevated apoptotic cell death compared to treatment with each agent individually [450].

An additional effective combination that was described here was that between Oxamic acid and paclitaxel. The competitive LDH inhibitor proved able to enhance the potency of the taxane on two breast cancer cell lines. Both the ER positive MCF7 line and the triple negative MDA-MB-231 line gave synergistic CI values for the lowest Oxamic acid concentrations used (Figures 5.17 to 5.20). Nonetheless Oxamic acid required great concentrations in the millimolar range which renders the possibility of further developing

this combination problematic. Research using Oxamic acid as a lead compound to synthesise a derivative exhibiting enhanced potency and membrane permeability is currently being conducted [368]. However for the potent selective LDHA inhibitor, NHI-1, no synergistic inhibitory interaction with paclitaxel was observed under the particular conditions of these experiments.

In their key study Zhou *et al* linked LDHA expression with resistance to paclitaxel in breast tumours. They observed elevated LDHA expression and activity in paclitaxel resistant breast cancer cells and demonstrated that LDHA siRNA knockdown or inhibition by Oxamic acid significantly enhanced their sensitivity to paclitaxel. The authors suggested that the combination of Oxamic acid with paclitaxel could be promising for the treatment of paclitaxel resistant mammary malignancy promoting apoptotic cell death [373]. The contribution of the current thesis lies in the observation of a synergistic interaction between Oxamic acid and paclitaxel in paclitaxel sensitive breast cancer cell lines. It is possible to hypothesise that combinatorial treatment of these two agents could delay or even prevent development of paclitaxel resistance. This would be of great importance and remains to be further investigated.

5.6.2 LDH inhibitors potentiated the antiproliferative effect of trastuzumab on breast cancer cells

Trastuzumab is a recombinant humanised monoclonal antibody against the HER2 receptor. It has revolutionised treatment of HER2 positive breast tumours however clinical resistance presents a major challenge [32]. In the present study I examined the effect of two LDH inhibitors combined with several constant concentrations of trastuzumab on cell growth of the HER2 amplified MDA-MB-361 breast cancer cell line. As shown in Figure 5.21 trastuzumab induced an invariable cytostatic effect on MDA-MB-361 cells reducing their cell number by 20%. For this reason it was not possible to analyse the data in the Calcusyn software and obtain quantitative CI values since sigmoidal growth inhibition curves from both single agents is a requirement of the used algorithm. As shown, the MDA-MB-361 cell line is moderately sensitive to trastuzumab treatment and therefore it has been used as a model system for the study of trastuzumab resistant disease [451].

Both LDH inhibitors enhanced the antiproliferative effect of trastuzumab on breast cancer cells. Even though quantitative characterisation was not possible it was obvious that in both cases the combination is much more effective than each single agent individually. This

according to the current predominant definition qualifies for synergism [402]. Oxamic acid enhanced the efficacy of several different trastuzumab concentrations, ranging from 10 to 80μg/ml, in a comparable way. In contrast, the novel selective LDHA inhibitor NHI-1 improved the inhibitory effect of low trastuzumab concentration (5μg/ml) more effectively compared to higher concentrations (40μg/ml). Interestingly, NHI-1 markedly increased the sensitivity of MDA-MB-361 cells to trastuzumab concentrations as low as 0.1 and 0.5μg/ml, (Figures 5.22 to 5.29). Taking into account that MDA-MB-361 cells represent trastuzumab resistant breast cancer these findings suggest that combination of LDH inhibitors with trastuzumab has the potential to be developed for the treatment of HER2 positive trastuzumab resistant breast malignancy.

Zhao *et al* were the first to report a synergistic interaction between trastuzumab and Oxamic acid. They observed that trastuzumab inhibits the glycolytic metabolism of HER2 positive tumours via heat shock factor 1 and LDHA downregulation and associated trastuzumab resistance with the elevated dependency of tumours on the glycolytic pathway. They demonstrated that Oxamic acid enhanced the antitumour activity of trastuzumab in both trastuzumab sensitive and resistant HER2 high breast cancers *in vitro* as well as *in vivo*. They proposed this combination as a strategy to battle trastuzumab resistance [372].

The present study confirms previous findings and contributes additional evidence that suggests that LDHA inhibition can potentially reverse trastuzumab resistance in HER2 amplified breast tumours. A favourable interaction between trastuzumab and the selective LDHA inhibitor NHI-1 appears not to have been described before. An important noteworthy finding is that the concentration of trastuzumab required to augment the NHI-1 effect on MDA-MB-361 cellular growth is considerably lower compared to the concentrations used for the pyruvate analogue Oxamic acid.

Zhao *et al* suggested that inhibition of the glycolytic metabolism of tumours is associated with the antitumour mechanism of trastuzumab. Therefore inhibition of the glycolytic pathway, broader than LDHA inhibition, could enhance the potency of trastuzumab on HER2 positive breast tumours. Additionally to Oxamic acid a synergistic interaction with 2DG has also been demonstrated [372]. A question arises as to whether inhibition of other glycolytic enzymes with more potent ‘next-generation’ compounds may have the same impact on trastuzumab efficacy. This remains to be further investigated and has great potential to bring a new era in treating trastuzumab resistant disease.

5.6.3 Metformin potentiated the antiproliferative effect of glycolytic inhibitors on breast and ovarian cancer cells

Metformin is a biguanide universally prescribed for the treatment of type 2 diabetes mellitus. Besides its anti-hyperglycaemic action metformin is known to inhibit the mitochondrial respiratory chain complex 1. Reduced ATP synthesis leads to an increased AMP/ATP intracellular ratio provoking AMPK activation and mTOR inhibition. In recent years, there has been an increasing volume of literature providing evidence of marked antitumour activity. Even though diabetic patients have a well substantiated elevated risk for the development of cancer a growing body of epidemiologic studies and meta-analyses have associated metformin treatment with decreased cancer incidence as well as with improved clinical outcome of diabetic cancer patients [389-392, 452, 453].

Metformin has received considerable critical attention and is currently a major area of extensive research and numerous clinical trials in various cancer types as chemoprevention, monotherapy or in combination with several chemotherapeutic agents [389-392, 452, 453].

Metformin is a very attractive candidate for combinatorial cancer treatment. There are several lines of evidence that recognise its antiproliferative properties; there is great experience in human administration coupled with a favourable toxicity profile and minimal cost. Nevertheless contradictory findings have recently emerged and a number of clinical trials have questioned metformin's antitumour value in non-diabetic patients. Further research and large scale clinical trials are required to elucidate the mechanisms and substantiate the anticancer efficacy of this biguanide [389, 390, 392, 452, 453].

A number of pre-clinical as well as epidemiological studies have revealed that metformin potentiates cancer therapeutics [389, 391, 452]. It has been suggested that metformin selectively targets cancer stem cells which are resistant to several chemotherapeutics. Hirsch *et al* reported that metformin in concert with doxorubicin was able to eradicate the stem cell and non-stem cell cancer cell population *in vitro* and the combination synergistically suppressed tumour growth and prolonged remission *in vivo* [454]. In a follow-up study Iliopoulos *et al* documented that metformin in combination with paclitaxel or carboplatin synergistically inhibited tumour growth and decreased the dosage of doxorubicin required to prevent relapse of breast, lung and prostate xenografts [455]. Consistent with the stem cell hypothesis, Cufi *et al* demonstrated that metformin preferentially targeted trastuzumab resistant breast cancer stem cells and resensitised breast tumours to trastuzumab in a

xenograft mouse model [456]. Moreover metformin has been evidenced to enhance the cytotoxic effects of cisplatin and paclitaxel on endometrial cancer cells [457, 458]. In another study Rattan *et al* reported that metformin attenuated tumour growth inhibiting angiogenesis and lung metastasis and also enhanced the therapeutic efficacy of cisplatin in established ovarian tumour xenografts [459].

To date far too little attention has been paid to a possible interaction among glycolytic inhibitors and the antidiabetic drug. In 2011 Sahra *et al* were the first to report that metformin in combination with 2DG synergistically attenuated prostate cancer cell growth. The combinatorial strategy was associated with ATP depletion, p53 dependent apoptotic cell death and G2-M cell cycle arrest [460]. A year later an independent research group verified the beneficial combination and reported suppressed tumour growth in a breast cancer mouse xenograft model [461]. Choi *et al* documented that DCA-mediated PDH activation enhanced metformin cytotoxicity in HeLa cells inducing oxidative stress resulting in cell death [462]. The synergism was further confirmed by Haugrud *et al* who demonstrated caspase dependent apoptotic cell death in breast cancer cells treated with the PDHK1 inhibitor along with metformin [463].

In the present study a synergistic beneficial effect was revealed between metformin and several compounds targeting the glycolytic pathway. It was observed that while low concentrations of the antidiabetic drug and the glycolytic inhibitors had only marginal effects on the growth of breast and ovarian cancer cell lines, in combination they induced a marked antitumour effect. The most robust synergistic relationship that was identified was with the novel GLUT1 inhibitor IOM-1190. Two separate metformin concentrations were used for each of the paired breast cancer cell lines. Metformin was shown to greatly enhance the antiproliferative potency of IOM-1190 in both the ER positive and the triple negative breast cancer cell lines. The great efficacy of this combination was reflected in very low CI values. All CI values generated for the whole range of concentrations used signified either strong or even very strong synergism (Figures 5.30 to 5.35).

Metformin was also found to augment STF31-induced cytotoxicity on both breast and ovarian cancer cells. The favourable interaction between the GLUT1 inhibitor and the antidiabetic agent was characterised by low synergistic CI values. Interestingly comparing the CI values the triple negative and more aggressive MDA-MB-231 line was more sensitive to the combination compared to the ER positive and of low invasive potential MCF7 line. Furthermore the two paired ovarian cancer cell lines the platinum naïve PEA1 and the platinum resistant PEA2 presented equally sensitive to this combination (Figures 5.36 to

5.43). The antiproliferative effect of another inhibitor of glucose transport (Phloretin) on the PEO1 ovarian cancer cell line was also enhanced by metformin. Low CI values indicating synergism were only generated for this platinum sensitive line while the combination was not effective on its paired platinum resistant line nor the breast cancer cell lines examined (Figures 5.44&5.45).

An additional beneficial interaction encountered while examining combinatorial treatments of glycolytic inhibitors with the most widely prescribed antidiabetic drug was with Oxamic acid. Metformin proved able to improve the antiproliferative efficacy of the established pyruvate analogue. The combination was effective on every breast and ovarian cancer cell line examined in this study giving synergistic CI values. Interestingly the two breast cancer cell lines as well as the PEO1 and PEO4 paired ovarian cancer cell lines demonstrated comparable sensitivity to Oxamic acid and metformin co-administration as inferred by the similar CI values generated. In contrast the combination was considerably more effective on the platinum naïve PEA1 cell line compared to its paired platinum resistant line (Figures 5.46 to 5.57). The last synergistic relationship of metformin identified in this thesis was with DCA. The two agents demonstrated a synergistic inhibitory effect on two breast cancer cell lines. Interestingly the CI values generated for the triple negative line were remarkably lower than the corresponding values of MCF7 cells (Figures 5.58 to 5.61). The synergistic effect on MCF7 cells demonstrated is in agreement with previous findings by Haugrud *et al* [463].

A reasonable concern regarding the clinical potential of these preliminary data is the relatively high concentrations of metformin used. Indeed the plasma concentration of the drug in a diabetic patient does not exceed 15μM [390]. However metformin remains stable, is not metabolised and accumulates in the liver, stomach, colon or salivary glands before being excreted through the kidneys [390, 464]. It has been reported that metformin does accumulate in tissues reaching significantly higher concentrations compared to the blood stream [464, 465]. Therefore low millimolar concentrations could be considered achievable *in vivo* and clinically relevant [465]. But this remains to be further evaluated in a clinical setting.

The antiproliferative action of metformin is postulated to be dependent on glucose availability. A number of studies have demonstrated that cells could be rescued in a rich glucose environment even following treatment with high metformin concentrations [462, 465]. It should be emphasised that all these experiments were conducted in physiologically relevant glucose conditions (5.56mM) differing from the majority of *in vitro* experiments that are mostly carried out in ‘unnaturally’ high glucose concentrations.

The tumour suppressor gene Liver kinase B1 (LKB1) is associated with metformin mediated hepatic gluconeogenesis inhibition. LKB1 is an upstream kinase that phosphorylates and activates AMPK leading to mTOR inhibition. This is currently the best characterised mechanism of the antiproliferative action of metformin [390, 452, 465]. The triple negative MDA-MB-231 breast cancer cell line is known to be LKB1 deficient. Sensitivity of this cell line to metformin even though it lacks a functional LKB1 gene corroborates previous findings from Zordoky *et al* [465]. Furthermore it verifies that metformin can also activate AMPK via an LKB1 independent mechanism [390, 452, 465]. An interesting observation was that in many cases this cell line proved more sensitive to metformin combinations compared to the MCF7 line that has a functional LKB1 gene.

The fact that a comparable synergistic interaction between metformin and several glycolytic inhibitors is identified provides an indication that the synergism is indeed a consequence of inhibition of glycolysis. It is hypothesised that simultaneous inhibition of two energy pathways, mitochondrial oxidative phosphorylation along with the glycolytic pathway induces ATP depletion that results in massive cell death. The present study provides substantial evidence and suggests that dual inhibition of the two energy pathways might be a promising antitumour therapeutic strategy.

5.6.4 Combinatorial treatment of STF31 and Metformin was associated with induction of apoptosis in breast cancer cells

The molecular mechanism of cellular death induced by the co-treatment of metformin with the GLUT1 inhibitor STF31was examined. This is a novel combination that appeared to be effective on both breast and ovarian cancer cells. Flow cytometric analysis provided evidence that STF31 in combination with metformin promoted apoptotic cell death in MDA-MB-231 breast cancer cells (Figures 5.62&5.63). Simultaneous inhibition of two energy pathways, the glycolytic pathway and oxidative phosphorylation, is expected to lead to massive ATP depletion. The current findings link this energy stress with apoptotic cell death.

The anti-hyperglycaemic agent when used individually has been extensively associated with apoptotic cell death. Metformin accumulates in the mitochondria and inhibits the mitochondrial respiratory chain complex I. The biguanide impairs mitochondrial respiration and induces oxidative stress leading to apoptosis [390, 463, 465]. Zhuang *et al* demonstrated caspase-dependent apoptosis in a number of breast cancer cell lines [466]. Caspase dependent apoptosis linked with oxidative damage and mitochondrial depolarisation has also been confirmed in glioma cells [467]. Another recent study revealed that metformin promoted apoptotic cell death in pancreatic cancer cells by downregulating the pro-survival

proteins Mcl-1 and Bcl-2 and increasing the expression of the pro-apoptotic proteins Bim and Puma [468].

The results of this study are consistent with previous findings indicating apoptosis following metformin treatment combined with glycolysis inhibition. Sahra *et al* reported that the combination of 2DG with metformin diminished the intracellular ATP levels and induced p-53 dependent apoptotic cell death in prostate cancer cells [460]. Moreover, recent evidence suggested that DCA augmented the metformin induced oxidative stress and synergistically enhanced the induction of caspase-dependent apoptosis in breast cancer cell line models [463].

5.6.5 Combinatorial treatments of glycolytic inhibitors and Metformin were associated with cell cycle arrest

In the last section of this chapter the effect of combinations of glycolytic inhibitors with metformin on cell cycle progression was investigated. The most successful metformin combinations were prioritised for these experiments as metformin is not currently in use as an antitumour agent and the novel combinations identified in this study are proposed for further evaluation as future treatment strategies. Interestingly the three combinations examined had differential effects on the distribution of MDA-MB-231 breast cancer cells in each phase of the cell cycle. Co-treatment of the novel GLUT1 inhibitor IOM-1190 with the antidiabetic drug was associated with cell cycle arrest in the G2/M phase. The proportion of co-treated cells in this phase was double compared to single treated cells with each individual inhibitor (Figure 5.66). In contrast the combination of STF31 with metformin did not affect cell cycle progression (Figure 5.67). Apoptotic cell death following this co-treatment was previously demonstrated but was not coupled with cell cycle arrest (section 5.4). Finally combinational treatment of Oxamic acid with metformin caused an accumulation of cells in the G0/G1 phase compared to the controls of cells treated with the agents individually (Figure 5.68).

In the literature metformin treatment of breast cancer cells has been associated with cell cycle arrest in the G0/G1 phase linked with cyclin D1 inhibition [469]. However very little is known regarding cell cycle arrest following combinatorial treatments of metformin with glycolytic inhibitors. The only relevant information identified was that the combination of 2DG with metformin induced G2/M phase cell cycle arrest in prostate cancer cells according to Sahra *et al* [460].

The primary aim of this research was to investigate the preclinical efficacy of combinatorial treatments among glycolytic inhibitors and traditional cancer therapies. This is the first study to explore the effectiveness of a wide range of such combinations in breast and ovarian cancer cell line models. Several combinations that synergistically inhibited tumour growth were identified and presented in this chapter. Among them the combination of the novel GLUT1 inhibitor IOM-1190 and metformin was the most potent one for the breast cancer cell lines. Impressively low CI values signifying strong synergism were generated for both the ER positive and the triple negative cell line. More importantly the MDA-MB-231 cell line, which represents triple negative aggressive breast cancer with limited treatment options, was particularly sensitive to this combination. Regarding the ovarian cancer cell lines the most promising combinatorial treatment identified was that between 3PO and cisplatin. Low CI values indicated a promising strategy to overcome platinum resistance.

Both IOM-1190 and 3PO are novel specific compounds. They were identified as the most potent growth inhibitors among the ones used in this study (Chapter 3). They are both believed to have great *in vivo* potential.

Further research should be undertaken to validate these promising *in vitro* pilot data and investigate their *in vivo* therapeutic potential. An *in vivo* model of triple negative breast cancer and one of platinum resistant ovarian cancer is proposed for each of them respectively. These models could further assess the mechanism of synergy between these agents and hopefully a positive outcome could serve as a translational platform which could potentially have a great impact on these subgroups of tumours that currently have very limited treatment options.

Chapter 6

Chapter 6: The effect of varying oxygen levels on sensitivity to glycolytic inhibition

6.1 The effect of glycolytic inhibitors on the growth of breast cancer cell lines under varying oxygen levels

Hypoxia is a common characteristic of the tumour microenvironment. It is well substantiated that adaptation to low oxygen conditions induces high flux through the glycolytic pathway and enhanced glycolytic rates [153, 470]. Therefore this study set out to examine the effect of varying oxygen levels on sensitivity to glycolysis inhibition. An array of eight glycolytic inhibitors was compared under a range of oxygen concentrations. Two representative breast cancer cell lines were selected for these experiments; the ER positive MCF7 and the triple negative MDA-MB-231 which were adapted in four oxygen concentrations 21, 7, 2 and 0.5% (cells were cultured in each of the oxygen levels for at least two weeks prior to the experiments). Cancer cell proliferation was examined by the SRB assay in each of the conditions after a 3 and a 5-day treatment period with the glycolytic inhibitors. The concentration response curves generated using SRB assays are presented below. These results depict the percentage of cell numbers remaining following treatment with increasing concentrations of each of the compounds under the four different oxygen levels. Tables 6.1 and 6.2 summarise the corresponding IC_{50} values calculated for MCF7 and MDA-MB-231 cells respectively.

It was observed that breast cancer cells grow more slowly in low oxygen conditions. Table 6.3 indicates the 3 and 5-day growth fold changes of the untreated MCF7 and MDA-MB-231 controls in the four different oxygen conditions. For both cell lines, comparable growth at the three low oxygen conditions was observed, and this was decreased 40 to 60% compared to the respective growth at 21% O_2 (with the only exception being the growth of MCF7 cells after 3 days that appeared unaffected by hypoxia). It was speculated that the reduced proliferation rate presented in hypoxic conditions could play a role in the sensitivity to the glycolytic inhibitors.

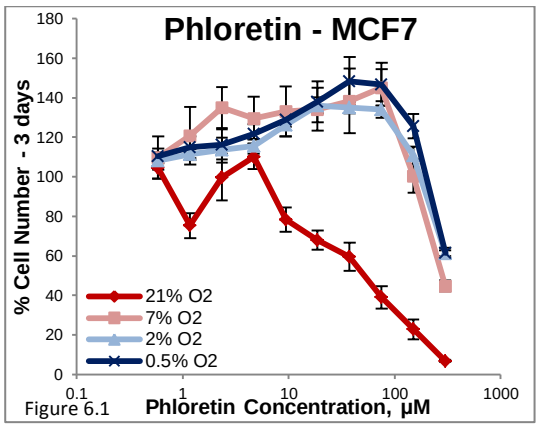

Figure 6.1

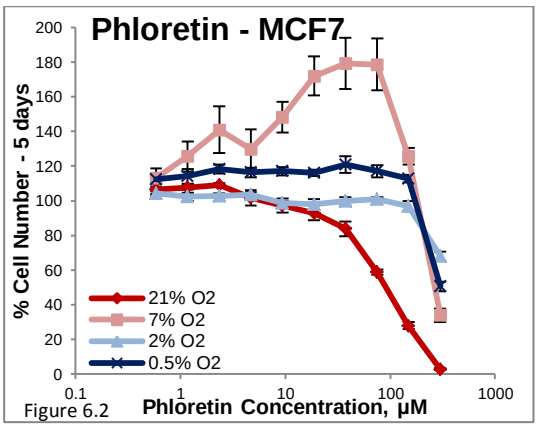

Figure 6.2

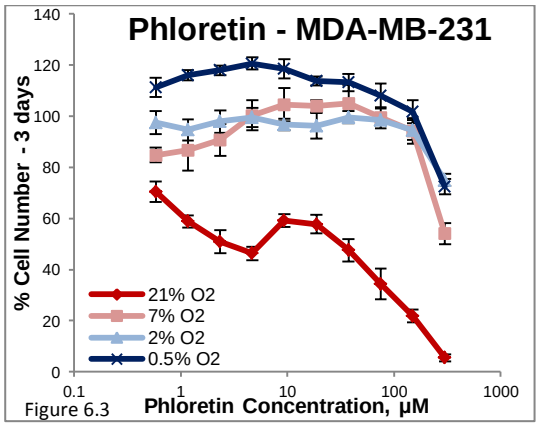

Figure 6.3

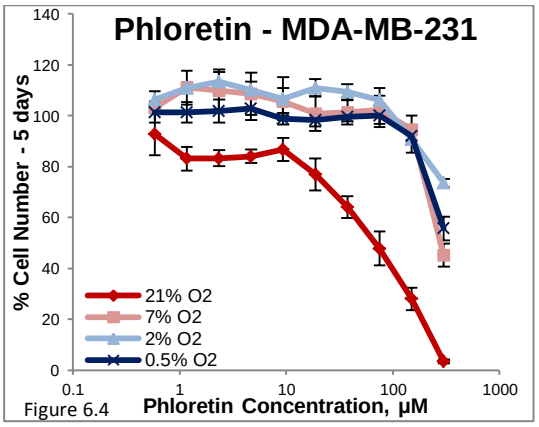

Figure 6.4

Figures 6.1 to 6.4: Concentration response curves of MCF7 (6.1 & 6.2) and MDA-MB-231 (6.3 & 6.4) breast cancer cells treated with Phloretin concentrations between 0.6-300µM under four different oxygen levels (21% - 7% - 2% - 0.5% O_2). Results for a three day treatment are presented on the left while those for a five day treatment are shown on the right. Cell viability was determined by an SRB assay. Mean results of 6 replicates are reported and error bars represent standard deviations. Values are shown as a percentage of control. A constant 0.3% DMSO concentration was used across the whole curve in each case (n=1).

Figures 6.1 and 6.2 present the concentration response curves of MCF7 breast cancer cells treated with a range of Phloretin concentrations under four different oxygen conditions for 3 and 5 days respectively. Results for MDA-MB-231 cells are presented in Figures 6.3 and 6.4. Both cell lines regardless of the duration of treatment responded to Phloretin in a very similar way at the three lower oxygen levels. Increased sensitivity can be observed from both MCF7 and MDA-MB-231 cells at 21% O_2, in parallel with enhanced resistance at 7, 2 and 0.5% O_2. An interesting observation is that Phloretin was found to induce proliferation of MCF7 cells (at concentrations up to 150µM) at the three lower O_2 levels after 3 days and at 7% O_2 after 5 days of treatment up to 160% compared to the untreated control.

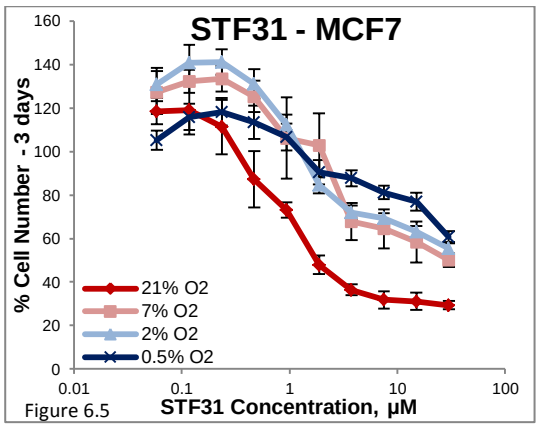

Figure 6.5

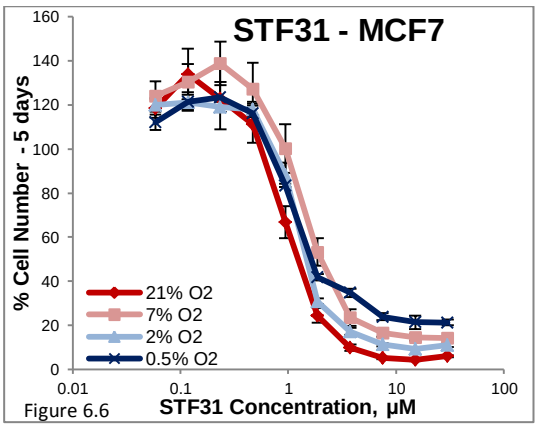

Figure 6.6

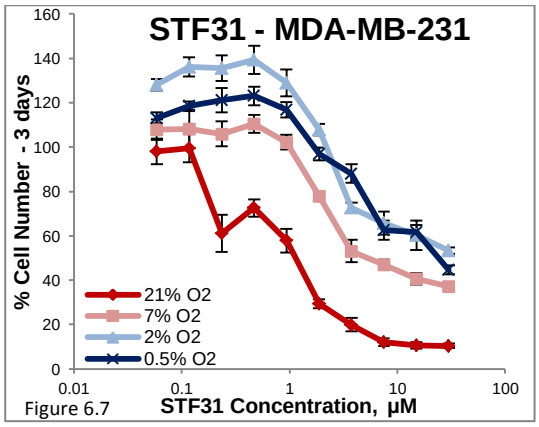

Figure 6.7

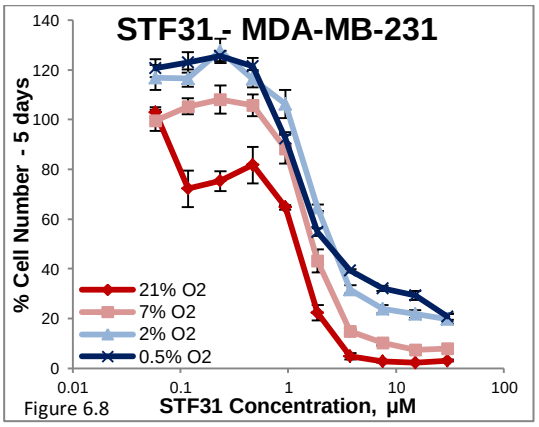

Figure 6.8

Figures 6.5 to 6.8: Concentration response curves of MCF7 (6.5 & 6.6) and MDA-MB-231 (6.7 & 6.8) breast cancer cells treated with STF31 concentrations between 0.06-30µM under four different oxygen levels (21% - 7% - 2% - 0.5% O_2). Results for a three day treatment are presented on the left while those for a five day treatment are shown on the right. Cell viability was determined by an SRB assay. Mean results of 6 replicates are reported and error bars represent standard deviations. Values are shown as a percentage of control. A constant 0.3% DMSO concentration was used across the whole curve in each case (n=1).

The above figures indicate the effect of the oxygen level on breast cancer cell sensitivity to STF31. Figures 6.5 and 6.7 show that both MCF7 and MDA-MB-231 cells were very sensitive to this GLUT1 inhibitor at 21% O_2 after 3 days of treatment. The triple negative cell line presented a fourfold increase in the IC_{50} value at 7% O_2 and even greater resistance at the lower oxygen conditions. Regarding MCF7 cells, a similar pattern of increased resistance at the three lower oxygen levels can be observed. Figure 6.6 indicates that the oxygen concentration did not have a great influence on the antiproliferative effect of STF31 after 5 days of treatment; the four generated IC_{50} values were comparable. In contrast Figure 6.8 demonstrates that MDA-MB-231 cells were more sensitive to the inhibitor at 21% O_2 compared to the three hypoxic conditions when treated for 5 days.

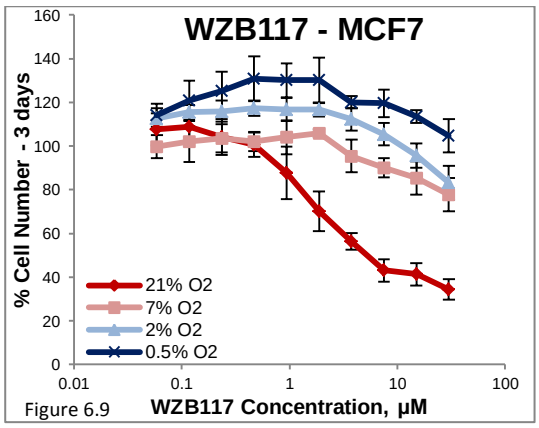

Figure 6.9

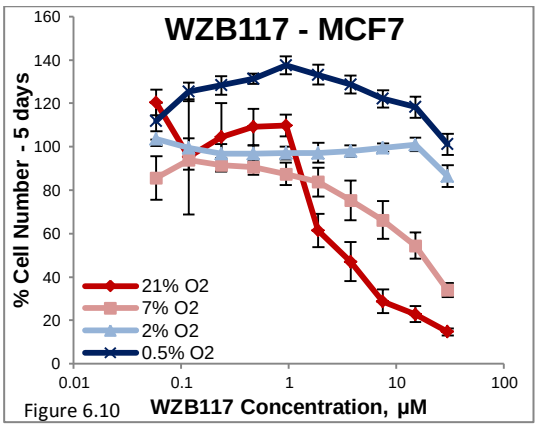

Figure 6.10

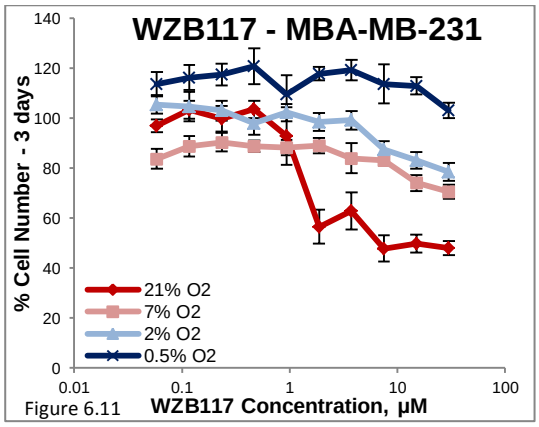

Figure 6.11

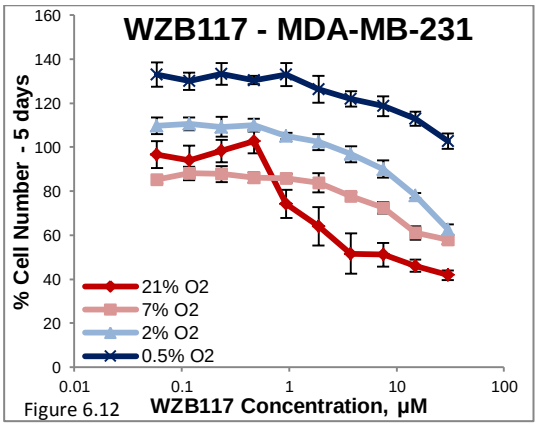

Figure 6.12

Figures 6.9 to 6.12: Concentration response curves of MCF7 (6.9 & 6.10) and MDA-MB-231 (6.11 & 6.12) breast cancer cells treated with WZB117 concentrations between 0.06-30µM under four different oxygen levels (21% - 7% - 2% - 0.5% O_2). Results for a three day treatment are presented on the left while those for a five day treatment are shown on the right. Cell viability was determined by an SRB assay. Mean results of 6 replicates are reported and error bars represent standard deviations. Values are shown as a percentage of control. A constant 0.3% Ethanol concentration was used across the whole curve in each case (n=1).

Figures 6.9 to 6.12 illustrate the effect of WZB117 on cell viability of two breast cancer cell lines under four different oxygenation conditions. Evidence is provided of enhanced activity of this GLUT1 inhibitor under normoxic conditions after either 3 or 5 days of treatment. Both MCF7 and MDA-MB-231 cells were found to be very sensitive to the compound at 21% O_2 while increased resistance was observed in the presence of lower oxygen. Under hypoxic conditions, 2 and 0.5% O_2, even the highest concentrations of WZB117 that were used were found unable to affect breast cancer cell growth.

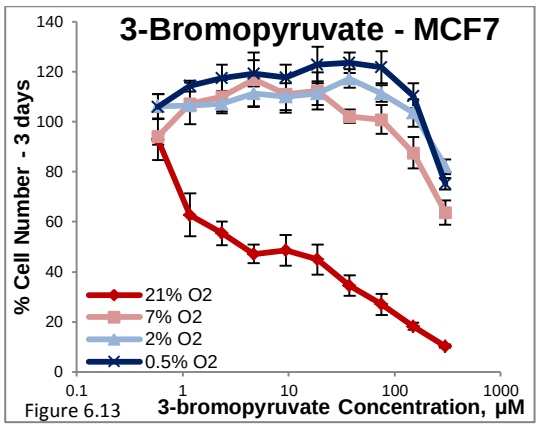

Figure 6.13

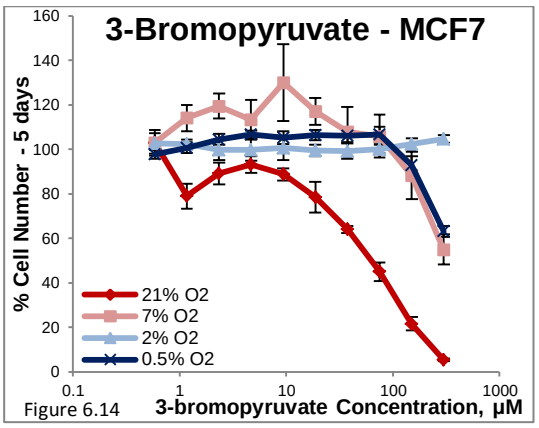

Figure 6.14

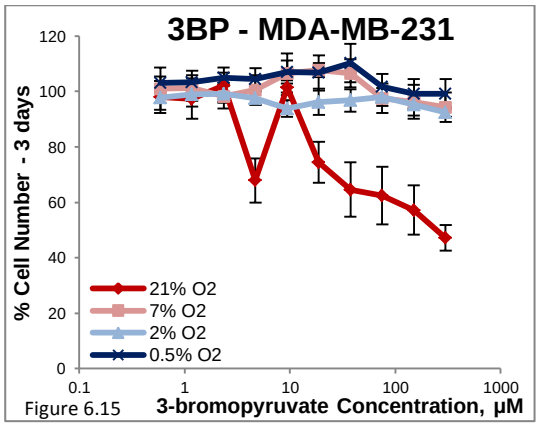

Figure 6.15

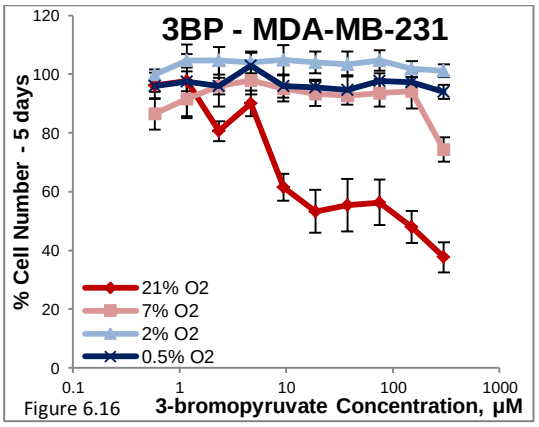

Figure 6.16

Figures 6.13 to 6.16: Concentration response curves of MCF7 (6.13 & 6.14) and MDA-MB-231 (6.15 & 6.16) breast cancer cells treated with 3-bromopyruvate concentrations between 0.6-300µM under four different oxygen levels (21% - 7% - 2% - 0.5% O_2). Results for a three day treatment are presented on the left while those for a five day treatment are shown on the right. Cell viability was determined by an SRB assay. Mean results of 6 replicates are reported and error bars represent standard deviations. Values are shown as a percentage of control (n=1).

The preceding figures (6.13 to 6.16) demonstrate that 3BP is only effective in attenuating breast cancer cell proliferation under normoxic conditions. An interesting observation is that varying the oxygen concentration between 7, 2 and 0.5% did not affect the efficacy of the HKII inhibitor. Both cell lines responded in an almost identical way to these lower oxygen levels. For MCF7 cells a reduction of cell number up to 40% was observed after treatment with 300µM 3BP in low oxygen conditions while in contrast MDA-MB-231 cells were found to be completely resistant even to the highest concentrations used in these conditions.

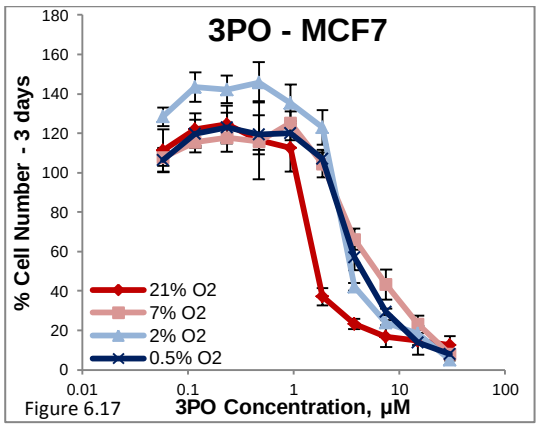

Figure 6.17

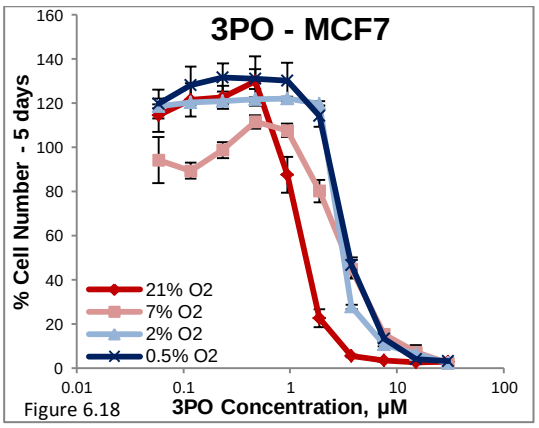

Figure 6.18

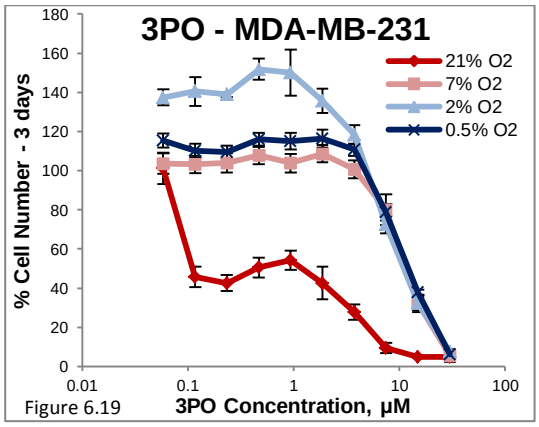

Figure 6.19

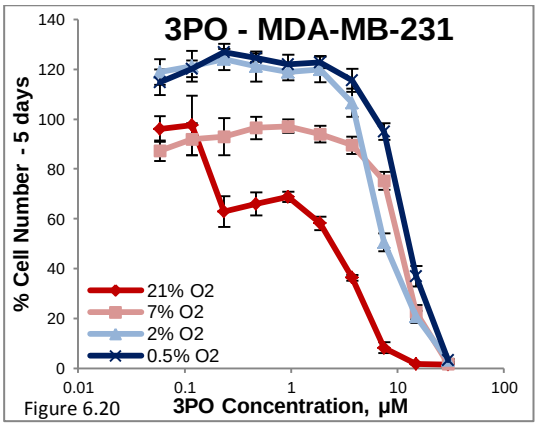

Figure 6.20

Figures 6.17 to 6.20: Concentration response curves of MCF7 (6.17 & 6.18) and MDA-MB-231 (6.19 & 6.20) breast cancer cells treated with 3PO concentrations between 0.06-30µM under four different oxygen levels (21% - 7% - 2% - 0.5% O_2). Results for a three day treatment are presented on the left while those for a five day treatment are shown on the right. Cell viability was determined by an SRB assay. Mean results of 6 replicates are reported and error bars represent standard deviations. Values are shown as a percentage of control. A constant 0.3% DMSO concentration was used across the whole curve in each case (n=1).

In the above graphs, evidence is provided that 3PO is more effective in inhibiting breast cancer cell proliferation when oxygen availability is at 21%, while variation of the oxygen concentration between 7, 2 and 0.5% did not alter the sensitivity to the compound. Figures 6.17 and 6.18 show that MCF7 cells demonstrated a twofold and a threefold increase of their IC_{50} value under low oxygen conditions compared to 21% O_2 after a 3 and a 5-day treatment with the PFKFB3 inhibitor respectively. For MDA-MB-231 cells the difference in sensitivity was even more profound. Triple negative cells increased their IC_{50} value 26 times when treated with the inhibitor for 3 days in low oxygen conditions and up to sevenfold following 5 days of treatment.

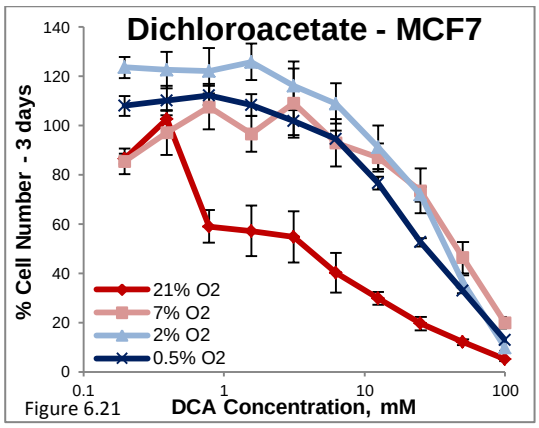

Figure 6.21

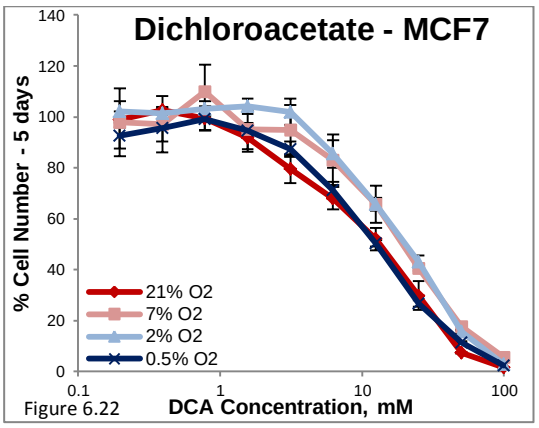

Figure 6.22

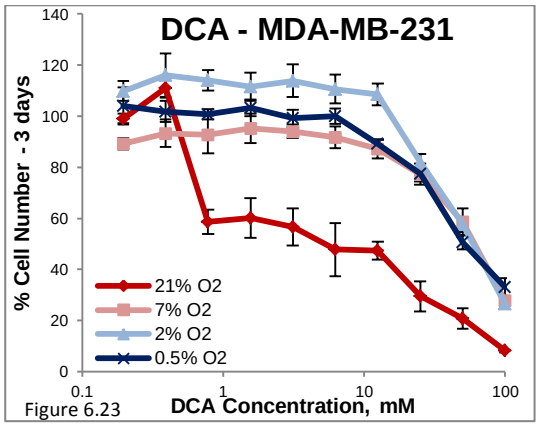

Figure 6.23

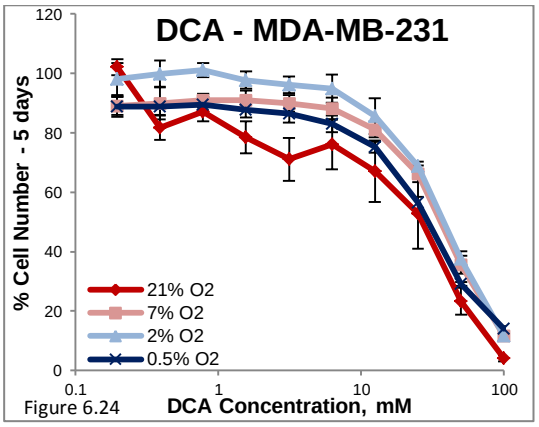

Figure 6.24

Figures 6.21 to 6.24: Concentration response curves of MCF7 (6.21 & 6.22) and MDA-MB-231 (6.23 & 6.24) breast cancer cells treated with Dichloroacetate concentrations between 0.4-100mM under four different oxygen levels (21% - 7% - 2% - 0.5% O_2). Results for a three day treatment are presented on the left while those for a five day treatment are shown on the right. Cell viability was determined by an SRB assay. Mean results of 6 replicates are reported and error bars represent standard deviations. Values are shown as a percentage of control (n=1).

The above figures indicate that DCA is effective in inhibiting breast cancer cell proliferation over the whole range of oxygen levels examined. Figures 6.21 and 6.23 show that MCF7 and MDA-MB-231 cells presented increased sensitivity to the PDHK1 inhibitor at 21% O_2 when treated for 3 days. Both cell lines were found to be more resistant to treatment at low oxygen conditions (7-2 and 0.5%) presenting a tenfold increase in their IC_{50} values. In contrast, as demonstrated in Figures 6.22 and 6.24 both breast cancer cell lines responded similarly to a 5-day treatment irrespective of oxygen availability. Little variation was detected in their IC_{50} values over the range of oxygen levels tested.

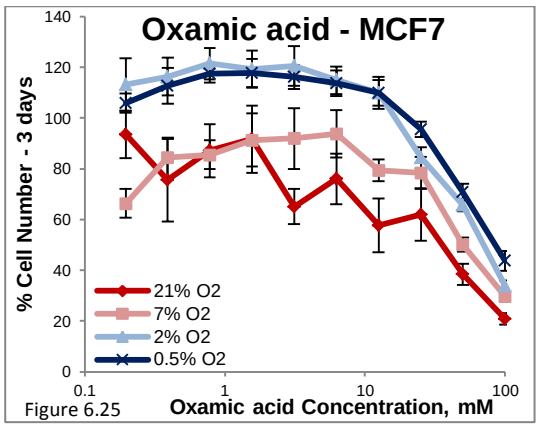

Figure 6.25

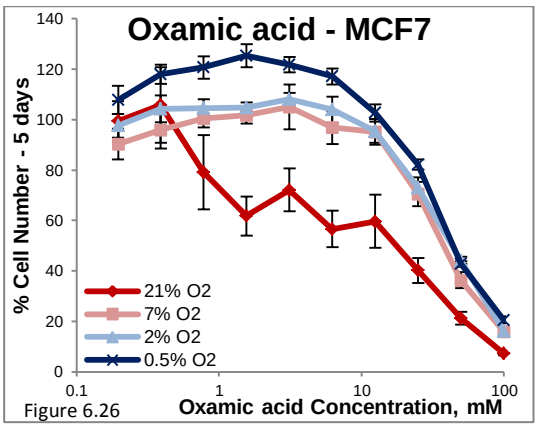

Figure 6.26

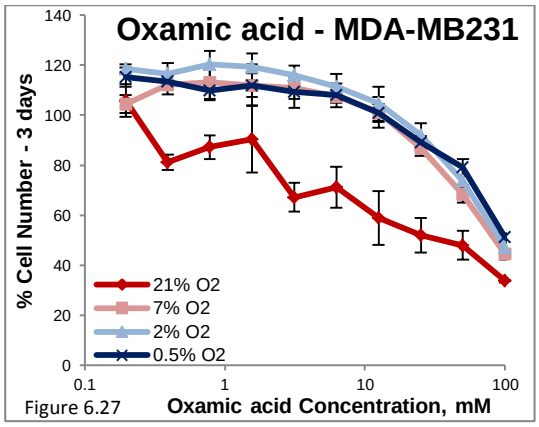

Figure 6.27

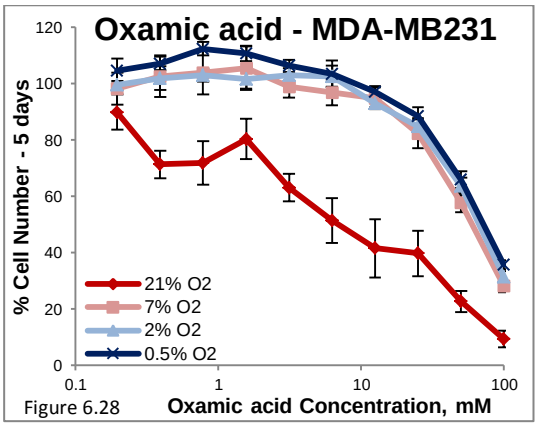

Figure 6.28

Figures 6.25 to 6.28: Concentration response curves of MCF7 (6.25 & 6.26) and MDA-MB-231 (6.27 & 6.28) breast cancer cells treated with Oxamic acid concentrations between 0.4-100mM under four different oxygen levels (21% - 7% - 2% - 0.5% O_2). Results for a three day treatment are presented on the left while those for a five day treatment are shown on the right. Cell viability was determined by an SRB assay. Mean results of 6 replicates are reported and error bars represent standard deviations. Values are shown as a percentage of control (n=1).

Both breast cancer cell lines were found sensitive to Oxamic acid in all examined conditions. Figure 6.25 demonstrates that the lower the oxygen level, the greater the resistance (higher the IC_{50} value) after a 3-day treatment of MCF7 cells. In contrast, Figure 6.26 illustrates that after 5 days of treatment MCF7 cells presented increased sensitivity at 21% O_2, but variation of the oxygen level between 7 and 0.5% did not affect the potency of the LDH inhibitor. MDA-MB-231 cells presented increased sensitivity at 21% O_2 (Figures 6.27 and 6.28) although response in the three lower oxygen levels was almost identical at both 3 and 5-day time points.

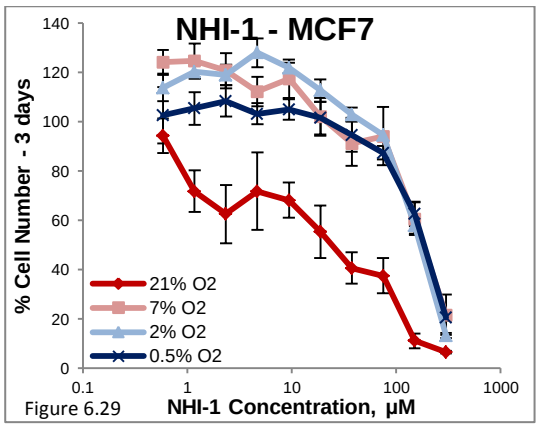

Figure 6.29

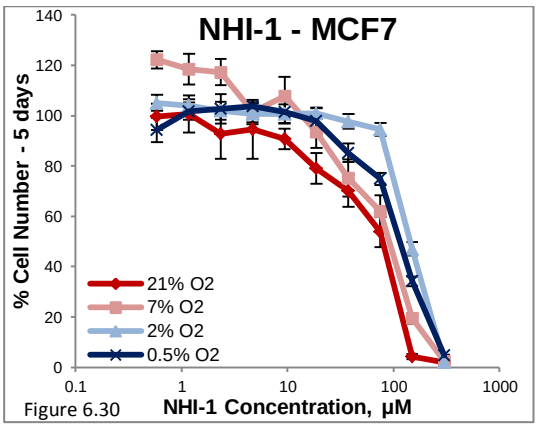

Figure 6.30

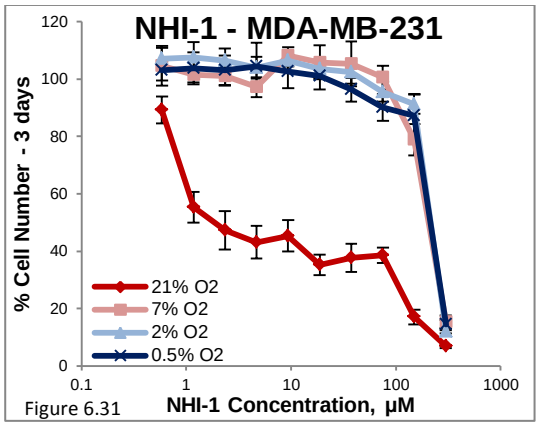

Figure 6.31

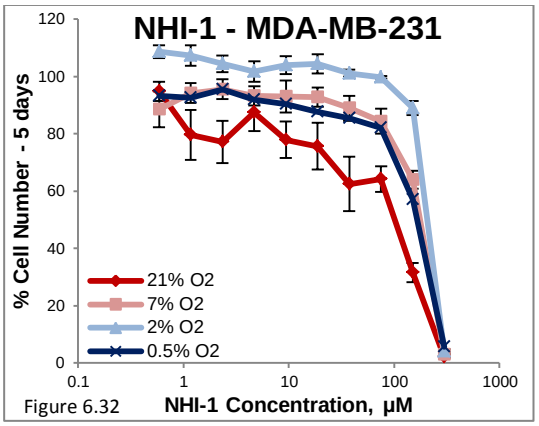

Figure 6.32

Figures 6.29 to 6.32: Concentration response curves of MCF7 (6.29 & 6.30) and MDA-MB-231 (6.31 & 6.32) breast cancer cells treated with NHI-1 concentrations between 0.6-300µM under four different oxygen levels (21% - 7% - 2% - 0.5% O_2). Results for a three day treatment are presented on the left while those for a five day treatment are shown on the right. Cell viability was determined by an SRB assay. Mean results of 6 replicates are reported and error bars represent standard deviations. Values are shown as a percentage of control. A constant 0.3% DMSO concentration was used across the whole curve in each case (n=1).

The above figures examine the effect of oxygen availability on the efficacy of NHI-1 as a breast cancer growth inhibitor. Figures 6.29 and 6.31 show that after 3 days of treatment both breast cancer cell lines were very sensitive to the novel LDHA inhibitor at 21% O_2 whereas resistance was presented at the three low oxygen conditions. This was demonstrated by the increase of the respective IC_{50} values up to 7 and 70 times higher for MCF7 and MDA-MB-231 cells respectively. The same pattern of increased sensitivity at 21% O_2 was followed in the 5-day treatment results as well that are shown in Figures 6.30 and 6.32 however the differences were not as great. Both cell lines became more resistant to the compound presenting a twofold increase in their IC_{50} values. It is interesting that while both cell lines at 7 and 2% O_2 increase their resistance at 0.5% O_2 their IC_{50} values presented a modest decrease.

IC_{50} values	MCF7 – 3 days				MCF7 – 5 days			
	21% O_2	**7% O_2**	**2% O_2**	**0.5% O_2**	**21% O_2**	**7% O_2**	**2% O_2**	**0.5% O_2**
Phloretin (µM)	49.7	294.4	>300	>300	90	295.2	>300	>300
STF31 (µM)	1.7	N/A	N/A	N/A	1.3	2.3	1.4	1.6
WZB117 (µM)	5	N/A	>30	>30	2.3	16.4	>30	>30
BP (µM)	5.8	>300	>300	>300	62.7	>300	N/A	>300
3PO (µM)	1.7	7.2	3.6	4.4	1.3	3.8	3.5	3.7
DCA (mM)	3.3	45.5	38.4	30.1	13	18.9	19.6	12.6
Oxamic (mM)	24.3	52.8	66.6	82.3	10.4	39.4	47.1	49.5
NHI-1 (µM)	24.2	178	174.4	185.5	61.8	80	150.1	111.5

Table 6.1: Summary of the IC_{50} concentrations generated for MCF7 breast cancer cells when treated with 8 glycolytic inhibitors under four different oxygen levels (21% - 7% - 2% - 0.5% O_2) for 3 or 5 days. N/A stands for not achieved in the range of tested concentrations.

IC_{50} values	MDA-MB-231 – 3 days				MDA-MB-231 – 5 days			
	21% O_2	**7% O_2**	**2% O_2**	**0.5% O_2**	**21% O_2**	**7% O_2**	**2% O_2**	**0.5% O_2**
Phloretin (µM)	28.3	>300	>300	>300	69.6	289.1	>300	>300
STF31 (µM)	0.99	4.3	N/A	25.6	1.2	1.8	2.4	2.2
WZB117 (µM)	14.7	N/A	N/A	>30	4.1	N/A	>30	N/A
BP (µM)	N/A	>300	N/A	N/A	39	>300	N/A	>300
3PO (µM)	0.47	12.3	11.3	12.2	1.5	11.2	8.6	12.9
DCA (mM)	5.7	61.5	55.9	58.8	23.3	38.9	37	31.1
Oxamic (mM)	30.3	83.4	93.3	>100	6.9	60.4	66.2	74
NHI-1 (µM)	3.7	229	266	260.5	93.6	190.1	227.6	174.1

Table 6.2: Summary of the IC_{50} concentrations generated for MDA-MB-231 breast cancer cells when treated with 8 glycolytic inhibitors under four different oxygen levels (21% - 7% - 2% - 0.5% O_2) for 3 or 5 days. N/A stands for not achieved in the range of tested concentrations.

Control growth fold change	MCF7		MDA-MB-231	
	3 days	**5 days**	**3 days**	**5 days**
21% O_2	4.1	16.3	5	15.7
7% O_2	3.5	10.7	3.3	7.9
2% O_2	5.1	9	3	5.6
0.5% O_2	4.1	10.8	3	6.7

Table 6.3: Summary of growth fold change presented from MCF7 and MDA-MB-231control breast cancer cells under four different oxygen levels (21% - 7% - 2% - 0.5% O_2) after 3 or 5 days.

5-day IC_{50} values – fold growth Pearson correlation	**r**	**two-tailed P value**
Phloretin	-0.8871	0.0033
STF31	-0.9136	0.0297
WZB117	-0.7568	0.0015
3-bromopyruvate	-0.8860	0.0034
3PO	-0.8197	0.0127
Dichloroacetate	-0.6883	*0.0591*
Oxamic acid	-0.9718	< 0.0001
NHI-1	-0.8845	0.0035

Table 6.4: Pearson correlation of sensitivity of two breast cancer cell lines to eight glycolytic inhibitors when treated for a five day period under four different oxygen levels (21% - 7% - 2% - 0.5% O_2) with their growth fold change in each of the conditions. Correlation coefficient (r) and Pearson two-tailed P-values are presented.

It was speculated that a reduced growth rate could contribute to increased resistance to the glycolytic inhibitors at low oxygen conditions. Therefore the fold growth of the cell lines in each of the conditions was correlated with sensitivity to the inhibitors. Correlation coefficient and Pearson P-values are presented in Table 6.4. A statistically significant inverse correlation is demonstrated between an increased proliferation rate at conditions of high oxygen availability and increased sensitivity to the glycolytic inhibitors, as indicated by a low IC_{50} value. When 5-day treatment data were taken into consideration all the growth rate-

inhibitor potency associations were statistically significant ($P<0.05$) with the only exemption being the DCA correlation ($P=0.0591$) and this was nearly of borderline significance. Based on these associations it appears that the low proliferation rate of breast cancer cells grown in hypoxic conditions is significantly correlated with decreased efficacy of the glycolytic inhibitors (high IC_{50} values).

However while greater resistance to the majority of glycolytic inhibitors in hypoxic conditions was observed following a 3-day treatment compared to 5 days low oxygen availability had a minimal impact on the proliferation of MCF7 cells. Thus at this time point the observed resistance at low oxygen conditions does not appear to correlate with a lower proliferation rate.

6.2 Protein expression of glycolytic targets under varying oxygen levels

In an attempt to gain a better understanding of how glycolysis inhibition is affected by oxygen availability the protein expression of the glycolytic targets of interest was examined in hypoxic conditions. It was hypothesised that relative resistance to glycolytic inhibitors in a low oxygen environment could be associated with upregulation of the targeted glycolytic enzymes. To investigate this further the protein expression of the glycolytic targets was examined in MCF7 and MDA-MB-231 cells under varying oxygen levels. The following figures (Figures 6.33 to 6.52) show the Western blot results for GLUT1, HKII, PFKFB3, PDHK1 and LDHA protein expression in whole lysates collected from cells cultured at 7%, 2% and 0.5% O_2 for a time course of 24, 48 or 72 hours. The expression was compared to the 21% O_2 control lysate. Data were normalised to α tubulin expression. Quantitative densitometric analysis of the immunoblots was performed and is presented below.

- **Glucose Transporter 1**

In the following figures the effect of the oxygen level on GLUT1 protein expression is examined. Figures 6.33 and 6.34 present the immunoblots showing the transporter's expression in MCF7 and MDA-MB-231 cells cultured in 7, 2 and 0.5% O2 for three different time points of 24, 48 and 72h. In Figures 6.35 and 6.36 the corresponding densitometric results are shown. GLUT1 expression in hypoxic conditions was found to be similar to the 21% O2 controls for both cell lines. Variation of the oxygen level in the examined conditions did not have a marked effect on expression of the transporter and no upregulation was detected. Rather, GLUT1 expression decreased by 30% at 0.5% O2 compared to the 21% O2 controls in MCF7 cells.

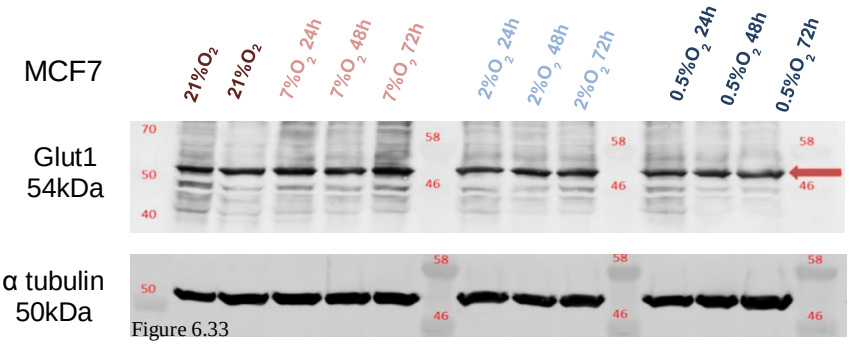

Figure 6.33

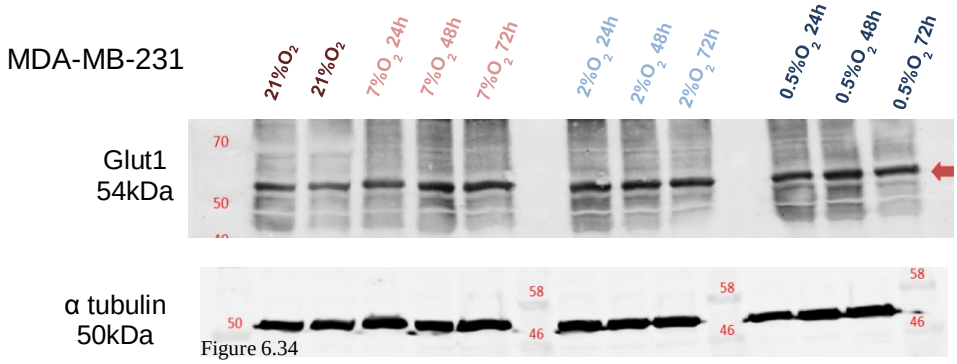

Figure 6.34

Figures 6.33 & 6.34: GLUT1 protein expression detected through Western blotting in MCF7 and MDA-MB-231 breast cancer cells under four different oxygen levels. Lysates were collected from cells cultured at 7%, 2% and 0.5% O_2 for 24, 48 and 72 hours and expression was compared to a 21% O_2 control lysate. Alpha tubulin was used as a loading control (n=1).

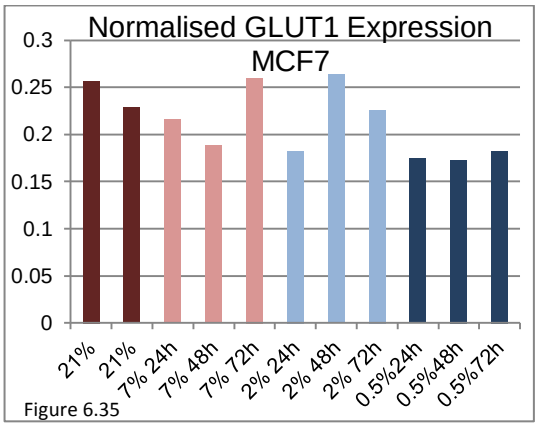

Figure 6.35

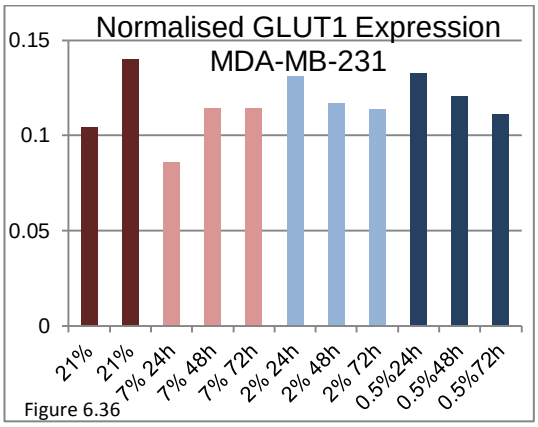

Figure 6.36

Figures 6.35 & 6.36: GLUT1 protein expression detected through Western blotting in MCF7 and MDA-MB-231 breast cancer cells under four different oxygen levels. Lysates were collected from cells cultured at 7%, 2% and 0.5% O_2 for 24, 48 and 72 hours and expression was compared to a 21% O_2 control lysate. Densitometry analysis was conducted using the Odyssey Infrared Imaging System software (Licor) and data were normalised to α tubulin expression.

- **Hexokinase II**

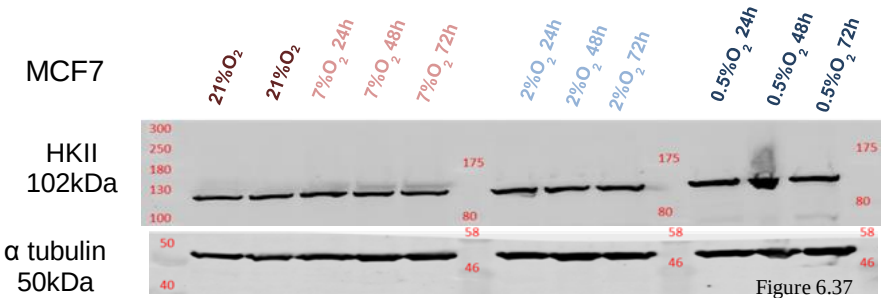

Figure 6.37

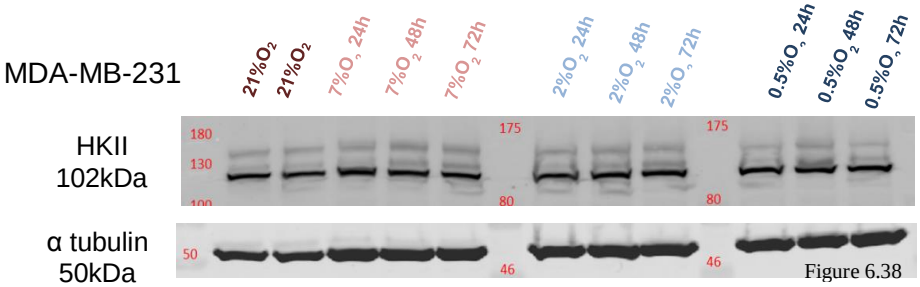

Figure 6.38

Figures 6.37 & 6.38: HKII protein expression detected through Western blotting in MCF7 and MDA-MB-231 breast cancer cells under four different oxygen levels. Lysates were collected from cells cultured at 7%, 2% and 0.5% O_2 for 24, 48 and 72 hours and expression was compared to a 21% O_2 control lysate. Alpha tubulin was used as a loading control (n=1).

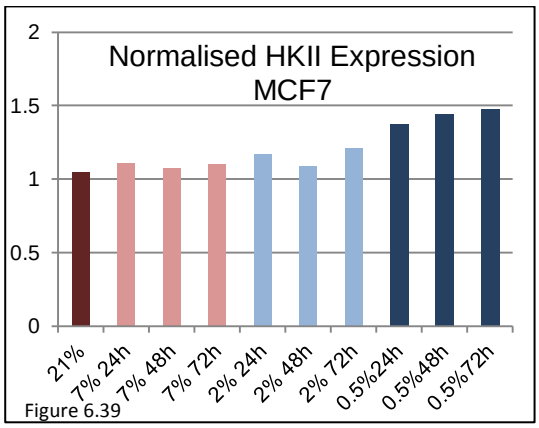

Figure 6.39

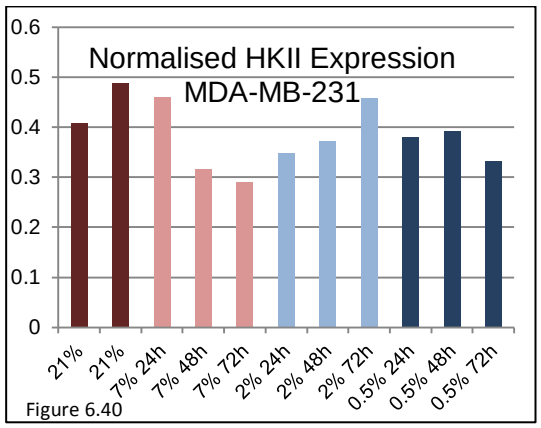

Figure 6.40

Figures 6.39 & 6.40: HKII protein expression detected through Western blotting in MCF7 and MDA-MB-231 breast cancer cells under four different oxygen levels. Lysates were collected from cells cultured at 7%, 2% and 0.5% O_2 for 24, 48 and 72 hours and expression was compared to a 21% O_2 control lysate. Densitometry analysis was conducted using the Odyssey Infrared Imaging System software (Licor) and data were normalised to α tubulin expression.

In Figures 6.37 and 6.38 the Western blot results of HKII expression of MCF7 and MDA-MB-231 breast cancer cells under varying oxygen concentrations are presented. Figures 6.39 and 6.40 show the densitometric analysis of the same blots. HKII expression of MCF7 cells at 7 and 2% O_2 was very comparable to that of the 21% O_2 control. However a gradual increase with time can be observed at the 0.5% O_2 level reaching 40% after 72h. No

upregulation was detected in MDA-MB-231 cells with expression of the enzyme being comparable between the four oxygen levels. The lowest expression was seen at 7% O_2 after 72h in MDA-MB-231 cells, with expression roughly 30% lower than the normoxic control.

- **PFKFB3**

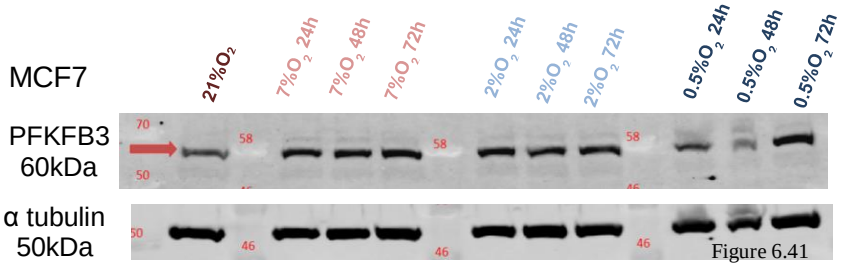

Figure 6.41

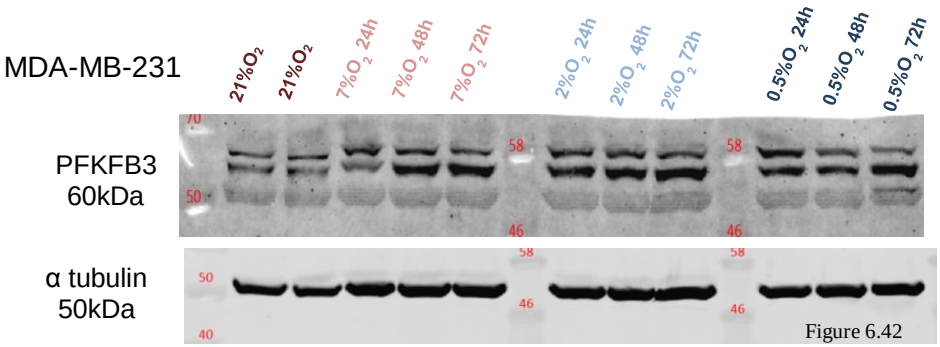

Figure 6.42

Figures 6.41 & 6.42: PFKFB3 protein expression detected through Western blotting in MCF7 and MDA-MB-231 breast cancer cells under four different oxygen levels. Lysates were collected from cells cultured at 7%, 2% and 0.5% O_2 for 24, 48 and 72 hours and expression was compared to a 21% O_2 control lysate. Alpha tubulin was used as a loading control (n=1).

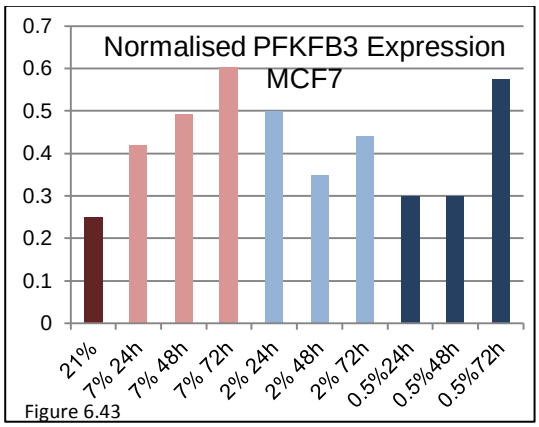

Figure 6.43

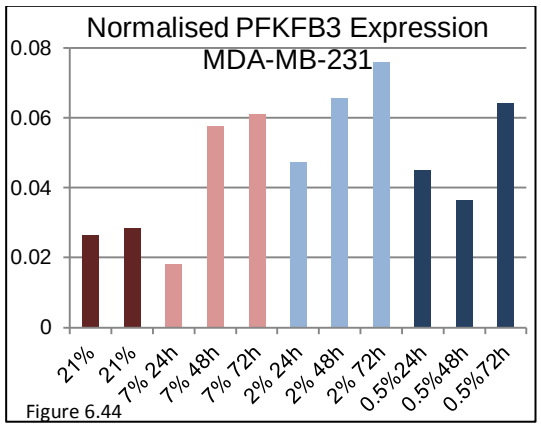

Figure 6.44

Figures 6.43 & 6.44: PFKFB3 protein expression detected through Western blotting in MCF7 and MDA-MB-231 breast cancer cells under four different oxygen levels. Lysates were collected from cells cultured at 7%, 2% and 0.5% O_2 for 24, 48 and 72 hours and expression was compared to a 21% O_2 control lysate. Densitometry analysis was conducted using the Odyssey Infrared Imaging System software (Licor) and data were normalised to α tubulin expression.

The effect of the oxygen level on PFKFB3 expression of two breast cancer cell lines was examined and the Western blots are presented in Figures 6.41 and 6.42. As can be seen from the densitometric analysis in Figures 6.43 and 6.44, both cell lines presented a threefold increase in PFKFB3 expression in low oxygen conditions at 72h. Regarding MCF7 cells, an upregulation compared to the control was observed under all 3 oxygen conditions, with highest expression at both 7 and 0.5% O_2 after 72h. A similar induction was demonstrated in MDA-MB-231 cells. An interesting observation was that under each condition, expression increased with time with a peak at 2% O_2 after 72h.

- **Pyruvate Dehydrogenase Kinase 1**

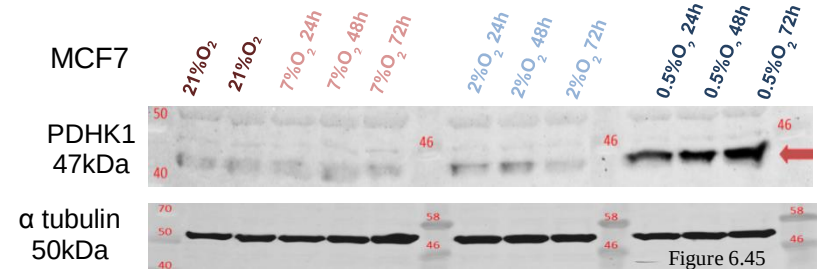

Figure 6.45

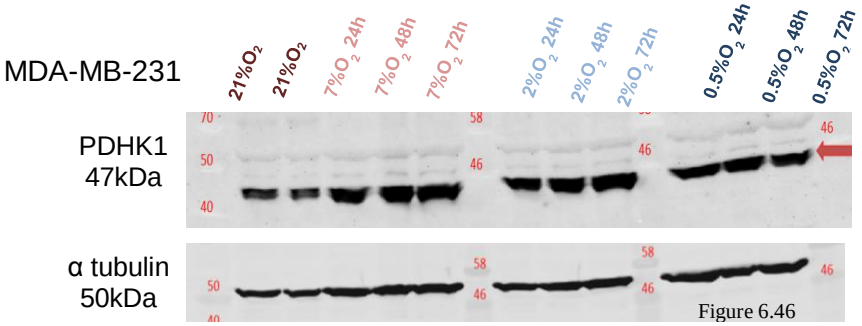

Figure 6.46

Figures 6.45 & 6.46: PDHK1 protein expression detected through Western blotting in MCF7 and MDA-MB-231 breast cancer cells under four different oxygen levels. Lysates were collected from cells cultured at 7%, 2% and 0.5% O_2 for 24, 48 and 72 hours and expression was compared to a 21% O_2 control lysate. Alpha tubulin was used as a loading control (n=1).

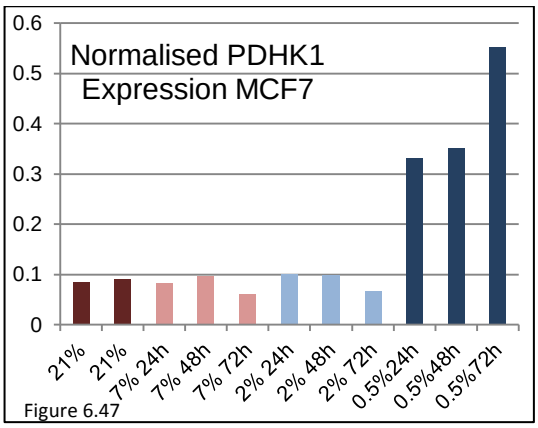

Figure 6.47

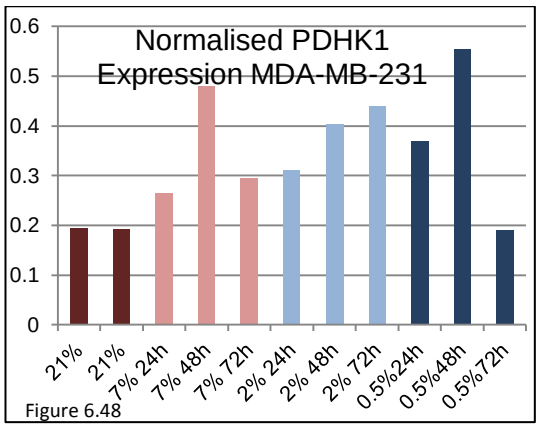

Figure 6.48

Figures 6.47 & 6.48: PDHK1 protein expression detected through Western blotting in MCF7 and MDA-MB-231 breast cancer cells under four different oxygen levels. Lysates were collected from cells cultured at 7%, 2% and 0.5% O_2 for 24, 48 and 72 hours and expression was compared to a 21% O_2 control lysate. Densitometry analysis was conducted using the Odyssey Infrared Imaging System software (Licor) and data were normalised to α tubulin expression.

The immunoblots in Figures 6.45 and 6.46 indicate PDHK1 expression of two breast cancer cell lines under four different oxygen conditions. As can be seen from the densitometric analysis displayed in Figures 6.47 and 6.48 a large induction was observed for both cell lines when oxygen availability was reduced. For MCF7 cells, PDHK1 expression was very low at 21, 7 and 2% O_2 but increased substantially at 0.5% O_2. A threefold increase was observed at 24 and 48h while a maximal fivefold induction was seen after 72h. In MDA-MB-231 cells, PDHK1 expression peaked at 0.5% O_2 after 48h (threefold increase compared to the normoxic control).

- **Lactate Dehydrogenase A**

The following Figures 6.49 and 6.50 present the Western blot results examining LDHA expression in the breast cancer cell lines under a range of oxygen concentrations. Based on the normalised results acquired from densitometric analysis, oxygen had a differential effect on LDHA expression in the two cell lines. Figure 6.51 shows that LDHA expression of MCF7 cells was low at 21, 7 and 2% O2 but was elevated at 0.5% O2. The highest twofold increase was observed after 24h and interestingly a 20 and 40% decline was noticed at 48 and 72h respectively. Regarding MDA-MB-231 cells, Figure 6.52 shows that no LDHA upregulation was seen in hypoxic conditions. Expression was actually reduced by half at 7% O2 after 48h and at 2% O2 after 24h compared to the normoxic controls.

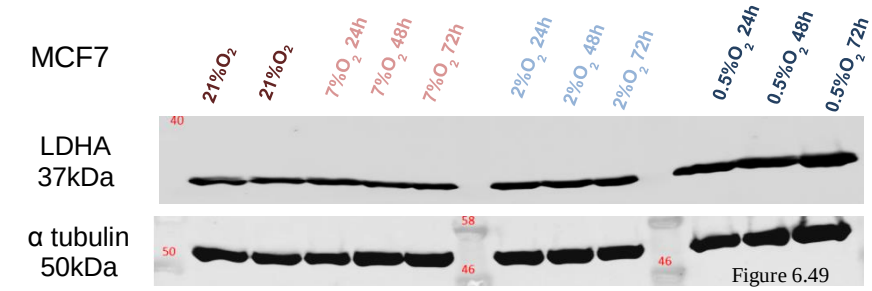

Figure 6.49

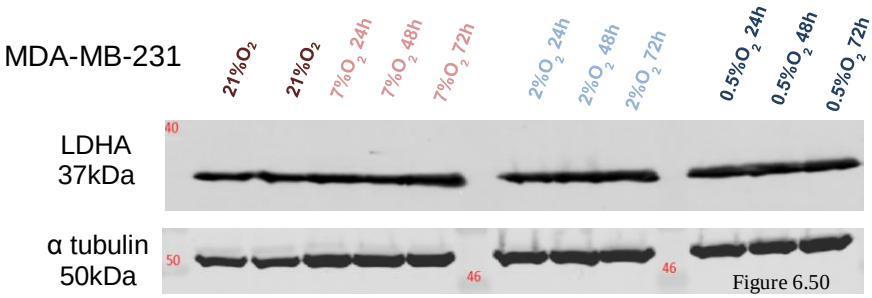

Figure 6.50

Figures 6.49 & 6.50: LDHA protein expression detected through Western blotting in MCF7 and MDA-MB-231 breast cancer cells under four different oxygen levels. Lysates were collected from cells cultured at 7%, 2% and 0.5% O_2 for 24, 48 and 72 hours and expression was compared to a 21% O_2 control lysate. Alpha tubulin was used as a loading control (n=1).

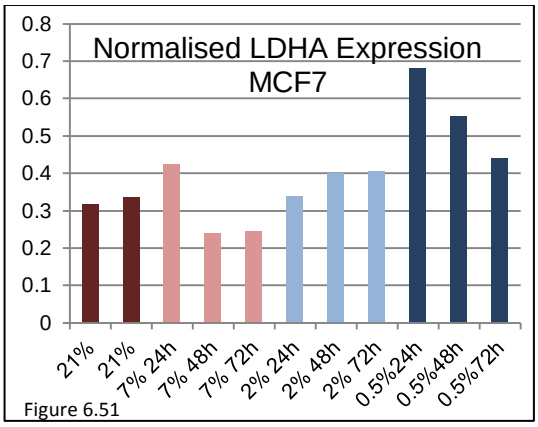

Figure 6.51

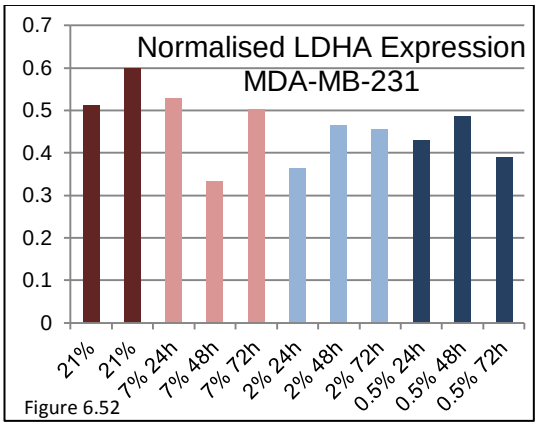

Figure 6.52

Figures 6.51 & 6.52: LDHA protein expression detected through Western blotting in MCF7 and MDA-MB-231 breast cancer cells under four different oxygen levels. Lysates were collected from cells cultured at 7%, 2% and 0.5% O_2 for 24, 48 and 72 hours and expression was compared to a 21% O_2 control lysate. Densitometry analysis was conducted using the Odyssey Infrared Imaging System software (Licor) and data were normalised to α tubulin expression.

6.3 The antiproliferative effect of the novel GLUT1 inhibitor IOM-1190 under hypoxic conditions

The effect of the oxygen level on sensitivity to the novel GLUT1 inhibitor was next examined. Sensitivity of breast cancer cells to IOM-1190 was compared under three different oxygenation conditions; normoxic cells cultured and treated at 21% O_2, acute hypoxic cells treated at 21% O_2, placed in the hypoxic chamber immediately after treatment and incubated at 0.5% O_2 for a 3-day period (not being preadapted to hypoxic conditions) and chronic hypoxic cells which were fully adapted to 0.5% O_2 conditions for 10 weeks before being treated with the inhibitor (inside the hypoxic chamber). MCF7 and MDA-MB-231 breast cancer cells were used for these experiments. Cancer cell proliferation was examined by the SRB assay in each of the conditions after a 3-day treatment period. The generated concentration response curves of MCF7 cells are presented in Figure 6.53 and for MDA-MB-231 cells in Figure 6.54. The corresponding IC_{50} values are shown in Table 6.5.

From the figures below it is apparent that the effect of the oxygen level on sensitivity to IOM-1190 was greater in MCF7 cells. The most striking observation was that both cell lines presented greater sensitivity to the inhibitor in acute hypoxic conditions. A fortyfold decrease was demonstrated from MCF7 cells in their IC_{50} value between cells that were treated at 21% O_2 and those that were incubated at 0.5% O_2 during treatment without preadaptation in low oxygen conditions. Comparatively MDA-MB-231 cells presented a fourfold decrease in their IC_{50} values in these conditions. Interestingly the response to IOM-1190 of chronically adapted cells in hypoxia was different between the two cell lines. MCF7 cells were more resistant compared to acute hypoxic cells but still more sensitive compared to normoxic cells. Their IC_{50} value was eightfold lower compared to 21% O_2 conditions. In contrast the MDA-MB-231 cells became more resistant in chronic hypoxic conditions increasing their IC_{50} value twofold compared to normoxic cells.

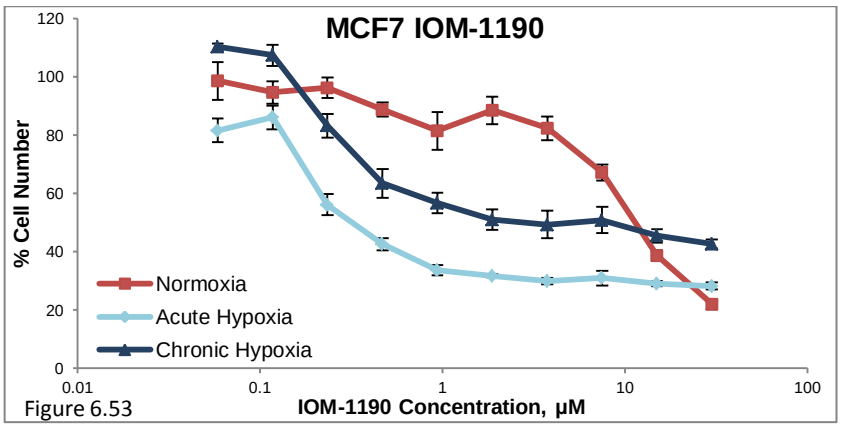

Figure 6.53

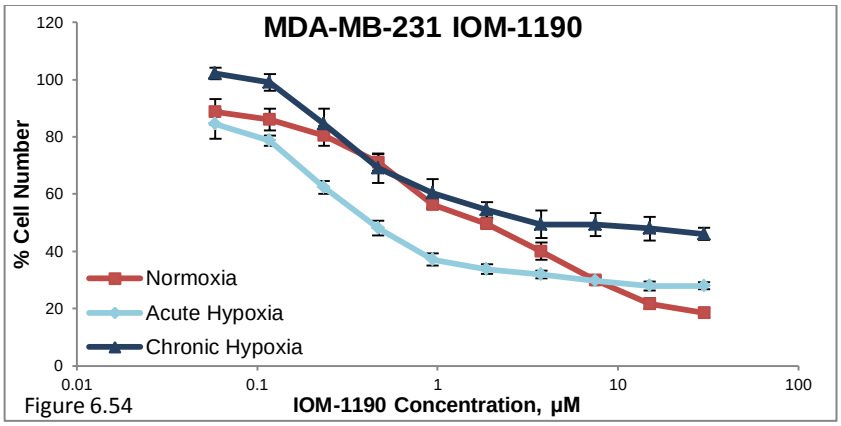

Figure 6.54

Figures 6.53 & 6.54: Concentration response curves of MCF7 and MDA-MB-231 breast cancer cells treated with IOM-1190 concentrations between 0.06-30µM under three different conditions (normoxic, acute and chronic hypoxic). Cell viability was determined by an SRB assay after a three day treatment. Mean results of 6 replicates are reported and error bars represent standard deviations. Values are shown as a percentage of control. A constant 0.3% DMSO concentration was used across the whole curve in each case (n=1).

IOM-1190 IC_{50} values (µM)	**Normoxia**	**Acute Hypoxia**	**Chronic Hypoxia**
MCF7	12.5	0.31	1.6
MDA-MB-231	1.9	0.43	3.5

Table 6.5: Summary of the IC_{50} concentrations generated for two breast cancer cell lines after a three day treatment with IOM-1190 under three different conditions (normoxic, acute and chronic hypoxic).

6.3.1 The effect of the combination of IOM-1190 with metformin under hypoxic conditions

The most robust synergist combination identified in Chapter 5 was between IOM-1190 and metformin (section 5.3.1). The effect of this combination on MCF7 and MDA-MB-231 breast cancer cells was therefore examined under hypoxic conditions. Chronic hypoxic cells adapted in hypoxic conditions for 10 weeks before co-treatment were used. These cells were treated with a range of concentrations of the GLUT1 inhibitor along with a constant concentration of metformin for 3 days. Cancer cell proliferation was assessed through SRB assays and the generated curves are presented in Figures 6.55 and 6.56 while the corresponding IC_{50} values can be seen in Table 6.6.

The combination was not effective under hypoxic conditions for both cell lines. The IOM-1190 single treatment curve was almost identical to the combination curves and remained unaffected from the addition of a constant metformin concentration either low (1mM for both cell lines) or higher (2mM for MCF7 cells). The only exception was the combination of IOM-1190 with 4mM metformin in MDA-MB-231 cells. MDA-MB-231 cells presented fivefold more sensitivity to this combination compared to single treatment with the glycolytic inhibitor (based on the IC_{50} values).

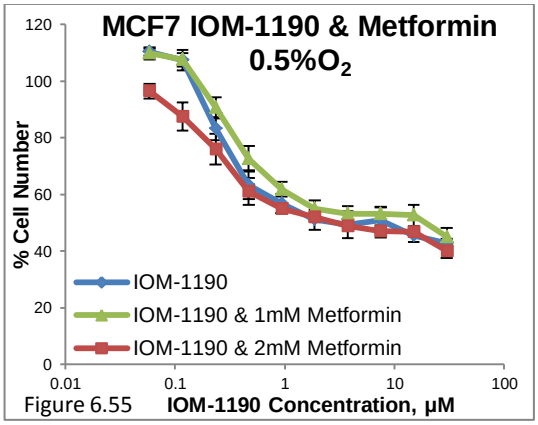

Figure 6.55

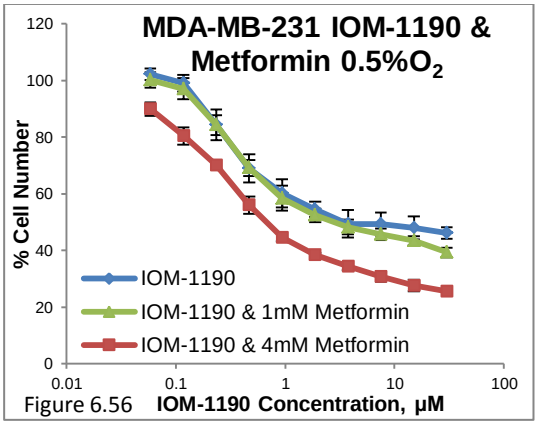

Figure 6.56

Figures 6.55 & 6.56: Concentration response curves of MCF7 and MDA-MB-231 breast cancer cells treated with IOM-1190 concentrations between 0.06-30µM alone (blue line) and combined with 1mM (green line) or 2/4mM Metformin (red line) at 0.5% O_2. Cell viability was determined by an SRB assay after a three day treatment. Mean results of 6 replicates are reported and error bars represent standard deviations. Values are shown as a percentage of control. A constant 0.3% DMSO concentration was used across the whole curve in all cases (n=1).

IC_{50} values (μM) $0.5\%O_2$	IOM-1190	IOM-1190 & 1mM Metformin	IOM-1190 & 2/4mM Metformin
MCF7	1.6	N/A	2.1
MDA-MB-231	3.5	2.2	0.72

Table 6.6: Summary of the IC_{50} concentrations generated for two breast cancer cell lines when treated with IOM-1190 alone or combined with two different Metformin concentrations at 0.5% O_2. N/A stands for not achieved in the range of used concentrations.

It was concluded that this combination, although potent in normoxic conditions generating CI values lower than 0.1, was not effective in hypoxic conditions. However the effect of metformin as single treatment on breast cancer cells at 0.5% O_2 provides an explanation, since a concentration range of metformin up to 64mM had no effect on viability of either breast cancer cell line under these hypoxic conditions (Figures 6.57&6.58). (The equivalent effect of metformin under normoxia is presented in the Appendix Figure A1.1).

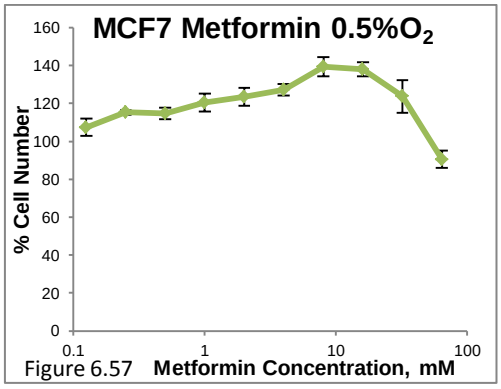

Figure 6.57

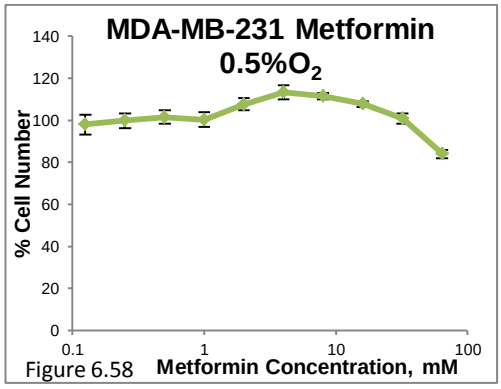

Figure 6.58

Figures 6.57& 6.58: Concentration response curves of MCF7 and MDA-MB-231 breast cancer cells treated with Metformin concentrations between 0.13-64mM at 0.5% O_2. Cell viability was determined by an SRB assay after a three day treatment. Mean results of 6 replicates are reported and error bars represent standard deviations. Values are shown as a percentage of control (n=1).

6.4 Analysis of the glycolytic pathway in hypoxia using transcriptomic data

The primary aim of this section was to elucidate further the role of glycolytic induction in hypoxic breast cancer and develop a better understanding of the observed resistance to the majority of glycolytic inhibitors (section 6.1) in hypoxia. A collaborative gene expression Illumina BeadChip analysis was undertaken with two colleagues, James Meehan and Ed Jarman, and separate analysis was incorporated in the three independent projects. Dr Arran Turnbull contributed significantly to the design of this experiment and assisted in data analysis.

Breast cancer cells (MCF7, MCF7-HER2, MDA-MB-231 and HBL100) were cultured in four distinct experimental conditions: normoxia (21% O_2), acute hypoxia (0.5% O_2 for 24h), chronic hypoxia (0.5% O_2 for 10 weeks) and treatment with $CoCl_2$, a hypoxia mimetic agent that chemically induces HIF-1. Approximately $3x10^6$ pelleted cells were collected and total RNA was extracted. The RNA was then reverse transcribed, amplified and biotinylated. Labelled RNA was hybridised to whole genome HumanHT-12 v4 Illumina BeadChips and arrays were scanned on the Illumina iScan. Raw gene expression files were processed, filtered and normalised as described in Chapter 2, section 2.10.

6.4.1 Differentially expressed genes between hypoxic and normoxic breast cancer cells

Gene expression profiles were obtained for breast cancer cells cultured in normoxia and hypoxia. Differentially expressed genes between chronic hypoxic and normoxic breast cancer cells were identified with the use of rank products (FDR cut-off P value 0.05). Functional enrichment analysis of differentially expressed genes was conducted using DAVID Bioinformatics Resources 6.7. Gene Ontology (GO) analysis was then performed and clusters of GO terms reflecting mutually modulated genes in three breast cancer cell lines between hypoxic and normoxic conditions were summarised and visualised using Revigo. The Revigo server applies a clustering algorithm in a list of GO terms and based on the concept of GO term semantic similarity, reduces functional redundancies and visualises representative clusters of GO terms [471].

The Venn diagrams presented below indicate the genes that were commonly deregulated in all three cell lines in the selected conditions. 30 genes were consistently downregulated and 20 were upregulated when comparing breast cancer cells in long term hypoxia and normoxia (Figures 6.59&6.61 left). The commonly deregulated genes are listed in tables in the Appendix (Tables A2.1&A2.2). Two dimensional scatterplots of GO terms reflecting mutually modulated genes in all three MCF7, MDA-MB-231 and HBL100 breast cancer cell lines were generated (Figures 6.59&6.61 right). These plots present the GO terms in a two dimensional scale by applying multidimensional scaling to a matrix of their semantic similarities [471]. Circle colour indicates the P value and their size reflects the frequency of the respective GO term in the GO Annotation database. The Tree maps depict the respective

GO terms in rectangles while superclusters, illustrated in different colours, associate related terms (Figures 6.60&6.62). The size of the rectangles reflects the P value.

Comparison of differentially expressed genes between culture at 0.5% O_2 for 10 weeks and normoxia revealed that 30 genes were commonly downregulated in three breast cancer cell lines while 20 were upregulated. The functional categories of genes downregulated in breast cancer cells following long term adaptation in hypoxia were mainly associated with nuclear division, mitotic cell cycle, mitotic M phase, chromosome localisation and translation (Figures 6.59&6.60). Genes upregulated in breast cancer cells chronically adapted in hypoxia were assigned to two main categories - the glycolytic process and response to hypoxia. Along with glucose metabolism the upregulated genes were involved in hexose and fructose metabolism, alcohol and carbohydrate catabolism (Figures 6.61&6.62).

Figure 6.59

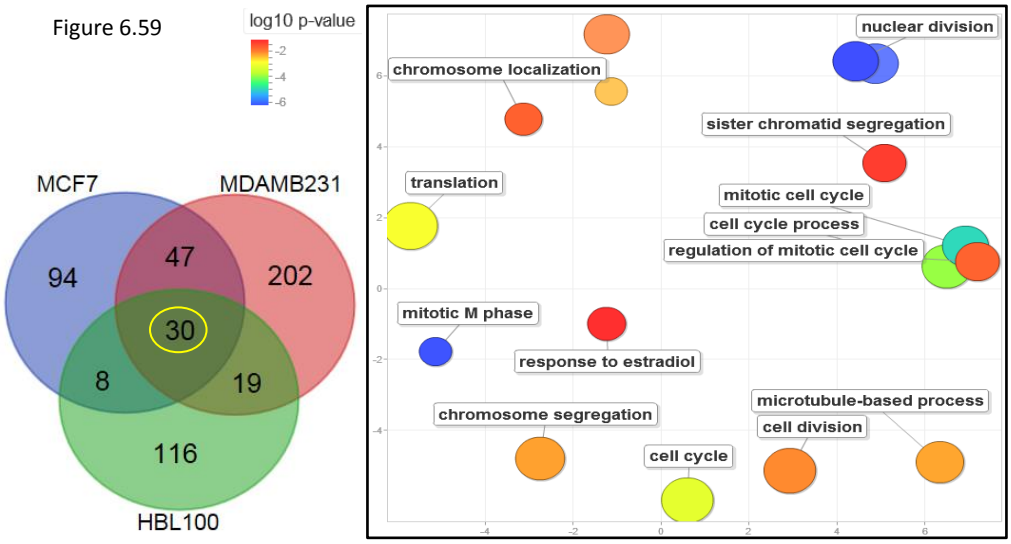

Figure 6.59: Gene Ontology analysis of downregulated genes in breast cancer cells under chronic hypoxia. The Venn diagram (on the left) indicates the number of downregulated genes in each cell line. The yellow circle highlights the number of genes mutually modulated in all three breast cancer cell lines. The Revigo scatterplot (on the right) visualises representative clusters of gene functional categories in accord with their semantic similarity. The colour of the circles indicates the P value and their size reflects the frequency of the respective Gene Ontology term in the Gene Ontology Annotation database.

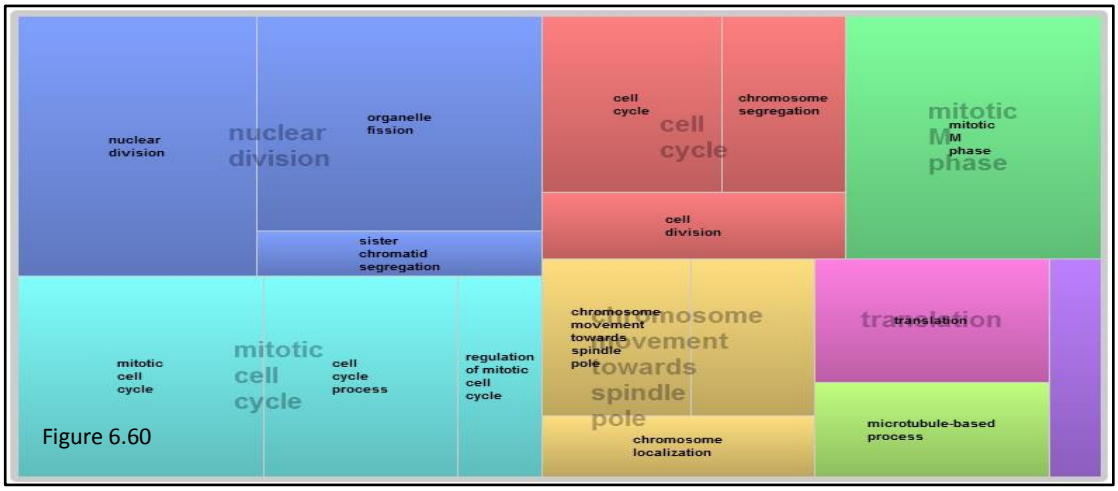

Figure 6.60: Revigo Tree map generated by Gene Ontology analysis of mutually downregulated genes in three breast cancer cell lines under chronic hypoxia. Each rectangle illustrates a representative cluster of Gene Ontology terms. Superclusters of each colour depict joined clusters of related terms. The size of the rectangles indicates the P value (the larger the rectangle the lower the P value). The lilac unnamed rectangle represents residual genes that do not fit the clusters.

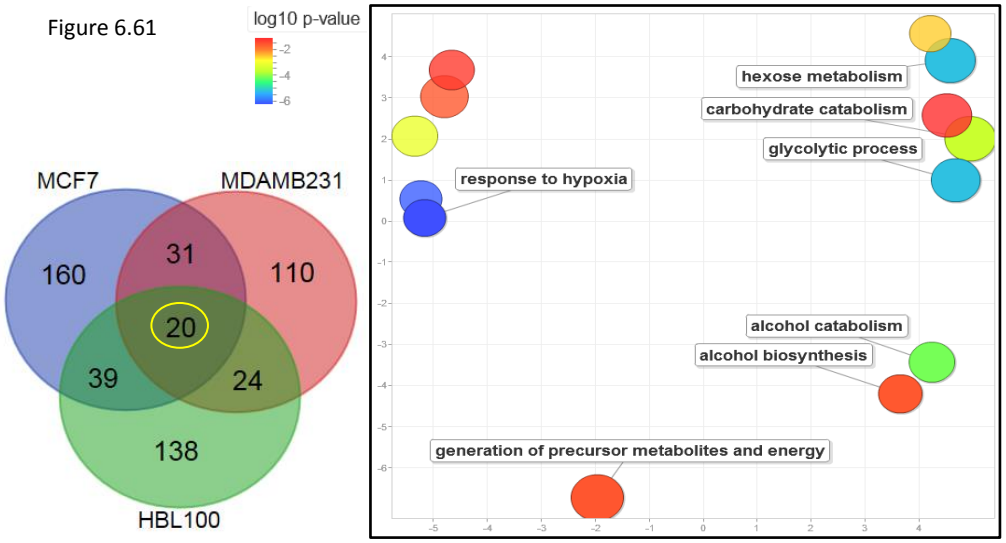

Figure 6.61: Gene Ontology analysis of upregulated genes in breast cancer cells under chronic hypoxia. The Venn diagram (on the left) indicates the number of downregulated genes in each cell line. The yellow circle highlights the number of genes mutually modulated in all three breast cancer cell lines. The Revigo scatterplot (on the right) visualises representative clusters of gene functional categories in accord with their semantic similarity. The colour of the circles indicates the P value and their size reflects the frequency of the respective Gene Ontology term in the Gene Ontology Annotation database.

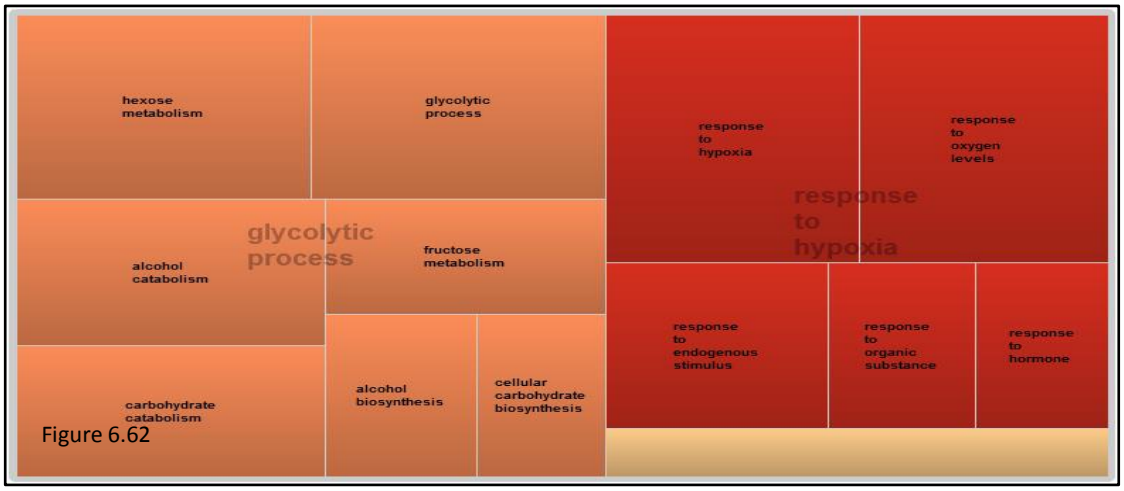

Figure 6.62: Revigo Tree map generated by Gene Ontology analysis of mutually upregulated genes in three breast cancer cell lines under chronic hypoxia. Each rectangle illustrates a representative cluster of Gene Ontology terms. Superclusters of each colour depict joined clusters of related terms. The size of the rectangles indicates the P value (the larger the rectangle the lower the P value). The beige unnamed rectangle represents residual genes that do not fit the clusters.

6.4.2 Modulation of the glycolytic pathway in chronic hypoxic breast cancer cells

Having established that the glycolytic process was commonly upregulated in hypoxic breast cancer cells attention was next focused on the glycolytic genes. The expression profiles of the genes implicated in the glycolytic pathway of four breast cancer cell lines between chronic hypoxic and normoxic conditions were compared. The genes are presented in a table in the Appendix (Table A2.3). Hierarchical clustering was performed using log2 fold change values and the following heatmap (Figure 6.63) summarises the differences in the expression patterns of MCF7, MCF7-HER2, MDA-MB-231 and HBL100 cells. Genes were clustered using average linkage and Euclidean distance metric.

The changes in expression after 10 weeks incubation in hypoxia as depicted in the heatmap verify that the glycolytic genes are upregulated in this condition. GLUT1 (SLC2A1), HKII and PFKFB3 were strongly upregulated following long term hypoxia in all four cell lines as indicated by the bright red colour. These three genes were clustered together in the same branch of the dendrogram. LDHA and PDHK1 were similarly modulated and were positioned in a separate branch. These genes demonstrated lower log2 gene expression fold changes as illustrated by darker red colours.

The only genes that presented signs of significant downregulation (bright green colouration highlighted with a green circle in the heatmap list of genes) especially for MDA-MB-231

cells were two isozymes of phosphoglucomutase (PGM). This enzyme catalyses the upstream transfer of a phosphate group and the interconversion of glucose-1-phosphate and glucose-6-phosphate [472]. Indeed this is virtually the sole glycolytic gene that has not been described as a HIF-1 or c-Myc target [113, 473].

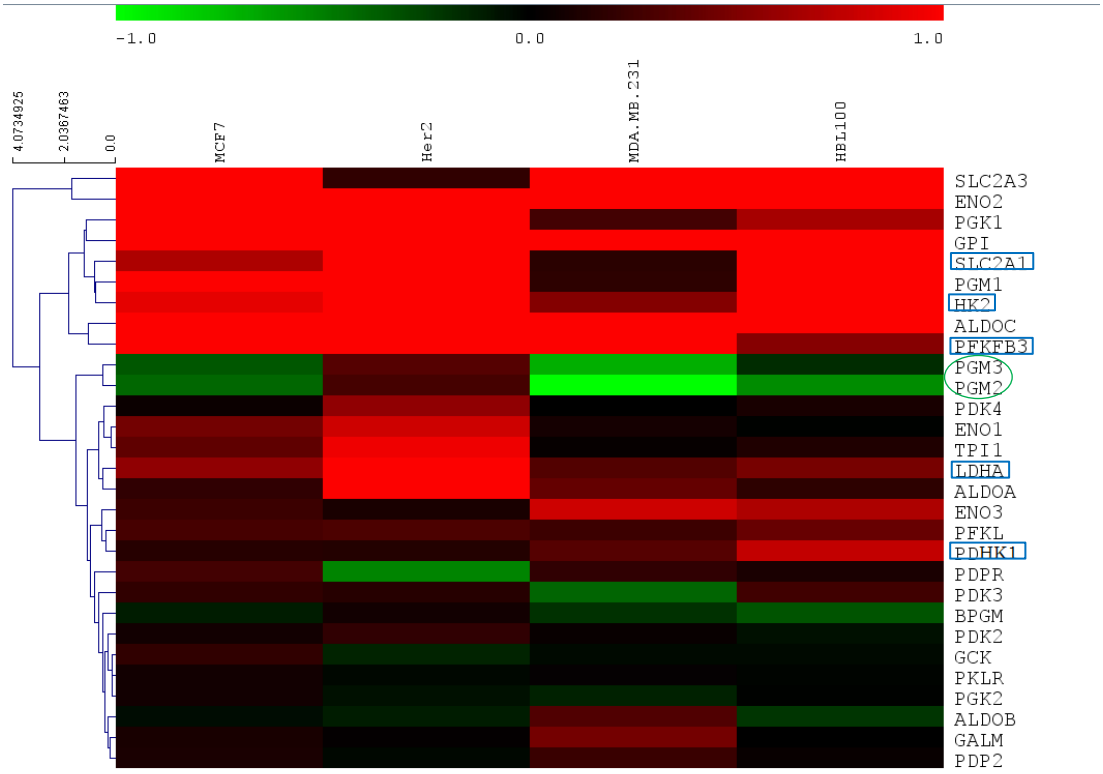

Figure 6.63: Heatmap visualisation of hierarchical clustering of glycolytic genes. The log2 fold change values of four breast cancer cell lines between chronic hypoxic and normoxic conditions were used. Red and green colours indicate relatively high and low log2 gene expression fold changes respectively. Average linkage clustering was performed and genes were ordered by Euclidean distance. List of glycolytic genes is presented on the right and genes of particular interest are highlighted.

6.4.3 Modulation of selected glycolytic enzymes in breast cancer cells under varying conditions of hypoxia

The final objective of this experiment was to evaluate the effect of hypoxia on the mRNA expression of the five glycolytic enzymes of particular interest to this study. Transcriptome levels of these enzymes in MCF7, MDA-MB-231 and HBL100 cells were assessed under chronic hypoxic and acute hypoxic conditions as well as following chemical induction of HIF-1 mediated responses via treatment with $CoCl_2$ and were compared to normoxic levels. mRNA data were determined using gene expression profiling as described in Chapter 2, section 2.10.

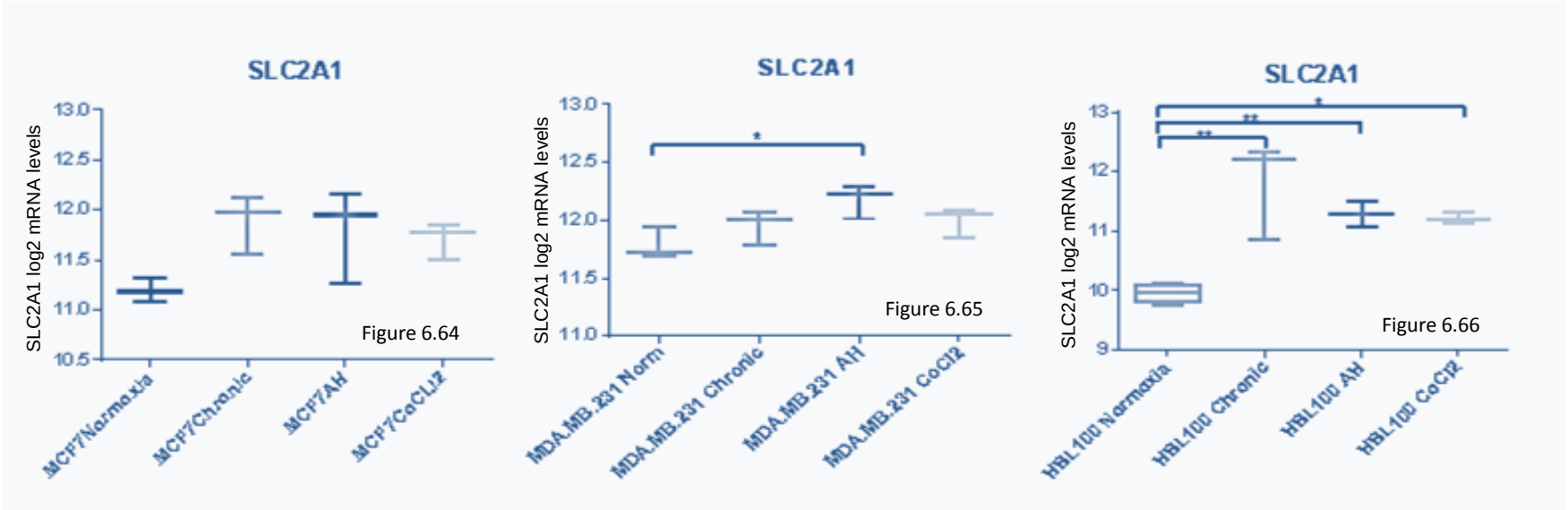

Figures 6.64 to 6.66: Log2 transformed SLC2A1 (GLUT1) mRNA levels in MCF7, MDA-MB-231 and HBL100 breast cancer cells cultured in normoxia (21% O_2), chronic hypoxia (0.5% O_2 for 10 weeks), acute hypoxia (0.5% O_2 for 24h) or treated with $CoCl_2$. Three replicate values are reported and error bars represent standard deviations. Statistical significance indications: * P<0.05, ** P<0.01 compared with the normoxic control (one-way ANOVA followed by Dunnett's multiple comparisons test).

The above figures (Figures 6.64 to 6.66) present the effect of varying conditions of hypoxia on GLUT1 expression in three breast cancer cell lines. GLUT1 was upregulated in every condition in all three cell lines (though only certain values were statistically significant). However the upregulation was greater in HBL100 cells and especially under chronic hypoxic conditions. In contrast in MDA-MB-231 cells the upregulation was statistically significant only following short term 24h incubation at 0.5% O_2. MCF7 cells demonstrated a similar induction across the examined conditions but the up-regulation did not reach significance.

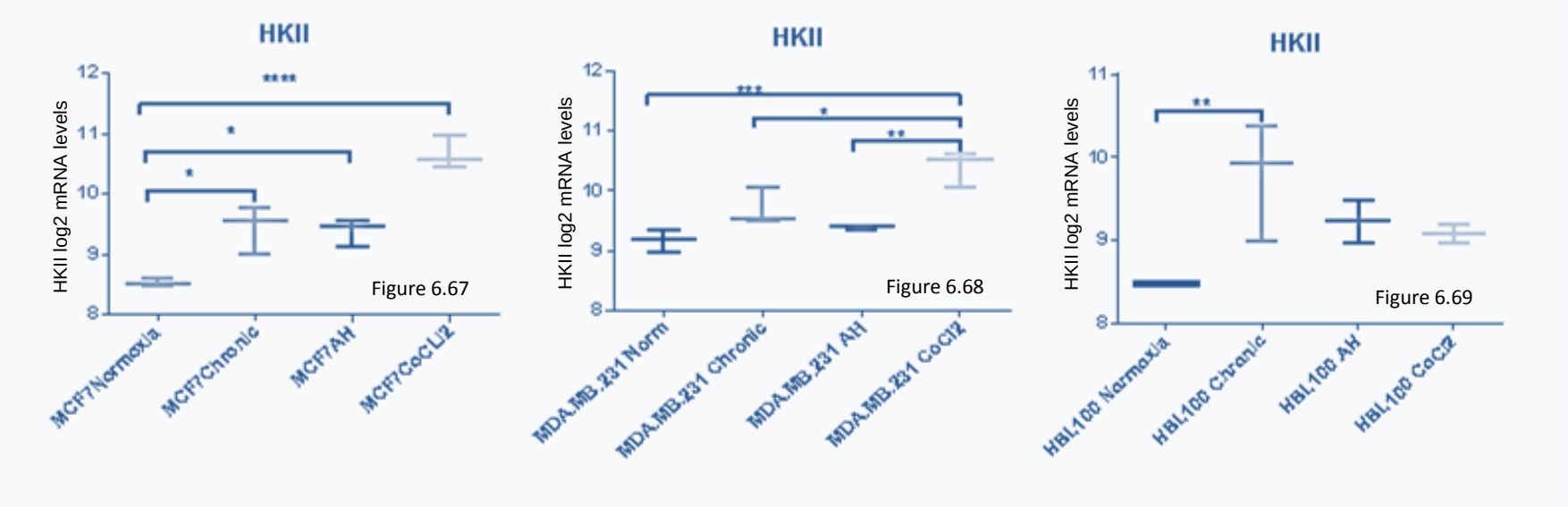

Figures 6.67 to 6.69: Log2 transformed HKII mRNA levels in MCF7, MDA-MB-231 and HBL100 breast cancer cells cultured in normoxia (21% O_2), chronic hypoxia (0.5% O_2 for 10 weeks), acute hypoxia (0.5% O_2 for 24h) or treated with $CoCl_2$. Three replicate values are reported and error bars represent standard deviations. Statistical significance indications: * P<0.05, ** P<0.01, *** P<0.001 compared with the normoxic control (one-way ANOVA followed by Dunnett's multiple comparisons test).

Figures 6.67 to 6.69 demonstrate the transcript levels of HKII in three breast cancer cell lines across several conditions of hypoxia. The upregulated levels of this target were comparable between acute and chronic hypoxic conditions in MCF7 and MDA-MB-231 cells. An interesting observation is that the hypoxia-mimetic agent $CoCl_2$ resulted in significantly higher HKII mRNA levels in these two cell lines. In contrast treatment with $CoCl_2$ did not significantly increase HKII expression in HBL100 cells suggesting that the upregulation observed in 0.5% O_2 conditions is only partially attributed to HIF-1 stabilisation in these cells. Statistically significant induction of this enzyme in HBL100 cells was only observed following long term incubation in low oxygen conditions.

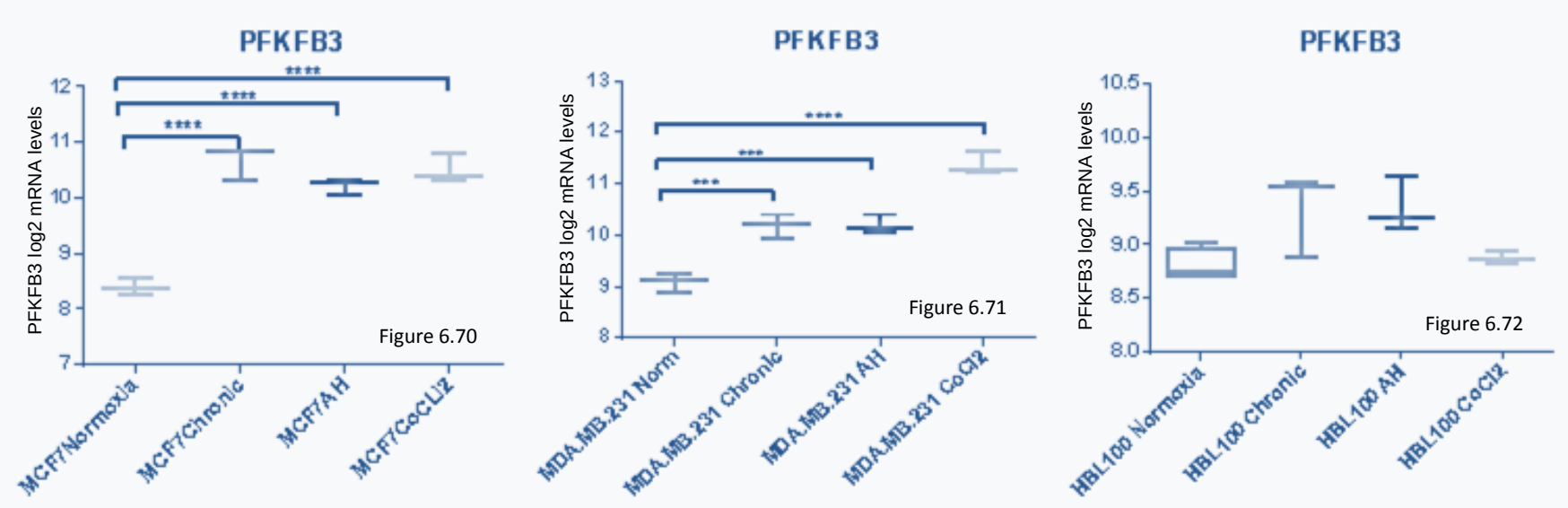

Figures 6.70 to 6.72: Log2 transformed PFKFB3 mRNA levels in MCF7, MDA-MB-231 and HBL100 breast cancer cells cultured in normoxia (21% O_2), chronic hypoxia (0.5% O_2 for 10 weeks), acute hypoxia (0.5% O_2 for 24h) or treated with $CoCl_2$. Three replicate values are reported and error bars represent standard deviations. Statistical significance indications: *** P<0.001, ****P<0.0001 compared with the normoxic control (one-way ANOVA followed by Dunnett's multiple comparisons test).

Figures 6.70 to 6.72 depict the response of PFKFB3 mRNA expression in MCF7, MDA-MB-231 and HBL100 cells respectively to variable conditions of hypoxia. The first two cell lines presented a marked induction of this target in hypoxic conditions. PFKFB3 expression was comparable in MCF7 cells across the examined conditions while higher mRNA levels following $CoCl_2$ treatment compared to low oxygenation were observed in MDA-MB-231 cells. In contrast no statistically significant changes in PFKFB3 expression were detected in HBL100 cells. Interestingly expression was unchanged in HBL100 cells treated with the hypoxia mimetic agent suggesting that HIF-1 does not affect PFKFB3 expression in this cell line.

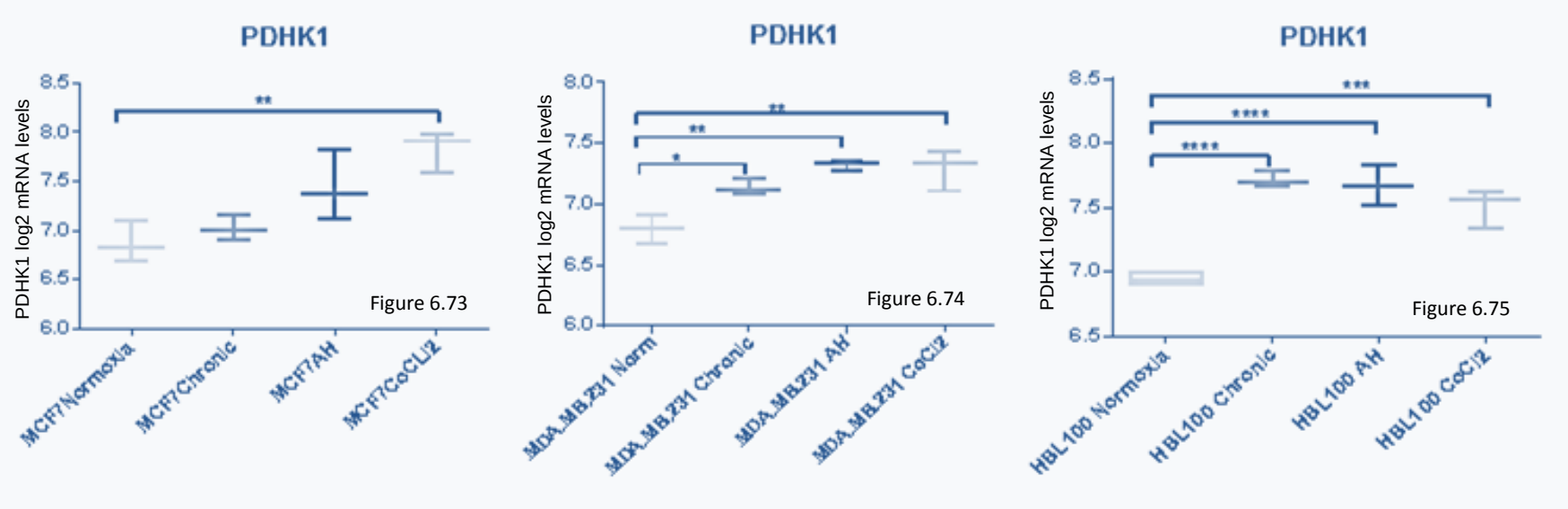

Figures 6.73 to 6.75: Log2 transformed PDHK1 mRNA levels in MCF7, MDA-MB-231 and HBL100 breast cancer cells cultured in normoxia (21% O_2), chronic hypoxia (0.5% O_2 for 10 weeks), acute hypoxia (0.5% O_2 for 24h) or treated with $CoCl_2$. Three replicate values are reported and error bars represent standard deviations. Statistical significance indications: * P<0.05, ** P<0.01, *** P<0.001, ****P<0.0001 compared with the normoxic control (one-way ANOVA followed by Dunnett's multiple comparisons test).

Results acquired from PDHKI gene expression analysis are shown in Figures 6.73 to 6.75. MCF7 cells demonstrated a modest induction when cultured in a low oxygen environment whereas statistically significant upregulation was only observed following treatment with $CoCl_2$. On the contrary MDA-MB-231 and HBL100 cells significantly upregulated PDHK1 expression in hypoxic conditions or conditions mimicking hypoxia. Both cell lines demonstrated comparable levels of this target across the three examined conditions.

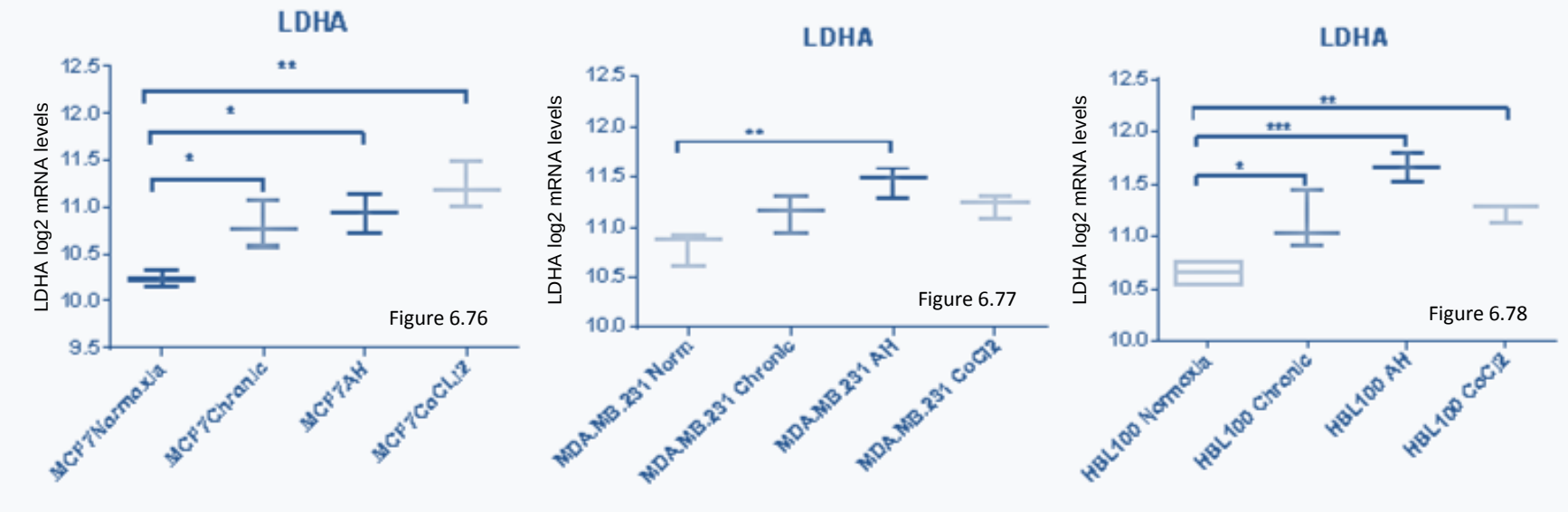

Figures 6.76 to 6.78: Log2 transformed LDHA mRNA levels in MCF7, MDA-MB-231 and HBL100 breast cancer cells cultured in normoxia (21% O_2), chronic hypoxia (0.5% O_2 for 10 weeks), acute hypoxia (0.5% O_2 for 24h) or treated with $CoCl_2$. Three replicate values are reported and error bars represent standard deviations. Statistical significance indications: * P<0.05, ** P<0.01, *** P<0.001 compared with the normoxic control (one-way ANOVA followed by Dunnett's multiple comparisons test).

Figures 6.76 to 6.78 provide evidence that breast cancer cells upregulate LDHA expression in hypoxia. MCF7 and HBL100 cells exhibited significantly increased LDHA expression following exposure to 0.5% O_2 or $CoCl_2$. In contrast significantly higher LDHA mRNA levels were only detected in acute hypoxic MDA-MB-231 cells.

6.5 Discussion

6.5.1 Breast cancer cells demonstrated increased sensitivity to glycolysis inhibition in high oxygen conditions

Hypoxia is a well substantiated prevalent characteristic of the tumour microenvironment. Solid tumours grow uncontrollably and outreach the diffusion distance of oxygen. Oxygen deficiency commonly arises as a result of the unrestricted tumour growth and the chaotic architecture of the tumour microvasculature. Hypoxia has important implications as it has been extensively associated with an aggressive phenotype, adverse clinical outcome and resistance to radiation therapy and several cytotoxic agents [142, 143, 474]. Previous research has established that advanced solid tumours frequently exhibit heterogeneously distributed hypoxic and anoxic areas. A number of studies have reported remarkable variability in the oxygenation status among individual tumours as well as within the same lesion [142-144]. In their major study Helmlinger *et al* employed high-resolution microscopy techniques to measure the oxygen tension *in vivo* in colon cancer xenograft models. They revealed pronounced gradients and heterogeneously distributed patterns with distinct variability in the oxygen pressure. Hypoxic regions (<5mmHg) were detected at a distance of 70-80μm from the nearest blood vessel wall while anoxic regions (0-0.5mmHg) at a distance greater than 150μm [475]. With regard to breast malignancies, Vaupel *et al* demonstrated differentially oxygenated populations within individual breast tumours and documented that at least 40% of examined breast carcinomas contained hypoxic tissue regions with O_2 tensions ranging from 0 to 2.5mmHg. The median oxygen level of 16 normal breast tissue samples was calculated at 8.6% O_2, while the respective value of 15 breast tumours was 4% [145].

The HIF family of transcription factors plays a leading role in cellular homeostasis and the adaptation of cancer cells in the hypoxic tumour microenvironment, particularly HIF-1. HIF-1 activation, either because of low oxygen tensions or through aberrant oncogenic signalling, is known to promote the glycolytic phenotype and suppress mitochondrial oxidative phosphorylation. The glycolytic enzymes of particular interest to this study, along with PDHK1, are known to be HIF-1 inducible [151, 446, 474]. Based on previous research supporting variability in the oxygenation of breast tumours and metabolic dependency on oxygen availability, this study set out to determine the efficacy of glycolysis inhibition in differing oxygen conditions. The effect of the panel of glycolytic inhibitors was assessed under a range of oxygenation levels. Two breast cancer cell lines were used in these

experiments and were treated with eight glycolytic inhibitors under four oxygen conditions, 21%, 7%, 2% and 0.5% O_2, for an either 3 or 5-day period.

The four different oxygenation levels were deliberately selected based on the HIF-1α activation status. As discussed in the introduction HIF-1 is the major regulator of cellular response to low oxygen tensions (Chapter 1, section 1.3.1). Jiang *et al* documented that HIF-1α protein levels increase exponentially in HeLa cells mainly when oxygen availability becomes lower than 6%. Thus the selected 7% O_2 condition aims to reflect an environment prior to HIF-1α activation. In the same study half maximal HIF-1α protein levels and HIF-1-DNA binding activity was observed at 2% while the maximal response occurred at 0.5% O_2 [476].

It is necessary to clarify that normoxia here denotes 21% O_2 conditions (150mmHg), the oxygen concentration in ambient air. The majority of *in vitro* cancer research experiments are currently conducted in this aerobic environment. Nevertheless these conditions are not physiologically relevant and the term 'normoxia' does not imply normal oxygen availability in mammalian tissue which is averaged between 2 and 9% O_2 [474].

The most important finding of this experiment was that breast cancer cells presented enhanced sensitivity to all eight glycolytic inhibitors in 21% O_2 conditions, compared to the three lower oxygen levels. Enhanced sensitivity in normoxia was consistent for both breast cancer cell lines and was confirmed at both time points examined. Higher IC_{50} values in hypoxia suggested increased resistance to the inhibitors in these conditions. Nevertheless, both cell lines were susceptible to glycolysis inhibition over the whole range of oxygen levels tested validating the strategy as effective anticancer treatment in the gradient of hypoxia observed in solid tumours. Modulation of the activity of the eight compounds targeted against multiple points of the glycolytic pathway was comparable across the varying levels of oxygen. This could be considered an indication of a shared mechanism of action and inhibition of a common pathway.

The most striking observation was the notable difference in the efficacy of the inhibitors between 21 and 7% O_2. Both cell lines markedly increased their IC_{50} values between 21 and 7% O_2 regardless of the duration of treatment. Breast cancer cells were found to be considerably more resistant to the whole panel of glycolytic inhibitors at 7% O_2 compared to 21% O_2 conditions. The respective IC_{50} values increased from 1.5 fold (MDA-MB-231 cells treated with STF31 for 5 days – Figure 6.8) up to 62 times (MDA-MB-231 cells treated with NHI-1 for 3 days – Figure 6.31). In contrast, variation in oxygen levels between 0.5 and 7%

seemed to have a relatively minimal effect on the sensitivity to the glycolytic inhibitors. Interestingly, the response of the breast cancer cells to the majority of the compounds in the three lower oxygen levels was comparable at both time points. However, in some cases cells enhanced their resistance increasing further their IC_{50} values (MCF7 cells treated with Oxamic acid for 3 days – Figure 6.25) or became slightly more sensitive demonstrating a modest decrease in their IC_{50} values (MCF7 and MDA-MB-231 treated with DCA – Figures 6.21 to 6.24). Taken together, breast cancer cells were found to be considerably more sensitive to the eight glycolytic inhibitors at 21% O_2 compared to any of the lower oxygen levels examined following a 3-day or a 5-day treatment period (Tables 6.1&6.2).

One unanticipated observation was that Phloretin actually enhanced the growth of MCF7 breast cancer cells following a 3-day treatment under the three low oxygen conditions as well as following a 5-day treatment at 7% O_2. Growth reached 160 and 180% compared to the untreated controls in each time point respectively (Figures 6.1&6.2). Taking into account that this effect was specific to the ER positive line this could possibly be attributed to the oestrogenic nature of this phytochemical. As discussed in the introduction (Chapter 1 section 1.5.1.1) these substances have been associated with a wide range of pharmacological responses. Several flavonoids possess oestrogenic activity as they resemble 17β-oestradiol and have the ability to interact directly and competitively bind the ER receptors [275, 477]. Phloretin has been described as a natural nonsteroidal oestrogen [478]. It has previously been reported that genistein, another flavonoid, induces proliferation of MCF7 breast cancer cells when used in low concentrations in an ER dependent way while it demonstrates antiproliferative action in high concentrations [275, 479]. However dependency of the effect on the oxygen availability has never been described and furthermore stimulation of cancer cell growth by Phloretin has not been reported. Further work needs to be undertaken to clarify this interesting observation.

This study has demonstrated amplified sensitivity to inhibition of the glycolytic pathway in normoxia. This outcome seems counter-intuitive as it is contrary to the notion of increased dependency on glycolysis under hypoxic conditions. In the absence of oxygen, cells rely primarily on the catabolism of glucose for the production of energy. Furthermore, it is now well established that HIF-1 induces the expression of glycolytic enzymes, promotes the glycolytic phenotype and suppresses mitochondrial oxidative phosphorylation as an adaptive response to support tumour growth in the hostile hypoxic tumour microenvironment [146, 446]. Hence mechanistically it would be anticipated that increased reliance on glycolysis would make its inhibition more effective. Nonetheless dependency on the glycolytic pathway

even in the presence of ample oxygen is in agreement with the seminal theory of Warburg [87].

An important factor that could possibly be related to the observed resistance to the inhibitors in hypoxia is the growth rate. Cells grow more slowly in low oxygen tensions and this may have influenced the response to the compounds. Significant associations between the potency of the inhibitors under the varying levels of oxygen and the proliferation rate in the corresponding conditions were revealed (Table 6.4). One conceivable explanation is that faster growing cells under high oxygen tensions are highly dependent on glycolysis for the production of energy and the metabolic intermediates required for the biosynthesis of macromolecules, and for that reason are more susceptible to glycolytic inhibitors. Greater resistance to glycolysis inhibition by slow growing cancer cells is in agreement with results presented in Chapter 3 section 3.3 demonstrating a correlation between response to certain glycolytic inhibitors and the proliferation rate across an extended panel of breast and ovarian cancer cell lines (Figures 3.39&3.40).

In the literature there has been little agreement on the efficacy of glycolysis inhibition in hypoxia in several cancer cell line models. Research in the field has generated disparate results. Although a number of studies demonstrated minimal changes in the potency of selected glycolytic inhibitors under normoxic and hypoxic conditions, some studies suggested enhanced activity in hypoxia while others showed the opposite. According to Cao *et al* Phloretin was equally effective in normoxia and hypoxia against SW620 colon cancer cells and K562 leukaemia cells [287]. In line with this Xiao *et al* reported that 3BP had a comparable effect on pancreatic cancer cells in normoxic and hypoxic conditions [480]. In contrast three independent studies demonstrated enhanced 3BP activity in hypoxic conditions using lymphoma and colon cancer cell lines, hepatocellular as well as pancreatic cancer cells [331, 481, 482]. Similarly increased sensitivity of A549 lung cancer cells to WZB117 in hypoxia has been evidenced by Liu *et al* [319]. Furthermore Liu *et al* developed anaerobic osteosarcoma cell model systems that exhibited hypersensitivity to 2-DG and Oxamic acid [483, 484]. Likewise Granchi *et al* documented that NHI-1 was particularly potent against various cancer cell line models in a low oxygen environment [378, 379]. However, in agreement with the findings of the present study, Anderson *et al* reported that DCA was more potent in attenuating the proliferation of HeLa and PANC-1 cells in normoxic conditions. Accordingly, Shahrzad *et al* confirmed that colorectal cancer cells were more susceptible to PDHK1 inhibition under normoxia both *in vitro* and *in vivo* [485]. Resistance to inhibition of pH regulating proteins (the CAIX inhibitor S4, the NHE1

inhibitor DMA and the V-ATPase inhibitor bafilomycin A1) under low oxygen availability has been recently demonstrated (James Meehan, personal communication, paper under review). Even though the concept of amplified sensitivity to glycolysis inhibition in hypoxia has been challenged there has been no detailed study investigating the effect of multiple inhibitors of the glycolytic pathway within a wide range of hypoxia.

This study offers valuable insights into the sensitivity to glycolysis inhibition under physiological levels of hypoxia. This is the first study to examine the effect of a series of glycolytic inhibitors on breast cancer cells in varying oxygenation levels in contrast to the previous research on the subject that has been mostly restricted to 21% O_2 conditions which are undoubtedly less relevant to the tumour microenvironment. Relative resistance of breast cancer cells in hypoxic conditions was consistently demonstrated for all eight of these inhibitors and may have implications for their use as antitumour agents. This important finding will be further investigated in this chapter.

6.5.2 Resistance of breast cancer cells to glycolysis inhibition in hypoxia was associated with target overexpression

The aim of this section was to interpret the observed resistance of breast cancer cells to glycolysis inhibition in varying levels of hypoxia. It was assessed whether the expression of the targeted glycolytic enzymes could have an impact on the efficacy of the inhibitors. The protein expression of the glycolytic targets of interest were evaluated by Western blotting in MCF7 and MDA-MB-231 cells cultured in a range of hypoxia levels (7, 2 and 0.5% O_2) for varying periods of time (24, 48 and 72h). The expression was compared to a 21% O_2 control.

This study has been unable to demonstrate GLUT1 protein upregulation in either of the breast cancer cell lines under the examined conditions (Figures 6.35&6.36). HKII and LDHA were upregulated compared to the normoxic control only in MCF7 cells at 0.5% O_2. Peak HKII expression was observed following 72h incubation at 0.5% O_2 while maximal LDHA expression as early as 24h (Figures 6.39&6.51). The most profound effect of oxygen depletion was on PDHK1 expression. Both breast cancer cell lines demonstrated a marked induction of this target. MCF7 cells exhibited a fivefold increase at 0.5% O_2 and MDA-MB-231 cells a threefold increase in the same conditions (Figures 6.47&6.48). Furthermore PFKFB3 expression was also increased in both cell lines. Both MCF7 and MDA-MB-231 cells had increased expression of this enzyme (up to threefold) when grown at 7 and 2% O_2 respectively (Figures 6.43&6.44).

An interesting observation was that the modulation of the targets in the triple negative basal B breast cancer cell line (MDA-MB-231) was less profound compared to the ER positive luminal A line (MCF7). Two of the targets were upregulated only in MCF7 cells while PDHK1 upregulation was greater in this cell line. A possible explanation for that could be that MDA-MB-231 cells harbouring an oncogenic K-Ras are highly glycolytic suggesting that the expression of the glycolytic enzymes is already elevated in normoxia and further induction in hypoxic conditions is modest. In agreement with this, Gaglio *et al* documented upregulation of several glycolytic enzymes in MDA-MB-231 cells compared to normal breast tissue [423].

This experiment examined the hypothesis that elevated expression of the targeted glycolytic enzymes could lead to increased resistance to glycolytic inhibitors in a low oxygen environment. Mechanistically it can conceivably be assumed that increased expression of an enzyme is likely to require increased amount of an inhibitor to be targeted. HIF-1α mediated upregulation of the glycolytic targets in hypoxia is well characterised [151, 446]. The glycolytic enzymes as verified HIF-1 targets are upregulated in hypoxic conditions however the majority of research in the field has only focused on mRNA expression levels. No study has been identified examining the modulation of protein expression levels of several glycolytic enzymes under a range of oxygen levels in breast cancer cells.

A limitation in this experiment is that it was only conducted once and so detailed statistical analysis is not feasible. An additional limitation lies in the absence of HIF-1 data. Ideally the expression of the glycolytic enzymes should be associated with the expression of the major hypoxia response regulator. Evaluation of the HIF-1 levels in the same lysates was attempted. However due to complications in the antibody optimisation process and because of stability issues of the protein reliable data were not acquired.

Further support for the concept of reduced sensitivity to glycolytic inhibitors in hypoxia mediated by elevated expression of the respective targets was provided by the findings of Maher *et al*. In their study the authors used several *in vitro* models (chemical restriction of oxidative phosphorylation, HIF-1 downregulation and HIF-1 deficient cells) and indicated that HIF-1 confers resistance to 2-DG. They suggested that HIF-1 activation upregulates the expression of the glycolytic enzymes reducing the sensitivity to glycolytic inhibitors as higher concentrations are required to block the pathway and induce the same antitumour effect. Corroborating the findings of the present study elevated resistance to 2-DG was associated with HKII upregulation [486]. The same mechanism of resistance has also been proposed for other chemotherapeutic agents. For example, development of resistance to

methotrexate in leukemia cells has been attributed to target gene amplification (dihydrofolate reductase) [487].

According to these data, it can be inferred that relative resistance to glycolysis inhibition in hypoxia can at least to some extent be attributed to upregulation of the targeted glycolytic enzymes. These findings enhance our understanding of the effect of oxygen availability on the glycolytic pathway and sensitivity to its inhibition and provide new insights into the interpretation of the impaired potency of glycolytic inhibitors in hypoxic conditions.

6.5.3 Breast cancer cells demonstrated enhanced sensitivity to the novel GLUT1 inhibitor IOM-1190 in low oxygen conditions

In chapter 3 the novel GLUT1 inhibitor IOM-1190 was identified as a potent inhibitor of breast cancer cell proliferation. In this section the effect of this inhibitor was assessed in hypoxic conditions. IOM-1190 was compared against MCF7 and MDA-MB-231 cells at 0.5% O_2 in two distinct situations. Acute hypoxic cells were incubated at 0.5% O_2 for 3 days during treatment while chronically hypoxic cells were perfectly preadapted to the oxygen level for 10 weeks prior to treatment. These conditions were selected to mirror the tumour microenvironment. It is known that the abnormal tumour vasculature gives rise to heterogeneously distributed alternating normoxic, hypoxic, anoxic necrotic and re-oxygenated areas [146]. Consequently acute hypoxic along with chronically hypoxic cells are a common feature of solid malignancies.

The single most important observation to emerge from these data is that breast cancer cells presented enhanced sensitivity to IOM-1190 in hypoxic conditions. Interestingly both breast cancer cell lines exhibited a marked reduction in their IC_{50} values between normoxic and acute hypoxic conditions that reached the fortyfold level in MCF7 cells. Long term adaptation in hypoxic conditions made breast cancer cells less sensitive to treatment with the GLUT1 inhibitor. However MCF7 cells were still eightfold more sensitive compared to 21% O_2 conditions while in contrast MDA-MB-231 cells presented a modest increase in their IC_{50} value compared to normoxic conditions (Figures 6.53&6.54 and Table 6.5).

Enhanced sensitivity to IOM-1190 in hypoxia is contrary to the findings with the majority of the other eight compounds tested (Tables 6.1&6.2). However these results corroborate the notion of elevated sensitivity to glycolysis inhibition stemming from increased dependency on the pathway under hypoxic conditions. Moreover, they are consistent with earlier studies demonstrating that a number of glycolytic inhibitors, including WZB117, 3BP, Oxamic acid and NHI-1, were more effective in hypoxic systems [319, 331, 378, 379, 481-484].

The glycolytic inhibitors have been evaluated in combination strategies with established chemotherapeutic and targeted agents. Several synergistic interactions were identified and are presented in Chapter 5. Robust synergy was revealed between IOM-1190 and the antidiabetic drug metformin as shown in section 5.3.1. Here this combination was assessed in hypoxic conditions. It was demonstrated that metformin did not enhance the antiproliferative effect of the GLUT1 inhibitor on chronically hypoxic breast cancer cells (Figures 6.53&6.54) suggesting that the interaction between the two compounds is less favourable in these conditions. However a high concentration of metformin (4mM) significantly augmented the action of IOM-1190 against MDA-MB-231 cells.

While IOM-1190 as a single agent is highly potent in hypoxic conditions, metformin did not affect breast cancer cell proliferation in a low oxygen environment, even over a broad range of concentrations (Figures 6.57&6.58). However, an inhibitor of mitochondrial oxidative phosphorylation is unlikely to have any influence in oxygen depleted conditions, if cells are not reliant on mitochondrial respiration. Nonetheless literature has recently emerged that offers contradictory findings. In agreement with the findings of the present study Garofalo *et al* documented that Ewing sarcoma cells were less sensitive to metformin in hypoxia either as single treatment or in combination with vincristine both *in vitro* and *in vivo*. They claimed that the limited efficacy was associated with impediment to AMPK activation and subsequent mTOR inhibition [488]. Along the same line Griss *et al* reported that metformin impaired the proliferation of osteosarcoma cells exclusively in aerobic conditions. The authors argued that the antiproliferative effect of metformin is not related to the activation of AMPK. The antitumour effect of the antidiabetic agent was attributed to impairment of the anabolic growth of tumour cells due to deficiency of mitochondrial metabolic intermediates (particularly for lipid biosynthesis). It was suggested that cells not reliant on mitochondria to replenish their biosynthetic precursors develop resistance to the biguanide. This includes hypoxic cells engaged in a reductive glutamine metabolism [489]. On the other hand Safari *et al* indicated that metformin was more effective against hypoxic than normoxic MCF7 breast cancer cells [490]. In agreement with this Wheaton *et al* associated the antitumour effect of the antidiabetic agent with inhibition of the mitochondrial respiratory chain complex I. They demonstrated that metformin inhibits HIF-1 activation and suggested that low glucose or oxygen availability augments the action of metformin [491].

One important result to emerge from these data is that the novel GLUT1 inhibitor exhibited significant antiproliferative action in hypoxic conditions. Cells chronically adapted in hypoxia are considered highly aggressive and are likely to be irresponsive to conventional

treatment including radiation therapy and several chemotherapeutic agents [142]. The observation that both ER positive and triple negative 'resistant' hypoxic breast cancer cells demonstrated amplified sensitivity to IOM-1190 in low concentrations is of great importance. The novel GLUT1 inhibitor is identified here as a potent cancer cell proliferation inhibitor. Evidence is provided that this compound has potential therapeutic value and could play a role in the future cancer therapy. However further studies need to be carried out in order to evaluate its efficacy in *in vivo* systems. Furthermore the combination of IOM-1190 and metformin needs further evaluation and may prove useful in the treatment of triple negative tumours. Although metformin did not increase the effectiveness of IOM-1190 as a single treatment in chronically hypoxic cells, the combination may be more effective in the range of oxygenation levels found in the microenvironment of solid tumours. IOM-1190 along with metformin is highly potent under high oxygen levels, while the GLUT1 inhibitor is effective by itself in low oxygen conditions.

6.5.4 Upregulation of the glycolytic pathway in breast cancer cells under hypoxia at the transcriptomic level

A genome-wide transcriptomic analysis on breast cancer cells under short term (24h) and long term (10 week) hypoxia as well as in conditions of chemically induced hypoxia (by $CoCl_2$ treatment) was undertaken. Illumina BeadChip analysis was conducted to evaluate the transcriptome changes between these conditions. The aim of this experiment was to determine the response of breast cancer cells to hypoxia and investigate the modulation of the glycolytic pathway in these conditions. To further explore the previously observed resistance to glycolysis inhibition in a low oxygen environment, the transcript levels of selected glycolytic enzymes were assessed.

It has been long appreciated that hypoxia has extensive effects on gene expression and enhances the glycolytic pathway. Adaptation to the hostile hypoxic microenvironment dictates high flux through the glycolytic pathway and enhanced glycolytic rates [153, 470]. However, the transcriptional response to oxygen deprivation is specific for each cell type [492]. It has been suggested that HIF-1 targets vary between cell types and are dependent on the expression profile of the α subunit as well as the severity of hypoxia [146, 492]. Therefore this study set out to investigate the control of the glycolytic enzymes expression in hypoxia in breast cancer cells using transcriptomic data.

Prolonged exposure to 0.5% O_2 had a great impact on gene expression in breast cancer cells. By comparing cells in chronic hypoxia with those in normoxia, a number of differentially expressed genes were identified; this indicates that substantial changes are induced at the transcriptomic level in hypoxic breast cancer cells. The gene expression profile in hypoxic breast cancer cells and the hypoxia-mediated transcriptional changes were studied. Genes that were consistently deregulated in three breast cancer cell lines (MCF7, MDA-MB-231 and HBL100) following 10 week incubation at 0.5% O_2 were established. Enrichment test and functional annotation GO analysis were performed to identify the gene functional categories among the differentially expressed genes and explore the key biological processes affected in chronic hypoxia. Transcriptional changes induced by long term adaptation in hypoxia are summarised in Figures 6.59 and 6.61. The Revigo server implementing a simple clustering procedure enabled the representation of clusters of semantically similar GO terms [471].

Functional analysis of the data revealed that genes commonly upregulated in chronic hypoxia in three breast cancer cell lines were associated with the glycolytic process and response to hypoxia (Figures 6.61&6.62). This finding provides evidence that the glycolytic pathway was strongly upregulated in hypoxic breast cancer cells despite the inherent differences among the cell lines. Similar data were generated in a recent study conducted by Sanzey *et al* in glioblastoma cells [493]. However, long term incubation at 0.5% O_2 led to the downregulation of transcripts involved in multiple pathways regulating primarily the mitotic cell cycle and nuclear division (Figures 6.59&6.60). This result is in agreement with the classic study by Hochachka *et al* where the authors argued that primary mechanisms contributing to cellular hypoxia tolerance include suppression of biosynthetic pathways (and subsequently mitosis) in order to diminish energy demand [494].

Further analysis was carried out to investigate hypoxia driven transcriptional changes on the glycolytic pathway. The log2 fold change expression values of the glycolytic genes calculated between chronic hypoxic and normoxic conditions in four breast cancer cell lines (MCF7, MCF7-HER2, MDA-MB-231 and HBL100) were used for hierarchical clustering. The generated heatmap shows that the genes involved in the glycolytic pathway were collectively upregulated under hypoxia (Figure 6.63). These results demonstrate that glycolysis is a major pathway mediating the response of breast cancer cells to oxygen deprivation. GLUT3 and ENO2 (enolase 2) formed a separate branch and were strongly induced by hypoxia. PGK1 (phosphoglycerate kinase 1), GPI (glucose-6-phosphate isomerase), GLUT1, PGM1 (phosphoglucomutase 1), HKII, ALDOC (aldolase, fructose-

bisphosphate C) and PFKFB3 were clustered together and demonstrated significant upregulation. The remaining glycolytic genes (including LDHA and PDHK1) were also upregulated however they were characterised by lower log2 gene expression fold changes.

The transcription factor HIF-1 orchestrates the cellular response to low oxygen availability. In hypoxia HIF-1 binds to hypoxia-response elements of hypoxia-sensitive genes and induces their transcriptional activation as an adaptive response to the hostile low oxygen tumour microenvironment. The HIF-1 responsive transcriptome is predominantly involved in angiogenesis, erythropoiesis and glucose metabolism [150, 153, 470]. Therefore increased mRNA expression of glycolytic genes in hypoxia stems primarily from stabilisation of HIF-1α. Virtually all the genes implicated in the glycolytic pathway are considered HIF-1 inducible [118, 473]. In their key study Iyer *et al* documented that HIF-1 activates the transcription of genes implicated in the glycolytic pathway. The authors demonstrated that HIF-1α was essential for their expression in embryonic stem cells and characterised the pathway as ‘‘a remarkable example of coordinate transcriptional regulation’’ [495]. Functional hypoxia-response elements in the promoters of several glycolytic genes have been characterised [470, 496, 497].

However, according to the Warburg effect many tumours preferentially rely on the glycolytic pathway irrespective of oxygen availability [87]. Analysis of NIH gene expression libraries show that at least 70% of human cancer cases worldwide exhibit inherent upregulation of glycolytic enzymes [498].

Gene expression changes occurring upon hypoxia were finally assessed in glycolytic enzymes of particular interest to this study. Comparison of hypoxia responses at the level of transcription between chronic and acute hypoxic cells as well as following treatment with $CoCl_2$ was carried out. Three of the breast cancer cell lines that have been included in the growth inhibition studies were used in this analysis (MCF7, MDA-MB-231 and HBL100).

$CoCl_2$ is a hypoxia mimetic agent that chemically induces HIF-1. Transition metals like cobalt mimic the effect of oxygen deprivation and stabilise HIF-1α. It has been evidenced that $CoCl_2$ inhibits prolyl hydroxylases (through iron substitution) that hydroxylate HIF-1α provoking its degradation and leads to the accumulation of active transcription factor complexes within the cell nucleus [154, 499]. However it has also been suggested that $CoCl_2$ inhibits the interaction between hydroxylated HIF-1α and pVHL and prevents its ubiquitination and degradation [500]. $CoCl_2$ treatment was used in this study to mirror the effects of HIF-1 activation and artificially induce the cellular responses mediated by HIF-1

in normoxia. Therefore it was possible to develop an understanding of the contribution of HIF-1 to the induction of the glycolytic enzymes in hypoxia. (Oxygen regulation of HIF-1α is discussed in Chapter 1 section 1.3.1)

The present study confirms previous findings and contributes additional evidence to a growing body of literature investigating the impact of oxygen concentration on the expression of glycolytic enzymes in breast cancer. The GLUT isoforms prevalent in breast cancer cells under low oxygen availability were GLUT1 and GLUT3. Both transporters demonstrated a marked induction in chronic hypoxic conditions in the examined cell lines (Figure 6.63). These isoforms have high affinity for glucose to ensure high glycolytic flux [501]. In a previous study Takagi *et al* reported GLUT1 mRNA in cultured bovine retinal endothelial cells increased ninefold after 12h at 0.5% O_2 [502]. Sorensen *et al* demonstrated a prompt induction (evident as early as 1h) of GLUT1 and LDHA expression in anoxia using cervix squamous cell carcinoma cells. Upregulation reached twelvefold after 6h and fivefold after 3h for the two genes respectively while maximal response was reported at 0.01% O_2 [503]. Minchenko *et al* documented HIF-1 mediated significant upregulation of PFKFB3 in several cancer cell lines. Furthermore in line with the observation of the present study that treatment with $CoCl_2$ failed to induce PFKFB3 mRNA expression in HBL100 cells (Figure 6.72), the authors reported a similar finding for HeLa cells [504]. PDHK1 has also been verified as a HIF-1 target and at least a fourfold mRNA upregulation has been demonstrated in hypoxic P493-6 Burkitt's lymphoma cells [161].

The most important finding of this analysis was that the glycolytic targets of interest were significantly induced in hypoxic conditions in all three breast cancer cell lines examined. Response between acute and chronic hypoxic conditions was primarily comparable suggesting that the glycolytic pathway is rapidly upregulated upon exposure to 0.5% O_2 and remains consistently activated following long term incubation. This is contrary to the acknowledged regulation of HIF-1α as the levels of this subunit get promptly induced upon exposure in a low oxygen environment but in chronic hypoxia, accumulation decreases [146, 505]. This has been described as a protective mechanism against necrosis mediated by activation of prolyl hydroxylases that cause HIF-1α degradation [505]. Another major difference is that HIF-1α expression is regulated by oxygen availability mainly at the post-translational level through inhibition of protein degradation whereas mRNA transcription is ubiquitous and constant [470]. Upregulation of the glycolytic enzymes is consistent with the hypothesis that increased expression of the glycolytic targets may lead to enhanced resistance to the respective glycolytic inhibitors suggested in section 6.2. Furthermore

treatment with the hypoxia mimetic agent corroborated that the upregulation of the glycolytic genes is mainly attributable to the activation of HIF-1 as $CoCl_2$ induced comparable effects to actual hypoxia.

Expression of the glycolytic enzymes was consistently a level of magnitude higher in MDA-MB-231 compared to MCF7 cells in normoxia. This corroborates previous findings from Gaglio *et al* that MDA-MB-231 cells, harbouring an oncogenic K-Ras, exhibit enhanced glycolytic activity and upregulation of several glycolytic enzymes [423]. Furthermore this finding further supports the view of a prevalent glycolytic phenotype in triple negative tumours [424, 506].

The protein levels of these targets have previously been assessed in MCF7 and MDA-MB-231 breast cancer cells under varying oxygenation levels through Western blotting (section 6.2). One of the examined conditions was incubation at 0.5% O_2 for 24h. This matches exactly the acute hypoxic conditions of this experiment. Therefore a direct comparison between mRNA and protein levels was enabled. HKII, PFKFB3 and PDHK1 upregulation was mirrored at both the mRNA and protein levels in both cell lines (Figures 6.39, 6.40&6.67,6.68 for HKII, Figures 6.43, 6.44&6.70, 6.71 for PFKFB3, Figures 6.47, 6.48&6.73, 6.74 for PDHK1). Although PFKFB3 mRNA expression in MCF7 cells was significantly induced at the $P<0.0001$ level while the effect of oxygen deprivation on the protein level was only marginal. Furthermore an apparent disconnect between mRNA and protein levels was observed for LDHA expression in MDA-MB-231 cells (Figures 6.52&6.77). Significant upregulation was demonstrated at the mRNA level whereas no effect was detected in protein expression. A similar disparity was also noticed as regards GLUT1 expression as this study failed to identify hypoxia mediated protein induction of this enzyme in either cell line (Figures 6.35&6.36).

The correlation between mRNA and protein expression levels is not always straightforward. Increased gene transcription does not always predict increased levels or enhanced activity of the protein product [507]. Nonetheless induction of glycolytic enzymes in low oxygen conditions at both the mRNA and protein levels as a result of HIF-1 activation has been substantiated [153].

In a very recent study Smith *et al* investigated the metabolic profile of colon cancer 3-D spheroid models cultured in severe hypoxia. Significant induction of the glycolytic flux was demonstrated following short term 16h exposure to 0.1% O_2 by a radioactivity assay. The increase in the glycolytic flux rate was associated with overexpression of GLUTs (GLUT1

and GLUT3) and enhanced enzymatic activity of PFK1. Nevertheless increased mRNA expression of key glycolytic enzymes, including HKII, PK and LDHA, was not reflected in protein expression and metabolic capacity in line with observations of the present study. The authors attributed reduced enzymatic levels to impaired protein synthesis in these conditions. Furthermore it was argued that their reduced expression serves the purpose to divert metabolic intermediates from biosynthetic pathways and diminish anabolic growth [508].

This study validates glycolysis as a major pathway mediating the response of breast cancer cells to an oxygen depleted environment. The present study enhances our understanding of the role of the glycolytic induction in hypoxic breast cancer.

Chapter 7

Chapter 7: Evaluation of glycolytic targets in ovarian tumours

7.1 Expression of selected glycolytic enzymes in ovarian tumours

To date much uncertainty still exists about the metabolism of ovarian tumours. Therefore the role of glycolysis in ovarian cancer was thoroughly investigated in this study by examining the level of protein expression of selected glycolytic enzymes in a series of clinical ovarian cancer samples. Expression of four glycolytic targets was assessed with *in situ* staining in 469 ovarian tumours using Automated Quantitative Analysis (AQUA). The objective of this experiment was to quantitatively evaluate the expression of glycolytic enzymes and associate expression with several clinicopathological parameters, as well as with survival outcome. Thus, the aim was to enhance our understanding of the role of the glycolytic pathway in ovarian carcinogenesis and reveal subtypes of tumours that might benefit from targeted inhibition of the glycolytic enzymes.

Tissue Microarrays (TMAs), constructed of formalin fixed, paraffin embedded samples of each of 469 ovarian tumours in triplicate, were obtained from the Division of Pathology Laboratories, Western General Hospital, University of Edinburgh. Details of patient characteristics of this cohort (summarised in the Appendix Table A3) and the procedure of TMA construction have been previously published [509, 510]. They are all primary ovarian tumours obtained from patients treated in the Edinburgh Cancer Centre the period between 1991 and 2006. Samples were collected prior to treatment. Antibodies targeting glycolytic markers of interest -GLUT1, HKII, PKM2 and LDHA- were optimised and a standard three label immunofluorescent protocol as described in Chapter 2 section 2.9 was followed. DAPI counterstain was used to identify the nuclei, pan-cytokeratin to visualise the epithelium and Cy-5 tyramide for target detection. AQUA analysis was employed as an automated scoring method to access the target's expression generating a quantitative score for each histospot. High resolution monochromatic images of each TMA core were obtained and analysed by the AQUA software. The Cy-5 fluorescent signal intensity of the target antigen was quantified in each image pixel. A score was attributed in each core based on the average Cy-5 signal within the epithelial tumour mask, as this was identified from the cytokeratin stain. For the four targets of interest, expression in the cytoplasmic compartment was assessed. Damaged cores or cores containing imaging errors as well as those consisting of less than 5% epithelium were excluded from further analysis. After filtering the data only the samples that had at least two replicate values were used. Average expression values from either two or three replicate cores were calculated.

Representative immunofluorescence images showing the expression of four glycolytic targets in TMA cores of ovarian cancers obtained from the AQUA image analysis software are presented below. Figure 7.1 presents representative examples of GLUT1 fluorescent staining. GLUT1 showed membranous as well as cytoplasmic localisation. In Figures 7.2, 7.3 and 7.4 images of HKII, PKM2 and LDHA expression are presented respectively. These three targets demonstrated mainly cytoplasmic localisation.

GLUT1

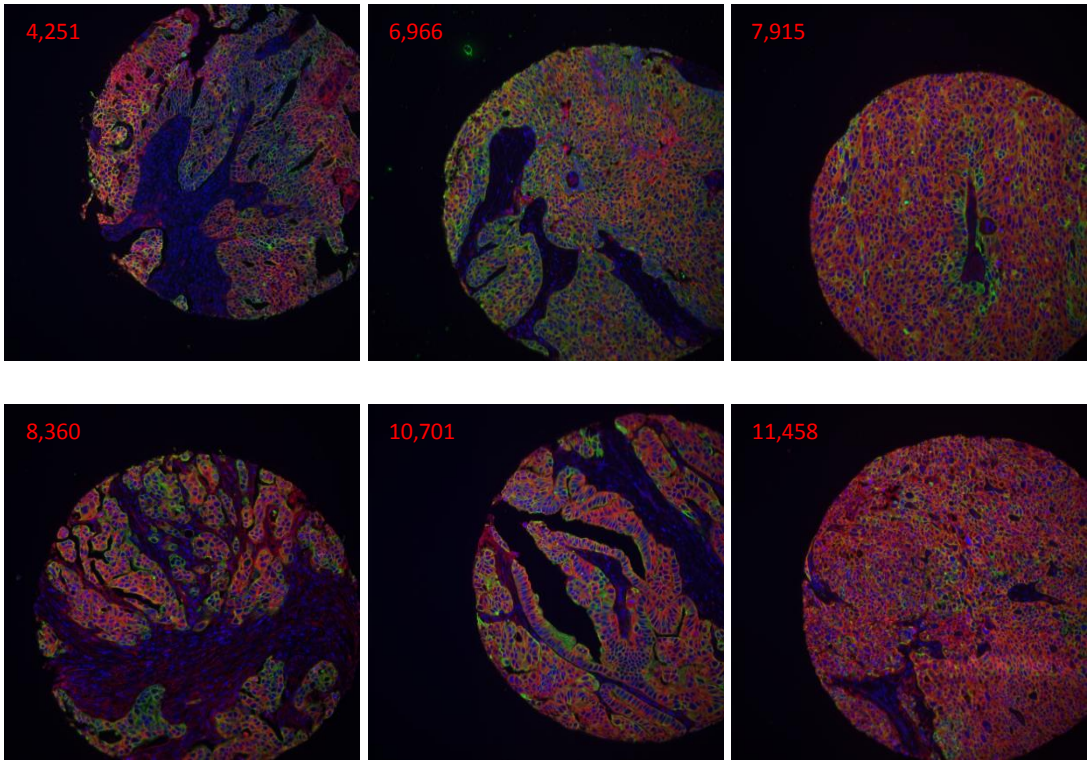

Figure 7.1: Representative immunofluorescence images showing GLUT1 expression in TMA cores of ovarian cancers. Blue colour visualises DAPI nuclear counterstain, green colour cytokeratin tumour mask and red colour GLUT1 staining. Quantified GLUT1 expression in the cytoplasmic compartment of each core is indicated.

HKII

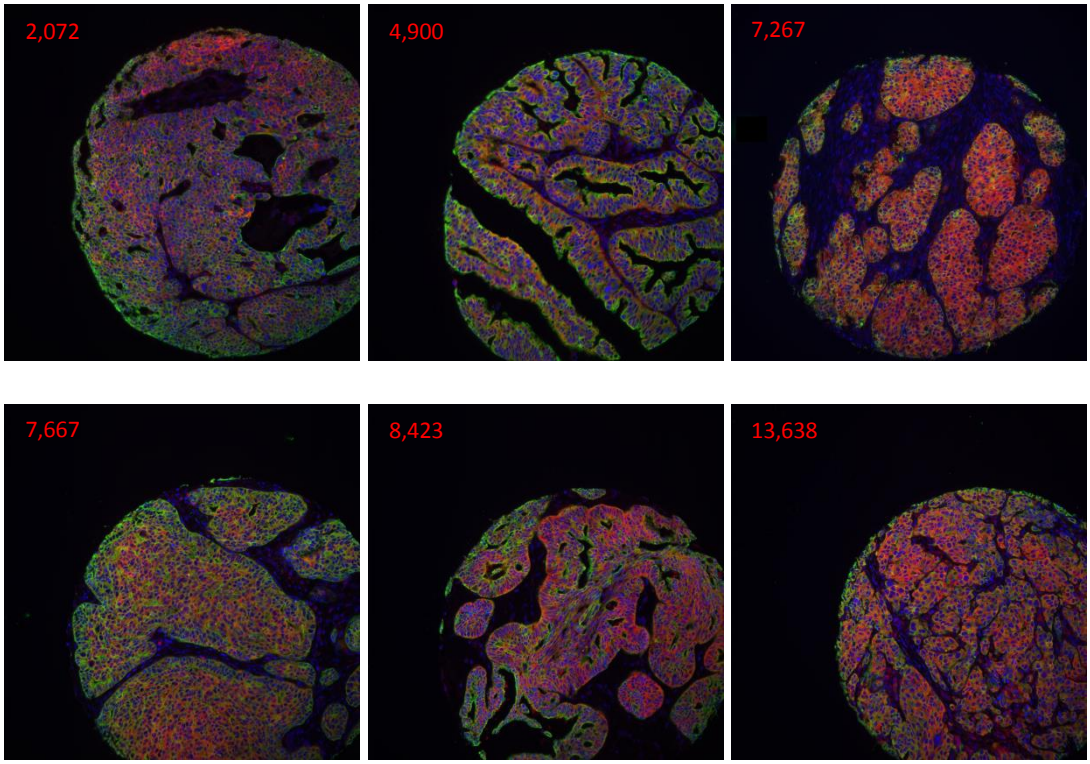

Figure 7.2: Representative immunofluorescence images showing HKII expression in TMA cores of ovarian cancers. Blue colour visualises DAPI nuclear counterstain, green colour cytokeratin tumour mask and red colour HKII staining. Quantified HKII expression in the cytoplasmic compartment of each core is indicated.

PKM2

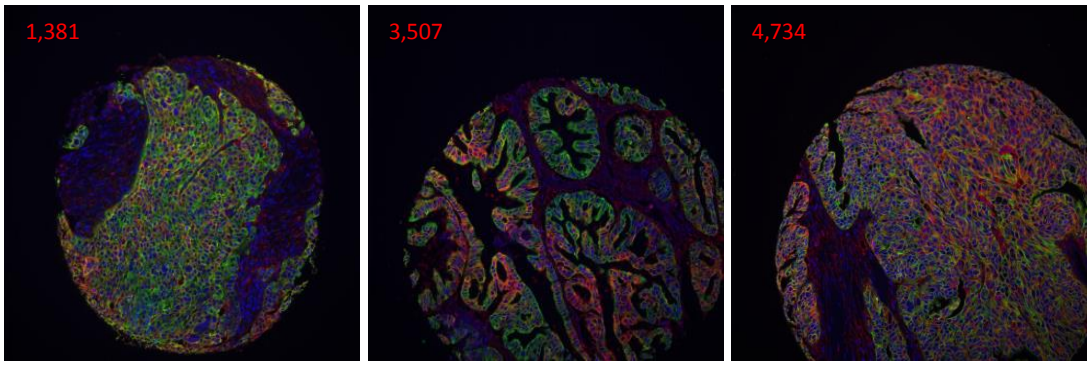

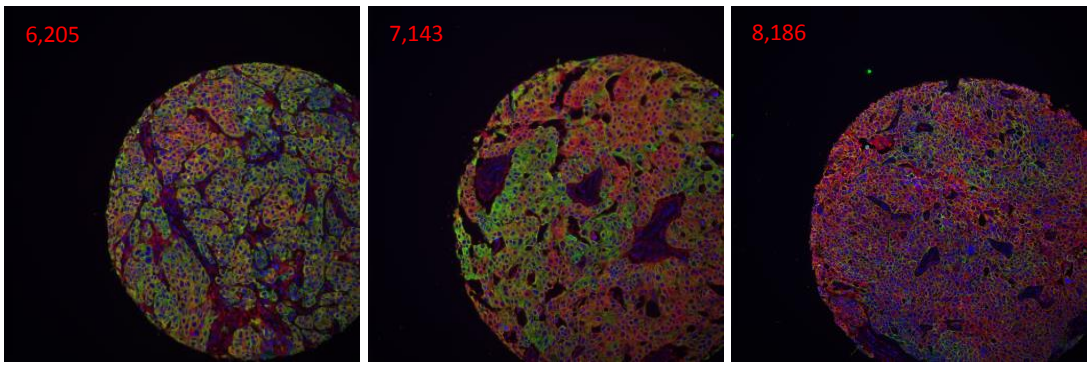

Figure 7.3: Representative immunofluorescence images showing PKM2 expression in TMA cores of ovarian cancers. Blue colour visualises DAPI nuclear counterstain, green colour cytokeratin tumour mask and red colour PKM2 staining. Quantified PKM2 expression in the cytoplasmic compartment of each core is indicated.

LDHA

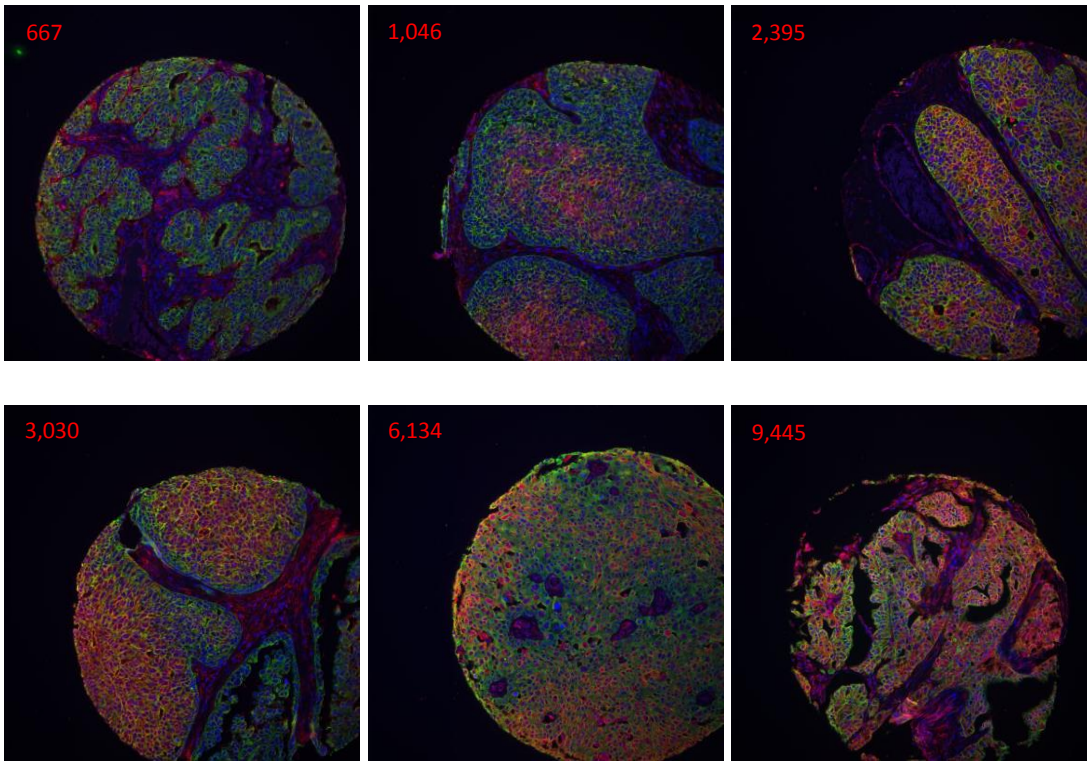

Figure 7.4: Representative immunofluorescence images showing LDHA expression in TMA cores of ovarian cancers. Blue colour visualises DAPI nuclear counterstain, green colour cytokeratin tumour mask and red colour LDHA staining. Quantified LDHA expression in the cytoplasmic compartment of each core is indicated.

In Figure 7.5 the expression of the four glycolytic targets is compared in one individual ovarian cancer case. Immunofluorescence images showing expression of the four glycolytic enzymes in TMA cores of a particular patient are presented. High expression of all four markers consistent with a glycolytic phenotype can be observed.

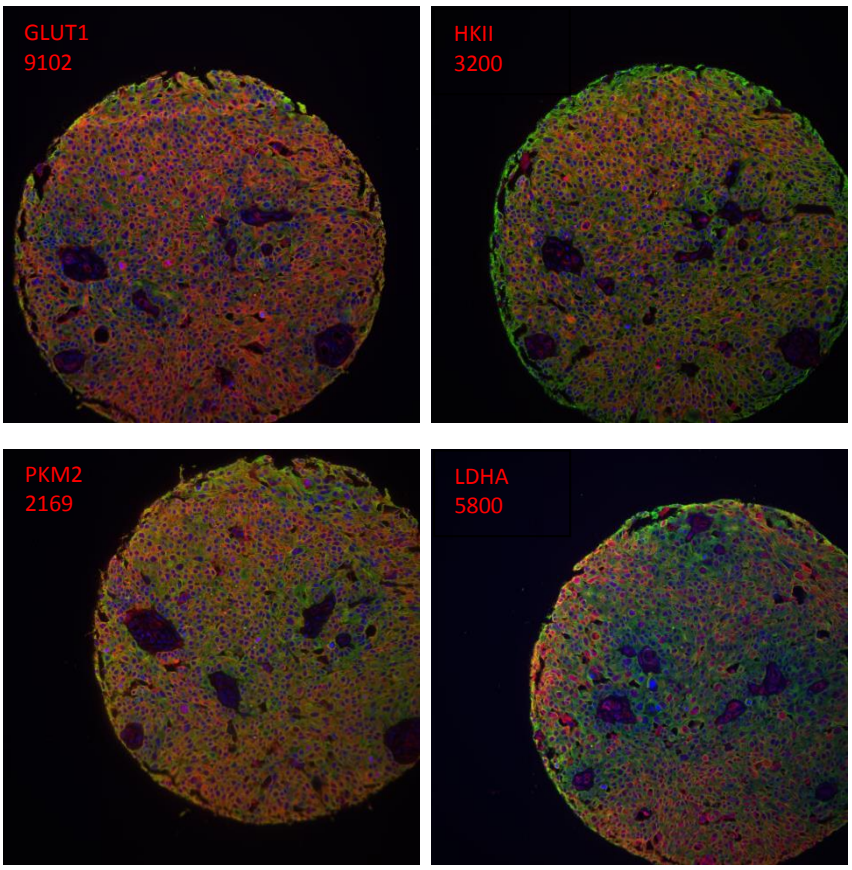

Figure 7.5: Immunofluorescence images showing expression of four glycolytic enzymes in TMA cores of an individual ovarian cancer patient. Blue colour visualises DAPI nuclear counterstain, green colour cytokeratin tumour mask and red colour staining of the target protein. Quantified target expression in the cytoplasmic compartment of each core is indicated.

The initial question addressed by this experiment was whether differential expression of glycolytic enzymes in ovarian tumours could be associated with discrete clinicopathological characteristics. The expression of each of the glycolytic markers was therefore compared across the different pathological stages and histological subtypes of ovarian tumours.

7.2 Association of the expression of glycolytic enzymes with ovarian cancer progression

The relationship between the level of expression of the four glycolytic enzymes and the pathological stage of ovarian cancer was examined and is presented below. Table 7.1 shows the number of patients of each stage that were included in the analysis for each of the markers.

Interestingly lower LDHA expression was associated with increasing tumour stage. LDHA expression was significantly higher in stage I tumours compared to stage III and IV (Figure 7.9). In contrast no statistically significant change in the expression of GLUT1, HKII and PKM2 across the different tumour stages was observed. (Figures 7.6 to 7.8).

Tumour stage	GLUT1	HKII	PKM2	LDHA
I	28	36	33	29
II	39	42	37	30
III	183	211	202	157
IV	54	63	58	48
Unknown	10	14	10	8
TOTAL	314	366	340	272

Table 7.1: Number of ovarian cancer patients of different tumour stages that gave adequate AQUA data for each of the four glycolytic markers.

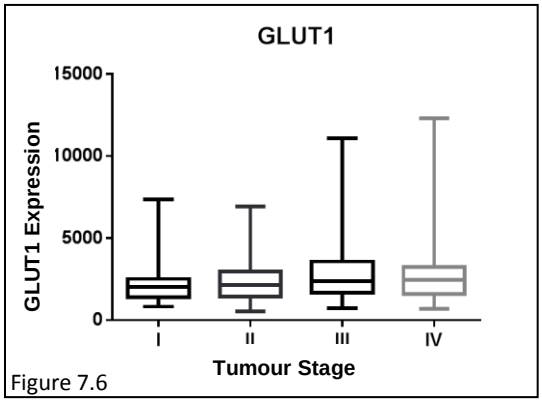

Figure 7.6

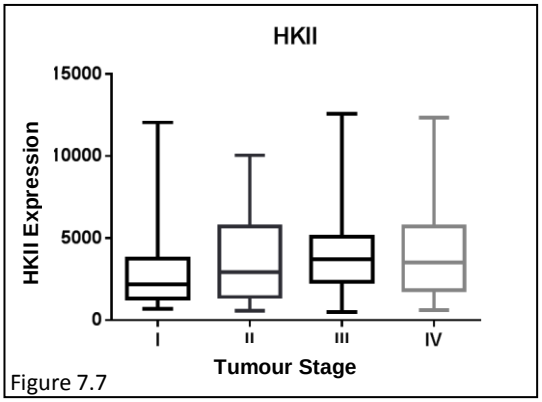

Figure 7.7

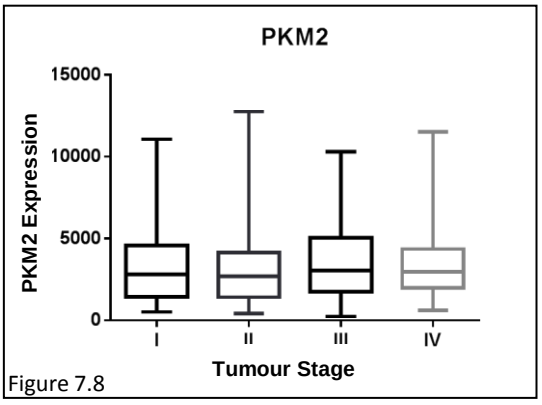

Figure 7.8

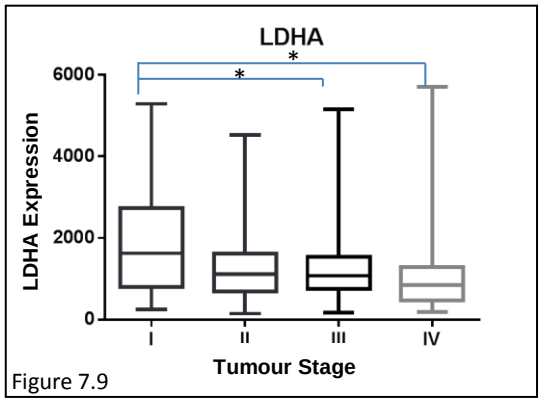

Figure 7.9

Figures 7.6 to 7.9: Expression of four glycolytic enzymes correlated with different stages of ovarian cancer. Statistical significance indication: * P<0.05 (one-way ANOVA followed by Tukey's multiple comparisons test).

7.3 Association of the expression of glycolytic enzymes with ovarian cancer histological subtype

The expression of the four glycolytic enzymes was compared across the different histological types of ovarian tumours. Table 7.2 shows the number of patients of each subtype that were included in the analysis for each of the markers.

GLUT1 appeared to be similarly expressed in all different histotypes (Figure 7.10). The analysis revealed that LDHA expression was heterogeneous between histological subtypes; significantly increased expression was demonstrated in clear cell tumours (Figure 7.13). The same trend was also observed for PKM2, but was not significant (Figure 7.12). In contrast clear cell carcinomas were significantly associated with lower HKII expression (Figure 7.11).

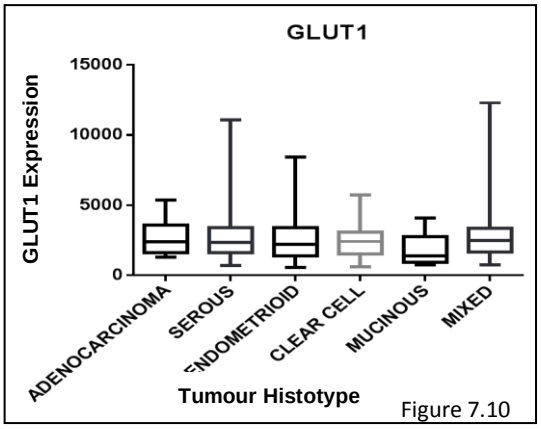

Figure 7.10

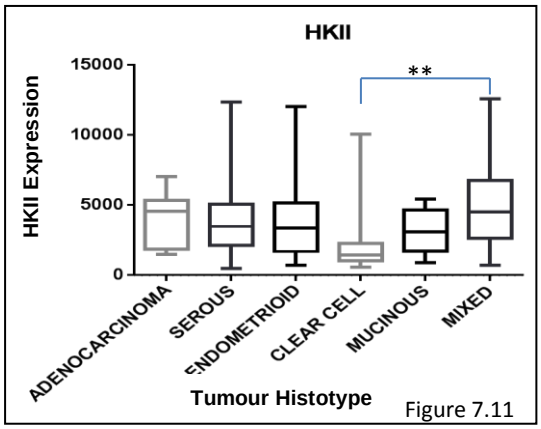

Figure 7.11

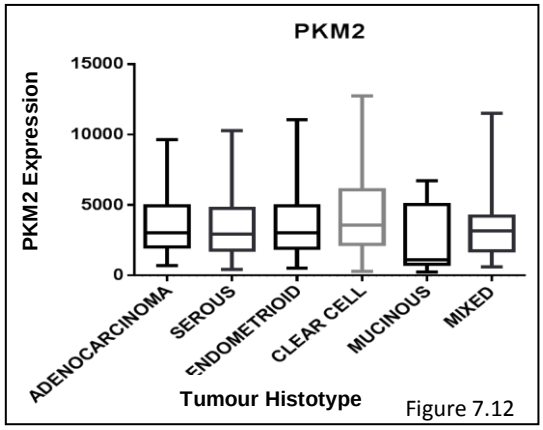

Figure 7.12

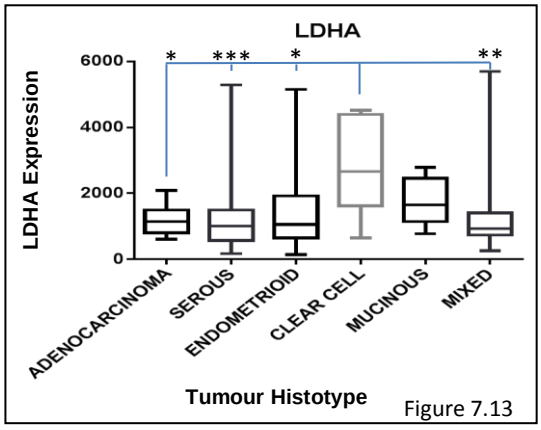

Figure 7.13

Figures 7.10 to 7.13: Expression of four glycolytic enzymes correlated with different histological subtypes of ovarian cancer. Statistical significance indications: * P<0.05, ** P<0.01, *** P<0.001 (one-way ANOVA followed by Tukey's multiple comparisons test).

Tumour Histotype	GLUT1	HKII	PKM2	LDHA
Adenocarcinoma	11	11	11	8
Serous	168	200	182	143
Endometrioid	63	74	71	61
Clear cell	16	20	18	11
Mucinous	8	10	10	8
Mixed	48	51	48	41
TOTAL	314	366	340	272

Table 7.2: Number of ovarian cancer patients of different histotypes that gave adequate AQUA data for each of the four glycolytic markers.

7.4 Correlation of the expression of glycolytic enzymes with other markers

The expression of the four glycolytic enzymes was then correlated with expression of several other molecular markers. These data were already available for the same cohort from previous independent projects that had used the same TMAs in the past [509]. Spearman nonparametric correlation was performed and the following correlation heatmaps were generated using TMA Navigator. Positive rho correlation values are displayed in bright yellow colours while negative rho values are displayed in dark blue colours. For this analysis all data had been log transformed, mean-centred and quantile-normalised to compensate for differences in the staining of different markers.

Figure 7.14 presents a heatmap correlating the expression of the four examined glycolytic enzymes. The expression of the four targets across the ovarian cancers gave positive rho correlation values when compared to each other. Based on the dendrogram, it can be concluded that LDHA expression appeared more closely correlated to PKM2 expression; while in contrast HKII expression was more distant to the expression of the other three markers.

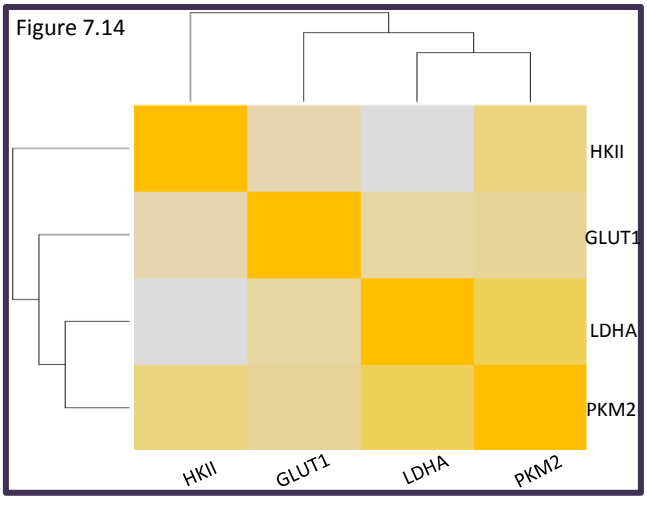

Figure 7.14: Heatmap correlating the expression of four glycolytic enzymes in a cohort of 469 ovarian cancers. Positive Spearman rho correlation values are displayed in bright yellow colours while negative Spearman rho correlation values in dark blue colours. The heatmap was generated through TMA Navigator.

Spearman correlation network analysis was conducted to further interpret the relationship between the glycolytic markers and evaluate their significance. The Spearman correlation coefficient was calculated for each pair of markers and statistical significance was determined using the Algorithm AS89 [511]. Spearman's correlation P-values were adjusted for multiple hypothesis testing according to Benjamini-Yekutieli FDR correction. The P-value significance threshold was set at 0.01. The Spearman correlation network of the expression of four glycolytic enzymes is presented in Figure 7.15. Significant relationships (FDR P <0.01) are drawn as lines that connect pairs of markers. Thickness of connection lines reflects significance. Positive significant relationships are displayed in grey colour. The colour of each marker indicates the number of significant connections. High number of significant connections is displayed in yellow colour while low in blue. Significant correlations (FDR P <0.01) are summarised in Table 7.3.

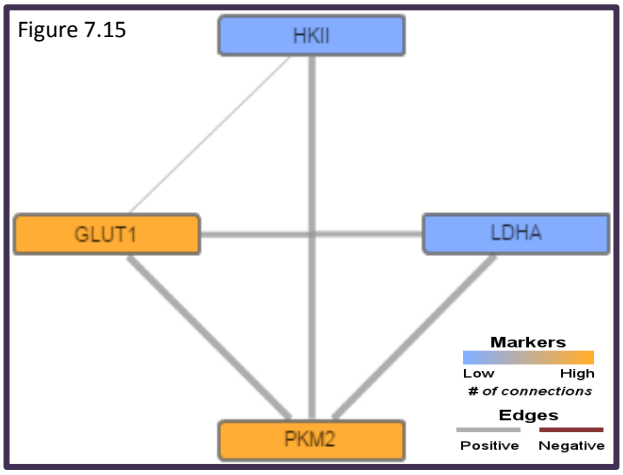

Figure 7.15: Spearman correlation network of the expression of four glycolytic enzymes in a cohort of 469 ovarian cancers. Statistically significant correlations thresholded at FDR P value <0.01 are presented. High number of significant connections is displayed in bright yellow colours while low in dark blue colours. Positive relationships are indicated in grey while negative in red. Thickness of connection lines reflects significance (the adjusted P value). The network was generated through TMA Navigator.

Nonparametric Correlation	GLUT1	HKII	PKM2	LDHA
GLUT1	*	0.20 0.0071	0.27 0.00024	0.23 0.0016
HKII	0.20 0.0071	*	0.34 0.0000018	-
PKM2	0.27 0.00024	0.34 0.0000018	*	0.46 $5.02e^{-12}$
LDHA	0.23 0.0016	-	0.46 $5.02e^{-12}$	*

Table 7.3: Spearman correlation of the expression of four glycolytic enzymes in a cohort of 469 ovarian cancers. Spearman rho correlation values (top value) along with the respective adjusted P value (bottom value) of statistically significant correlations thresholded at FDR P value <0.01 are summarised.

A large dataset detailing the expression of important oncogenic markers in the same ovarian cancer patient cohort was available and already published elsewhere [509]. The heatmap in Figure 7.15 shows the correlation of the expression of the four glycolytic enzymes with the expression of proliferation (Ki67, histone H3), apoptosis (caspase 3), cell cycle (RB), DNA damage response (H2AX, BRCA1, p53) and various signalling markers (ER, ERK, STAT3, AKT, NFκB). The four glycolytic markers appeared clustered together giving positive rho correlation values when compared to each other. GLUT1 expression was more closely correlated to HKII expression while PKM2 to LDHA. Regarding the relationship with the expression of the other non-glycolytic markers the most distinct positive correlations were observed with AKT, BRCA1 and ERβ2 while the most apparent negative correlations were with the expression of caspase 3, Snail and ERβ1.

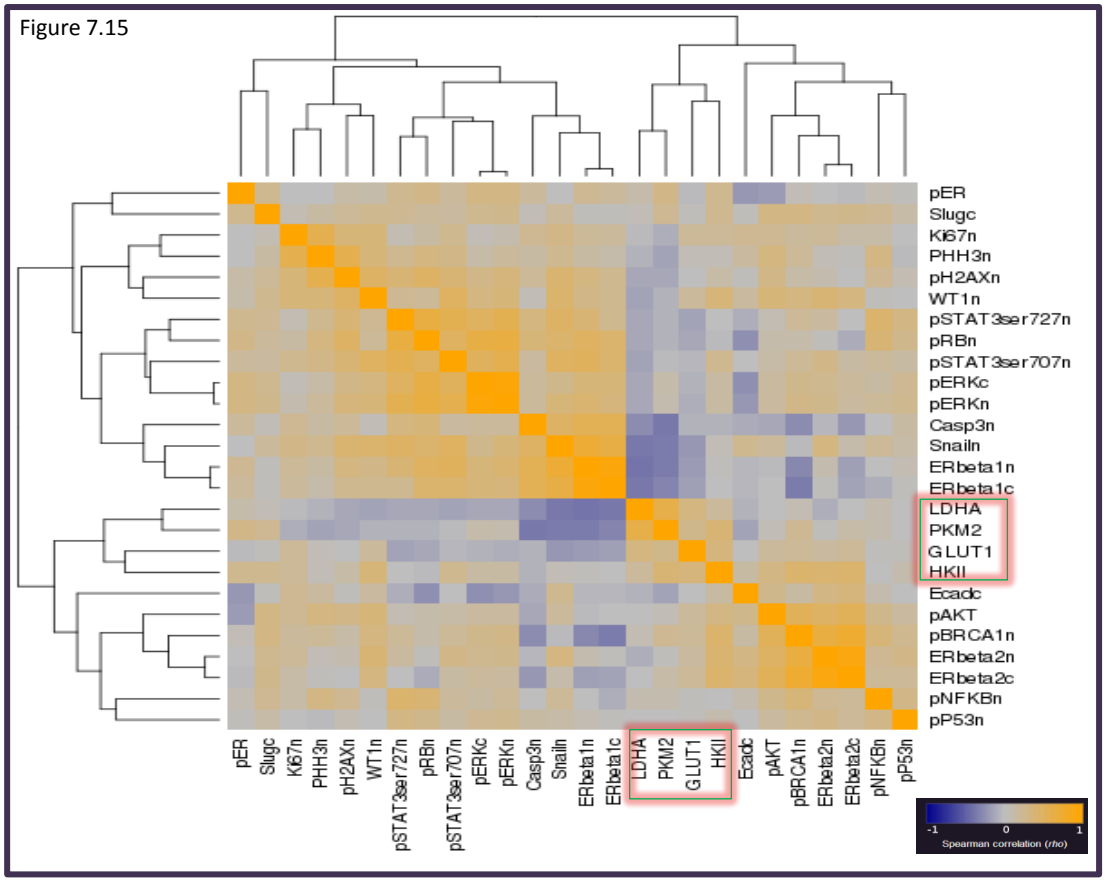

Figure 7.15: Heatmap correlating the expression of four glycolytic enzymes with the expression of various proliferation, apoptosis and signalling markers previously examined in the same cohort of 469 ovarian cancers. Data of the expression of the oncogenic markers were obtained from Faratian *et al* [509]. Positive Spearman rho correlation values are displayed in bright yellow colours while negative Spearman rho correlation values in dark blue colours. The heatmap was generated through TMA Navigator. (n and c indicate nuclear and cytoplasmic expression).

The relationship with this set of markers was further interpreted and their significance was evaluated. Spearman's correlation P-values were adjusted for multiple hypothesis testing by Benjamini-Yekutieli FDR correction. The P-value significance threshold was set at 0.01. The significant correlations (FDR P <0.01) detected for each of the glycolytic markers are summarised in Table 7.4. The previously described correlations among them were not included in this table.

Nonparametric Correlation	**Molecular markers**	**Spearman rho**	**adjusted P value**
GLUT1	-	-	-
HKII	BRCA1	0.44	$3.4e^{-7}$
	ERβ2 c	0.44	$3.6e^{-7}$
	ERβ2 n	0.42	0.0000012
	WNT1	0.37	0.000040
	pAKT	0.33	0.00049
PKM2	Caspase 3	-0.35	0.00021
	Snail	-0.34	0.00030
	ERβ1 n	-0.33	0.00042
LDHA	ERβ1 n	-0.38	0.000023
	Snail	-0.35	0.00013
	ERβ1 c	-0.35	0.00013

Table 7.4: Spearman correlation of the expression of four glycolytic enzymes with the expression of various proliferation, apoptosis and signalling markers previously examined in the same cohort of 469 ovarian cancers. Spearman rho correlation values along with the respective adjusted P value of statistically significant correlations thresholded at FDR P value <0.01 are summarised. (n and c indicate nuclear and cytoplasmic expression).

7.5 Association of the expression of glycolytic enzymes with clinical outcome

The expression of the four glycolytic targets was assessed for association between the behaviour of tumours and the survival outcome of the ovarian cancer patients. Overall survival data calculated from the day of initial surgical diagnosis until the date of death by ovarian cancer were used. Patients who discontinued medical supervision or died from a different cause were censored. No association was found between the expression of the markers and the clinical outcome of the total patient cohort. Therefore, whether the expression of the targets in separate histopathological subtypes could be associated with the survival outcome was examined.

The following figures present the survival analysis of endometrioid ovarian cancer patients. Optimised cut-off values, dividing the target expression into either low, moderate or high; were generated in X-Tile and enabled the association to be made between protein expression and the clinical outcome. Miller–Siegmund P-value correction was applied. Based on these cut-off points Kaplan-Meier survival curves were created. Figures 7.19 and 7.18 show that low LDHA and low PKM2 expression were correlated with improved survival of endometrioid ovarian cancer patients. The corresponding P values determined through the Log-Rank survival analysis test were 0.0038 and 0.0006 respectively. The same trend was also observed for GLUT1 but it was not statistically significant.

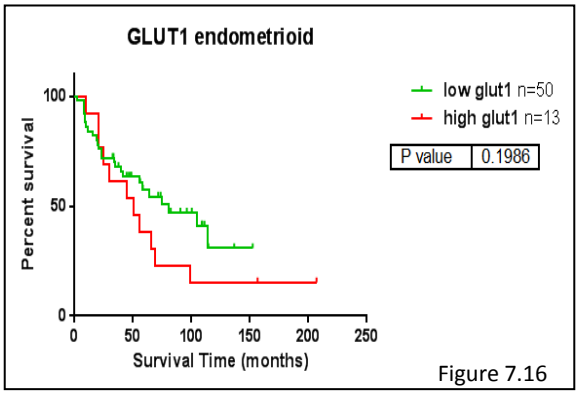

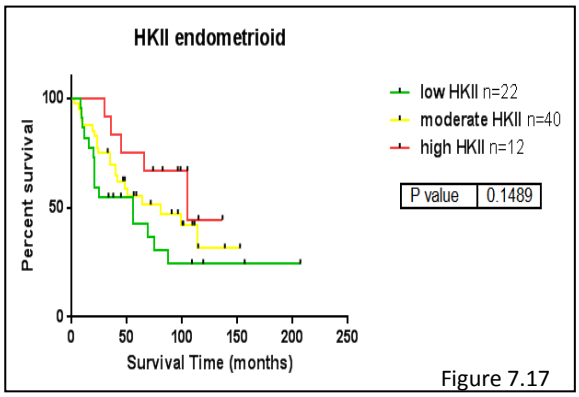

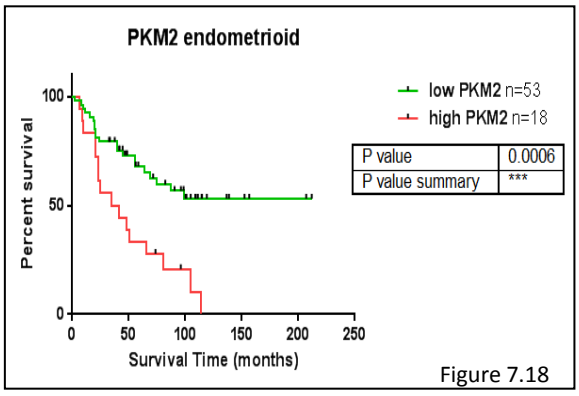

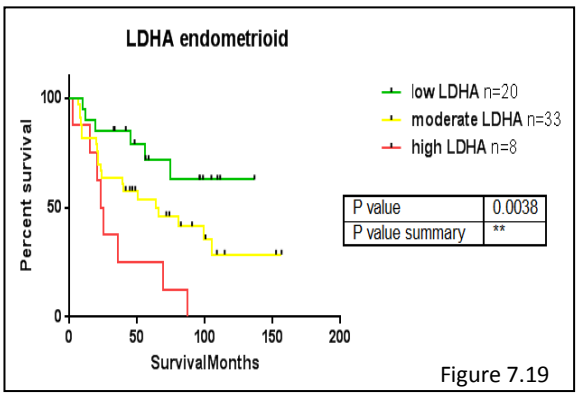

Figures 7.16 to 7.19: Kaplan-Meier survival curves showing relationship between the expression of four glycolytic enzymes and overall survival of endometrioid ovarian cancer patients. Statistical significance was determined using the Log-Rank survival analysis test and optimised cut-off values were generated in X-Tile.

7.6 Discussion

Little attention to date has been paid on the glycolytic pathway in ovarian tumours as a target for new therapies. This chapter sought to identify the subtypes of ovarian tumours in which inhibition of glycolysis might be a beneficial strategy. The expression of four glycolytic enzymes was examined in clinical ovarian tumours with *in situ* immunofluorescent staining and quantitated automatically. Two upstream targets, GLUT1 and HKII, as well as two downstream targets, PKM2 and LDHA, were selected. No previous study has reported the expression of multiple glycolytic enzymes in ovarian tumours.

AQUA is a novel technology that enables accurate, efficient and reproducible assessment of biomarker expression in hundreds of tissue sections. Traditional widely used IHC techniques involve the subjective semi-quantitation interpretation of staining intensity characterised 'by eye' on a scoring system as weak, moderate or strong. In contrast AQUA provides an opportunity to automatically quantitate the protein expression of biomarkers in TMA cores. Mathematical algorithms generate a score of immunofluorescence intensity for each histospot. This is based on the average Cy-5 fluorescent signal intensity of the target antigen in a subcellular compartment of choice within the epithelial tumour mask, as this was defined by Cy-3 cytokeratin staining [512, 513]. For the targets of interest here the cytoplasmic compartment was selected.

The expression of the glycolytic enzymes varied considerably across the ovarian tumours. Representative immunofluorescence images exhibiting a wide range of quantitated expression of each of the targets are presented in Figures 7.1 to 7.4. An example demonstrating variable expression of each of the enzymes in the same cancer is shown in Figure 7.5. Prior to further analysis data were filtered and expression values from either two or three replicate cores were averaged. However, lost TMA cores and absence of at least two replicate values resulted in some missing data.

The initial step of the analysis of this dataset was to associate the expression of the glycolytic enzymes with tumour progression and the histopathological subtype. The relationship between these discrete variables and target expression was investigated by comparing the mean expression level in each subgroup by one-way ANOVA. Statistical significance was determined by Tukey's multiple comparisons test.

Correlation of the level of expression of the four glycolytic enzymes with the pathological stage of the disease revealed interesting associations. Significantly higher LDHA expression was detected in stage I tumours compared to stage III and IV. Regarding the other three

targets, no statistically significant change in their expression across the different tumour stages was detected (Figures 7.6 to 7.9).

The expression of the glycolytic enzymes was also compared across the different ovarian cancer histological types. The analysis revealed that GLUT1 expression was comparable among the different histotypes. In contrast the other three markers were differentially expressed. Significantly higher LDHA expression was detected in clear cell carcinomas. Similarly higher PKM2 expression was also observed in clear cell tumours. However this histotype was significantly associated with lower HKII expression (Figures 7.10 to 7.13).

The existing literature has repeatedly reported a possible role for GLUT1 in ovarian carcinogenesis. Several studies have demonstrated gradually elevated GLUT1 expression from healthy ovarian epithelium to benign and borderline tumours to malignant ovarian adenocarcinomas and the transporter has been suggested as a potential marker of ovarian malignancy [189, 191, 192]. Increased GLUT1 expression in advanced stage ovarian tumours has also been reported [193]. In line with these findings a trend was also observed here but it did not reach significance. Moreover a number of studies have documented elevated GLUT1 expression in serous adenocarcinomas [189, 193-195]. In contrast to earlier findings however the present study indicated comparable GLUT1 expression among the different ovarian cancer histological types. The findings of this research seem to be consistent with data published by Rudlowski *et al* which found no significant association between GLUT1 expression and disease progression or histotype following IHC of 78 invasive ovarian tumour samples [192]. The mitochondrial-bound HKII is the predominant isoform expressed in many tumours [206]. A graduation in elevated HKII expression from benign and borderline tissues to malignant tumours has been noted in ovarian cancer [219]. Jin *et al* documented increased HKII expression in serous carcinomas compared to non-serous tumours while in contrast another study reported that HKII expression was correlated with neither the tumour stage nor the histotype [218, 219]. Decreased HKII expression in clear cell carcinomas as observed here has not previously been described. Elevated LDHA and PKM2 expression (although not significantly in the second case) in clear cell tumours is consistent with recent findings indicating that these cancers are highly dependent on the glycolytic pathway. The transcription factor HNF1β, frequently overexpressed in this histotype, suppresses oxidative phosphorylation and promotes glycolytic metabolism. The glycolytic phenotype of clear cell carcinomas has been described as a protective mechanism against oxidative stress and has been linked with chemoresistance [514]. Confirmation of increased expression of glycolytic enzymes in these tumours has not been reported before

and is of great importance as it may have therapeutic significance in future treatment of these highly resistant tumours. The observed discrepancy with the upstream glycolytic targets, GLUT1 and HKII, might be an indication that additional GLUT or HK isoforms might be involved. Nevertheless, a weakness of this analysis was the relatively small sample size of clear cell cancers (18 patients were included for PKM2 and 11 for LDHA – Table 7.2).

Further work is required to investigate the role of other GLUTs in ovarian carcinogenesis. Although a few studies have highlighted the importance of GLUT1 in ovarian cancer much less is known about the role of other GLUTs and contradictory findings have been generated. In their study Rudlowski *et al* reported weak GLUT3 expression in ovarian tumours while GLUT2 and GLUT4 were not detected [192]. In contrast Tsukioka *et al* demonstrated strong GLUT3 and GLUT4 expression when examining 154 ovarian tumour samples using IHC [193].

The expression of the four glycolytic enzymes across the ovarian cancers was correlated. Positive rho correlation values indicated a positive relationship consistent with activation of a single pathway. The expression of the two downstream enzymes PKM2 and LDHA appeared more closely related to each other while in contrast HKII expression was the least related to the expression of the other three markers (Figure 7.14).

A large dataset of the expression of several oncogenic markers in the same ovarian cancer patient cohort was available from preceding independent research projects [509]. The expression of the four glycolytic enzymes was compared with the expression of a series of oncogenic biomarkers including proliferation (Ki67, histone H3), apoptosis (caspase 3), cell cycle (RB), DNA damage response (H2AX, BRCA1, P53) and signalling markers (ER, ERK, STAT3, AKT, NFκB). In the heatmap correlating the expression of all these proteins, the most apparent observation was that the four glycolytic enzymes clustered together and were characterised by a relatively strong positive relationship as anticipated of enzymes belonging to the same pathway. Interestingly the upstream targets, GLUT1 and HKII, as well as the downstream ones, PKM2 and LDHA, appeared closely related to each other. From the dendrogram it can be observed that the four enzymes formed a separate branch quite distant from the other markers (Figure 7.15). Regarding the non-glycolytic markers a positive correlation between GLUT1 and ki-67 has been previously described and was further verified here. Semman *et al* correlated high GLUT1 expression with high ki-67 levels following IHC evaluation in 213 primary ovarian tumours correlating the glycolytic metabolism with the high proliferation index of ovarian tumours [194].

The most significant positive correlations revealed in the present study were among HKII and the DNA damage response related tumour suppressor gene BRCA1, the oestrogen receptor β splice variant 2 ERβ2, the regulator of the oncogenic Wnt signalling pathway WNT1 and the effector of the PI3K pathway AKT. A tight relationship between signalling cell survival and metabolic pathways has previously been described. AKT is known to stimulate glycolysis and has been shown to regulate HKII activity and mitochondrial association [515]. Interestingly it has been demonstrated that AKT directly phosphorylates HKII (in an Akt consensus sequence) enhancing the mitochondrial binding of the glycolytic target. The interaction between the two kinases has been associated with a protective anti-apoptotic survival mechanism [515, 516]. The tumour suppressor gene BRCA1 is known to downregulate AKT oncogenic activity [517]. This interaction has been linked with the effect of BRCA1 on cancer cell metabolism. A recent study reported that BRCA1 suppresses glycolysis and promotes mitochondrial oxidative phosphorylation in breast cancer cells. Contradicting the strong positive correlation between BRCA1 and HKII observed in this study the authors presented that the expression of key glycolytic enzymes (including HKII) was significantly downregulated in wild type BRCA1 breast tumours [518].

The most significant negative correlations detected were between PKM2 and LDHA and the apoptosis marker caspase 3, the transcriptional repressor Snail and the oestrogen receptor β splice variant 1 ERβ1 (Table 7.4). The observed negative association between the glycolytic enzymes PKM2 and LDHA and Snail contradicts the current state of knowledge. The epithelial–mesenchymal transition inducer and regulator of multiple signalling pathways has been shown to promote the glycolytic metabolism of tumours. In their key study Dong *et al* provided evidence that Snail directly represses fructose-1,6-bisphosphatase expression by promoter methylation in basal-like breast tumours (this enzyme catalyses the conversion of fructose-1,6-bisphosphate to fructose 6-phosphate in gluconeogenesis). Loss of fructose-1,6-bisphosphatase induced glycolytic metabolism, activated tetrameric PKM2 and suppressed mitochondrial respiration and ROS production. The Snail-mediated glycolytic reprogramming was suggested to enhance tumourigenesis and invasiveness in these tumours [519]. Along similar lines Tao *et al* documented that downregulation of Snail suppressed prostate cancer cell growth and glucose metabolism and lowered PKM2 as well as HIF-1α (major regulator of the expression of glycolytic enzymes in hypoxia) expression [520]. Negative association between PKM2 and caspase 3 expression is in line with recent findings by Stetak *et al*. In their study the authors documented that in response to apoptotic agents PKM2 translocates to the nucleus and induces caspase independent cell death [521]. On the contrary, Tang *et al* who identified PKM2 as an apoptosis regulator in a murine model of

Crohn's disease argued that upregulated PKM2 correlated with increased caspase 3 expression. The authors showed that high levels of PKM2 and active caspase 3 co-localised in intestinal epithelial cells [522]. Oestrogen and ERs are major cellular regulators and have been reported to regulate glucose homeostasis, enhance glucose uptake and promote glycolysis [523-525]. It has been demonstrated that estradiol stimulates glucose consumption and lactate production in MCF7 breast cancer cells while glycolysis was suppressed by tamoxifen [526]. Investigation of the estradiol effect on rat brain and mouse neuroblastoma cells revealed that hormonal treatment induced the activity of the glycolytic enzymes HK, PFK and PK [527]. Furthermore enolase β and PKM2 have been characterised as oestrogen regulated enzymes in a bone proteome study while glucose metabolism was found to be suppressed by oophorectomy [528]. Previous research is in agreement with the currently detected robust correlation between HKII and ERβ2 expression in the examined cohort of ovarian tumours but does not support the finding of a significantly negative association between ERβ1 and the glycolytic targets PKM2 and LDHA.

An interesting observation is that the upstream glycolytic targets demonstrated only positive significant associations while in contrast the downstream targets negative. This research has gone some way towards enhancing our knowledge of the interaction between the glycolytic metabolism and oncogenic signalling pathways in ovarian cancer. Several significant associations between the expression of glycolytic enzymes and key oncogenic molecular markers were revealed. However, further investigation is required for the interpretation and evaluation of their potential significance.

Finally the relationship between the expression of the enzymes and the clinical outcome of ovarian cancer patients was investigated. Levels of expression of the glycolytic enzymes did not associate with the survival outcome. GLUT1 has been proposed as a marker of adverse prognosis in ovarian cancer [195]. However this study has been unable to demonstrate an association between increased GLUT1 expression and poor survival outcome as has previously been reported. Cantuaria *et al* associated GLUT1 overexpression with poor disease free survival rate in 89 advanced stage ovarian carcinomas [190]. Semaan *et al* demonstrated that high GLUT1 expression had a negative impact on the overall survival of 213 ovarian cancer patients [194]. Cho *et al* consistently reported a reverse statistically significant relationship among overall survival of 50 patients and high GLUT1 expression [195]. On the other hand Rudlowski *et al* failed to identify any evidence of an association between GLUT1 expression and disease clinical outcome [192]. Much less information is available regarding the other glycolytic enzymes. Suh *et al* examined HKII expression by

IHC in 111 ovarian tumours and documented that high HKII was correlated with chemoresistance and disease recurrence as well as decreased progression free survival [218]. In agreement with our data Hjerpe *et al* were unable to demonstrate an association between PKM2 expression and disease free or overall survival of 54 ovarian cancer patients [529]. LDHA overexpression has been reported in several tumour types and has been frequently associated with poor survival [259, 262]. Nevertheless LDHA expression in ovarian tumours had never been reported before.

To explore the associations with the clinical outcome further the histopathological subtypes were examined separately. Indeed low PKM2 and LDHA expression appeared significantly correlated with improved survival of endometrioid ovarian cancer patients. Low PKM2 and LDHA expression was proportional to decreased relative risk of death in patients with this tumour histotype. A similar association was also observed for GLUT1 expression but it did not reach significance.

Endometrioid and clear cell tumours have similar pathology associated with the endometrial epithelium as they both arise from endometrioid cysts [51, 61]. It has been suggested that the carcinogenic process associated with this microenvironment selects for a highly glycolytic phenotype as a survival mechanism against ROS production which contributes to an aggressive resistant behaviour. This hypothesis has recently been proposed for clear cell carcinomas based on the upregulation of HNF1β [514]. However due to the shared site of origin it is possible that endometrioid tumours favour the same metabolic pathway (i.e. glycolysis). In this case, the observed correlation of enhanced GLUT1, PKM2 and LDHA expression with poor clinical outcome would be in line with the association of glycolytic metabolism with cell survival and chemoresistance as suggested for clear cell tumours. Further support that endometrioid tumours favour a glycolytic phenotype was obtained in Chapter 3, where TOV112D endometrioid ovarian cancer cells demonstrated enhanced sensitivity to an array of glycolytic inhibitors. They were identified as the most sensitive cells to 7 out of 9 compounds compared to 3 other non-endometrioid ovarian cancer cell lines (Chapter 3.3).

The discrepancy with previous studies may be related to the nature of the disease. As discussed in the introduction ovarian cancer is a highly heterogeneous disease and the diversity of findings might be attributed to the great disease heterogeneity and population variability [78]. Other possible explanations could be related to the specificity of the used antibodies or other technical differences affecting the sensitivity of immunostaining of the

various studies. That being said, this present study is the first to report expression using an automated quantitative technique for the detection of glycolytic enzymes in ovarian tumours.

To the best of my knowledge this is the first study evaluating the expression of a series of glycolytic enzymes in a large cohort of ovarian tumours. Taken together, the results of this research show that the glycolytic pathway plays a significant role in epithelial ovarian tumours. This is corroborated by previous research indicating enhanced tracer FDG uptake by ovarian cancers [530, 531], and by a study from Anderson *et al* that used a murine model of progressive ovarian cancer to demonstrate that along with progression of ovarian cancer, the glycolytic phenotype increasingly prevails and oxidative phosphorylation is repressed [532].

Most importantly, evidence is provided for the first time of an association among glycolytic metabolism and endometrium related tumours. Inhibition of the glycolytic pathway, specifically LDHA, is proposed as a promising strategy for the treatment of resistant clear cell cancers and furthermore PKM2 and LDHA are identified as prognostic markers of adverse survival in endometrioid cancers. These findings could possibly have therapeutic implication however further research in experimental and clinical settings is essential to validate them and explore them further.

Chapter 8

Chapter 8: Concluding Discussion

Despite important advances in diagnosis and treatment, breast and ovarian cancers still present major health care concerns. Significant challenges remain to be faced (including adverse effects of widely used treatment modalities, clinical resistance and poor survival rates of certain tumour types) and there is an urgent need for more efficient targeted treatments. This project examined the hypothesis that the differential metabolism of glucose by cancer cells, in comparison to normal cells, could offer a possible therapeutic target for new drugs in these cancer types. Therefore this study aimed to investigate the role of aerobic glycolysis in breast and ovarian cancer cells and identify a therapeutically exploitable glycolytic target or a translatable combinatorial strategy for the development of novel cancer drug therapies.

The data obtained provided further evidence that the glycolytic pathway is a potential target for breast and ovarian cancer treatment. Initially, strong reliance on glucose availability for cancer cell proliferation was established and further work confirmed that breast and ovarian cancer cell proliferative growth is dependent on the glycolytic pathway. Ten compounds targeting key enzymes of the glycolytic pathway were selected for investigation in this study and were compared against a panel of breast and ovarian cancer cell line models. Each of these inhibitors blocked the glycolytic pathway and attenuated breast and ovarian cancer cell proliferation in a concentration-dependent manner. The antiproliferative effects of the compounds were demonstrated to be associated with induction of apoptosis along with G0/G1 cell cycle arrest in selected cancer cell lines.

Hypoxia is a well substantiated common characteristic of the tumour microenvironment. Therefore the effects of the selected glycolytic inhibitors were assessed under a range of oxygen conditions. Interestingly, and in contrast to the notion of enhanced dependency on glycolysis in hypoxia, cancer cells presented increased sensitivity to glycolytic inhibitors at 21% O_2 conditions relative to lower O_2 conditions. Nevertheless, breast cancer cells were found to be susceptible to glycolysis inhibition over a wide range of oxygen levels, including the physiologically relevant low oxygen conditions found in solid tumours. Moreover, dependency on the glycolytic pathway even in the presence of oxygen sufficiency, corroborates Warburg's theory [87]. The relative lack of sensitivity to the glycolytic inhibitors in hypoxia was associated with slow proliferation rates as well as overexpression of the targeted glycolytic enzymes as demonstrated at both protein and mRNA levels. The modulation of the glycolytic targets of interest was assessed under varying levels of hypoxia

by Western blotting. Furthermore genome-wide transcriptomic analysis identified glycolysis as a major pathway mediating the response of breast cancer cells to oxygen deprivation.

Based on these findings, the glycolytic pathway is proposed as a potential target for breast and ovarian cancer treatment. All compounds tested, inhibiting major enzymes of the glycolytic pathway, proved effective at inhibiting cancer cell proliferation, even under varying levels of hypoxia. However, all these compounds do not have the same potential for further development as antitumour agents. Established inhibitors including Phloretin, Quercetin, 3BP, DCA and Oxamic acid served as reference compounds and enabled comparative inhibition of the whole pathway. However it is well substantiated that they affect more than one target and they required high concentrations to exert antitumour activity. These concentrations would likely be associated with high systemic toxicity. Even among "next generation" inhibitors that demonstrated promising anticancer activity at low concentrations specificity issues do exist, for example STF31 targeting NAMPT [315-317].

The most promising glycolytic targets identified in this study were GLUT1 and LDHA at the very top and bottom of the glycolytic pathway, as well as the intermediate regulator PFKFB3. LDHA seems an ideal candidate as its inhibition is anticipated to cause minimal adverse effects in normal tissue [257, 258]. In this study, evaluation of this target by siRNA knockdown demonstrated that suppressing LDHA expression was sufficient to significantly impair breast cancer cell proliferation. However NHI-1 had low potency, even though it has been characterised as a specific LDHA inhibitor and proved a valuable tool compound in this research. Further research using NHI-1 as a lead molecule to synthesise a derivative exhibiting enhanced potency and efficacy would be useful. PFKFB3 is a critical enzyme that plays a key role in the glycolytic phenotype of tumours promoting the high glycolytic rate by regulating F2,6BP the allosteric activator of PFK1 [221, 222]. 3PO was identified here as a potent inhibitor of breast and ovarian cancer cell proliferation and is believed to have potential as an antitumour agent. Similar antiproliferative action against several adenocarcinoma and haematological cell lines was also documented in the identification study of the compound conducted by Clem and colleagues. Additional evidence supporting the potential of PFKFB3 inhibition as an antitumour strategy was provided in the referred study as 3PO treatment suppressed the tumourigenic growth of established leukaemia, lung and breast adenocarcinomas *in vivo* [343]. PFK15, a recently developed 3PO derivative, demonstrated 100 fold enhanced potency against the enzymatic activity of recombinant PFKFB3 compared to the parent compound. The authors reported that PFK15 attenuated tumour growth in glioblastoma, colorectal and pancreatic tumour xenograft models [349].

However the effect of the optimised derivative compound on breast and ovarian cancer remains to be investigated.

Glucose transport is the first key rate-limiting step controlling the metabolism of glucose [176]. The novel GLUT1 inhibitor IOM-1190 demonstrated antitumour activity in a low concentration range and was characterised as a very potent cancer cell growth inhibitor in this study. Importantly, resistant cancer cells, including the triple negative breast cancer cell line MDA-MB-231 and the platinum resistant PEO4 ovarian cancer cell line were sensitive to IOM-1190 treatment. Furthermore, the compound was highly effective against hypoxic cancer cells, in contrast to the other anti-glycolytic molecules tested. Both IOM-1190 and 3PO exhibited very promising antiproliferative action supporting their potential for continued *in vivo* evaluation and appear to hold promise for development as antitumour agents.

Targeting the glycolytic pathway for cancer treatment requires some caution as the glycolytic enzymes are not tumour specific and are ubiquitously expressed. However normal cells are expected to exhibit metabolic plasticity and be able to better tolerate inhibition of the glycolytic pathway. Ample oxygen availability combined with intact mitochondrial function enables energy generation through mitochondrial respiration using alternative energy substrates such as fatty acids and amino acids [94, 100]. Preclinical evidence that antiglycolytic agents are well tolerated derives from studies documenting that several of these compounds, including WZB117 and 3PO, were associated with minimal adverse effects in xenograft models [319, 343, 349]. Preferential reliance on glycolysis has been acknowledged as a hallmark of tumourigenesis and has been described as a ‘vulnerable Achilles’ heel’ providing an opportunity to target cancer cells [90, 92]. Metabolic reconfiguration and lost cellular homeostasis renders cancer cells highly susceptible to inhibition of the glycolytic pathway which is anticipated to deplete their energy supply, severely disrupting their proliferation rate and eventually lead to apoptosis [100, 103]. Nonetheless a logical concern raised regards tissues intrinsically engaging a glycolytic metabolism. A few tissues, most importantly the brain, but also the testes and retina, are known to use glucose as their primary energy source [533-535]. Further research is required to establish the safety profile for glycolytic inhibitors. One way to avoid neurological toxicity would be to use molecules unable to cross the blood-brain barrier [100]. However this would compromise effectiveness against brain metastases. An additional limitation is that the majority of tool molecules currently available for inhibiting the glycolytic enzymes are rather nonspecific and have limited efficacy, demanding high pharmacological

concentrations [100]. Targeting the metabolic phenotype of tumours even though it presents an exciting and promising anticancer strategy is still in its infancy and further progress is required to translate it to the clinic. Future research should concentrate on the identification of molecules exhibiting enhanced specificity and potency.

Despite glycolysis inhibition being a promising antitumour strategy its value as monotherapy has been questioned [105]. Therefore the glycolytic inhibitors were assessed in combination strategies with established chemotherapeutic and targeted agents. Multiple co-treatments were investigated and indeed several synergistic combinations characterised by low combination index values were revealed. Two distinct goals were achieved in this study. Firstly, to improve the efficacy of currently used chemotherapeutics using a glycolytic inhibitor and resensitise resistant cancer cells to treatment, and secondly, to identify a novel combination of inhibitors with potential to be developed as a future anticancer strategy. The PFKFB3 inhibitor, 3PO, enhanced the cytotoxic effect of cisplatin against both platinum sensitive and platinum resistant ovarian cancer cells. This combination suggested a promising approach to overcome platinum resistance and future work should evaluate it in a relevant *in vivo* model. Moreover, combination of IOM-1190 with the antidiabetic agent metformin demonstrated a robust synergistic antiproliferative effect on breast cancer cells. MDA-MB-231 triple negative highly aggressive breast cancer cells exhibited enhanced sensitivity to this combination. This combination is anticipated to hold possible promise for the treatment of triple negative breast cancer disease and future research should focus on determining its efficacy *in vivo*. Both combinatorial strategies presented preclinical efficacy in subgroups of tumours. Such novel approaches are important and may have potential for continued development. Nevertheless, these results are exploratory pilot data and future work should focus on evaluating these combinations to assess their therapeutic index in *in vivo* and clinical models.

This research focused on two malignancies, breast and ovarian cancer. Interestingly, breast and ovarian cancer cell line models exhibited comparable sensitivity to glycolysis inhibition. Metabolism of breast tumours has been extensively studied in the past. It has been shown that triple negative tumours depend on a highly glycolytic Warburg metabolism while in contrast ER positive breast cancers primarily demonstrate a reverse Warburg phenotype [506]. This is a symbiotic metabolic model in which cancer cells induce a glycolytic metabolism in the neighbouring fibroblastic stroma and they rely on the secreted lactate and pyruvate to fuel their mitochondrial TCA cycle [536]. The glycolytic phenotype of triple negative tumours has been repeatedly verified and associated with aggressiveness and rapid

proliferation [506]. A number of studies have documented significantly enhanced tracer FDG uptake compared to other breast cancer subtypes [424, 537, 538]. Thus triple negative breast tumours seem an ideal candidate cancer type for future research on glycolysis inhibition. This could possibly have important therapeutic implications as these tumours lack specific treatment options [428].

In contrast, relatively few studies have considered the metabolism of ovarian tumours. This study sought to investigate the glycolytic phenotype of ovarian cancer. The expression of several glycolytic markers was examined across a large cohort of ovarian tumours by AQUA. The role of the glycolytic profile in ovarian cancer was explored. Results suggested that inhibition of the glycolytic pathway, specifically LDHA, could be a promising strategy for the treatment of clear cell cancers. PKM2 and LDHA were identified as prognostic markers of adverse survival in patients with endometrioid carcinomas. The findings of the present study, for the first time, suggest a significant role for glycolytic metabolism in endometrium related tumours. Further experimental investigations however are needed to verify this association. Future studies should focus on therapeutically exploiting the glycolytic phenotype of clear cell ovarian tumours. This is of paramount importance as these tumours exhibit chemoresistance and are associated with adverse clinical outcome [52, 54].

A natural progression of this work would be to validate these preliminary preclinical data, by assessing the efficacy of the most promising glycolytic inhibitors and identifying the combinatorial strategies that inhibit growth and invasion of 3-D spheroid culture models, which mimic more closely the tumour microenvironment. Future *in vivo* studies should focus on the subtypes of breast and ovarian cancers identified as more susceptible to inhibition of the glycolytic pathway. The effect of IOM-1190 as monotherapy and in combination with metformin should be evaluated in xenograft models of triple negative breast tumours. Additionally further research should determine the efficacy of the optimised derivative of 3PO, PFK15 (characterised by enhanced potency and improved pharmacokinetic properties) as a single agent or combined with cisplatin against xenograft models of platinum resistant clear cell ovarian tumours.

In recent years, there has been renewed interest in the dysregulated metabolic pathways characterising malignant transformation and tumour metabolism has emerged as a promising strategy for selective tumour targeting [272, 539-541]. In addition to the glycolytic phenotype of tumours, the well-known Warburg effect, alterations in several metabolic pathways supporting the high proliferative demands of tumours have been characterised [539, 541, 542]. Examples include the upregulation of the pentose phosphate pathway,

essential for ribonucleotide synthesis and NADPH generation, as well as the serine and glycine metabolic pathway which plays an important role in nucleotide, amino acid and lipids synthesis and redox homeostasis [540, 543-545]. A number of inhibitors targeting the altered metabolic pathways in tumours are currently under development or undergoing clinical trials [105, 272]. In their key study Folger *et al* developed a genome-wide cancer metabolic model and identified a wide range of metabolic enzymes essential for the proliferation of cancer cell lines. 52 of these targets, the majority of them novel, were predicted to have cytostatic antitumour action. Synergistic combinations of synthetic lethal metabolic targets were proposed as a tumour-selective approach. The pentose phosphate pathway along with pyruvate metabolism was identified as an attractive target in synthetic lethal strategies [546].

Overall it should be highlighted that the glycolytic phenotype of tumours studied in the present study is only one aspect of the aberrant metabolism of tumours that potentially can offer an opportunity of selective tumour targeting. Furthermore targeting tumour metabolism for cancer treatment is far from a novel therapeutic strategy. Antimetabolites including nucleoside analogues (e.g. 5‑fluorouracil and gemcitabine) and antifolate agents (pemetrexed) as well as L-asparaginase (for the treatment of acute lymphoblastic leukaemia) all have unique metabolic targets and are widely and effectively used in the clinic [272]. However the principal challenge to exploit the altered expression of tumour specific enzyme isoforms and the dependency of tumours on particular metabolic pathways to achieve selectivity remains to be translated into clinical practice [272, 540]. In recent years pharmaceutical industry has shown an increased interest demonstrating enhanced commercial activity and investment around cancer metabolism supporting the therapeutic potential in this field. The pipeline of several pharmaceutical companies is focused on the discovery and development of novel small molecules disrupting cancer cell metabolism. Examples include the GLUT1 inhibitor IOM-1190 (IOmet Pharma), the IDH1 and IDH2 mutant inhibitors AG-120, AG-221 and AG-881 (Agios in collaboration with Celgene), the glutaminase inhibitor CB-839 (Calithera BioSciences) as well as the arginase inhibitor CB-1158 (Calithera BioSciences) [141, 324, 547, 548].

The present study contributes further to our understanding of the role of glycolytic metabolism in breast and ovarian cancer. The metabolic reconfiguration of tumours is indicated as a promising anticancer target. Inhibition of the glycolytic pathway is suggested as a potential strategy for future assessment especially against triple negative breast and clear cell ovarian tumours.

Appendices

Appendix 1: Supplementary figures of Chapter 5

The following tables correspond to the drug interaction studies presented in Chapter 5. The specific concentrations of each pair of compounds that were used in the combination experiments are indicated along with the growth inhibition effect (fraction affected) of each combination point and the respective CI values as they were generated through the Calcusyn software. The figure of Chapter 5 that each table relates to is specified.

PEA1 (Figure 5.1) Table A1.1

3PO (μM)	Cisplatin (μM)	Fa	CI
0.9	1	0.094	**1.339**
1.9	1	0.509	**0.22**
3.8	1	0.505	**0.351**
7.5	1	0.546	**0.566**
15	1	0.782	**0.716**

PEA2 (Figure 5.2) Table A1.2

3PO (μM)	Cisplatin (μM)	Fa	CI
0.9	4	0.158	-
1.9	4	0.476	**0.457**
3.8	4	0.463	**0.553**
7.5	4	0.502	**0.716**
15	4	0.687	**0.923**

PEO1 (Figure 5.5) Table A1.3

3PO (μM)	Cisplatin (μM)	Fa	CI
0.9	0.5	0.096	**1.662**
1.9	0.5	0.176	**1.098**
3.8	0.5	0.430	**0.568**
7.5	0.5	0.507	**0.757**
15	0.5	0.839	**0.434**

PEO4 (Figure 5.6) Table A1.4

3PO (μM)	Cisplatin (μM)	Fa	CI
0.9	1	-	-
1.9	1	0.197	**0.626**
3.8	1	0.244	**0.602**
7.5	1	0.275	**0.763**
15	1	0.353	**1.054**

PEA1 (Figure 5.9) Table A1.5

3PO (μM)	Paclitaxel (μM)	Fa	CI
0.9	0.001	0.125	-
1.9	0.001	0.526	**0.125**
3.8	0.001	0.517	**0.253**
7.5	0.001	0.490	**0.524**
15	0.001	0.699	**0.794**

PEA2 (Figure 5.10) Table A1.6

3PO (μM)	Paclitaxel (μM)	Fa	CI
0.9	0.002	0.515	**0.262**
1.9	0.002	0.496	**0.327**
3.8	0.002	0.499	**0.415**
7.5	0.002	0.532	**0.535**
15	0.002	0.613	**0.657**

PEO1 (Figure 5.13) Table A1.7

3PO (μM)	Paclitaxel (μM)	Fa	CI
0.9	0.002	0.534	**0.542**
1.9	0.002	0.542	**0.602**
3.8	0.002	0.581	**0.669**
7.5	0.002	0.670	**0.712**
15	0.002	0.885	**0.444**

PEO4 (Figure 5.14) Table A1.8

3PO (μM)	Paclitaxel (μM)	Fa	CI
0.9	0.002	0.370	**1.077**
1.9	0.002	0.399	**1.044**
3.8	0.002	0.356	**1.617**
7.5	0.002	0.428	**1.458**
15	0.002	0.640	**0.645**

MCF7 (Figure 5.17) Table A1.9			
Oxamic acid (µM)	**Paclitaxel (µM)**	**Fa**	**CI**
4,700	0.001	0.280	**0.607**
9,400	0.001	0.512	**0.457**
18,800	0.001	0.557	**0.656**
37,500	0.001	0.653	**0.814**
75,000	0.001	0.756	**0.943**

MDA-MB-231 (Figure 5.18) Table A1.10			
Oxamic acid (µM)	**Paclitaxel (µM)**	**Fa**	**CI**
4,600	0.001	0.369	**0.363**
9,400	0.001	0.430	**0.436**
18,800	0.001	0.334	**1.02**
37,500	0.001	0.523	**0.94**
75,000	0.001	0.680	**1.002**

MCF7 (Figure 5.30) Table A1.11						
IOM-1190 (µM)	**Metformin (µM)**	**Fa**	**CI**	**Metformin (µM)**	**Fa**	**CI**
0.1	1000	0.310	**0.421**	2000	0.660	**0.147**
0.2	1000	0.306	**0.46**	2000	0.744	**0.094**
0.5	1000	0.308	**0.512**	2000	0.852	**0.044**
0.9	1000	0.589	**0.152**	2000	0.866	**0.042**
1.9	1000	0.607	**0.184**	2000	0.865	**0.05**
3.8	1000	0.668	**0.196**	2000	0.857	**0.069**
7.5	1000	0.728	**0.224**	2000	0.879	**0.078**
15	1000	0.811	**0.218**	2000	0.890	**0.109**

MDA-MB-231 (Figure 5.33) Table A1.12						
IOM-1190 (µM)	**Metformin (µM)**	**Fa**	**CI**	**Metformin (µM)**	**Fa**	**CI**
0.1	1000	0.513	**0.167**	4000	0.754	**0.121**
0.2	1000	0.495	**0.246**	4000	0.861	**0.051**
0.5	1000	0.687	**0.108**	4000	0.888	**0.04**
0.9	1000	0.739	**0.116**	4000	0.895	**0.043**
1.9	1000	0.788	**0.13**	4000	0.898	**0.054**
3.8	1000	0.845	**0.128**	4000	0.918	**0.056**
7.5	1000	0.859	**0.202**	4000	0.926	**0.077**
30	1000	0.904	**0.377**	4000	0.927	**0.243**

MCF7 (Figure 5.36) Table A1.13			
STF31 (µM)	**Metformin (µM)**	**Fa**	**CI**
0.2	2000	0.426	**0.485**
0.4	2000	0.374	**0.721**
0.9	2000	0.633	**0.39**
1.8	2000	0.707	**0.568**
3.5	2000	0.773	**0.951**

MDA-MB-231 (Figure 5.37) Table A1.14			
STF31 (µM)	**Metformin (µM)**	**Fa**	**CI**
0.9	3000	0.343	**0.36**
1.9	3000	0.634	**0.182**
3.8	3000	0.707	**0.251**
7.5	3000	0.681	**0.522**
15	3000	0.722	**0.882**

PEA1 (Figure 5.40) Table A1.15			
STF31 (µM)	**Metformin (µM)**	**Fa**	**CI**
0.9	1000	0.775	**0.101**
1.9	1000	0.817	**0.138**
3.8	1000	0.829	**0.236**
7.5	1000	0.835	**0.431**
15	1000	0.818	**0.957**

PEA2 (Figure 5.41) Table A1.16			
STF31 (µM)	**Metformin (µM)**	**Fa**	**CI**
0.9	1000	0.510	**0.11**
1.9	1000	0.697	**0.147**
3.8	1000	0.727	**0.276**
7.5	1000	0.727	**0.549**
15	1000	0.749	**1.056**

PEO1 (Figure 5.44) Table A1.17			
Phloretin (μM)	**Metformin (μM)**	**Fa**	**CI**
18.8	3000	0.396	**0.351**
37.5	3000	0.394	**0.448**
75	3000	0.298	**0.701**
150	3000	0.567	**0.884**
300	3000	0.914	**1.002**

MCF7 (Figure 5.46) Table A1.18			
Oxamic acid (mM)	**Metformin (mM)**	**Fa**	**CI**
4.7	2	0.236	**1.903**
9.4	2	0.428	**0.825**
18.8	2	0.683	**0.388**
37.5	2	0.777	**0.414**
75	2	0.846	**0.493**

MDA-MB-231 (Figure 5.47) Table A1.19			
Oxamic acid (mM)	**Metformin (mM)**	**Fa**	**CI**
4.7	4	0.390	**0.467**
9.4	4	0.357	**0.73**
18.8	4	0.569	**0.483**
37.5	4	0.783	**0.336**
75	4	0.865	**0.382**

PEA1 (Figure 5.50) Table A1.20			
Oxamic acid (mM)	**Metformin (mM)**	**Fa**	**CI**
3.1	1	0.821	**0.052**
6.3	1	0.882	**0.055**
12.5	1	0.895	**0.085**
25	1	0.862	**0.211**
50	1	0.895	**0.303**

PEA2 (Figure 5.51) Table A1.21			
Oxamic acid (mM)	**Metformin (mM)**	**Fa**	**CI**
3.1	1	0.203	**0.352**
6.3	1	0.364	**0.273**
12.5	1	0.519	**0.272**
25	1	0.658	**0.305**
50	1	0.847	**0.235**

PEO1 (Figure 5.54) Table A1.22			
Oxamic acid (mM)	**Metformin (mM)**	**Fa**	**CI**
3.1	2	0.713	**0.154**
6.3	2	0.742	**0.205**
12.5	2	0.819	**0.24**
25	2	0.770	**0.539**
50	2	0.845	**0.702**

PEO4 (Figure 5.55) Table A1.23			
Oxamic acid (mM)	**Metformin (mM)**	**Fa**	**CI**
3.1	0.5	0.573	**0.123**
6.3	0.5	0.747	**0.11**
12.5	0.5	0.737	**0.217**
25	0.5	0.751	**0.392**
50	0.5	0.788	**0.627**

MCF7 (Figure 5.58) Table A1.24			
DCA (mM)	**Metformin (mM)**	**Fa**	**CI**
3.1	1	0.291	**0.938**
6.3	1	0.555	**0.448**
12.5	1	0.630	**0.603**
25	1	0.685	**0.903**
50	1	0.890	**0.4**

MDA-MB-231 (Figure 5.47) Table A1.25			
DCA (mM)	**Metformin (mM)**	**Fa**	**CI**
3.1	3	0.426	**0.203**
6.3	3	0.419	**0.292**
12.5	3	0.460	**0.405**
25	3	0.471	**0.689**
50	3	0.879	**0.404**

Tables A1.1 to A1.25: Concentration range of a glycolytic inhibitor that was combined with a constant concentration of a chemotherapy or targeted inhibitor for the treatment of the referred breast or ovarian cancer cell line. The growth inhibition effect of each combination point (fraction affected) along with the respective combination index value generated through Calcusyn are presented. In brackets the figure of Chapter 5 that each combination is depicted is indicated.

The following figures correspond to the metformin drug interaction studies presented in Chapter 5 section 5.3. Concentration response curves of metformin single treatments for a panel of three paired breast and ovarian cancer cell lines are presented here as reference.

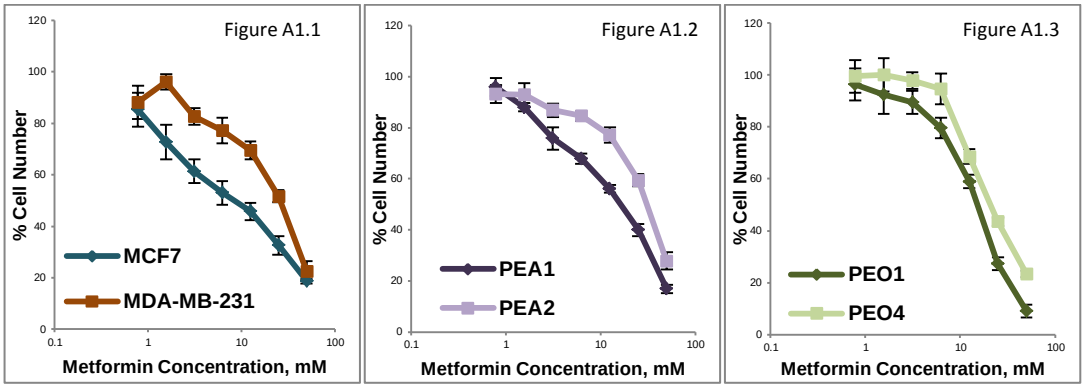

Figures A1.1 to A1.3: Concentration response curves of three paired breast and ovarian cancer cell lines (MCF7 and MDA-MB-231, PEA1 and PEA2, PEO1 and PEO4) treated with metformin concentrations between 0.8-50mM for a three day period. Cell viability was determined by an SRB assay. Averaged results of 6 replicates are reported and error bars represent standard deviations. Values are shown as a percentage of control.

Below some examples of unfavourable non-synergistic combinations that were encountered in this study are presented. The combinations of Phloretin, Oxamic acid and NHI-1 with cisplatin as well as 3PO with metformin gave rise to high CI values (>1) indicating an antagonistic relationship.

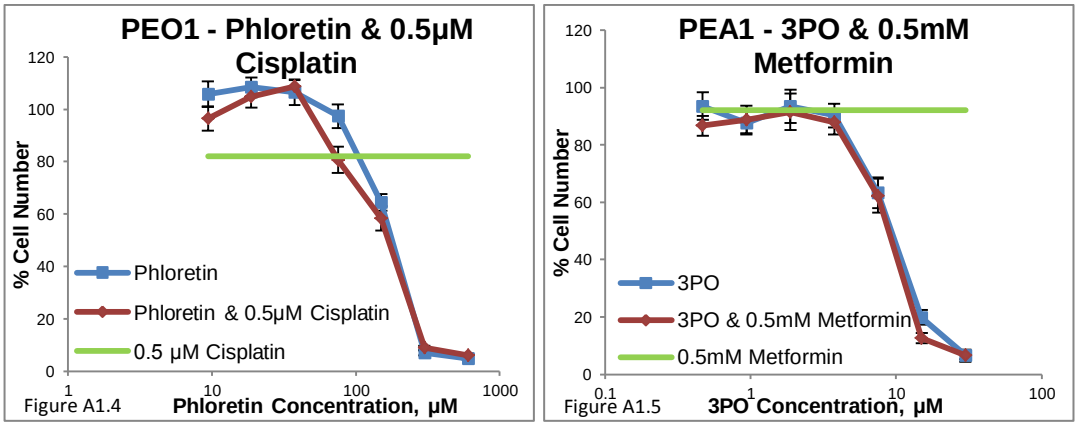

Figures A1.4 & A1.5: Concentration response curves of PEO1 ovarian cancer cells treated with Phloretin concentrations between 9.4-600μM alone (blue line) or combined with 0.5μM Cisplatin (red line) on the left (A1.4) as well as concentration response curves of PEA1 ovarian cancer cells treated with 3PO concentrations between 0.5-30μM alone (blue line) or combined with 0.5mM Metformin (red line) on the right (A1.5). Cell viability was determined by an SRB assay after a 3 day treatment. Averaged results of 6 replicates are reported and error bars represent standard deviations. Values are shown as a percentage of control. In green the effect of the constant concentration of Cisplatin or Metformin on cell viability is indicated.

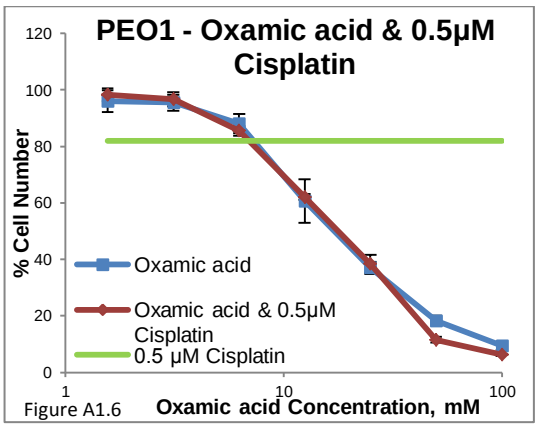

Figure A1.6

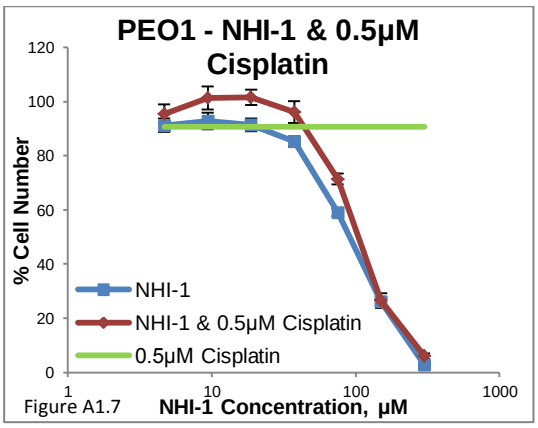

Figure A1.7

Figures A1.6 & A1.7: Concentration response curves of PEO1 ovarian cancer cells treated with Oxamic acid concentrations between 1.6-100mM alone (blue line) or combined with 0.5µM Cisplatin (red line) on the left (A1.6) as well as treated with NHI-1 concentrations between 4.7-300µM alone (blue line) or combined with 0.5µM Cisplatin (red line) on the right (A1.7). Cell viability was determined by an SRB assay after a 3 day treatment. Averaged results of 6 replicates are reported and error bars represent standard deviations. Values are shown as a percentage of control. In green the effect of 0.5µM Cisplatin on cell viability is indicated.

The following figures correspond to the flow cytometric analysis of induction of apoptosis of the drug interaction studies presented in Chapter 5 section 5.4. They are the controls of untreated MDA-MB-231 cells at 24 and 48h respectively related to the examination of apoptosis of STF31 and metformin co-treated cells in Figures 5.62 and 5.63.

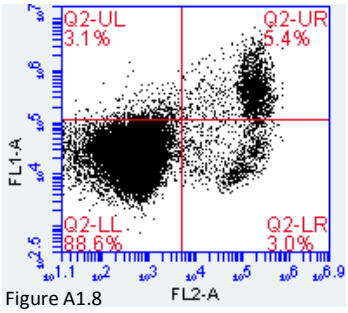

Figure A1.8

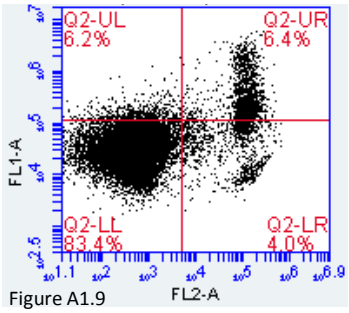

Figure A1.9

Figures A1.8 & A1.9: Flow cytometric analysis of untreated MDA-MB-231 breast cancer cells at 24 and 48h. FL1 (annexin V) versus FL2 (PI) scatter plots of gated cells double stained with FITC-conjugated annexin V and propidium iodide are presented. The percentage of cells in each quadrant is indicated in red.

Figure A1.10 corresponds to the flow cytometric cell cycle analysis of the drug interaction studies presented in Chapter 5 section 5.5. It is the control of untreated MDA-MB-231 cells related to the examination of cell cycle progression of cells treated with three glycolytic inhibitors, IOM-1190, STF31 and Oxamic acid, combined with metformin in Figures 5.66 to 5.68.

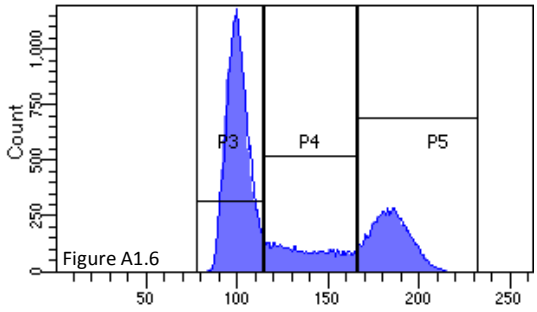

Untreated Cells	
G0/G1	56.2
S	17.8
G2/M	26

Figure A1.10: Flow cytometric analysis of cellular DNA content of untreated MDA-MB-231 breast cancer cells at 24h. In the histogram fluorescence of the DNA bound propidium iodide, indicating the DNA content in X-axis, is plotted against the number of cells in the Y-axis. The percentage of cells in each cell cycle phase is demonstrated on the right.

Appendix 2: Supplementary tables of Chapter 6

ENSM Gene ID	Gene Symbol	DAVID Gene Name
ENSG00000003436	TFPI	tissue factor pathway inhibitor
ENSG00000006747	SCIN	scinderin
ENSG00000087586	AURKA	aurora kinase A
ENSG00000088325	TPX2	TPX2, microtubule nucleation factor
ENSG00000089009	RPL6	ribosomal protein L6
ENSG00000090889	KIF4A	kinesin family member 4A
ENSG00000101447	FAM83D	family with sequence similarity 83 member D
ENSG00000112984	KIF20A	kinesin family member 20A
ENSG00000124802	EEF1E1	eukaryotic translation elongation factor 1 epsilon 1
ENSG00000126787	DLGAP5	DLG associated protein 5
ENSG00000131747	TOP2A	topoisomerase (DNA) II alpha
ENSG00000138778	CENPE	centromere protein E
ENSG00000145220	LYAR	Ly1 antibody reactive
ENSG00000145386	CCNA2	cyclin 2
ENSG00000147224	PRPS1	phosphoribosyl pyrophosphate synthetase 1
ENSG00000148459	PDSS1	prenyl (decaprenyl) diphosphate synthase, subunit 1
ENSG00000154719	MRPL39	mitochondrial ribosomal protein L39
ENSG00000156802	ATAD2	ATPase family, AAA domain containing 2
ENSG00000163170	BOLA3	bolA family member 3
ENSG00000163319	MRPS18C	mitochondrial ribosomal protein S18C
ENSG00000165264	NDUFB6	NADH:ubiquinone oxidoreductase subunit B6
ENSG00000165672	PRDX3	peroxiredoxin 3
ENSG00000171863	RPS7	ribosomal protein S7
ENSG00000172172	MRPL13	mitochondrial ribosomal protein L13
ENSG00000183527	PSMG1	proteasome assembly chaperone 1
ENSG00000214810	CYCSP55	cytochrome c, somatic pseudogene 55
ENSG00000233966	UBE2SP1	ubiquitin conjugating enzyme E2 S pseudogene 1
ENSG00000235001	EIF4A1P2	eukaryotic translation initiation factor 4A1 pseudogene 2
ENSG00000238249	HMGN2P17	high mobility group nucleosomal binding domain 2 pseudogene 17
ENSG00000242616	GNG10	G protein subunit gamma 10

Table A2.1: Genes mutually downregulated in three breast cancer cell lines (MCF7, MDA-MB-231, HBL100) under chronic hypoxia. The Ensembl gene identifiers, the official gene symbol and the DAVID gene name are referred.

ENSM Gene ID	Gene Symbol	DAVID Gene Name
ENSG00000059804	SLC2A3	solute carrier family 2 member 3
ENSG00000100906	NFKBIA	NFKB inhibitor alpha
ENSG00000104419	NDRG1	N-myc downstream regulated 1
ENSG00000105220	GPI	glucose-6-phosphate isomerase
ENSG00000107159	CA9	carbonic anhydrase 9
ENSG00000109107	ALDOC	aldolase, fructose-bisphosphate C
ENSG00000111674	ENO2	enolase 2
ENSG00000114268	PFKFB4	6-phosphofructo-2-kinase/fructose-2,6-biphosphatase 4
ENSG00000115548	KDM3A	lysine demethylase 3A
ENSG00000122884	P4HA1	prolyl 4-hydroxylase subunit alpha 1
ENSG00000124145	SDC4	syndecan 4
ENSG00000134107	BHLHE40	basic helix-loop-helix family member e40
ENSG00000138166	DUSP5	dual specificity phosphatase 5
ENSG00000143847	PPFIA4	PTPRF interacting protein alpha 4
ENSG00000145901	TNIP1	TNFAIP3 interacting protein 1
ENSG00000164463	CREBRF	CREB3 regulatory factor
ENSG00000167702	KIFC2	kinesin family member C2
ENSG00000168209	DDIT4	DNA damage inducible transcript 4
ENSG00000176171	BNIP3	BCL2 interacting protein 3
ENSG00000186352	ANKRD37	ankyrin repeat domain 37

Table A2.2: Genes mutually upregulated in three breast cancer cell lines (MCF7, MDA-MB-231, HBL100) under chronic hypoxia. The Ensembl gene identifiers, the official gene symbol and the DAVID gene name are referred.

ENSM Gene ID	Gene Symbol	DAVID Gene Name
ENSG00000149925	ALDOA	aldolase A, fructose-bisphosphate
ENSG00000136872	ALDOB	aldolase B, fructose-bisphosphate
ENSG00000109107	ALDOC	aldolase C, fructose-bisphosphate
ENSG00000172331	BPGM	2,3-bisphosphoglycerate mutase
ENSG00000074800	ENO1	enolase 1 (alpha)
ENSG00000111674	ENO2	enolase 2 (gamma, neuronal)
ENSG00000108515	ENO3	enolase 3 (beta, muscle)
ENSG00000143891	GALM	galactose mutarotase (aldose 1-epimerase)
ENSG00000106633	GCK	glucokinase (hexokinase 4)
ENSG00000105220	GPI	glucose phosphate isomerase
ENSG00000159399	HK2	hexokinase 2 pseudogene; hexokinase 2
ENSG00000134333	LDHA	lactate dehydrogenase A
ENSG00000152256	PDK1	pyruvate dehydrogenase kinase, isozyme 1
ENSG00000005882	PDK2	pyruvate dehydrogenase kinase, isozyme 2
ENSG00000067992	PDK3	pyruvate dehydrogenase kinase, isozyme 3
ENSG00000004799	PDK4	pyruvate dehydrogenase kinase, isozyme 4
ENSG00000172840	PDP2	pyruvate dehydrogenase phosphatase catalytic subunit 2
ENSG00000090857	PDPR	pyruvate dehydrogenase phosphatase regulatory subunit
ENSG00000170525	PFKFB3	6-phosphofructo-2-kinase/fructose-2,6-biphosphatase 3
ENSG00000141959	PFKL	phosphofructokinase, liver
ENSG00000102144	PGK1	phosphoglycerate kinase 1
ENSG00000170950	PGK2	phosphoglycerate kinase 2
ENSG00000079739	PGM1	phosphoglucomutase 1
ENSG00000169299	PGM2	phosphoglucomutase 2
ENSG00000013375	PGM3	phosphoglucomutase 3
ENSG00000143627	PKLR	pyruvate kinase, liver and RBC
ENSG00000117394	SLC2A1	solute carrier family 2 (facilitated glucose transporter), member 1
ENSG00000059804	SLC2A3	solute carrier family 2 (facilitated glucose transporter), member 3
ENSG00000111669	TPI1	TPI1 pseudogene; triosephosphate isomerase 1

Table A2.3: Probes of interest in this study indicating genes involved in the glycolytic pathway and its regulation. The Ensembl gene identifiers, the official gene symbol and the DAVID gene name are referred.

Appendix 3: Supplementary table of Chapter 7

Spot Number	Tumour Stage	Tumour Histotype	Survival Months	Event Occurred
1	III	ADENO	29.20	1
2	III	ENDO	20.87	1
3	IV	Serous PAP	1.23	1
4	IV	ENDO	20.03	1
5	III	Serous PAP	20.10	1
6	I	ENDO	207.07	0
7	I	ENDO	87.27	1
8	III	Serous PAP	15.10	1
9	IV	Serous PAP	10.97	1
10	III	CLEAR CELL	5.47	1
11	III	Serous PAP	47.87	1
12	III	Serous PAP	10.07	1
13	III	Serous PAP	178.00	0
14	III	ENDO	20.70	1
15	I	Serous PAP	169.43	1
16	I	Serous PAP	149.30	1
17	III	Serous PAP	16.43	1
18	III	Serous PAP	29.23	1
19	III	ENDO	211.90	0
20	III	Serous PAP	44.37	1
21	III	Serous PAP	7.03	1
22	IV	Serous PAP	33.47	1
23	III	Serous PAP	21.70	1
24	I	Serous PAP	29.63	1
25	III	ENDO	35.83	1
26	III	Serous PAP	14.27	1
27	II	Serous PAP	6.60	1
28	IV	MIXED	7.57	1
29	III	Serous PAP	76.50	1
30	III	Serous PAP	19.07	1
31	III	ENDO	39.40	1
32	III	ENDO	69.13	1
33	III	ENDO	25.10	1
34	III	ENDO	31.93	1
35	III	Serous PAP	10.60	1
36	I	CLEAR CELL	158.40	0
37	III	ENDO	50.40	1
38	III	Serous PAP	21.47	1
39	III	ENDO	20.30	1

40	III	Serous PAP	39.17	1
41	II	ENDO	30.57	1
42	III	Serous PAP	13.40	1
43	III	Serous PAP	23.30	1
44	III	ENDO	23.20	1
45	III	Serous PAP	12.93	1
46	III	ENDO	51.03	1
47	III	Serous PAP	37.33	1
48	III	Serous PAP	18.53	1
49	III	Serous PAP	15.40	1
50	III	Serous PAP	5.37	1
51	III	ADENO	12.03	1
52	IV	CLEAR CELL	34.30	1
53	III	MUCINOUS	48.67	1
54	IV	ENDO	2.30	1
55	III	Serous PAP	11.90	1
56	IV	Serous PAP	15.00	1
57	III	ENDO	8.27	1
58	II	MUCINOUS	145.13	0
59	III	Serous PAP	16.83	1
60	IV	ENDO	11.57	1
61	IV	ADENO	20.33	1
62	III	Serous PAP	149.37	0
63	III	Serous PAP	5.57	1
64	III	Serous PAP	105.50	1
65	III	Serous PAP	24.00	1
66	II	CLEAR CELL	158.07	0
67	III	Serous PAP	33.73	1
68	III	Serous PAP	11.90	1
69	III	Serous PAP	124.10	1
70	III	ENDO	152.47	0
71	I	MIXED	143.80	0
72	IV	Serous PAP	9.90	1
73	III	Serous PAP	45.30	1
74	II	ENDO	156.63	0
75	III	Serous PAP	41.50	1
76	III	Serous PAP	43.47	1
77	III	Serous PAP	45.00	1
78	III	Serous PAP	13.07	1
79	IV	Serous PAP	19.83	1
80	II	MUCINOUS	5.83	1
81	III	Serous PAP	11.57	1
82	III	Serous PAP	25.17	1
83	III	ENDO	20.83	1

84	III	Serous PAP	8.83	1
85	III	Serous PAP	50.93	1
86	IV	Serous PAP	1.90	1
87	III	Serous PAP	70.47	1
88	IV	Serous PAP	18.67	1
89	III	Serous PAP	46.00	1
90	III	Serous PAP	15.00	1
91	III	ENDO	65.83	1
92	III	MUCINOUS	21.40	1
93	I	MUCINOUS	133.03	0
94	I	ENDO	137.73	0
95	IV	Serous PAP	49.73	1
96	unknown	ENDO	138.67	0
97	III	Serous PAP	20.00	1
98	III	Serous PAP	25.03	1
99	IV	ENDO	9.67	1
100	III	Serous PAP	6.47	1
101	III	MUCINOUS	138.57	0
102	III	ENDO	7.87	1
103	I	ENDO	23.03	1
104	III	ADENO	97.87	1
105	III	MIXED	19.63	1
106	III	CLEAR CELL	31.60	1
107	III	MIXED	144.20	0
108	I	ENDO	136.60	0
109	IV	Serous PAP	7.57	1
110	I	CLEAR CELL	132.37	0
111	IV	Serous PAP	53.67	1
112	II	MIXED	78.10	1
113	III	Serous PAP	10.43	1
114	III	Serous PAP	2.53	1
115	III	Serous PAP	65.53	1
116	IV	Serous PAP	79.27	1
117	III	Serous PAP	20.80	1
118	II	Serous PAP	133.00	0
119	III	ADENO	13.03	1
120	I	Serous PAP	14.83	1
121	IV	Serous PAP	7.67	1
122	III	Serous PAP	132.07	0
123	III	ENDO	37.07	1
124	III	Serous PAP	34.67	1
125	III	MIXED	10.40	1
126	III	Serous PAP	89.93	1
127	III	Serous PAP	10.63	1

128	III	Serous PAP	80.83	1
129	III	ENDO	8.90	1
130	III	ENDO	6.47	1
131	II	ENDO	74.67	1
132	III	Serous PAP	12.13	1
133	IV	Serous PAP	18.03	1
134	III	ENDO	48.40	1
135	III	Serous PAP	10.40	1
136	III	ADENO	13.23	1
137	III	Serous PAP	78.97	1
138	III	Serous PAP	59.63	1
139	IV	Serous PAP	13.93	1
140	I	ADENO	44.70	1
141	IV	MIXED	30.47	1
142	IV	Serous PAP	13.20	1
143	III	Serous PAP	16.67	1
144	IV	Serous PAP	30.27	1
145	I	ENDO	105.13	1
146	III	ADENO	7.10	1
147	IV	Serous PAP	37.40	1
148	II	ENDO	55.37	1
149	I	MIXED	117.27	0
150	II	MIXED	10.13	1
151	III	Serous PAP	12.07	1
152	III	Serous PAP	53.63	1
153	III	Serous PAP	29.03	1
154	III	Serous PAP	48.37	1
155	III	MIXED	71.40	1
156	III	Serous PAP	41.00	1
157	III	ENDO	34.57	1
158	I	Serous PAP	121.80	0
159	III	ENDO	23.57	1
160	III	Serous PAP	12.17	1
161	III	Serous PAP	18.73	1
162	III	Serous PAP	12.43	1
163	III	ENDO	111.23	0
164	III	Serous PAP	13.67	1
165	II	Serous PAP	40.00	1
166	IV	Serous PAP	15.30	1
167	IV	Serous PAP	8.17	1
168	III	Serous PAP	11.83	1
169	III	ENDO	114.03	1
170	III	Serous PAP	108.50	0
171	IV	ENDO	39.63	1

172	II	ENDO	109.27	0
173	IV	ENDO	18.80	1
174	IV	Serous PAP	12.50	1
175	III	MIXED	46.23	1
176	IV	MIXED	12.27	1
177	I	Serous PAP	104.83	1
178	III	MIXED	34.77	1
179	III	Serous PAP	65.07	1
180	II	ENDO	64.03	1
181	I	MIXED	80.27	1
182	III	MIXED	28.53	1
183	II	Serous PAP	63.63	1
184	III	ENDO	114.57	0
185	III	Serous PAP	3.67	1
186	IV	ENDO	15.47	1
187	III	Serous PAP	94.87	1
188	II	CLEAR CELL	78.63	1
189	III	MUCINOUS	20.93	1
190	III	Serous PAP	16.20	1
191	unknown	CLEAR CELL	46.30	1
192	I	ADENO	44.73	1
193	III	Serous PAP	50.77	1
194	II	MIXED	10.33	1
195	I	MUCINOUS	30.43	1
196	IV	Serous PAP	104.90	0
197	IV	MIXED	9.40	1
198	III	Serous PAP	1.80	1
199	III	Serous PAP	50.07	1
200	III	Serous PAP	104.10	0
201	III	MIXED	8.83	1
202	III	Serous PAP	11.70	1
203	I	ENDO	104.77	0
204	I	ENDO	108.83	0
205	III	Serous PAP	110.00	0
206	IV	Serous PAP	29.33	1
207	I	ENDO	106.70	0
208	II	MIXED	112.00	0
209	I	Serous PAP	55.07	1
210	III	ENDO	9.40	1
211	IV	Serous PAP	5.07	1
212	III	MIXED	36.57	1
213	II	ENDO	114.77	0
214	III	ENDO	99.20	1
215	III	Serous PAP	24.73	1

216	III	ADENO	2.27	1
217	III	ENDO	80.53	1
218	II	ENDO	96.20	0
219	III	Serous PAP	13.10	1
220	unknown	MIXED	14.83	1
221	III	Serous PAP	34.53	1
222	I	ENDO	100.40	0
223	III	Serous PAP	12.93	1
224	III	Serous PAP	5.27	1
225	III	Serous PAP	41.37	1
226	III	Serous PAP	56.93	1
227	I	CLEAR CELL	73.20	1
228	I	ENDO	101.03	0
229	III	Serous PAP	25.63	1
230	IV	Serous PAP	31.57	1
231	II	ENDO	7.30	1
232	II	Serous PAP	5.50	1
233	IV	Serous PAP	56.50	1
234	III	Serous PAP	97.37	0
235	I	ENDO	119.10	0
236	IV	Serous PAP	31.53	1
237	IV	Serous PAP	35.40	1
238	III	Serous PAP	18.63	1
239	III	Serous PAP	27.50	1
240	unknown	ENDO	96.10	0
241	II	MIXED	76.20	1
242	unknown	ENDO	98.60	0
243	I	MIXED	23.00	1
244	II	Serous PAP	47.10	1
245	III	MIXED	7.50	1
246	III	Serous PAP	10.73	1
247	III	Serous PAP	37.50	1
248	III	ENDO	39.37	1
249	III	MIXED	100.37	0
250	III	Serous PAP	93.07	1
251	III	ENDO	45.07	1
252	II	Serous PAP	97.37	0
253	III	Serous PAP	32.40	1
254	II	MUCINOUS	96.67	0
255	II	MIXED	24.17	1
256	IV	ENDO	30.03	1
257	IV	Serous PAP	49.80	1
258	III	Serous PAP	44.63	1
259	III	Serous PAP	39.80	1

260	III	Serous PAP	47.27	1
261	III	Serous PAP	44.23	1
262	III	Serous PAP	46.67	1
263	I	ENDO	35.13	1
264	III	Serous PAP	12.63	1
265	II	ENDO	57.90	1
266	IV	Serous PAP	14.87	1
267	III	Serous PAP	8.73	1
268	III	Serous PAP	97.23	0
269	unknown	Serous PAP	12.73	1
270	III	Serous PAP	9.20	1
271	III	Serous PAP	29.73	1
272	I	CLEAR CELL	43.83	1
273	III	ENDO	44.73	1
274	III	Serous PAP	35.83	1
275	II	ENDO	9.27	1
276	I	MUCINOUS	90.13	0
277	II	CLEAR CELL	71.17	1
278	III	CLEAR CELL	26.17	1
279	III	Serous PAP	27.00	1
280	IV	Serous PAP	77.93	0
281	III	MIXED	51.13	1
282	unknown	Serous PAP	14.30	1
283	I	MUCINOUS	75.83	0
284	III	Serous PAP	44.37	1
285	III	Serous PAP	46.03	1
286	III	ENDO	55.60	1
287	III	CLEAR CELL	7.37	1
288	III	ENDO	90.53	0
289	IV	Serous PAP	21.07	1
290	III	Serous PAP	87.90	0
291	III	Serous PAP	29.00	1
292	III	Serous PAP	78.60	0
293	IV	MIXED	1.37	1
294	III	Serous PAP	48.23	1
295	III	Serous PAP	5.60	1
296	IV	Serous PAP	31.37	1
297	III	MIXED	83.03	0
298	IV	ENDO	41.30	1
299	III	MIXED	46.87	1
300	III	Serous PAP	22.63	1
301	III	Serous PAP	31.10	1
302	III	Serous PAP	41.47	1
303	II	Serous PAP	60.90	1

304	III	MIXED	38.10	1
305	III	Serous PAP	15.53	1
306	III	MIXED	75.77	1
307	III	Serous PAP	81.00	1
308	III	ENDO	15.33	1
309	III	Serous PAP	11.73	1
310	III	ENDO	82.27	0
311	III	Serous PAP	42.37	1
312	III	MIXED	20.03	1
313	II	Serous PAP	72.50	0
314	III	Serous PAP	31.33	1
315	III	ENDO	34.43	1
316	III	Serous PAP	51.53	1
317	II	CLEAR CELL	42.20	1
318	III	Serous PAP	27.60	0
319	III	Serous PAP	73.97	0
320	III	Serous PAP	14.33	1
321	IV	Serous PAP	4.07	1
322	III	Serous PAP	21.83	1
323	IV	Serous PAP	20.97	1
324	IV	Serous PAP	20.57	1
325	III	Serous PAP	28.20	1
326	IV	Serous PAP	8.40	1
327	III	Serous PAP	52.77	1
328	II	Serous PAP	73.23	0
329	II	ENDO	64.97	0
330	III	MIXED	33.27	1
331	III	Serous PAP	41.00	1
332	III	Serous PAP	71.77	0
333	III	Serous PAP	13.37	1
334	III	Serous PAP	67.77	1
335	III	MIXED	42.10	1
336	III	Serous PAP	34.27	1
337	unknown	ENDO	71.53	0
338	I	CLEAR CELL	29.63	1
339	III	ADENO	17.83	1
340	III	Serous PAP	8.93	1
341	III	Serous PAP	66.57	0
342	III	Serous PAP	19.37	1
343	IV	Serous PAP	27.83	1
344	III	MIXED	31.10	1
345	IV	Serous PAP	14.63	1
346	III	Serous PAP	31.77	1
347	II	CLEAR CELL	7.27	1

348	II	CLEAR CELL	59.00	0
349	III	Serous PAP	68.43	0
350	I	ENDO	73.67	0
351	III	Serous PAP	30.33	1
352	II	Serous PAP	57.17	0
353	IV	ENDO	48.07	0
354	IV	Serous PAP	49.63	1
355	III	Serous PAP	59.07	0
356	III	Serous PAP	17.00	1
357	III	Serous PAP	56.43	0
358	III	Serous PAP	23.10	1
359	II	Serous PAP	50.77	0
360	IV	MIXED	16.93	1
361	III	ENDO	58.43	0
362	unknown	Serous PAP	54.80	0
363	III	Serous PAP	3.30	1
364	II	ENDO	59.30	0
365	III	MIXED	22.73	1
366	II	ENDO	56.20	0
367	III	MIXED	10.00	1
368	IV	MIXED	59.30	0
369	unknown	Serous PAP	33.80	1
370	III	Serous PAP	30.10	1
371	III	Serous PAP	56.77	0
372	III	Serous PAP	3.83	1
373	I	MIXED	55.60	0
374	unknown	MIXED	8.53	1
375	unknown	CLEAR CELL	52.30	0
376	IV	ENDO	7.97	1
377	III	MIXED	24.23	1
378	II	MIXED	45.23	0
379	II	ENDO	48.07	0
380	I	ENDO	56.73	0
381	IV	MIXED	52.60	0
382	III	Serous PAP	37.87	1
383	I	ENDO	41.57	0
384	IV	Serous PAP	23.30	1
385	III	Serous PAP	24.50	1
386	II	ENDO	48.60	0
387	III	ENDO	53.73	0
388	IV	Serous PAP	18.00	1
389	II	ENDO	46.40	0
390	II	MIXED	51.77	0
391	III	MIXED	51.07	0

392	IV	MIXED	16.03	1
393	IV	Serous PAP	20.10	1
394	IV	Serous PAP	47.50	1
395	III	Serous PAP	47.10	0
396	II	CLEAR CELL	28.70	1
397	III	Serous PAP	49.87	0
398	III	Serous PAP	34.47	1
399	IV	Serous PAP	53.47	0
400	III	Serous PAP	17.93	1
401	I	ENDO	34.30	1
402	III	Serous PAP	21.50	1
403	I	ENDO	44.57	0
404	IV	Serous PAP	48.57	0
405	III	Serous PAP	21.30	1
406	III	MIXED	19.63	1
407	III	Serous PAP	41.30	1
408	III	Serous PAP	25.87	1
409	III	Serous PAP	14.63	1
410	III	MIXED	19.83	1
411	II	MIXED	45.57	0
412	III	Serous PAP	36.73	1
413	I	MIXED	38.77	0
414	II	MIXED	43.17	0
415	III	Serous PAP	44.77	0
416	IV	MIXED	30.20	1
417	II	CLEAR CELL	46.70	0
418	III	Serous PAP	11.90	1
419	III	MUCINOUS	5.30	1
420	III	MIXED	18.63	1
421	III	Serous PAP	11.20	1
422	unknown	Serous PAP	9.17	1
423	III	CLEAR CELL	16.50	1
424	unknown	MIXED	14.13	1
425	III	Serous PAP	22.00	1
426	unknown	ADENO	26.87	1
427	IV	ENDO	41.53	0
428	III	Serous PAP	41.23	0
429	III	MIXED	41.03	0
430	IV	Serous PAP	9.07	1
431	IV	Serous PAP	41.80	0
432	III	Serous PAP	30.93	1
433	II	ENDO	37.53	0
434	I	Serous PAP	13.07	1
435	IV	Serous PAP	24.17	1

436	IV	Serous PAP	5.17	1
437	III	MIXED	22.00	1
438	IV	Serous PAP	36.37	0
439	I	MUCINOUS	39.20	0
440	II	MIXED	29.70	1
441	III	Serous PAP	21.37	1
442	III	Serous PAP	33.23	0
443	III	Serous PAP	26.07	1
444	III	Serous PAP	25.93	1
445	III	MUCINOUS	28.93	1
446	unknown	MIXED	35.77	0
447	III	MIXED	36.00	0
448	II	CLEAR CELL	26.10	0
449	III	Serous PAP	13.60	1
450	III	Serous PAP	29.30	0
451	I	CLEAR CELL	35.40	0
452	I	ENDO	32.63	0
453	II	ENDO	20.00	1
454	IV	Serous PAP	19.20	1
455	unknown	ENDO	33.33	0
456	I	Serous PAP	32.20	0
457	IV	Serous PAP	19.50	1
458	III	Serous PAP	34.03	0
459	III	Serous PAP	35.23	0
460	III	Serous PAP	14.07	1
461	IV	Serous PAP	32.73	1
462	III	Serous PAP	30.63	0
463	unknown	Serous PAP	27.63	1
464	III	Serous PAP	43.90	0
465	III	Serous PAP	27.93	1
466	III	Serous PAP	29.30	0
467	II	CLEAR CELL	29.83	0
468	II	Serous PAP	32.23	0
469	III	Serous PAP	unknown	unknown

Table A3: Patient characteristics (tumour stage, histotype and survival data) of the cohort of 469 ovarian tumours used in the Tissue Microarrays of Chapter 7. ADENO stands for Adenocarcinoma, Serous PAP for Serous and ENDO for Endometrioid. Event described is death, 0 indicates no event (censored patients) and 1 indicates event occurrence i.e. death from ovarian cancer.

Appendix 4: Published Manuscript

www.impactjournals.com/oncotarget/ Oncotarget, Vol. 6, No. 28

A comparative analysis of inhibitors of the glycolysis pathway in breast and ovarian cancer cell line models

Chrysi Xintaropoulou[1], Carol Ward[1], Alan Wise[2], Hugh Marston[2,4], Arran Turnbull[3], Simon P. Langdon[1]

[1]Division of Pathology, Institute of Genetics and Molecular Medicine, University of Edinburgh, Western General Hospital, Edinburgh, EH4 2XU, UK

[2]IOMET Pharma, Nine, Edinburgh BioQuarter, Edinburgh, EH16 4UX, UK

[3]Breakthrough Breast Unit, Institute of Genetics and Molecular Medicine, University of Edinburgh, Western General Hospital, Edinburgh, EH4 2XU, UK

[4]Current Address: Eli Lilly Research and Development, Windlesham, Surrey, GU20 6PH, UK

Correspondence to:
Simon P. Langdon, **e-mail:** Simon.Langdon@ed.ac.uk

Keywords: *glycolysis, inhibitors, ovarian cancer, breast cancer*

Received: *May 12, 2015* ***Accepted:*** *June 29, 2015* ***Published:*** *July 16, 2015*

ABSTRACT

Many cancer cells rely on aerobic glycolysis for energy production and targeting of this pathway is a potential strategy to inhibit cancer cell growth. In this study, inhibition of five glycolysis pathway molecules (GLUT1, HKII, PFKFB3, PDHK1 and LDH) using 9 inhibitors (Phloretin, Quercetin, STF31, WZB117, 3PO, 3-bromopyruvate, Dichloroacetate, Oxamic acid, NHI-1) was investigated in panels of breast and ovarian cancer cell line models. All compounds tested blocked glycolysis as indicated by increased extracellular glucose and decreased lactate production and also increased apoptosis. Sensitivity to several inhibitors correlated with the proliferation rate of the cell lines. Seven compounds had IC_{50} values that were associated with each other consistent with a shared mechanism of action. A synergistic interaction was revealed between STF31 and Oxamic acid when combined with the antidiabetic drug metformin. Sensitivity to glycolysis inhibition was also examined under a range of O_2 levels (21% O_2, 7% O_2, 2% O_2 and 0.5% O_2) and greater resistance to the inhibitors was found at low oxygen conditions (7% O_2, 2% O_2 and 0.5% O_2) relative to 21% O_2 conditions. These results indicate growth of breast and ovarian cancer cell lines is dependent on all the targets examined in the glycolytic pathway with increased sensitivity to the inhibitors under normoxic conditions.

INTRODUCTION

In the 1920s, Otto Warburg demonstrated that cancer cells exhibit an alteration in their metabolism when compared with non-malignant cells. Normal cells in the presence of oxygen use primarily the mitochondrial tricarboxylic acid (TCA) cycle and oxidative phosphorylation for the production of energy and rely on glycolysis only when their oxygen supply is limited. In contrast, cancer cells frequently utilise glycolysis even in the presence of sufficient amounts of oxygen [1, 2]. This persistence of aerobic glycolysis in many cancers is now well substantiated and considered a 'hallmark' of advanced cancers [3]. The fact that cancer cells reduce their dependence on mitochondrial oxidative phosphorylation and are more reliant on glycolysis provides a wide range of potential targets for therapy. Targeting aerobic glycolysis is a promising strategy to preferentially kill cancer cells which are dependent on this pathway and in recent years multiple glycolytic inhibitors have been developed [4–6]. However, to date only a few agents have been assessed within *in vivo* experiments and even fewer have undergone clinical trials [4–6].

The glycolytic pathway comprises a series of ten reactions (Figure 1). All of the enzymes within the glycolysis pathway potentially represent targets for anticancer treatment and inhibitors have been developed that target molecular components of this pathway [4–6]

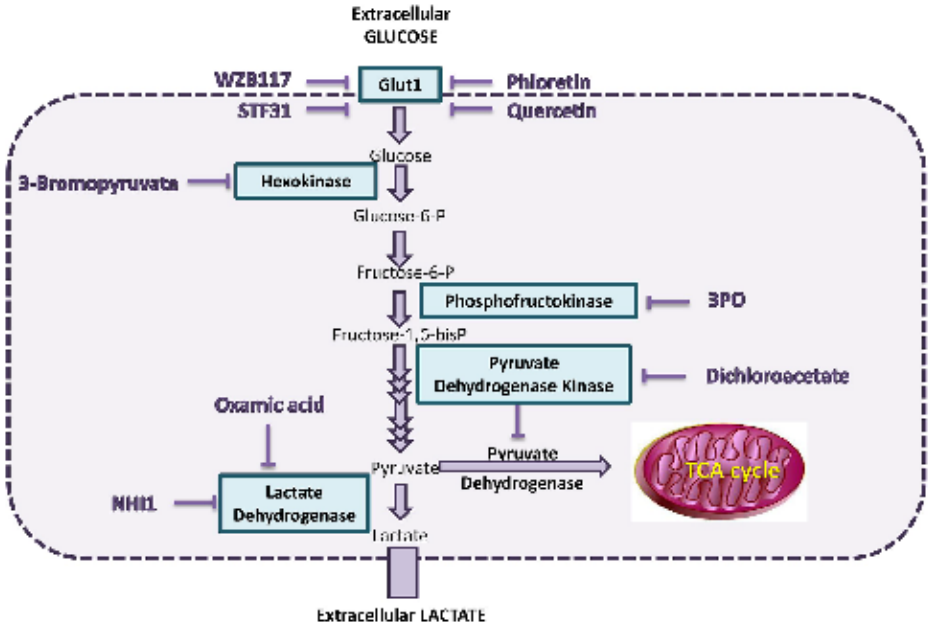

Figure 1: Scheme of selected components of the glycolysis pathway and the inhibitors studied. One molecule of glucose is catabolised to two molecules of pyruvate releasing two ATP molecules. Glucose is transported into the cell by the glucose transporter (GLUT) family of molecules and, once inside the cell, is phosphorylated to glucose-6-phosphate (G6P) by hexokinase. After conversion of G6P to fructose-6-phosphate, a second phosphate group is added to fructose-6-phosphate by 6-phosphofructo-1-kinase (PFK1). Several more enzyme reactions eventually produce pyruvate. In normal tissues under aerobic conditions, pyruvate is directed into the mitochondrion by pyruvate dehydrogenase (PDH). Under anaerobic conditions, pyruvate is converted to lactate by lactate dehydrogenase (LDH) and this is also facilitated by the increased activity of pyruvate dehydrogenase kinase 1 (PDHK1), which blocks PDH activity. In malignant cells, this conversion of pyruvate to lactate occurs even under aerobic conditions and has been denoted the Warburg effect.

(Figure 1). Inhibitors of glucose transporter 1 (GLUT1) include the flavonoids Phloretin and Quercetin [7]. Flavonoids are polyphenolic substances, abundantly distributed in plants, fruits and vegetables and are well known for their powerful anti-oxidative and anti-inflammatory effects [8]. Furthermore, they have been shown to inhibit glucose transmembrane transport and proven to have preclinical anticancer activity [7, 8]. Phloretin, mainly found in the members of the *Rosaceae* family, has been demonstrated to induce apoptosis in breast cancer cells as well as in hepatocellular carcinoma both *in vitro* and *in vivo* [9, 10]. Quercetin has been shown to induce apoptosis in breast and colon cancer cell lines [11, 12]. Recently, Chan *et al*. identified STF31, a compound which induces cell death selectively in VHL-deficient renal cell carcinoma cells by binding specifically to GLUT1 and impairing glucose uptake [13]. WZB117 is a novel specific GLUT1 inhibitor causing suppression of glucose metabolism, inhibition of cellular proliferation both *in vitro* and *in vivo* and cell-cycle arrest leading to senescence and necrosis [14].

Inhibitors of hexokinase II include 3-bromopyruvate (3BP) [15, 16]. This compound has demonstrated anticancer effects both *in vitro* and *in vivo*. It directly inhibits mitochondrial bound hexokinase-II which is up-regulated in many types of cancer. A cytotoxic inhibitory effect has been documented in many types of cancer including melanoma, glioblastoma, mesothelioma, as well as pancreatic, hepatocellular and breast carcinoma [15, 16]. 3-(3-Pyridinyl)-1-(4-pyridinyl)-2-propen-1-one](3PO) is a novel small molecule inhibitor of PFKFB3, an isozyme which is a component of fructose-2, 6-bisphosphate (Fru-2, 6-BP), an allosteric activator of PFK1 [17]. It has been shown that 3PO suppresses phosphofructokinase activity, decreases glucose uptake and induces growth inhibition in several cell lines, including Ras–transformed cells and additionally in established tumors *in vivo* [17]. PFK158, an optimised 3PO compound, is now undergoing a clinical trial [18].

Dichloroacetate (DCA) is a pyruvate analogue which inhibits pyruvate dehydrogenase kinase (PDHK1),

an enzyme which inhibits the mitochondrial pyruvate dehydrogenase (PDH). In this way it suppresses glycolysis and stimulates oxidative phosphorylation. It is reported to have antitumor activity both *in vitro*, in several types of cancer, and *in vivo* [19, 20]. DCA is now currently undergoing clinical trials [21] and while promising results were obtained in 3 of 5 glioblastoma patients treated with DCA alongside temozolomide and radiotherapy [22], combination therapy trials with platinum have so far failed to show activity against non-small cell lung cancer [23]. Furthermore, the drug is not without toxicity and at high concentrations produces peripheral neuropathy [22]. Oxamic acid is an established pyruvate analogue and a competitive lactate dehydrogenase (LDH) inhibitor. Some promising anti-proliferative effects have been documented *in vitro* using cervical adenocarcinoma and hepatocellular carcinoma cell lines [24, 25]. In 2011 Granchi *et al*. published the identification of several novel N-hydroxyindole-based (NHI) LDH Inhibitors [26]. NHI-1 (aka compound 1j) is a competitive isoform selective LDH A inhibitor [26]. It has been shown to diminish lactate production and inhibit cell proliferation in a variety of cancer cell lines [26, 27].

This study examined the effects of these inhibitors on breast and ovarian cancer cell lines by using cell proliferation, glucose and lactate assays, to assess impact on aerobic glycolysis. While there are reports of these agents showing activity against various cancer cell line models, we are not aware of any detailed comparative studies of multiple inhibitors against panels of either breast or ovarian cancer cell line models. We sought to understand why certain cell lines were more sensitive to inhibitors of these pathways.

Metformin is a biguanide widely prescribed for the treatment of type 2 diabetes mellitus. An increasing number of epidemiologic studies have associated metformin with a decreased risk of several types of cancer and improved clinical outcome in diabetic cancer patients [28]. Metformin inhibits the mitochondrial respiratory chain complex I and its anticancer effect is mainly attributed to the activation of the AMP-activated protein kinase (AMPK) resulting in decreased hepatic gluconeogenesis [28–30]. Here we hypothesized that since metformin decreases ATP production, inhibiting mitochondrial oxidative phosphorylation, a combined inhibition of the glycolytic pathway could possibly result in a complete depletion of cellular ATP and lead to increased cell death.

An additional objective of this study was to evaluate the effect of these inhibitors under varying oxygenation levels. Previous reports have revealed considerable intratumoral heterogeneity in oxygenation status, as well as increased variability among individual solid tumors [31]. For breast cancers, Vaupel *et al*. reported marked variability in oxygen levels (from 13%–0% oxygen) even when comparing tumors of the same stage, grade and histology. Furthermore, they demonstrated great heterogeneity in the oxygenation of individual tumors with hypoxic and anoxic areas distributed within the same tumor tissue [31]. Hypoxia is a well substantiated common feature of the tumor microenvironment that contributes to resistance to radiotherapy, chemotherapy and tumor relapse. The transcription factor HIF-1 (Hypoxia Inducible Factor 1) is induced by hypoxia and regulates expression of proteins that enable cells to survive hypoxia [32]. Many of the glycolytic enzymes, including all the targets selected here (GLUT1, Hexokinase II, PFKFB3, PDHK1 and LDHA), are known to be HIF1-inducible [32]. Previous studies using these inhibitors have demonstrated both reduced and increased potency in hypoxic conditions dependent on the inhibitor and cancer model, hence we were interested to ascertain their effects in breast and ovarian cancer cell line models. To date, most experimental studies have been carried out under normoxic conditions. This study investigated the sensitivity of breast cancer cells to glycolytic inhibitors at a range of oxygen levels (21% –7% –2% –0.5% O_2), the latter three representing more closely the microenvironment of clinical cancers.

RESULTS

Targeted inhibition of the glycolysis pathway in breast and ovarian cancer cell lines

The effect of inhibitors targeted against upstream components of the glycolysis pathway (GLUT1, hexokinase II, PFKFB3) and the downstream component LDH-A were compared on cell proliferation. These were also compared with an inhibitor (DCA) of PDHK1 which promotes conversion of pyruvate to acetyl-CoA. Proliferation was assessed by use of a sulphorhodamine B (SRB) assay and growth was assayed after a 5-day treatment period. Concentration response curves for the breast and ovarian cancer cell lines (Supplementary Table 1) are illustrated in Figures 2 and 3 respectively and IC_{50} values are recorded in Table 1.

Four breast cancer cell lines (MCF-7, MDA-MB-231, HBL100 and BT549) were first investigated (Figure 2). Four GLUT1 inhibitors, Phloretin, Quercetin, STF31 and WZB117, were compared. The flavonoids Phloretin and Quercetin had similar effects on the growth of the cell lines. For Phloretin, the IC_{50} values ranged between 36–135 μM while IC_{50} values ranged between 44–106 μM for Quercetin. STF31 produced a much larger differential effect between the cell lines. MCF-7 and HBL100 cells were very sensitive while BT549 cells showed resistance to the compound. The IC_{50} values varied markedly and ranged between 0.2–18 μM. In contrast, WZB117 had a very similar effect on all four cell lines with IC_{50} values ranging between 5.2–6.6 μM. 3BP which targets hexokinase II had IC_{50} values that ranged between 10–84 μM; MCF-7, HBL100 and BT549 cells had a similar response, while MDA-MB-231 cells were

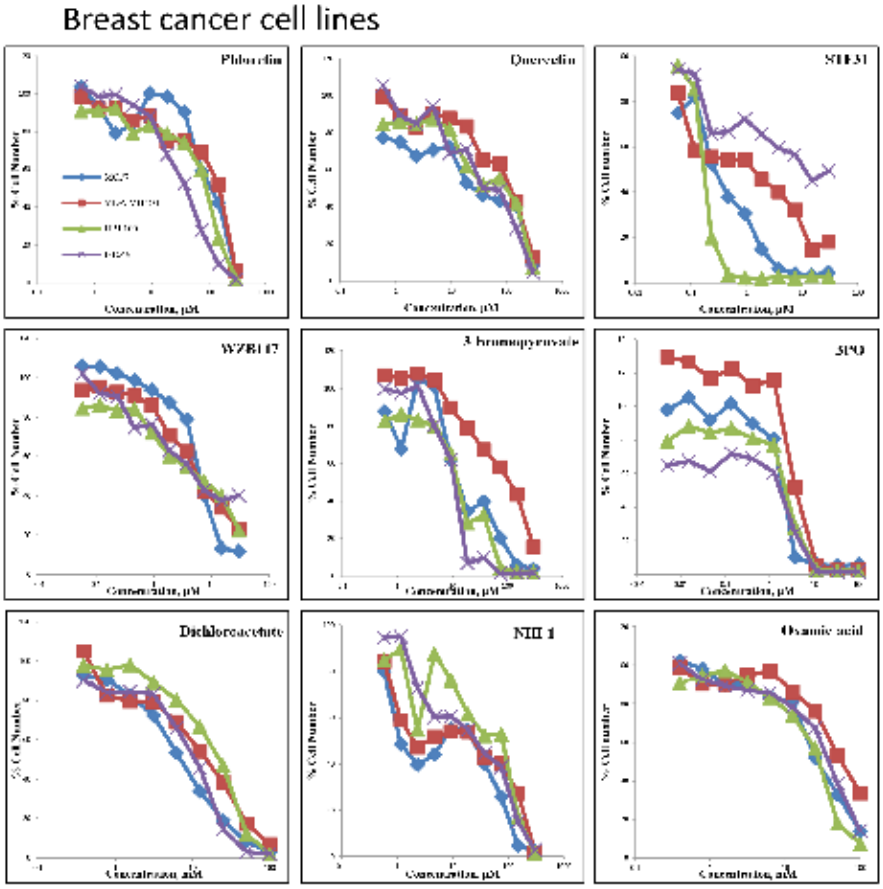

Figure 2: Concentration response curves of four breast cancer cell lines (MCF-7, MDA-MB-231, HBL100, BT549) treated with nine glycolytic inhibitors. Breast cancer cells were treated with Phloretin concentrations between 0.6–300 μM, Quercetin concentrations between 0.6–300 μM, STF31 concentrations between 0.06–30 μM, WZB117 concentrations between 0.06–30 μM, 3BP concentrations between 0.6–300 μM, 3PO concentrations between 0.005–100 μM, DCA concentrations between 0.4–100 mM, Oxamic acid concentrations between 0.2–100 mM and NHI-1 concentrations between 0.6–300 μM. An SRB assay was performed on day 5. Results shown here are in replicates of 6. Constant 0.3% DMSO concentration was used across the whole curve for Phloretin, Quercetin, STF31 and NH-1. Constant 0.3% ethanol concentration was used across the whole curve for WZB117.

more resistant. All cell lines responded in a similar way to 3PO which targets PFKFB3 having IC_{50} values between 2.1–3.8 μM. For DCA the concentrations needed were higher compared to the previous inhibitors and were in the millimolar concentration range. MCF-7 proved the most sensitive breast cancer cell line (IC_{50} 6.8 mM), while HBL100 (IC_{50} 18.9 mM) was least sensitive. Finally, for NHI-1 and Oxamic acid which target LDH-A, the IC_{50} values ranged between 27–58 mM for Oxamic acid and between 8–53 μM for NHI-1. The MDA-MB-231 cell line was found more resistant to several of the inhibitors.

For the 4 ovarian cancer cell lines, similar datasets were obtained (Figure 3). Phloretin inhibited cell proliferation with IC_{50} values ranging between 51–197 μM and Quercetin with values between 21–240 μM. STF31 and WZB117 produced increased differential effects

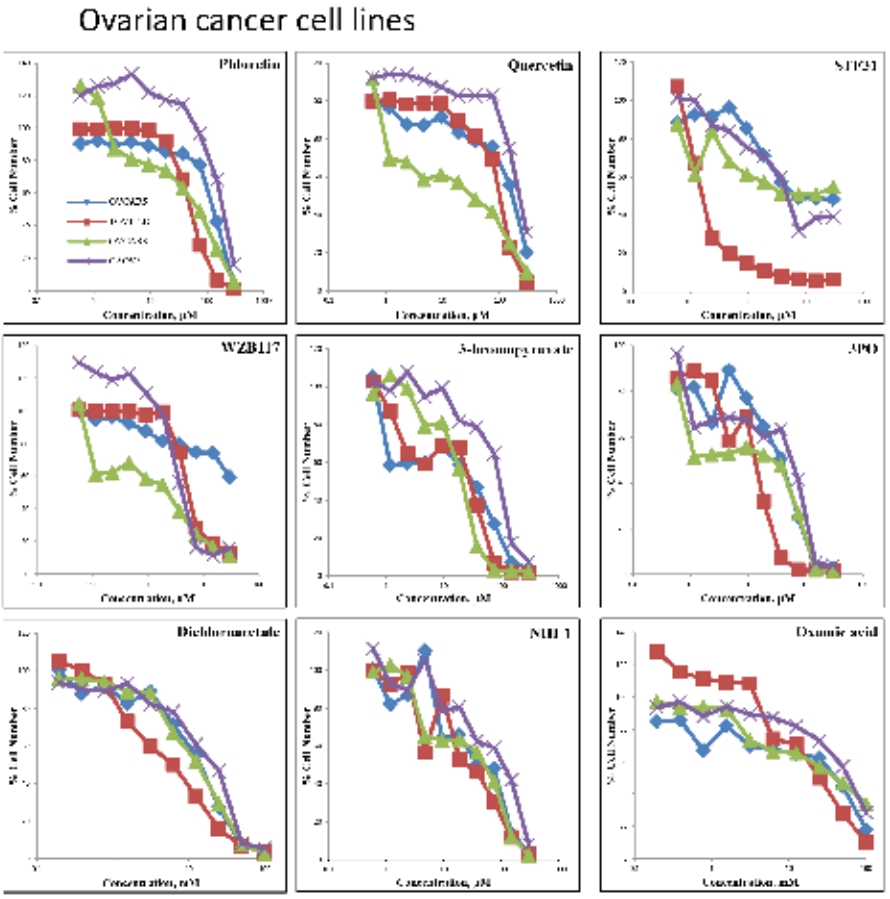

Figure 3: Concentration response curves of four ovarian cancer cell lines (OVCAR5, TOV112D, OVCAR3, CAOV3) treated with nine glycolytic inhibitors. Ovarian cancer cells were treated with Phloretin concentrations between 0.6–300 μM, Quercetin concentrations between 0.6–300 μM, STF31 concentrations between 0.06–30 μM, WZB117 concentrations between 0.06–30 μM, 3BP concentrations between 0.6–300 μM, 3PO concentrations between 0.06–30 μM, DCA concentrations between 0.4–100 mM, Oxamic acid concentrations between 0.2–100 mM and NHI-1 concentrations between 0.6–300 μM. An SRB assay was performed on day 5. Results shown here are in replicates of 6. Constant 0.3% DMSO concentration was used across the whole curve for Phloretin, Quercetin, STF31 and NH-1. Constant 0.3% ethanol concentration was used across the whole curve for WZB117

between the cell lines. The IC_{50} values ranged between 0.2 to greater than 30 μM for STF31 and between 1.4 to greater than 30 μM for WZB117. OVCAR3 cells demonstrated resistance to STF31 and OVCAR5 cells were resistant to WZB117. For 3BP, the IC_{50} values ranged between 16–84 μM with the CAOV3 cell line demonstrating most resistance to this compound. Regarding 3PO, the TOV112D cell line was the most sensitive with IC_{50} value almost 1.2 μM while CAOV3 was least sensitive, with an IC_{50} 5 times higher. DCA and Oxamic acid again required much greater (millimolar) concentrations compared to the other compounds. In both cases, TOV112D cell line showed the lowest IC_{50} values (5.5 mM for DCA and 24 mM for Oxamic acid) while CAOV3 had the highest (20 mM for DCA and 59 mM for Oxamic acid). Finally, for NHI-1 the IC_{50} values ranged between 28–91 μM.

Table 1: Summary of the IC_{50} concentrations obtained from four breast and four ovarian cancer cell lines when treated with the indicated glycolytic inhibitors for 5 days

	MCF-7	MDA-MB-231	HBL100	BT549	OVCAR5	TOV112D	OVCAR3	CAOV3
Phloretin (μM)	122	135	69	36	119	51	54	197
Quercetin (μM)	44	105	76	44	154	94	21	240
STF31 (μM)	0.31	0.81	0.17	18	7.4	0.15	>30	4.9
WZB117 (μM)	6.4	6.3	5.2	6.6	>30	5.9	1.4	4.3
Bromopyruvate (μM)	18	84	15	10	20	16	20	84
3PO (μM)	2.1	3.8	2.7	2.3	3.9	1.2	2.8	5.8
Dichloroacetate (mM)	6.8	13	19	9.1	14	5.5	13	20
Oxamic acid (mM)	28	58	27	39	38	24	34	59
NHI-1 (μM)	8	20	53	22	45	28	35	91

Glucose uptake and lactate production are inhibited by all of the studied inhibitors

The effects of the above inhibitors were next examined on glucose uptake and lactate production in HBL100 and MCF-7 cells (Figure 4). Glucose concentrations remaining in the media and extracellular lactate production into the medium after a 24 h treatment with the indicated compound are shown. The range of concentrations used for each compound was based on the corresponding IC_{50} values, derived from the SRB

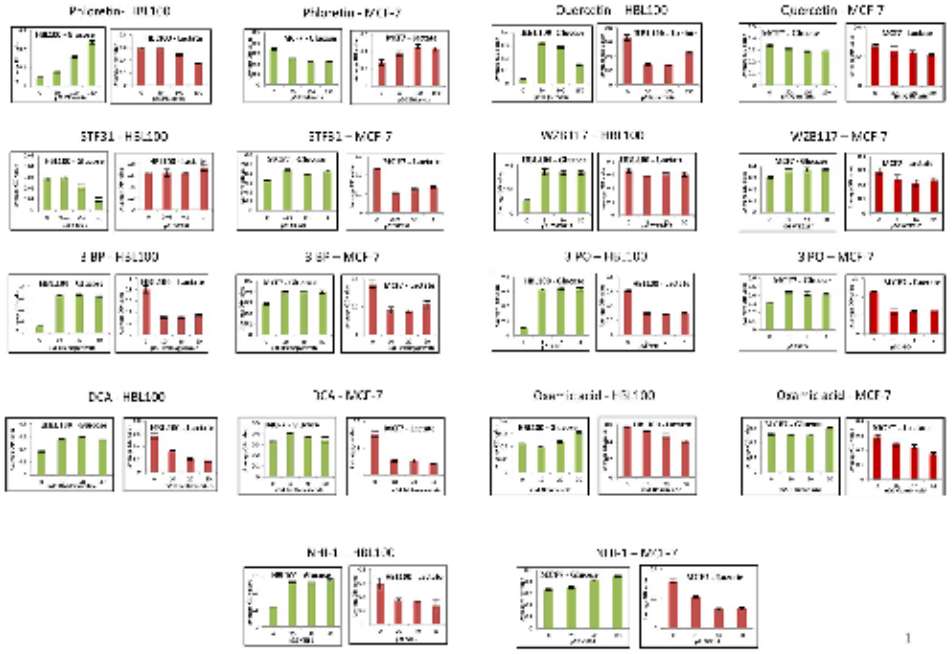

Figure 4: Extracellular glucose remaining in the media and extracellular lactate secreted against increasing concentration of the nine glycolytic inhibitors after a 24 h treatment of MCF-7 or HBL100 cells. Results are reported as the mean of three repeats and error bars represent standard deviations.

assay, for each specific cell line. Both sets of measurements were conducted on the same day from the same sample.

All the inhibitors tested proved effective in blocking glycolysis in at least one of the two cell lines tested (Figure 4). Increasing concentrations of Phloretin caused an increase in the glucose remaining in the media while lactate production decreased following the same pattern. Regarding the other three glucose transport inhibitors Quercetin, STF31 and WZB117, even the lowest concentration used produced a maximal effect causing accumulation of glucose and depletion of lactate in the culture media. 3BP, 3PO and DCA were also effective in inhibiting glycolysis. Low concentrations of each compound caused a large increase in the glucose accumulating in the media and a corresponding decline in the secreted lactate. The inhibition of glycolysis hit a plateau with treatment of 10 μM 3BP, 10 μM 3PO or 10 mM DCA and no apparent additional effect was detected with increasing concentrations. The lactate dehydrogenase inhibitors likewise suppressed glycolysis. Following treatment with NHI-1 and Oxamic acid, cells demonstrated a modest increase in glucose and a more profound depletion of lactate in their culture media.

Glycolytic inhibitors induced apoptosis

To investigate whether the growth inhibitory effect of these compounds was associated with induction of apoptotic cell death, flow cytometric analysis was performed. MCF-7 cells were treated with 9 glycolytic inhibitors for 48 h, stained with FITC-conjugated Annexin V and PI and analysed using flow cytometry. Cells were separated into four different groups, the lower left quadrant represents intact viable cells (Annexin negative and PI negative), the upper left quadrant represents early apoptotic cells (Annexin positive and PI negative), the upper right quadrant represents late apoptotic cells (Annexin positive and PI positive) and the lower right quadrant represents necrotic cells (Annexin negative and PI positive). Cells stained with Annexin-FITC were collectively considered as apoptotic cells (upper region). As shown in Figure 5A there

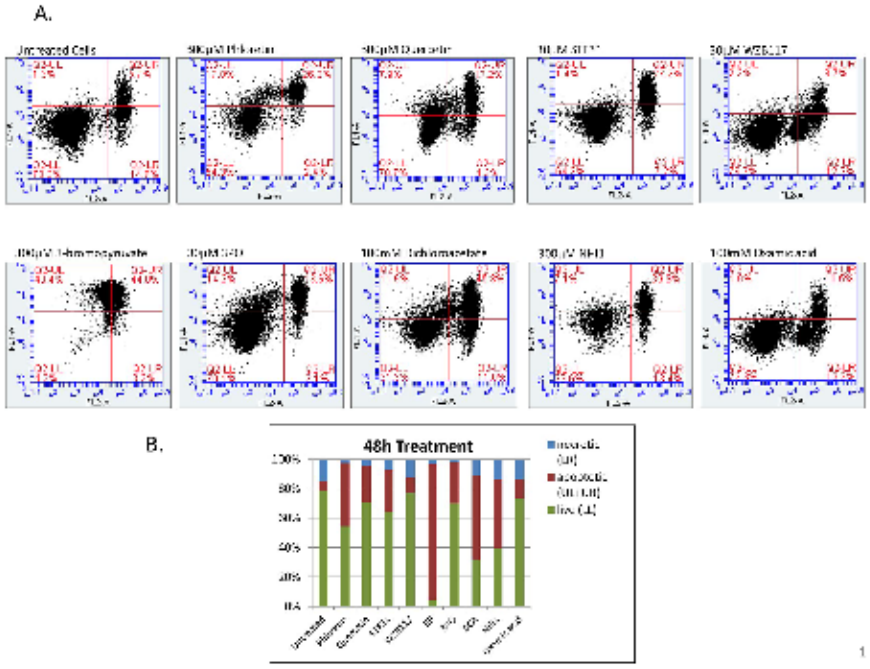

Figure 5: A. Two- dimensional scatter plots of Annexin V (FL1) vs PI (FL2) generated from flow cytometry analysis of MCF-7 cells when treated with 9 glycolytic inhibitors for 48 h. After treatment cells were harvested, washed with cold PBS and resuspended in 1X Binding Buffer. 5 μl of FITC Annexin and 5 μl of PI were added to the suspension and cells were incubated for 15min in the dark prior to analysis with the BD Accuri C6. The numbers in the quadrants of each plot indicate the percentage of cells in this region. Cells in LL represent intact viable cells (Annexin negative and PI negative), in UL represent early apoptotic cells (Annexin positive and PI negative), in UR represent late apoptotic cells (Annexin positive and PI positive) and in LL represent necrotic cells (Annexin negative and PI positive). B. Percentage of apoptotic, necrotic and live cells after a 48 h treatment with 300 μM Phloretin, 300 μM Quercetin, 30 μM STF31, 30 μM WZB117, 300 μM 3BP,30 μm 3PO, 100 mM DCA, 300 μM NHI-1 and 100mM Oxamic acid compared to untreated cells.

is an induction of both early and late phases of apoptosis after treatment with the glycolytic inhibitors compared to untreated cells. Untreated cells showed 7% apoptosis (Annexin positive) whereas for cells treated with 300 μM Phloretin the percentage of apoptotic cells increased to 43%, with 300 μM Quercetin to 25%, with 30 μM STF31 to 29%, with 30 μM WZB117 to 11%, with 300 μM 3BP to 92%, with 30 μM 3PO to 28%, with 100 mM DCA to 58%, with 300 μM NHI-1 to 47% and with 100 mM Oxamic acid to 13% (Figure 5B).

Correlation analysis of IC_{50} concentrations and cell proliferation rate

The association of IC_{50} values against the panel of 8 cell lines was assessed for each pair of drugs indicating that sensitivity to 7 of these inhibitors correlated with each other (Supplementary Table 2). The correlation heatmap in Figure 6A illustrated that 7 inhibitors (Phloretin, Quercetin, 3BP, 3PO, DCA, NHI-1 and Oxamic acid) had IC_{50} concentrations that gave high Pearson R correlation values when compared to each other. This is consistent with these agents sharing a common mechanism of action targeting the same pathway. STF31 and WZB117 did not significantly correlate with any of the other agents. The expression levels of GLUT1, hexokinase II, PFKFB3, PDHK1 and LDHA were examined in the cell line panel (Supplementary Figure 1). No significant correlation between the expression of the targets in the eight cell lines and their sensitivity to the inhibitors was detected

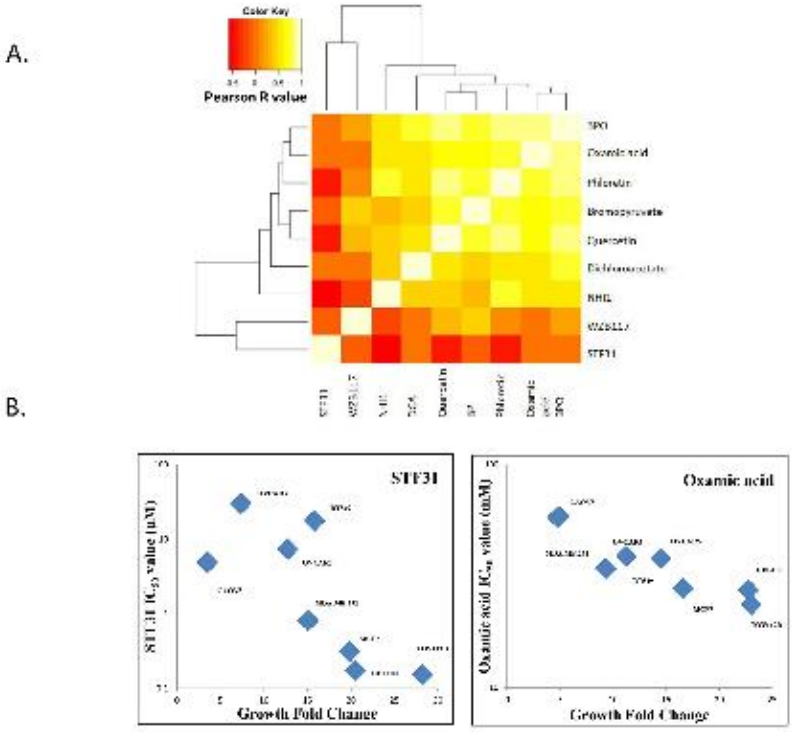

Figure 6: A. Correlation heat-map demonstrating that seven glycolytic inhibitors had IC_{50} concentrations that correlated with each other in the panel of cell lines. This is consistent with a shared mechanism of action. Dark orange colours indicate negative Pearson R correlation values while bright white colours indicate positive Pearson R correlation values. B. STF31 and Oxamic acid IC_{50} values of the panel of four breast and four ovarian cancer cell lines plotted against the growth fold change of the respective cell line. Non-parametric Spearman correlation r = -0.7619 with two-tailed *P* value 0.0368 for STF31; considered significant. Non-parametric Spearman correlation r = -0.9048 with two-tailed *P* value 0.0046 for Oxamic acid; considered very significant.

(data not shown). Sensitivity to STF31 and Oxamic acid was found to correlate significantly with the proliferation rate of the cell lines, giving *p* values of 0.0368 and 0.0046 respectively. The fastest growing cell lines were more sensitive to these compounds while the slowest growing cell lines presented greater resistance (Figure 6B).

Combination of metformin and glycolytic inhibitors synergistically inhibited cancer cell growth of a triple negative breast cancer cell line

The interaction between glycolytic inhibitors and the antidiabetic drug metformin was examined. A range of different concentrations of two glycolytic inhibitors, STF31 and Oxamic acid, was used in combination with a constant fixed concentration of metformin and incubation lasted for 72 h. Metformin enhanced the potency of both STF31 and Oxamic acid to inhibit cancer cell proliferation compared to the effect of these drugs individually (Figure 7A). To evaluate the efficacy of the combinations, data were analysed using the Calcusyn Software and Combination Index (CI) values were generated (Tables 2a, 2b). Examples of synergistic combinations are depicted in Figure 7B. For example, 1.9 μM of STF31 alone reduced the percentage of cell number to 78% and 3mM of metformin to 87% while the combination of both drugs reduced the cell number to 37% compared to untreated cells. For this combination a CI value equal to 0.182 is generated which is characterised as

A.

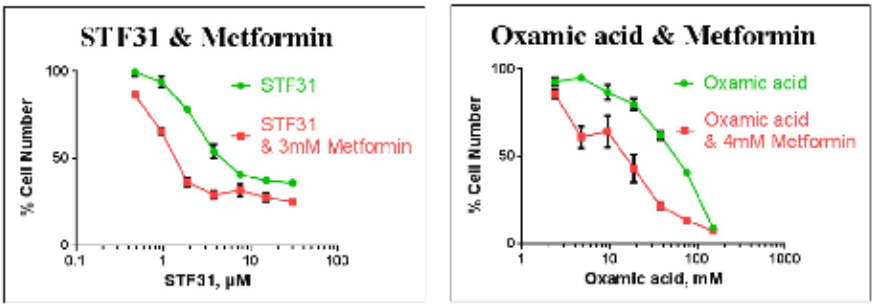

B.

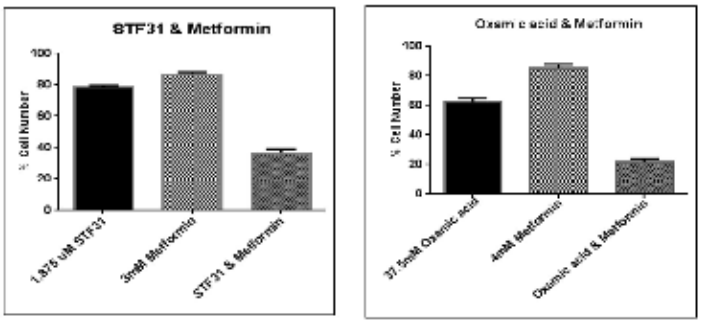

Figure 7: A. Concentration response curves of drug interaction studiesMDA-MB-231 cells were treated with STF31 concentrations between 0.5–30 μM and Oxamic acid concentrations between 2.3–150 mM alone or in combination with a constant concentration of 3mM or 4 mM metformin respectively. An SRB assay was performed on day 3. Error bars shown here represent SD ($n = 6$). B. Effect of 2 μM STF31 alone or in combination with 3 mM metformin and of 38 mM Oxamic acid alone or in combination with 4 mM metformin on cell viability. Both combinations are characterised synergistic based on their CI values generated using the Calcusyn Software. Error bars shown here represent SD ($n = 6$).

Table 2: Summary of drug interaction studies

a.

STF31 (μM)	Metformin (μM)	Fa	CI
0.46875	3000	0.134506	**1.183**
0.9375	3000	0.343076	**0.36**
1.875	3000	0.63395	**0.182**
3.75	3000	0.706688	**0.251**
7.5	3000	0.68129	**0.522**
15	3000	0.721799	**0.882**
30	3000	0.747518	**1.585**

b.

Oxamic acid (mM)	Metformin (mM)	Fa	CI
2.34375	4	0.144005	**1.683**
4.6875	4	0.389971	**0.467**
9.375	4	0.356693	**0.73**
18.75	4	0.568973	**0.483**
37.5	4	0.783404	**0.336**
75	4	0.864651	**0.382**
150	4	0.926606	**0.411**

Tables show concentration range of STF31 (2a) and Oxamic acid (2b) used with a constant concentration of Metformin. FA-fraction affected represents the growth inhibition for each tested combination and CI represents the combination index values generated through Calcusyn. Values lower than 0.8 indicate synergism, values between 0.8 and 1.2 indicate additivity and values higher than 1.2 indicate antagonism

strong synergy. Similarly, 37.5 mM of Oxamic acid reduced cell number to 62% and 4 mM of metformin to 85% while their combination reduced the cell number to 22%. The CI value generated for this combination was 0.336 characterised as synergy.

Growth inhibition at varying oxygen tensions

We next sought to examine the effect of the oxygen level on sensitivity to these glycolytic inhibitors. For this purpose two breast cancer cell lines were selected, the ER positive, luminal A MCF-7 and the basal B, triple negative MDA-MB-231 lines. The breast cancer cells were adapted to the different oxygen conditions, before being treated with eight of the glycolytic inhibitors. The SRB assay was performed after a five day treatment. In Figure 8 is depicted the percentage of cell number for the two cell lines against increasing concentration of each of the eight compounds under four different oxygen conditions 21% O_2, 7% O_2, 2% O_2, 0.5% O_2. Table 3 presents the corresponding IC_{50} values.

Both cell lines were sensitive to all the inhibitors in hypoxic conditions. The most striking observation was the increase presented in the IC_{50} values between 21% O_2 and 7% O_2. Both cell lines when treated with the eight inhibitors under 7% O_2 followed the same pattern and their IC_{50} values were increased from 1.5 fold (MDA-MB-231 cells treated with STF31 – Figure 8b) up to 9 fold (MDA-MB-231 cells treated with Oxamic acid – Figure 8g) with an average of 4 fold. (Table 3)

The response of the breast cancer cell lines at the lower oxygen levels (2% O_2 and 0.5% O_2) differed between the compounds. In some cases, cells became even more resistant to the compounds increasing further their IC_{50} value (e.g. MDA-MB-231 cells treated with Oxamic acid – Figure 8g), or presented a modest decrease (e.g. MDA-MB-231 cells treated with DCA – Figure 8f). In the majority of the treatments, response between the three lower levels was similar. Both cell lines were more resistant to the whole panel of glycolytic inhibitors under any of the lower oxygen levels tested compared to 21% O_2 conditions (Table 3).

When drug IC_{50} was correlated with growth rate under the range of differing O_2 concentrations for both cell lines, there was in general a significant inverse association between higher growth rates and lower IC_{50} with increasing oxygen level (Supplementary Table 3).

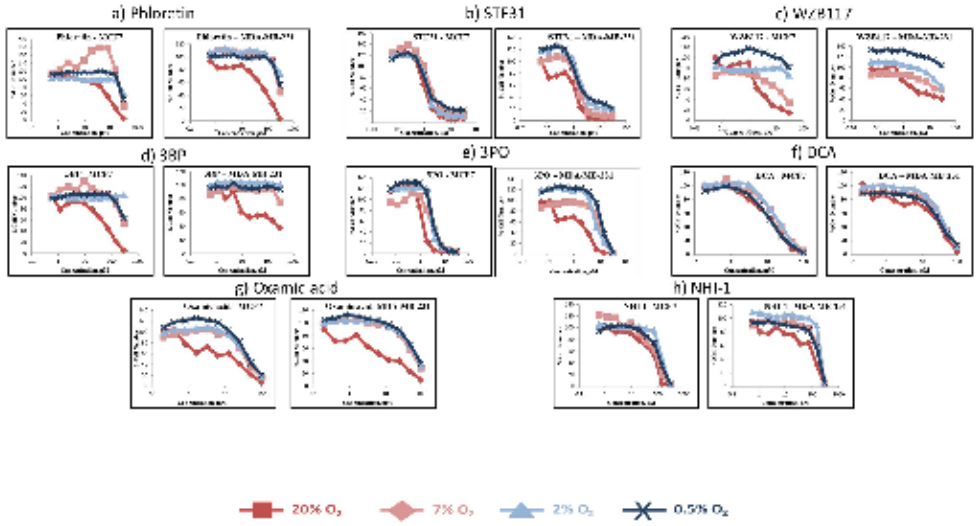

Figure 8: Concentration response curves of two breast cancer cell lines (MCF-7, MDA-MB-231) treated with eight glycolytic inhibitors under four different oxygen conditions (21% O_2, 7% O_2, 2% O_2, 0.5% O_2). Breast cancer cells were treated with STF31 concentrations between 0.06–30 μM (Figure 8a), WZB117 concentrations between 0.06–30 μM (Figure 8b), Phloretin concentrations between 0.6–300 μM (Figure 8c), 3BP concentrations between 0.6–300 μM (Figure 8d), 3PO concentrations between 0.06–30 μM (Figure 8e), DCA concentrations between 0.2–100 mM (Figure 8f), Oxamic acid concentrations between 0.2–100 mM (Figure 8g) and NHI-1 concentrations between 0.6–300 μM (Figure 8h). An SRB assay was performed on day 5. Results shown here are in replicates of 6. Constant 0.3% DMSO concentration was used across the whole curve in Figures 8a, 8c, 8e and 8h. Constant 0.3% Ethanol concentration was used across the whole curve in Figure 8b.

Table 3: Summary of the IC_{50} concentrations presented from two breast cancer cell lines (MCF-7, MDA-MB-231) when treated with the indicated glycolytic inhibitors for 5 days under four different oxygen conditions (21% O_2, 7% O_2, 2% O_2, and 0.5% O_2)

IC_{50}	MCF-7				MDA-MB-231			
	21% O_2	7% O_2	2% O_2	0.5% O_2	21% O_2	7% O_2	2% O_2	0.5% O_2
STF31 (μM)	1.284	2.277	1.445	1.613	1.243	1.803	2.367	2.162
WZB117 (μM)	2.3	16.419	>30	>30	4.079	N/A	>30	N/A
Phloretin (μM)	90.016	295.224	>300	>300	69.644	289.107	>300	>300
BP (μM)	62.659	>300	N/A	>300	38.989	>300	N/A	>300
3PO (μM)	1.34	3.759	3.481	3.673	1.486	11.232	8.574	12.9
DCA (mM)	13.043	18.91	19.558	12.569	23.3	38.904	36.967	31.079
NHI1 (μM)	61.778	80.026	150.111	111.495	93.628	190.059	227.572	174.091
Oxamic acid(mM)	10.4	39.368	47.089	49.478	6.944	60.431	66.192	73.993

Modulation of target expression levels under different O_2 levels

We speculated that decreased sensitivity to the glycolytic inhibitors in hypoxic conditions could be attributed to up-regulation of the respective target. In an attempt to understand the increased resistance to the inhibitors under lower levels of oxygen the expression of the five glycolytic targets of interest was examined in these conditions.

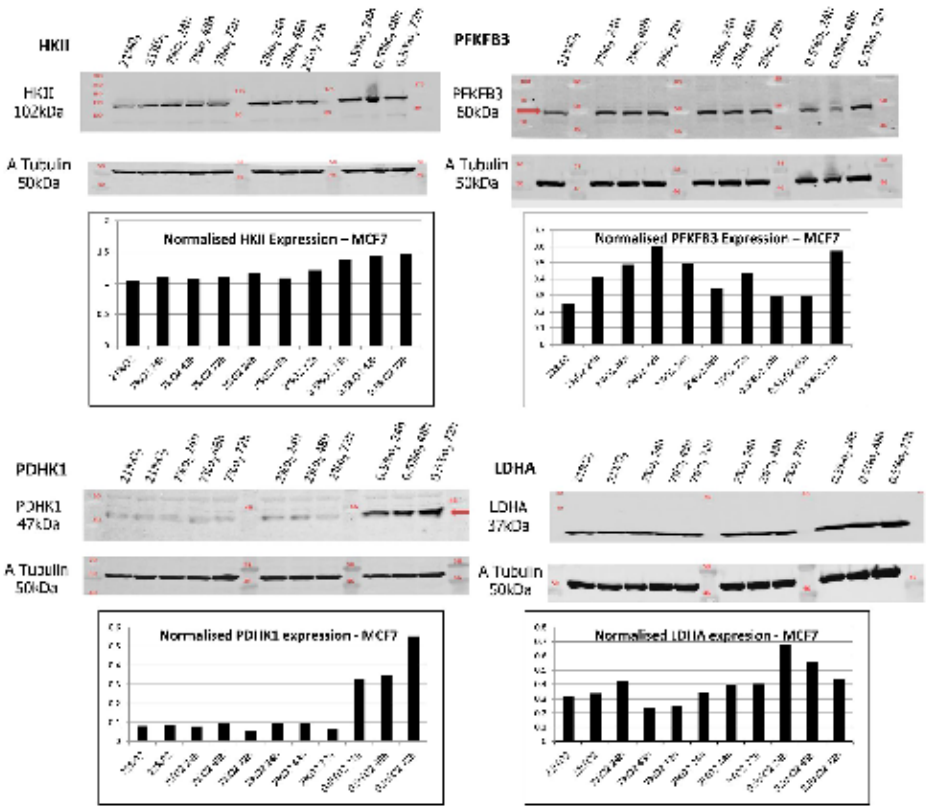

Figure 9: HKII, PFKFB3, PDHK1 and LDHA expression were examined in MCF-7 cells at different O_2 levels. Lysates were taken from cells cultured in 0.5% O_2, 2% O_2 and 7% O_2 for different periods of time, 24 h, 48 h and 72 h. Samples are presented as follows: 21% O_2, 21% O_2, 7% O_2 24 h, 7% O_2 48 h, 7% O_2 72 h, 2% O_2 24 h, 2% O_2 48 h, 2% O_2 72 h, 0.5% O_2 24 h, 0.5% O_2 48 h and 0.5% O_2 72 h. Tubulin expression was examined in the same samples as a loading control. Densitometric analysis of HKII, PFKFB3, PDHK1 and LDHA expression was performed using the Odyssey Infrared Imaging System software (Licor).

Expression of the GLUT1 transporter as well as of the Hexokinase II, PFKFB3, PDHK1 and LDHA enzymes were examined in MCF-7 and MDA-MB-231 cells cultured in 0.5% O_2, 2% O_2 as well as 7% O_2 for different periods of time, 24 h, 48 h and 72 h and compared with expression at 21% O_2 (Figure 9 - Supplementary Figures 2, 3). PFKFB3 and PDHK1 were up-regulated under hypoxic conditions in both cancer cell lines, while Hexokinase II and LDHA were up-regulated only in MCF-7 cells at 0.5% O_2.

DISCUSSION

The purpose of this study was to evaluate the effects of a series of inhibitors targeted against multiple points of the glycolysis pathway in breast and ovarian cancer cell line models. All inhibitors induced apoptosis and blocked glycolysis irrespective of their target and point of action in the pathway. The majority of these compounds had IC_{50} concentrations that correlated significantly with each other consistent with sharing a common mechanism of action. A second objective was to examine the effect of selected glycolytic inhibitors in combination with the antidiabetic drug metformin. The third aim of the study was to investigate the impact of varying levels of O_2 on inhibitor efficacy - increasing concentrations of oxygen resulted in more rapid cell growth rates and increased potency of the inhibitors.

This study provides confirmation that all 9 of these inhibitors block the glycolytic pathway. All the tested

inhibitors caused glucose accumulation in the media of cultured cells combined with a decline in the production of lactate, the final product of glycolysis (Figure 4). It is noteworthy that even when targeting the final step of the pathway an effect on the uptake of glucose can be observed. This is attributed to the tight allosteric regulation of the key glycolytic enzymes [33]. All the tested compounds inhibited cell proliferation of both breast and ovarian cancer cells, in a concentration-dependent manner at concentrations associated with glycolytic inhibition (Figures 2, 3). Each of the inhibitors presented a different potential in attenuating cell proliferation. More recently developed compounds (STF31, WZB117, 3PO and NHI-1) proved more potent and inhibited tumor cell growth at lower concentrations. The compounds Phloretin, 3PO, DCA, NHI1 and 3BP had clear cytotoxic effects on the majority of cell lines while Quercetin, WZB117 and Oxamic acid showed cytostatic effects (judged based on the comparison of the cell number on day 0 –the day of treatment- and day 5 of treatment; data not shown). The breast and ovarian cancer cell line models studied demonstrated similar sensitivities to these agents.

GLUT1 facilitates basal glucose transport across the plasma membrane. In breast cancer, increased expression of GLUT1 has been reported to be associated with high grade tumors, basal-like subtype, high proliferative index as measured by Ki-67 and poor survival [34–37]. Similarly, an association between high GLUT1 expression and poor outcome has been observed for ovarian cancer [38] suggesting GLUT1 might be a promising target for therapeutic inhibition. The novel GLUT1 inhibitors, STF31 and WZB117 proved inhibitory at lower concentrations when compared to the flavonoids Phloretin and Quercetin. STF31 demonstrated a marked differential effect between the cell lines. It caused a potent cytotoxic effect in the HBL100 breast and TOV112D ovarian cell lines (with an IC_{50} as low as 0.1 μM) whereas the BT549 breast and OVCAR3 ovarian cancer cell lines were found to be highly resistant to the compound. Its activity was first reported in renal cell cancer cell line models [13] and we are unaware of antitumor data being reported in breast or ovarian cancer systems. While the breast cancer cell lines exhibited a similar response to WZB117, with almost identical IC_{50} values, ovarian cancer cell lines showed a significant variation in their response. OVCAR3 cells showed increased sensitivity (IC_{50} 1.4 μM) while OVCAR5 cells were found resistant. In the only published report to date of WZB117, the IC_{50} in MCF-7 cells (approximately 10 μM) was similar to the value (6.4 μM) observed here [14]. (Table 1).

Hexokinase II catalyses the ATP-dependent phosphorylation of glucose. Hexokinase II (HKII), the mitochondrial-bound isozyme, is associated with poor outcome in both breast [39] and ovarian cancers [40]. 3BP proved a potent compound causing a concentration-dependent reduction in the number of viable cancer cells. Breast and ovarian cancer cells presented similar sensitivity. The anti-glycolytic effect of 3BP has previously been demonstrated by decreased FDG uptake in a rat breast cancer model [41]. 3BP has also been shown to have possible value in targeting ovarian cancer tumor initiating cells [42].

PFKFB3 catalyses the ATP-dependent phosphorylation of fructose-6-phosphate and produces Fru-2, 6-BP an allosteric activator of PFK1. It is more highly expressed in breast and ovarian cancers relative to normal tissue [42]. 3PO, a PFKFB3 inhibitor, proved a potent inhibitor in these cell lines. Breast cancer cells lines responded in a similar way while the ovarian cancer cell lines exhibited greater variation in their response. 3PO has already demonstrated promising activity in an MDA-MB-231 breast cancer xenograft model and since these other breast cancer cell lines tested here have increased sensitivity, while the ovarian cancer cell lines have similar sensitivities to the MDA-MB-231 cell line, this would suggest that *in vivo* activity might be obtained in further models [17].

PDHK1 phosphorylates and inactivates PDH and in this way prevents pyruvate from entering the mitochondrial TCA cycle. DCA effectively attenuated cell proliferation in millimolar concentrations in these cell lines and IC_{50} values varied between 5 and 20 mM (Table 1). While it is feasible to achieve concentrations of 1mM in patients [23], these concentrations are insufficient for single agent consideration and combination approaches which require lower concentrations of inhibitors are more likely to be beneficial.

The final target of the glycolytic pathway examined was LDH, a tetramer of A and B subunits that catalyses the reduction of pyruvate to lactate coupled with NADH oxidation. NHI-1 was found to be a much more potent inhibitor than Oxamic acid. Breast and ovarian cancer cells had a similar response to Oxamic acid (Table 1). NHI-1 has been shown to produce synergistic activity when used in combination with gemcitabine in pancreatic cancer cell line models [27] and it may be that combination with cytotoxic drugs would be worth exploring within breast and ovarian cancer models.

The mechanism of action of these inhibitors was also investigated using flow cytometric analysis of treated cells stained with FITC-conjugated Annexin V and Propidium Iodide. Annexin V is a calcium dependent protein that binds to phosphatidylserine when exposed to the extracellular membrane of apoptotic cells. The viability dye PI is excluded from the intact cell membrane of viable cells. With this staining it is possible to distinguish between early apoptotic (Annexin V positive), late apoptotic (Annexin V and PI positive) and necrotic cells (PI positive). Evidence was obtained that all 9 of these inhibitors induce apoptosis. After a 48 h treatment all of them caused an induction of both early and late apoptosis (Figures 5a, 5b), consistent with targeting a common pathway.

The expression levels of the glycolytic targets did not vary markedly in this panel of cell lines (Supplementary Figure 1) and no clear association between expression level and inhibitor response was apparent. We observed though that sensitivity to STF31 (GLUT1 inhibitor) and Oxamic acid (LDHA inhibitor) correlated significantly with the proliferation rate of the cell lines (Figure 6B). The differential effect of these compounds to the various cell lines can be explained by the difference in their growth rate. The most rapidly growing cell lines were found to be more sensitive to these compounds and these are likely to be more dependent on glycolysis for the production of energy and the metabolic intermediates needed for the biosynthesis of macromolecules and for that reason more sensitive to the glycolytic inhibitors.

Seven inhibitors demonstrated a correlation in their IC_{50} values in the panel of cell lines and these were Phloretin, Quercetin, 3BP, 3PO, DCA, NHI-1 and Oxamic acid. This would be consistent with their possessing a common mechanism of action i.e. inhibition of the glycolysis pathway. The two remaining inhibitors, STF31 and WZB117, did not correlate and it is feasible that inhibition of other (non-glycolytic pathway) targets may be responsible for their actions. Certainly, for STF31, a recent report has indicated that it can also inhibit nicotinamide phosphoribosyltransferase (NAMPT) which may contribute to its growth inhibitory activity [43].

Recently, there has been an increasing interest in the anti-proliferative effects of metformin. This widely prescribed antidiabetic drug, because of its low toxicity profile and its established efficacy to target metabolism, has attracted a great deal of attention. A considerable volume of literature has associated metformin with a decreased cancer risk and in addition metformin has been shown in many cases to increase sensitivity to chemotherapy [28, 29]. Currently metformin is undergoing several clinical trials in various cancer types as monotherapy or in combination with other drugs [28]. It has been shown to enhance cisplatin and paclitaxel efficacy in endometrial cancer cells [44] as well as cisplatin efficacy in ovarian cancer cells *in vivo* inhibiting also metastasis in the lung [45]. In another study Iliopoulos *et al*. showed a synergistic effect between metformin and Doxorubicin in a xenograft model using prostate and lung cancer cells [46]. Regarding glycolytic inhibitors two separate research groups, Sahra *et al*. in 2010 and Cheong *et al*. in 2011, demonstrated a synergistic effect between metformin and 2-deoxyglucose (2DG) in prostate cancer cells and mouse xenograft models respectively [47, 48]. Moreover in 2014 Choi *et al*. reported that DCA enhanced metformin potency in inducing cell death in HeLa cells [49].

Encouraged by promising evidence in previous studies we hypothesised that targeting two energy pathways simultaneously; the glycolytic pathway and mitochondrial oxidative phosphorylation, could result in greater energy depletion and enhance cell death of cancer cells. The selected cell line for combination experiments was the triple negative MDA-MB-231. These tumors are considered aggressive and invasive and have limited treatment options [50]. In addition this cell line lacks the functional tumor suppressor gene LKB1 [51]. This is an upstream kinase responsible for the activation of AMPK and is considered important for metformin's antitumor effect [29]. Our results are in agreement with findings from Zordoky *et al*. which showed that MDA-MB-231 cells are sensitive to metformin even though they are LKB1 deficient [51]. In terms of the culture conditions it should be mentioned that these experiments were contacted in 5.56 mM glucose medium equivalent to physiological serum glucose levels, taking into consideration findings from previous studies indicating dependence of metformin's action on glucose availability [49, 51]. We provide evidence of a synergistic interaction between STF31 and metformin as well as between Oxamic acid and metformin (Figure 7A). The CI values generated for both combinations were lower than 0.8 and indicate synergy. The concentrations of 3 and 4 mM Metformin tested are relatively high but millimolar concentrations of the drug have been demonstrated to be achievable *in vivo* as the drug, being stable and not metabolized, can accumulate in tissues at much higher concentrations than in the blood [52]. These findings suggest a potential strategy for triple negative breast cancer treatment.

A key objective of this study was to investigate the sensitivity to the glycolytic inhibitors under varying levels of hypoxia. A published report of a series of normal and malignant breast tissues had indicated a median oxygen level of 8.6% O_2 in normal breast tissue ($n = 16$) compared to a median value of 4% O_2 in a series ($n = 15$) of malignant breast cancers [31]. Multiple measurements obtained within individual breast cancers demonstrated values varying between 0 and 13% O_2 indicating the diversity and mixture of differentially oxygenated populations that co-exist within individual tumors [31]. To test sensitivity, two representative breast cancer cell lines were selected. Dependence on glycolysis was examined over a range of oxygen levels varying from 21% to 0.5% O_2 and both cell lines examined were more sensitive to all glycolytic inhibitors at 21% O_2 conditions.

Previous studies investigating these inhibitors in normoxic and hypoxic conditions against other cancer cell lines have demonstrated widely contrasting results with some studies suggesting enhanced activity under normoxic conditions, other studies suggesting enhanced activity under hypoxic conditions and the majority of studies showing equivalent activity or minimally changed activity under both normoxic and hypoxic conditions [53–59]. For example, Phloretin is equally effective under normoxic and hypoxic conditions against the SW620 colon and K562 leukemia cell lines [53] while WZB117 is more effective against hypoxic than normoxic cells [14]. 3BP has previously been shown to be minimally more

cytotoxic under hypoxic conditions [54–56] than normoxic conditions although the effects in these studies were very modest and are not dissimilar to other studies which indicate no difference between normoxia and hypoxia [57]. The LDH inhibitor NHI-1 is more effective in hypoxic than normoxic systems [27]. In contrast, several studies have shown that DCA is more cytotoxic in normoxic than hypoxic conditions [58, 59].

Increased dependency under hypoxic conditions might arise through up-regulation of the drug target providing a greater stimulus in cells hence its blockade might be more effective. Equally, increased drug target might also require more inhibitor to block its efficacy and furthermore other pathway components will also be up-regulated by hypoxia, requiring more drug to produce inhibition compared to normoxic conditions. The modulation of the drug targets was examined under these varying oxygen conditions and of the five targets examined, PFKFB3 and PDHK1 were up-regulated under hypoxic conditions in both cancer cell lines, while Hexokinase II and LDHA were up-regulated only in MCDF-7 cells at 0.5% O_2. Therefore relative resistance to the compounds at low O_2 levels could be attributed at least in part to increased expression of the targets.

Another factor that should be taken into consideration is that cells grow more slowly in low O_2 concentration and this might contribute to the decreased sensitivity to the compounds. There were significant associations for most of the compounds between growth rate and drug potency (i.e. IC_{50}) across the panel of cell lines (Supplementary Table 3).

Together, these data indicate that inhibition of glycolysis is associated with growth inhibition in these breast and ovarian cancer cell lines. Combination of glycolytic inhibitors with metformin is proposed as a promising strategy for triple negative breast cancer treatment. Variation in oxygen levels between 0.5 and 7% has a relatively small effect on the efficacy of the inhibitors however these compounds are, in general, more effective at 21% O_2 which appears to correlate with an increased growth rate. We are currently assessing the effects of these inhibitors in combination with various cytotoxic and targeted therapies to assess how these might integrate with established therapies.

MATERIALS AND METHODS

Cell culture and inhibitors

A panel of eight cell lines was used; four breast cancer (MCF-7, MDA-MB-231, HBL100 and BT549) and four ovarian cancer cell lines (OVCAR5, TOV112D, OVCAR3, CAOV3). Key features of the cell lines are summarised in Supplementary Table 1. All cell lines were authenticated utilizing Short Tandem Repeat (STR) profiling. They were maintained in Dulbecco's Modified Eagle Medium without HEPES modification (DMEM 31885–023, Invitrogen), including low glucose (5.56 mM), sodium pyruvate (110 mg/L) and L-glutamine (3.97 mM). The medium was supplemented with 10% fetal calf serum and 1% penicillin-streptomycin. The cells were incubated in a humidified incubator at 37°C with 5% CO_2. They were grown in T175cm^3 culture flasks, until reaching approximately 70–80% confluence, and were sub-cultured as follows. Medium was removed and cells were washed with phosphate buffered saline (PBS). Trypsin was used to cause cell detachment. Medium containing serum was added to neutralize the enzyme and cells were pelleted at 400G for 5min. Finally, cells were resuspended in media and passaged into fresh flasks or dishes (ratio 1:10). When necessary, cells were counted using a Neubauer hemocytometer. All procedures were performed under sterile conditions in a Laminar Air Flow hood. Hypoxia experiments were conducted at 37°C with 5% CO_2 and 7%, 2% or 0.5% O_2 using the H35 Hypoxystation (Don Whitley Scientific, Shipley, UK). Prior to hypoxia experiments, cells were allowed to adapt to each oxygen level for at least 5 days.

Phloretin, Quercetin, 3BP, DCA and Oxamic acid were obtained from Sigma Aldrich. STF31 and Metformin were obtained from Tocris Bioscience, WZB117 and 3PO from Merck Millipore and NHI-1 from Mercachem. Stock solutions of compounds were prepared in DMSO except for WZB117 which was dissolved in ethanol and DCA, Oxamic acid, 3BP and Metformin in PBS.

Sulphorhodamine B assay (SRB)

The SRB assay is a cell density assay based on the measurement of cellular protein content [60]. Cells (0.5 - 2x10^3 cells/well, depending on the proliferation rate of each cell line) were seeded in 96-well plates. Forty-eight hours later, cells were treated with or without the indicated concentration of the inhibitors. A 10-point dilution series with 1:2 steps in six replicates was performed. For the compounds dissolved in dimethylsulphoxide (DMSO) or ethanol, a constant DMSO/ ethanol concentration was used across the whole concentration- response curve. After a five day incubation period, cell monolayers were fixed with cold 25% trichloroacetic acid (Sigma) and stained with the SRB dye solution (Sigma). Unbound excess dye was removed by 1% acetic acid washes. The protein-bound stain was solubilized in 10mM Tris buffer solution (pH 10.5). Finally absorbance was measured at 540 nm using a microplate reader (BP800, Biohit Health Care). Measurements were corrected for background absorbance and presented as percentage of absorbance in untreated cells

The half maximal inhibitory concentration (IC_{50}) was used as a measure of the effectiveness of each compound. It indicates the concentration needed to reduce cell number by half. Sigmoidal concentration response curves were fitted and the IC_{50} values were defined using the XL fit tool within the Microsoft Excel.

For drug interaction studies a range of 7 different concentrations of glycolytic inhibitors was used in combination with a fixed concentration of metformin (around the IC_{20}). Both drugs were administered at the same time and the SRB assay was performed after a three day treatment. Data were analysed using the Calcusyn Software generating combination index values (CI) for each single combination point [61].

Glucose uptake assay

Cells were seeded in 12-well plates at 1 x 10^5 to 2 x 10^5 cells per well. The following day, cells were treated with or without the indicated concentration of inhibitor. The concentrations used for each compound were determined based on the corresponding IC_{50} values derived from the SRB assays. Culture media was collected at 24 h. Glucose remaining in the media was measured using the Amplex Red Glucose/Glucose Oxidase Assay Kit (Invitrogen), according to the manufacturer's instructions. Samples were diluted 1:50 in 1xReaction Buffer provided in the kit. A 96-well plate format with triplicates was used. After a 30 min incubation period with the reaction reagent solution, protected from light, absorbance was measured at 540 nm using the microplate reader. Measurements were corrected for background absorbance, subtracting the value derived from the no-glucose control [62].

Lactate assay

Lactate was measured in the same samples as used for the glucose assay, as described above. Lactate produced in the media was measured using the Lactate Assay Kit (Trinity Biotech), according to the manufacturer's instructions. A 96-well plate format with triplicates was used. 2 µl of sample was added to the wells followed by 200 µl of lactate reagent. The reagent was used as a 50% solution in distilled water. Plates were incubated in the dark for 7 min and absorbance was measured at 540 nm using the microplate reader. Measurements were corrected for background absorbance, subtracting the value derived from the no-lactate control [63].

Flow cytometry analysis

Detection of compound-induced cell death was carried out by dual staining with FITC-conjugated Annexin V and Propidium Iodide (PI) followed by flow cytometry. Briefly, 3 x 10^5 cells were seeded in 6-well plates and the following day they were treated with or without the indicated concentration of inhibitor. After a 48 h treatment, cells were harvested and stained using the FITC Annexin V Apoptosis Detection Kit I (BD Pharmingen) according to the manufacturer's instructions. Data acquisition and analysis of 30,000 events for each sample was performed using the flow cytometer BD Accuri C6 (BD Biosciences). Annexin V single positive cells were identified as early apoptotic, while cells both Annexin V and PI positive were identified as end stage apoptotic cells and PI positive cells as necrotic.

Western blotting

Cells were seeded in cell culture dishes and, when approximately 80% confluent, were washed with ice cold PBS and then treated with ice cold isotonic lysis buffer (50mM Tris pH7.5, 5 mM EGTA pH8.5, 150 mM NaCl, 1 "Complete Protease Inhibitor Tablet" (Roche), 100 µl Phosphatase Inhibitor Cocktail 2 (Sigma), 100µl Phosphatase Inhibitor Cocktail 3 (Sigma), 50 µl Aprotinin (Sigma), 100 µl Triton-X 100 (Sigma)). Subsequently cells were scraped and after centrifugation lysate supernatant was collected and stored at -70ºC. The Bicinchoninic Acid Assay (BCA) was performed to determine lysate protein concentration and absorbance was measured at 540nm using a microplate reader. Sodium dodecyl sulphate polyacrylamide gel electrophoresis (SDS-PAGE) was performed to separate proteins according to their molecular weight. Following electrophoresis, proteins were transferred onto a methanol-activated Immobilon-P polyvinylidene fluoride (PVDF) Transfer Membrane (Immobilon) using the Bio-Rad Protean Transfer Cell equipment. Transfer was performed at 100V for 1 h in ice-cold Tris-Glycine transfer buffer at 4ºC. After transfer the membrane was blocked for 1 h at RT, in 1:1 PBS/Odyssey Blocking Buffer to prevent non-specific binding. Following blocking, the membrane was incubated in primary antibody solution at 4 ºC overnight. The following primary antibodies were used: GLUT1 (07-1401; Millipore), HKII (2867; CST), PFKFB3 (13123; CST), PDHK1 (3820; CST), LDHA (3582; CST) and α-Tubulin (ab7291; Abcam). As antibody diluent, PBS/Odyssey Blocking Buffer or 5%w/v bovine serum albumin (BSA, Sigma) in 1X PBS containing 0.1% Tween-20 were used. After primary antibody incubation, the membrane was washed with PBS-0.1% Tween 20, to remove excess antibody. Secondary fluorescent antibody (anti-rabbit IR Dye 800CW (926-32211; Odyssey) and anti-mouse IR Dye 680LT (926-68020; Odyssey)) were employed, raised against the species of the primary antibody and diluted in PBS/Odyssey Blocking Buffer containing 0.001% SDS. Incubation was performed for 45 min at room temperature, protected from light. Finally the membrane was washed with PBS-0.1% Tween 20. Visualization of proteins was achieved by scanning on the Odyssey Infrared Imaging System (Licor). This machine is equipped with two infrared channels for direct fluorescence detection allowing two separate targets to be probed simultaneously.

Statistics

To evaluate the significance of differences between treated samples and untreated controls, ANOVA followed by the Tukey-Kramer Multiple Comparisons Test was used. To correlate the expression of the glycolytic enzymes in the panel of the eight cancer cell lines with their sensitivity to the inhibitors the non-Parametric Spearman correlation test was performed. Statistical tests were undertaken using GraphPad software.

ACKNOWLEDGMENTS

We thank Elisabeth Freyer (Flow Cytometry Facility IGMM, University of Edinburgh UK) for assistance with the FACs analysis.

CONFLICTS OF INTEREST

The authors declare that they have no competing interests.

FINANCIAL SUPPORT

We are grateful to Medical Research Scotland for support of this study.

REFERENCES

1. Hsu PP, Sabatini DM. Cancer cell metabolism: Warburg and beyond. Cell. 2008; 134:703–707.
2. Heiden MGV, Cantley LC, Thompson CB. Understanding the warburg effect: The metabolic requirements of cell proliferation. Science. 2009; 324:1029–1033.
3. Hanahan D, Weinberg RA. Hallmarks of cancer: The next generation. Cell. 2011; 144:646–674.
4. Zhao Y, Butler EB, Tan M. Targeting cellular metabolism to improve cancer therapeutics. Cell Death and Disease. 2013; 4:e532.
5. Tennant DA, Durán RV, Gottlieb E. Targeting metabolic transformation for cancer therapy. Nature Reviews Cancer. 2010; 10:267–277.
6. Madhok BM, Yeluri S, Perry SL, Hughes TA, Jayne DG. Targeting glucose metabolism: An emerging concept for anticancer therapy. American Journal of Clinical Oncology: Cancer Clinical Trials. 2011; 34:628–635.
7. Martin HJ, Kornmann F, Fuhrmann GF. The inhibitory effects of flavonoids and antiestrogens on the Glut1 glucose transporter in human erythrocytes. Chemico-Biological Interactions. 2003; 146:225–235.
8. Romano B, Pagano E, Montanaro V, Fortunato AL, Milic N, Borrelli F. Novel insights into the pharmacology of flavonoids. Phytotherapy Research. 2013; 27:1588–1596.
9. Kim MS, Kwon JY, Kang NJ, Lee KW, Lee HJ. Phloretin induces apoptosis in H-Ras MCF10A human breast tumor cells through the activation of p53 via JNK and p38 mitogen-activated protein kinase signaling. Ann NY Acad Sci. 2009; 1171:479–483.
10. Wu CH, Ho YS, Tsai CY, Wang YJ, Tseng H, Wei PL, Lee CH, Liu RS, Lin SY. *In vitro* and *in vivo* study of phloretin-induced apoptosis in human liver cancer cells involving inhibition of type II glucose transporter. International Journal of Cancer. 2009; 124:2210–2219.
11. Zhang H, Zhang M, Yu L, Zhao Y, He N, Yang X. Antitumor activities of quercetin and quercetin-5′, 8- disulfonate in human colon and breast cancer cell lines. Food and Chemical Toxicology. 2012; 50:1589–1599.
12. Kim HS, Wannatung T, Lee S, Yang WK, Chung SH, Lim JS, Choe W, Kang I, Kim SS, Ha J. Quercetin enhances hypoxia-mediated apoptosis via direct inhibition of AMPK activity in HCT116 colon cancer. Apoptosis. 2012; 17:938–949.
13. Chan DA, Sutphin PD, Nguyen P, Turcotte S, Lai EW, Banh A, Reynolds GE, Chi JT, Wu J, Solow-Cordero DE, Bonnet M, Flanagan JU, Bouley DM, et al. Targeting GLUT1 and the Warburg effect in renal cell carcinoma by chemical synthetic lethality. Science Translational Medicine. 2011; 3:94ra70.
14. Liu Y, Cao Y, Zhang W, Bergmeier S, Qian Y, Akbar H, Colvin R, Ding J, Tong L, Wu S, Hines J, Chen X. A small-molecule inhibitor of glucose transporter 1 downregulates glycolysis, induces cell-cycle arrest, and inhibits cancer cell growth *in vitro* and *in vivo*. Molecular Cancer Therapeutics. 2012; 11:1672–1682.
15. Cardaci S, Desideri E, Ciriolo MR. Targeting aerobic glycolysis: 3-Bromopyruvate as a promising anticancer drug. Journal of Bioenergetics and Biomembranes. 2012; 44:17–29.
16. Pedersen PL. 3-Bromopyruvate (3BP) a fast acting, promising, powerful, specific, and effective "small molecule" anti-cancer agent taken from labside to bedside: Introduction to a special issue. Journal of Bioenergetics and Biomembranes. 2012; 44:1–6.
17. Clem B, Telang S, Clem A, Yalcin A, Meier J, Simmons A, Rasku MA, Arumugam S, Dean WL, Eaton J, Lane A, Trent JO, Chesney J. Small-molecule inhibition of 6- phosphofructo-2-kinase activity suppresses glycolytic flux and tumor growth. Molecular Cancer Therapeutics. 2008; 7:110–120.
18. Granchi C, Fancelli D, Minutolo F. An update on therapeutic opportunities offered by cancer glycolytic metabolism. Bioorganic and Medicinal Chemistry Letters. 2014; 24:4915–4925.
19. Wong JYY, Huggins GS, Debidda M, Munshi NC, De Vivo I. Dichloroacetate induces apoptosis in endometrial cancer cells. Gynecologic Oncology. 2008; 109:394–402.

20. Sun RC, Fadia M, Dahlstrom JE, Parish CR, Board PG, Blackburn AC. Reversal of the glycolytic phenotype by dichloroacetate inhibits metastatic breast cancer cell growth *in vitro* and *in vivo*. Breast Cancer Research and Treatment. 2010; 120:253–260.
21. Michelakis ED, Webster L, Mackey JR. Dichloroacetate (DCA) as a potential metabolic-targeting therapy for cancer. British Journal of Cancer. 2008; 99:989–994.
22. Michelakis ED, Sutendra G, Dromparis P. Metabolic Modulation of Glioblastoma with Dichloroacetate. Science translational medicine. 2010; 2:31ra34.
23. Garon EB, Christofk HR, Hosmer W, Britten CD, Bahng A, Crabtree MJ, Hong CS, Kamranpour N, Pitts S, Kabbinavar F, Patel C, Euw EV, Black A, et al. Dichloroacetate should be considered with platinum-based chemotherapy in hypoxic tumors rather than as a single agent in advanced non-small cell lung cancer. J Cancer Res Clin Oncol. 2014; 140:443–452.
24. Fiume L, Manerba M, Vettraino M, Di Stefano G. Impairment of aerobic glycolysis by inhibitors of lactic dehydrogenase hinders the growth of human hepatocellular carcinoma cell lines. Pharmacology. 2010; 86:157–162.
25. Fiume L, Vettraino M, Manerba M, Di Stefano G. Inhibition of lactic dehydrogenase as a way to increase the anti-proliferative effect of multi-targeted kinase inhibitors. Pharmacological Research. 2011; 63:328–334.
26. Granchi C, Roy S, Giacomelli C, MacChia M, Tuccinardi T, Martinelli A, Lanza M, Betti L, Giannaccini G, Lucacchini A, Funel N, León LG, Giovannetti E, et al. Discovery of N-hydroxyindole-based inhibitors of human lactate dehydrogenase isoform A (LDH-A) as starvation agents against cancer cells. Journal of Medicinal Chemistry. 2011; 54:1599–1612.
27. Maftouh M, Avan A, Sciarrillo R, Granchi C, Leon LG, Rani R, Funel N, Smid K, Honeywell R, Boggi U, Minutolo F, Peters GJ, Giovannetti E. Synergistic interaction of novel lactate dehydrogenase inhibitors with gemcitabine against pancreatic cancer cells in hypoxia. British Journal of Cancer. 2014; 110:172–182.
28. Rizos CV, Elisaf MS. Metformin and cancer. European Journal of Pharmacology. 2013; 705:96–108.
29. Quinn BJ, Kitagawa H, Memmott RM, Gills JJ, Dennis PA. Repositioning metformin for cancer prevention and treatment. Trends in Endocrinology and Metabolism. 2013; 24:469–480.
30. Viollet B, Guigas B, Sanz Garcia N, Leclerc J, Foretz M, Andreelli F. Cellular and molecular mechanisms of metformin: An overview. Clinical Science. 2012; 122:253–270.
31. Vaupel P, Schlenger K, Knoop C, Höckel M. Oxygenation of human tumors: Evaluation of tissue oxygen distribution in breast cancers by computerized O2 tension measurements. Cancer Research. 1991; 51:3316–3322.
32. Wenger RH. Cellular adaptation to hypoxia: O2-sensing protein hydroxylases, hypoxia-inducible transcription factors, and O2-regulated gene expression. FASEB Journal. 2002; 16:1151–1162.
33. Porporato PE, Dhup S, Dadhich RK, Copetti T, Sonveaux P. Anticancer targets in the glycolytic metabolism of tumors: A comprehensive review. Frontiers in Pharmacology. 2011; 2:49.
34. Pinheiro C, Sousa B, Albergaria A, Paredes J, Dufloth R, Vieira D, Schmitt F, Baltazar F. GLUT1 and CAIX expression profiles in breast cancer correlate with adverse prognostic factors and MCT1 overexpression. Histology and Histopathology. 2011; 26:1279–1286.
35. Kang SS, Chun YK, Hur MH, Lee HK, Kim YJ, Hong SR, Lee JH, Lee SG, Park YK. Clinical significance of glucose transporter 1 (GLUT1) expression in human breast carcinoma. Japanese Journal of Cancer Research. 2002; 93:1123–1128.
36. Younes M, Brown RW, Mody DR, Fernandez L, Laucirica R. GLUT1 expression in human breast carcinoma: Correlation with known prognostic markers. Anticancer Research. 1995; 15:2895–2898.
37. Jang SM, Han H, Jang KS, Jun YJ, Jang SH, Min KW, Chung MS, Paik SS. The glycolytic phenotype is correlated with aggressiveness and poor prognosis in invasive ductal carcinomas. Journal of Breast Cancer. 2012; 15:172–180.
38. Cantuaria G, Fagotti A, Ferrandina G, Magalhaes A, Nadji M, Angioli R, Penalver M, Mancuso S, Scambia G. GLUT-1 expression in ovarian carcinoma: Association with survival and response to chemotherapy. Cancer. 2001; 92:1144–1150.
39. Sato-Tadano A, Suzuki T, Amari M, Takagi K, Miki Y, Tamaki K, Watanabe M, Ishida T, Sasano H, Ohuchi N. Hexokinase II in breast carcinoma: A potent prognostic factor associated with hypoxia-inducible factor-1α and Ki-67. Cancer Science. 2013; 104:1380–1388.
40. Suh DH, Kim MA, Kim H, Kim MK, Kim HS, Chung HH, Kim YB, Song YS. Association of overexpression of hexokinase II with chemoresistance in epithelial ovarian cancer. Clinical and Experimental Medicine. 2014; 14:345–353.
41. Buijs M, Vossen JA, Geschwind JFH, Ishimori T, Engles JM, Acha-Ngwodo O, Wahl RL, Vali M. Specificity of the anti-glycolytic activity of 3-bromopyruvate confirmed by FDG uptake in a rat model of breast cancer. Investigational New Drugs. 2009; 27:120–123.
42. Wintzell M, Löfstedt L, Johansson J, Pedersen AB, Fuxe J, Shoshan M. Repeated cisplatin treatment can lead to a multiresistant tumor cell population with stem cell features and sensitivity to 3-bromopyruvate. Cancer Biology and Therapy. 2012; 13:1454–1462.
43. Adams DJ, Ito D, Rees MG, Seashore-Ludlow B, Puyang X, Ramos AH, Cheah JH, Clemons PA, Warmuth M, Zhu P, Shamji AF, Schreiber SL. NAMPT Is the Cellular Target of STF-31-Like Small-Molecule Probes. ACS Chem Biol. 2014; 9:2247–2254.

44. Dong L, Zhou Q, Zhang Z, Zhu Y, Duan T, Feng Y. Metformin sensitizes endometrial cancer cells to chemotherapy by repressing glyoxalase I expressionjog. Journal of Obstetrics and Gynaecology Research. 2012; 38:1077–1085.
45. Rattan R, Graham RP, Maguire JL, Giri S, Shridhar V. Metformin suppresses ovarian cancer growth and metastasis with enhancement of cisplatin cytotoxicity *in Vivo*. Neoplasia. 2011; 13:483–491.
46. Iliopoulos D, Hirsch HA, Struhl K. Metformin decreases the dose of chemotherapy for prolonging tumor remission in mouse xenografts involving multiple cancer cell types. Cancer Research. 2011; 71:3196–3201.
47. Sahra IB, Laurent K, Giuliano S, Larbret F, Ponzio G, Gounon P, Le Marchand-Brustel Y, Giorgetti-Peraldi S, Cormont M, Bertolotto C, Deckert M, Auberger P, Tanti JF, et al. Targeting cancer cell metabolism: The combination of metformin and 2-deoxyglucose induces p53-dependent apoptosis in prostate cancer cells. Cancer Research. 2010; 70:2465–2475.
48. Cheong JH, Park ES, Liang J, Dennison JB, Tsavachidou D, Nguyen-Charles C, Cheng KW, Hall H, Zhang D, Lu Y, Ravoori M, Kundra V, Ajani J, et al. Dual inhibition of tumor energy pathway by 2-deoxyglucose and metformin is effective against a broad spectrum of preclinical cancer models. Molecular Cancer Therapeutics. 2011; 10:2350–2362.
49. Choi YW, Lim IK. Sensitization of metformin-cytotoxicity by dichloroacetate via reprogramming glucose metabolism in cancer cells. Cancer Letters. 2014; 346:300–308.
50. Griffiths CL, Olin JL. Triple negative breast cancer: A brief review of its characteristics and treatment options. Journal of Pharmacy Practice. 2012; 25:319–323.
51. Zordoky BNM, Bark D, Soltys CL, Sung MM, Dyck JRB. The anti-proliferative effect of metformin in triple-negative MDA-MB-231 breast cancer cells is highly dependent on glucose concentration: Implications for cancer therapy and prevention. Biochimica et Biophysica Acta - General Subjects. 2014; 1840:1943–1957.
52. Wilcock C, Bailey CJ. Accumulation of metformin by tissues of the normal and diabetic mouse. Xenobiotica. 1994; 24:49–57.
53. Cao X, Fang L, Gibbs S, Huang Y, Dai Z, Wen P, Zheng X, Sadee W, Sun D. Glucose uptake inhibitor sensitizes cancer cells to daunorubicin and overcomes drug resistance in hypoxia. Cancer Chemotherapy and Pharmacology. 2007; 59:495–505.
54. Xu RH, Pelicano H, Zhou Y, Carew JS, Feng L, Bhalla KN, Keating MJ, Huang P. Inhibition of glycolysis in cancer cells: A novel strategy to overcome drug resistance associated with mitochondrial respiratory defect and hypoxia. Cancer Research. 2005; 65:613–621.
55. Cao X, Bloomston M, Zhang T, Frankel WL, Jia G, Wang B, Hall NC, Koch RM, Cheng H, Knopp MV, Sun D. Synergistic antipancreatic tumor effect by simultaneously targeting hypoxic cancer cells with HSP90 inhibitor and glycolysis inhibitor. Clinical Cancer Research. 2008; 14:1831–1839.
56. Gwak GY, Yoon JH, Kim KM, Lee HS, Chung JW, Gores GJ. Hypoxia stimulates proliferation of human hepatoma cells through the induction of hexokinase II expression. Journal of Hepatology. 2005; 42:358–364.
57. Xiao H, Li S, Zhang D, Liu T, Yu M, Wang F. Separate and concurrent use of 2-deoxy-D-glucose and 3-bromopyruvate in pancreatic cancer cells. Oncol Rep. 2013; 29:329–334.
58. Anderson KM, Jajeh J, Guinan P, Rubenstein M. *In vitro* effects of dichloroacetate and CO2 on hypoxic HeLa cells. Anticancer Research. 2009; 29:4579–4588.
59. Shahrzad S, Lacombe K, Adamcic U, Minhas K, Coomber BL. Sodium dichloroacetate (DCA) reduces apoptosis in colorectal tumor hypoxia. Cancer Letters. 2010; 297:75–83.
60. Vichai V, Kirtikara K. Sulforhodamine B colorimetric assay for cytotoxicity screening. Nat. Protocols. 2006; 1:1112–1116.
61. Irene V, Bijnsdorp EG, Godefridus J. Peters, Analysis of Drug Interactions, in Cancer Cell Culture, Methods and Protocols, I.A. Cree, Editor 2011: Humana Press. p. 421–434.
62. http://products.invitrogen.com/ivgn/product/A22189.
63. http://www.trinitybiotech.com/ClinicalChemistry/Pages/ProductDetails.aspx?ProductNumber=735–10&Filter=*735–10*.

Bibliography

Bibliography

1. *Cancer Research UK*. 2016; Available from: http://www.cancerresearchuk.org/.
2. American Cancer Society. 2016; Available from: http://www.cancer.org/.
3. Kluttig A, Schmidt-Pokrzywniak A. Established and suspected risk factors in breast cancer aetiology. Breast Care. 2009; 4: 82-87.
4. Singletary SE. Rating the Risk Factors for Breast Cancer. Annals of Surgery. 2003; 237: 474-482.
5. McPherson K, Steel CM, Dixon JM. ABC of breast diseases: Breast cancer - Epidemiology, risk factors, and genetics. British Medical Journal. 2000; 321: 624-628.
6. Ripperger T, Gadzicki D, Meindl A, Schlegelberger B. Breast cancer susceptibility: Current knowledge and implications for genetic counselling. European Journal of Human Genetics. 2009; 17: 722-731.
7. Ford D, Easton DF. The genetics of breast and ovarian cancer. British Journal of Cancer. 1995; 72: 805-812.
8. NHS. *NHS choises*. 2016; Available from: http://www.nhs.uk/.
9. Dean A. Primary breast cancer: risk factors, diagnosis and management. Nursing standard (Royal College of Nursing (Great Britain) : 1987). 2008; 22: 47-55; quiz 58, 60.
10. Davies EL. Breast cancer. Medicine. 2012; 40: 5-9.
11. Bloom HJ, Richardson WW. Histological grading and prognosis in breast cancer; a study of 1409 cases of which 359 have been followed for 15 years. British Journal of Cancer. 1957; 11: 359-377.
12. Singletary SE, Allred C, Ashley P, Bassett LW, Berry D, Bland KI, Borgen PI, Clark G, Edge SB, Hayes DF, Hughes LL, Hutter RVP, Morrow M, et al. Revision of the American Joint Committee on cancer staging system for breast cancer. Journal of Clinical Oncology. 2002; 20: 3628-3636.
13. Wellings SR, Jensen HM, Marcum RG. An atlas of subgross pathology of the human breast with special reference to possible precancerous lesions. Journal of the National Cancer Institute. 1975; 55: 231-273.
14. Malhotra GK, Zhao X, Band H, Band V. Histological, molecular and functional subtypes of breast cancers. Cancer Biology and Therapy. 2010; 10: 955-960.
15. Weigelt B, Geyer FC, Reis-Filho JS. Histological types of breast cancer: How special are they? Molecular Oncology. 2010; 4: 192-208.
16. Virnig BA, Tuttle TM, Shamliyan T, Kane RL. Ductal carcinoma in Situ of the breast: A systematic review of incidence, treatment, and outcomes. Journal of the National Cancer Institute. 2010; 102: 170-178.
17. Payne SJL, Bowen RL, Jones JL, Wells CA. Predictive markers in breast cancer - The present. Histopathology. 2008; 52: 82-90.
18. Zardavas D, Irrthum A, Swanton C, Piccart M. Clinical management of breast cancer heterogeneity. Nature Reviews Clinical Oncology. 2015; 12: 381-394.
19. Perou CM, Sørile T, Eisen MB, Van De Rijn M, Jeffrey SS, Ress CA, Pollack JR, Ross DT, Johnsen H, Akslen LA, Fluge Ø, Pergammenschlkov A, Williams C, et al. Molecular portraits of human breast tumours. Nature. 2000; 406: 747-752.
20. Brenton JD, Carey LA, Ahmed A, Caldas C. Molecular classification and molecular forecasting of breast cancer: Ready for clinical application? Journal of Clinical Oncology. 2005; 23: 7350-7360.
21. Yersal O, Barutca S. Biological subtypes of breast cancer: Prognostic and therapeutic implications. World Journal of Clinical Oncology. 2014; 5: 412-424.
22. Prat A, Perou CM. Deconstructing the molecular portraits of breast cancer. Molecular Oncology. 2011; 5: 5-23.

23. Kirova YM. Recent advances in breast cancer radiotherapy: Evolution or revolution, or how to decrease cardiac toxicity?
24. Fisher B, Anderson S, Bryant J, Margolese RG, Deutsch M, Fisher ER, Jeong JH, Wolmark N. Twenty-year follow-up of a randomized trial comparing total mastectomy, lumpectomy, and lumpectomy plus irradiation for the treatment of invasive breast cancer. New England Journal of Medicine. 2002; 347: 1233-1241.
25. Giuliano AE, Dale PS, Turner RR, Morton DL, Evans SW, Krasne DL, Foster RS, Gardner B, Cady B, Howard JM, Kauffman GL. Improved axillary staging of breast cancer with sentinel lymphadenectomy. Annals of Surgery. 1995; 222: 394-401.
26. McArthur HL, Hudis CA. Breast cancer chemotherapy. Cancer Journal. 2007; 13: 141-147.
27. Santa-Maria CA, Camp M, Cimino-Mathews A, Harvey S, Wright J, Stearns V. Neoadjuvant therapy for early-stage breast cancer: Current practice, controversies, and future directions. ONCOLOGY (United States). 2015; 29:
28. Relevance of breast cancer hormone receptors and other factors to the efficacy of adjuvant tamoxifen: Patient-level meta-analysis of randomised trials. The Lancet. 2011; 378: 771-784.
29. Ignatiadis M, Sotiriou C. Luminal breast cancer: From biology to treatment. Nature Reviews Clinical Oncology. 2013; 10: 494-506.
30. Slamon D, Eiermann W, Robert N, Pienkowski T, Martin M, Press M, Mackey J, Glaspy J, Chan A, Pawlicki M, Pinter T, Valero V, Liu MC, et al. Adjuvant trastuzumab in HER2-positive breast cancer. The New England journal of medicine. 2011; 365: 1273-1283.
31. Ahmed S, Sami A, Xiang J. HER2-directed therapy: current treatment options for HER2-positive breast cancer. Breast Cancer. 2015; 22: 101-116.
32. Hudis CA. Trastuzumab - Mechanism of action and use in clinical practice. New England Journal of Medicine. 2007; 357: 39-51.
33. Amiri-Kordestani L, Blumenthal GM, Xu QC, Zhang L, Tang SW, Ha L, Weinberg WC, Chi B, Candau-Chacon R, Hughes P, Russell AM, Miksinski SP, Chen XH, et al. FDA approval: ado-trastuzumab emtansine for the treatment of patients with HER2-positive metastatic breast cancer. Clinical cancer research : an official journal of the American Association for Cancer Research. 2014; 20: 4436-4441.
34. Arteaga CL, Sliwkowski MX, Osborne CK, Perez EA, Puglisi F, Gianni L. Treatment of HER2-positive breast cancer: Current status and future perspectives. Nature Reviews Clinical Oncology. 2012; 9: 16-32.
35. Langdon SP, Cameron DA. Pertuzumab for the treatment of metastatic breast cancer. Expert Review of Anticancer Therapy. 2013; 13: 907-918.
36. Baselga J, Campone M, Piccart M, Burris Iii HA, Rugo HS, Sahmoud T, Noguchi S, Gnant M, Pritchard KI, Lebrun F, Beck JT, Ito Y, Yardley D, et al. Everolimus in postmenopausal hormone-receptor-positive advanced breast cancer. New England Journal of Medicine. 2012; 366: 520-529.
37. Finn RS, Crown JP, Lang I, Boer K, Bondarenko IM, Kulyk SO, Ettl J, Patel R, Pinter T, Schmidt M, Shparyk Y, Thummala AR, Voytko NL, et al. The cyclin-dependent kinase 4/6 inhibitor palbociclib in combination with letrozole versus letrozole alone as first-line treatment of oestrogen receptor-positive, HER2-negative, advanced breast cancer (PALOMA-1/TRIO-18): A randomised phase 2 study. The Lancet Oncology. 2015; 16: 25-35.
38. Zardavas D, Baselga J, Piccart M. Emerging targeted agents in metastatic breast cancer. Nature Reviews Clinical Oncology. 2013; 10: 191-210.
39. Cannistra SA. Cancer of the ovary. New England Journal of Medicine. 2004; 351: 2519-2529+2565.

40. Salehi F, Dunfield L, Phillips KP, Krewski D, Vanderhyden BC. Risk factors for ovarian cancer: An overview with emphasis on hormonal factors. Journal of Toxicology and Environmental Health - Part B: Critical Reviews. 2008; 11: 301-321.
41. Sueblinvong T, Carney ME. Current understanding of risk factors for ovarian cancer. Current Treatment Options in Oncology. 2009; 10: 67-81.
42. Hunn J, Rodriguez GC. Ovarian cancer: Etiology, risk factors, and epidemiology. Clinical Obstetrics and Gynecology. 2012; 55: 3-23.
43. Rooth C. Ovarian cancer: Risk factors, treatment and management. British Journal of Nursing. 2013; 22: S23-S30.
44. Søgaard M, Kjær SK, Gayther S. Ovarian cancer and genetic susceptibility in relation to the BRCA1 and BRCA2 genes. Occurrence, clinical importance and intervention. Acta Obstetricia et Gynecologica Scandinavica. 2006; 85: 93-105.
45. Prat J, Ribé A, Gallardo A. Hereditary ovarian cancer. Human Pathology. 2005; 36: 861-870.
46. Al Bakir M, Gabra H. The molecular genetics of hereditary and sporadic ovarian cancer: Implications for the future. British Medical Bulletin. 2014; 112: 57-69.
47. Malander S, Rambech E, Kristoffersson U, Halvarsson B, Ridderheim M, Borg Å, Nilbert M. The contribution of the hereditary nonpolyposis colorectal cancer syndrome to the development of ovarian cancer. Gynecologic Oncology. 2006; 101: 238-243.
48. Sundar S, Neal RD, Kehoe S. Diagnosis of ovarian cancer. BMJ (Online). 2015; 351:
49. Menon U, Griffin M, Gentry-Maharaj A. Ovarian cancer screening - Current status, future directions. Gynecologic Oncology. 2014; 132: 490-495.
50. Menon U, Ryan A, Kalsi J, Gentry-Maharaj A, Dawnay A, Habib M, Apostolidou S, Singh N, Benjamin E, Burnell M, Davies S, Sharma A, Gunu R, et al. Risk algorithm using serial biomarker measurements doubles the number of screen-detected cancers compared with a single-threshold rule in the United Kingdom Collaborative Trial of Ovarian Cancer Screening. Journal of Clinical Oncology. 2015; 33: 2062-2071.
51. Bast Jr RC, Hennessy B, Mills GB. The biology of ovarian cancer: New opportunities for translation. Nature Reviews Cancer. 2009; 9: 415-428.
52. McCluggage WG. Morphological subtypes of ovarian carcinoma: A review with emphasis on new developments and pathogenesis. Pathology. 2011; 43: 420-432.
53. Kaku T, Ogawa S, Kawano Y, Ohishi Y, Kobayashi H, Hirakawa T, Nakano H. Histological classification of ovarian cancer. Medical Electron Microscopy. 2003; 36: 9-17.
54. Soslow RA. Histologic subtypes of ovarian carcinoma: An overview. International Journal of Gynecological Pathology. 2008; 27: 161-174.
55. Naora H. The heterogeneity of epithelial ovarian cancers: Reconciling old and new paradigms. Expert Reviews in Molecular Medicine. 2007; 9: 1-12.
56. Seidman J. Advances in sub-classification of ovarian carcinomas by cell type: An update. Diagnostic Histopathology. 2014; 20: 351-356.
57. Prat J. New insights into ovarian cancer pathology. Annals of Oncology. 2012; 23:
58. Lee Y, Miron A, Drapkin R, Nucci MR, Medeiros F, Saleemuddin A, Garber J, Birch C, Mou H, Gordon RW, Cramer DW, McKeon FD, Crum CP. A candidate precursor to serous carcinoma that originates in the distal fallopian tube. Journal of Pathology. 2007; 211: 26-35.
59. Kurman RJ, Shih IM. The origin and pathogenesis of epithelial ovarian cancer: A proposed unifying theory. American Journal of Surgical Pathology. 2010; 34: 433-443.

60. Bowtell DD, Böhm S, Ahmed AA, Aspuria PJ, Bast RC, Beral V, Berek JS, Birrer MJ, Blagden S, Bookman MA, Brenton JD, Chiappinelli KB, Martins FC, et al. Rethinking ovarian cancer II: Reducing mortality from high-grade serous ovarian cancer. Nature Reviews Cancer. 2015; 15: 668-679.
61. Marquez RT, Baggerly KA, Patterson AP, Liu J, Broaddus R, Frumovitz M, Atkinson EN, Smith DI, Hartmann L, Fishman D, Berchuck A, Whitaker R, Gershenson DM, et al. Patterns of gene expression in different histotypes of epithelial ovarian cancer correlate with those in normal fallopian tube, endometrium, and colon. Clinical Cancer Research. 2005; 11: 6116-6126.
62. Kurman RJ, Shih IM. Pathogenesis of ovarian cancer: Lessons from morphology and molecular biology and their clinical implications. International Journal of Gynecological Pathology. 2008; 27: 151-160.
63. Shih IM, Kurman RJ. Ovarian Tumorigenesis: A Proposed Model Based on Morphological and Molecular Genetic Analysis. American Journal of Pathology. 2004; 164: 1511-1518.
64. Meinhold-Heerlein I, Hauptmann S. The heterogeneity of ovarian cancer. Archives of Gynecology and Obstetrics. 2014; 289: 237-239.
65. Pignata S, Cannella L, Leopardo D, Pisano C, Bruni GS, Facchini G. Chemotherapy in epithelial ovarian cancer. Cancer Letters. 2011; 303: 73-83.
66. Bohra U. Recent advances in management of epithelial ovarian cancer. Apollo Medicine. 2012; 9: 212-218.
67. Kim A, Ueda Y, Naka T, Enomoto T. Therapeutic strategies in epithelial ovarian cancer. Journal of Experimental and Clinical Cancer Research. 2012; 31:
68. Bast Jr RC. Molecular approaches to personalizing management of ovarian cancer. Annals of Oncology. 2011; 22: 5-15.
69. Yap TA, Carden CP, Kaye SB. Beyond chemotherapy: Targeted therapies in ovarian cancer. Nature Reviews Cancer. 2009; 9: 167-181.
70. Moss C, Kaye SB. Ovarian cancer: Progress and continuing controversies in management. European Journal of Cancer. 2002; 38: 1701-1707.
71. Kalachand R, Hennessy BT, Markman M. Molecular targeted therapy in ovarian cancer: what is on the horizon? Drugs. 2011; 71: 947-967.
72. Ashworth A. A synthetic lethal therapeutic approach: Poly(ADP) ribose polymerase inhibitors for the treatment of cancers deficient in DNA double-strand break repair. Journal of Clinical Oncology. 2008; 26: 3785-3790.
73. Burger RA. Overview of anti-angiogenic agents in development for ovarian cancer. Gynecologic Oncology. 2011; 121: 230-238.
74. Liu JF, Cannistra SA. Emerging role for bevacizumab in combination with chemotherapy for patients with platinum-resistant ovarian cancer. Journal of Clinical Oncology. 2014; 32: 1287-1289.
75. Pliarchopoulou K, Pectasides D. Epithelial ovarian cancer: Focus on targeted therapy. Critical Reviews in Oncology/Hematology. 2011; 79: 17-23.
76. Telli ML, Sledge GW. The future of breast cancer systemic therapy: the next 10 years. Journal of Molecular Medicine. 2015; 93: 119-125.
77. Sims AH, Howell A, Howell SJ, Clarke RB. Origins of breast cancer subtypes and therapeutic implications. Nature Clinical Practice Oncology. 2007; 4: 516-525.
78. Vaughan S, Coward JI, Bast RC, Berchuck A, Berek JS, Brenton JD, Coukos G, Crum CC, Drapkin R, Etemadmoghadam D, Friedlander M, Gabra H, Kaye SB, et al. Rethinking ovarian cancer: Recommendations for improving outcomes. Nature Reviews Cancer. 2011; 11: 719-725.
79. Lheureux S, Karakasis K, Kohn EC, Oza AM. Ovarian cancer treatment: The end of empiricism? Cancer. 2015; 121: 3203-3211.

80. Takano M, Tsuda H, Sugiyama T. Clear cell carcinoma of the ovary: Is there a role of histology-specific treatment? Journal of Experimental and Clinical Cancer Research. 2012; 31:
81. Warburg O, Wind F, Negelein E. THE METABOLISM OF TUMORS IN THE BODY. The Journal of general physiology. 1927; 8: 519.
82. Warburg O. On the origin of cancer cells. Science. 1956; 123: 309-314.
83. Koppenol WH, Bounds PL, Dang CV. Otto Warburg's contributions to current concepts of cancer metabolism. Nature Reviews Cancer. 2011; 11: 325-337.
84. Weinhouse S, Warburg O, Burk D, Schade AL. On respiratory impairment in cancer cells. Science. 1956; 124: 267-272.
85. Ferreira LMR. Cancer metabolism: The Warburg effect today. Experimental and Molecular Pathology. 2010; 89: 372-380.
86. Nobel Media AB. *Nobelprize.org*. 2016; Available from: http://www.nobelprize.org/nobel_prizes/medicine/laureates/1931/.
87. Heiden MGV, Cantley LC, Thompson CB. Understanding the warburg effect: The metabolic requirements of cell proliferation. Science. 2009; 324: 1029-1033.
88. DeBerardinis RJ, Lum JJ, Hatzivassiliou G, Thompson CB. The Biology of Cancer: Metabolic Reprogramming Fuels Cell Growth and Proliferation. Cell Metabolism. 2008; 7: 11-20.
89. Racker E. Bioenergetics and the problem of tumor growth. American Scientist. 1972; 60: 56-63.
90. Ward PS, Thompson CB. Metabolic Reprogramming: A Cancer Hallmark Even Warburg Did Not Anticipate. Cancer Cell. 2012; 21: 297-308.
91. Hsu PP, Sabatini DM. Cancer cell metabolism: Warburg and beyond. Cell. 2008; 134: 703-707.
92. Hanahan D, Weinberg RA. Hallmarks of cancer: The next generation. Cell. 2011; 144: 646-674.
93. Yeluri S, Madhok B, Prasad KR, Quirke P, Jayne DG. Cancer's craving for sugar: An opportunity for clinical exploitation. Journal of Cancer Research and Clinical Oncology. 2009; 135: 867-877.
94. Chen Z, Lu W, Garcia-Prieto C, Huang P. The Warburg effect and its cancer therapeutic implications. Journal of Bioenergetics and Biomembranes. 2007; 39: 267-274.
95. Senyilmaz D, Teleman AA. Chicken or the egg: Warburg effect and mitochondrial dysfunction. F1000Prime Reports. 2015; 7:
96. Bensinger SJ, Christofk HR. New aspects of the Warburg effect in cancer cell biology. Seminars in Cell and Developmental Biology. 2012; 23: 352-361.
97. Kelloff GJ, Hoffman JM, Johnson B, Scher HI, Siegel BA, Cheng EY, Cheson BD, O'Shaughnessy J, Guyton KZ, Mankoff DA, Shankar L, Larson SM, Sigman CC, et al. Progress and promise of FDG-PET imaging for cancer patient management and oncologic drug development. Clinical Cancer Research. 2005; 11: 2785-2808.
98. Lunt SY, Vander Heiden MG, *Aerobic glycolysis: Meeting the metabolic requirements of cell proliferation*, in *Annual Review of Cell and Developmental Biology*2011. p. 441-464.
99. Chen X, Qian Y, Wu S. The Warburg effect: Evolving interpretations of an established concept. Free Radical Biology and Medicine. 2015; 79: 253-263.
100. Pelicano H, Martin DS, Xu RH, Huang P. Glycolysis inhibition for anticancer treatment. Oncogene. 2006; 25: 4633-4646.
101. Madhok BM, Yeluri S, Perry SL, Hughes TA, Jayne DG. Targeting glucose metabolism: An emerging concept for anticancer therapy. American Journal of Clinical Oncology: Cancer Clinical Trials. 2011; 34: 628-635.

102. Granchi C, Fancelli D, Minutolo F. An update on therapeutic opportunities offered by cancer glycolytic metabolism. Bioorganic and Medicinal Chemistry Letters. 2014; 24: 4915-4925.
103. Gatenby RA, Gillies RJ. Glycolysis in cancer: A potential target for therapy. International Journal of Biochemistry and Cell Biology. 2007; 39: 1358-1366.
104. Zhao Y, Liu H, Riker AI, Fodstad O, Ledoux SP, Wilson GL, Tan M. Emerging metabolic targets in cancer therapy. Frontiers in Bioscience. 2011; 16: 1844-1860.
105. Tennant DA, Durán RV, Gottlieb E. Targeting metabolic transformation for cancer therapy. Nature Reviews Cancer. 2010; 10: 267-277.
106. Weinhouse S. The Warburg hypothesis fifty years later. Zeitschrift für Krebsforschung und Klinische Onkologie. 1976; 87: 115-126.
107. Kim JW, Dang CV. Cancer's molecular sweet tooth and the warburg effect. Cancer Research. 2006; 66: 8927-8930.
108. Manning BD, Cantley LC. AKT/PKB Signaling: Navigating Downstream. Cell. 2007; 129: 1261-1274.
109. Elstrom RL, Bauer DE, Buzzai M, Karnauskas R, Harris MH, Plas DR, Zhuang H, Cinalli RM, Alavi A, Rudin CM, Thompson CB. Akt stimulates aerobic glycolysis in cancer cells. Cancer Research. 2004; 64: 3892-3899.
110. Kohn AD, Summers SA, Birnbaum MJ, Roth RA. Expression of a constitutively active Akt Ser/Thr kinase in 3T3-L1 adipocytes stimulates glucose uptake and glucose transporter 4 translocation. Journal of Biological Chemistry. 1996; 271: 31372-31378.
111. Taha C, Liu Z, Jin J, Al-Hasani H, Sonenberg N, Klip A. Opposite translational control of GLUT1 and GLUT4 glucose transporter mRNAs in response insulin. Role of mammalian target of rapamycin, protein kinase B, and phosphatidylinositol 3-kinase in GLUT1 mRNA translation. Journal of Biological Chemistry. 1999; 274: 33085-33091.
112. Robey RB, Hay N. Mitochondrial hexokinases, novel mediators of the antiapoptotic effects of growth factors and Akt. Oncogene. 2006; 25: 4683-4696.
113. Gordan JD, Thompson CB, Simon MC. HIF and c-Myc: Sibling Rivals for Control of Cancer Cell Metabolism and Proliferation. Cancer Cell. 2007; 12: 108-113.
114. Osthus RC, Shim H, Kim S, Li Q, Reddy R, Mukherjee M, Xu Y, Wonsey D, Lee LA, Dang CV. Deregulation of glucose transporter 1 and glycolytic gene expression by c-Myc. Journal of Biological Chemistry. 2000; 275: 21797-21800.
115. Bensaad K, Tsuruta A, Selak MA, Vidal MNC, Nakano K, Bartrons R, Gottlieb E, Vousden KH. TIGAR, a p53-Inducible Regulator of Glycolysis and Apoptosis. Cell. 2006; 126: 107-120.
116. Matoba S, Kang JG, Patino WD, Wragg A, Boehm M, Gavrilova O, Hurley PJ, Bunz F, Hwang PM. p53 regulates mitochondrial respiration. Science. 2006; 312: 1650-1653.
117. Rempel A, Mathupala SP, Griffin CA, Hawkins AL, Pedersen PL. Glucose catabolism in cancer cells: Amplification of the gene encoding type II hexokinase. Cancer Research. 1996; 56: 2468-2471.
118. Semenza GL. HIF-1: upstream and downstream of cancer metabolism. Current Opinion in Genetics and Development. 2010; 20: 51-56.
119. Kaelin Jr WG. Molecular basis of the VHL hereditary cancer syndrome. Nature Reviews Cancer. 2002; 2: 673-682.
120. Lu H, Forbes RA, Verma A. Hypoxia-inducible factor 1 activation by aerobic glycolysis implicates the Warburg effect in carcinogenesis. Journal of Biological Chemistry. 2002; 277: 23111-23115.
121. Gottlieb E, Tomlinson IPM. Mitochondrial tumour suppressors: A genetic and biochemical update. Nature Reviews Cancer. 2005; 5: 857-866.

122. Porporato PE, Dhup S, Dadhich RK, Copetti T, Sonveaux P. Anticancer targets in the glycolytic metabolism of tumors: A comprehensive review. Frontiers in Pharmacology. 2011; AUG:
123. López-Lázaro M. The Warburg effect: Why and how do cancer cells activate glycolysis in the presence of oxygen? Anti-Cancer Agents in Medicinal Chemistry. 2008; 8: 305-312.
124. Zheng J. Energy metabolism of cancer: Glycolysis versus oxidative phosphorylation (review). Oncology Letters. 2012; 4: 1151-1157.
125. Gatenby RA, Gillies RJ. Why do cancers have high aerobic glycolysis? Nature Reviews Cancer. 2004; 4: 891-899.
126. Gatenby RA, Gillies RJ. A microenvironmental model of carcinogenesis. Nature Reviews Cancer. 2008; 8: 56-61.
127. Deberardinis RJ, Cheng T. Q's next: The diverse functions of glutamine in metabolism, cell biology and cancer. Oncogene. 2010; 29: 313-324.
128. Wise DR, Thompson CB. Glutamine addiction: a new therapeutic target in cancer. Trends in Biochemical Sciences. 2010; 35: 427-433.
129. Daye D, Wellen KE. Metabolic reprogramming in cancer: Unraveling the role of glutamine in tumorigenesis. Seminars in Cell and Developmental Biology. 2012; 23: 362-369.
130. Hensley CT, Wasti AT, DeBerardinis RJ. Glutamine and cancer: Cell biology, physiology, and clinical opportunities. Journal of Clinical Investigation. 2013; 123: 3678-3684.
131. Reitzer LJ, Wice BM, Kennell D. Evidence that glutamine, not sugar, is the major energy source for cultured HeLa cells. Journal of Biological Chemistry. 1979; 254: 2669-2676.
132. DeBerardinis RJ, Mancuso A, Daikhin E, Nissim I, Yudkoff M, Wehrli S, Thompson CB. Beyond aerobic glycolysis: Transformed cells can engage in glutamine metabolism that exceeds the requirement for protein and nucleotide synthesis. Proceedings of the National Academy of Sciences of the United States of America. 2007; 104: 19345-19350.
133. Gao P, Tchernyshyov I, Chang TC, Lee YS, Kita K, Ochi T, Zeller KI, De Marzo AM, Van Eyk JE, Mendell JT, Dang CV. C-Myc suppression of miR-23a/b enhances mitochondrial glutaminase expression and glutamine metabolism. Nature. 2009; 458: 762-765.
134. Wise DR, Deberardinis RJ, Mancuso A, Sayed N, Zhang XY, Pfeiffer HK, Nissim I, Daikhin E, Yudkoff M, McMahon SB, Thompson CB. Myc regulates a transcriptional program that stimulates mitochondrial glutaminolysis and leads to glutamine addiction. Proceedings of the National Academy of Sciences of the United States of America. 2008; 105: 18782-18787.
135. Robinson MM, McBryant SJ, Tsukamoto T, Rojas C, Ferraris DV, Hamilton SK, Hansen JC, Curthoys NP. Novel mechanism of inhibition of rat kidney-type glutaminase by bis-2-(5-phenylacetamido-1,2,4-thiadiazol-2-yl)ethyl sulfide (BPTES). Biochemical Journal. 2007; 406: 407-414.
136. Sigma-Aldrich Co. 2016; Available from: http://www.sigmaaldrich.com/.
137. Le A, Lane AN, Hamaker M, Bose S, Gouw A, Barbi J, Tsukamoto T, Rojas CJ, Slusher BS, Zhang H, Zimmerman LJ, Liebler DC, Slebos RJC, et al. Glucose-independent glutamine metabolism via TCA cycling for proliferation and survival in b cells. Cell Metabolism. 2012; 15: 110-121.
138. Seltzer MJ, Bennett BD, Joshi AD, Gao P, Thomas AG, Ferraris DV, Tsukamoto T, Rojas CJ, Slusher BS, Rabinowitz JD, Dang CV, Riggins GJ. Inhibition of glutaminase preferentially slows growth of glioma cells with mutant IDH1. Cancer Research. 2010; 70: 8981-8987.

139. Emadi A, Jun SA, Tsukamoto T, Fathi AT, Minden MD, Dang CV. Inhibition of glutaminase selectively suppresses the growth of primary acute myeloid leukemia cells with IDH mutations. Experimental Hematology. 2014; 42: 247-251.
140. Hudson CD, Savadelis A, Nagaraj AB, Joseph P, Avril S, DiFeo A, Avril N. Altered glutamine metabolism in platinum resistant ovarian cancer. Oncotarget. 2016;
141. Calithera BioSciences. *CB-839 has the potential to be an important new therapeutic agent with a novel mechanism of action for the treatment of a broad range of cancers*. 2016; Available from: http://www.calithera.com/programs/cb-839/.
142. Vaupel P, Mayer A. Hypoxia in cancer: Significance and impact on clinical outcome. Cancer and Metastasis Reviews. 2007; 26: 225-239.
143. Vaupel P, Mayer A, Höckel M, *Tumor Hypoxia and Malignant Progression*, in *Methods in Enzymology*2004. p. 335-354.
144. Vaupel P, Briest S, Höckel M. Hypoxia in breast cancer: Pathogenesis, characterization and biological/therapeutic implications. Wiener Medizinische Wochenschrift. 2002; 152: 334-342.
145. Vaupel P, Schienger K, Knoop C, Höckel M. Oxygenation of human tumors: Evaluation of tissue oxygen distribution in breast cancers by computerized O2 tension measurements. Cancer Research. 1991; 51: 3316-3322.
146. Eales KL, Hollinshead KER, Tennant DA. Hypoxia and metabolic adaptation of cancer cells. Oncogenesis. 2016; 5: e190.
147. Dang CV, Semenza GL. Oncogenic alterations of metabolism. Trends in Biochemical Sciences. 1999; 24: 68-72.
148. Østergaard L, Tietze A, Nielsen T, Drasbek KR, Mouridsen K, Jespersen SN, Horsman MR. The Relationship between tumor blood flow, angiogenesis, tumor hypoxia, and aerobic glycolysis. Cancer Research. 2013; 73: 5618-5624.
149. Semenza GL. Hypoxia-inducible factor 1: Master regulator of O2 homeostasis. Current Opinion in Genetics and Development. 1998; 8: 588-594.
150. Ke Q, Costa M. Hypoxia-inducible factor-1 (HIF-1). Molecular Pharmacology. 2006; 70: 1469-1480.
151. Semenza GL. Regulation of cancer cell metabolism by hypoxia-inducible factor 1. Seminars in Cancer Biology. 2009; 19: 12-16.
152. Salceda S, Caro J. Hypoxia-inducible factor 1α (HIF-1α) protein is rapidly degraded by the ubiquitin-proteasome system under normoxic conditions. Its stabilization by hypoxia depends on redox-induced changes. Journal of Biological Chemistry. 1997; 272: 22642-22647.
153. Wenger RH. Cellular adaptation to hypoxia: O2-sensing protein hydroxylases, hypoxia-inducible transcription factors, and O2-regulated gene expression. FASEB Journal. 2002; 16: 1151-1162.
154. Epstein ACR, Gleadle JM, McNeill LA, Hewitson KS, O'Rourke J, Mole DR, Mukherji M, Metzen E, Wilson MI, Dhanda A, Tian YM, Masson N, Hamilton DL, et al. C. elegans EGL-9 and mammalian homologs define a family of dioxygenases that regulate HIF by prolyl hydroxylation. Cell. 2001; 107: 43-54.
155. Maxwell PH, Wlesener MS, Chang GW, Clifford SC, Vaux EC, Cockman ME, Wykoff CC, Pugh CW, Maher ER, Ratcliffe PJ. The tumour suppressor protein VHL targets hypoxia-inducible factors for oxygen-dependent proteolysis. Nature. 1999; 399: 271-275.
156. Ivan M, Kondo K, Yang H, Kim W, Valiando J, Ohh M, Salic A, Asara JM, Lane WS, Kaelin W.G, Jr. HIFα targeted for VHL-mediated destruction by proline hydroxylation: Implications for O2 sensing. Science. 2001; 292: 464-468.
157. Mahon PC, Hirota K, Semenza GL. FIH-1: A novel protein that interacts with HIF-1α and VHL to mediate repression of HIF-1 transcriptional activity. Genes and Development. 2001; 15: 2675-2686.

158. Lando D, Peet DJ, Gorman JJ, Whelan DA, Whitelaw ML, Bruick RK. FIH-1 is an asparaginyl hydroxylase enzyme that regulates the transcriptional activity of hypoxia-inducible factor. Genes and Development. 2002; 16: 1466-1471.
159. Dang CV, Kim JW, Gao P, Yustein J. The interplay between MYC and HIF in cancer. Nature Reviews Cancer. 2008; 8: 51-56.
160. Kim JW, Tchernyshyov I, Semenza GL, Dang CV. HIF-1-mediated expression of pyruvate dehydrogenase kinase: A metabolic switch required for cellular adaptation to hypoxia. Cell Metabolism. 2006; 3: 177-185.
161. Papandreou I, Cairns RA, Fontana L, Lim AL, Denko NC. HIF-1 mediates adaptation to hypoxia by actively downregulating mitochondrial oxygen consumption. Cell Metabolism. 2006; 3: 187-197.
162. Kim JW, Gao P, Liu YC, Semenza GL, Dang CV. Hypoxia-inducible factor 1 and dysregulated c-Myc cooperatively induce vascular endothelial growth factor and metabolic switches hexokinase 2 and pyruvate dehydrogenase kinase 1. Molecular and Cellular Biology. 2007; 27: 7381-7393.
163. Doherty JR, Cleveland JL. Targeting lactate metabolism for cancer therapeutics. Journal of Clinical Investigation. 2013; 123: 3685-3692.
164. Halestrap AP. The monocarboxylate transporter family-Structure and functional characterization. IUBMB Life. 2012; 64: 1-9.
165. Draoui N, Feron O. Lactate shuttles at a glance: From physiological paradigms to anti-cancer treatments. DMM Disease Models and Mechanisms. 2011; 4: 727-732.
166. Shime H, Yabu M, Akazawa T, Kodama K, Matsumoto M, Seya T, Inoue N. Tumor-secreted lactic acid promotes IL-23/IL-17 proinflammatory pathway. Journal of Immunology. 2008; 180: 7175-7183.
167. Fischer K, Hoffmann P, Voelkl S, Meidenbauer N, Ammer J, Edinger M, Gottfried E, Schwarz S, Rothe G, Hoves S, Renner K, Timischl B, Mackensen A, et al. Inhibitory effect of tumor cell-derived lactic acid on human T cells. Blood. 2007; 109: 3812-3819.
168. Végran F, Boidot R, Michiels C, Sonveaux P, Feron O. Lactate influx through the endothelial cell monocarboxylate transporter MCT1 supports an NF-kB/IL-8 pathway that drives tumor angiogenesis. Cancer Research. 2011; 71: 2550-2560.
169. Sonveaux P, Végran F, Schroeder T, Wergin MC, Verrax J, Rabbani ZN, De Saedeleer CJ, Kennedy KM, Diepart C, Jordan BF, Kelley MJ, Gallez B, Wahl ML, et al. Targeting lactate-fueled respiration selectively kills hypoxic tumor cells in mice. Journal of Clinical Investigation. 2008; 118: 3930-3942.
170. Semenza GL. Tumor metabolism: Cancer cells give and take lactate. Journal of Clinical Investigation. 2008; 118: 3835-3837.
171. McCracken AN, Edinger AL. Nutrient transporters: The Achilles' heel of anabolism. Trends in Endocrinology and Metabolism. 2013; 24: 200-208.
172. Adekola K, Rosen ST, Shanmugam M. Glucose transporters in cancer metabolism. Current Opinion in Oncology. 2012; 24: 650-654.
173. Thorens B, Mueckler M. Glucose transporters in the 21st Century. American Journal of Physiology - Endocrinology and Metabolism. 2010; 298: E141-E145.
174. Macheda ML, Rogers S, Best JD. Molecular and cellular regulation of glucose transporter (GLUT) proteins in cancer. Journal of Cellular Physiology. 2005; 202: 654-662.
175. Szablewski L. Expression of glucose transporters in cancers. Biochimica et Biophysica Acta - Reviews on Cancer. 2013; 1835: 164-169.
176. Aparicio LA, Calvo MB, Figueroa A, Pulido EG, Campelo RG. Potential role of sugar transporters in cancer and their relationship with anticancer therapy. International Journal of Endocrinology. 2010; 2010:
177. Augustin R. The protein family of glucose transport facilitators: It's not only about glucose after all. IUBMB Life. 2010; 62: 315-333.

178. Carvalho KC, Cunha IW, Rocha RM, Ayala FR, Cajaíba MM, Begnami MD, Vilela RS, Paiva GR, Andrade RG, Soares FA. GLUT1 expression in malignant tumors and its use as an immunodiagnostic marker. Clinics. 2011; 66: 965-972.
179. Grover-McKay M, Walsh SA, Seftor EA, Thomas PA, Hendrix MJC. Role for glucose transporter 1 protein in human breast cancer. Pathology and Oncology Research. 1998; 4: 115-120.
180. Xu G, Feng J, Li J *Comparison of MCF-7, a Poorly Invasive Human Breast Tumor Cell Line, and MDA-MB-231, a Highly Invasive Human Breast Tumor Cell Line*. 2012. Ori-Medsci.
181. Brown RS, Wahl RL. Overexpression of Glut-1 glucose transporter in human breast cancer: An immunohistochemical study. Cancer. 1993; 72: 2979-2985.
182. Younes M, Brown RW, Mody DR, Fernandez L, Laucirica R. GLUT1 expression in human breast carcinoma: Correlation with known prognostic markers. Anticancer Research. 1995; 15: 2895-2898.
183. Brown RS, Goodman TM, Zasadny KR, Greenson JK, Wahl RL. Expression of hexokinase II and Glut-1 in untreated human breast cancer. Nuclear Medicine and Biology. 2002; 29: 443-453.
184. Kang SS, Chun YK, Hur MH, Lee HK, Kim YJ, Hong SR, Lee JH, Lee SG, Park YK. Clinical significance of glucose transporter 1 (GLUT1) expression in human breast carcinoma. Japanese Journal of Cancer Research. 2002; 93: 1123-1128.
185. Jang SM, Han H, Jang KS, Jun YJ, Jang SH, Min KW, Chung MS, Paik SS. The glycolytic phenotype is correlated with aggressiveness and poor prognosis in invasive ductal carcinomas. Journal of Breast Cancer. 2012; 15: 172-180.
186. Pinheiro C, Sousa B, Albergaria A, Paredes J, Dufloth R, Vieira D, Schmitt F, Baltazar F. GLUT1 and CAIX expression profiles in breast cancer correlate with adverse prognostic factors and MCT1 overexpression. Histology and Histopathology. 2011; 26: 1279-1286.
187. Krzeslak A, Wojcik-Krowiranda K, Forma E, Jozwiak P, Romanowicz H, Bienkiewicz A, Brys M. Expression of GLUT1 and GLUT3 glucose transporters in endometrial and breast cancers. Pathology and Oncology Research. 2012; 18: 721-728.
188. Alò PL, Visca P, Botti C, Galati GM, Sebastiani V, Andreano T, Di Tondo U, Pizer ES. Immunohistochemical expression of human erythrocyte glucose transporter and fatty acid synthase in infiltrating breast carcinomas and adjacent typical/atypical hyperplastic or normal breast tissue. American Journal of Clinical Pathology. 2001; 116: 129-134.
189. Cantuaria G, Magalhaes A, Penalver M, Angioli R, Braunschweiger P, Gomez-Marin O, Kanhoush R, Gomez-Fernandez C, Nadji M. Expression of GLUT-1 glucose transporter in borderline and malignant epithelial tumors of the ovary. Gynecologic Oncology. 2000; 79: 33-37.
190. Cantuaria G, Fagotti A, Ferrandina G, Magalhaes A, Nadji M, Angioli R, Penalver M, Mancuso S, Scambia G. GLUT-1 expression in ovarian carcinoma: Association with survival and response to chemotherapy. Cancer. 2001; 92: 1144-1150.
191. Kalir T, Wang BY, Goldfischer M, Haber RS, Reder I, Demopoulos R, Cohen CJ, Burstein DE. Immunohistochemical staining of GLUT1 in benign, borderline, and malignant ovarian epithelia. Cancer. 2002; 94: 1078-1082.
192. Rudlowski C, Moser M, Becker AJ, Rath W, Buttner R, Schroder W, Schurmann A. GLUT1 mRNA and protein expression in ovarian borderline tumors and cancer. Oncology. 2004; 66: 404-410.
193. Tsukioka M, Matsumoto Y, Noriyuki M, Yoshida C, Nobeyama H, Yoshida H, Yasui T, Sumi T, Honda KI, Ishiko O. Expression of glucose transporters in

epithelial ovarian carcinoma: Correlation with clinical characteristics and tumor angiogenesis. Oncology Reports. 2007; 18: 361-367.
194. Semaan A, Munkarah AR, Arabi H, Bandyopadhyay S, Seward S, Kumar S, Qazi A, Hussein Y, Morris RT, Ali-Fehmi R. Expression of GLUT-1 in epithelial ovarian carcinoma: Correlation with tumor cell proliferation, angiogenesis, survival and ability to predict optimal cytoreduction. Gynecologic Oncology. 2011; 121: 181-186.
195. Cho H, Lee YS, Kim J, Chung JY, Kim JH. Overexpression of glucose transporter-1 (GLUT-1) predicts poor prognosis in epithelial ovarian cancer. Cancer Investigation. 2013; 31: 607-615.
196. Lamkin DM, Spitz DR, Shahzad MMK, Zimmerman B, Lenihan DJ, Degeest K, Lubaroff DM, Shinn EH, Sood AK, Lutgendorf SK. Glucose as a prognostic factor in ovarian carcinoma. Cancer. 2009; 115: 1021-1027.
197. Edinger AL. Controlling cell growth and survival through regulated nutrient transporter expression. Biochemical Journal. 2007; 406: 1-12.
198. Barthel A, Okino ST, Liao J, Nakatani K, Li J, Whitlock Jr JP, Roth RA. Regulation of GLUT1 gene transcription by the serine/threonine kinase Akt1. Journal of Biological Chemistry. 1999; 274: 20281-20286.
199. Flier JS, Mueckler MM, Usher P, Lodish HF. Elevated levels of glucose transport and transporter messenger RNA are induced by ras or src oncogenes. Science. 1987; 235: 1492-1495.
200. Yun J, Rago C, Cheong I, Pagliarini R, Angenendt P, Rajagopalan H, Schmidt K, Willson JKV, Markowitz S, Zhou S, Diaz Jr LA, Velculescu VE, Lengauer C, et al. Glucose deprivation contributes to the development of KRAS pathway mutations in tumor cells. Science. 2009; 325: 1555-1559.
201. Chen C, Pore N, Behrooz A, Ismail-Beigi F, Maity A. Regulation of glut1 mRNA by hypoxia-inducible factor-1: Interaction between H-ras and hypoxia. Journal of Biological Chemistry. 2001; 276: 9519-9525.
202. Schwartzenberg-Bar-Yoseph F, Armoni M, Karnieli E. The Tumor Suppressor p53 Down-Regulates Glucose Transporters GLUT1 and GLUT4 Gene Expression. Cancer Research. 2004; 64: 2627-2633.
203. Young CD, Lewis AS, Rudolph MC, Ruehle MD, Jackman MR, Yun UJ, Ilkun O, Pereira R, Abel ED, Anderson SM. Modulation of glucose transporter 1 (GLUT1) expression levels alters mouse mammary tumor cell growth in vitro and in vivo. PLoS ONE. 2011; 6:
204. Leen WG, Klepper J, Verbeek MM, Leferink M, Hofste T, Van Engelen BG, Wevers RA, Arthur T, Bahi-Buisson N, Ballhausen D, Bekhof J, Van Bogaert P, Carrilho I, et al. Glucose transporter-1 deficiency syndrome: The expanding clinical and genetic spectrum of a treatable disorder. Brain. 2010; 133: 655-670.
205. Mathupala SP, Ko YH, Pedersen PL. Hexokinase II: Cancer's double-edged sword acting as both facilitator and gatekeeper of malignancy when bound to mitochondria. Oncogene. 2006; 25: 4777-4786.
206. Pedersen PL, Mathupala S, Rempel A, Geschwind JF, Ko YH. Mitochondrial bound type II hexokinase: A key player in the growth and survival of many cancers and an ideal prospect for therapeutic intervention. Biochimica et Biophysica Acta - Bioenergetics. 2002; 1555: 14-20.
207. Mathupala SP, Ko YH, Pedersen PL. Hexokinase-2 bound to mitochondria: Cancer's stygian link to the "Warburg effect" and a pivotal target for effective therapy. Seminars in Cancer Biology. 2009; 19: 17-24.
208. Wilson JE. Isozymes of mammalian hexokinase: Structure, subcellular localization and metabolic function. Journal of Experimental Biology. 2003; 206: 2049-2057.
209. Pastorino JG, Hoek JB. Hexokinase II: The integration of energy metabolism and control of apoptosis. Current Medicinal Chemistry. 2003; 10: 1535-1551.

210. Pastorino JG, Shulga N, Hoek JB. Mitochondrial binding of hexokinase II inhibits Bax-induced cytochrome c release and apoptosis. Journal of Biological Chemistry. 2002; 277: 7610-7618.
211. Azoulay-Zohar H, Israelson A, Abu-Hamad S, Shoshan-Barmatz V. In self-defence: Hexokinase promotes voltage-dependent anion channel closure and prevents mitochondria-mediated apoptotic cell death. Biochemical Journal. 2004; 377: 347-355.
212. Roberts DJ, Tan-Sah VP, Ding EY, Smith JM, Miyamoto S. Hexokinase-II Positively Regulates Glucose Starvation-Induced Autophagy through TORC1 Inhibition. Molecular Cell. 2014; 53: 521-533.
213. Tan VP, Miyamoto S. HK2/hexokinase-II integrates glycolysis and autophagy to confer cellular protection. Autophagy. 2015; 11: 963-964.
214. Mathupala SP, Rempel A, Pedersen PL. Aberrant glycolytic metabolism of cancer cells: A remarkable coordination of genetic, transcriptional, post-translational, and mutational events that lead to a critical role for Type II hexokinase. Journal of Bioenergetics and Biomembranes. 1997; 29: 339-443.
215. Goel A, Mathupala SP, Pedersen PL. Glucose metabolism in cancer: Evidence that demethylation events play a role in activating type II hexokinase gene expression. Journal of Biological Chemistry. 2003; 278: 15333-15340.
216. Sato-Tadano A, Suzuki T, Amari M, Takagi K, Miki Y, Tamaki K, Watanabe M, Ishida T, Sasano H, Ohuchi N. Hexokinase II in breast carcinoma: A potent prognostic factor associated with hypoxia-inducible factor-1α and Ki-67. Cancer Science. 2013; 104: 1380-1388.
217. Palmieri D, Fitzgerald D, Shreeve SM, Hua E, Bronder JL, Weil RJ, Davis S, Stark AM, Merino MJ, Kurek R, Mehdorn HM, Davis G, Steinberg SM, et al. Analyses of resected human brain metastases of breast cancer reveal the association between up-regulation of hexokinase 2 and poor prognosis. Molecular Cancer Research. 2009; 7: 1438-1445.
218. Suh DH, Kim MA, Kim H, Kim MK, Kim HS, Chung HH, Kim YB, Song YS. Association of overexpression of hexokinase II with chemoresistance in epithelial ovarian cancer. Clinical and Experimental Medicine. 2014; 14: 345-353.
219. Jin Z, Gu J, Xin X, Lp Y, Wang H. Expression of hexokinase 2 in epithelial ovarian tumors and its clinical significance in serous ovarian cancer. European Journal of Gynaecological Oncology. 2014; 35: 519-524.
220. Mor I, Cheung EC, Vousden KH, *Control of glycolysis through regulation of PFK1: Old friends and recent additions*, in *Cold Spring Harbor Symposia on Quantitative Biology*2011. p. 211-216.
221. Yalcin A, Telang S, Clem B, Chesney J. Regulation of glucose metabolism by 6-phosphofructo-2-kinase/fructose-2,6-bisphosphatases in cancer. Experimental and Molecular Pathology. 2009; 86: 174-179.
222. Ros S, Schulze A. Balancing glycolytic flux: the role of 6-phosphofructo-2-kinase/fructose 2,6-bisphosphatases in cancer metabolism. Cancer & Metabolism. 2013; 1:8:
223. Atsumi T, Chesney J, Metz C, Leng L, Donnelly S, Makita Z, Mitchell R, Bucala R. High expression of inducible 6-phosphofructo-2-kinase/fructose-2,6-bisphosphatase (iPFK-2; PFKFB3) in human cancers. Cancer Research. 2002; 62: 5881-5887.
224. Chesney J, Mitchell R, Benigni F, Bacher M, Spiegel L, Al-Abed Y, Han JH, Metz C, Bucala R. An inducible gene product for 6-phosphofructo-2-kinase with an AU-rich instability element: Role in tumor cell glycolysis and the Warburg effect. Proceedings of the National Academy of Sciences of the United States of America. 1999; 96: 3047-3052.

225. Novellasdemunt L, Obach M, Millán-ariño L, Manzano A, Ventura F, Rosa JL, Jordan A, Navarro-Sabate À, Bartrons R. Progestins activate 6-phosphofructo-2-kinase/fructose-2,6-bisphosphatase 3 (PFKFB3) in breast cancer cells. Biochemical Journal. 2012; 442: 345-356.
226. Bando H, Atsumi T, Nishio T, Niwa H, Mishima S, Shimizu C, Yoshioka N, Bucala R, Koike T. Phosphorylation of the 6-phosphofructo-2-kinase/fructose 2,6-bisphosphatase/PFKFB3 family of glycolytic regulators in human cancer. Clinical Cancer Research. 2005; 11: 5784-5792.
227. Telang S, Yalcin A, Clem AL, Bucala R, Lane AN, Eaton JW, Chesney J. Ras transformation requires metabolic control by 6-phosphofructo-2-kinase. Oncogene. 2006; 25: 7225-7234.
228. Almeida A, Bolaños JP, Moncada S. E3 ubiquitin ligase APC/C-Cdh1 accounts for the Warburg effect by linking glycolysis to cell proliferation. Proceedings of the National Academy of Sciences of the United States of America. 2010; 107: 738-741.
229. Garcia-Cao I, Song MS, Hobbs RM, Laurent G, Giorgi C, De Boer VCJ, Anastasiou D, Ito K, Sasaki AT, Rameh L, Carracedo A, Vander Heiden MG, Cantley LC, et al. Systemic elevation of PTEN induces a tumor-suppressive metabolic state. Cell. 2012; 149: 49-62.
230. Yalcin A, Clem BF, Simmons A, Lane A, Nelson K, Clem AL, Brock E, Siow D, Wattenberg B, Telang S, Chesney J. Nuclear targeting of 6-phosphofructo-2-kinase (PFKFB3) increases proliferation via cyclin-dependent kinases. Journal of Biological Chemistry. 2009; 284: 24223-24232.
231. Yalcin A, Clem BF, Imbert-Fernandez Y, Ozcan SC, Peker S, O'Neal J, Klarer AC, Clem AL, Telang T, Chesney J. 6-Phosphofructo-2-kinase (PFKFB3) promotes cell cycle progression and suppresses apoptosis via Cdk1-mediated phosphorylation of p27. Cell Death and Disease. 2014; 5:
232. De Bock K, Georgiadou M, Schoors S, Kuchnio A, Wong BW, Cantelmo AR, Quaegebeur A, Ghesquière B, Cauwenberghs S, Eelen G, Phng LK, Betz I, Tembuyser B, et al. Role of PFKFB3-driven glycolysis in vessel sprouting. Cell. 2013; 154: 651-663.
233. Seo M, Lee YH. PFKFB3 regulates oxidative stress homeostasis via its S-glutathionylation in cancer. Journal of Molecular Biology. 2014; 426: 830-842.
234. Iqbal MA, Gupta V, Gopinath P, Mazurek S, Bamezai RNK. Pyruvate kinase M2 and cancer: An updated assessment. FEBS Letters. 2014; 588: 2685-2692.
235. Israelsen WJ, Vander Heiden MG. Pyruvate kinase: Function, regulation and role in cancer. Seminars in Cell and Developmental Biology. 2015; 43: 43-51.
236. David CJ, Chen M, Assanah M, Canoll P, Manley JL. HnRNP proteins controlled by c-Myc deregulate pyruvate kinase mRNA splicing in cancer. Nature. 2010; 463: 364-368.
237. Wong N, Ojo D, Yan J, Tang D. PKM2 contributes to cancer metabolism. Cancer Letters. 2015; 356: 184-191.
238. Jiang L, Deberardinis RJ. Cancer metabolism: When more is less. Nature. 2012; 489: 511-512.
239. Christofk HR, Vander Heiden MG, Wu N, Asara JM, Cantley LC. Pyruvate kinase M2 is a phosphotyrosine-binding protein. Nature. 2008; 452: 181-186.
240. Hitosugi T, Kang S, Vander Heiden MG, Chung TW, Elf S, Lythgoe K, Dong S, Lonial S, Wang X, Chen GZ, Xie J, Gu TL, Polakiewicz RD, et al. Tyrosine phosphorylation inhibits PKM2 to promote the warburg effect and tumor growth. Science Signaling. 2009; 2:
241. Gao X, Wang H, Yang JJ, Liu X, Liu ZR. Pyruvate Kinase M2 Regulates Gene Transcription by Acting as a Protein Kinase. Molecular Cell. 2012; 45: 598-609.

242. Yang W, Xia Y, Ji H, Zheng Y, Liang J, Huang W, Gao X, Aldape K, Lu Z. Nuclear PKM2 regulates β-catenin transactivation upon EGFR activation. Nature. 2011; 480: 118-122.
243. Yang W, Xia Y, Hawke D, Li X, Liang J, Xing D, Aldape K, Hunter T, Alfred Yung WK, Lu Z. PKM2 phosphorylates histone H3 and promotes gene transcription and tumorigenesis. Cell. 2012; 150: 685-696.
244. Luo W, Hu H, Chang R, Zhong J, Knabel M, O'Meally R, Cole RN, Pandey A, Semenza GL. Pyruvate kinase M2 is a PHD3-stimulated coactivator for hypoxia-inducible factor 1. Cell. 2011; 145: 732-744.
245. Luo W, Semenza GL. Pyruvate kinase M2 regulates glucose metabolism by functioning as a coactivator for hypoxia-inducible factor 1 in cancer cells. Oncotarget. 2011; 2: 551-556.
246. Christofk HR, Vander Heiden MG, Harris MH, Ramanathan A, Gerszten RE, Wei R, Fleming MD, Schreiber SL, Cantley LC. The M2 splice isoform of pyruvate kinase is important for cancer metabolism and tumour growth. Nature. 2008; 452: 230-233.
247. Anastasiou D, Yu Y, Israelsen WJ, Jiang JK, Boxer MB, Hong BS, Tempel W, Dimov S, Shen M, Jha A, Yang H, Mattaini KR, Metallo CM, et al. Pyruvate kinase M2 activators promote tetramer formation and suppress tumorigenesis. Nature Chemical Biology. 2012; 8: 839-847.
248. Vander Heiden MG, Christofk HR, Schuman E, Subtelny AO, Sharfi H, Harlow EE, Xian J, Cantley LC. Identification of small molecule inhibitors of pyruvate kinase M2. Biochemical Pharmacology. 2010; 79: 1118-1124.
249. Bluemlein K, Grüning NM, Feichtinger RG, Lehrach H, Kofler B, Ralser M. No evidence for a shift in pyruvate kinase PKM1 to PKM2 expression during tumorigenesis. Oncotarget. 2011; 2: 393-400.
250. Desai S, Ding M, Wang B, Lu Z, Zhao Q, Shaw K, Alfred Yung WK, Weinstein JN, Tan M, Yao J. Tissue-specific isoform switch and DNA hypomethylation of the pyruvate kinase PKM gene in human cancers. Oncotarget. 2014; 5: 8202-8210.
251. Cortés-Cros M, Hemmerlin C, Ferretti S, Zhang J, Gounarides JS, Yin H, Muller A, Haberkorn A, Chene P, Sellers WR, Hofmann F. M2 isoform of pyruvate kinase is dispensable for tumor maintenance and growth. Proceedings of the National Academy of Sciences of the United States of America. 2013; 110: 489-494.
252. Jeoung NH. Pyruvate dehydrogenase kinases: Therapeutic targets for diabetes and cancers. Diabetes and Metabolism Journal. 2015; 39: 188-197.
253. Patel MS, Nemeria NS, Furey W, Jordan F. The pyruvate dehydrogenase complexes: Structure-based function and regulation. Journal of Biological Chemistry. 2014; 289: 16615-16623.
254. Sugden MC, Holness MJ. Recent advances in mechanisms regulating glucose oxidation at the level of the pyruvate dehydrogenase complex by PDKs. American Journal of Physiology - Endocrinology and Metabolism. 2003; 284: E855-E862.
255. Sutendra G, Michelakis ED. Pyruvate dehydrogenase kinase as a novel therapeutic target in oncology. Frontiers in Oncology. 2013; 3 MAR:
256. Hitosugi T, Fan J, Chung TW, Lythgoe K, Wang X, Xie J, Ge Q, Gu TL, Polakiewicz RD, Roesel JL, Chen GZ, Boggon TJ, Lonial S, et al. Tyrosine Phosphorylation of Mitochondrial Pyruvate Dehydrogenase Kinase 1 Is Important for Cancer Metabolism. Molecular Cell. 2011; 44: 864-877.
257. Fiume L, Manerba M, Vettraino M, Di Stefano G. Inhibition of lactate dehydrogenase activity as an approach to cancer therapy. Future Medicinal Chemistry. 2014; 6: 429-445.
258. Granchi C, Bertini S, Macchia M, Minutolo F. Inhibitors of lactate dehydrogenase isoforms and their therapeutic potentials. Current Medicinal Chemistry. 2010; 17: 672-697.

259. Augoff K, Hryniewicz-Jankowska A, Tabola R. Lactate dehydrogenase 5: An old friend and a new hope in the war on cancer. Cancer Letters. 2015; 358: 1-7.
260. Goldberg E, Eddy EM, Duan C, Odet F. LDHC: The ultimate testis-specific gene. Journal of Andrology. 2010; 31: 86-94.
261. Gupta GS. LDH-C4: A target with therapeutic potential for cancer and contraception. Molecular and Cellular Biochemistry. 2012; 371: 115-127.
262. Miao P, Sheng S, Sun X, Liu J, Huang G. Lactate dehydrogenase a in cancer: A promising target for diagnosis and therapy. IUBMB Life. 2013; 65: 904-910.
263. Koukourakis MI, Kontomanolis E, Giatromanolaki A, Sivridis E, Liberis V. Serum and tissue ldh levels in patients with breast/gynaecological cancer and benign diseases. Gynecologic and Obstetric Investigation. 2009; 67: 162-168.
264. Dennison JB, Molina JR, Mitra S, González-Angulo AM, Balko JM, Kuba MG, Sanders ME, Pinto JA, Gómez HL, Arteaga CL, Brown RE, Mills GB. Lactate dehydrogenase B: A metabolic marker of response to neoadjuvant chemotherapy in breast cancer. Clinical Cancer Research. 2013; 19: 3703-3713.
265. Leiblich A, Cross SS, Catto JWF, Phillips JT, Leung HY, Hamdy FC, Rehman I. Lactate dehydrogenase-B is silenced by promoter hypermethylation in human prostate cancer. Oncogene. 2006; 25: 2953-2960.
266. Wang ZY, Loo TY, Shen JG, Wang N, Wang DM, Yang DP, Mo SL, Guan XY, Chen JP. LDH-A silencing suppresses breast cancer tumorigenicity through induction of oxidative stress mediated mitochondrial pathway apoptosis. Breast Cancer Research and Treatment. 2012; 131: 791-800.
267. Fan J, Hitosugi T, Chung TW, Xie J, Ge Q, Gu TL, Polakiewicz RD, Chen GZ, Boggon TJ, Lonial S, Khuri FR, Kang S, Chen J. Tyrosine phosphorylation of lactate dehydrogenase a is important for NADH/NAD + redox homeostasis in cancer cells. Molecular and Cellular Biology. 2011; 31: 4938-4950.
268. Grosse F, Nasheuer HP, Scholtissek S, Schomburg U. Lactate dehydrogenase and glyceraldehyde-phosphate dehydrogenase are single-stranded DNA-binding proteins that affect the DNA-polymerase-α-primase complex. European Journal of Biochemistry. 1986; 160: 459-467.
269. Dai RP, Yu FX, Goh SR, Chng HW, Tan YL, Fu JL, Zheng L, Luo Y. Histone 2B (H2B) expression is confined to a proper NAD+/NADH redox status. Journal of Biological Chemistry. 2008; 283: 26894-26901.
270. He H, Lee MC, Zheng LL, Zheng L, Luo Y. Integration of the metabolic/redox state, histone gene switching, DNA replication and S-phase progression by moonlighting metabolic enzymes. Bioscience Reports. 2013; 33: 187-197.
271. Fantin VR, St-Pierre J, Leder P. Attenuation of LDH-A expression uncovers a link between glycolysis, mitochondrial physiology, and tumor maintenance. Cancer Cell. 2006; 9: 425-434.
272. Vander Heiden MG. Targeting cancer metabolism: A therapeutic window opens. Nature Reviews Drug Discovery. 2011; 10: 671-684.
273. Xintaropoulou C, Ward C, Wise A, Marston H, Turnbull A, Langdon SP. A comparative analysis of inhibitors of the glycolysis pathway in breast and ovarian cancer cell line models. Oncotarget. 2015; 6: 25677-25695.
274. Di Carlo G, Mascolo N, Izzo AA, Capasso F. Flavonoids: Old and new aspects of a class of natural therapeutic drugs. Life Sciences. 1999; 65: 337-353.
275. Middleton Jr E, Kandaswami C, Theoharides TC. The effects of plant flavonoids on mammalian cells: Implications for inflammation, heart disease, and cancer. Pharmacological Reviews. 2000; 52: 673-751.
276. Romano B, Pagano E, Montanaro V, Fortunato AL, Milic N, Borrelli F. Novel insights into the pharmacology of flavonoids. Phytotherapy Research. 2013; 27: 1588-1596.

277. Martin HJ, Kornmann F, Fuhrmann GF. The inhibitory effects of flavonoids and antiestrogens on the Glut1 glucose transporter in human erythrocytes. Chemico-Biological Interactions. 2003; 146: 225-235.
278. Kobori M, Shinmoto H, Tsushida T, Shinohara K. Phloretin-induced apoptosis in B16 melanoma 4A5 cells by inhibition of glucose transmembrane transport. Cancer Letters. 1997; 119: 207-212.
279. Kim MS, Kwon JY, Kang NJ, Lee KW, Lee HJ, *Phloretin induces apoptosis in H-Ras MCF10A human breast tumor cells through the activation of p53 via JNK and p38 mitogen-activated protein kinase signaling*, in *Annals of the New York Academy of Sciences*2009. p. 479-483.
280. Lefevre PF, Marshall JK. The atachment of phloretin and analogues to human erythrocytes in connection with inhibition of sugar transport. The Journal of Biological Chemistry. 1959; 234: 3022-3026.
281. Nelson JAS, Falk RE. The efficacy of phloridzin and phloretin on tumor cell growth. Anticancer Research. 1993; 13: 2287-2292.
282. Nelson JAS, Falk RE. Phloridzin and phloretin inhibition of 2-deoxy-D-glucose uptake by tumor cells in vitro and in vivo. Anticancer Research. 1993; 13: 2293-2299.
283. Kobori M, Iwashita K, Shinmoto H, Tsushida T. Phloretin-induced apoptosis in B16 melanoma 4A5 cells and HL60 human leukemia cells. Bioscience, Biotechnology and Biochemistry. 1999; 63: 719-725.
284. Wu CH, Ho YS, Tsai CY, Wang YJ, Tseng H, Wei PL, Lee CH, Liu RS, Lin SY. In vitro and in vivo study of phloretin-induced apoptosis in human liver cancer cells involving inhibition of type II glucose transporter. International Journal of Cancer. 2009; 124: 2210-2219.
285. Min J, Li X, Huang K, Tang H, Ding X, Qi C, Qin X, Xu Z. Phloretin induces apoptosis of non-small cell lung carcinoma A549 cells via JNK1/2 and p38 MAPK pathways. Oncology Reports. 2015; 34: 2871-2879.
286. Gonzalez-Menendez P, Hevia D, Rodriguez-Garcia A, Mayo JC, Sainz RM. Regulation of GLUT transporters by flavonoids in androgen-sensitive and-insensitive prostate cancer cells. Endocrinology. 2014; 155: 3238-3250.
287. Cao X, Fang L, Gibbs S, Huang Y, Dai Z, Wen P, Zheng X, Sadee W, Sun D. Glucose uptake inhibitor sensitizes cancer cells to daunorubicin and overcomes drug resistance in hypoxia. Cancer Chemotherapy and Pharmacology. 2007; 59: 495-505.
288. Yang KC, Tsai CY, Wang YJ, Wei PL, Lee CH, Chen JH, Wu CH, Ho YS. Apple polyphenol phloretin potentiates the anticancer actions of paclitaxel through induction of apoptosis in human Hep G2 cells. Molecular Carcinogenesis. 2009; 48: 420-431.
289. Sak K. Site-specific anticancer effects of dietary flavonoid quercetin. Nutrition and Cancer. 2014; 66: 177-193.
290. Miles SL, McFarland M, Niles RM. Molecular and physiological actions of quercetin: Need for clinical trials to assess its benefits in human disease. Nutrition Reviews. 2014; 72: 720-734.
291. Russo GL, Russo M, Spagnuolo C, Tedesco I, Bilotto S, Iannitti R, Palumbo R, *Quercetin: A pleiotropic kinase inhibitor against cancer*, in *Cancer Treatment and Research*2014. p. 185-205.
292. U.S. National Institutes of Health. *ClinicalTrials.gov*. 2016; Available from: https://clinicaltrials.gov/ct2/results?term=quercetin&brwse-force=true.
293. Cossarizza A, Gibellini L, Pinti M, Nasi M, Montagna JP, De Biasi S, Roat E, Bertoncelli L, Cooper EL. Quercetin and cancer chemoprevention. Evidence-based Complementary and Alternative Medicine. 2011; 2011:

294. Pérez A, Ojeda P, Ojeda L, Salas M, Rivas CI, Vera JC, Reyes AM. Hexose transporter GLUT1 harbors several distinct regulatory binding sites for flavones and tyrphostins. Biochemistry. 2011; 50: 8834-8845.
295. Strobel P, Allard C, Perez-Acle T, Calderon R, Aldunate R, Leighton F. Myricetin, quercetin and catechin-gallate inhibit glucose uptake in isolated rat adipocytes. Biochemical Journal. 2005; 386: 471-478.
296. Moreira L, Araújo I, Costa T, Correia-Branco A, Faria A, Martel F, Keating E. Quercetin and epigallocatechin gallate inhibit glucose uptake and metabolism by breast cancer cells by an estrogen receptor-independent mechanism. Experimental Cell Research. 2013; 319: 1784-1795.
297. Deng XH, Song HY, Zhou YF, Yuan GY, Zheng FJ. Effects of quercetin on the proliferation of breast cancer cells and expression of survivin in vitro. Experimental and Therapeutic Medicine. 2013; 6: 1155-1158.
298. Ren MX, Deng XH, Ai F, Yuan GY, Song HY. Effect of quercetin on the proliferation of the human ovarian cancer cell line SKOV-3 in vitro. Experimental and Therapeutic Medicine. 2015; 10: 579-583.
299. Ranganathan S, Halagowder D, Sivasithambaram ND. Quercetin suppresses twist to induce apoptosis in MCF-7 breast cancer cells. PLoS ONE. 2015; 10:
300. Tao SF, He HF, Chen Q. Quercetin inhibits proliferation and invasion acts by up-regulating miR-146a in human breast cancer cells. Molecular and Cellular Biochemistry. 2015; 402: 93-100.
301. Seo HS, Ku JM, Choi HS, Choi YK, Woo JK, Kim M, Kim I, Na CH, Hur H, Jang BH, Shin YC, Ko SG. Quercetin induces caspase-dependent extrinsic apoptosis through inhibition of signal transducer and activator of transcription 3 signaling in HER2-overexpressing BT-474 breast cancer cells. Oncology Reports. 2016; 36: 31-42.
302. Zhang H, Zhang M, Yu L, Zhao Y, He N, Yang X. Antitumor activities of quercetin and quercetin-5',8-disulfonate in human colon and breast cancer cell lines. Food and Chemical Toxicology. 2012; 50: 1589-1599.
303. Liao H, Bao X, Zhu J, Qu J, Sun Y, Ma X, Wang E, Guo X, Kang Q, Zhen Y. O-Alkylated derivatives of quercetin induce apoptosis of MCF-7 cells via a caspase-independent mitochondrial pathway. Chemico-Biological Interactions. 2015; 242: 91-98.
304. Zhao X, Wang Q, Yang S, Chen C, Li X, Liu J, Zou Z, Cai D. Quercetin inhibits angiogenesis by targeting calcineurin in the xenograft model of human breast cancer. European Journal of Pharmacology. 2016; 781: 60-68.
305. Wang H, Tao L, Qi K, Zhang H, Feng D, Wei W, Kong H, Chen T, Lin Q. Quercetin reverses tamoxifen resistance in breast cancer cells. Journal of B.U.ON. 2015; 20: 707-713.
306. Minaei A, Sabzichi M, Ramezani F, Hamishehkar H, Samadi N. Co-delivery with nano-quercetin enhances doxorubicin-mediated cytotoxicity against MCF-7 cells. Molecular Biology Reports. 2016; 43: 99-105.
307. Maciejczyk A, Surowiak P. Quercetin inhibits proliferation and increases sensitivity of ovarian cancer cells to cisplatin and paclitaxel. Ginekologia Polska. 2013; 84: 590-595.
308. Yang Z, Liu Y, Liao J, Gong C, Sun C, Zhou X, Wei X, Zhang T, Gao Q, Ma D, Chen G. Quercetin induces endoplasmic reticulum stress to enhance cDDP cytotoxicity in ovarian cancer: Involvement of STAT3 signaling. FEBS Journal. 2015; 282: 1111-1125.
309. Yi L, Zongyuan Y, Cheng G, Lingyun Z, Guilian Y, Wei G. Quercetin enhances apoptotic effect of tumor necrosis factor-related apoptosis-inducing ligand (TRAIL) in ovarian cancer cells through reactive oxygen species (ROS) mediated CCAAT

enhancer-binding protein homologous protein (CHOP)-death receptor 5 pathway. Cancer Science. 2014; 105: 520-527.
310. Ferry DR, Smith A, Malkhandi J, Fyfe DW, DeTakats PG, Anderson D, Baker J, Kerr DJ. Phase I clinical trial of the flavonoid quercetin: Pharmacokinetics and evidence for in vivo tyrosine kinase inhibition. Clinical Cancer Research. 1996; 2: 659-668.
311. Lorenzo GD, Pagliuca M, Perillo T, Zarrella A, Verde A, Placido SD, Buonerba C. Complete response and fatigue improvement with the combined use of cyclophosphamide and quercetin in a patient with metastatic bladder cancer a case report. Medicine (United States). 2016; 95:
312. Chan DA, Sutphin PD, Nguyen P, Turcotte S, Lai EW, Banh A, Reynolds GE, Chi JT, Wu J, Solow-Cordero DE, Bonnet M, Flanagan JU, Bouley DM, et al. Targeting GLUT1 and the Warburg effect in renal cell carcinoma by chemical synthetic lethality. Science Translational Medicine. 2011; 3:
313. Tocris Bioscience. 2016; Available from: https://www.tocris.com.
314. Matsumoto T, Jimi S, Migita K, Takamatsu Y, Hara S. Inhibition of glucose transporter 1 induces apoptosis and sensitizes multiple myeloma cells to conventional chemotherapeutic agents. Leukemia Research. 2016; 41: 103-110.
315. Adams DJ, Ito D, Rees MG, Seashore-Ludlow B, Puyang X, Ramos AH, Cheah JH, Clemons PA, Warmuth M, Zhu P, Shamji AF, Schreiber SL. NAMPT is the cellular target of STF-31-like small-molecule probes. ACS Chemical Biology. 2014; 9: 2247-2254.
316. Dragovich PS, Zhao G, Baumeister T, Bravo B, Giannetti AM, Ho YC, Hua R, Li G, Liang X, Ma X, O'Brien T, Oh A, Skelton NJ, et al. Fragment-based design of 3-aminopyridine-derived amides as potent inhibitors of human nicotinamide phosphoribosyltransferase (NAMPT). Bioorganic and Medicinal Chemistry Letters. 2014; 24: 954-962.
317. Kropp EM, Oleson BJ, Broniowska KA, Bhattacharya S, Chadwick AC, Diers AR, Hu Q, Sahoo D, Hogg N, Boheler KR, Corbett JA, Gundry RL. Inhibition of an NAD+ salvage pathway provides efficient and selective toxicity to human pluripotent stem cells. Stem Cells Translational Medicine. 2015; 4: 483-493.
318. Liu Y, Zhang W, Cao Y, Bergmeier S, Chen X. Small compound inhibitors of basal glucose transport inhibit cell proliferation and induce apoptosis in cancer cells via glucose-deprivation-like mechanisms. Cancer Letters. 2010; 298: 176-185.
319. Liu Y, Cao Y, Zhang W, Bergmeier S, Qian Y, Akbar H, Colvin R, Ding J, Tong L, Wu S, Hines J, Chen X. A small-molecule inhibitor of glucose transporter 1 downregulates glycolysis, induces cell-cycle arrest, and inhibits cancer cell growth in vitro and in vivo. Molecular Cancer Therapeutics. 2012; 11: 1672-1682.
320. Merck Millipore M. 2016; Available from: http://www.merckmillipore.com/.
321. Liu W, Fang Y, Wang XT, Liu J, Dan X, Sun LL. Overcoming 5-Fu resistance of colon cells through inhibition of glut1 by the specific inhibitor WZB117. Asian Pacific Journal of Cancer Prevention. 2014; 15: 7037-7041.
322. Zhao F, Ming J, Zhou Y, Fan L. Inhibition of Glut1 by WZB117 sensitizes radioresistant breast cancer cells to irradiation. Cancer Chemotherapy and Pharmacology. 2016; 1-10.
323. Shibuya K, Okada M, Suzuki S, Seino M, Seino S, Takeda H, Kitanaka C. Targeting the facilitative glucose transporter GLUT1 inhibits the self-renewal and tumor-initiating capacity of cancer stem cells. Oncotarget. 2015; 6: 651-661.
324. IOmet Pharma. 2016; Available from: http://iometpharma.com/research/cancer-metabolism-2/.
325. Pedersen PL. 3-Bromopyruvate (3BP) a fast acting, promising, powerful, specific, and effective "small molecule" anti-cancer agent taken from labside to bedside:

Introduction to a special issue. Journal of Bioenergetics and Biomembranes. 2012; 44: 1-6.
326. Cardaci S, Desideri E, Ciriolo MR. Targeting aerobic glycolysis: 3-Bromopyruvate as a promising anticancer drug. Journal of Bioenergetics and Biomembranes. 2012; 44: 17-29.
327. Chen Z, Zhang H, Lu W, Huang P. Role of mitochondria-associated hexokinase II in cancer cell death induced by 3-bromopyruvate. Biochimica et Biophysica Acta - Bioenergetics. 2009; 1787: 553-560.
328. Shoshan MC. 3-bromopyruvate: Targets and outcomes. Journal of Bioenergetics and Biomembranes. 2012; 44: 7-15.
329. Majkowska-Skrobek G, Augustyniak D, Lis P, Bartkowiak A, Gonchar M, Ko YH, Pedersen PL, Goffeau A, Ułaszewski S. Killing multiple myeloma cells with the small molecule 3-bromopyruvate: Implications for therapy. Anti-Cancer Drugs. 2014; 25: 673-682.
330. Queirós O, Preto A, Pacheco A, Pinheiro C, Azevedo-Silva J, Moreira R, Pedro M, Ko YH, Pedersen PL, Baltazar F, Casal M. Butyrate activates the monocarboxylate transporter MCT4 expression in breast cancer cells and enhances the antitumor activity of 3-bromopyruvate. Journal of Bioenergetics and Biomembranes. 2012; 44: 141-153.
331. Xu RH, Pelicano H, Zhou Y, Carew JS, Feng L, Bhalla KN, Keating MJ, Huang P. Inhibition of glycolysis in cancer cells: A novel strategy to overcome drug resistance associated with mitochondrial respiratory defect and hypoxia. Cancer Research. 2005; 65: 613-621.
332. Philippe I, Xiao-Dong Z, Edwige L, Marie-Hélène L, Stéphane A, Hubert L, Laurent P. Experimental results using 3-bromopyruvate in mesothelioma: In vitro and in vivo studies. Journal of Bioenergetics and Biomembranes. 2012; 44: 81-90.
333. Zou X, Zhang M, Sun Y, Zhao S, Wei Y, Zhang X, Jiang C, Liu H. Inhibitory effects of 3-bromopyruvate in human nasopharyngeal carcinoma cells. Oncology Reports. 2015; 34: 1895-1904.
334. Wintzell M, Löfstedt L, Johansson J, Pedersen AB, Fuxe J, Shoshan M. Repeated cisplatin treatment can lead to a multiresistant tumor cell population with stem cell features and sensitivity to 3-bromopyruvate. Cancer Biology and Therapy. 2012; 13: 1454-1462.
335. Ko YH, Pedersen PL, Geschwind JF. Glucose catabolism in the rabbit VX2 tumor model for liver cancer: Characterization and targeting hexokinase. Cancer Letters. 2001; 173: 83-91.
336. Ko YH, Smith BL, Wang Y, Pomper MG, Rini DA, Torbenson MS, Hullihen J, Pedersen PL. Advanced cancers: Eradication in all cases using 3-bromopyruvate therapy to deplete ATP. Biochemical and Biophysical Research Communications. 2004; 324: 269-275.
337. Buijs M, Vossen JA, Geschwind JFH, Ishimori T, Engles JM, Acha-Ngwodo O, Wahl RL, Vali M. Specificity of the anti-glycolytic activity of 3-bromopyruvate confirmed by FDG uptake in a rat model of breast cancer. Investigational New Drugs. 2009; 27: 120-123.
338. Ko YH, Verhoeven HA, Lee MJ, Corbin DJ, Vogl TJ, Pedersen PL. A translational study "case report" on the small molecule "energy blocker" 3-bromopyruvate (3BP) as a potent anticancer agent: From bench side to bedside. Journal of Bioenergetics and Biomembranes. 2012; 44: 163-170.
339. El Sayed SM, Mohamed WG, Hassan Seddik MA, Ahmed Ahmed AS, Mahmoud AG, Amer WH, Helmy Nabo MM, Hamed AR, Ahmed NS, Abd-Allah AAR. Safety and outcome of treatment of metastatic melanoma using 3-bromopyruvate: A concise literature review and case study. Chinese Journal of Cancer. 2014; 33: 356-364.

340. Periera da Silva AP, El-Bacha T, Kyaw N, dos Santosa RS, da-Silva WS, Almeida FC, da Poian AT, Galina A. Inhibition of energy-producing pathways of HepG2 cells by 3-bromopyruvate. Biochemical Journal. 2009; 417: 717-726.
341. Dell'Antone P. Targets of 3-bromopyruvate, a new, energy depleting, anticancer agent. Medicinal Chemistry. 2009; 5: 491-496.
342. Kwiatkowska E, Wojtala M, Gajewska A, Soszyński M, Bartosz G, Sadowska-Bartosz I. Effect of 3-bromopyruvate acid on the redox equilibrium in non-invasive MCF-7 and invasive MDA-MB-231 breast cancer cells. Journal of Bioenergetics and Biomembranes. 2016; 48: 23-32.
343. Clem B, Telang S, Clem A, Yalcin A, Meier J, Simmons A, Rasku MA, Arumugam S, Dean WL, Eaton J, Lane A, Trent JO, Chesney J. Small-molecule inhibition of 6-phosphofructo-2-kinase activity suppresses glycolytic flux and tumor growth. Molecular Cancer Therapeutics. 2008; 7: 110-120.
344. Klarer A, O'Neal J, Imbert-Fernandez Y, Clem A, Ellis S, Clark J, Clem B, Chesney J, Telang S. Inhibition of 6-phosphofructo-2-kinase (PFKFB3) induces autophagy as a survival mechanism. Cancer & Metabolism. 2014; 2:2:
345. Trefely S, Khoo PS, Krycer JR, Chaudhuri R, Fazakerley DJ, Parker BL, Sultani G, Lee J, Stephan JP, Torres E, Jung K, Kuijl C, James DE, et al. Kinome screen identifies PFKFB3 and glucose metabolism as important regulators of the insulin/insulin-like growth factor (IGF)-1 signaling pathway. Journal of Biological Chemistry. 2015; 290: 25834-25846.
346. Schoors S, De Bock K, Cantelmo AR, Georgiadou M, Ghesquière B, Cauwenberghs S, Kuchnio A, Wong BW, Quaegebeur A, Goveia J, Bifari F, Wang X, Blanco R, et al. Partial and transient reduction of glycolysis by PFKFB3 blockade reduces pathological angiogenesis. Cell Metabolism. 2014; 19: 37-48.
347. Telang S, Clem BF, Klarer AC, Clem AL, Trent JO, Bucala R, Chesney J. Small molecule inhibition of 6-phosphofructo-2-kinase suppresses t cell activation. Journal of Translational Medicine. 2012; 10:
348. Seo M, Kim JD, Neau D, Sehgal I, Lee YH. Structure-based development of small molecule PFKFB3 inhibitors: A framework for potential cancer therapeutic agents targeting the Warburg effect. PLoS ONE. 2011; 6:
349. Clem BF, O'Neal J, Tapolsky G, Clem AL, Imbert-Fernandez Y, Kerr Ii DA, Klarer AC, Redman R, Miller DM, Trent JO, Telang S, Chesney J. Targeting 6-phosphofructo-2-kinase (PFKFB3) as a therapeutic strategy against cancer. Molecular Cancer Therapeutics. 2013; 12: 1461-1470.
350. U.S. National Institutes of Health. *Phase 1 Safety Study of ACT-PFK-158, 2HCl in Patients With Advanced Solid Malignancies*. 2016; Available from: https://clinicaltrials.gov/ct2/show/study/NCT02044861.
351. Telang S, O'Neal J, Tapolsky G, Clem B, Kerr A, Imbert-Ferndandez Y, Chesney J. Discovery of a PFKFB3 inhibitor for phase I trial testing that synergizes with the B-Raf inhibitor vemurafenib. Cancer & Metabolism. 2014; 2: P14-P14.
352. Michelakis ED, Webster L, Mackey JR. Dichloroacetate (DCA) as a potential metabolic-targeting therapy for cancer. British Journal of Cancer. 2008; 99: 989-994.
353. Kankotia S, Stacpoole PW. Dichloroacetate and cancer: New home for an orphan drug? Biochimica et Biophysica Acta - Reviews on Cancer. 2014; 1846: 617-629.
354. Kaufmann P, Engelstad K, Wei Y, Jhung S, Sano MC, Shungu DC, Millar WS, Hong X, Gooch CL, Mao X, Pascual JM, Hirano M, Stacpoole PW, et al. Dichloroacetate causes toxic neuropathy in MELAS: A randomized, controlled clinical trial. Neurology. 2006; 66: 324-330.
355. Stacpoole PW, Kerr DS, Barnes C, Bunch S, Carney PR, Fennell EM, Felitsyn NM, Gilmore RL, Greer M, Henderson GN, Hutson AD, Neiberger RE, O'Brien RG, et al. Controlled clinical trial of dichloroacetate for treatment of congenital lactic acidosis in children. Pediatrics. 2006; 117: 1519-1531.

356. Dunbar EM, Coats BS, Shroads AL, Langaee T, Lew A, Forder JR, Shuster JJ, Wagner DA, Stacpoole PW. Phase 1 trial of dichloroacetate (DCA) in adults with recurrent malignant brain tumors. Investigational New Drugs. 2014; 32: 452-464.
357. Saed GM, Fletcher NM, Jiang ZL, Abu-Soud HM, Diamond MP. Dichloroacetate induces apoptosis of epithelial ovarian cancer cells through a mechanism involving modulation of oxidative stress. Reproductive Sciences. 2011; 18: 1253-1261.
358. Sun RC, Fadia M, Dahlstrom JE, Parish CR, Board PG, Blackburn AC. Reversal of the glycolytic phenotype by dichloroacetate inhibits metastatic breast cancer cell growth in vitro and in vivo. Breast Cancer Research and Treatment. 2010; 120: 253-260.
359. Sun RC, Board PG, Blackburn AC. Targeting metabolism with arsenic trioxide and dichloroacetate in breast cancer cells. Molecular Cancer. 2011; 10:
360. Gang BP, Dilda PJ, Hogg PJ, Blackburn AC. Targeting of two aspects of metabolism in breast cancer treatment. Cancer Biology and Therapy. 2014; 15: 1533-1541.
361. Bonnet S, Archer SL, Allalunis-Turner J, Haromy A, Beaulieu C, Thompson R, Lee CT, Lopaschuk GD, Puttagunta L, Harry G, Hashimoto K, Porter CJ, Andrade MA, et al. A Mitochondria-K+ Channel Axis Is Suppressed in Cancer and Its Normalization Promotes Apoptosis and Inhibits Cancer Growth. Cancer Cell. 2007; 11: 37-51.
362. Sutendra G, Dromparis P, Kinnaird A, Stenson TH, Haromy A, Parker JMR, McMurtry MS, Michelakis ED. Mitochondrial activation by inhibition of PDKII suppresses HIF1a signaling and angiogenesis in cancer. Oncogene. 2013; 32: 1638-1650.
363. Lin G, Hill DK, Andrejeva G, Boult JKR, Troy H, Fong ACLFWT, Orton MR, Panek R, Parkes HG, Jafar M, Koh DM, Robinson SP, Judson IR, et al. Dichloroacetate induces autophagy in colorectal cancer cells and tumours. British Journal of Cancer. 2014; 111: 375-385.
364. Dhar S, Lippard SJ. Mitaplatin, a potent fusion of cisplatin and the orphan drug dichloroacetate. Proceedings of the National Academy of Sciences of the United States of America. 2009; 106: 22199-22204.
365. Michelakis ED, Sutendra G, Dromparis P, Webster L, Haromy A, Niven E, Maguire C, Gammer TL, Mackey JR, Fulton D, Abdulkarim B, McMurtry MS, Petruk KC. Metabolic modulation of glioblastoma with dichloroacetate. Science Translational Medicine. 2010; 2:
366. Garon EB, Christofk HR, Hosmer W, Britten CD, Bahng A, Crabtree MJ, Hong CS, Kamranpour N, Pitts S, Kabbinavar F, Patel C, Von Euw E, Black A, et al. Dichloroacetate should be considered with platinum-based chemotherapy in hypoxic tumors rather than as a single agent in advanced non-small cell lung cancer. Journal of Cancer Research and Clinical Oncology. 2014; 140: 443-452.
367. Strum SB, Adalsteinsson O, Black RR, Segal D, Peress NL, Waldenfels J. Case report: Sodium dichloroacetate (DCA) inhibition of the "warburg Effect" in a human cancer patient: Complete response in non-Hodgkin's lymphoma after disease progression with rituximab-CHOP. Journal of Bioenergetics and Biomembranes. 2013; 45: 307-315.
368. Granchi C, Paterni I, Rani R, Minutolo F. Small-molecule inhibitors of human LDH5. Future Medicinal Chemistry. 2013; 5: 1967-1991.
369. Thornburg JM, Nelson KK, Clem BF, Lane AN, Arumugam S, Simmons A, Eaton JW, Telang S, Chesney J. Targeting aspartate aminotransferase in breast cancer. Breast Cancer Research. 2008; 10:
370. Fiume L, Manerba M, Vettraino M, Di Stefano G. Impairment of aerobic glycolysis by inhibitors of lactic dehydrogenase hinders the growth of human hepatocellular carcinoma cell lines. Pharmacology. 2010; 86: 157-162.

371. Fiume L, Vettraino M, Manerba M, Di Stefano G. Inhibition of lactic dehydrogenase as a way to increase the anti-proliferative effect of multi-targeted kinase inhibitors. Pharmacological Research. 2011; 63: 328-334.
372. Zhao Y, Liu H, Liu Z, Ding Y, LeDoux SP, Wilson GL, Voellmy R, Lin Y, Lin W, Nahta R, Liu B, Fodstad O, Chen J, et al. Overcoming trastuzumab resistance in breast cancer by targeting dysregulated glucose metabolism. Cancer Research. 2011; 71: 4585-4597.
373. Zhou M, Zhao Y, Ding Y, Liu H, Liu Z, Fodstad O, Riker AI, Kamarajugadda S, Lu J, Owen LB, Ledoux SP, Tan M. Warburg effect in chemosensitivity: Targeting lactate dehydrogenase-A re-sensitizes Taxol-resistant cancer cells to Taxol. Molecular Cancer. 2010; 9:
374. Miskimins WK, Ahn HJ, Kim JY, Ryu S, Jung YS, Choi JY. Synergistic anti-cancer effect of phenformin and oxamate. PLoS ONE. 2014; 9:
375. Zhai X, Yang Y, Wan J, Zhu R, Wu Y. Inhibition of LDH-A by oxamate induces G2/M arrest, apoptosis and increases radiosensitivity in nasopharyngeal carcinoma cells. Oncology Reports. 2013; 30: 2983-2991.
376. Yang Y, Su D, Zhao L, Zhang D, Xu J, Wan J, Fan S, Chen M. Different effects of LDH-A inhibition by oxamate in non-small cell lung cancer cells. Oncotarget. 2014; 5: 11886-11896.
377. Zhao Z, Han F, Yang S, Wu J, Zhan W. Oxamate-mediated inhibition of lactate dehydrogenase induces protective autophagy in gastric cancer cells: Involvement of the Akt-mTOR signaling pathway. Cancer Letters. 2015; 358: 17-26.
378. Granchi C, Roy S, Giacomelli C, MacChia M, Tuccinardi T, Martinelli A, Lanza M, Betti L, Giannaccini G, Lucacchini A, Funel N, León LG, Giovannetti E, et al. Discovery of N-hydroxyindole-based inhibitors of human lactate dehydrogenase isoform A (LDH-A) as starvation agents against cancer cells. Journal of Medicinal Chemistry. 2011; 54: 1599-1612.
379. Granchi C, Roy S, De Simone A, Salvetti I, Tuccinardi T, Martinelli A, MacChia M, Lanza M, Betti L, Giannaccini G, Lucacchini A, Giovannetti E, Sciarrillo R, et al. N-Hydroxyindole-based inhibitors of lactate dehydrogenase against cancer cell proliferation. European Journal of Medicinal Chemistry. 2011; 46: 5398-5407.
380. Granchi C, Calvaresi EC, Tuccinardi T, Paterni I, Macchia M, Martinelli A, Hergenrother PJ, Minutolo F. Assessing the differential action on cancer cells of LDH-A inhibitors based on the N-hydroxyindole-2-carboxylate (NHI) and malonic (Mal) scaffolds. Organic and Biomolecular Chemistry. 2013; 11: 6588-6596.
381. Maftouh M, Avan A, Sciarrillo R, Granchi C, Leon LG, Rani R, Funel N, Smid K, Honeywell R, Boggi U, Minutolo F, Peters GJ, Giovannetti E. Synergistic interaction of novel lactate dehydrogenase inhibitors with gemcitabine against pancreatic cancer cells in hypoxia. British Journal of Cancer. 2014; 110: 172-182.
382. Zhao Y, Butler EB, Tan M. Targeting cellular metabolism to improve cancer therapeutics. Cell Death and Disease. 2013; 4:
383. Butler EB, Zhao Y, Muñoz-Pinedo C, Lu J, Tan M. Stalling the engine of resistance: Targeting cancer metabolism to overcome therapeutic resistance. Cancer Research. 2013; 73: 2709-2717.
384. Dasari S, Bernard Tchounwou P. Cisplatin in cancer therapy: Molecular mechanisms of action. European Journal of Pharmacology. 2014; 740: 364-378.
385. *Cisplatin.org*. 2016; Available from: http://www.cisplatin.org/.
386. Parness J, Horwitz SB. Taxol binds to polymerized tubulin in vitro. Journal of Cell Biology. 1981; 91: 479-487.
387. Gelmon K. The taxoids: paclitaxel and docetaxel. The Lancet. 1994; 344: 1267-1272.
388. Weaver BA. How Taxol/paclitaxel kills cancer cells. Molecular Biology of the Cell. 2014; 25: 2677-2681.

389. Morales DR, Morris AD, *Metformin in cancer treatment and prevention*, in *Annual Review of Medicine*2015. p. 17-29.
390. Quinn BJ, Kitagawa H, Memmott RM, Gills JJ, Dennis PA. Repositioning metformin for cancer prevention and treatment. Trends in Endocrinology and Metabolism. 2013; 24: 469-480.
391. Chae YK, Arya A, Malecek MK, Shin DS, Carneiro B, Chandra S, Kaplan J, Kalyan A, Altman JK, Platanias L, Giles F. Repurposing metformin for cancer treatment: current clinical studies. Oncotarget. 2016; 7 40767-40780.
392. Heckman-Stoddard BM, Gandini S, Puntoni M, Dunn BK, Decensi A, Szabo E. Repurposing old drugs to chemoprevention: The case of metformin. Seminars in Oncology. 2016; 43: 123-133.
393. Levenson AS, Jordan VC. MCF-7: The first hormone-responsive breast cancer cell line. Cancer Research. 1997; 57: 3071-3078.
394. Neve RM, Chin K, Fridlyand J, Yeh J, Baehner FL, Fevr T, Clark L, Bayani N, Coppe JP, Tong F, Speed T, Spellman PT, DeVries S, et al. A collection of breast cancer cell lines for the study of functionally distinct cancer subtypes. Cancer Cell. 2006; 10: 515-527.
395. The Global Bioresourse Center. *ATCC*. 2015; Available from: www.atcc.org.
396. Gaffney EV. A cell line (HBL-100) established from human breast milk. Cell and Tissue Research. 1982; 227: 563-568.
397. Benz CC, Scott GK, Sarup JC, Johnson RM, Tripathy D, Coronado E, Shepard HM, Osborne CK. Estrogen-dependent, tamoxifen-resistant tumorigenic growth of MCF-7 cells transfected with HER2/neu. Breast Cancer Research and Treatment. 1992; 24: 85-95.
398. Hamilton TC, Young RC, McKoy WM, Grotzinger KR, Green JA, Chu EW, Whang-Peng J, Rogan AM, Green WR, Ozols RF. Characterization of a human ovarian carcinoma cell line (NIH:OVCAR-3) with androgen and estrogen receptors. Cancer Research. 1983; 43: 5379-5389.
399. Langdon SP, Lawrie SS, Hay FG, Hawkes MM, McDonald A, Hayward IP, Schol DJ, Hilgers J, Leonard RCF, Smyth JF. Characterization and properties of nine human ovarian adenocarcinoma cell lines. Cancer Research. 1988; 48: 6166-6172.
400. Cooke SL, Ng CKY, Melnyk N, Garcia MJ, Hardcastle T, Temple J, Langdon S, Huntsman D, Brenton JD. Genomic analysis of genetic heterogeneity and evolution in high-grade serous ovarian carcinoma. Oncogene. 2010; 29: 4905-4913.
401. Vichai V, Kirtikara K. Sulforhodamine B colorimetric assay for cytotoxicity screening. Nat. Protocols. 2006; 1: 1112-1116.
402. Irene V. Bijnsdorp EG, and Godefridus J. Peters, *Analysis of Drug Interactions*, in *Cancer Cell Culture, Methods and Protocols*, I.A. Cree, Editor 2011: Humana Press. p. 421 - 434.
403. Thermo Fisher Scientific. *Amplex® Red Glucose/Glucose Oxidase Assay Kit*. 2015; Available from: https://www.thermofisher.com/order/catalog/product/A22189.
404. Trinity Biotech. *Lactate Kit*. 2015; Available from: http://www.trinitybiotech.com/products/lactate-kit-reagent-10-x-10ml/.
405. BD Pharmingen. *FITC Annexin V Apoptosis Detection Kit I* 2015; Available from: http://www.bdbiosciences.com/us/applications/research/apoptosis/apoptosis-kits-sets/fitc-annexin-v-apoptosis-detection-kit-i/p/556547.
406. Thermo Fisher Scientific. *FxCycle™ PI/RNase Staining Solution*. 2015; Available from: https://www.thermofisher.com/order/catalog/product/F10797.
407. Qiagen. *miRNeasy Mini Kit*. 2015; Available from: https://www.qiagen.com/gb/shop/sample-technologies/rna/rna-preparation/mirneasy-mini-kit.

408. Thermo Fisher Scientific. *Illumina® TotalPrep™ RNA Amplification Kit*. 2015; Available from: https://www.thermofisher.com/order/catalog/product/AMIL1791.
409. Gerich JE. Control of glycaemia. Bailliere's Clinical Endocrinology and Metabolism. 1993; 7: 551-586.
410. Birsoy K, Possemato R, Lorbeer FK, Bayraktar EC, Thiru P, Yucel B, Wang T, Chen WW, Clish CB, Sabatini DM. Metabolic determinants of cancer cell sensitivity to glucose limitation and biguanides. Nature. 2014; 508: 108-112.
411. Walsh NP, Blannin AK, Robson PJ, Gleeson M. Glutamine, exercise and immune function: Links and possible mechanisms. Sports Medicine. 1998; 26: 177-191.
412. Maestri NE, McGowan KD, Brusilow SW. Plasma glutamine concentration: A guide in the management of urea cycle disorders. The Journal of Pediatrics. 1992; 121: 259-261.
413. Yang L, Moss T, Mangala LS, Marini J, Zhao H, Wahlig S, Armaiz-Pena G, Jiang D, Achreja A, Win J, Roopaimoole R, Rodriguez-Aguayo C, Mercado-Uribe I, et al. Metabolic shifts toward glutamine regulate tumor growth, invasion and bioenergetics in ovarian cancer. Molecular Systems Biology. 2014; 10:
414. Mathews EH, Stander BA, Joubert AM, Liebenberg L. Tumor cell culture survival following glucose and glutamine deprivation at typical physiological concentrations. Nutrition. 2014; 30: 218-227.
415. Aykin-Burns N, Ahmad IM, Zhu Y, Oberley LW, Spitz DR. Increased levels of superoxide and H_2O_2 mediate the differential susceptibility of cancer cells versus normal cells to glucose deprivation. Biochemical Journal. 2009; 418: 29-37.
416. Graham NA, Tahmasian M, Kohli B, Komisopoulou E, Zhu M, Vivanco I, Teitell MA, Wu H, Ribas A, Lo RS, Mellinghoff IK, Mischel PS, Graeber TG. Glucose deprivation activates a metabolic and signaling amplification loop leading to cell death. Molecular Systems Biology. 2012; 8:
417. Yuneva M, Zamboni N, Oefner P, Sachidanandam R, Lazebnik Y. Deficiency in glutamine but not glucose induces MYC-dependent apoptosis in human cells. Journal of Cell Biology. 2007; 178: 93-105.
418. Van Tonder A, Joubert AM, Cromarty AD. Limitations of the 3-(4,5-dimethylthiazol-2-yl)-2,5-diphenyl-2H-tetrazolium bromide (MTT) assay when compared to three commonly used cell enumeration assays. BMC Research Notes. 2015; 8:
419. Ganapathy-Kanniappan S, Geschwind JFH, Kunjithapatham R, Buijs M, Syed LH, Rao PP, Ota S, Vali M. The pyruvic acid analog 3-bromopyruvate interferes with the tetrazolium reagent MTS in the evaluation of cytotoxicity. Assay and Drug Development Technologies. 2010; 8: 258-262.
420. Mosmann T. Rapid colorimetric assay for cellular growth and survival: Application to proliferation and cytotoxicity assays. Journal of Immunological Methods. 1983; 65: 55-63.
421. National Cancer Institute. *Developmental Therapeutics Program*. 2016; Available from: https://dtp.cancer.gov/.
422. Guiyan Xu JF, Jianyi Li. *Comparison of MCF-7, a Poorly Invasive Human Breast Tumor Cell Line, and MDA-MB-231, a Highly Invasive Human Breast Tumor Cell Line*. 2012; Available from: www.ori-medsci.com.
423. Gaglio D, Metallo CM, Gameiro PA, Hiller K, Danna LS, Balestrieri C, Alberghina L, Stephanopoulos G, Chiaradonna F. Oncogenic K-Ras decouples glucose and glutamine metabolism to support cancer cell growth. Molecular Systems Biology. 2011; 7:
424. Kim S, Kim DH, Jung WH, Koo JS. Metabolic phenotypes in triple-negative breast cancer. Tumor Biology. 2013; 34: 1699-1712.
425. Yaginuma Y, Westphal H. Abnormal structure and expression of the p53 gene in human ovarian carcinoma cell lines. Cancer Research. 1992; 52: 4196-4199.

426. Shayesteh L, Lu Y, Kuo WL, Baldocchi R, Godfrey T, Collins C, Pinkel D, Powell B, Mills GB, Gray JW. PlK3CA is implicated as an oncogene in ovarian cancer. Nature Genetics. 1999; 21: 99-102.
427. Bhattacharya B, Low SHH, Soh C, Kamal Mustapa N, Beloueche-Babari M, Koh KX, Loh J, Soong R. Increased drug resistance is associated with reduced glucose levels and an enhanced glycolysis phenotype. British Journal of Pharmacology. 2014; 171: 3255-3267.
428. Griffiths CL, Olin JL. Triple negative breast cancer: A brief review of its characteristics and treatment options. Journal of Pharmacy Practice. 2012; 25: 319-323.
429. Wise A, *Identification of novel inhibitors of GLUT1 as potent cancer cell-killing agents*, in *26th EORTC-NCI-AACR Symposium*2014: Barcelona, Spain.
430. van Genderen H, Kenis H, Lux P, Ungeth L, Maassen C, Deckers N, Narula J, Hofstra L, Reutelingsperger C. In vitro measurement of cell death with the annexin A5 affinity assay. Nature Protocols. 2006; 1: 363-367.
431. Vermes I, Haanen C, Steffens-Nakken H, Reutellingsperger C. A novel assay for apoptosis Flow cytometric detection of phosphatidylserine expression on early apoptotic cells using fluorescein labelled Annexin V. Journal of Immunological Methods. 1995; 184: 39-51.
432. Riccardi C, Nicoletti I. Analysis of apoptosis by propidium iodide staining and flow cytometry. Nature Protocols. 2006; 1: 1458-1461.
433. Cooper. GM, *The Cell, A Molecular Approach*. 2nd ed2000: Sunderland (MA): Sinauer Associates.
434. Pozarowski P, Darzynkiewicz Z. Analysis of cell cycle by flow cytometry. Methods in molecular biology (Clifton, N.J.). 2004; 281: 301-311.
435. Zong WX, Thompson CB. Necrotic death as a cell fate. Genes and Development. 2006; 20: 1-15.
436. White E. The role for autophagy in cancer. Journal of Clinical Investigation. 2015; 125: 42-46.
437. Cheong H, Lu C, Lindsten T, Thompson CB. Therapeutic targets in cancer cell metabolism and autophagy. Nature Biotechnology. 2012; 30: 671-678.
438. Giacinti C, Giordano A. RB and cell cycle progression. Oncogene. 2006; 25: 5220-5227.
439. Zhang C, Liu J, Liang Y, Wu R, Zhao Y, Hong X, Lin M, Yu H, Liu L, Levine AJ, Hu W, Feng Z. Tumour-associated mutant p53 drives the Warburg effect. Nature Communications. 2013; 4:
440. Wang YD, Li SJ, Liao JX. Inhibition of glucose transporter 1 (GLUT1) chemosensitized head and neck cancer cells to cisplatin. Technology in Cancer Research and Treatment. 2013; 12: 525-535.
441. Sargeant RJ, Paquet MR. Effect of insulin on the rates of synthesis and degradation of GLUT1 and GLUT4 glucose transporters in 3T3-L1 adipocytes. Biochemical Journal. 1993; 290: 913-919.
442. Khayat ZA, McCall AL, Klip A. Unique mechanism of GLUT3 glucose transporter regulation by prolonged energy demand: Increased protein half-life. Biochemical Journal. 1998; 333: 713-718.
443. Hsu PD, Lander ES, Zhang F. Development and applications of CRISPR-Cas9 for genome engineering. Cell. 2014; 157: 1262-1278.
444. Sheng SL, Liu JJ, Dai YH, Sun XG, Xiong XP, Huang G. Knockdown of lactate dehydrogenase A suppresses tumor growth and metastasis of human hepatocellular carcinoma. FEBS Journal. 2012; 279: 3898-3910.
445. Allison SJ, Knight JRP, Granchi C, Rani R, Minutolo F, Milner J, Phillips RM. Identification of LDH-A as a therapeutic target for cancer cell killing via (i) p53/NAD(H)-dependent and (ii) p53-independent pathways. Oncogenesis. 2014; 3:

446. Nakazawa MS, Keith B, Simon MC. Oxygen availability and metabolic adaptations. Nature Reviews Cancer. 2016; 16: 663-673.
447. Adeva-Andany M, López-Ojén M, Funcasta-Calderón R, Ameneiros-Rodríguez E, Donapetry-García C, Vila-Altesor M, Rodríguez-Seijas J. Comprehensive review on lactate metabolism in human health. Mitochondrion. 2014; 17: 76-100.
448. Chou TC. Drug combination studies and their synergy quantification using the chou-talalay method. Cancer Research. 2010; 70: 440-446.
449. Nakano A, Tsuji D, Miki H, Cui Q, El Sayed SM, Ikegame A, Oda A, Amou H, Nakamura S, Harada T, Fujii S, Kagawa K, Takeuchi K, et al. Glycolysis inhibition inactivates ABC transporters to restore drug sensitivity in malignant cells. PLoS ONE. 2011; 6:
450. Liang H, Tong J, Xie G, He J, Li J, Pan F. Synergistic antitumor effect of dichloroacetate in combination with 5-fluorouracil in colorectal cancer. Journal of Biomedicine and Biotechnology. 2011; 2011:
451. Narayan M, Wilken JA, Harris LN, Baron AT, Kimbler KD, Maihle NJ. Trastuzumab-lnduced HER reprogramming in "Resistant" breast carcinoma cells. Cancer Research. 2009; 69: 2191-2194.
452. Rizos CV, Elisaf MS. Metformin and cancer. European Journal of Pharmacology. 2013; 705: 96-108.
453. Coperchini F, Leporati P, Rotondi M, Chiovato L. Expanding the therapeutic spectrum of metformin: From diabetes to cancer. Journal of Endocrinological Investigation. 2015; 38: 1047-1055.
454. Hirsch HA, Iliopoulos D, Tsichlis PN, Struhl K. Metformin selectively targets cancer stem cells, and acts together with chemotherapy to block tumor growth and prolong remission. Cancer Research. 2009; 69: 7507-7511.
455. Iliopoulos D, Hirsch HA, Struhl K. Metformin decreases the dose of chemotherapy for prolonging tumor remission in mouse xenografts involving multiple cancer cell types. Cancer Research. 2011; 71: 3196-3201.
456. Cufí S, Corominas-Faja B, Vazquez-Martin A, Oliveras-Ferraros C, Dorca J, Bosch-Barrera J, Martin-Castillo B, Menendez JA. Metformin-induced preferential killing of breast cancer initiating CD44 +CD24 -/low cells is sufficient to overcome primary resistance to trastuzumab in HER2+ human breast cancer xenografts. Oncotarget. 2012; 3: 395-398.
457. Dong L, Zhou Q, Zhang Z, Zhu Y, Duan T, Feng Y. Metformin sensitizes endometrial cancer cells to chemotherapy by repressing glyoxalase I expressionjog. Journal of Obstetrics and Gynaecology Research. 2012; 38: 1077-1085.
458. Hanna RK, Zhou C, Malloy KM, Sun L, Zhong Y, Gehrig PA, Bae-Jump VL. Metformin potentiates the effects of paclitaxel in endometrial cancer cells through inhibition of cell proliferation and modulation of the mTOR pathway. Gynecologic Oncology. 2012; 125: 458-469.
459. Rattan R, Graham RP, Maguire JL, Giri S, Shridhar V. Metformin suppresses ovarian cancer growth and metastasis with enhancement of cisplatin cytotoxicity in Vivo. Neoplasia. 2011; 13: 483-491.
460. Sahra IB, Laurent K, Giuliano S, Larbret F, Ponzio G, Gounon P, Le Marchand-Brustel Y, Giorgetti-Peraldi S, Cormont M, Bertolotto C, Deckert M, Auberger P, Tanti JF, et al. Targeting cancer cell metabolism: The combination of metformin and 2-deoxyglucose induces p53-dependent apoptosis in prostate cancer cells. Cancer Research. 2010; 70: 2465-2475.
461. Cheong JH, Park ES, Liang J, Dennison JB, Tsavachidou D, Nguyen-Charles C, Cheng KW, Hall H, Zhang D, Lu Y, Ravoori M, Kundra V, Ajani J, et al. Dual inhibition of tumor energy pathway by 2-deoxyglucose and metformin is effective against a broad spectrum of preclinical cancer models. Molecular Cancer Therapeutics. 2011; 10: 2350-2362.

462. Choi YW, Lim IK. Sensitization of metformin-cytotoxicity by dichloroacetate via reprogramming glucose metabolism in cancer cells. Cancer Letters. 2014; 346: 300-308.
463. Haugrud AB, Zhuang Y, Coppock JD, Miskimins WK. Dichloroacetate enhances apoptotic cell death via oxidative damage and attenuates lactate production in metformin-treated breast cancer cells. Breast Cancer Research and Treatment. 2014; 147: 539-550.
464. Wilcock C, Bailey CJ. Accumulation of metformin by tissues of the normal and diabetic mouse. Xenobiotica. 1994; 24: 49-57.
465. Zordoky BNM, Bark D, Soltys CL, Sung MM, Dyck JRB. The anti-proliferative effect of metformin in triple-negative MDA-MB-231 breast cancer cells is highly dependent on glucose concentration: Implications for cancer therapy and prevention. Biochimica et Biophysica Acta - General Subjects. 2014; 1840: 1943-1957.
466. Zhuang Y, Miskimins WK. Metformin induces both caspase-dependent and poly(ADP-ribose) polymerase-dependent cell death in breast cancer cells. Molecular Cancer Research. 2011; 9: 603-615.
467. Isakovic A, Harhaji L, Stevanovic D, Markovic Z, Sumarac-Dumanovic M, Starcevic V, Micic D, Trajkovic V. Dual antiglioma action of metformin: Cell cycle arrest and mitochondria-dependent apoptosis. Cellular and Molecular Life Sciences. 2007; 64: 1290-1302.
468. Yue W, Zheng X, Lin Y, Yang CS, Xu Q, Carpizo D, Huang H, DiPaola RS, Tan XL. Metformin combined with aspirin significantly inhibit pancreatic cancer cell growth in vitro and in vivo by suppressing antiapoptotic proteins Mcl-1 and Bcl-2. Oncotarget. 2015; 6: 21208-21224.
469. Zhuang Y, Keith WK. Cell cycle arrest in Metformin treated breast cancer cells involves activation of AMPK, downregulation of cyclin D1, and requires p27Kip1 or p21Cip1. Journal of Molecular Signaling. 2008; 3:
470. Semenza GL, *Regulation of mammalian O2 homeostasis by hypoxia-inducible factor 1*, in *Annual Review of Cell and Developmental Biology*1999. p. 551-578.
471. Supek F, Bošnjak M, Škunca N, Šmuc T. Revigo summarizes and visualizes long lists of gene ontology terms. PLoS ONE. 2011; 6:
472. Lu M, Kleckner N. Molecular cloning and characterization of the pgm gene encoding phosphoglucomutase of Escherichia coli. Journal of Bacteriology. 1994; 176: 5847-5851.
473. Yeung SJ, Pan J, Lee MH. Roles of p53, MYC and HIF-1 in regulating glycolysis - The seventh hallmark of cancer. Cellular and Molecular Life Sciences. 2008; 65: 3981-3999.
474. Bertout JA, Patel SA, Simon MC. The impact of O2 availability on human cancer. Nature Reviews Cancer. 2008; 8: 967-975.
475. Helmlinger G, Yuan F, Dellian M, Jain RK. Interstitial pH and pO<inf>2</inf> gradients in solid tumors in vivo: High-resolution measurements reveal a lack of correlation. Nature Medicine. 1997; 3: 177-182.
476. Jiang BH, Semenza GL, Bauer C, Marti HH. Hypoxia-inducible factor 1 levels vary exponentially over a physiologically relevant range of O <inf>2</inf> tension. American Journal of Physiology - Cell Physiology. 1996; 271:
477. Martinez-Perez C, Ward C, Cook G, Mullen P, McPhail D, Harrison DJ, Langdon SP. Novel flavonoids as anti-cancer agents: Mechanisms of action and promise for their potential application in breast cancer. Biochemical Society Transactions. 2014; 42: 1017-1023.
478. Miksicek RJ. Interaction of naturally occurring nonsteroidal estrogens with expressed recombinant human estrogen receptor. Journal of Steroid Biochemistry and Molecular Biology. 1994; 49: 153-160.

479. Wang TTY, Sathyamoorthy N, Phang JM. Molecular effects of genistein on estrogen receptor mediated pathways. Carcinogenesis. 1996; 17: 271-275.
480. Xiao H, Li S, Zhang D, Liu T, Yu M, Wang F. PhosphogluSeparate and concurrent use of 2-deoxy-D-glucose and 3-bromopyruvate in pancreatic cancer cells. Oncology Reports. 2013; 29: 329-334.
481. Gwak GY, Yoon JH, Kim KM, Lee HS, Chung JW, Gores GJ. Hypoxia stimulates proliferation of human hepatoma cells through the induction of hexokinase II expression. Journal of Hepatology. 2005; 42: 358-364.
482. Cao X, Bloomston M, Zhang T, Frankel WL, Jia G, Wang B, Hall NC, Koch RM, Cheng H, Knopp MV, Sun D. Synergistic antipancreatic tumor effect by simultaneously targeting hypoxic cancer cells with HSP90 inhibitor and glycolysis inhibitor. Clinical Cancer Research. 2008; 14: 1831-1839.
483. Liu H, Hu YP, Savaraj N, Priebe W, Lampidis TJ. Hypersensitization of tumor cells to glycolytic inhibitors. Biochemistry. 2001; 40: 5542-5547.
484. Liu H, Savaraj N, Priebe W, Lampidis TJ. Hypoxia increases tumor cell sensitivity to glycolytic inhibitors: A strategy for solid tumor therapy (Model C). Biochemical Pharmacology. 2002; 64: 1745-1751.
485. Shahrzad S, Lacombe K, Adamcic U, Minhas K, Coomber BL. Sodium dichloroacetate (DCA) reduces apoptosis in colorectal tumor hypoxia. Cancer Letters. 2010; 297: 75-83.
486. Maher JC, Wangpaichitr M, Savaraj N, Kurtoglu M, Lampidis TJ. Hypoxia-inducible factor-1 confers resistance to the glycolytic inhibitor 2-deoxy-D-glucose. Molecular Cancer Therapeutics. 2007; 6: 732-741.
487. Bertino JR, Carman MD, Weiner HL, Cashmore A, Moroson BA, Srimatkandada S, Schornagel JH, Medina WD, Dube SK. Gene amplification and altered enzymes as mechanisms for the development of drug resistance. Cancer Treatment Reports. 1983; 67: 901-904.
488. Garofalo C, Capristo M, Manara MC, Mancarella C, Landuzzi L, Belfiore A, Lollini PL, Picci P, Scotlandi K. Metformin as an adjuvant drug against pediatric sarcomas: Hypoxia limits therapeutic effects of the drug. PLoS ONE. 2013; 8:
489. Griss T, Vincent EE, Egnatchik R, Chen J, Ma EH, Faubert B, Viollet B, DeBerardinis RJ, Jones RG. Metformin Antagonizes Cancer Cell Proliferation by Suppressing Mitochondrial-Dependent Biosynthesis. PLoS Biology. 2015; 13:
490. Safari Z, Safaralizadeh R, Seyedzadeh MH, Orang AV, Zare A, Feizi MAH, Kardar GA. The induction of metformin inhibitory effects on tumor cell growth in hypoxic condition. Iranian Journal of Allergy, Asthma and Immunology. 2015; 14: 605-614.
491. Wheaton WW, Weinberg SE, Hamanaka RB, Soberanes S, Sullivan LB, Anso E, Glasauer A, Dufour E, Mutlu GM, Scott Budigner GR, Chandel NS. Metformin inhibits mitochondrial complex I of cancer cells to reduce tumorigenesis. eLife. 2014; 2014:
492. Chi JT, Wang Z, Nuyten DSA, Rodriguez EH, Schaner ME, Salim A, Wang Y, Kristensen GB, Helland Å, Børresen-Dale AL, Giaccia A, Longaker MT, Hastie T, et al. Gene expression programs in response to hypoxia: Cell type specificity and prognostic significance in human cancers. PLoS Medicine. 2006; 3: 395-409.
493. Sanzey M, Abdul Rahim SA, Oudin A, Dirkse A, Kaoma T, Vallar L, Herold-Mende C, Bjerkvig R, Golebiewska A, Niclou SP. Comprehensive analysis of glycolytic enzymes as therapeutic targets in the treatment of glioblastoma. PLoS ONE. 2015; 10:
494. Hochachka PW, Buck LT, Doll CJ, Land SC. Unifying theory of hypoxia tolerance: Molecular/metabolic defense and rescue mechanisms for surviving oxygen lack. Proceedings of the National Academy of Sciences of the United States of America. 1996; 93: 9493-9498.

495. Iyer NV, Kotch LE, Agani F, Leung SW, Laughner E, Wenger RH, Gassmann M, Gearhart JD, Lawler AM, Yu AY, Semenza GL. Cellular and developmental control of O2 homeostasis by hypoxia- inducible factor 1α. Genes and Development. 1998; 12: 149-162.
496. Semenza GL, Jiang BH, Leung SW, Passantino R, Concordat JP, Maire P, Giallongo A. Hypoxia response elements in the aldolase A, enolase 1, and lactate dehydrogenase a gene promoters contain essential binding sites for hypoxia-inducible factor 1. Journal of Biological Chemistry. 1996; 271: 32529-32537.
497. Firth JD, Ebert BL, Pugh CW, Ratcliffe PJ. Oxygen-regulated control elements in the phosphoglycerate kinase 1 and lactate dehydrogenase A genes: Similarities with the erythropoietin 3′ enhancer. Proceedings of the National Academy of Sciences of the United States of America. 1994; 91: 6496-6500.
498. Altenberg B, Greulich KO. Genes of glycolysis are ubiquitously overexpressed in 24 cancer classes. Genomics. 2004; 84: 1014-1020.
499. Ho VT, Bunn HF. Effects of transition metals on the expression of the erythropoietin gene: Further evidence that the oxygen sensor is a heme protein. Biochemical and Biophysical Research Communications. 1996; 223: 175-180.
500. Triantafyllou A, Liakos P, Tsakalof A, Georgatsou E, Simos G, Bonanou S. Cobalt induces hypoxia-inducible factor-1α (HIF-1α) in HeLa cells by an iron-independent, but ROS-, PI-3K- and MAPK-dependent mechanism. Free Radical Research. 2006; 40: 847-856.
501. Gould GW, Holman GD. The glucose transporter family: Structure, function and tissue-specific expression. Biochemical Journal. 1993; 295: 329-341.
502. Takagi H, King GL, Aiello LP. Hypoxia upregulates glucose transport activity through an adenosine- mediated increase of GLUT1 expression in retinal capillary endothelial cells. Diabetes. 1998; 47: 1480-1488.
503. Sørensen BS, Hao J, Overgaard J, Vorum H, Honoré B, Alsner J, Horsman MR. Influence of oxygen concentration and pH on expression of hypoxia induced genes. Radiotherapy and Oncology. 2005; 76: 187-193.
504. Minchenko A, Leshchinsky I, Opentanova I, Sang N, Srinivas V, Armstead V, Caro J. Hypoxia-inducible factor-1-mediated expression of the 6-phosphofructo-2-kinase/fructose-2,6-bisphosphatase-3 (PFKFB3) gene: Its possible role in the warburg effect. Journal of Biological Chemistry. 2002; 277: 6183-6187.
505. Ginouvès A, Ilc K, Macías N, Pouysségur J, Berra E. PHDs overactivation during chronic hypoxia "desensitizes" HIFα and protects cells from necrosis. Proceedings of the National Academy of Sciences of the United States of America. 2008; 105: 4745-4750.
506. Elia I, Schmieder R, Christen S, Fendt SM, *Organ-specific cancer metabolism and its potential for therapy*, in *Handbook of Experimental Pharmacology*2016. p. 321-353.
507. De Sousa Abreu R, Penalva LO, Marcotte EM, Vogel C. Global signatures of protein and mRNA expression levels. Molecular BioSystems. 2009; 5: 1512-1526.
508. Smith H, Board M, Pellagatti A, Turley H, Boultwood J, Callaghan R. The Effects of Severe Hypoxia on Glycolytic Flux and Enzyme Activity in a Model of Solid Tumors. Journal of Cellular Biochemistry. 2016; 1890-1901.
509. Faratian D, Um I, Wilson DS, Mullen P, Langdon SP, Harrison DJ. Phosphoprotein pathway profiling of ovarian carcinoma for the identification of potential new targets for therapy. European Journal of Cancer. 2011; 47: 1420-1431.
510. Graham AD, Faratian D, Rae F, Thomas JSJ. Tissue microarray technology in the routine assessment of HER-2 status in invasive breast cancer: A prospective study of the use of immunohistochemistry and fluorescence in situ hybridization. Histopathology. 2008; 52: 847-855.

511. Best DJ, Roberts DE. Algorithm AS 89: The Upper Tail Probabilities of Spearman's Rho. Journal of the Royal Statistical Society. Series C (Applied Statistics). 1975; 24: 377-379.
512. Camp RL, Chung GG, Rimm DL. Automated subcellular localization and quantification of protein expression in tissue microarrays. Nature Medicine. 2002; 8: 1323-1327.
513. McCabe A, Dolled-Filhart M, Camp RL, Rimm DL. Automated quantitative analysis (AQUA) of in situ protein expression, antibody concentration, and prognosis. Journal of the National Cancer Institute. 2005; 97: 1808-1815.
514. Mandai M, Amano Y, Yamaguchi K, Matsumura N, Baba T, Konishi I. Ovarian clear cell carcinoma meets metabolism; HNF-1β confers survival benefits through the Warburg effect and ROS reduction. Oncotarget. 2015; 6: 30704-30714.
515. Roberts DJ, Miyamoto S. Hexokinase II integrates energy metabolism and cellular protection: Akting on mitochondria and TORCing to autophagy. Cell Death and Differentiation. 2015; 22: 248-257.
516. Roberts DJ, Tan-Sah VP, Smith JM, Miyamoto S. Akt phosphorylates HK-II at Thr-473 and increases mitochondrial HK-II association to protect cardiomyocytes. Journal of Biological Chemistry. 2013; 288: 23798-23806.
517. Xiang T, Ohashi A, Huang Y, Pandita TK, Ludwig T, Powell SN, Yang Q. Negative regulation of AKT activation by BRCA1. Cancer Research. 2008; 68: 10040-10044.
518. Privat M, Radosevic-Robin N, Aubel C, Cayre A, Penault-Llorca F, Marceau G, Sapin V, Bignon YJ, Morvan D. BRCA1 induces major energetic metabolism reprogramming in breast cancer cells. PLoS ONE. 2014; 9:
519. Dong C, Yuan T, Wu Y, Wang Y, Fan TWM, Miriyala S, Lin Y, Yao J, Shi J, Kang T, Lorkiewicz P, St Clair D, Hung MC, et al. Loss of FBP1 by snail-mediated repression provides metabolic advantages in basal-like breast cancer. Cancer Cell. 2013; 23: 316-331.
520. Tao T, Li G, Dong Q, Liu D, Liu C, Han D, Huang Y, Chen S, Xu B, Chen M. Loss of SNAIL inhibits cellular growth and metabolism through the miR-128-mediated RPS6KB1/HIF-1α/PKM2 signaling pathway in prostate cancer cells. Tumor Biology. 2014; 35: 8543-8550.
521. Steták A, Veress R, Ovádi J, Csermely P, Kéri G, Ullrich A. Nuclear translocation of the tumor marker pyruvate kinase M2 induces programmed cell death. Cancer Research. 2007; 67: 1602-1608.
522. Tang Q, Ji Q, Xia W, Li L, Bai J, Ni R, Qin Y. Pyruvate Kinase M2 Regulates Apoptosis of Intestinal Epithelial Cells in Crohn's Disease. Digestive Diseases and Sciences. 2015; 60: 393-404.
523. Mauvais-Jarvis F, Clegg DJ, Hevener AL. The role of estrogens in control of energy balance and glucose homeostasis. Endocrine Reviews. 2013; 34: 309-338.
524. Chen JQ, Brown TR, Russo J. Regulation of energy metabolism pathways by estrogens and estrogenic chemicals and potential implications in obesity associated with increased exposure to endocrine disruptors. Biochimica et Biophysica Acta - Molecular Cell Research. 2009; 1793: 1128-1143.
525. Arias-Loza PA, Kreissl MC, Kneitz S, Kaiser FR, Israel I, Hu K, Frantz S, Bayer B, Fritzemeier KH, Korach KS, Pelzer T. The estrogen receptor-α is required and sufficient to maintain physiological glucose uptake in the mouse heart. Hypertension. 2012; 60: 1070-1077.
526. Furman E, Rushkin E, Margalit R, Bendel P, Degani H. Tamoxifen induced changes in MCF7 human breast cancer: In vitro and in vivo studies using nuclear magnetic resonance spectroscopy and imaging. Journal of Steroid Biochemistry and Molecular Biology. 1992; 43: 189-195.

527. Kostanyan A, Nazaryan K. Rat brain glycolysis regulation by estradiol-17β. BBA - Molecular Cell Research. 1992; 1133: 301-306.
528. Pastorelli R, Carpi D, Airoldi L, Chiabrando C, Bagnati R, Fanelli R, Moverare S, Ohlsson C. Proteome analysis for the identification of in vivo estrogen-regulated proteins in bone. Proteomics. 2005; 5: 4936-4945.
529. Hjerpe E, Egyhazi Brage S, Carlson J, Frostvik Stolt M, Schedvins K, Johansson H, Shoshan M, Åvall-Lundqvist E. Metabolic markers GAPDH, PKM2, ATP5B and BEC-index in advanced serous ovarian cancer. BMC Clinical Pathology. 2013; 13:
530. Karantanis D, Allen-Auerbach M, Czernin J. Relationship among glycolytic phenotype, grade, and histological subtype in ovarian carcinoma. Clinical Nuclear Medicine. 2012; 37: 49-53.
531. Kurokawa T, Yoshida Y, Kawahara K, Tsuchida T, Okazawa H, Fujibayashi Y, Yonekura Y, Kotsuji F. Expression of GLUT-1 glucose transfer, cellular proliferation activity and grade of tumor correlate with [F-18]-fluorodeoxyglucose uptake by positron emission tomography in epithelial tumors of the ovary. International Journal of Cancer. 2004; 109: 926-932.
532. Anderson AS, Roberts PC, Frisard MI, McMillan RP, Brown TJ, Lawless MH, Hulver MW, Schmelz EM. Metabolic changes during ovarian cancer progression as targets for sphingosine treatment. Experimental Cell Research. 2013; 319: 1431-1442.
533. Mergenthaler P, Lindauer U, Dienel GA, Meisel A. Sugar for the brain: The role of glucose in physiological and pathological brain function. Trends in Neurosciences. 2013; 36: 587-597.
534. Winkler BS, Arnold MJ, Brassell MA, Puro DG. Energy metabolism in human retinal Muller cells. Investigative Ophthalmology and Visual Science. 2000; 41: 3183-3190.
535. Setchell BP, Hinks NT. The importance of glucose in the oxidative metabolism of the testis of the conscious ram and the role of the pentose cycle. Biochemical Journal. 1967; 102: 623-630.
536. Pavlides S, Whitaker-Menezes D, Castello-Cros R, Flomenberg N, Witkiewicz AK, Frank PG, Casimiro MC, Wang C, Fortina P, Addya S, Pestell RG, Martinez-Outschoorn UE, Sotgia F, et al. The reverse Warburg effect: Aerobic glycolysis in cancer associated fibroblasts and the tumor stroma. Cell Cycle. 2009; 8: 3984-4001.
537. Groheux D, Giacchetti S, Moretti JL, Porcher R, Espié M, Lehmann-Che J, De Roquancourt A, Hamy AS, Cuvier C, Vercellino L, Hindié E. Correlation of high 18F-FDG uptake to clinical, pathological and biological prognostic factors in breast cancer. European Journal of Nuclear Medicine and Molecular Imaging. 2011; 38: 426-435.
538. Koo HR, Park JS, Kang KW, Cho N, Chang JM, Bae MS, Kim WH, Lee SH, Kim MY, Kim JY, Seo M, Moon WK. 18F-FDG uptake in breast cancer correlates with immunohistochemically defined subtypes. European Radiology. 2014; 24: 610-618.
539. Yizhak K, Chaneton B, Gottlieb E, Ruppin E. Modeling cancer metabolism on a genome scale. Molecular Systems Biology. 2015; 11:
540. Hay N. Reprogramming glucose metabolism in cancer: Can it be exploited for cancer therapy? Nature Reviews Cancer. 2016; 16: 635-649.
541. Tennant DA, Durán RV, Boulahbel H, Gottlieb E. Metabolic transformation in cancer. Carcinogenesis. 2009; 30: 1269-1280.
542. Vazquez A, Kamphorst JJ, Markert EK, Schug ZT, Tardito S, Gottlieb E. Cancer metabolism at a glance. Journal of Cell Science. 2016; 129: 3367-3373.

543. Patra KC, Hay N. The pentose phosphate pathway and cancer. Trends in Biochemical Sciences. 2014; 39: 347-354.
544. Yang M, Vousden KH. Serine and one-carbon metabolism in cancer. Nature Reviews Cancer. 2016; 16: 650-662.
545. Locasale JW. Serine, glycine and one-carbon units: Cancer metabolism in full circle. Nature Reviews Cancer. 2013; 13: 572-583.
546. Folger O, Jerby L, Frezza C, Gottlieb E, Ruppin E, Shlomi T. Predicting selective drug targets in cancer through metabolic networks. Molecular Systems Biology. 2011; 7:
547. Agios. *Pipeline - IDH Mutant Inhibitors*. 2016; Available from: http://www.agios.com/pipeline-idh.php.
548. Calithera BioSciences. *We are leveraging our core expertise in tumor biology and medicinal chemistry to develop small molecule selective arginase inhibitors*. 2016; Available from: http://www.calithera.com/programs/arginase-inhibitors/.